City, University of London Institutional Repository

THE BEHAVIOUR OF CLAY IN

SIMPLE SHEAR AND TRIAXIAL TESTS

by

William Hon Wai LAU

B.Sc., M.Sc., D.I.C.

A thesis submitted for the degree of

Doctor of Philosophy

at

The City University

Civil Engineering Department

May 1988

CONTENTS

List of tables

Acknowledgements

Declaration

I grant powers of discretion to the University Librarian to allow this thesis to be copied in whole or in part without further reference to me. This permission covers only single copies made for study purposes, subject to normal conditions of acknowledgement.

Abstract

The main objective of this work is to study the applications of critical state soil mechanics to simple shear testing. The problems with the simple shear apparatus and the approach for interpreting simple shear test results are described. Laboratory tests were conducted using the NGI simple shear apparatus, standard shear box and computer controlled stress path testing equipment for samples with 38 mm and 100 mm diameter. The test programme comprised simple shear and shear box tests on remoulded, reconstituted and undisturbed samples of Cowden till and London clay, undrained triaxial tests on reconstituted and undisturbed London clay and stress probing tests on undisturbed London clay. Simple shear samples were tested under either constant effective vertical stress σ_v' or constant volume condition. Basic results for one-dimensional compression and for shearing obtained from 72 simple shear tests , 27 shear box tests and 16 stress path tests are presented.

Analyses of the simple shear test results indicate that the critical state friction angle for horizontal planes ρ_{cs}' is dependent on whether the sample was sheared under constant σ_v' or constant volume condition and on the pre-shearing value of K_O which is a function of overconsolidation ratio. A theory for the critical states of simple shear tests which takes into account the influence of K_O is proposed. The normalised test data show that the overall patterns of the simple shear and triaxial tests are as predicted by the critical state model. Tangent stiffnesses instead of secant stiffnesses were calculated . For simple shear tests, the shear stiffnesses obtained from constant σ_v' shearing are the same as those obtained from constant volume shearing. For London clay, the normalised shear moduli for undrained triaxial tests have the same order of magnitude as those for constant volume simple shear tests. Results of probing tests show that undisturbed London clay is linear anisotropic elastic. The elastic parameters for the constitutive equations can be measured from special stress paths.

List of symbols

A^e to D^e	parameters in constitutive equations for cross-anisotropic elastic material
A_s to E_s	parameters in constitutive equations for elasto-plastic material under simple shear
A	activity
A	area
E	Young's modulus
E'	Young's modulus in terms of effective stresses
E_u	Young's modulus for undrained (constant volume) loading in terms of total stress
F	flow parameter
F_s	flow parameter for simple shear
F_a	axial force
G'	elastic shear modulus
G_u	elastic shear modulus for undrained loading in terms of total stress
G_s'	elastic shear modulus for simple shear
G_{us}	elastic shear modulus for constant volume loading in terms of total stress for simple shear
G_s, H_s	hardening parameters for simple shear
G_s	specific gravity of soil grains
H	maximum drainage path
K'	elastic bulk modulus
K_s'	elastic one-dimensional bulk modulus for simple shear
K_{us}	elastic one-dimensional bulk modulus for constant volume loading in terms of total stress for simple shear
K_o	coefficient of earth pressure at rest
L	length
LL	liquid limit

LI	liquidity index
N_v	normal load on horizontal planes of simple shear sample
OCR	overconsolidation ratio in terms of $\sigma_v{}'$
PL	plastic limit
PI	plasticity index
R_p	overconsolidation ratio in terms of p'
S_v	shear load on horizontal planes of simple shear sample
T_v	time factor
U_t	average degree of consolidation
V	volume
V_w	volume of water
W	work done

b	$(\sigma_2{}'-\sigma_3{}')/(\sigma_1{}'-\sigma_3{}')$
c'	cohesion
c_u	undrained shear strength
c_v	coefficient of consolidation
d	diameter
d_h, d_v	horizontal displacement, vertical displacement
e	voids ratio
g,h	soil constants defining the Hvorslev surface
g_s, h_s	soil constants defining the Hvorslev surface for simple shear
h	height
k	coefficient of permeability
k	soil constant in the empirical relationship $\tau_{yx}{}'/\sigma_y{}' = k \tan\theta$ for simple shear
m_v	coefficient of volume compressibility
n	porosity

p'	$(1/3)(\sigma_1'+\sigma_2'+\sigma_3')$
p_{cs}'	value of p' at critical state
p_e'	equivalent stress — value of p' on the normal compression line at the same specific volume
p_o'	pre-shearing value of p'
p_p'	maximum previous stress —— value of p' at the intersecting point of the normal compression line and the swelling line of an overconsolidated sample
p_{peak}'	value of p' at peak q'/p' state
p	$(1/3)(\sigma_1+\sigma_2+\sigma_3)$
q'	$(1/\sqrt{2})[(\sigma_1'-\sigma_2')^2+(\sigma_2'-\sigma_3')^2+(\sigma_3'-\sigma_1')^2]^{\frac{1}{2}}$
q_{cs}'	value of q' at critical state
q_o'	pre-shearing value of q'
q_{peak}'	value of q' at peak q'/p' state
q_y'	yield stress
q	$(1/\sqrt{2})[(\sigma_1-\sigma_2)^2+(\sigma_2-\sigma_3)^2+(\sigma_3-\sigma_1)^2]^{\frac{1}{2}}$
r	radius
t	time
t_1	time for calculation of c_v in $\sqrt{(time)}$ curve fitting method
t	thickness
u	pore pressure
u_o	steady-state pore pressure
$\bar{u}$	excess pore pressure
v	specific volume
v_{cs}	value of v at critical state
v_o	pre-shearing value of v
v_p	value of v at peak τ_v'/σ_v' state for simple shear and shear box
v_{peak}	value of v at peak q'/p' state
$v_{\kappa o}$	specific volume of one-dimensionally overconsolidated soil swelled to $p'=1.0$ kPa

$v_{\kappa s}, v_{\kappa b}$	specific volume of one-dimensionally overconsolidated soil swelled to $\sigma_v'=1.0$ kPa for simple shear and shear box
v_λ	specific volume on reference section with $p'=1.0$ kPa
$v_{\lambda s}$	specific volume on reference section with $\sigma_v'=1.0$ kPa for simple shear
w	water content
x,y,z	reference axes (y for vertical)

Γ	specific volume on reference section with $p'=1.0$ kPa at critical state
Γ_s	specific volume on reference section with $\sigma_v'=1.0$ kPa at critical state for simple shear
Δ	large increment of
M	slope of critical state line on p',q' plane
M_c	value of M for triaxial compression test
M_e	value of M for triaxial extension test
N	specific volume of isotropically normally compressed soil at $p'=1.0$ kPa
N_o	specific volume of one-dimensionally normally compressed soil at $p'=1.0$ kPa
N_s, N_b	specific volume of one-dimensionally normally compressed soil at $\sigma_v'=1.0$ kPa for simple shear and shear box
Σ	sum of

α	$45°+(\phi'/2)$, angle defining planes with maximum τ'/σ'
α_s	pore pressure parameter for simple shear
β	$45°+(\psi/2)$, angle defining directions of zero strain increment
γ	engineer's shear strain; shear strain parameter for simple shear and shear box
γ	unit weight
γ_w	unit weight of water

ε_n, γ_n	strains for planes parallel with the directions of zero strain increment
δ	small increment of
ε	strain
$\varepsilon_a, \varepsilon_r$	axial strain, radial strain
ε_s	$(\sqrt{2}/3)[(\varepsilon_1-\varepsilon_2)^2+(\varepsilon_2-\varepsilon_3)^2+(\varepsilon_3-\varepsilon_1)^2]^{\frac{1}{2}}$
ε_v	$(\varepsilon_1+\varepsilon_2+\varepsilon_3)$; volumetric strain parameter for simple shear and shear box
$\varepsilon_1, \varepsilon_2, \varepsilon_3$	principal strains (subscripts 1,2,3 denote major, intermediate and minor respectively)
η'	q'/p'
η_s'	τ_v'/σ_v'
θ	angle of rotation of directions of principal stresses
θ	angle of rotation of directions of principal strain increments
κ	slope of swelling line on $v, \ln p'$ plane
κ_s, κ_b	slope of swelling line on $v, \ln \sigma_v'$ plane for simple shear and shear box
λ	slope of normal compression line on $v, \ln p'$ plane
λ_s, λ_b	slope of normal compression line on $v, \ln \sigma_v'$ plane for simple shear and shear box
μ'	$K'/3G'$
μ_s'	K_s'/G_s'
μ	factor for calculating rate of dissipation of excess pore pressure in Equation (E.3)
ν	Poisson's ratio
ν_u	0.5, Poisson's ratio for constant volume (undrained) loading in terms of total stresses
ρ'	angle of shearing resistance on horizontal planes
ρ_{cs}'	angle of shearing resistance on horizontal planes at critical state
ρ	settlement
σ'	effective normal stress

σ	total normal stress
σ_a', σ_r'	effective axial stress, effective radial stress
σ_h'	effective normal stress on vertical planes
σ_{oct}'	effective octahedral normal stress
σ_v'	effective normal stress parameter for simple shear and shear box
$(\sigma_v')_{cs}$	value of σ_v' at critical state for simple shear and shear box
$(\sigma_v')_p$	value of σ_v' at peak τ_v'/σ_v' state for simple shear and shear box
σ_{ve}'	equivalent stress — value of σ_v' on the normal compression line at the same specific volume for simple shear
σ_{vo}'	pre-shearing value of σ_v'
σ_{vp}'	maximum previous stress — value of σ_v' at the intersecting point of the normal compression line and the swelling line of an overconsolidated sample for simple shear and shear box
σ_1', σ_2', σ_3'	effective principal stresses (subscripts 1,2,3 denote major, intermediate and minor respectively)
τ'	effective shear stress
τ	total shear stress
τ_v'	effective shear stress parameter for simple shear and shear box
$(\tau_v')_{cs}$	value of τ_v' at critical state for simple shear and shear box
$(\tau_v')_p$	value of τ_v' at peak τ_v'/σ_v' state for simple shear and shear box
τ_{oct}'	effective octahedral shear stress
ϕ'	maximum angle of shearing resistance
ϕ_{cs}'	maximum angle of shearing resistance at critical state
ϕ_p'	maximum angle of shearing resistance at peak shear stress
ψ	angle of dilation
ω'	angle of shearing resistance on vertical planes
ω_{cs}'	angle of shearing resistance on vertical planes at critical state

Superscripts

'	effective stress e.g. σ'
e	elastic
p	plastic

Subscripts

a	axial
b	shear box
cs	critical state
e	equivalent stress — stress on the normal compression line at the same specific volume e.g. σ_{ve}'
h	horizontal
o	ordinary strain
oct	octahedral
ps	plane strain
r	radial
s	simple shear
u	undrained; constant volume
v	vertical
x,y,z	reference axes (y for vertical)
o	K_o condition

CHAPTER 1   INTRODUCTION

Over the last twenty years critical state soil mechanics have been developed into a simple and powerful model for understanding the mechanical behaviour of soils. The strength of the model lies in its unification of the fundamental concepts of consolidation, compression, yielding and failure of soils for both undrained and drained loading. Most of the ideas in the critical state theory originated from and are supported by laboratory test results obtained from the triaxial apparatus. There are, however, various loading conditions in the field which are not simulated by the triaxial test. One of these conditions is simple shear loading characterized by shearing associated with the rotation of principal stress directions under plane strain conditions. Such a loading condition occurs, for example, in slope stability problems, adjacent to friction piles or beneath foundations of off-shore platforms. Although the simple shear test existed even before the development of the critical state theory, there have been very few studies which relate simple shear testing to the critical state model. The main objective of this project is to examine the applications of the critical state theory to simple shear tests on saturated clays. A secondary objective is to compare soil behaviour in triaxial tests and simple shear tests.

The layout of this thesis follows the usual conventions observed by most dissertations based on experimental work. Chapter 2 outlines the basic concepts of the critical state model to provide a framework for the analyses of data obtained from laboratory tests. The current knowledge on simple shear testing and on the two clays, Cowden till and London clay are described in Chapter 3. Chapter 4 gives the engineering geology background of the two clays which is useful for understanding the behaviour of undisturbed samples. The equipment used and the testing procedures followed are described in Chapter 5 and the raw test data are presented in Chapter 6. Chapter 7 brings together the previous chapters to develop new understanding of simple shear tests, triaxial tests and critical state soil

mechanics through analyses and discussions. Chapter 8 sums up the conclusions drawn in Chapter 7 and recommends possible future work.

CHAPTER 2   BASIC THEORY

2.1   Introduction

The purpose of this chapter is to form a basis for the theory which will be used to analyse the test data presented in Chapter 6.   In the beginning of the chapter, the preliminaries section defines the parameters to be used and the conventions to be adopted. Then, the approach for analysing the states of stress and strain in simple shear samples will be outlined and the basic concepts of elasticity and plasticity will be described in terms of idealised stress-strain behaviour. The critical state model will provide the overall framework for analyses and discussions in Chapter 7. Finally, procedures for normalising test data which enable experimental results to be compared with theoretical predictions will be given.

2.2   Preliminaries

2.2.1   Stresses and strains in soils

In the analysis of stress and strain in soils, the soil mass is approximated to a continuum so that all infinitesimal elements have the same properties as the mass. The normal and shear stresses acting on a small two-dimensional element OABC are shown in Figure 2.1(a) and the associated normal and shear strains are shown in Figure 2.1(b). The same orientation of the orthogonal reference axes x , y and z as defined in Figure 2.1 will be used throughout this study. Compressive normal stresses and strains are defined as positive and shear stresses and shear strains associated with increases in the angles in the positive quadrants of the element are defined as positive. Therefore, all the stresses and strains shown in Figure 2.1 are positive quantities.

2.2.2   The principle of effective stress

The principle of effective stress was first stated by Terzaghi (1936). Based on results from numerous experiments on various saturated materials including sand and clay over a wide range of total normal stresses σ and pore pressures u, Terzaghi concluded that all the measurable effects of a change of stress, such as deformation and a change of shearing resistance, are exclusively due to changes of effective stresses σ' where

$$\sigma' = \sigma - u \qquad (2.1)$$

For engineering purposes, zero value of the stresses σ and u is atmospheric pressure.

2.2.3   Pure shear strain and engineer's shear strain

Figure 2.2(a) shows the strained element O'A'B'C' with shear strains ε_{xy} and ε_{yx}. By rotating the element counter-clockwise about O' through an angle ε_{xy}, Figure 2.2(b) is obtained. This shows that

$$\gamma_{yx} = \varepsilon_{xy} + \varepsilon_{yx} \qquad (2.2)$$

but

$$\varepsilon_{xy} = \varepsilon_{yx} \qquad (2.3)$$

therefore,

$$\gamma_{yx} = 2\varepsilon_{yx} \qquad (2.4)$$

Similarly,

$$\gamma_{xy} = 2\varepsilon_{xy} \qquad (2.5)$$

ε_{xy} and ε_{yx} are pure shear strains and γ_{xy} and γ_{yx} are engineer's shear strains. The engineer's shear strain consists of a component of pure shear strain together with a numerically equal component of body rotation. It gives a measure of the change of angle between two initially orthogonal fibres embedded in the x,y plane.

2.2.4   Mohr's circles of stress and strain

The Mohr's circle of stress and Mohr's circle of strain corresponding

to the states of stress and strain in Figure 2.1 are shown in Figure 2.3. For plotting Mohr's circles, counter-clockwise shear stresses and shear strains are defined as positive. Hence, the counter-clockwise shear stress τ_{yx} and shear strain $\frac{1}{2}\gamma_{yx}$ in Figure 2.1 are positive in Figure 2.3 and the clockwise shear stress τ_{xy} and shear strain $\frac{1}{2}\gamma_{xy}$ are negative. Stresses and strains associated with the element at different orientations with respect to the x,y axes can be obtained from the pole of planes P.

2.2.5   Definition of stress parameters

For triaxial tests, the stress parameters used are stress invariants which are independent of the orientation of the reference axes and are measures of the three-dimensional stress states of the samples. The invariants for effective normal and shear stresses are p' and q' respectively. In terms of effective axial stress σ_a' and effective radial stress σ_r' which are principal stresses, p' and q' are defined as

$$p' = (1/3)(\sigma_a' + 2\sigma_r') \qquad (2.6)$$

$$q' = (\sigma_a' - \sigma_r') \qquad (2.7)$$

For general states of stress, where σ_2' may not be equal to σ_3', p' and q' are defined as

$$p' = (1/3)(\sigma_1' + \sigma_2' + \sigma_3') \qquad (2.8)$$

$$q' = (1/\sqrt{2})[(\sigma_1' - \sigma_2')^2 + (\sigma_2' - \sigma_3')^2 + (\sigma_3' - \sigma_1')^2]^{\frac{1}{2}} \qquad (2.9)$$

For simple shear tests and shear box tests, the stress parameters are not invariants. They are the average stresses determined from the normal load N_v and shear load S_v acting on the horizontal boundaries of the sample. The forces N_v, S_v acting on a simple shear sample are shown in Figure 2.4. The total normal stress and shear stress parameters are defined as

$$\sigma_v = N_v/A \qquad \text{and} \qquad \tau_v = S_v/A \qquad (2.10)$$

where A is the horizontal cross-sectional area.   For shear box tests

the current horizontal cross-sectional area is used in calculating both normal stress and shear stress. The corresponding effective stress parameters are

$$\sigma_v' = \sigma_v - u \qquad \text{and} \qquad \tau_v' = \tau_v \qquad (2.11)$$

where u is the pore pressure in the sample.

2.2.6   Definition of strain parameters

For triaxial tests, the strain parameters used are strain invariants which are independent of the orientation of the reference axes and are measures of the three-dimensional states of strain of the samples. The invariants for volumetric strain and shear strain are ε_v and ε_s respectively.   In terms of axial strain ε_a and radial strain ε_r which are principal strains, ε_v and ε_s are defined as

$$\varepsilon_v = (\varepsilon_a + 2\varepsilon_r) \qquad (2.12)$$

$$\varepsilon_s = (2/3)(\varepsilon_a - \varepsilon_r) \qquad (2.13)$$

For general states of strain, where ε_2 may not be equal to ε_3, they are defined as

$$\varepsilon_v = (\varepsilon_1 + \varepsilon_2 + \varepsilon_3) \qquad (2.14)$$

$$\varepsilon_s = (\sqrt{2}/3)[(\varepsilon_1 - \varepsilon_2)^2 + (\varepsilon_2 - \varepsilon_3)^2 + (\varepsilon_3 - \varepsilon_1)^2]^{\frac{1}{2}} \qquad (2.15)$$

For simple shear tests and shear box tests, the strain parameters are not invariants.   They are strains determined from increments of vertical displacement δy and increments of horizontal displacement δx measured at the boundaries of the sample. The volumetric strain and shear strain parameters are defined as

$$\varepsilon_v = \Sigma(-\delta y/h) \qquad \text{and} \qquad \gamma = \Sigma(-\delta x/h) \qquad (2.16)$$

where h is the current height of the sample.

37

2.2.7   Correspondence between parameters for stress and strain

Stress and strain parameters are correctly chosen if the sum of the products of corresponding parameters of stress and of strain gives the work done by external loads and pressures.   The work done by external loads and pressures is an invariant but the corresponding stress and strain parameters are not necessarily invariants.

For triaxial tests,   the correspondence between the stress parameters p', q' and the strain parameters ε_v, ε_s have already been demonstrated by Atkinson and Bransby (1978).

For simple shear tests, the correspondence between the stress parameters σ_v', τ_v' and the strain parameters ε_v, γ can be demonstrated in a similar manner. The work done by external loads and pressures is first calculated by considering the sample under simple shear shown in Figure 2.4.   During a small time interval,   the vertical force N_v and shear force S_v acting on the horizontal boundaries of the sample caused the deformations $-\delta x$ and $-\delta y$. Assuming the pore pressure has a constant value u and the volume of water expelled is δV_w , the work done δW by the external loads and pressures is

$$\delta W = S_v(-\delta x) + N_v(-\delta y) - u\,V_w \qquad (2.17)$$

Hence, the work done per unit volume is

$$\frac{\delta W}{V} = \frac{S_v}{A}\left(-\frac{\delta x}{h}\right) + \frac{N_v}{A}\left(-\frac{\delta y}{h}\right) + u\,\frac{\delta V}{V}$$

where δV is the change in volume of the sample.   Therefore,

$$\delta W/V = \tau_v \delta\gamma + \sigma_v \delta\varepsilon_v - u\delta\varepsilon_v$$

$$= \tau_v \delta\gamma + (\sigma_v - u)\delta\varepsilon_v \qquad (2.18)$$

Using Equation (2.11),

$$\delta W/V = \tau_v'\delta\gamma + \sigma_v'\delta\varepsilon_v \qquad (2.19)$$

The work done per unit volume calculated from the stress and strain

parameters is

$$\delta W/V = \tau_v' \delta \gamma + \sigma_v' \delta \varepsilon_v \qquad (2.20)$$

Since Equations (2.19) and (2.20) lead to identical expressions for $\delta W/V$, the strain parameters γ, ε_v are correctly associated with the stress parameters τ_v', σ_v' for simple shear tests.

2.2.8   Relationships between ordinary strains and natural strains

The importance of using natural strains in the analysis of soil test data has been considered by Richardson (1984a). To distinguish between ordinary strains and natural strains a subscript 'o' is added to ordinary strain parameters.

For normal strains the relationship between ordinary strains and natural strains is

$$\varepsilon = -\ln(1 - \varepsilon_o) \qquad (2.21)$$

Equation (2.21) allows natural strain parameters $\varepsilon_1, \varepsilon_3$ to be calculated from ordinary strain parameters $\varepsilon_{1o}, \varepsilon_{3o}$. The triaxial natural strain parameters ε_v, ε_s are then calculated from $\varepsilon_1, \varepsilon_3$ using Equations (2.12) and (2.13).

For simple shear tests, the relationship between ordinary and natural volumetric strain is derived as

$$\delta \varepsilon_v = -\delta y/h \qquad (2.22)$$

since $\delta y = \delta h$, the accumulated strain is

$$\int_0^{\varepsilon_v} \delta \varepsilon_v = \int_{h_o}^{h} -\frac{1}{h} \delta h$$

where h_o is the reference height at the start of the test. Therefore,

$$\varepsilon_v = -\ln(h/h_o) \qquad (2.23)$$

but, $$\varepsilon_{vo} = -(h-h_o)/h_o \qquad (2.24)$$

giving $\qquad h_0/h = 1-\varepsilon_{vo}$ $\qquad$ (2.25)

so, $\qquad \varepsilon_v = -\ln(1-\varepsilon_{vo})$ $\qquad$ (2.26)

For simple shear strains, an increment of natural strain is shown in Figure 2.4. By geometry,

$$\delta\gamma = \tan^{-1}\left(\frac{-x-\delta x}{h+\delta h}\right) - \tan^{-1}\left(\frac{-x}{h}\right) \qquad (2.27)$$

For small increments of shear strain, Equation (2.27) can be written as

$$\delta\gamma = \left(\frac{-x-\delta x}{h+\delta h}\right) - \left(\frac{-x}{h}\right) \qquad (2.28)$$

and for small increments of δh, Equation (2.28) can be written as

$$\delta\gamma = -\delta x/h \qquad (2.29)$$

The accumulated strain is therefore

$$\int_0^\gamma \delta\gamma = \int_0^x -\frac{1}{h} \delta x \qquad (2.30)$$

There is no explicit solution for Equation (2.30) because x and h are independent variables. Values of γ can only be calculated numerically by summing up individual values of $\delta\gamma$.

2.3   Analysis of stresses and strains in simple shear tests

2.3.1   Analysis of stresses

In an ideal simple shear test, effective stresses as shown in Figure 2.5 are uniformly imposed on the sample. The Mohr's circle of stress corresponding to the state of stress in Figure 2.5 is shown in Figure 2.6. The major principal effective stress σ_1' and minor principal effective stress σ_3' rotate through an angle θ during shearing. The intermediate principal effective stress σ_2' coincides with σ_z' because shear stresses τ_{zx}' and τ_{zy}' acting on the x,y plane are both zero. The pole of planes is at P and the principal planes for σ_1' and σ_3' are rotated through the angle θ.

40

From the geometry of Figure 2.6 the maximum angle of shearing resistance mobilised in the soil mass ϕ' is defined as

$$\phi' = \sin^{-1}\left(\frac{\sigma_1' - \sigma_3'}{\sigma_1' + \sigma_3'}\right) \tag{2.31}$$

The angle of shearing resistance mobilised on the horizontal plane is defined as

$$\rho' = \tan^{-1}\left(\frac{\tau_{yx}'}{\sigma_y'}\right) \tag{2.32}$$

and the angle of shearing resistance mobilised on the vertical plane is defined as

$$\omega' = \tan^{-1}\left(\frac{\tau_{xy}'}{\sigma_x'}\right) \tag{2.33}$$

The angles ϕ', ρ' and ω' vary during shearing and at critical state, the theory of which will be outlined later, they become ϕ_{cs}', ρ_{cs}' and ω_{cs}'. The angle ϕ_{cs}' is assumed to be a soil constant.

For tests in the NGI simple shear apparatus, assuming the stresses in the sample are uniform, the stresses σ_v', τ_v' measured are the stresses σ_y', τ_{yx}'. The angle ρ' can be obtained from σ_y', τ_{yx}' using Equation (2.32). However, without also knowing σ_x' or θ, the Mohr's circle of stress cannot be drawn and the stress state of the sample cannot be determined. Furthermore, the angle ϕ' and the soil constant ϕ_{cs}' cannot be calculated from the stresses σ_y', τ_{yx}' alone. Methods of estimating the stress state, and hence, ϕ_{cs}' will be discussed in Section 3.3.2.

The relationships among the parameters ϕ', ρ' and θ can be obtained from the geometry of Figure 2.6. For the case of $\sigma_y' > \sigma_x'$ before shearing,

$$\phi' = \sin^{-1}\left[\frac{1}{\dfrac{\sin(2\theta)}{\tan \rho'} - \cos(2\theta)}\right] \tag{2.34}$$

$$\rho' = \tan^{-1}\left[\frac{\sin(2\theta)}{\dfrac{1}{\sin \phi'} + \cos(2\theta)}\right] \tag{2.35}$$

$$\theta = \frac{1}{2}\left[\sin^{-1}\left(\frac{\sin \rho'}{\sin \phi'}\right) + \rho'\right] \quad \text{for } 2\theta \leqslant 90°+\phi' \qquad (2.36a)$$

$$\theta = 90° - \frac{1}{2}\left[\sin^{-1}\left(\frac{\sin \rho'}{\sin \phi'}\right) - \rho'\right] \quad \text{for } 2\theta \geqslant 90°+\phi' \qquad (2.36b)$$

For the case of $\sigma_y' < \sigma_x'$ before shearing,

$$\phi' = \sin^{-1}\left[\frac{1}{\dfrac{\sin(2\theta)}{\tan \rho'} + \cos(2\theta)}\right] \qquad (2.37)$$

$$\rho' = \tan^{-1}\left[\frac{\sin(2\theta)}{\dfrac{1}{\sin \phi'} - \cos(2\theta)}\right] \qquad (2.38)$$

$$\theta = \frac{1}{2}\left[\sin^{-1}\left(\frac{\sin \rho'}{\sin \phi'}\right) - \rho'\right] \quad \text{for } 2\theta \leqslant 90°-\phi' \qquad (2.39a)$$

$$\theta = 90° - \frac{1}{2}\left[\sin^{-1}\left(\frac{\sin \rho'}{\sin \phi'}\right) + \rho'\right] \quad \text{for } 2\theta \geqslant 90°-\phi' \qquad (2.39b)$$

Similar equations which apply to critical state can be written by substituting the parameters ϕ', ρ', θ by the critical state parameters $\phi_{cs}', \rho_{cs}', \theta_{cs}$. Equations (2.36a) and (2.36b) show that knowing ρ' and ϕ' there are two possible values of θ. This is because each point (σ_y', τ_{yx}') is associated with two possible Mohr's circles, one with $2\theta < 90°+\phi'$ and the other with $2\theta > 90°+\phi'$. For the special case when (σ_y', τ_{yx}') lies on the ϕ' envelope, there is only one possible Mohr's circle and both Equations (2.36a) and (2.36b) become $\theta = \frac{1}{2}(90°+\rho')$.

Figure 2.7 shows that two planes are subjected to a maximum stress ratio of $\tan \phi'$. The directions of these two planes are defined by the angle α and from the geometry of Figure 2.7,

$$\alpha = 45° + \tfrac{1}{2} \phi' \qquad\qquad (2.40)$$

2.3.2 Anaylsis of strains

In a simple shear test, if the intended boundary conditions are met and the strains are uniform, the incremental strains occurring in the sample are as shown in Figure 2.8. Since no radial deformation is allowed,

$$\varepsilon_x = , \varepsilon_z = 0 \qquad\qquad (2.41)$$

From the definitions of the parameters ε_v, γ given by Equation (2.16),

$$\delta\varepsilon_y = -\delta y/h = \delta\varepsilon_v \qquad\qquad (2.42)$$

$$\delta\gamma_{yx} = -\delta x/h = \delta\gamma \qquad\qquad (2.43)$$

Equation (2.43) shows that a simple shear strain increment is an engineer's shear strain increment. Mohr's circles of strain increment for a compressing sample and for a dilating sample are shown in Figures 2.9(a) and (b) respectively. The major principal strain increment $\delta\varepsilon_1$ and minor principal strain increment $\delta\varepsilon_3$ rotate through an angle θ during shearing. The intermediate principal strain increment $\delta\varepsilon_2$ coincides with $\delta\varepsilon_z$ because shear strains γ_{zx} and γ_{zy} are both zero and from Equation (2.41),

$$\delta\varepsilon_2 = 0 \qquad\qquad (2.44)$$

Equation (2.44) indicates that the sample deforms under plane strain condition. The pole of planes is at P and the principal planes for $\delta\varepsilon_1$ and $\delta\varepsilon_3$ are rotated through the angle θ. From the geometry of Figure 2.9,

$$\delta\varepsilon_1 = \frac{\delta\varepsilon_v + \sqrt{[(\delta\varepsilon_v)^2 + (\delta\gamma)^2]}}{2} \qquad\qquad (2.45a)$$

$$\delta\varepsilon_3 = \frac{\delta\varepsilon_v - \sqrt{[(\delta\varepsilon_v)^2 + (\delta\gamma)^2]}}{2} \qquad\qquad (2.45b)$$

Combining Equations (2.15), (2.44), (2.45a) and (2.45b),

$$\delta \mathcal{E}_s = \frac{2}{3} \left[(\delta \mathcal{E}_v)^2 + \frac{3}{4} (\delta \gamma)^2 \right]^{\frac{1}{2}} \tag{2.46}$$

The angle of dilation ψ which represents the relative magnitudes of normal and shear strains is defined as

$$\psi = -\sin^{-1}\left(\frac{\delta \mathcal{E}_1 + \delta \mathcal{E}_3}{\delta \mathcal{E}_1 - \delta \mathcal{E}_3}\right) \tag{2.47}$$

and, in terms of the simple shear strain parameters,

$$\psi = -\tan^{-1}\left(\frac{\delta \mathcal{E}_v}{\delta \gamma}\right) \tag{2.48}$$

The angle ψ is positive for negative (dilational) volumetric strain and negative for positive (compressive) volumetric strain. Hence, from the geometry of Figure 2.9,

$$\psi = 2\theta - 90° \tag{2.49}$$

In each of Figures 2.9(a) and (b), there are two planes represented by broken lines for which increments of normal strain are zero and the directions of zero strain increment (also called zero extension lines) are normal to these planes. One of these planes is vertical and the other, from the geometry of Figure 2.9 is inclined at an angle of ψ to the horizontal.

Figure 2.10 shows the directions of zero strain increment corresponding to the planes represented by the broken lines in Figure 2.9(a). One of these directions is horizontal and the other, from the geometry of Figure 2.9(a), is inclined at an angle of ψ to the vertical. The directions of zero strain increment can also be defined by the angle β which, from the geometry of Figure 2.10, is given by

$$\beta = \theta = 45° + \frac{1}{2}\psi \tag{2.50}$$

The increments of shear and normal strains for planes parallel with the directions of zero strain increment are marked as $\delta \gamma_n, \delta \mathcal{E}_n$. From the geometry of Figure 2.10, $\delta \mathcal{E}_n = \delta \mathcal{E}_v$, $\delta \gamma_n = \delta \gamma$ and the tangents to the Mohr's circle at the points $(\delta \mathcal{E}_n, \frac{1}{2}\delta \gamma_n)$ make an angle ψ with

44

the $\delta\epsilon$ axis.

For the case of constant volume shearing, for which no volume change
is allowed to take place during shearing, Equation (2.48) shows that
ψ is zero. According to Equation (2.49), θ becomes a constant value
of $45°$ so that there is no rotation of $\delta\epsilon_1$ and $\delta\epsilon_3$ during constant
volume shearing and the Mohr's circle of strain increment is as shown
in Figure 2.11. Equation (2.50) shows that for $\psi = 0$, the directions
of zero strain increment are the horizontal and vertical directions.
This is so because during constant volume shearing the sample is not
allowed to deform in the horizontal and vertical directions.

2.4   Elasticity and plasticity for soils

2.4.1   Purely elastic stress-strain behaviour

When a purely elastic material is loaded, the energy transferred from
external forces to the material is fully recoverable when the material
is unloaded. Elastic strain increments are related to increments of
stress and the stress-strain behaviour of an ideal isotropic elastic
material is given by the generalised form of Hooke's law as

$$\delta\epsilon_x^e = (1/E')(\delta\sigma_x' - \gamma'\delta\sigma_y' - \gamma'\delta\sigma_z') \qquad (2.51a)$$

$$\delta\epsilon_y^e = (1/E')(\delta\sigma_y' - \gamma'\delta\sigma_z' - \gamma'\delta\sigma_x') \qquad (2.51b)$$

$$\delta\epsilon_z^e = (1/E')(\delta\sigma_z' - \gamma'\delta\sigma_x' - \gamma'\delta\sigma_y') \qquad (2.51c)$$

$$\delta\gamma_{xy}^e = (2/E')(1 + \gamma')\,\delta\tau_{xy}' \qquad (2.51d)$$

$$\delta\gamma_{yz}^e = (2/E')(1 + \gamma')\,\delta\tau_{yz}' \qquad (2.51e)$$

$$\delta\gamma_{zx}^e = (2/E')(1 + \gamma')\,\delta\tau_{zx}' \qquad (2.51f)$$

where E' and γ' are the Young's modulus and Poisson's ratio for
changes of effective stress. If the material is linear elastic E'
and γ' are constants.

When the reference axes x, y, z coincide with the axes for principal

stresses and strains, Equations (2.51) become

$$\delta \varepsilon_1^e = (1/E')(\delta\sigma_1' - \nu'\delta\sigma_2' - \nu'\delta\sigma_3')$$

$$\delta \varepsilon_2^e = (1/E')(\delta\sigma_2' - \nu'\delta\sigma_3' - \nu'\delta\sigma_1') \qquad (2.52)$$

$$\delta \varepsilon_3^e = (1/E')(\delta\sigma_3' - \nu'\delta\sigma_1' - \nu'\delta\sigma_2')$$

For triaxial tests, with $\delta\sigma_2' = \delta\sigma_3'$ and $\delta\varepsilon_2 = \delta\varepsilon_3$, Equations (2.52) give

$$\delta\varepsilon_s^e = \frac{2(1+\nu')}{3E'} \delta q' = \frac{1}{3G'} \delta q' \qquad (2.53)$$

$$\delta\varepsilon_v^e = \frac{3(1-2\nu')}{E'} \delta p' = \frac{1}{K'} \delta p' \qquad (2.54)$$

where G' is the shear modulus, K' is the bulk modulus, and they are related to E' and ν' by

$$G' = E'/[2(1+\nu')] \qquad \text{and} \qquad K' = E'/[3(1-2\nu')] \qquad (2.55)$$

For simple shear tests, Equation (2.51d) gives

$$\delta\gamma^e = \frac{2}{E'} (1+\nu') \delta\tau_v' = \frac{1}{G_s'} \delta\tau_v' \qquad (2.56)$$

where G_s' is the shear modulus and it is related to E' and ν' by

$$G_s' = E'/[2(1+\nu')] \qquad (2.57)$$

The subscript 's' of G_s' indicates that the parameter G_s' is appropriate for simple shear tests, and from now on subscripts 's' will be added to all simple shear parameters. Although the stress and strain parameters for triaxial and simple shear tests are different, Equations (2.55) and (2.57) show that the shear moduli for the two types of tests are the same.

Substituting Equation (2.41) into Equations (2.51a) and (2.51c) gives

$$\delta\sigma_x' - \gamma' \delta\sigma_y' - \gamma' \delta\sigma_z' = 0$$

$$\delta\sigma_z' - \gamma' \delta\sigma_x' - \gamma' \delta\sigma_y' = 0$$

hence,
$$\delta\sigma_x' = \delta\sigma_z' = [\gamma'/(1-\gamma')] \delta\sigma_y' \qquad (2.58)$$

Substituting Equation (2.58) into Equation (2.51b),

$$\delta\varepsilon_v^e = \frac{1}{E'} \frac{(1+\gamma')(1-2\gamma')}{(1-\gamma')} \delta\sigma_v' = \frac{1}{K_s'} \delta\sigma_v' \qquad (2.59)$$

and the modulus K_s' is related to E' and γ' by

$$K_s' = [(1-\gamma')E'] / [(1+\gamma')(1-2\gamma')] \qquad (2.60)$$

From Equations (2.54) and (2.59), it can be seen that both the bulk modulus K' and the modulus K_s' relate an effective normal stress increment to an elastic volumetric strain increment. On the other hand, K' is appropriate for three-dimensional stress and strain increments whileas K_s' is only appropriate for one-dimensional stress and strain increments. Therefore, K_s' is referred to as an one-dimensional bulk modulus.

Equations (2.53) and (2.56) demonstrate that increments of elastic shear strains are dependent only on the corresponding increments of shear stresses and Equations (2.54) and (2.59) demonstrate that increments of elastic volumetric strains are dependent only on the corresponding increments of normal stresses. As a result, the stress and strain increments of an isotropic elastic material are said to be decoupled.

Using Equations (2.51a) to (2.51c), it can be shown that for both constant volume and constant σ_v' simple shear tests on isotropic elastic material, $\delta\sigma_x' = \delta\sigma_y' = 0$. Hence, the Mohr's circle of stress increment is as shown in Figure 2.12. Such stress increments, with $\delta\sigma_1' = -\delta\sigma_3'$, are known as pure shear stress increments. The effect of superposing pure shear increments on any initial stress state is that the Mohr's circle of stress will change in size but the centre of the Mohr's circle remains unchanged. From the geometry of Figure 2.12, $\delta\sigma_1'$ is inclined to the vertical at an angle of 45°. If σ_1' is

vertical before shearing, the inclination of σ_1' to the vertical, θ, will be intermediate between 0° and 45° during shearing. The exact value will depend on the relative magnitudes of the initial σ_1' and the changes in stress.

Soils which are deposited one-dimensionally are cross-anisotropic with an axis of symmetry in the vertical direction. To describe the stress-strain behaviour of a cross-anisotropic elastic material requires five independent elastic parameters: Young's modulus in the vertical direction E_v', Young's modulus in any horizontal direction E_h', Poisson's ratio for horizontal normal strain increments due to vertical normal stress increments ν_{vh}' Poisson's ratio for horizontal normal strain increments due to orthogonal horizontal normal stress increments ν_{hh}' and the shear modulus for shear strain increments for vertical planes G_{vh}'.

When the axes of principal stresses and strains coincide with the vertical and horizontal directions, the stress-strain relationships for a cross-anisotropic elastic material can be written as

$$\delta\varepsilon_s^e = A^e \; \delta q' + B^e \; \delta p' \qquad (2.61a)$$

$$\delta\varepsilon_v^e = C^e \; \delta q' + D^e \; \delta p' \qquad (2.61b)$$

with the relationships between the parameters A^e to D^e and the parameters E_v', E_h', ν_{vh}' and ν_{hh}' as shown in Appendix A. From Equations (A.1) to (A.3) of Appendix A it can be deduced that for the case of isotropy $B^e = C^e = 0$ and Equations (2.61a) and (2.61b) become Equations (2.53) and (2.54) respectively.

For an anisotropic elastic material the stress and strain increments are coupled. Equation (2.61a) shows that elastic shear strain increments are dependent on both shear stress increments and normal stress increments and Equation (2.61b) shows that elastic volumetric strain increments are also dependent on both shear stress increments and normal stress increments.

In practice, the elastic parameters A^e to D^e can be determined

from triaxial tests using the stress path testing equipment described in Chapter 5. The parameters A^e and C^e can be measured by subjecting the sample to changes in q' while holding p' constant and the parameters B^e and D^e can be measured by subjecting the sample to changes in p' while holding q' constant.

2.4.2   Purely plastic stress-strain behaviour

A material is considered to be purely plastic if it does not suffer from any elastic deformation but only deforms plastically. For a plastic strain increment, all the energy transferred from external forces to the material is dissipated as friction and is, therefore, irrecoverable when the material is unloaded.

Figure 2.13(a) shows an example of an idealised purely plastic soil tested in triaxial condition. When the material is loaded from A to B there is no straining until the stress reaches q_y' at B when plastic straining occurs. The stress q_y' is known as yield stress and the material is said to be yielding when plastic straining occurs. When the material is unloaded from C to D, none of the plastic strain is recovered. On reloading from D yielding occurs again at C and if the stress is maintained at q_y' straining will occur indefinitely.

Figure 2.13(b) shows the behaviour of a purely plastic soil which strain hardens. At F, no straining will occur unless the stress is increased above the yield stress q_{y1}'. As the stress is increased the material strains and moves to G when it is unloaded to H. On reloading from H, no straining will occur unless the stress is increased above the yield stress q_{y2}'. Hence, due to straining from F to G the yield stress of the material has been increased from q_{y1}' to q_{y2}'. When the material is loaded beyond G it continues to strain harden until it reaches J. At J, if the stress is maintained at q_{y3}' straining will occur indefinitely. A purely plastic material which strain softens behaves similarly except that the yield stress has to be reduced for straining to occur.

For a purely plastic soil with a certain specific volume, combinations of p',q' at yield in triaxial tests or combinations of σ_v',τ_v' at yield in simple shear tests can be plotted to form a yield curve.

Figure 2.14 shows three yield curves KJL, NGP and QFR for three different specific volumes. An infinite number of yield curves with the same shape but different sizes each associated with a particular specific volume form a yield surface in the three-dimensional p',q',v space for triaxial tests and σ_v',τ_v',v space for simple shear tests. The state of a soil may be on or within the yield surface but cannot lie outside it, therefore, the yield surface represents a boundary for all possible states.

When a purely plastic soil is loaded, if the state of the soil remains inside the yield surface, it can only move along a vertical plane corresponding to a particular yield curve such as plane MNGP in Figure 2.14. Also, no straining will occur so that any changes in stress will encounter a rigid response. However, once the state reaches the yield surface, any further increment of stress which causes the state to move from one yield curve to another will result in a plastic strain increment. Hence, no plastic straining occurs unless the state path moves along the yield surface crossing over different yield curves.

Figure 2.14 shows the state path followed by the soil tested in Figure 2.13(b). This path together with the yield curves of Figure 2.14 are projected onto the p',q' plane in Figure 2.15. Figures 2.13 to 2.15 show that as the state path moves from F to G, the yield stress increases from q_{y1}' to q_{y2}' and the yield curve NGP associated with G is larger than the yield curve QFR associated with F. This illustrates the usual behaviour of strain hardening being accompanied by an expansion of the current yield curve. Likewise, strain softening is usually accompanied by a contraction of the current yield curve.

When yielding occurs the direction of the plastic strain increment vector is dependent only on the state of stress and is independent of the direction of the stress increment. The precise relationship between the direction of the vector of plastic strain increment and the stress state is given by a flow rule. For triaxial tests the flow rule has a general form of

$$\delta \varepsilon_s^p / \delta \varepsilon_v^p = F \qquad (2.62a)$$

and for simple shear tests,

$$\delta \gamma^p \, / \, \delta \varepsilon_v^p = F_s \qquad\qquad (2.62b)$$

where F and F_s are flow parameters which depend on the shape of the yield curves. If the plastic strain increment vector is everywhere normal to the yield curve the flow rule is described as associated and the normality condition applies.

The relationship between the magnitude of a plastic strain increment and the magnitude of the corresponding stress increment is given by a hardening law. For simple shear tests the hardening law has the form of

$$\delta \varepsilon_v^p = H_s \, \delta \tau_v{}' + G_s \, \delta \sigma_v{}' \qquad\qquad (2.63)$$

and from Equations (2.62b) and (2.63),

$$\delta \gamma^p = F_s H_s \, \delta \tau_v{}' + F_s G_s \, \delta \sigma_v{}' \qquad\qquad (2.64)$$

Equations similar to Equations (2.63) and (2.64) can be written for triaxial tests.

2.4.3   Elasto-plastic stress-strain behaviour

The behaviour of an elasto-plastic material is a combination of the behaviour of a purely elastic material and the behaviour of a purely plastic material. Figure 2.16 shows an example of an elasto-plastic soil tested in triaxial condition. When the material is loaded from A to B it deforms purely elastically so that when unloaded to A all the strains are recovered. On reloading to B yielding occurs once the stress is increased above $q_{y1}{}'$. As the soil moves along path BC to C it suffers from both elastic and plastic strains. At C, the strain that is due to elastic straining $(\varepsilon_s^e)_c$ and the strain that is due to plastic straining $(\varepsilon_s^p)_c$ are as illustrated. During unload and reload between C and D the behaviour is again purely elastic and reversible. When the stress is increased above $q_{y2}{}'$ the soil continues to strain harden until it reaches E. If the stress is maintained at $q_{y3}{}'$ at E straining will occur indefinitely.

In the three-dimensional p', q', v space for triaxial tests and the σ_v', τ_v', v space for simple shear tests, the yield surface separates states which cause only elastic strains from states which cause both elastic and plastic strains. During loading if the state of the soil remains inside the yield surface, it can only move along a certain surface known as an elastic wall. For an isotropic material the elastic walls are vertical surfaces as shown in Figure 2.17. There is a direct analogy between elastic walls and the vertical planes shown in Figure 2.14. State paths on an elastic wall will only cause elastic strains and state paths which traverse the yield surface will cause both elastic and plastic strains.

For any increment of stress in a simple shear test, the resulting increment of strain can be expressed as the sum of its elastic and plastic components,

$$\delta \gamma = \delta \gamma^e + \delta \gamma^p \tag{2.65}$$

$$\delta \varepsilon_v = \delta \varepsilon_v^e + \delta \varepsilon_v^p \tag{2.66}$$

The elastic components for an isotropic material are given by Equations (2.56) and (2.59), and the plastic components are given by Equations (2.63) and (2.64). Therefore, Equations (2.65) and (2.66) can be written as

$$\delta \gamma = (F_s H_s + 1/G_s') \, \delta \tau_v' + F_s G_s \, \delta \sigma_v' \tag{2.67}$$

$$\delta \varepsilon_v = H_s \, \delta \tau_v' + (G_s + 1/K_s') \, \delta \sigma_v' \tag{2.68}$$

Naylor et al (1981) showed that if the coaxiality condition holds and the flow rule is associated, then

$$F_s G_s = H_s \tag{2.69}$$

Hence, Equations (2.67) and (2.68) become

$$\delta \gamma = (F_s H_s + 1/G_s') \, \delta \tau_v' + H_s \, \delta \sigma_v' \tag{2.70}$$

$$\delta \varepsilon_v = H_s \, \delta \tau_v' + (H_s/F_s + 1/K_s) \, \delta \sigma_v' \tag{2.71}$$

Equations similar to Equations (2.65) to (2.71) can be written for triaxial tests.

2.5   The critical state model

The crucial idea of the critical state model is that the mechanical behaviour of a soil can be specified with reference to a unique state boundary surface. The state boundary surface represents a boundary to all possible states of stresses and specific volume. It is assumed that the behaviour of soil is elasto-plastic and that the state boundary surface is the yield surface. Therefore, the behaviour of samples of soil whose states are inside the state boundary surface is purely elastic and plastic strains occur as the state of a sample traverses the state boundary surface.

The critical state model for triaxial tests on isotropically compressed samples has been described in detail by Atkinson and Bransby (1978). A diagram of the complete state boundary surface given in Atkinson and Bransby is reproduced in Figure 2.18. A constant specific volume section of the state boundary surface is shown in Figure 2.19(a). Figure 2.19(b) illustrates the difference between samples which are on the wet side and on the dry side of critical. As shown in Figure 2.19(a) normally consolidated and lightly overconsolidated samples are wet of critical and samples dry of critical are heavily overconsolidated. It will be assumed that the general features of this state boundary surface apply also for triaxial tests and simple shear tests on one-dimensionally compressed samples.

2.5.1   One-dimensional compression

During one-dimensional compression and swelling the effective horizontal and vertical stresses are related by

$$\sigma_h' = K_o \, \sigma_v' \qquad\qquad (2.72)$$

where K_o is the coefficient of earth pressure at rest.

The normal compression line and swelling lines for triaxial tests are

$$v = N_o - \lambda \ln p' \tag{2.73}$$

$$v = v_{ko} - \kappa \ln p' \tag{2.74}$$

where N_o is the specific volume at $p' = 1.0$ kN/m^2 and the subscript 'o' of N_o and v_{ko} denotes K_o condition. The corresponding equations for simple shear tests are

$$v = N_s - \lambda_s \ln \sigma_v' \tag{2.75}$$

$$v = v_{ks} - \kappa_s \ln \sigma_v' \tag{2.76}$$

Each swelling line is associated with a particular elastic wall. Therefore, when an overconsolidated soil is loaded it can only either move along the swelling line or the associated elastic wall.

Combining Equations (2.6) and (2.72),

$$p' = (1/3)(1+2K_o) \, \sigma_v' \tag{2.77}$$

and
$$\ln p' = \ln[(1/3)(1+2K_o)] + \ln \sigma_v' \tag{2.78}$$

During one-dimensional compression K_o has a constant value so that differentiating Equation (2.78) gives

$$d(\ln p') = d(\ln \sigma_v') \tag{2.79}$$

Differentiating Equations (2.73) and (2.75) gives

$$d(v)/d(\ln p') = -\lambda \quad \text{and} \quad d(v)/d(\ln \sigma_v') = -\lambda_s \tag{2.80}$$

and from Equation (2.79),

$$\lambda = \lambda_s \tag{2.81}$$

Therefore, for any particular soil the normal compression line has the same slope when plotted on $v, \ln p'$ plane and $v, \ln \sigma_v'$ plane. Substituting Equation (2.78) into Equation (2.73),

$$v = N_O - \lambda \ln[(1/3)(1+2K_O)] - \lambda \ln \sigma_v' \qquad (2.82)$$

Comparing Equation (2.75) with Equation (2.82) and applying Equation (2.81),

$$N_S = N_O - \lambda \ln[(1/3)(1+2K_O)] \qquad (2.83)$$

For triaxial tests, the overconsolidation ratio is defined as

$$R_p = p_p'/p' \qquad (2.84a)$$

and for simple shear tests,

$$OCR = \sigma_{vp}'/\sigma_v' \qquad (2.84b)$$

where p_p' and σ_{vp}' are maximum previous values of p' and σ_v' respectively.

Combining Equations (2.77), (2.84a) and (2.84b), R_p and OCR are related as

$$R_p = \left[\frac{1+2(K_O)_{nc}}{1+2K_O} \right] (OCR) \qquad (2.85)$$

where $(K_O)_{nc}$ is the value of K_O for normal compression.

2.5.2 One-dimensional consolidation

For a layer of saturated soil with a steady-state pore pressure u_O , if an increment of total stress $\Delta\sigma_v$ is suddenly applied at time t=0 on the soil surface, excess pore pressures $\bar{u}$ will be generated in the layer. As time passes, water will be squeezed out of the pores and the excess pore pressures will dissipate. By considering stresses, pore pressures, seepage and compressibility of an element in the layer, the theory of one-dimensional consolidation states that the change of these excess pore pressures with time at different depths y of the layer is described by the partial differential equation

$$c_v \frac{\partial^2 \bar{u}}{\partial y^2} = \frac{\partial \bar{u}}{\partial t} \qquad (2.86)$$

The coefficient of consolidation c_v is given by

$$c_v = k/(m_v \gamma_w) \qquad (2.87)$$

where k is the coefficient of permeability and m_v is the coefficient of volume compressibility. The coefficient m_v is defined as

$$\delta \varepsilon_v = m_v \, \delta \sigma_v' \qquad (2.88)$$

where $\delta \varepsilon_v$ is an increment of volumetric strain caused by an increment of effective stress $\delta \sigma_v'$ over a time interval δt. Both k and m_v are assumed to remain constant throughout the consolidation.

The solution of Equation (2.86) is given by Taylor (1948) in the form of a Fourier series. In the solution, t appears as a multiple of c_v/H^2 where H is the maximum drainage path so that c_v/H^2 is a constant for any particular boundary conditions. Since $(c_v t)/H^2$ is dimensionless, it is convenient to define the time factor T_v as

$$T_v = (c_v t)/H^2 \qquad (2.89)$$

The average degree of consolidation U_t at time t is defined as

$$U_t = \rho_t / \rho_\infty \qquad (2.90)$$

where ρ_t is the overall settlement of the surface of the soil layer at time t and ρ_∞ is the final overall settlement when all the excess pore pressures have dissipated. In terms of T_v and U_t the solution of Equation (2.86) is

$$U_t = 1 - \sum_{m=0}^{\infty} (2/M^2) \exp(-M^2 T_v) \qquad (2.91)$$

where m is any integer and $M = (\pi/2)(2m+1)$.

The value of c_v may be determined from the results of a consolidation stage in a simple shear test using the $\sqrt{}$(time) curve

fitting method. Figure 2.20(a) shows the results from a consolidation stage of a simple shear test plotted as U_t against $\sqrt{t}$ with the slope of the initially linear part of the curve defined as $\sqrt{t_1}$. Figure 2.20(b) shows the theoretical curve given by Equation (2.91) with the slope of the initial linear part of the curve approximately equal to $\sqrt{\pi}/2$. Therefore, at $t=t_1$ the value of T_v is $\pi/4$ and from Equation (2.89),

$$c_v = (\pi/4)(H^2/t_1) \qquad (2.92)$$

2.5.3   Critical states

If a soil is sheared continuously it will fail when it reaches a critical state, a state at which deformations occur with no change in stresses or in specific volume. At this state the soil behaves as a frictional fluid so that all the energy transferred from external forces to the soil is dissipated as friction and the strains are purely plastic.

For triaxial tests the critical states form a unique critical state line in p',q',v space with its projections on the p',q' and p',v planes given by

$$q_{cs}' = M \, p_{cs}' \qquad (2.93)$$

$$v_{cs} = \Gamma - \lambda \ln p_{cs}' \qquad (2.94)$$

where M and Γ are soil constants and Γ is defined as the specific volume at $p_{cs}'=1.0$ kN/m^2. Equation (2.93) is an extended Von Mises failure criterion and it states that the strength of soil is purely frictional, and Equation (2.94) states that the critical state specific volume of soil varies logarithmically with p_{cs}'.

Different relationships between the soil parameters M and ϕ_{cs}' defined in Equation (2.31) apply for triaxial compression tests and extension tests. This is because the criteria M = constant and ϕ_{cs}' = constant lead to different general three-dimensional stresses at critical state. If M is the same in compression and extension, then

$$\phi_{cs}' \text{ for compression} = \sin^{-1}[3M/(6+M)] \qquad (2.95a)$$

$$\phi_{cs}' \text{ for extension} = \sin^{-1}[3M/(6-M)] \qquad (2.95b)$$

In an undrained triaxial test the sample is sheared with drainage prevented so that the pre-shearing specific volume v_o is the same as the critical state specific volume v_{cs}. The undrained shear strength, usually denoted by c_u, is defined as the maximum of the shear stress τ' mobilised in the sample at critical state. From the Mohr's circle of stress c_u is the radius of the circle and is equal to $\frac{1}{2}q_{cs}'$. Combining $v_{cs} = v_o$ and $c_u = \frac{1}{2}q_{cs}'$ with Equations (2.93) and (2.94) and rearranging

$$c_u = \frac{1}{2}M \exp[(\Gamma - v_o)/\lambda] \qquad (2.96)$$

which shows that c_u decreases exponentially with v_o. Samples with the same v_o have the same c_u irrespective of overconsolidation ratio.

For simple shear tests the critical state line on the σ_v', τ_v' plane is represented by

$$(\tau_v')_{cs} = (\tan \rho_{cs}')(\sigma_v')_{cs} \qquad (2.97)$$

where ρ_{cs}' is the critical state angle of shearing resistance mobilised on the horizontal plane as described in Section 2.3.1. Equation (2.97) is a Mohr-Coulomb failure criterion which is usually expressed in the form

$$\tau' = c' + (\tan \phi')\sigma' \qquad (2.98)$$

and, so, Equation (2.97) states that soil has no cohesive strength. In Section 2.3.1 it has been shown in Equations (2.35) and (2.38) that ρ_{cs}' is dependent on θ_{cs} which is not a soil constant. Hence, ρ_{cs}' itself is not a soil constant.

58

From the geometry of the Mohr's circle of stress shown in Figure 2.6 it is reasonable to expect that the value of $\rho_{cs}{'}$ is, at least partly, affected by the ratio of $\sigma_x{'}$ to $\sigma_y{'}$ before shearing. This ratio is equal to K_O which varies with the overconsolidation ratio OCR. Therefore, a relationship between $\rho_{cs}{'}$ and the pre-shearing K_O value will be proposed here. Figure 2.21 shows a Mohr's circle of stress for a sample with pre-shearing stresses $\sigma_{vo}{'}$, $K_O\sigma_{vo}{'}$. By assuming that the stress increments applied during shearing are pure shear stress increments and that $\sigma_v{'}$ remains unchanged during shearing the Mohr's circle at critical state is also constructed. The meaning of pure shear stress increments has been explained in Section 2.4.1. As a result of the two assumptions the value of K_O also remains unchanged during shearing. From the geometry of Figure 2.21,

$$r_O = \left(\frac{K_O-1}{2}\right) \sigma_{vo}{'} \tag{2.99}$$

$$r_{cs} = \left(\frac{1+K_O}{2}\right) (\sigma_{vo}{'})\sin \phi_{cs}{'} \tag{2.100}$$

therefore,

$$(\tau_v{'})_{cs} = \left[\left(\frac{1+K_O}{2}\right)^2 (\sigma_{vo}{'})^2\sin^2\phi_{cs}{'} - \left(\frac{K_O-1}{2}\right)^2 (\sigma_{vo}{'})^2\right]^{\frac{1}{2}} \tag{2.101}$$

Since $\sigma_{vo}{'} = (\sigma_v{'})_{cs}$, substituting Equation (2.97) into Equation (2.101) gives

$$\tan \rho_{cs}{'} = \frac{1}{2}[(\sin^2\phi_{cs}{'}-1)+2(\sin^2\phi_{cs}{'}+1)K_O+(\sin^2\phi_{cs}{'}-1)K_O^2]^{\frac{1}{2}} \tag{2.102}$$

Equation (2.102) shows that $\rho_{cs}{'}$ is not a soil constant but depends on K_O which is a function of OCR. The equation also applies when $\sigma_{vo}{'} \geqslant K_O\sigma_{vo}{'}$. However, because of the assumption of $\sigma_v{'}$ remaining unchanged during shearing, Equation (2.102) will not give good predictions for constant volume tests on normally compressed samples where $\sigma_v{'}$ reduces during shearing. Two special cases can be deduced from the geometry of the Mohr's circle at critical state. Firstly, the maximum value of K_O

that can be reached during K_o swelling is

$$K_o = (1+\sin \phi_{cs}')/(1-\sin \phi_{cs}') \qquad (2.103)$$

and, secondly, ρ_{cs}' becomes the same as ϕ_{cs}' when

$$K_o = (1+\sin^2\phi_{cs}')/(1-\sin^2\phi_{cs}') \qquad (2.104)$$

For simple shear tests it is not obvious how the critical state line can be represented on the σ_v',v plane. In Equation (2.94) the unique critical state line on the p',v plane is defined by the soil constants λ and Γ. It is proposed here to locate the critical state line on the σ_v',v plane also in terms of λ and Γ by relating $(\sigma_v')_{cs}$ to p_{cs}'. At critical state Equation (2.8) becomes

$$p_{cs}' = (1/3)(\sigma_1'+\sigma_2'+\sigma_3')_{cs} \qquad (2.105)$$

Making the assumptions that the stress increments applied during shearing are pure shear stress increments and that σ_v' remains unchanged during shearing, the geometry of Figure 2.21 gives

$$(\sigma_1'+\sigma_3')_{cs} = (\sigma_v'+\sigma_h')_{cs} \qquad (2.106)$$

where σ_h' is the normal stress acting on the ends of the sample corresponding to σ_x' in Figure 2.5. Using Equation (2.106) and by assuming that

$$(\sigma_2')_{cs} = (\sigma_h')_{cs} \qquad (2.107)$$

Equation (2.105) becomes

$$p_{cs}' = (1/3)(1+2K_o)(\sigma_v')_{cs} \qquad (2.108)$$

The relationship between σ_2' and σ_h' will be discussed further in Section 3.3.2. Substituting Equation (2.108) into Equation (2.94),

$$v_{cs} = \Gamma - \lambda\ln\left(\frac{1+2K_o}{3}\right) - \lambda\ln(\sigma_v')_{cs} \qquad (2.109)$$

60

which can be written as

$$v_{cs} = \Gamma_s - \lambda_s \ln(\sigma_v')_{cs} \qquad (2.110)$$

where

$$\lambda_s = \lambda \qquad (2.111)$$

and

$$\Gamma_s = \Gamma - \lambda \ln \left(\frac{1+2K_o}{3}\right) \qquad (2.112)$$

Equation (2.112) shows that Γ_s is not a soil constant but depends on K_o which is a function of OCR.

The proposed representation of the critical state line for simple shear tests is illustrated in Figure 2.22. In Figure 2.22(a) the critical state lines are given by Equation (2.97) with the influence of K_o on ρ_{cs}' described by Equation (2.102). In Figure 2.22(b) the critical state lines are given by Equation (2.110) with the influence of K_o on Γ_s described by Equation (2.112).

In a constant volume simple shear test the sample is sheared without volume change so that v_o is the same as v_{cs}. From the geometry of Figure 2.6, the stress $(\tau_v')_{cs}$ measured from constant volume shearing is related to the undrained shear strength c_u by

$$c_u = (\tau_v')_{cs} / \sin(2\theta_{cs}) \qquad (2.113)$$

Since θ_{cs} can be related to ρ_{cs}' and ϕ_{cs}' as shown in Equations (2.36a), (2.36b), (2.39a) and (2.39b), c_u can be expressed in terms of $(\tau_v')_{cs}$, ρ_{cs}' and ϕ_{cs}'. For example, for samples with $\sigma_v' > \sigma_h'$ before shearing and $2\theta_{cs} \leqslant 90° + \phi_{cs}'$, combining Equations (2.36a) and (2.113) gives

$$c_u = \frac{(\tau_v')_{cs}}{\sin\left[\sin^{-1}\left(\frac{\sin\rho_{cs}'}{\sin\phi_{cs}'}\right) + \rho_{cs}'\right]} \qquad (2.114)$$

Hence, for any soil with a known value of ϕ_{cs}', the parameters $(\tau_v')_{cs}$ and ρ_{cs}' measured from a constant volume simple shear test at v_o can be used to calculate the undrained shear strength c_u for the same v_o. For the special case of $2\theta_{cs} = 90°$, ρ_{cs}' and ϕ_{cs}' are related as $\sin \phi_{cs}' = \tan \rho_{cs}'$ which when substituted into Equation (2.114) gives $c_u = (\tau_v')_{cs}$.

2.5.4 The state boundary surface

The first complete theoretical state boundary surface was proposed by Schofield and Wroth (1968) in the Cam-clay model. Slightly different shapes for the state boundary surface have been proposed since then. For example, Roscoe and Burland (1968) derived the Modified Cam-clay model to give better predictions of strain increments. Atkinson and Bransby (1978) proposed a state boundary surface based on triaxial test results, and a summary of the state boundary surfaces for triaxial tests and plane strain tests is given in Atkinson (1981). All these models apply to isotropically compressed soil, but more recently a state boundary surface for K_o compressed soil is proposed by Atkinson et al (1987).

The Roscoe surface defines a curved three-dimensional yield surface linking the normal compression line to the critical state line. All normally consolidated samples loaded to failure will traverse the Roscoe surface to reach the critical state line. The Cam-clay model and Modified Cam-clay model have slightly different assumptions made in deriving the two models. The procedure for deriving the Modified Cam-clay model will be followed here to obtain an analogous Roscoe surface for simple shear tests.

The total energy per unit volume transmitted to a simple shear sample has already been given by Equation (2.19). Using Equations (2.65) and (2.66),

$$W = W^e + W^p \qquad (2.115)$$

$$\delta W^e = \tau_v' \, \delta \gamma^e + \sigma_v' \, \delta \varepsilon_v^e \qquad (2.116a)$$

$$\delta W^p = \tau_v' \, \delta \gamma^p + \sigma_v' \, \delta \varepsilon_v^p \qquad (2.116b)$$

The work done δW^e due to elastic straining is stored within the soil skeleton and is recoverable on unloading while the work done δW^p is dissipated within the sample as friction. During one-dimensional compression, both τ_v' and $\delta \gamma^p$ are zero so that Equation (2.116b) becomes

$$\delta W^p = \sigma_v' \, \delta \varepsilon_v^p \qquad (2.117)$$

At critical state, $\delta \varepsilon_v^p$ is equal to zero and substituting Equation (2.97) into Equation (2.116b),

$$\delta W^p = (\sigma_v')_{cs} \tan \rho_{cs}' \, \delta \gamma^p \qquad (2.118)$$

A general expression which satisfies both particular conditions is

$$\delta W^p = \sigma_v' \, \sqrt{[(\delta \varepsilon_v^p)^2 + (\tan \rho_{cs}' \, \delta \gamma^p)^2]} \qquad (2.119)$$

Combining Equations (2.116b) and (2.119) gives the flow rule as

$$\frac{\delta \gamma^p}{\delta \varepsilon_v^p} = \frac{2 \, \eta_s'}{\tan^2 \rho_{cs}' - (\eta_s')^2} \qquad (2.120)$$

where $\eta_s' = \tau_v'/\sigma_v'$. Equation (2.120) is analogous to the flow rule for triaxial tests and the Roscoe surface is given by

$$v = \Gamma_s - \lambda_s \ln \sigma_v' - (\lambda_s - \kappa_s) \ln \left[\frac{\tan^2 \rho_{cs}' + (\eta_s')^2}{2 \tan^2 \rho_{cs}'} \right] \qquad (2.121)$$

The Hvorslev surface adopted by Atkinson and Bransby (1978) was defined by considering results of drained and undrained triaxial tests on overconsolidated clay samples. By analogy, the Hvorslev surface for simple shear tests is

$$\tau_v' = (\tan \rho_{cs}' - h_s) \, \exp \left(\frac{\Gamma_s - v}{\lambda_s}\right) + h_s \sigma_v' \qquad (2.122)$$

In a constant specific volume section of the state boundary surface, Equation (2.122) is a straight line with slope h_s .

The tension failure surface exists because soil cannot withstand tensile effective stress. Since σ_3' has the lowest value of normal effective stress in a soil sample, the tension failure surface represents all states with σ_3' equal to zero. For simple shear tests, Figure 2.6 shows that if σ_3' becomes zero, then, by geometry, $\tau_{yx}'/\sigma_y' = \tan \theta$. Since θ changes during shearing, the tension failure surface in the σ_v', τ_v', v space is any plane passing through the v axis and angled at θ to the horizontal σ_v', v plane.

2.5.5 Stress-strain relationships inside the state boundary surface

So long as the state of a sample is inside the state boundary surface, its behaviour is purely elastic and the state remains on an elastic wall. The stress-strain behaviour of an isotropic linear elastic soil has been described in Section 2.4.1 and the stress-strain relationships are given by Equations (2.56) and (2.59). As the state of a sample remains on an elastic wall, the change of specific volume is given by

$$\delta v = -\kappa_s \, \delta(\ln \sigma_v') = -\kappa_s \frac{\delta \sigma_v'}{\sigma_v'} \qquad (2.123)$$

or
$$\delta \varepsilon_v^e = \frac{\kappa_s}{v \sigma_v'} \, \delta \sigma_v' \qquad (2.124)$$

Hence, from Equations (2.56), (2.59) and (2.124),

$$K_s' = (v \sigma_v') / \kappa_s \qquad (2.125)$$

$$G_s' = \frac{v\sigma_v'}{K_s} \frac{(1-2\ \gamma')}{2(1-\gamma')} \tag{2.126}$$

$$\mu_s' = \frac{K_s'}{G_s'} = \frac{2(1-\gamma')}{(1-2\ \gamma')} \tag{2.127}$$

For constant volume loading, Equations (2.56) and (2.59) become

$$\delta\gamma^e = (2/E_u)(1+\gamma_u)\ \delta\tau_v = (1/G_{us})\ \delta\tau_v \tag{2.128}$$

$$\delta\mathcal{E}_v^e = \frac{1}{E_u} \frac{(1+\gamma_u)(1-2\ \gamma_u)}{(1-\gamma_u)} \delta\sigma_v = \frac{1}{K_{us}} \delta\sigma_v \tag{2.129}$$

where the subscripts 'u' indicate that the elastic parameters are appropriate for constant volume loading. Since $\delta\tau_v = \delta\tau_v'$, $G_{us} = G_s'$ and since $\delta\mathcal{E}_v = 0$, K_{us} is infinite and $\gamma_u = \frac{1}{2}$. Substituting $\gamma_u = \frac{1}{2}$ into Equation (2.128) gives $G_{us} = (1/3)E_u$.

2.5.6   Stress-strain relationships on the state boundary surface

The behaviour of a sample whose state is moving on the state boundary surface is elasto-plastic with the stress-strain relationships described by Equations (2.70) and (2.71). For the Roscoe surface, the parameter F_s has already been given in Equation (2.120) as

$$F_s = \frac{2\ \eta_s'}{\tan^2\rho_{cs}' - (\eta_s')^2} \tag{2.130}$$

and the parameter H_s can be obtained from the equation for the Roscoe surface, Equation (2.121), as

$$H_s = \frac{(\lambda_s - \kappa_s)(2\ \eta_s')}{v\sigma_v'\ [(\tan^2\rho_{cs}' + (\eta_s')^2]} \tag{2.131}$$

For the Hvorslev surface, the parameters F_s and H_s can be obtained from the equation for the Hvorslev surface, Equation (2.122), as

$$F_s = - \left[\frac{1}{\left(\frac{K_s}{\lambda_s}\right)(\eta_s'-h_s) + h_s} \right]$$

(2.132)

$$H_s = \frac{\lambda_s}{v\sigma_v'(\eta_s'-h_s)}$$

(2.133)

2.6 Normalising test data

In order to compare experimental results with predictions of the critical state theory, soil test data have to be analysed and plotted in a way which can expose the pattern of soil behaviour. Normalising procedures for scaling triaxial test data obtained from tests with different effective stresses and different specific volumes have been described by Atkinson (1984a).

2.6.1 Idealised soil behaviour

The idealised behaviour of an isotropic soil in undrained triaxial compression tests is illustrated in Figure 2.23. Three samples were normally compressed to A1 and then two of them were swelled to overconsolidation ratios R_p of 2 and 4 at A2 and A4 respectively. One sample was normally compressed to a higher value of p' at C1 . When sheared, the normally consolidated samples A1 and C1 move along the Roscoe surface to reach the critical state line at B1 and D1 respectively. Sample A2 is directly below the critical state line and so it stays inside the state boundary surface until it fails at B2 . The heavily overconsolidated sample A4 first reaches the Hvorslev surface at J4 where the stress ratio q'/p' is a maximum and then moves along the Hvorslev surface to the critical state line at B4 . Figure 2.23(c) shows that the q'/p' versus $v\epsilon_s$ curves for samples A1 and C1 coincide. The reason for this will be explained in Section 2.6.4.

The idealised behaviour of an isotropic soil in constant p' triaxial compression tests is illustrated in Figure 2.24. Three samples were

normally compressed to E1 and then two of them were swelled to overconsolidation ratios of 2 and 4 at E2 and E4 respectively. One sample was normally compressed to a higher value of p' at G1 . When sheared, the normally consolidated samples E1 and G1 move along the Roscoe surface to reach the critical state line at F1 and H1 respectively. Sample E2 stays inside the state boundary surface until it fails at F2 . The heavily overconsolidated sample E4 first reaches the Hvorslev surface at K4 where the stress ratio q'/p' is a maximum and then moves along the Hvorslev surface to the critical state line at F4 . Figure 2.24(c) shows that the q'/p' versus $v\varepsilon_s$ curves for samples E1 and G1 coincide. The reason for this will be explained in Section 2.6.4.

The normalised behaviour of these eight ideal tests is illustrated in Figure 2.25. Figure 2.25(a) shows the normalised constant v section of the paths with the normalising parameter p_e' defined as

$$p_e' = \exp\left[(N-v)/\lambda\right] \qquad (2.134)$$

and Figure 2.25(b) shows the normalised constant p' section of the paths with the normalising parameter v_λ defined as

$$v_\lambda = v + \lambda \ln p' \qquad (2.135)$$

The normalised paths for all four normally consolidated samples A1, C1, E1 and G1 are the same and the normalised paths for the two heavily overconsolidated samples A4 and E4 are the same when they traverse the Hvorslev surface. The reason for this will be discussed in Section 2.6.3.

2.6.2 Normalised critical states

As shown in Figure 2.25 the critical state line becomes a critical state point in a normalised section of the state boundary surface. This, however, is not the case for simple shear tests. Figure 2.22 shows that for simple shear tests different values of K_o correspond to different critical state lines. Therefore, different values of K_o will correspond to different critical state points in a normalised section.

67

For a simple shear sample at state A in Figure 2.26, the constant v section normalising parameter $\sigma_{ve}{}'$ is defined as

$$\sigma_{ve}{}' = \exp\left[(N_s - v)/\lambda_s\right] \qquad (2.136)$$

and the constant $\sigma_v{}'$ section normalising parameter $v_{\lambda s}$ is defined as

$$v_{\lambda s} = v + \lambda_s \ln \sigma_v{}' \qquad (2.137)$$

Equations (2.136) and (2.137) are analogous to Equations (2.134) and (2.135) respectively.

Considering Figure 2.22(b), from Equation (2.136) the normal compression line is defined as

$$v = N_s - \lambda_s \ln \sigma_{ve}{}' \qquad (2.138)$$

From Equation (2.109), for any particular value of K_o, a critical state line is defined as

$$v_{cs} = \Gamma - \lambda \ln \left(\frac{1+2K_o}{3}\right) - \lambda \ln(\sigma_v{}')_{cs} \qquad (2.109)$$

For any constant v section, the value of v for Equation (2.138) will be the same as the value of v_{cs} for Equation (2.109). Hence, combining Equations (2.138) and (2.109) and applying Equation (2.111),

$$\left(\frac{\sigma_v{}'}{\sigma_{ve}{}'}\right)_{cs} = \exp\left[\frac{\Gamma - N_s}{\lambda_s} - \ln\left(\frac{1+2K_o}{3}\right)\right] \qquad (2.139)$$

and from Equation (2.97),

$$\left(\frac{\tau_v{}'}{\sigma_{ve}{}'}\right)_{cs} = \exp\left[\frac{\Gamma - N_s}{\lambda_s} - \ln\left(\frac{1+2K_o}{3}\right)\right] \tan \rho_{cs}{}' \qquad (2.140)$$

Equations (2.139) and (2.140) together define a critical state point on the normalised constant v section for any particular value of K_O .

Figure 2.26 shows that at critical state $v_{\lambda s}$ becomes Γ_s which is defined by Equation (2.112) as

$$\Gamma_s = \Gamma - \lambda \ln \left(\frac{1+2K_O}{3}\right) \qquad (2.112)$$

and from Equation (2.97),

$$(\tau_v{}'/\sigma_v{}')_{cs} = \tan \rho_{cs}{}' \qquad (2.141)$$

Equations (2.112) and (2.141) together define a critical state point on the normalised constant $\sigma_v{}'$ section for any particular value of K_O .

2.6.3 Normalised state paths

The equation for the Roscoe surface has already been given in Equation (2.121). At $\eta_s{}' = 0$, $v + \lambda_s \ln \sigma_v{}' = N_s$ so that Equation (2.121) becomes

$$N_s = \Gamma_s + (\lambda_s - \kappa_s) \ln 2 \qquad (2.142)$$

Substituting Equations (2.136) and (2.142) into Equation (2.121) and rearranging, the normalised constant v section of the Roscoe surface is

$$\left(\frac{\tau_v{}'}{\sigma_{ve}{}'}\right) = (\tan \rho_{cs}{}')\left(\frac{\sigma_v{}'}{\sigma_{ve}{}'}\right)\left[\left(\frac{\sigma_v{}'}{\sigma_{ve}{}'}\right)^{\left(\frac{-\lambda_s}{\lambda_s-\kappa_s}\right)} - 1\right]^{\frac{1}{2}} \qquad (2.143)$$

Substituting Equations (2.137) and (2.142) into Equation (2.121) and rearranging, the normalised constant $\sigma_v{}'$ section of the Roscoe surface is

$$\left(\frac{\tau_v{'}}{\sigma_v{'}}\right) = (\tan \rho_{cs}{'}) \left[\exp \left(\frac{N_s - v_{\lambda s}}{\lambda_s - \kappa_s}\right) - 1 \right]^{\frac{1}{2}} \qquad (2.144)$$

The equation for the Hvorslev surface has already been given in Equation (2.122). Dividing Equation (2.122) by $\sigma_{ve}{'}$ and applying Equation (2.136), the normalised constant v section of the Hvorslev surface is

$$\left(\frac{\tau_v{'}}{\sigma_{ve}{'}}\right) = (\tan \rho_{cs}{'} - h_s) \exp \left(\frac{\Gamma_s - N_s}{\lambda_s}\right) + h_s \left(\frac{\sigma_v{'}}{\sigma_{ve}{'}}\right) \qquad (2.145)$$

which can be written as

$$\left(\frac{\tau_v{'}}{\sigma_{ve}{'}}\right) = g_s + h_s \left(\frac{\sigma_v{'}}{\sigma_{ve}{'}}\right) \qquad (2.146)$$

where $\qquad g_s = (\tan \rho_{cs}{'} - h_s) \exp \left(\frac{\Gamma_s - N_s}{\lambda_s}\right) \qquad (2.147)$

Equation (2.146) shows that the surface is a straight line with slope h_s and intercept g_s on the $\tau_v{'}/\sigma_{ve}{'}$ axis. Dividing Equation (2.122) by $\sigma_v{'}$ and applying Equation (2.137), the normalised constant $\sigma_v{'}$ section of the Hvorslev surface is

$$\left(\frac{\tau_v{'}}{\sigma_v{'}}\right) = (\tan \rho_{cs}{'} - h_s) \exp \left(\frac{\Gamma_s - v_{\lambda s}}{\lambda_s}\right) + h_s \qquad (2.148)$$

Equations (2.143), (2.144), (2.145) and (2.148) are analogous to the corresponding equations for triaxial tests.

Equations (2.143) and (2.144) show that for triaxial tests the shapes of the normalised sections of the Roscoe surface depend only on the soil constants M , N , λ and κ . Therefore, in Figure 2.25 the four normally consolidated samples which traverse the Roscoe surface have the same normalised paths. Similarly, Equations (2.145) and (2.148) show that for triaxial tests the shapes

of the normalised sections of the Hvorslev surface depend only on the soil constants M , N , Γ , λ and h . Therefore, in Figure 2.25 both heavily overconsolidated samples which traverse the Hvorslev surface have the same normalised paths.

2.6.4 Normalised tangent stiffnesses

Since the stress-strain behaviour of most soils are non-linear, the stiffness of a soil varies with strain and is the tangent to its stress-strain curve. The advantages of defining stiffness parameters as tangents rather than secants have been discussed by Atkinson et al (1986).

To derive the normalised tangent stiffness parameters for simple shear tests Equation (2.70) and (2.71) are written as

$$(v\sigma_v') \, \delta\gamma = A_s \, \delta\tau_v' + B_s \, \delta\sigma_v' \qquad (2.149)$$

$$(v\sigma_v') \, \delta\varepsilon_v = C_s \, \delta\tau_v' + D_s \, \delta\sigma_v' \qquad (2.150)$$

The full expressions for the parameters A_s to D_s for both Roscoe surface and Hvorslev surface are given in Appendix B . As explained in Section 2.4.3 the parameters A_s to D_s are appropriate for elasto-plastic stress-strain behaviour. Hence, they are different to the parameters A^e to D^e described in Section 2.4.1 which are for purely elastic stress-strain behaviour.

For constant volume simple shear tests on normally consolidated samples, it is shown in Appendix B that

$$v \, \delta\gamma = E_s \, \delta(\tau_v'/\sigma_v') \qquad (2.151)$$

with the full expression for E_s given in Appendix B . Since E_s depends only on λ_s , k_s , ρ_{cs}' , μ_s' and η_s' , and η_s' varies between 0 and $\tan\rho_{cs}'$ for samples with any pre-shearing states, the variation of τ_v'/σ_v' with v γ is the same for all constant volume tests. Similarly, the variation of q'/p' with $v\varepsilon_s$ is the same for all undrained triaxial tests on normally compressed samples as suggested in Section 2.6.1. Also, for

constant volume tests, Equation (2.150) becomes

$$C_s \, \delta \tau_v' + D_s \, \delta \sigma_v' = 0 \qquad (2.152)$$

Substituting Equation (2.152) into Equation (2.149) and rearranging,

$$\frac{\delta \tau_v'}{(v\sigma_v') \, \delta \gamma} = \frac{D_s}{A_s D_s - B_s^2} \qquad (2.153)$$

The term $\delta \tau_v'/(v\sigma_v' \, \delta \gamma)$ represents the normalised tangent stiffness. The values of A_s, B_s and D_s depend only on λ_s, κ_s, ρ_{cs}', μ_s' and η_s', and the relationship between η_s' and $v\gamma$ is the same for all constant volume tests, as a result, the variation of $\delta \tau_v'/(v\sigma_v' \, \delta \gamma)$ with $v\gamma$ is also the same for all constant volume tests.

For constant σ_v' simple shear tests on normally compressed samples Equation (2.149) gives

$$(v\sigma_v') \, \delta \gamma = A_s \, \delta \tau_v' \qquad (2.154)$$

Since σ_v' is constant, Equation (2.154) can be written as

$$v \, \delta \gamma = A_s \, \delta(\tau_v'/\sigma_v') \qquad (2.155)$$

Because A_s depends only on ρ_{cs}', λ_s, κ_s, μ_s' and η_s', and η_s' varies between 0 and $\tan \rho_{cs}'$ for samples with any pre-shearing states, the variation of τ_v'/σ_v' with $v\gamma$ is the same for all constant σ_v' tests. Similarly, the variation of q'/p' with $v\varepsilon_s$ is the same for all constant p' triaxial tests on normally compressed samples as suggested in Section 2.6.1. Also, rearranging Equation (2.154) gives

$$\frac{\delta \tau_v'}{(v\sigma_v') \, \delta \gamma} = \frac{1}{A_s} \qquad (2.156)$$

72

which shows that $\delta\tau_v'/(v\sigma_v'\delta\gamma)$ depends only on ρ_{cs}' , λ_s , κ_s , μ_s' and η_s' . Since the relationship between η_s' and $v\gamma$ is the same for all constant σ_v' tests, the variation of $\delta\tau_v'/(v\sigma_v'\delta\gamma)$ with $v\gamma$ is also the same for all constant σ_v' tests.

2.7 Summary

In a NGI simple shear test the measured stresses are σ_v' , τ_v' defined by Equations (2.10) and (2.11) and the complete stress state is not known. From the geometry of the Mohr's circle of stress each of the parameters ρ' , ϕ' and θ can be expressed independently in terms of the other two as shown in Equations (2.34) to (2.39b). The strains measured are ε_v , γ defined in Equation (2.16). From the geometry of the Mohr's circle of strain increments the principal strain increments $\delta\varepsilon_1$, $\delta\varepsilon_3$ can be calculated from $\delta\varepsilon_v$, $\delta\gamma$ so that the complete state of strain increment is known.

The stress-strain behaviour for purely elastic material are described in Section 2.4.1. For an isotropic material the shear moduli and bulk moduli for triaxial and simple shear tests are defined in Equations (2.53), (2.54), (2.56) and (2.59). For a cross-anisotropic material the constitutive equations are

$$\delta\varepsilon_s^e = A^e \, \delta q' + B^e \, \delta p' \qquad (2.61a)$$

$$\delta\varepsilon_v^e = C^e \, \delta q' + D^e \, \delta p' \qquad (2.61b)$$

For a purely plastic material straining only occurs when the state path moves along the yield surface crossing over different yield curves. The relationship between the direction of the plastic strain increment vector and the stress state is described by a flow rule. The magnitude of a plastic strain increment and the magnitude of the corresponding stress increment are related by a hardening law. The general form of the constitutive equations for an elasto-plastic material is given by Equations (2.70) and (2.71).

The critical state model specifies a unique state boundary surface for soil. A sample whose states are inside the state boundary surface is purely elastic and the states remain on an elastic wall. Plastic strains only occur when the state of the sample moves on the state boundary surface. The critical state line for triaxial tests is

$$q_{cs}' = M \, p_{cs}' \tag{2.93}$$

$$v_{cs} = \Gamma - \lambda \ln p_{cs}' \tag{2.94}$$

where M, Γ and λ are soil constants. The critical state line for simple shear tests can be expressed in the same form as Equations (2.93) and (2.94),

$$(\tau_v')_{cs} = (\tan \rho_{cs}')(\sigma_v')_{cs} \tag{2.97}$$

$$v_{cs} = \Gamma_s - \lambda_s \ln(\sigma_v')_{cs} \tag{2.110}$$

But, ρ_{cs}' and Γ_s are not soil constants. It is proposed that ρ_{cs}' and Γ_s are dependent on K_o which is a function of OCR. The proposed relationships are

$$\tan \rho_{cs}' = \tfrac{1}{2}[(\sin^2\phi_{cs}'-1)+2(\sin^2\phi_{cs}'+1)K_o+(\sin^2\phi_{cs}'-1)K_o^2]^{\frac{1}{2}} \tag{2.102}$$

$$\Gamma_s = \Gamma - \lambda \ln \left(\frac{1+2K_o}{3}\right) \tag{2.112}$$

The undrained shear strength c_u is defined as $\tfrac{1}{2}q_{cs}'$ which can be obtained from triaxial tests. The parameters $(\tau_v')_{cs}$ and ρ_{cs}' measured from constant volume simple shear tests where $\sigma_v' > \sigma_h'$ before shearing and $2\theta_{cs} \leqslant 90° + \phi_{cs}'$ are related to c_u by

$$c_u = \frac{(\tau_v')_{cs}}{\sin\left[\sin^{-1}\left(\dfrac{\sin \rho_{cs}'}{\sin \phi_{cs}'}\right) + \rho_{cs}'\right]} \tag{2.114}$$

Similar equations can be written for samples with $2\theta_{cs} \geqslant 90°+\phi_{cs}'$ and for samples with $\sigma_h' > \sigma_v'$ before shearing.

Following the procedure of deriving the Roscoe surface for Modified Cam-clay, an analogous Roscoe surface for simple shear tests is written in Equation (2.121). A Hvorslev surface for simple shear tests analogous to that given by Atkinson and Bransby (1978) is written in Equation (2.122).

To compare experimental results with the critical state theory, test data have to be normalised to account for the effects of different pre-loading states. The idealised behaviour of an isotropic soil in undrained and constant p' triaxial compression tests are illustrated in Section 2.6.1.

For simple shear tests, different values of K_o correspond to different critical state points in a normalised section of the state boundary surface. Using the proposed relationships in Equations (2.102) and (2.112), the critical state points in a constant v section are given by Equations (2.139) and (2.140) and the critical state points in a constant σ_v' section are given by Equations (2.112) and (2.141).

Stiffness parameters are defined as tangents to stress-strain curves rather than secants (Atkinson et al, 1986). To derive the normalised tangent stiffness parameters for an isotropic elasto-plastic soil, the constitutive equations are written as

$$(v\sigma_v') \, \delta\gamma = A_s \, \delta\tau_v' + B_s \, \delta\sigma_v' \qquad (2.149)$$

$$(v\sigma_v') \, \delta\varepsilon_v = C_s \, \delta\tau_v' + D_s \, \delta\sigma_v' \qquad (2.150)$$

with the full expressions for the parameters A_s to D_s for Roscoe surface and Hvorslev surface given in Appendix B .

The normalised shear stiffness $\delta\tau_v'/(v\sigma_v' \, \delta\gamma)$ for constant volume and constant σ_v' simple shear tests are defined in Equations (2.153) and (2.156) respectively. For each type of test the variation of $\delta\tau_v'/(v\sigma_v' \, \delta\gamma)$ with $v\gamma$ is independent of the pre-shearing state of the sample.

CHAPTER 3   A REVIEW OF PREVIOUS WORK

3.1   Introduction

A description of the current state of knowledge is necessary before
further understanding of the subject can be achieved. Section 3.2
describes the simple shear test as one form of shear testing among
others.   Sections 3.3 and 3.4 provide important information about
simple shear testing which will be useful to the analysis of test data
in Chapter 7.   A summary of previous test results which already
exist outside this study is given in Section 3.5 to allow comparison
of results to be made. .

3.2   Shear testing of soils

3.2.1   Shear testing apparatus

Ideally a soil testing apparatus should be able to impose a completely.
general state of stress in the sample and it should be able to vary
the state of stress so that the principal planes may rotate. These
requirements are technically very difficult to achieve and all
existing apparatus are only able to load the soil in some restricted
ways.

Soil testing apparatus can be divided into two classes with respect to
the boundary conditions applied to the sample. The first class of
apparatus have smooth rigid platens or flexible membranes as a result
of which the sample boundaries are principal planes of stress and of
strain and no rotation of principal axes is allowed. Examples of
this class of apparatus are the triaxial apparatus, oedometer,
plane strain apparatus and true triaxial apparatus. The second
class of apparatus consists of the shear testing apparatus with rough
rigid platens which may rotate so that the sample boundaries need not
be principal planes and rotation of principal axes occurs during
loading.   Shear testing apparatus which are commercially available
and used in some commercial laboratories are the shear box, simple

shear apparatus and ring shear apparatus.

The shear box is the simplest and earliest shear testing apparatus, but it has two major problems. First, the sample is constrained to deform in such a way that the strains are concentrated in an indeterminate narrow portion of the sample. Consequently, the stresses and strains calculated from the forces and displacements measured at the boundary are not representative of the stresses and strains in the sample. Second, even if the stresses in the sample are assumed to be uniform, the stresses measured do not provide sufficient information to define the complete stress state of the soil. Hence, the shear box is unsuitable for studying the stress-strain behaviour of soils and it is better suited for finding the stresses on a particular plane at failure. It is most suitable for determining the strength of pre-existing surfaces in a soil sample.

The first problem of the shear box has been largely overcome by the development of the simple shear apparatus. The strains imposed on a simple shear sample are relatively uniform but the simple shear apparatus has its own problem of applying non-uniform stresses to the sample. Except for the more sophisticated versions of the apparatus, the stresses measured by most simple shear apparatus are also insufficient to define the complete stress state of the sample. The problems associated with the simple shear apparatus will be discussed in more detail in Section 3.3.

The ring shear apparatus (Bromhead, 1979) measures the residual strength of clay by causing one block of clay to slide over another for very large displacements. In contrast to the conditions at critical state when shear strains are of the order of several tens of percent and the orientation of the clay particles are random, the ring shear sample suffers from displacements of the order of several metres and the platey clay particles have become aligned to the directions of shearing.

Other shear testing apparatus which are only used for research purposes include the hollow cylinder apparatus and the directional shear cell. The hollow cylinder apparatus (Hight et al, 1983) subjects a hollow cylindrical soil sample to combined axial load,

torque and internal and external radial pressures. Under stress control, the directions of σ_1' and σ_3' can be rotated and the magnitude of σ_2' can be varied. The complete stress state of the sample can be calculated from the measured stresses, but in common with the other shear testing apparatus already described the hollow cylinder apparatus also has the problem of applying non-uniform stresses to the sample. The problem arises from the frictional restraints and stiffness of the platens which affect all apparatus with rough rigid platens; in addition, the applied stresses vary across the hollow cylindrical sample in the radial direction when either torque or different internal and external pressures are applied.

The directional shear cell (Arthur et al, 1980) applies normal and shear stresses to four faces of a cubical sample under plane strain conditions. By varying the applied stresses the directions of σ_1' and σ_3' can be rotated. Flexible rubber boundaries are used to reduce stress non-uniformities.

In general, the first class of apparatus has the advantage that the principal stresses and strains imposed on the sample are known and hence the complete states of stress and strain can be readily determined. On the other hand, the shear testing apparatus offers the capability of rotation of principal axes of stress and strain which can be useful in simulating states of anisotropic soils near building foundations and slopes. The problem with most shear testing apparatus is that non-uniform stresses and hence strains are imposed on the sample and in the cases of the shear box and simple shear apparatus the complete stress states cannot be determined.

3.2.2   Basic designs of simple shear apparatus

There are currently two basic designs of simple shear apparatus. One of them was first built at the Swedish Geotechnical Institute by Kjellman (1951). In this apparatus a sample, circular in plan, was enclosed in a rubber membrane surrounded by a series of aluminium rings as illustrated in Figure 3.1(a). The purpose of the rings was to maintain the

horizontal cross-section of the sample constant during shearing. This apparatus was later modified by Bjerrum and Landva (1966) at the Norwegian Geotechnical Institute (NGI). The modification was essentially the replacement of the aluminium rings by a wire reinforced rubber membrane as illustrated in Figure 3.1(b). This version of the apparatus became commercially available and the most widely used. Further descriptions of the NGI simple shear apparatus are given in Section 5.3.

The other basic design of simple shear apparatus was initiated by Roscoe (1953) at the Cambridge University. In this apparatus a sample, rectangular in plan, was completely surrounded by rigid platens with the end platens allowed to rotate about hinges as shown in Figure 3.1(c). The top and bottom platens were rough but the platens in contact with the four sides of the sample had to be made smooth for uniform straining. A small portion of the sample remained undeformed during shearing but this was eliminated in a later version of the apparatus constructed by Bassett (1967) by means of a different arrangement of hinges and platens as shown in Figure 3.1(d).

In the more recent versions of the Cambridge simple shear apparatus the sample is usually surrounded by contact load cells (Bransby, 1973) incorporated in the rigid platens. These contact load cells are capable of measuring normal load, shear load and eccentricity of normal load; the most successful version of these was designed by Stroud (1971). An example of the arrangement of load cells in one of the versions of Cambridge simple shear apparatus, SSA.Mk.7R , used by Budhu and Wood (1979) is shown in Figure 3.2. There are five load cells on each of the top and bottom platens and another four load cells one at each of the vertical platens. From the stresses measured by the load cells at the end platens the stresses σ_x' , τ_{xy}' can be calculated and hence the Mohr's circle of stress can be drawn. The stress σ_2' acting perpendicular to the plane of shearing is measured by the load cells at each side of the sample. Hence, the complete general stress state of the sample can be determined.

Different versions of the Cambridge simple shear apparatus have been used for testing dry sands by Cole (1967), Stroud (1971) and

79

Budhu (1979). The only major study on clay using this apparatus was by Borin (1973). For testing clay samples, water drainage and pore pressure can be controlled; the sample is enclosed in a rubber membrane and a lubricant applied between the membrane and the vertical platens.

Although the stress state of the sample in the elaborately instrumented Cambridge simple shear apparatus can be calculated, the apparatus remains a piece of research equipment because it is too complicated to be widely used in practice. The NGI simple shear apparatus has the attractive advantage that it is simple to use, and less importantly, field samples which are usually circular can be easily installed in the apparatus. To tackle the problem of estimating the stress states of NGI simple shear samples, the general approach has been to study the behaviour of soils in simple shear using the Cambridge simple shear apparatus and make recommendations for the interpretation of results obtained from the NGI simple shear apparatus. Some of the methods recommended are described in Section 3.3.2.

3.3   Problems with simple shear apparatus

3.3.1   Non-uniformities of stresses and strains

In the NGI simple shear apparatus the vertical boundaries of the sample are surrounded by a smooth rubber membrane and in the Cambridge simple shear apparatus the end platens are made smooth to allow unrestricted deformation. Therefore, during shearing when the shear stresses τ_{yx}' are applied, neither of the two basic designs of the simple shear apparatus provides the complementary shear stresses τ_{xy}' which should be applied to the ends of the sample. As a result, the shear stresses τ_{yx}' over the horizontal boundaries are non-uniformly distributed and the normal stresses σ_y' also become non-uniform in order to maintain moment equilibrium. The expected general pattern of these non-uniform stress distributions is illustrated in Figure 3.3.

The non-uniformities of the stress and strain distributions have been studied theoretically by several authors. Unless otherwise stated all the studies to be described assumed isotropic, linear elastic material properties.

Roscoe (1953) performed a mathematical analysis to calculate the stress distributions on a sample, square in plan, with height to width ratio of 1 to 3. For constant volume shearing with initial $\sigma_v' = 0$, the results are as shown in Figure 3.4 with the stresses σ_y', τ_{yx}' and σ_x' divided by τ_v' which represents the average shear stress across the horizontal boundaries of the sample. Figure 3.4 shows that as a result of the absence of the stress τ_{xy}', non-uniform compressive and tensile normal stresses act on the horizontal surfaces and the ends of the sample. The moments due to the resultants of these non-uniform stresses exactly counterbalanced the moment due to τ_{yx}'. It was concluded that the distributions of both the stresses σ_y' and τ_{yx}' over the central third of the surface of the sample, away from the influence of the ends, were uniform.

Lucks et al (1972) performed a finite element analysis on a sample, circular in plan, with height to diameter ratio of 1 to 4 to simulate the stresses acting on a sample under constant volume shearing in the NGI simple shear apparatus. The results, with the value of initial σ_v' adjusted to zero, are shown in Figure 3.5. Lucks et al suggested that if the shear stress τ_{xy}' had been provided, the stresses would have been uniform with the horizontal shear stress τ_{yx}' given by the equation

$$\tau_{yx}' = \tau_{xy}' = \frac{E'}{2(1+ \nu')} \gamma_{yx} \qquad (3.1)$$

It was concluded that there were high normal stresses at the edges of the sample, but these stress concentrations were considered to be quite local. Approximately 70 % of the sample was found to have remarkably uniform stress distributions. Within the zone of uniform stresses the value of τ_{yx}' predicted by the finite element analysis was greater than the value of τ_{yx}' calculated by Equation (3.1) by less than 2 % of the

latter value. Therefore, the magnitude of the shear stress within this zone was only very slightly affected by the non-uniform stress conditions.

Prevost and Høeg (1976) performed a mathematical analysis on a sample with height to length ratio of 1 to 4. The analysis included an investigation into the effects of slippage between the top and bottom platens and the sample during constant volume shearing. The assumed distribution of slippage is shown in Figure 3.6(a) and the results are shown in Figures 3.6(b) to (d). Figure 3.6(b) shows that the stresses σ_y' and τ_{yx}' are uniform over approximately 70 % of the sample when no slippage occurs ($\lambda=0$), but slippage induces normal stresses and reduces shear stresses. Figure 3.6(d) shows that the vertical displacements are close to zero over 80 % of the sample.

Budhu and Britto (1987) used the finite element program CRISP (Gunn and Britto, 1984) to study the distribution of effective vertical stresses on NGI simple shear samples. A purely elastic model and the elasto-plastic Modified Cam-clay model were used to simulate constant σ_v' and constant volume tests on kaolin. The sample size was chosen as 110 mm diameter and 20 mm height to allow direct comparisons with experimental results. At $\gamma = 10 \%$, both models predicted that approximately 70 % of the sample was uniformly stressed but the elastic analyses produced greater stress concentrations at the ends of the sample than analyses based on Modified Cam-clay.

Duncan and Dunlop (1969) performed a two-dimensional finite element analysis using anisotropic, non-linear stress-strain properties. The variation of the tangential Young's moduli E_{uh} and E_{uv} with shear strain γ and the variation of E_u with the direction of σ_1' are shown in Figures 3.7(a) and (b) respectively. The moduli E_{uh} and E_{uv} in Figure 3.7(a) are normalised with respect to σ_{10}' which are the pre-shearing values of σ_1' . The finite element mesh used, with a height to length ratio of 1 to 3, is shown in Figure 3.7(c). The results of the analyses corresponding to average shear strains from 5 % to 10 % are shown in Figure 3.7(d). The dotted areas indicate zones where the shear stress has reached the

undrained shear strength of the material. Progressive failure
begins near the ends of the sample at 6 % shear strain. It
was concluded that the stress conditions were sufficiently non-
uniform to cause local failures within the sample.

A simple shear apparatus was developed at Cambridge
University by Budhu and Wood (1979) to study the non-
uniformities of stresses and strains in the NGI simple shear
samples experimentally. The basic design of this apparatus was
similar to that of the NGI simple shear apparatus, but contact
load cells were placed in the top and bottom platens for measuring
distributions of stresses and provision was made for the
determination of internal strains by lead shot markers and
radiographic techniques. Budhu (1979) and Airey (1980) used the
first version of this apparatus, CSSA.Mk.1 , to study the non-
uniformities of stresses and strains in samples of dry sand.
It was found that for sand the stress and strain distributions
were less uniform. than those predicted by theoretical
analyses.

A comprehensive study of the non-uniformities of stresses and
strains in kaolin samples was performed by Airey (1984) using
the CSSA.Mk.2 , a modified version of CSSA.Mk.1 . Three
areas of the sample, the principal third, the central third and
the sample core, are defined as in Figure 3.8. Examples of the
results obtained are given in Figures 3.9 and 3.10. Figure 3.9
shows the stress distributions on the principal third after one-
dimensional consolidation and at different stages during
constant σ_v' and constant volume shearing of normally
consolidated samples. It was concluded that the normal stress
and shear stress were uniform over 80 % and 50 % of the
sample respectively. Figure 3.10 shows that the average shear
stress τ_v' determined from the applied load was 10 % less
than the shear stress τ_{yx}' measured at the sample core.
Other results also showed that the average normal stress σ_v'
determined from the applied load was 10 % greater than the
normal stress σ_y' measured at the sample core. On the whole,
the stress distributions for clay samples were considerably more
uniform than those for sand samples. From the results of
internal strain measurements, it was concluded that the

distributions of normal and shear strains were uniform and the strains determined from boundary displacements were representative of the strains within the sample until the formation of the first slip plane. During constant $\sigma_v{}'$ and constant volume tests slip planes did not develop until shear strains γ reached 25 % and 15 % respectively. The difference between the measured zero strain increment directions and the slip planes varied from 3 to 10 degrees.

Considering all the work mentioned in this section, it can be concluded that the general patterns of the non-uniform stress distributions predicted theoretically by Roscoe, Lucks et al, Prevost and Høeg and Budhu and Britto were all the same and they also agreed with the pattern of stress distributions obtained experimentally by Airey. Both theoretical and experimental results indicated that approximately 70 % of the sample was uniformly stressed. Because of non-uniformities, the stresses determined from the applied loads differed from the stresses measured at the sample core by about 10 % . The theoretical analysis by Duncan and Dunlop showed that progressive failure occurred within the sample during shearing. This might not be important for normally consolidated samples but it might affect the results of heavily overconsolidated samples. In spite of the stress non-uniformities, experimental results obtained by Airey showed that the distributions of strains within the samples were uniform until the formation of slip planes at later stages of the tests.

3.3.2   Methods for estimating states of stress

In the NGI simple shear apparatus, the stresses measured are the average stresses $\sigma_v{}'$, $\tau_v{}'$ applied to the horizontal surface of the sample. Even if uniform stress distributions are assumed, this information can only fix one point $(\sigma_y{}' , \tau_{yx}{}')$ on the Mohr's circle of stress and it is therefore insufficient to determine the complete stress state of the sample. Various theoretical and empirical methods for estimating the stress state have been proposed by various authors. These methods will be briefly described and their applications to clay samples will

be discussed.

Duncan and Dunlop (1969) suggested that the stress increments of a simple shear sample could be approximated by pure shear stress increments. The definition of pure shear stress increments has been given in Section 2.4.1. Using such an approximation the complete stress state of the sample can be defined and from the geometry of Mohr's circle of stress,

$$\sigma_1' = \tfrac{1}{2}(1+K_o)\sigma_{yo}' + \left[\frac{\sigma_{yo}'(1-K_o)^2}{4} + (\tau_{yx}')^2 \right]^{\tfrac{1}{2}} \qquad (3.2)$$

$$\sigma_3' = \tfrac{1}{2}(1+K_o)\sigma_{yo}' - \left[\frac{\sigma_{yo}'(1-K_o)^2}{4} + (\tau_{yx}')^2 \right]^{\tfrac{1}{2}} \qquad (3.3)$$

where K_o is the pre-shearing coefficient of earth pressure at rest and σ_{yo}' is the pre-shearing value of σ_y'. Randolph and Wroth (1981) also suggested that for simple shear tests on overconsolidated samples, in the early stages of the tests before plastic straining occurs, the stress increments can be expected to be pure shear stress increments.

De Josselin de Jong (1972) studied possible failure mechanism for a simple shear sample shearing at critical state with constant volume. It was assumed that slip planes could only form along zero extension lines so that the slip planes were either horizontal or vertical. It was further assumed that the slip planes were planes subjected to the maximum of the stress ratio τ'/σ'. As a result, there are two possible modes of failure as shown in Figure 3.11. De Josselin de Jong argued that the failure mode represented by the bottom half of Figure 3.11 requires the application of the smallest shear stress and is therefore the most likely failure mode. Randolph and Wroth (1981) and Wroth (1984 and 1987) presented the results of an undrained test on normally compressed kaolin as shown in Figure 3.12. The results were obtained by Borin (1973) using the Cambridge simple shear apparatus with the complete stress states of the sample recorded. The Mohr's circle of stress in Figure 3.12 is

drawn for the condition of maximum τ_{yx}' and it appears to touch the failure envelope given by $\phi_{ps}' = 23°$ at point E which corresponds to stresses on the vertical planes. Based on this, Wroth suggested that the supposition of De Josselin de Jong might be valid.

Ladd and Edgers (1972) performed constant volume tests on clay samples in the NGI simple shear apparatus in an attempt to relate the maximum shear stress τ_{yx}' and the maximum stress ratio τ_{yx}'/σ_y' to undrained shear strengths c_u and friction angles ϕ' measured in other forms of laboratory tests. They concluded that at failure the effective stress circle is tangent to the Mohr-Coulomb failure envelope defined by ϕ' as shown in Figure 3.13. At maximum τ_{yx}' the ratio τ_{yx}'/σ_y' is less than $\tan \phi'$ for the soil, thus the horizontal plane is not a plane of maximum stress ratio and the stress state (σ_y', τ_{yx}') at maximum τ_{yx}' is not at point A in Figure 3.13. They predicted that the failure state lies somewhere between points A and C in Figure 3.13. Similar suggestions were made by Parry and Swain (1977) in a discussion about the stress state in clay soils adjacent to piles.

Various procedures for computing the complete stress states of a sample tested in the Cambridge simple shear apparatus have been proposed by Bassett (1967), Cole (1967) and Stroud (1971). Figure 3.14 shows a typical set of forces acting on the boundaries of the principal third of the sample measured by eight load cells in the Cambridge simple shear apparatus. The principal third of the sample is regarded as three separate elements rather than a single element due to stress non-uniformities already described in Section 3.3.1. The more recent procedures proposed by Drescher et al (1978) and Wood et al (1980) adopted the concept of an average stress tensor to determine a representative stress state in the central part of the sample. A difficulty in the application of the concept of the average stress tensor was the requirement of equilibrium of all boundary forces and their moments. Because of experimental inaccuracies in the measurement of forces, and friction at the vertical sides of the sample, the measured boundary forces did not

86

usually satisfy force or moment equilibrium. Different correction procedures to achieve equilibrium might produce different results.

Since the complete states of strain of the samples in both Cambridge and NGI simple shear apparatus are known, the complete states of stress can be determined if coaxiality, defined as the coincidence of the principal axes of stress and principal axes of strain increment, applies. For sands, results of tests performed by Budhu and Wood (1979) in the Cambridge simple shear apparatus showed that coaxiality was applicable. But for clays, an example of the results obtained by Borin (1973) shown in Figure 3.15 indicates that coaxiality does not apply at any stage during shearing.

Oda and Konishi (1974) conducted simple shear tests on cylindrical rods and observed the relationship

$$\frac{\tau_{yx}{}'}{\sigma_y{}'} = k \tan \theta \qquad (3.4)$$

where k is a material constant and θ is the inclination of the major principal stress $\sigma_1{}'$ to the vertical. Wood et al (1980) presented test results with the ratio $\tau_{yx}{}'/\sigma_y{}'$ for the central part of the sample plotted against $\tan \theta$ as shown in Figure 3.16(a). The results were from constant $\sigma_v{}'$ tests and constant volume tests performed in the Cambridge simple shear apparatus on samples of Leighton Buzzard sand with different initial voids ratios and stress states. Hence, Figure 3.16(a) demonstrates that the relationship given by Equation (3.4) applies to sand. Airey (1984) plotted $\tau_{yx}{}'/\sigma_y{}'$ against $\tan \theta$ using data from Borin as shown in Figure 3.16(b) and suggested that Equation (3.4) might also be applicable for normally consolidated clays. No test data is available to assess whether Equation (3.4) can be applied to overconsolidated clays. Using Equation (3.4) the complete stress states of samples tested in the NGI simple shear apparatus can be defined. From a consideration of the geometry of Mohr's circle of stress,

$$\sigma_1' = \left[1 + \frac{1}{k}\left(\frac{\tau_{yx}'}{\sigma_y'}\right)^2\right]\sigma_y' \tag{3.5}$$

$$\sigma_3' = (1 - k)\,\sigma_y' \tag{3.6}$$

$$\sin \phi' = \frac{[k^2 + (\tau_{yx}'/\sigma_y')^2]}{[k(2-k) + (\tau_{yx}'/\sigma_y')^2]} \tag{3.7}$$

Ideally, the value of k for any particular material can be determined in an instrumented simple shear apparatus and then Equation (3.4) can be applied to results obtained from the less complex apparatus. But in practice this is impossible and some other means of evaluating k is needed.

It has been shown in Section 2.3.2 that when a sample is sheared with no volume change allowed, the major principal strain increment $\delta\epsilon_1$ is inclined at 45° to the vertical. Ochiai (1975) suggested that at critical state, when shearing occurs with no volume change, the principal axes of strain increment and stress coincide, so that the major principal stress σ_1' is also inclined at 45° to the vertical. Hence, from Equation (3.4) and from the geometry of Mohr's circle of stress,

$$k = \left(\frac{\tau_{yx}'}{\sigma_y'}\right)_{cs} = \sin \phi_{cs}' \tag{3.8}$$

Airey (1980) demonstrated that Equation (3.8) underpredicts values of k. The evaluation of k will be further discussed later in this section.

For simple shear samples which are circular in plan, attempts have been made to measure the radial stress σ_r' acting on the curved boundaries of the sample by using the reinforcement wire of the membrane as a transducer. Examples of such attempts are

Soydemir (1976), Dyvik et al (1981) and Airey (1984). Although the radial stress can be measured, the complete stress state during shearing still cannot be determined because the intermediate principal stress σ_2' acting perpendicular to the plane of shearing might not be the same as the normal stress σ_x' acting on the ends of the sample in which case σ_r' might not be equal to either σ_2' or σ_x'. For sands, results obtained by Budhu and Wood (1979) using the Cambridge simple shear apparatus showed that during shearing the variation of σ_r' was completely different from the variations of σ_x' and σ_2'. For clays, Borin (1973) did not measure σ_2' and so no test data is available for predicting the relationships among the stresses σ_r', σ_x' and σ_2'.

Airey (1984) used both Equation (3.4) and radial stress measurement to estimate the Mohr's circle of stress at failure for a constant volume test on a kaolin sample. The results are reproduced in Figure 3.17. In order to calculate σ_x' from measurements of σ_r', Airey assumed that during shearing the change in radial stress $\delta\sigma_r'$ is the average of the change in intermediate principal stress $\delta\sigma_2'$ and the change in normal stress $\delta\sigma_x'$ on the ends of the sample. Plane strain test results were used to estimate $\delta\sigma_2'$. It was concluded that radial stress measurement can be used to give a reasonable estimate of the complete stress state.

The application to clays of the methods described will be discussed now. It has already been explained in Section 2.4.1 that simple shear stress increments can only be described as pure shear stress increments when the material is isotropic and elastic. This limits the applicability of the Duncan and Dunlop method to overconsolidated samples and before yielding starts.

The theory put forward by De Josselin de Jong requires the coincidence of slip planes and zero extension lines. Houlsby and Wroth (1980) demonstrated theoretically that contrary to what had frequently been stated there was no kinematic requirement that slip planes should occur along zero extension lines. Only for certain constitutive relations, for example those with associated flow rules, did the additional statical requirements

89

result in slip planes coinciding with zero extension lines. Experimental evidence for coincidence of slip planes and zero extension lines in dense sand has been provided by Arthur et al (1977) and by Budhu (1979). Experimental evidence for clay by Airey (1984) indicated that slip planes were close to but not coincident with zero extension directions.

The suggestion by Wroth that the De Josselin de Jong theory might be valid was based on just one set of test data by Borin. More experimental evidence on different soils with different friction angles ϕ_{cs}' and angles of rotation of principal stress axes θ_{cs} are required before any conclusions can be drawn. In order to provide further information, a set of basic test data reported by Dyvik and Zimmie (1983), shown in Figure 3.18, will now be interpreted. The tests were performed on three different normally consolidated clays under constant volume condition using the NGI simple shear apparatus with radial stress measurement. Dyvik and Zimmie assumed that the radial stress σ_r' was equal to the normal stress σ_h' on the sample ends. The stresses have been divided by the pre-shearing effective vertical stress σ_{vo}' which was equal to 50 kPa for all three clays. The stress paths traced out by the stresses on the horizontal planes and the stresses on the vertical planes are plotted in Figure 3.19. The Mohr's circles of stress shown correspond to stress states at γ = 18 % . It can be seen that for all three clays at γ = 18 % the vertical planes are not planes subjected to the maximum of the stress ratio τ'/σ' . Because of the lack of experimental evidence which supports the De Josselin de Jong theory, this theory will not be used for the analysis of test data in Chapter 7.

So far, the most suitable method for estimating the stress states in NGI simple shear samples is by using the relationship τ_{yx}'/σ_y' = k tan θ . This relationship was obeyed by sands and normally consolidated kaolin under constant volume and constant σ_v' shearing and at different voids ratios and stress states. The relationship between k and ϕ_{cs}' for sands and kaolin was plotted by Airey (1984) as shown in Figure 3.20. The relationship given by Equation (3.8)

which underpredicts values of k is also plotted. The scarcity of data for clays is mainly because instrumented simple shear apparatus are complicated to use, and as mentioned before, the sample cannot strictly be considered as a single element due to stress non-uniformities which makes the determination of stress states much more complicated than in triaxial tests. The data reported by Dyvik and Zimmie (1983) will again be used here to provide more information. In Figure 3.21, values of τ_{yx}'/σ_y' are plotted against tan θ for the three clays. It appears that the relationship $\tau_{yx}'/\sigma_y' = k \tan θ$ also applied to these clays. The values of ϕ_{cs}' for the three clays have been calculated from the stresses corresponding to $\gamma = 18$ % and the relationship between k and ϕ_{cs}' plotted in Figure 3.20. The data points for the three clays lie just below the curve drawn by Airey for sands and kaolin. This could be due to inaccuracies in values of σ_h' originated from the assumption $\sigma_h' = \sigma_r'$. Nevertheless, Figure 3.20 can be used to give a reasonable estimate of k for any soil with a known value of ϕ_{cs}'. The relationship $\tau_{yx}'/\sigma_y' = k \tan θ$ together with Figure 3.20 will be used in the analysis of test data in Chapter 7.

3.4 Application of triaxial parameters to plane strain conditions

In Chapter 2 it has been mentioned that simple shear samples deform under plane strain conditions and the angle ρ_{cs}' measured is dependent on ϕ_{cs}' as shown in Equations (2.35), (2.38) and (2.102). For the purpose of applying values of ϕ_{cs}' obtained from triaxial tests to the analyses of simple shear test data, it is necessary to be able to assess the difference in the value of ϕ_{cs}' under axial symmetry and plane strain condition for any particular soil.

Leussink and Wittke (1963) compared the shear strengths of glass and steel balls under axial symmetry and plane strain conditions for different packing arrangements. Theoretical predictions were made by considering the forces acting at the points of contact of the balls and experiments were carried out

using the triaxial apparatus and plane strain apparatus. It was concluded that both theoretical predictions and experimental results indicated that plane strain condition led to higher shear strength than axial symmetry condition.

In conventional triaxial tests and plane strain tests where no rotation of principal axes is allowed, compression tests are usually carried out by increasing the total major principal stress σ_1 while maintaining the total minor principal stress σ_3 constant. In triaxial tests the intermediate principal stress σ_2' is the same as σ_3' but in plane strain tests because straining along the intermediate principal direction is restricted σ_2' will become greater than σ_3'. To describe the relative magnitude of σ_2' the parameter $b = (\sigma_2'-\sigma_3')/(\sigma_1'-\sigma_3')$ is usually used. For triaxial compression tests b is zero and for plane strain tests b varies between 0 and 1.

There have been many studies of the influence of σ_2' on the strengths of sands using the true triaxial apparatus. Ladd et al (1977) summarised results of some of the studies including, for example, Reades and Green (1974) and Lade and Duncan (1973) to show that the shear strength of sand increased as the value of b increased from zero to the value corresponding to plane strain conditions. The friction angle at peak shear stress ϕ_p' was used as the shear strength parameter in these studies. Cornforth (1964) performed triaxial tests and plane strain tests on K_o compressed samples of Brasted sand with various initial porosities. The results were plotted as shown in Figure 3.22(a) and it was suggested that plane strain samples had greater strengths. However, Cornforth also presented results as shown in Figures 3.22(b) and (c) which demonstrate that the ultimate strengths were independent of initial porosity. Although the average value of b at ultimate states was 0.20 for plane strain tests compared to zero for triaxial tests, the average ultimate friction angle of 32° in plane strain tests and 33° in triaxial tests were sufficiently close to suggest that the ultimate friction angle in both types of tests were the same.

Test data for clays are not as abundant as for sands, but there is slightly more information on values of the critical state friction angle ϕ_{cs}' . Hambly and Roscoe (1969) performed tests on normally consolidated kaolin using a biaxial plane strain apparatus and concluded that at failure a unique Mohr-Coulomb failure criterion applied to both triaxial and plane strain conditions. Atkinson (1973) performed triaxial and plane strain tests on the heavily-overconsolidated undisturbed London clay and found that ϕ_p' was 22° for both types of tests. Ladd et al (1977) summarised most of the results on clays to show that the ratio of undrained strength c_u for triaxial tests to c_u for plane strain tests was 0.92 ± 0.05 in compression and 0.82 ± 0.02 in extension.

Duncan and Seed (1966) performed undrained plane strain tests on samples of undisturbed San Francisco Bay mud which were normally consolidated under K_o condition. Two series of tests were performed with the major principal stress oriented vertically in one and horizontally in the other and the values of ϕ_{cs}' obtained varied between 35° and 38° . The value of ϕ_{cs}' obtained from undrained triaxial tests on isotropically consolidated samples of the same material was 35° . Vaid and Campanella (1974) performed plane strain and triaxial tests on samples of undisturbed Haney clay which were normally consolidated under K_o conditions. They reported that for undrained compression tests the values of c_u/σ_{vo}' was 0.30 in plane strain tests and 0.27 in triaxial tests and the values of ϕ_{cs}' was 32° in plane strain tests and 30° in triaxial tests. It was concluded that plane strain condition gave rise to stiffer stress-strain response, higher undrained strength and angle of shearing resistance, and that when the test data were plotted in terms of octahedral stress and strain parameters the stress-strain behaviours in the two types of tests were the same.

Henkel and Wade (1966) performed undrained plane strain tests on samples of remoulded Weald clay which were normally consolidated under K_o condition. The results were compared with a parallel series of triaxial tests on the same soil by

Sowa (1963). The results, reproduced in Figure 3.23, show that c_u/σ_{vo}' was 0.28 for plane strain tests and 0.26 for triaxial tests and the value of ϕ_{cs}' was 27° for plane strain tests and 26° for triaxial tests. The value of b at critical state was 0.35. It was also found that on σ_{oct}', τ_{oct}' plane triaxial and plane strain stress paths had the same shape but terminated at different states. This led to the conclusion that the effective stress paths were uniquely defined by octahedral stresses which took account of values of σ_2' but the critical states were governed by the Mohr-Coulomb criterion which ignored the effects of σ_2'.

As a conclusion, most reports in literature tended to suggest that plane strain shear strengths were higher than triaxial shear strengths. This was so if for sands the peak strength parameter ϕ_p' was used and for clays the undrained strength parameter c_u was used. In terms of the critical state parameter ϕ_{cs}', results on sand by Cornforth and results on normally consolidated clays all demonstrated that at critical state Mohr-Coulomb failure criterion governed and the value of ϕ_{cs}' for any particular soil was the same under axial symmetry and plane strain conditions. Therefore, values of ϕ_{cs}' obtained from triaxial tests will be applied directly to the analyses of simple shear test data in Chapter 7.

3.5   Previous test results

3.5.1   Results on Cowden till

Most previous test results on Cowden till have arisen from the study of the engineering properties of glacial tills currently undertaken by the BRE. The location and geology of the BRE Cowden till test bed site are given in Chapter 4. There have been many reports on results of in-situ testing, for example, Powell et al (1983), Marsland and Powell (1985) and Powell and Uglow (1985 and 1986). Reports on laboratory test results are less abundant and fall into two categories. In the

first category are results from tests of research quality
largely on remoulded and reconstituted samples, for example,
Gens and Hight (1979) and Ng (1988). In the second category
are results from tests on undisturbed samples carried out by
BRE, mainly undrained triaxial tests on samples with 100 mm
diameter, for example, Lewin and Powell (1985).

Gens and Hight (1979) investigated whether the behaviour of
undisturbed samples of the till can be determined from remoulded
samples. The till tested was from the BRE test bed site and
a typical grading curve and the Atterberg limits obtained
are shown in Figure 3.24(a). Undrained triaxial compression
tests were carried out on undisturbed samples and on
remoulded samples with a maximum particle size of 2 mm. To
check whether the elimination of gravel sized particles
affected the mechanical properties of the soil, tests were
performed on samples with different gravel contents. The
gravel content of the undisturbed samples ranged between 5 %
and 12 % and it was found that no significant differences in
mechanical properties were produced by varying the gravel
content between 0 % and 12 % . No pre-shearing compression
or swelling was applied to the undisturbed samples and both
isotropically and K_O compressed and swelled remoulded
samples were tested. All samples gave a critical state friction
angle ϕ_{cs}' of 26° ± 1° . It was suggested that because of
experimental difficulties in accurately measuring stiffness
parameters, the effective stress paths served as a better
criterion for comparing behaviours of undisturbed and remoulded
samples. The effective stress paths obtained from the
undisturbed samples are reproduced in Figure 3.24(b). All six
undisturbed samples were taken from a single borehole between
4 m and 6 m depth and their water contents were between
14 % and 18 % . It was suggested that the stress paths of
the undisturbed samples were simulated better by the
remoulded samples which were compressed and swelled under K_O
condition than by the isotropic ones.

Ng (1988) studied the behaviour of Cowden till within the
framework of critical state soil mechanics. Stress path tests
were performed using the stress path testing equipment for

samples with 38 mm diameter described in Section 5.4. The samples were remoulded and reconstituted with particles greater than 2 mm eliminated. At the time of writing Ng's data have not been fully interpreted and written up and only limited results are available for comparison with the author's simple shear test results. The value of K_o for the normally compressed samples was measured to be 0.59 and the critical state parameters obtained are summarised in Table 3.1. For the reconstituted samples which were compressed and swelled under K_o condition, the effective stress paths for drained and undrained tests on samples with overconsolidation ratios $R_p = 1$, 2, 4 and 6 were normalised with respect to p_e' and it was found that a unique state boundary surface existed for the soil. For the undrained tests, the normalised tangent shear stiffness $dq'/(vp'd\epsilon_s)$ at $\epsilon_s = 0.06$ % ranged from 40 to 195.

Atkinson et al (1985a) compared undrained triaxial compression test results on isotropically compressed remoulded and reconstituted samples obtained by Ng (1988) with results on undisturbed samples obtained by Lewin and Powell (1985). The effective stress paths, reproduced in Figure 3.25, show that the behaviours of the remoulded and reconstituted samples were very similar and by comparing Figures 3.25(a) and (b) with Figure 3.25(c) it was suggested that the undrained stress paths for undisturbed samples resemble the paths for the overconsolidated remoulded and reconstituted samples. Figure 3.26 shows that the states corresponding to the ends of the tests on the undisturbed samples fall close to the extension of the critical state line for the remoulded and reconstituted samples defined by $M = 1.1$ and $\phi_{cs}' = 28°$.

3.5.2   Results on London clay

The mechanical properties of London clay have been the subject of extensive study for many years because of the large number of structures founded on the clay. A full description of the existing knowledge about London clay is outside the scope of

this work.   Instead, some of the general features of the
behaviour of London clay in terms of one-dimensional compression
and consolidation properties, shear   strength and   stiffness will
be highlighted and then any laboratory test results on the
London clay at Brent will be described.

Reports on in-situ testing   of London clay have been given by,
for example, Marsland (1971a and b),   Windle and Wroth (1977),
Marsland and Randolph (1977)   and   Powell and Uglow (1986).
St. John (1975)   reported that   stiffnesses of   London clay
measured in the   laboratory were   much lower than those
measured from full-scale   structures.   Simpson et al (1979)
suggested that this was due to the   lack of understanding of
threshold effects in soils and they described a non-linear
stress-strain model for London clay   which took account of
threshold effects for use in finite element analyses.   Since
then the influence of threshold effects on the stiffness of
London clay has been   studied by Richardson (1988).

As undisturbed samples of London clay can be quite easily
obtained,   there are   plenty of laboratory   test data on the
behaviour of undisturbed samples but   much less data on the
behaviour of remoulded and reconstituted samples.   A summary of
the classification test results from various sites is given in
Table 3.2.   The value of K_O for normally compressed London
clay was measured by Brooker and Ireland (1965).   A remoulded
sample was compressed in an instrumented oedometer and the
value measured was 0.62.   Som (1968)   performed standard
oedometer tests on London clay from Ongar.   Undisturbed
samples and a sample reconstituted from a slurry with initial
water content of   90 %   were tested with the results as shown in
Figure 3.27.   The values of λ and   N   for the normal
compression line of the slurry sample were 0.155 and 2.791
respectively and the value of k for an approximate linear
swelling line for the undisturbed samples was   0.040.
Atkinson et al (1984) and   Richardson (1984b) performed stress
path tests on remoulded samples of London clay from Bell
Common.   Results from K_O compression indicated that
K_O = 0.66, λ = 0.13, k = 0.04   and N_O = 2.54.

Values of the coefficient of consolidation c_v for undisturbed samples of London clay have been given by many authors. For example, Skempton and Henkel (1957) presented results of oedometer tests on 25 different undisturbed samples of London clay taken from various depths at Paddington, Victoria and South Bank which showed that values of c_v were very consistent and were between 7×10^{-9} m²/s and 50×10^{-9} m²/s and values of the coefficient of permeability k were between 2×10^{-12} m/s and 30×10^{-12} m/s. Average values of c_v reported by Sandroni (1977) for undisturbed samples of London clay from Broadoak and University of Kent were 20×10^{-9} m²/s and 9×10^{-9} m²/s respectively both of which lay within the range of values given by Skempton and Henkel.

Som (1968) carried out two strain controlled oedometer tests to evaluate the maximum previous effective vertical stress σ_{vp}' which acted on undisturbed samples of London clay from Ongar due to overburden in the ground. Effective vertical stresses σ_v' up to 48 MPa were applied to samples with a diameter of 76 mm and an initial thickness of 19 mm. A constant rate of straining slow enough to cause negligible excess pore pressures measured at the sample base was selected. The method used for estimating σ_{vp}', as illustrated in Figure 3.28, was proposed by Schmertmann (1953) based on the assumption that the swelling line due to erosion in the ground had a similar shape to the swelling line obtained from oedometer tests. The value of σ_{vp}' was estimated to be 1.8 MPa which suggested that the depth of ground eroded was 165 m.

When undisturbed samples of the heavily overconsolidated London clay are sheared, slip planes will form before the samples reach critical state. In most reports in literature the shear strength of heavily overconsolidated soils is associated with the peak shear stress state and the undrained strength c_u is defined as the maximum value of $(\sigma_1' - \sigma_3')/2$. It has been discussed in Section 3.4 that c_u is dependent on the strain condition imposed during shearing and is therefore not a soil constant. Since London clay was formed by deposition followed

by one-dimensional compression the soil can be expected to have anisotropic stress-strain properties and it is likely that the peak undrained strength c_u will depend on the orientation of the principal stress axes. Webb (1966) and Agarwal (1967) both performed undrained triaxial compression tests on undisturbed samples of London clay with 38 mm diameter to measure c_u with the samples at three different orientations: vertical axis of sample coinciding with the vertical in the ground (V), with the horizontal in the ground (H) and with the direction at 45° to the horizontal in the ground (D). They both found that $c_u(H) > c_u(V) > c_u(D)$.

Due to the presence of fissures in London clay, study of the behaviour of the clay requires testing samples which are large enough to represent the soil mass. Agarwal (1967) performed undrained triaxial tests on undisturbed samples of London clay from Wraysbury with diameters of 13 mm, 38 mm, 102 mm, 152 mm and 305 mm. It was concluded that the undrained strength decreased with increasing sample size and approached a constant value when the sample diameter was increased to 102 mm. Sandroni (1977) performed undrained triaxial compression tests on undisturbed samples of London clay from Broadoak with diameters of 38 mm, 71 mm, 152 mm, and 254 mm. For the samples with diameters of 152 mm and 254 mm pore pressures were measured by inserting probes in the side of the samples. States of stress at failure, defined as the peak deviator stress, are as shown in Figure 3.29. It can be seen from Figure 3.29 that the peak deviator stress was not influenced by the difference in sample size. Sandroni suggested that this was due to the unusually close spacing of the fissures in the London clay from this particular site.

Apted (1977) performed undrained triaxial tests on undisturbed samples of London clay from South Ockendon to study the effects of weathering on the properties of the clay. No pre-shearing compression or swelling was applied and the results for samples with 100 mm diameter are reproduced in Figure 3.30. Figure 3.30(a) shows typical effective stress paths and Figure 3.30(b) shows the stress states at peak deviator stress. Standard shear box tests were conducted by

Agarwal (1967) on undisturbed samples of London clay from Wraysbury. The rate of shearing was 1.4×10^{-3} mm/min and the stress states corresponding to peak shear stress are as shown in Figure 3.31 with no area correction applied in calculating the stresses.

There are only very few studies on the behaviour of London clay within the framework of critical state soil mechanics. Results of the tests performed by Atkinson et al (1984) mentioned earlier indicated that at critical state $\phi_{cs}' = 22°$ (M = 0.86) for compression and $\phi_{cs}' = 24°$ (M = 0.70) for extension. Atkinson and Richardson (1987) in an investigation into the effects of local drainage on the undrained strength of overconsolidated clay performed triaxial compression tests on reconstituted samples of London clay from Bell Common with 38 mm diameter. The samples were isotropically compressed before shearing and the critical state parameters obtained were M = 0.90 ($\phi_{cs}' = 23°$) and $\Gamma = 2.58$.

Although there are plenty of previous laboratory test results on the stiffness of London clay, for example Atkinson (1973), Sandroni (1977) and Costa Filho (1980), most of the results were presented in terms of secant moduli. The differences between secant modulus and tangent modulus and the advantages of using tangent modulus have been explained by Atkinson et al (1986). Since the results from this study will be plotted in terms of tangent modulus in Chapter 7, mainly examples of stress-strain curves will be given here. Stress-strain curves obtained by Sandroni (1977) for samples with 254 mm diameter are reproduced in Figure 3.32 with the failure modes also shown. Costa Filho (1980) studied the effects of bedding errors on the determination of stiffness at small strains by measuring axial strains with displacement transducers mounted directly onto undisturbed triaxial samples of London clay from South Ockendon with 38 mm diameter. Different pre-shearing stress paths were applied and the results with deviator stress plotted against axial strain measured from the middle third of the samples are as shown in

Figure 3.33. These stress-strain curves were not plotted up to failure due to erratic readings from the transducers once slip planes were formed. Costa Filho suggested that a main feature of Figure 3.33 is the non-linearity of the curves, which was also observed in many other reports in literature. Skempton and Henkel (1957) performed undrained triaxial tests on undisturbed samples of London clay from South Bank and calculated the undrained Young's modulus E_u from the initial linear part of the stress-strain curves. It was found that the values of E_u for extension tests were 2 to 4 times greater than those for compression tests. Jardine et al (1984) studied soil stiffness at small strains using electrolytic level gauges mounted on triaxial samples. The gauges were capable of resolving to less than 1 μm corresponding to an axial strain of approximately 0.001 % for a 76 mm long sample. Two undisturbed London clay samples from Canon's Park with 98 mm diameter were tested in undrained compression with no pre-shearing compression or swelling. At ε_a = 0.1 % , the two samples had values for the normalised secant modulus E_u/p_o' of 198 and 228.

No Laboratory tests of research quality on the London clay at Brent are reported in the literature. Only results from tests on undisturbed samples carried out by BRE are available. Marsland (1971b) reported results of undrained triaxial compression tests on both samples with 38 mm diameter and samples with 98 mm diameter. No pre-shearing compression or swelling was applied and the stiffness of the triaxial samples were compared with stiffnesses determined from plate loading tests for various depths.

3.6   Summary

This chapter has reviewed aspects of simple shear tests on clay samples and it has reviewed knowledge about the two soils tested in this research. Attention has been drawn to the problems of simple shear tests and the important points as

regards simple shear testing are summarised as follows :

(1) Both theoretical and experimental studies showed that approximately two thirds of the sample was under uniform stresses. Because of non-uniformities, the average shear stress τ_v' was about 10 % less than the shear stress τ_{yx}' at sample core and the average normal stress σ_v' was about 10 % greater than the normal stress σ_y' at sample core.

(2) Among the various proposed methods for estimating the stress states of clay samples, the method using the relation $\tau_{yx}'/\sigma_y' = k \tan \theta$ was supported by experimental results and it will be used in the analyses of test data in Chapter 7.

(3) At critical state the shear strength of soils is governed by the Mohr-Coulomb failure criterion which does not take into account the effects of σ_2'. Hence, the value of ϕ_{cs}' obtained from triaxial tests can be applied directly to the analyses of data from simple shear tests which impose plane strain conditions on the samples.

The principal characteristics of Cowden till and London clay have been summarised. Two categories of test results on the Cowden till have been described. Results from tests of research quality presented included a summary of the critical state parameters for Cowden till. Existing knowledge about London clay has been described generally in terms of one-dimensional compression and consolidation properties, strength and stress-strain behaviour. There are very little data available on the London clay at Brent.

CHAPTER 4   ENGINEERING GEOLOGY

4.1   Introduction

This chapter gives the engineering geology background that is needed for a better understanding of the mechanical behaviours of the soils studied. All Cowden till and London clay samples used in this study were obtained from BRE test bed sites which were established for in-situ testing. Cowden till was chosen for investigation by BRE because more knowledge was required for the design of foundations of offshore structures in the North Sea and Cowden till was a typical lowland glacial till which occurred both in central and eastern England and the southern North Sea. The section on regional geology will describe the geological history and depositional environment of each soil and the section on drift geology will describe the soil profile and index properties of the soil at each site.

4.2   Locations of soils

4.2.1   Cowden till

The BRE Cowden till test bed site is located at Cowden about 23 km north east of Hull and 2 km north of Aldbrough. Figure 4.1 shows that the site is at Ordnance Survey map reference 5245 4403 (sheet 107).

4.2.2   London clay

The BRE London clay test bed site is located at Brent about 10 km north west of central London. Figure 4.2 shows that the site is at OS map reference 5232 1874 (sheet 176).

4.3   Regional geology

4.3.1   Cowden till deposit

The test bed site at Cowden was selected by BRE because of the
known presence of a deep sequence of predominantly clayey glacial
deposits. A description of the geology of the area has been
given by Marsland and Powell (1985). Up to 25 m of the deposits
are exposed in cliffs which extended for about 40 km along
the coast about 800 m to the east of the site. The glacial
deposits are underlain by Cretaceous Chalk the surface contours
of which are shown in Figure 4.3. During the Ice Age
(Quaternary) which was characterised by a sequence of
alternating cold and temperate stages, the area was glaciated
in the last three cold stages: Anglian (200,000 years ago),
Wolstonian (125,000 years ago) and Devensian (75,000 years ago).
Each cold stage comprised more than one ice advance but much
of the material deposited during earlier advances was eroded
and redeposited from the ice during the Devensian stage. The
possible maximum extent of the ice along the east coast was
suggested by West (1968) as shown in Figure 4.4. Straw and
Clayton (1979) suggested that at least three significant
ice advances occurred during the Devensian as shown in Figure 4.5.
The build up of ice particularly in North America during the
Devensian lowered the sea levels by 130 m or more below
present levels. As a result the Cowden area lay well within
a permafrost desert and the tills formed were inorganic.

Various field documentation of the till sequences along the coast have
been made over the last 50 years. The earlier work has been re-
examined and the latest formulation of the stratigraphy was given
by Catt and Madgett (1981). Data from stratigraphical and
sedimentological studies indicated that a large proportion of the
tills at Cowden are late Devensian. It is still uncertain whether
they were deposited during successive advances of the ice or by
melting of a single ice sheet. Recent studies by
Derbyshire et al (1985) which considered the nature of the soils
eroded during the advance of the ice indicated relatively small
variations of the ice fronts. Data obtained from offshore borings

suggested that the Late Devensian tills stretch as a continuous stratum for at least 200 km east of the coast. It is likely that the deposits were derived from a large, active, oscillating ice lobe which extended well south of the general extent of the ice in the North Sea as shown in Figure 4.4. Sedimentological studies by Derbyshire et al indicated that most of the till were deposited from the base of the glacier so that the till was compacted under pressure. As a result no size sorting occurred and crushing of particles was intense. The fabric of the material and the crushed chalk particles also indicated post-depositional remoulding and shearing of the till at the base of the glacier.

4.3.2   London clay deposit

The geology of London clay has been the subject of extensive study for many years. An account of the geology of the area consisting of Greater London was given by Som (1968). The solid geology of the sedimentary formation in the London basin presented by Som is reproduced in Figure 4.6. A cross-section through the London basin given by Sherlock (1962) is shown in Figure 4.7. The Palaeozoic rocks are the deepest known formation in the area and under London itself the rocks are located at about 300 m below sea-level. Overlying the Palaeozoic rocks are the Jurassic rocks followed by the Cretaceous deposits. The Jurassic rocks are absent all over the London area so that the Cretaceous deposits lie directly over the Palaeozoic rocks. The Gault clay was the first of the Cretaceous formations to be deposited on the Palaeozoic rocks across the London area. Overlying the Gault clay is the Chalk which is about 200 m thick outcropping in the north-west and in the south. Overlying the Chalk is the Eocene beds the early deposits of which are the Thanet Sands and the Woolwich and Reading beds, collectively known as the Lower London Tertiaries.

The London clay which overlies the Lower London Tertiaries was deposited under marine and estuarine conditions. The deposition of London clay as a result of a series of marine invasions due

to changes of the land surface relative to sea-level was described by Burnett and Fookes (1974). The lowest part of the London clay, known as the Basement bed, is sandy but above it, the clay is very uniform and is originally about 120 m thick. The London clay was originally overlain by the Claygate beds and the Bagshot, Bracklesham and Barton Beds, all predominantly sandy with occasional clay layers. The total thickness of the original deposit was possibly 200 to 250 m. In the London area, subsequent uplift and erosion have removed the overlying deposits together with considerable thickness of the London clay so that the remaining clay is heavily overconsolidated. In central London only between 20 to 50 m of the London clay is left, for example, Skempton and Henkel (1957) reported that the thickness of London clay on the South Bank was 42 m. The geology of the area around the test bed site at Brent is shown in Figure 4.8. The cross-section along AB in Figure 4.8 is shown in Figure 4.9. In many areas gravels and alluvium were later deposited, but as Figure 4.8 shows, the London clay at Brent extends to the ground surface.

In several places the full thickness of the London clay has been preserved as indicated by the overlying Claygate Beds, for example, Wimbledon (130 m), Hampstead (120 m), Ingatestone (160 m) and Sheppey (160 m). Skempton (1961) estimated that erosion has reduced the thickness of London clay at Bradwell from 200 m to 50 m.

4.4   Drift geology

4.4.1   Cowden till test bed site

Inspection of the coastal cliff exposures indicated that the glacial drift in this area is composed mainly of a clay matrix dominated till typically found in eastern England. The clays are interspersed with layers and lenses of sand and gravel of varying extent. Results of tests carried out by BRE both on the test bed area and other areas towards the coast indicated that

the tills are of uniform composition and the index and strength properties are consistent. The largest variability occurs in the surface weathered layers.

General descriptions and index properties down a typical profile in the test site area given by Marsland and Powell (1985) are shown in Figure 4.10. There is a distinct change of colour from brown to very dark greyish brown at a depth of 4 to 5 m. This level varies considerably throughout the region and is considered to be a boundary above which surface weathering occurred. For depths between 3 and 17 m, the unit weights are almost constant with values between 21.6 and 22.0 kN/m^3. Down to a depth of 17 m the moisture contents gradually decrease with depth and are close to or just below the plastic limit. The plastic and liquid limits also show a gradual decrease with depth. The percentages by weight of clay sized particles down to 17 m depth are mostly within the range of 30 to 40 % of the material passing a 2 mm sieve. The results of eight particle size distribution tests performed by BRE fall within the envelope shown in Figure 4.11. Allowing for an average gravel content of about 10 % the typical overall clay content of the till is 30 %. The clay and silt accounts for about 60 % of the total dry weight and 66 % of the in-situ volume of the till. Therefore, the sand and gravel particles are generally separated by silty clay. Marsland and Powell also reported that when five samples of particles greater than 2 mm were counted, 43 to 76 % of the particles were chalk and the remainder were sandstone, siltstone, mudstone, limestone, flint, and quartzite. The cobbles or boulders are mainly resistant igneous materials and are considered to be sufficiently widely spread to be of little geotechnical significance.

The mineral contents of the till were identified by BRE. Minerals that were within the 0.25 to 0.63 mm range originated from northern England to Scotland and Scandinavia. Clay minerals constituted the major particle types in the material less than 2 μm with the non-clay minerals calcite, dolomite, and quartz comprising only a small proportion. Standard x-ray defraction techniques identified the clay minerals kaolinite, mica, chlorite and vermiculite. Values of the coefficient of consolidation c_v and the coefficient of permeability k

were measured from undisturbed oedometer samples by BRE (Gallagher, 1983) and it was found that values of c_v ranged between 32×10^{-9} and 476×10^{-9} m²/s and values of k ranged between 9×10^{-12} and 381×10^{-12} m/s.

4.4.2   London clay test bed site

General descriptions and index properties down a typical profile in the test site given by Powell and Uglow (1986) are shown in Figure 4.12.   Down to a depth of 9 m the clay was oxidised to a brown colour and consisted of hard lumps set in a clay matrix.   The sizes of the lumps increased gradually from a few millimeters near the surface to 6 to 50 mm at 9 m depth. Below 9 m the clay was stiff, greyish-blue and fissured with the spacing of the fissures increasing from between 6 and 50 mm at 9 m depth to between 75 and 325 mm at 25 m depth. The fissures were inclined at all angles but with a tendency towards near vertical and near horizontal. Powell and Uglow also reported that inspection of the clay in large diameter boreholes showed that below a depth of 17 m there were traces of silt and fine sand on some of the horizontal bedding planes.   The index properties of the soil as shown in Figure 4.12 are relatively uniform.   The unit weights are almost constant with values between 18.6 and 19.6 kN/m³. Down to a depth of 18 m the moisture contents gradually decrease with depth and are close to or just above the plastic limit.   The liquid limits also show a slight gradual decrease with depth.   The percentages by weight of clay sized particles down to 22 m are within the range of 55 to 65 % .   Results of oedometer tests performed by BRE indicated that the coefficient of permeability of the clay was of the order of 30×10^{-12} m/s.

The mineralogy of London clay was studied by Burnett (1974). The mineral compositions for different particle sizes for a sandy London clay sample presented by Burnett and Fookes (1974) is shown in Figure 4.13.   It illustrates that the coarser material is dominated by quartz and the finer material is mainly clay minerals.   In general, the mineral contents of London clay is not unusual for a marine sediment and they were found to be essentially uniform everywhere.

CHAPTER 5   EQUIPMENT AND TESTING PROCEDURES

5.1   Introduction

This chapter is divided into two parts. The first part, Sections 5.2 to 5.6, describes the laboratory testing equipment which have been used. The stress path testing equipment, the NGI simple shear apparatus and the standard shear box were all situated in the Geotechnical Engineering Research Centre at The City University. The shear box with automatic data logging was located in BRE. Methods of calibration and assessments of accuracies of measurements will be given. The second part, Sections 5.7 to 5.13, describes the procedures of preparing the different types of samples and the procedures of one-dimensionally compressing and loading these samples in the various types of apparatus used.

The objectives of the simple shear tests were to establish the critical state line and to examine whether a unique state boundary surface exists. These objectives were met by conducting tests on samples with different overconsolidation ratios and pre-shearing states under different drainage conditions. The remoulded and reconstituted samples allowed the testing of samples with any required OCR and, in particular, the testing of normally compressed samples enabled the Roscoe surface to be studied. The purpose of the stress path tests on samples with 38 mm diameter was to measure the basic critical state parameters for London clay which were useful to the analyses of simple shear test results. Reconstituted samples were used because, usually, normally compressed samples are more likely to reach critical states than overconsolidated samples. The normally compressed samples were compressed to different pre-shearing states so that when sheared they reached different critical states to define the critical state line. The stress path tests on samples with 100 mm diameter were performed mainly for the purpose of studying the behaviour of undisturbed London clay. Samples with 100 mm diameter instead of 38 mm diameter were tested because the larger samples were more representative of the fissured soil mass. The stress probing

tests included constant p' and constant q' probes for obtaining the elastic parameters in the constitutive relationships represented by Equations (2.61a) and (2.61b).

5.2 Equipment for sample preparation and setting up

5.2.1 Simple shear samples

Figure 5.1 shows the accessories used including : (1) Geonor sample trimming apparatus; (2) membrane stretcher; (3) sharp-edged steel former (80 mm diameter and 33 mm height); (4) Perspex disc (79.5 mm diameter and 15 mm thick); (5) porous stone (79 mm diameter); (6) bottom filter holder with porous stone in place and (7) top filter holder with porous stone removed. The sample trimming apparatus and the membrane stretcher have already been described by Geonor (1968). The trimming apparatus was designed for use with soft clay samples and, as Figure 5.1 shows, only part of the apparatus was used here. Other equipment used were :

(a) a Wykeham Farrance manually operated hydraulic extruder (model 52286) for extruding 100 mm diameter samples;

(b) a Hobart mechanical mixer (model AE125) with a three speed gearbox and a device for adjusting the position of the mixing bowl in relation to the whip;

(c) a Wykeham Farrance loading bench with a weight hanger.

5.2.2 Triaxial samples with 38 mm diameter

The following equipment were used :

(a) A Perspex oedometer which comprised a tube (38 mm inner diameter); a bottom piston; a top piston and a bath.

(b) a Wykeham Farrance Bishop ram which consisted of a

piston, connected to a threaded piston rod, fitted inside a cylinder with 200 c.c. capacity. The piston was driven up and down in the cylinder by turning a handwheel. At the end of the cylinder were two valves, one connected to a water container and the other to a tubing;

(c) a Wykeham Farrance loading bench with a weight hanger.

5.2.3 Triaxial samples with 100 mm diameter

(a) a manually operated hydraulic extruder as described in Section 5.2.1;

(b) a Bishop ram as described in Section 5.2.2.

5.2.4 Shear box samples

A sample cutter (60 mm square in plan and 25 mm deep) and an extruder for pushing sample out of cutter.

5.3 NGI simple shear apparatus

5.3.1 General description

The NGI simple shear apparatus, model h-12, manufactured by Geonor was used in this study. A full description of the apparatus has been given by Geonor (1968). The principal components of the apparatus are (a) sample assembly; (b) vertical loading system; and (c) horizontal loading system. A diagram of the apparatus is shown in Figure 5.2 and each component will be briefly described.

(a) The sample assembly

The sample assembly consisted of a pedestal (1), the upper and lower filter holders (2) and a plastic container. A cylindrical soil

111

sample (3) 80 mm diameter and approximately 18 mm thick was held between two porous stones located in the filter holders. The porous stone had small steel pins 2.0 mm high projecting from their faces in a regular array. The pins were intended to ensure transmission of shear stresses across the top and bottom surfaces of the sample. The bottom filter holder was located on the pedestal which was firmly clamped to the base of the apparatus. The sample was surrounded by a reinforced rubber membrane (4) which was about 0.5 mm thick. For the standard reinforced membrane, the constantan wire used for reinforcement had a diameter of 0.15 mm, a Young's modulus of 152×10^3 MPa and a tensile strength of 570 MPa. The reinforcement winding was 20 turns for every 10 mm height. This standard reinforced membrane was used for all tests performed, tabulated in Tables 6.6 and 6.7, except for the tests with $\sigma_{vo}' = 776$ kPa where a stiffer reinforced membrane was used. For the stiffer reinforced membrane, iron nickel wire with a diameter of 0.20 mm was used as reinforcement and the winding was 30 turns for every 10 mm height. Drainage tubes were provided at the top and bottom filter holders for injecting water into the assembly.

(b) The vertical loading system

The vertical loading system consisted of the loading plate (5), the adjusting mechanism (6), the lever arm (7), the proving ring (8), the piston (9) which slid in a precision bearing (10), the dial gauge (11) and the sliding box (12). The lever arm had a ratio of 1 : 10 and could be locked for controlled movements upwards or downwards by means of the adjusting mechanism. The applied load on the hanger was transferred to the sample via the lever arm, the piston, the proving ring and the sliding box. The top half of the sliding box was rigidly attached to the piston and was constrained to move vertically. The dial gauge measured the displacement of the top of the box relative to the base of the apparatus.

(c) The horizontal loading system

The horizontal loading system consisted of the drive unit (13), the proving ring (14), the piston (15) which slid in a

112

precision bearing (16), the dial gauge (17) and the connection fork (18). A constant rate of displacement was provided by the drive unit and different speeds could be obtained by using different motors and gear ratios giving a speed range of 1.2×10^{-3} mm/min to 12 mm/min. The horizontal load was transmitted to the sample through the proving ring, the piston and the connection fork. The bottom half of the sliding box, and the top filter holder which was clamped to it, moved horizontally. The two halves of the sliding box were separated by bearings to prevent tilting of the filter holders. The dial gauge measured the relative displacement of the two halves of the sliding box.

(d) Logging , storage and analysis of test data

All test data were recorded manually during the tests. An Epson QX-10 microcomputer together with programs written in the Basic language were used for storing the data on floppy disks and for carrying out analyses.

5.3.2   Calibration and accuracy

The proving rings were calibrated for compression by dismounting them and applying weights on them by means of a hanger. The readings on the rings were recorded both during loading and unloading. Typical calibration curves obtained during loading of both proving rings are shown in Figure 5.3. When the vertical proving ring was dismounted, it had a reading greater than zero even under no load condition. When mounted this reading was counterbalanced by the self-weight of the piston, the sliding box and the top filter holder so that the ring read zero when no load was applied to the sample.

The accuracies of the measurements were affected by a number of factors. The magnitudes of the inaccuracies caused by each factor will be estimated.

The calibration constants for the proving rings were determined from the calibration curves obtained during loading. By

comparison with the data obtained during unloading, the maximum error that could arise from hysteresis was $\pm$ 2 kPa. The friction in the vertical loading system was measured by applying small loads to the loading plate until the lever arm started to move. It was found to have varying magnitudes along the travel of the piston with a maximum of 50 gm on the loading plate corresponding to 1 kPa on the sample. Friction between the sample and the membrane would cause different vertical stresses to be applied on the top and bottom surfaces of the sample. The difference was measured by Airey (1984) in his instrumented simple shear apparatus to be less than 1 kPa. The friction in the horizontal loading system was determined by moving the sliding box forwards and backwards manually. The maximum load recorded on the proving ring was 0.5 division corresponding to less than 1 kPa on the sample. The shear resistance of the reinforced membrane can be determined by shearing a water sample which has no shear strength. The curve of shear stress versus shear strain provided by Geonor shown in Figure 5.4 indicates that the shear resistance is less than 2 kPa for shear strains up to 30 % . To prepare a water sample, the drainage openings at the top and bottom filter holders were sealed with araldite and rubber O-rings were used to grip the reinforced membrane against the filter holders. This method of confining the water allowed a vertical stress of only 6 kPa to be applied without too much leakage. At such stress, the shear resistances of the standard reinforced membrane and the stiffer reinforced membrane were within 2 kPa and 3 kPa respectively.

Volumetric strains were calculated by assuming that the horizontal cross-sectional area of the sample remained constant throughout the test, therefore, deformations of the reinforced membrane due to changes in radial stress would lead to errors. A calculation in Appendix C shows that the maximum error in volumetric strain that could result from changes in radial stress in any of the tests performed is estimated to be $\pm$ 0.07 % . Because the dial gauge measuring vertical displacements was situated on top of the sliding box, compliances of the sliding box, filter holders, porous stones and pedestal would affect the readings. A steel dummy sample was placed between the filter holders and the variation of vertical stress against displacement recorded on the

dial gauge was obtained (Figure 5.5). The porous stones were taken out because of the pins on their surfaces. Corrections have been applied to all vertical dial gauge readings. Assuming that the volume of the sample was increased by the volume of the pins, the initial height of the sample was increased by approximately 0.05 mm. This would have changed the volumetric strains by less than 0.01 % . The effect of the pins on the measurement of shear strain and the problem of slips which occurred in some of the tests performed are considered in Appendix D. No correction for either of these effects was applied.

A summary of the estimated maximum values for all inaccuracies described is given in Table 5.1.

5.4   Stress path testing equipment for samples with 38 mm diameter

5.4.1   General description

Microcomputer controlled stress path testing equipment developed at the City University, called the Spectra system, was used. The developments in microcomputer controlled stress path testing equipment have been described by Atkinson et al (1985b). An introduction to the Spectra system and detailed instructions for operating the equipment were given in the operating manual (Atkinson et al, 1983). Only a brief description of the system will be given here.

The Spectra system consists of six Bishop and Wesley hydraulic stress path cells connected to a single central microcomputer which provided automatic control and data logging. Two of the cells, cells no. 2 and 4, have been used in the course of this study. The major components of the system can be listed as

(a) the Bishop and Wesley hydraulic stress path cell;

(b) instrumentation for measuring stresses and strains;

(c) pressure and axial strain control;

(d) microcomputer hardware and software.

A diagram of the system is shown in Figure 5.6 and each component will be briefly described.

(a)   The Bishop and Wesley hydraulic stress path cell

The Bishop and Wesley hydraulic stress path cell has been described in detail by Wesley (1975) and Bishop and Wesley (1975). Both cells no. 2 and 4 of the Spectra system have been slightly modified.   The bodies have been enlarged to 200 mm diameter and the arrangement of the drainage connections have been redesigned.   Drainage was provided only from the bottom of the sample.   Figure 5.7   shows one of the cells used.

(b)   Instrumentation for measuring stresses and strains

The instruments attached to the cell recorded the axial force F_a , the radial stress σ_r , the pore pressure u , the change of sample length δL and the change of sample volume δV .   The arrangement of the instruments can also be seen in Figure 5.7.

All the instruments were of resistive type, measuring the distortions of resistors in a Wheatstone bridge.   An axial force was measured by an Imperial College load cell with a capacity of 4.4 kN.   Both cell and pore pressures were recorded using Druck pressure transducers with a range of 0-1000 kPa.   Axial displacements were measured both by a dial gauge and a MPE displacement transducer with 25 mm travel. Volume changes were recorded by an Imperial College volume gauge with 50 c.c. capacity.

(c)   Pressure and axial strain control

The pressures required by the six cells were supplied by a mains pressure generated in a Motivair air compressor.   The air from the compressor was cleaned and dried and passed through a Compair

air pressure regulator (model M) which allowed a maximum of 750 kPa to be supplied to the equipment. This regulator also ensured that the supply was smooth, unaffected by the varying output of the compressor. The air supply was then passed to the cells.

At each cell, each of the cell pressure, back pressure and pressure in the bottom pressure chamber was regulated by a Fairchild air pressure regulator (model 10). Each regulator was driven by a motor via a reduction gearbox. The motors were controlled by the central microcomputer and were AC motors capable of rotating in both clockwise and anticlockwise directions. The gearboxes had a ratio which allowed a maximum rate of change of stress of about 60 kPa/hr to be achieved with the motor running continuously. Pressures in the cell fluid and bottom pressure chamber fluid were generated from the air pressures using air-water interfaces.

When axial strain control was required, the bottom pressure chamber of the Bishop and Wesley cell was disconnected from pressure control but remained connected only to the Bishop ram by closing valve A (Figure 5.6). This allowed a fixed volume of incompressible fluid to be displaced to or from the Bishop ram. The Bishop ram was driven by a motor via a gearbox. The motor was controlled by the microcomputer and was the same as those for pressure control. The gearbox had a ratio which gave a maximum strain rate of about 2 % per hr .

(d) Microcomputer hardware and software

The microcomputer which controlled and monitored the six cells was an Intercole Spectra xb microcomputer with 32 K memory. Its peripherals included a keyboard, a visual display unit (VDU) and a cartridge tape drive. The VDU and keyboard were used as control console and the cartridge tape drive held the control program 'SPCTRA' and the systems programs for operating the peripherals.

The microcomputer was interfaced to the outputs from the transducers by a set of 48 analogue input channels. Each cell

was allocated six of these channels for the load cell, pore pressure and cell pressure transducers, axial displacement transducer and volume gauge leaving one spare channel. The channels were scanned at 10 s intervals and the analogue signals amplified and converted to 15-bit digital signals. The resolutions of the analogue to digital conversions were therefore $1/(2^{15})$ i.e. 1/32,768 of the full ranges of the analogue input channels. The digital signals were then converted to stresses and strains through suitable calibration constants. The resolutions of the measurements in terms of stresses and strains are given in Table 5.2. Every hour the current values of stresses and strains were recorded. The microcomputer was interfaced to the pressure and axial strain control by a set of 48 data output relay channels. Seven of these channels were allocated to each cell for controlling the motors.

The microcomputer was linked to another system, the Epson system, comprising a QX-10 microcomputer with 192 K memory, a keyboard, a VDU, two disc drives and a printer. The QX-10 microcomputer was loaded with a constantly running program 'LINK' which opened files to store the hourly readings. Each day the data stored were printed and at the end of a test the data were dumped to floppy disc for permanent storage. The program 'LINK' could be interrupted in order to use the QX-10 microcomputer for data analyses.

The control program 'SPCTRA' was written in BASIC and the main feed-back control loop of the program is shown in Figure 5.8. This loop was run continuously but could be interrupted to perform various operations.

At the beginning of a test stage the stress path was set by specifying the starting state, rate of loading, finishing state and limit of control. The limit of control represented the maximum deviation from the specified values allowed.

The stresses and strains were computed as

$$\varepsilon_{ao} = - \delta L/L_o \qquad\qquad (5.1)$$

118

$$\epsilon_{vo} = - \delta V/V_o \qquad\qquad (5.2)$$

$$\epsilon_{ro} = \tfrac{1}{2}(\epsilon_{vo} - \epsilon_{ao}) \qquad\qquad (5.3)$$

where L_o and V_o were the initial length and volume respectively when the strains were set to zero. Pore pressure u and radial stress σ_r were computed from the readings of the transducers and the axial stress was computed as

$$\sigma_a = F_a/A + \sigma_r \qquad\qquad (5.4)$$

where F_a was the axial force measured by the load cell and by assuming that the sample remained a right cylinder as it deformed and the current area A was calculated as

$$A = A_o \left(\frac{1 - \epsilon_v}{1 - \epsilon_a} \right) \qquad\qquad (5.5)$$

where A_o is the initial area. Corrections for the stiffness of the rubber membrane and the side drains were not included in the program.

5.4.2   Calibration and accuracy

Each instrument was calibrated by applying known displacements, loads or pressures to the device and the stresses or strains displayed at the console were compared with the applied stresses or strains.   Adjustments to the calibration constants could be calculated by

$$\begin{pmatrix} \text{Revised} \\ \text{constant} \end{pmatrix} = \begin{pmatrix} \text{Existing} \\ \text{constant} \end{pmatrix} \begin{pmatrix} \dfrac{\text{applied value}}{\text{displayed value}} \end{pmatrix} \qquad (5.6)$$

The load cell was calibrated for compressive stresses by inverting the cell and placing weights directly on top of it. For tensile stresses, weights were applied via a hanger attached to the load cell.

The pore pressure and cell pressure transducers were calibrated using a Druck digital pressure indicator (model DPI101) connected to a Bishop ram as shown in Figure 5.9. Valves D and E were for de-airing the system. Pressures were applied to the transducers by turning the Bishop ram with valves B and C open and valves A, D and E closed. The applied pressures were displayed by the indicator to an accuracy of $\pm$ 0.04 % . The indicator itself was calibrated by a Budenberg dead weight calibrator which could apply pressures to within $\pm$ 0.03 % of the stated values. The pressure transducers were mounted at the same level as the indicator to eliminate any difference in pressure due to difference in elevation.

The axial displacement transducer was calibrated by mounting the transducer and a micrometer on a block as shown in Figure 5.10. Displacements were applied by turning the barrel of the micrometer and noting the readings on the vernier.

The volume gauge was calibrated by connecting it to the Bishop ram. Water was displaced in and out of the volume gauge by turning the handwheel of the Bishop ram and noting the exact number of turns. The inner diameter of the cylinder of the Bishop ram was 38.0 mm and the pitch of the threads was 0.98 mm giving the volume of water per turn as 1.11 c.c.

Factors which affected the accuracies of the instruments were hysteresis, drift and noise. The errors due to hysteresis were obtained from the calibration curves. Drift arose from changes of gauge resistance under constant stress or strain conditions. Noise was any signal which was transmitted in addition to the instrument output and was caused by magnetic fields generated by other devices in the surroundings. Inaccuracies due to drift and noise were checked by observing the variation of readings when constant stresses or strains were applied. Inaccuracies due to temperature changes were eliminated by keeping the temperature of the laboratory constant. A summary of typical values of inaccuracies for each instrument is given in Table 5.3.

As shown in Equation (5.4) the axial stress σ_a was calculated as the sum of the cell pressure σ_r and the deviator stress $\sigma_a-\sigma_r$. It was, therefore, subject to inaccuracies related to both stresses resulting in worst errors of $\pm$ 6 kPa.

Hysteresis of the volume gauge was found to be of the order of 0.1 % . However, the calibration curves for both compression and swelling were linear and had the same slope so that it was possible to eliminate the effect of hysteresis by adopting the test procedure described in Section 5.11.2.

Further inaccuracies arose from the flexibilities of various parts of the testing apparatus. The design of the load cell was based on relating the applied deviator stress to a small deformation of the load cell measured by strain gauges. Therefore, a component of the axial strain measured by the axial displacement transducer was due to the compression of the load cell. To measure this compressibility, a steel dummy sample was set up like a real sample and was loaded in both compression and extension. The variation of deviator stress with axial strain was obtained and corrections were applied to the test results. Since a constant back pressure was applied in all tests the compressibility of the volume gauge did not cause any inaccuracies.

For those tests which involved crossing the isotropic axis, a sudden jump in the axial strain measurement could occur as the strain gauges in the load cell moved from compression to extension. Such jumps could be identified in the test results and corrected accordingly. Any leakage in the drainage system would have resulted in errors in volumetric strains. Checks were carried out by sealing the openings of the drainage paths at the pedestal. Leakage through any of the drainage connections would then be registered as volume change.

Errors would also have been introduced by the non-uniform straining of the samples. As the top and bottom platens were not perfectly smooth, shear stresses developed along these boundaries prevented the sample from maintaining the shape of a

right cylinder when deforming. There was no simple method for estimating the errors involved.

In general, the accuracy of the system was acceptable for stress path testing and the summary of inaccuracies given in Table 5.3 gives a reasonable estimate of the limits of accuracy of the measurements obtained.

5.5 Stress path testing equipment for samples with 100 mm diameter

5.5.1 General description

The microcomputer controlled stress path testing equipment for samples with 100 mm diameter was developed from the Spectra system described in Section 5.4. A detailed description of the equipment has been given by Clinton (1987). Unlike the Spectra system, these equipment used a single microcomputer for the control and logging of a single stress path cell. Therefore, the equipment was in the form of individual units each with the following major components :

(a) a hydraulic stress path cell;

(b) instrumentation for measuring stresses and strains;

(c) pressure and axial strain control;

(d) microcomputer hardware and software.

A diagram of the arrangement of the components is shown in Figure 5.11 and each component will be briefly described.

(a) The hydraulic stress path cell

The layout of the cell, shown diagrammatically in Figure 5.12, is very similar to the Bishop and Wesley stress path cell. The

upper part of the cell comprised an aluminium pressure vessel with an internal diameter of 275 mm and two round steel plates which formed the ends of the vessel. The top plate was held in position by three steel tie bars located inside the vessel. The load cell was mounted to the top plate by a screw threaded connection and the top platen of the sample was bolted to the load cell. The cell pressure transducer was attached to the bottom plate.

The pedestal with a diameter of 100 mm was mounted at the top of the loading ram which had a diameter of 97 mm. Bellofram rolling seals were used to retain the cell fluid and the ram travelled up and down a linear bearing. The base of the loading ram had a diameter of 140 mm so that the ratio of the area of the base of the ram to the area of the sample was 2 : 1. The bottom pressure chamber was sealed by a second rolling Bellofram. A cross-arm attached to the loading ram moved up and down in slots in the portion of the cell between the bearing housing and the bottom pressure chamber to deflect a dial gauge and the axial displacement transducer.

Two drainage passages from the pedestal were connected via separate tubes to two separate chambers attached to the bottom plate of the vessel. The pore pressure transducer was attached to one of the chambers and the other chamber was connected to the volume gauge by a tube.

(b) Instrumentation for measuring stresses and strains

The arrangement of the instruments has been shown in Figure 5.11. All instruments were of resistive type, based on changes of resistance of strain gauges arranged as a Wheatstone bridge. An axial force was measured by an Imperial College load cell with a capacity of 26.5 kN. Both cell and pore pressures were recorded by Druck pressure transducers with a range of 0-1000 kPa. Axial displacements were measured both by a dial gauge and a MPE displacement transducer with 50 mm travel. Volume changes were recorded by an Imperial College volume gauge with 100 c.c. capacity.

123

(c) Pressure and axial strain control

Pressures were supplied by a mains pressure generated in a Motivair air compressor. The air was cleaned and dried and passed through a Compair air pressure regulator (model M) which allowed a maximum of 800 kPa to be supplied to the equipment. Each of the cell pressure, back pressure and pressure in the bottom pressure chamber was regulated by a John Watson and Smith electromanostat (model EMC) controlled by the microcomputer. Each electromanostat consisted of an air pressure regulator driven by a stepper motor via a reduction gearbox. The stepper motors were 12 V DC motors with a step angle of 7.5° . Each step corresponded to a pressure change of 0.4 kPa. The gearboxes had a ratio of 60 : 1 . Pressures in the cell fluid and bottom pressure chamber fluid were generated from the air pressures using air-water interfaces.

When axial strain control was required, the bottom pressure chamber was disconnected from pressure control but remained connected only to the Bishop ram by closing valve A (Figure 5.11). This resulted in a fixed volume of incompressible fluid displaced to or from the Bishop ram which was driven by a stepper motor via a gearbox. The stepper motor was controlled by the microcomputer and was the same as those for pressure control. The gearbox had a ratio of 125 : 1 .

(d) Microcomputer hardware and software

The microcomputer which performed the feed-back control and data logging was an Acorn BBC microcomputer (model B+) with a 64 K ram. Its peripherals included a keyboard, a VDU, a disc drive and a printer.

The microcomputer was interfaced to the pressure and axial strain control and to the outputs from the transducers by an Intercole Spectra Micro-ms interface unit. Digital commands from the microcomputer for pressure and axial strain control were sent down an RS423 serial bus to the interface unit. The unit converted these commands into analogue signals and passed them to an Intercole relay box (model CM62). The signals operated the relays

to generate pulses which were sent to the stepper motors causing them to turn in the required directions for the required number of steps.

Analogue outputs from the transducers were transmitted to input channels of the interface unit. The analogue signals were then converted to digital signals with 11 bits. Hence, the resolutions of the conversions were $1/(2^{11})$ i.e. $1/(2048)$ of the full ranges of the channels. The resolutions of the measurements from each instrument in terms of stresses and strains are given in Table 5.4. The digital signals were then passed to the microcomputer via the RS423 bus.

The control program 'TRIAX.+' has been fully described in the user manual (Clinton, 1986). The main control loop was run continuously but could be interrupted to perform various operations. At the beginning of a test stage the stress path was set by specifying the starting state, rate of loading and finishing state. The intervals at which the transducers were scanned and the intervals at which readings from the transducers were recorded were also specified by the operator. The stresses and strains were computed as given by Equations (5.1) to (5.5).

5.5.2   Calibration and accuracy

Except for the method used for calibrating the load cell in compression, the methods used for calibrating the instruments were the same as those used for the Spectra system described in Section 5.4.2.

The calibration of the load cell for compressive deviator stresses was divided into two parts. For stresses below 100 kPa, the load cell was inverted and weights were placed directly on top of it. For stresses above 100 kPa, an oedometer frame made by Wykeham Farrance (model 2400) was used. The load cell was removed from the top plate and placed inverted on the platform where an oedometer sample would usually be placed. Weights applied to the hanger were transferred to the load cell via the lever arm which had a ratio of 1 : 11.2 .

125

Sources of inaccuracies were the same as those which affected the Spectra system described in Section 5.4.2. A summary of typical values of inaccuracies for each instrument is given in Table 5.4. The inaccuracy of axial stress σ_a measurements was the sum of the inaccuracies of the radial stress σ_r and deviator stress $\sigma_a-\sigma_r$ and was therefore $\pm$ 3.7 kPa.

The compressibility of the load cell was measured by setting up a steel sample in the stress path cell and loading it in compression and extension. At the beginning of a test stage, the compressibility was input as test data and the control program automatically corrected the axial strain measurements. Different ranges of deviator stress gave rise to different values of compressibility so that it was necessary to adjust the value used as testing progressed. The flexibility of the volume gauge was obtained by varying the back pressure and observing the volume change measured. This was also corrected by the control program during testing. Checks on leakage in the drainage system were carried out in the same way as for the Spectra system.

In general, the accuracy of the system was acceptable for stress path testing and the summary of inaccuracies given in Table 5.4 gives a reasonable estimate of the limits of accuracy of the measurements obtained.

5.6   Shear box apparatus

5.6.1   General description

A standard shear box was used by the author for testing samples BMB1 to BMB4 and all other tests, shown in Table 6.8, were performed by BRE using a standard shear box with automatic data logging. A detailed description of the standard shear box has been given by Head (1982). The standard shear boxes used, manufactured by Wykeham Farrance, accommodated samples 60 mm square in plan and were typical of that used for routine testing. The principal components of the apparatus

126

are (a) sample assembly; (b) vertical loading system; and (c) horizontal loading system.

(a) The sample assembly

The sample assembly consisted of a container, two halves of a split box, top and bottom platens, top and bottom porous stones and top and bottom perforated grid plates. The soil sample approximately 25 mm thick was held between the two grid plates which ensured transmission of shear stresses across the top and bottom surfaces of the sample. The two halves of the box could be temporarily fixed together by means of two clamping screws located at opposite corners of the box. The remaining two corners could be inserted with lifting screws for lifting the top half so as to separate the two halves of the box.

(b) The vertical loading system

The vertical loading system consisted of a loading yoke and weight hanger and a dial gauge. The dial gauge measured the displacement of the top platen relative to the steel frame which supported the apparatus.

(c) The horizontal loading system

The horizontal loading system consisted of a motor-gear unit, a screw jack, roller bearings, a dial gauge, a connection fork and a proving ring. The screw jack driven by the motor-gear unit pushed the container along the roller bearings at a constant rate of displacement. The lower half of the split box was constrained to move with the container. The horizontal load was transmitted to the proving ring via the sample, the upper half of the box and the connection fork. The point of contact between the connection fork and the proving ring was in line with the plane of separation of the two halves of the box. The deformation of the proving ring was calibrated to give the horizontal load and the dial gauge mounted on the container measured the relative displacement of the two halves of the box.

(d)   Storage and analysis of test data

An Epson Qx-10 microcomputer together with programs written in the Basic language were used for storing the data on floppy disks and for carrying out analyses.

5.6.2   Calibration and accuracy

The proving ring was calibrated for compression by dismounting it and applying weights on it by means of a hanger. The maximum error that could arise from hysteresis was $\pm$ 1 kPa . The dial gauges recorded to the nearest 0.01 mm so that for a sample 20 mm thick the limits of accuracy for volumetric strain and shear strain were both 0.05 % . For the automatic data logging system used by BRE, the accuracies of the measurements were estimated by Powell (1988) to be $\pm$ 0.2 kPa for shear stress and 0.01 mm for horizontal displacement.

5.7   Procedures for preparation of simple shear samples

All Cowden till and London clay samples were supplied by BRE in 100 mm diameter thin wall tubes taken from the test bed sites. The borehole numbers and depths of the tubes used for preparing undisturbed simple shear samples are given in Table 5.5. The procedures followed for preparing Cowden till and London clay samples are very similar, therefore, in Sections 5.7.2 and 5.7.4 only the procedures which are different to those for Cowden till samples will be mentioned.

5.7.1   Undisturbed Cowden till

Due to difficulty in extruding the soil from the sample tubes, for the preparation of each sample, a 40 mm length of the sample tube containing the soil was sawn off with a power driven hack-saw. The sawn-off section was held by a lathe and the annulus of steel was sawn off with a hand operated hack-saw.

128

The short length of clay was transferred onto the pedestal of the Geonor sample trimming apparatus. The sharp-edged steel former was placed on top of the sample and the yoke of the trimming apparatus lowered to press against the former. By pushing the yoke down, the sharp edge of the former was driven into the sample and a knife was used to cut away the material which had been pushed aside. Any particles which hindered the advance of the former were removed and replaced by pressing in small lumps of the clay. This process of pushing the yoke down followed by trimming the edges of the sample was repeated until the full height of the former was filled with soil.

One end of the sample was trimmed square using a knife and a spatula and the Perspex disc was pushed into the former from this end. The other end of the sample was then also trimmed square producing a sample of 18 mm height. Any sand or gravel sized particles on the horizontal surfaces of the sample which might prevent the pins from proper penetration were removed and replaced by the clay. The sample was weighed and the water content of the trimmings determined.

5.7.2   Undisturbed London clay (brown and blue)

No difficulty was encountered in extruding the soil from the sample tubes so that a 40 mm length of the clay was extruded using the hydraulic extruder. The extruded length of clay was then cut off with a knife.

5.7.3   Remoulded Cowden till

Material from the sample tube was soaked in water for a few days to allow it to soften. The material was transferred to the mechanical mixer where any remaining aggregations were broken up. The speed of mixing and the distance between the bowl and the whip were monitored to avoid crushing of the particles. The material was then wet-sieved on a 2 mm sieve, air-dried, and gently broken up into a powder with a mortar and a pestle.

129

About 200 gm of the powder was placed in an evaporating dish and dried in the oven at 105°C . De-aired distilled water weighing 25 % of the weight of the dried powder was added onto the dish and mixed with the powder using spatulas. The amount of water added was chosen on the basis that it should provide the mixture with a convenient moulding consistency. Mixing was carefully confined within the evaporating dish so that no loss of the intended amounts of soil and water could occur during mixing. The mixture was then kneaded into a homogeneous mass and packed into the steel former with the Perspex disc inside the former. Care was taken to avoid inclusion of air. The ends of the sample were levelled off to give a sample of 18 mm height.

5.7.4   Remoulded London clay (brown and blue)

Neither breaking up aggregations of soil with a mechanical mixer nor wet-sieving was necessary with this material. Water weighing 40 % of the weight of the dried powder was added.

5.7.5   Reconstituted Cowden till

A powder prepared in the same way as that for the remoulded samples was mixed with de-aired distilled water in a mixing bowl to form a slurry. The weights of powder and water used were 260 gm and 150 gm respectively providing the slurry with a convenient viscosity for pouring. Care was taken not to trap air or lose any material during mixing.

The steel former was fitted onto the bottom filter holder with the porous stone in place to form an oedometer. The slurry was poured slowly from a scoop into the oedometer while continuously stirring to avoid trapping air. The surface of the slurry was levelled off flush with the edge of the former. A filter paper disc of 79 mm diameter was placed on top of the slurry and the porous stone was placed on top of the filter paper disc. The top filter holder was used as the top piston for the oedometer.

The oedometer was transferred to the loading bench and vertical

stresses were applied to the sample by means of the hanger and weights. The vertical stress was increased gradually over a few hours up to 16 kPa. The sample was then allowed to consolidate overnight to a thickness of about 20 mm. Figure 5.13 shows a sample under consolidation and Figure 5.14 shows a sample after consolidation ready for setting up.

5.8   Procedures for preparation of triaxial samples

All samples were taken from the BRE test bed site at Brent in tubes. The borehole numbers and depths of the tubes used for preparing undisturbed triaxial samples are given in Table 5.5.

5.8.1   Reconstituted London clay (blue) with 38 mm diameter

Material from the sample tube was air dried and then gently broken up into a powder with a mortar and a pestle. The powder weighing 190 gm was mixed with 210 gm of de-aired distilled water in a mixing bowl to form a slurry. This ratio of soil and water was chosen by trial and error to give a viscosity convenient for handling.

The Perspex tube and the bottom piston with a filter paper disc on top of it were placed in position in the bath to form an oedometer. The slurry was poured from a scoop into the oedometer slowly and continuously to avoid trapping air. It was found that 240 gm of the slurry would provide a sample of about 76 mm height after consolidation. A filter paper disc was placed on top of the slurry and the top piston was placed on top of the filter paper disc.

The oedometer was transferred to the loading bench and vertical stresses were applied to the sample by means of the hanger and weights. The vertical stress was increased gradually over a few hours up to 52 kPa. The tube was then lifted in relation to the bottom piston in order to have the same stresses acting on the top and bottom halves of the sample. The sample was allowed to consolidate overnight and a sample under consolidation is shown in Figure 5.15.

131

5.8.2   Undisturbed London clay (brown and blue) with 100 mm diameter

A 250 mm length of the clay was extruded from the sample tube using the hydraulic extruder.   The extruded clay was cut off with a knife and placed on a cradle.   The length of the sample was gradually trimmed down to about 200 mm using the knife and the ends were made even by pressing a straight edge firmly against the ends of the cradle and scraping material off the surfaces.   No trimming of the sides was necessary.   The length and diameter of the sample were measured by calipers and the weight of the sample recorded.   The water content of the trimmings was determined.

5.9   Procedures for preparation of shear box samples

All Cowden till and London clay samples were taken from the BRE test bed site in tubes.   The borehole numbers and depths of the tubes used for preparing undisturbed shear box samples are given in Table 5.5.

5.9.1   Undisturbed Cowden till

A length of the clay was extruded from the sample tube and cut off with a knife.   The sample cutter was driven into the clay and the material pushed aside was cut away.   Any particles which hindered the advance of the cutter were removed and replaced by pressing in small lumps of the clay.   After the cutter was filled with the soil, the ends of the sample were trimmed flat using a knife and a straight edge.   Any sand or gravel sized particles on the horizontal surfaces of the sample which might prevent the grid plates from gripping the soil were removed and replaced by the clay.   The sample was weighed and the water content of the trimmings determined.

5.9.2   Undisturbed London clay (brown)

Same as for undisturbed Cowden till described in Section 5.9.1.

132

5.9.3 Remoulded Cowden till

A powder of the material was prepared in the same manner as
described in Section 5.7.3. The powder was mixed with de-
aired distilled water using spatulas in a mixing bowl. The
cutter was placed on a flat glass plate and the soil kneaded
into the cutter while keeping the cutter firmly in contact with
the glass plate. Care was taken to avoid including any air.
The ends of the sample were trimmed level.

5.9.4 Remoulded London clay (brown)

A powder of the material was prepared in the same manner as
described in Section 5.7.4. About 200 gm of the powder was
placed in an evaporating dish and dried in the oven at
105°C . De-aired distilled water weighing 40 % of the weight
of the dried powder was added onto the dish and mixed with the
powder. The mixture was kneaded into the cutter and the ends of
the sample levelled off.

5.10 Procedures for simple shear tests

5.10.1 Setting up

The undisturbed and remoulded samples were extruded from the steel
former onto the bottom filter holder seated on top of the pedestal.
In the case of the reconstituted samples, this step was eliminated
because the samples were consolidated on top of the bottom filter
holder. The purpose was to avoid disturbing the reconstituted
samples which were much softer than the undisturbed and remoulded
samples.

The wire-reinforced part of the membrane was placed inside the
stretcher and the unreinforced rubber folded over the ends. A
vacuum was applied using a suction pump through the tubing of the
stretcher to stretch out the membrane which was then slid over the
sample. Before the suction was released it was checked that the

full height of the sample would be covered by reinforcement. The top filter holder, the drainage tubes and the plastic container were placed in position and the complete sample assembly was transferred to the shear apparatus.

In the case of the undisturbed samples, the pins were bedded into the sample by applying a vertical stress of 300 kPa on the sample and removing the stress as quickly as possible to avoid disturbance. Weights which gave the intended vertical stress for compression were left on the loading plate and water was injected through the drainage tubes to fill the sample assembly.

5.10.2   One-dimensional compression and consolidation

After setting up, vertical stresses were applied to the samples by applying weights on the loading plate. The samples were allowed to consolidate or swell until they reached equilibrium at these stresses. The sequence and the values of the vertical stresses applied on each sample are tabulated in Table 5.6.

Each vertical stress was applied suddenly and vertical dial gauge readings at elapsed time t after the application of the vertical stress were taken at t (min) = 1/4, 1/2, 1, 2, 4, 8, 16, 30, 60, ... etc. The only exception to this was when a vertical stress of 388 kPa was to be applied to a disturbed sample as the first stress in the sequence. In this case the vertical stress was raised by 4 equal increments of 97 kPa at approximately hourly intervals.

At each vertical stress the sample was left overnight for it to reach equilibrium. When the excess pore pressure had fully dissipated so that further changes in sample volume became negligible, the final vertical dial gauge reading was noted and the next vertical stress in the sequence applied.

5.10.3   Shearing

All samples of Cowden till and London clay were sheared at a

constant rate of horizontal displacement of 0.52 mm/hr corresponding to a shear strain rate of approximately 3 % per hr . Readings of the proving rings and dial gauges were taken at approximately 20 min intervals.

Two types of shearing were performed, constant σ_v' shearing and constant volume shearing. In both types of shearing, there were no provisions for drainage prevention and pore water pressure measurement. The samples were considered to have zero pore pressure all the time. Appendix E shows that the excess pore pressures in both Cowden till and London clay samples were acceptably small.

Before shearing started, the horizontal dial gauge was adjusted to zero, and any slack in the horizontal loading system was taken up manually until the horizontal proving ring just started to move. In the case of constant volume shearing, the loading plate was clamped to the adjusting mechanism while taking care to maintain the vertical stress at σ_{vo}' . After the clamping all weights were removed. Initial readings of the proving rings and dial gauges were taken and the drive unit was switched on.

During constant σ_v' shearing, the weights on the loading plate were left unchanged so that the effective vertical stress remained constant at σ_{vo}' throughout shearing.

During constant volume shearing, as the sample tended to compress or dilate the vertical stress on the sample was adjusted to keep the sample height constant. Assuming there was no excess pore pressure, at any time during shearing the applied vertical stress was also the effective vertical stress.

5.10.4   Post-shearing

At the end of each test the total vertical stress was reduced to 20 kPa and the sample left to swell for several hours. The vertical dial gauge reading was recorded just before the sample assembly was taken out. The sample was then removed from the membrane and its water content determined.

135

5.11   Procedures for stress path tests on samples with 38 mm diameter

5.11.1   Setting up

The Bishop and Wesley cell was half filled with water and the zero readings from the load cell and the pressure transducers were taken. The cell was emptied and the upper part of the cell removed again. The drainage passages of the cell base and the volume gauge were flushed with de-aired distilled water using the Bishop ram leaving a meniscus on the pedestal. A porous stone saturated with water was placed on the pedestal by sliding it across the meniscus to avoid trapping air. High vacuum grease was applied along the sides of the pedestal and the top cap. A filter paper disc was placed on the porous stone.

A dial gauge mounted on a holder was placed on the loading bench next to the Perspex oedometer. The gauge spindle was set to rest on the top cross-arm of the hanger and the gauge reading was noted. The tube containing the sample was transferred to the Bishop and Wesley cell where it was held over the cell base and the sample pushed out of the tube onto the filter paper disc on the pedestal.

A filter paper disc saturated with water was placed on the top of the sample and the top cap was placed in position. A filter paper side drain also saturated with water was wrapped round the sample overlapping the porous stone at the bottom end. A 'fish-net' type side drain described by Richardson (1988) was used for extension tests to minimise the effect of stiffness of the paper. A rubber membrane was placed inside a membrane stretcher with the ends folded over and a vacuum was applied by sucking through the mouthpiece to stretch out the membrane. The vacuum was sustained by pressing a finger over the mouthpiece while the membrane was slid over the sample slowly without touching it. The suction was released so that the membrane contracted on to the sample and the ends of the membrane were slipped off the stretcher. A good contact between the membrane and the greased parts of the pedestal and top cap was ensured by stroking the membrane. Two rubber O-rings were used to grip the membrane against the pedestal and

another two were used for gripping the membrane against the top cap. The suction cap was screwed onto the top cap and the cell was filled with water.

The cell pressure was increased so that the pore pressure became the same as the required back pressure. The back pressure was set at the required value. The Bishop ram was connected to the valve at the top of the pore pressure transducer chamber and both this valve and the drainage valve between the sample and the volume gauge were opened. By unwinding the handwheel of the Bishop ram water was drawn from the volume gauge, passed the base of the sample, through the pore pressure transducer chamber into the Bishop ram. The drawing of water was continued until no air bubbles came out of the de-airing valve. The valves were closed again and the Bishop ram disconnected.

In order to check that the value of Skempton's pore pressure parameter B was at least 0.98 the cell pressure was raised by 50 kPa and the pore pressure response observed. The cell pressure was then lowered so that the pore pressure became the required back pressure again. The Bishop ram was connected to the valve at the top of the cell, and the ram pressure was increased to bring the suction cap upwards slowly towards the load cell. With the suction cap fitted over the load cell the valve at the top of the cell was opened and water between the top cap and the load cell was drawn out. Care was taken to keep the deviator stress at zero all the time. The Bishop ram was disconnected and the valve left opened.

A dummy Perspex sample was set up in the oedometer in the same way the soil sample was. The reading of the dial gauge above the hanger was noted and the height of the soil sample was calculated from the height of the dummy sample and the dial gauge readings.

Zero readings for the strains were taken from the displacement transducers. The required test data were entered at the console and the test stage started. As soon as the pressures were under control by the microcomputer the drainage valve was opened.

137

5.11.2   One-dimensional compression

The sample was compressed from its initial isotropic stress state to $p' = 107$ kPa and $q' = 51$ kPa which was close to a K_o stress state. A linear stress path was followed using stress control at 2 kPa/hr . At the end of the stress path the test stage was ended. A new test stage was started to compress the sample under K_o condition by controlling the axial stress to increase at 3 kPa/hr and at the same time controlling the radial strain to remain constant. On completion of the stress path the stresses were automatically held constant and any excess pore pressure was allowed to dissipate fully before the test stage was ended.

For tests which required K_o swelling, the drainage valve between the sample and the volume gauge was closed and approximately 3 c.c. of water was released through the valve at the top of the volume gauge. This reversed the direction of movement of the Bellofram and the displacement transducer of the volume gauge, hence, eliminating any hysteresis effect. The drainage valve was re-opened. Zero readings of strains were taken from the displacement transducers and the current sample dimensions were entered as test data. A test stage was then started to swell the sample under K_o condition by controlling the axial stress to reduce at 3 kPa/hr while keeping the radial strain at zero. The test stage was ended when the required value of R_p was reached. A new test stage was started to hold the axial stress constant and the radial strain at zero and any excess pore pressure was allowed to dissipate fully before ending the test stage.

5.11.3   Shearing

The drainage valve between the sample and the volume gauge was closed. Zero readings for strains were taken and current sample dimensions were entered as test data. For compression tests, the axial stress was controlled to increase at 5 kPa/hr , and for extension tests, the axial stress was controlled to decrease at 5 kPa/hr . In both cases, the radial stress was kept constant.

138

When the rate of change of axial strain reached 0.5 % per hr in the compression tests and -0.5 % per hr in the extension tests, loading was changed from stress control to axial strain control. Strain rates of 0.5 % per hr and -0.5 % per hr were used for compression and extension tests respectively.

5.11.4   Post-shearing

At the end of each test the top cap was disconnected from the load cell and the cell pressure was reduced to zero. The sample was removed from the membrane and its water content determined. It was checked that the load cell and pressure transducers were all giving zero readings.

5.12   Procedures for stress path tests on samples with 100 mm diameter

5.12.1   Setting up

Zero readings for the load cell and the pressure transducers were taken. The drainage passages of the cell base and the volume gauge were flushed with de-aired distilled water using the Bishop ram leaving a meniscus on the pedestal. A porous stone saturated with water was placed on the pedestal by sliding it across the meniscus. High vacuum grease was applied along the sides of the pedestal and the top cap. A filter paper disc was placed on the porous stone.

The sample was placed on the pedestal and a filter paper disc saturated with water was placed on the top face of the sample. The top cap was placed in position and a filter paper side drain saturated with water was wrapped round the sample overlapping the porous stone at the bottom end. A 'fish-net' type side drain was used for extension tests. A rubber membrane was placed inside a membrane stretcher with the ends folded over and a vacuum was applied through the opening by a suction pump to stretch out the membrane. The vacuum was sustained by pressing a finger over the opening while the membrane was slid over the sample

slowly without touching it. The suction was released and the ends of the membrane were slipped off the stretcher. Two rubber O-rings were used to grip the membrane against the pedestal and another two were used for gripping the membrane against the top cap. The positions of the loading ram and the load cell were adjusted to connect the top cap and the load cell. The pressure vessel was placed in position and filled with water.

Both radial stress and axial stress were adjusted to 30 kPa. Zero readings for the strains were taken from the displacement transducers. A test stage was started to increase the total stresses isotropically from 30 kPa to 300 kPa with the drainage valve between the sample and the volume gauge remaining closed.

5.12.2   Pre-shearing and pre-probing

The sample was left at the isotropic total stress of 300 kPa overnight for the pore pressures to reach equilibrium. The test stage was stopped and the back pressure set to the same value as the pore pressure. The base of the sample, the drainage passages and the pore pressure transducer chamber were flushed using the same procedures as described in Section 5.11.1. The pore pressure parameter B was measured by carrying out a test stage to increase the total stresses isotropically by 50 kPa and observing the change in pore pressure. The sample was left for air to dissolve and the value of B checked every 2 to 3 days until a value of at least 0.98 was obtained.

A test stage was then performed to change the total stresses isotropically so that the pore pressure became the required back pressure which was kept constant throughout each test. The drainage valve between the sample and the volume gauge was opened.

For shearing tests TUL1 to TUL4, linear stress paths illustrated in Figure 5.16 were followed. At A, B, C and D the stresses were automatically held constant and any excess pore pressures were allowed to dissipate fully.

For stress probing tests TUB1 and TUL5, the samples were swelled isotropically at 2 kPa/hr to isotropic states with values of p' equal to 125 kPa and 200 kPa respectively.

5.12.3 Shearing and stress probing

Zero readings for strains were taken and current sample dimensions were entered as test data for the next stage.

For undrained shearing, the drainage valve was closed. For loading in compression, the axial stress was controlled to increase at 3 kPa/hr and for loading in extension, the axial stress was controlled to decrease at 2 kPa/hr . In both cases, the radial stress was kept constant. When the rate of change of axial strain reached 0.1 % per hr in compression tests and -0.1 % per hr in extension tests, loading was changed from stress control to axial strain control. Strain rates of 0.1 % per hr and -0.1 % per hr were used for compression and extension tests respectively.

For stress probing test TUB1, the drainage valve was left open. A test stage was started with the specified effective stress path A'B' and specified rate of loading along A'B' as shown in Figure 5.17. At the end of loading, the stresses were automatically held constant to allow any excess pore pressures to dissipate fully. The test stage was ended and the same procedure was repeated for the specified stress path B'C' and so on.

For stress probing test TUL5, the drainage valve was closed. A test stage was started with the specified total stress path AB and specified rate of loading along AB as shown in Figure 5.18(a). At the end of the stress path, with the total stress state at B , the stresses were automatically held constant to allow the pore pressures to reach equilibrium. The test stage was ended and the same procedure followed for the total stress path BC. After the pore pressures reached equilibrium at total stress state C , the corresponding effective stress state was C' . The drainage valve was then opened and a test

141

stage started with the specified effective stress path C'D' and specified rate of loading along C'D' as shown in Figure 5.18(a). At the end of loading, the stresses were automatically held constant and any excess pore pressures were allowed to dissipate before the test stage was ended. The same procedure was repeated for the specified stress path D'E' and so on until stress path R'S' , shown in Figure 5.18(b), which was the last stress path specified for stress probing. The stress state S' represented the end of stress probing.

5.12.4   Post-testing

For the shearing tests and stress probing test TUB1, the drainage valve and the valve to the bottom pressure chamber were closed. The cell pressure was reduced to zero and the water in the pressure vessel was emptied. The top cap was disconnected from the load cell and the sample was removed from the membrane to have its water content determined. It was then checked that the load cell and the pressure transducers were all giving zero readings.

For stress probing test TUL5, the sample was unloaded using two test stages with the specified effective stress paths S'A' and A'T' as shown in Figure 5.18(b). The same procedures as those for the shearing tests and test TUB1 were then followed.

5.13   Procedures for shear box tests

5.13.1   Setting up

The two halves of the split box were fixed together by the clamping screws and placed in position in the container. The bottom platen followed by the bottom porous stone and the bottom grid plate were placed in position. The sample was pushed from the cutter into the box using the extruder. The top grid plate followed by the top porous stone and the top platen were

placed on top of the sample. The grid plates were placed such that the serrations were at right-angles to the direction of shear.

The loading yoke was set on top of the top platen. The dial gauge was fixed in position and the reading noted. Weights which gave the intended vertical stress for compression were placed on the hanger. Water was poured into the space between the container and the box.

5.13.2   One-dimensional compression

The weights were left on the hanger for the stresses in the sample to reach equilibrium. When changes in the vertical dial gauge readings became negligible the final reading was recorded.

5.13.3   Shearing

Any slack in the horizontal loading system was taken up by moving the screw jack towards the container manually. The two clamping screws were removed and the lifting screws inserted until they just came into contact with the lower half of the box. The lifting screws were then rotated together for a further half-turn to raise the top half of the box relative to the bottom half. The horizontal dial gauge was fixed in position and initial readings of the dial gauges were taken. The motor-gear unit was switched on and all samples of Cowden till and London clay were sheared at a constant rate of horizontal displacement of 0.59 mm/hr . The weights on the hanger were left unchanged so that the effective vertical stress remained constant at σ_{vo}' throughout shearing.

5.13.4   Post-shearing

The vertical stress was removed and the split box with the sample in it was taken out of the container as quickly as possible. The sample was removed from the box and its water content determined.

CHAPTER 6   TEST RESULTS

6.1   Introduction

This chapter presents the results obtained from the simple shear tests, shear box tests and stress path tests. Data obtained during one-dimensional compression are shown to an extent which will allow normal compression lines and swelling lines and the specific volumes before shearing to be determined. The data for shearing will allow the stress state and specific volume at any point during shearing to be calculated. No analysis of the results will be given in this chapter.

6.2   Classification tests

Results of the measurement of unit weight γ , water content w , plastic limit PL , liquid limit LL , plasticity index PI , clay fraction, activity A and specific gravity G_s are shown in Table 6.1. Each value of unit weight is obtained by taking the average of the unit weights of all undisturbed simple shear samples and each value of water content is obtained by taking the average of the water contents of the trimmings of all undisturbed simple shear samples. Results of the particle size distribution tests are shown in Figures 6.1(a) and (b).

6.3   One-dimensional compression

Results of one-dimensional compression and swelling obtained from the simple shear tests, shear box tests and stress path tests will be given in this section. For the simple shear and shear box data which are plotted on $\ln \sigma_v'$, v plane, all points correspond to states of compression which had reached equilibrium with zero excess pore pressure. For the triaxial data, however, the data points plotted on $\ln p'$, v plane represent the relationship between specific volume and the

observed effective stress $p - u_o$. The changes in specific volume, at the end of the constant stress rate loadings, due to dissipation of excess pore pressures $\bar{u}$ are also shown.

6.3.1 Cowden till

The results for remoulded, reconstituted and undisturbed simple shear samples are given in Figures 6.2(a) to (c). For samples MC1 to MC8 and CC1 to CC8 the specific volumes at $\sigma_v' = 388$ kPa and at σ_{vo}' before shearing are shown. For samples MC9, MC10 and CC9 states obtained during normal compression are shown and for sample CC10 states obtained during normal compression and then swelling are shown. For samples UC1 to UC12 specific volumes at σ_{vo}' before shearing are plotted. For samples UC9 and UC10 states obtained at stresses lower than σ_{vo}' are also shown.

The results for remoulded and undisturbed shear box samples are given in Figures 6.3(a) and (b). All data points are states of the samples before shearing.

6.3.2 London clay (brown)

The results for remoulded and undisturbed simple shear samples are given in Figures 6.4(a) and (b). For samples MB1 to MB8 the specific volumes at $\sigma_v' = 388$ kPa and at σ_{vo}' are shown. For sample MB9 states obtained during normal compression are shown and for sample MB10 states obtained during normal compression and then swelling are shown. For samples UB1 to UB10 states at σ_{vo}' are shown and for samples UB1, UB2, UB3, UB5, UB6, UB9 and UB10 states obtained at stresses lower than σ_{vo}' are also shown.

The results for remoulded and undisturbed shear box samples are given in Figures 6.5(a) and (b). For the undisturbed samples the data points represent states at σ_{vo}'.

6.3.3.   London clay (blue)

The results for remoulded and undisturbed simple shear samples are given in Figures 6.6(a) and (b). For samples ML1 to ML8 the specific volumes at σ_v' = 388 kPa and at σ_{vo}' are shown and for samples ML9 and ML10 states obtained during normal compression are shown. For samples UL1 to UL10 states at σ_{vo}' are shown and for sample UL9 states obtained at stresses lower than σ_{vo}' are also shown.

The results for reconstituted triaxial samples are given in Figures 6.7(a) and (b).   In Figure 6.7(b), for the compression of each sample, at the end of loading both the state when loading has just stopped and the state when the excess pore pressures have dissipated fully are plotted.   For the swelling of each of samples TCL2 , TCL3 , TCL7 and TCL8 , at the end of unloading both the state when unloading has just stopped and the state when the excess pore pressures have dissipated fully are plotted.

6.3.4   Normal compression lines and swelling lines

For the results obtained from remoulded and reconstituted simple shear and shear box samples (Figures 6.2(a) and (b), 6.3(a), 6.4(a), 6.5(a) and 6.6(a)), curves which give the best fit of the data points have been drawn.   The straight portions of the curves joining the points obtained during normal compression are taken as normal compression lines.   Straight lines have been used as swelling lines.

On the plots of results for the undisturbed simple shear and shear box samples (Figures 6.2(c), 6.3(b), 6.4(b),   6.5(b) and 6.6(b)), the broken lines are the normal compression lines for remoulded samples of the same material tested in the same apparatus.   It is assumed that these broken lines are the normal compression lines of the undisturbed samples.   Straight lines which give the best fit of the data points have been drawn as swelling lines.

For the results from reconstituted triaxial samples

(Figure 6.7(b)), a curve which follows the pattern of the data points obtained during compression and gives the best fit of the points corresponding to zero excess pore pressure has been drawn. The linear portion of this curve is taken as the normal compression line. A straight line which follows the slope of the data points obtained during swelling and gives the best fit of the points corresponding to zero excess pore pressures has been drawn as the swelling line.

A summary of the values of the compression and swelling parameters obtained for the various materials in the various apparatus is shown in ⸱Table 6.2.

6.4   One-dimensional consolidation

Results of one-dimensional consolidation obtained from the simple shear apparatus will be given in this section. The values of the coefficient of volume compressibility m_v were calculated using Equation (2.88). The value of the coefficient of consolidation c_v were determined using the $\sqrt{}$(time) curve fitting method described in Section 2.5.2 and the values of the coefficient of permeability k were calculated using Equation (2.87).

6.4.1   Cowden till

The results for remoulded and undisturbed samples are given in Table 6.3. An example of the variation of the average degree of consolidation U_t with $\sqrt{}$(time) is given in Figure 6.8(a).

6.4.2   London clay (brown)

The results for remoulded and undisturbed samples are given in Table 6.4.

147

6.4.3   London clay (blue)

The results for remoulded and undisturbed samples are given in Table 6.5.   An example of the variation of U_t with $\sqrt{(time)}$ is given in Figure 6.8(b).

6.5   Simple shear tests

Summaries of the states before shearing and the type of shearing performed for each sample are given in Tables 6.6 and 6.7.   The values of the specific volume before shearing v_o were taken from the normal compression lines and swelling lines already described in Section 6.3.4.

6.5.1   Cowden till

Figures 6.9(a) to (g) show the basic data for the remoulded samples, Figures 6.10(a) to (g) show the basic data for the reconstituted samples and Figures 6.11(a) to (h) show the basic data for the undisturbed samples.

6.5.2   London clay (brown)

Figures 6.12(a) to (d) show the basic data for the remoulded samples and Figures 6.13(a) to (g) show the basic data for the undisturbed samples.

6.5.3   London clay (blue)

Figures 6.14(a) to (d) show the basic data for the remoulded samples and Figures 6.15(a) to (g) show the basic data for the undisturbed samples.

6.6   Shear box tests

A summary of the states before shearing for each sample is given in Table 6.8.   The values of the specific volume before shearing v_O were taken from the normal compression lines and swelling lines already described in Section 6.3.4.

In calculating the shear stresses τ_v' and normal stresses σ_v', the current areas of the sample between the two halves of the box were used.

6.6.1   Cowden till

Figure 6.16 shows the basic data for the undisturbed samples. Figure 6.16(a) shows the shear stress τ_v' against horizontal displacement d_h curves and Figure 6.16(b) shows the vertical displacement d_v against horizontal displacement d_h curves.

Figures 6.17(a) and (b) show the basic data for the remoulded samples.

6.6.2   London clay (brown)

Figures 6.18(a) to (h) show the basic data for the undisturbed samples and Figures 6.19(a) and (b) show the basic data for the remoulded samples.

6.7   Stress path tests on samples with 38mm diameter

6.7.1   London clay (blue)

A summary of the states before undrained shearing of the reconstituted samples and whether the sample was sheared in compression or extension is given in Table 6.9.   The values

of the specific volume before shearing v_o were taken from the normal compression line and swelling line described in Section 6.3.4.

Figures 6.20(a) to (e) show the basic data. The values of σ_r which remained constant throughout shearing are shown in Figures 6.20(a) and (c).

6.8   Stress path tests on samples with 100 mm diameter

6.8.1   London clay (brown and blue)

A summary of the states before undrained shearing of the undisturbed samples and whether the sample was sheared in compression or extension is given in Table 6.10. A summary of the states before probing of the undisturbed samples and whether the probe was drained or undrained is given in Table 6.11. In both Tables 6.10 and 6.11 the values of the specific volume before loading v_o were values back calculated from the water contents measured after testing as described in Section 5.12.4.

For the undrained shearing tests, the basic data are shown in Figures 6.21(a) to (e). Figures 6.21 (a) and (c) show the values of σ_r which remained constant throughout shearing.

For probing test TUB1, the basic data are shown in Figures 6.22(a) to (j) and Figure 6.24(a). A back pressure of 200 kPa was used throughout this test.

For probing test TUL5, the basic data are shown in Figures 6.23(a) to (j) and Figure 6.24(b). In Figure 6.23(a) the variation of u against ε_s for the undrained probe AC is also shown. A back pressure of 200 kPa was used for the drained probes A'E' to A'S'.

150

CHAPTER 7   ANALYSES AND DISCUSSIONS

7.1   Introduction

In this chapter the test results presented in Chapter 6
will be analysed using the basic theory outlined in Chapter 2.
The purpose is to advance the current state of knowledge on
soil behaviour under simple shear and triaxial loading.
Discussions will focus on one-dimensional compression, critical
states, state paths and stiffnesses.

7.2   Discussion on classification test results

7.2.1   Cowden till

The average unit weight of the undisturbed simple shear
samples given in Table 6.1 as 21.5 kN/m^3 is close to the
range of unit weights of 21.6 to 22.0 kN/m^3 obtained by
BRE described in Section 4.4.1. The average water content of
the undisturbed simple shear samples given in Table 6.1 as
14.9 % is within the range of water contents of 14 to 18 %
for the undisturbed triaxial samples tested by Gens and
Hight (1979) described in Section 3.5.1 and it is also close to
the water contents given by Marsland and Powell (1985) in
Figure 4.10. The plastic limit and liquid limit of 16 and
34 respectively given in Table 6.1 are very close to the
plastic and liquid limits of 16 and 32 obtained by Gens
and Hight shown in Figure 3.24(a). For the typical profile
obtained by BRE shown in Figure 4.10, at depths between 3
and 17 m the plastic limit varies between 11 and 20 and the
liquid limit varies between 33 and 38 and so the plastic
and liquid limits obtained in this study lie within these
ranges of values obtained by BRE. The clay fraction by weight
given in Table 6.1 as 33 % agrees with the value of 30 %
estimated by BRE in Section 4.4.1. A comparison of the
grading curves obtained by the author, by BRE and by Gens and
Hight is shown in Figure 7.1. The results obtained by the

author lie within the envelope for the BRE results.

It can be concluded that the classification test results for the samples used in this study are similar to those obtained by BRE and Gens and Hight. The unit weights and water contents indicated that the states of the undisturbed samples used in this study are similar to the others and the Atterberg limits and the grading curves suggested that the mineralogy of the clay and the particle size distribution of the samples used in this study are also similar to the others. The similarity exists because the samples used by the author, by BRE and by Gens and Hight were all from the same test bed site which has a uniform composition.

7.2.2   London clay (brown)

The average unit weight of the undisturbed simple shear samples given as 19.1 kN/m^3 in Table 6.1 lies within the range of unit weights of 18.6 to 19.6 kN/m^3 obtained by BRE described in Section 4.4.2 and it also lies within the range of 18.8 to 20.1 kN/m^3 for the various sites shown in Table 3.2. The average water content of the undisturbed simple shear samples given as 29.6 % in Table 6.1 is close to the values obtained by Powell and Uglow (1986) in Figure 4.12. The plastic limit of 32 given in Table 6.1 is just outside the range of plastic limits of 23 to 29 for the brown clay down to 9 m depth in the typical profile obtained by BRE shown in Figure 4.12. It is also just outside the range of 27 to 30 for the various sites shown in Table 3.2. The liquid limit of 72 given in Table 6.1 is within the range of 71 to 85 in Figure 4.12 and is also within the range of 63 to 95 in Table 3.2. The clay fraction by weight of 64 % given in Table 6.1 is within the range of 55 to 65 % obtained by BRE as described in Section 4.4.2 and is also within the range of 48 to 64 % for the various sites shown in Table 3.2.

It can be concluded that the results obtained in this study are similar to those obtained by BRE and that the grading and

mineralogy of the brown London clay at the BRE test bed site is typical of London clay which is essentially uniform everywhere.

7.2.3 London clay (blue)

The average unit weight of the undisturbed simple shear samples given as 19.7 kN/m^3 in Table 6.1 lies just outside the range of unit weights of 18.6 to 19.6 kN/m^3 obtained by BRE described in Section 4.4.2 and it lies within the range of 18.8 to 20.1 kN/m^3 for the various sites shown in Table 3.2. The average water content of the undisturbed simple shear samples given as 26.0 % in Table 6.1 is close to the values obtained by Powell and Uglow (1986) in Figure 4.12. The plastic limit of 26 given in Table 6.1 lies within the range of plastic limits of 22 to 29 for the blue clay between 9 m and 22 m depth in the typical profile obtained by BRE shown in Figure 4.12. Also, it lies just outside the range of 27 to 30 for the various sites shown in Table 3.2 . The liquid limit of 71 given in Table 6.1 is within the range of 65 to 77 in Figure 4.12 and is also within the range of 63 to 95 in Table 3.2. The clay fraction by weight of 59 % given in Table 6.1 is within the range of 55 to 65 % obtained by BRE as described in Section 4.4.2 and is also within the range of 48 to 64 % for the various sites shown in Table 3.2.

It can be concluded that the results obtained in this study are similar to those obtained by BRE and that the grading and mineralogy of the blue London clay at the BRE test bed site is also typical of London clay.

7.3 Discussion on one-dimensional compression

7.3.1 Cowden till

For the results of the remoulded and reconstituted samples,

shown in Figures 6.2(a) and (b) and 6.3(a), the curves which give the best fit of the data points give a close fit for all points. At any particular value of σ_v' the maximum deviation of the data points from the best fit curves is 0.016 in specific volume. Samples MC1 to MC10 which were all normally compressed to $\sigma_v' = 388$ kPa have a scatter in specific volume of between 1.460 and 1.491 at $\sigma_v' = 388$ kPa. Samples CC1 to CC10 which were also compressed to 388 kPa have a scatter in specific volume of between 1.505 and 1.529. The scatter of the data points for the undisturbed samples in Figures 6.2(c) and 6.3(b) are larger due to the more variable nature of undisturbed samples. The maximum deviations from the best fit lines in specific volume are 0.020 in Figure 6.2(c) and 0.036 in Figure 6.3(b).

For the normal compression curves of the remoulded and reconstituted simple shear samples (Figures 6.2(a) and (b)), at lower stresses before the straight line portions are reached, the curve for the reconstituted samples curves upwards due to the higher specific volume used during sample preparation and the curve for the remoulded samples curves downwards due to the lower specific volume used during sample preparation. A comparison of the three normal compression curves shown in Figures 6.2(a) and (b) and 6.3(a) is given in Figure 7.2(a). As Table 6.2 indicates, the values of λ_s , λ_b and N_s , N_b for the three normal compression lines differ only slightly and Figure 7.2(a) shows that the three lines are converging as the effective vertical stress increases. During one-dimensional compression the boundary conditions in the shear box are the same as those in an oedometer with rigid vertical boundaries while in the NGI simple shear apparatus the reinforced membrane may deform slightly radially as discussed in Appendix C. However, Figure 7.2(a) shows that the results obtained from the simple shear apparatus are similar to those obtained from the shear box.

In Figure 6.2(b) the data points obtained during swelling for sample CC10 suggest that although the linear swelling line gives a good fit of the points, the exact path followed by the

points is slightly curved. Table 6.2 shows that the values of K_s obtained in the simple shear apparatus for the remoulded, reconstituted and undisturbed samples range between 0.010 and 0.020 but the value of K_b obtained in the shear box for the undisturbed samples is at a higher value of 0.045. However, the data points for the undisturbed shear box samples (Figure 6.3(b)) are too scattered for accurate determination of the value of K_b.

It can be concluded that the behaviour of Cowden till during one-dimensional compression and swelling is governed by Equations (2.75) and (2.76) for simple shear tests and by equivalent equations for shear box tests. The different methods of sample preparation used and the different testing equipment used gave similar values for the parameters λ_s, λ_b and N_s, N_b for compression and K_s, K_b for swelling.

7.3.2   London clay (brown)

For the results of the remoulded samples, shown in Figures 6.4(a) and 6.5(a), the best fit curves give a close fit of the data points. At any particular value of σ_v' the maximum deviation of the data points from the best fit curves is 0.032 in specific volume. Samples MB1 to MB10 which were all normally compressed to $\sigma_v' = 388$ kPa have a scatter in specific volume of between 1.886 and 1.957 at $\sigma_v' = 388$ kPa. The scatter of the data points for the undisturbed samples in Figures 6.4(b) and 6.5(b) are much larger. The maximum deviations from the best fit lines in specific volume are 0.095 in Figure 6.4(b) and 0.070 in Figure 6.5(b).

A comparison of the two normal compression curves shown in Figures 6.4(a) and 6.5(a) is given in Figure 7.2(b). As Table 6.2 indicates the values of λ_s, λ_b and N_s, N_b for the two normal compression lines are very close and Figure 7.2(b) shows that the two lines are converging as the stresses increase.

The data points obtained during swelling of sample MB10 in Figure 6.4(a) and during swelling of sample BMB4 in Figure 6.5(a) indicate that although the linear swelling lines give good fits of the points, the exact paths followed by the points are slightly curved. Table 6.2 shows that the two values of κ_s , κ_b for the remoulded samples are close to each other but the values of κ_s , κ_b for the undisturbed samples are higher. However, the data points for the undisturbed samples (Figures 6.4(b) and 6.5(b)) are too scattered for accurate determination of κ_s , κ_b values.

It can be concluded that the behaviour of the brown London clay during one-dimensional compression and swelling are described by Equations (2.75) and (2.76) for simple shear tests and by equivalent equations for shear box tests. The values of the parameters λ_s , λ_b and N_s , N_b for compression and κ_s , κ_b for swelling obtained from the NGI simple shear apparatus and the shear box for the remoulded samples are very similar.

7.3.3   London clay (blue)

For the results of the remoulded samples, shown in Figure 6.6(a) the best fit curves give a close fit of the data points. At any particular value of σ_v' , the maximum deviation of the data points from the best fit curves is 0.016 in specific volume. Samples ML1 to ML10 were all normally compressed to σ_v' = 388 kPa and the scatter in specific volume is between 1.846 and 1.885 at σ_v' = 388 kPa. The scatter of the data points for the undisturbed samples in Figure 6.6(b) is very large with a maximum deviation from the best fit line of 0.080 in specific volume. Table 5.5 shows that samples UL8 to UL10 which have higher specific volumes were from different sample tubes as samples UL1 to UL7 . In Figure 6.7(a), at any particular value of p' the maximum scatter of the data points in the value of .q' are 10 kPa during K_o compression and 20 kPa during K_o swelling. In Figure 6.7(b) at any particular value of p' the maximum scatter of the data points in specific volume are 0.020 during K_o

compression and 0.026 during K_O swelling.

During K_O compression of the reconstituted samples the total stresses were increased at a constant rate so that the pore pressures in the samples were greater than the steady state pore pressures measured at the sample base. At the end of loading when the total stresses were held constant, the excess pore pressures dissipated and the resulting changes in specific volumes are shown in Figure 6.7(b). The relationship between this change in specific volume and the average excess pore pressure $\bar{u}$ has been given by Atkinson (1984b) as $\bar{u} = -(p' \delta v)/\lambda$. For example, for test TCL5 , at the end of loading the values of δv and p' are given in Figure 6.7(b) as -0.008 and 445 kPa respectively and as shown in Table 6.2, λ is 0.192, hence, giving $\bar{u} = 19$ kPa.

In order to compare the two normal compression curves shown in Figures 6.6(a) and 6.7(b), the normal compression line in Figure 6.7(b) which is plotted on $\ln p'$, v plane will be plotted on $\ln \sigma_v'$, v plane. The relationships between the parameters λ_s , N_s and the parameters λ , N_O have been given in Equations (2.81) and (2.83). The value of K_O is shown in Figure 6.7(a) as 0.57 and the values of λ and N_O are given in Table 6.2 as 0.192 and 3.037 respectively. Substituting these values into Equations (2.81) and (2.83), the values of λ_s and N_s for the normal compression line of the reconstituted samples are 0.192 and 3.102 respectively. The two normal compression curves are plotted together on $\ln \sigma_v'$, v plane in Figure 7.2(c). At relatively low stresses the curve for the reconstituted samples lies well above the curve for the remoulded samples. This is because a much higher specific volume was used for the reconstituted samples during sample preparation. But, as the stresses increase the two curves converge.

The data points obtained during K_O swelling of samples TCL2 , TCL3 , TCL7 and TCL8 in Figure 6.7(b) show that the

157

exact paths followed by the points are linear except for the initial portions of the paths. Since the reconstituted samples were tested in the stress path testing equipment, during K_O swelling both effective horizontal and vertical stresses were known and the values of K_O can be calculated. The variation of K_O with OCR will be discussed later.

It can be concluded that the behaviour of the blue London clay during one-dimensional compression and swelling is governed by Equations (2.75) and (2.76) for simple shear tests and by Equations (2.73) and (2.74) for triaxial tests. The normal compression line for the reconstituted samples lie above the normal compression line for the remoulded samples on $\ln \sigma_v'$, v plane but the two lines converge as stresses increase.

7.4   Discussion on one-dimensional consolidation

7.4.1   Cowden till

The values of the coefficient of consolidation c_v obtained from the remoulded and undisturbed simple shear samples, shown in Table 6.3, range from 24×10^{-9} to 269×10^{-9} m^2/s with the values for the undisturbed samples higher than those for the remoulded samples. The range of values of 32×10^{-9} to 476×10^{-9} m^2/s measured from undisturbed oedometer samples from the same site by BRE, described in Section 4.4.1, is similar. The values of the coefficient of permeability k obtained, shown in Table 6.3, range from 21×10^{-12} to 472×10^{-12} m/s. This is similar to the range of values of 9×10^{-12} to 381×10^{-12} m/s measured by BRE described in Section 4.4.1.

It can be concluded that the range of values of c_v and k for Cowden till measured from remoulded and undisturbed simple shear samples are similar to those measured from undisturbed oedometer samples taken from the same site.

7.4.2 London clay (brown)

The values of c_v obtained from the remoulded and undisturbed simple shear samples, shown in Table 6.4, range from 6×10^{-9} to 31×10^{-9} m²/s . The range of values of 7×10^{-9} to 50×10^{-9} m²/s measured from undisturbed oedometer samples from different sites by Skempton and Henkel (1957), described in Section 3.5.2, is similar. The values of k obtained, shown in Table 6.4, range from 6×10^{-12} to 74×10^{-12} m/s . The value of 30×10^{-12} m/s measured from undisturbed oedometer samples from the same site by BRE, described in Section 4.4.2, falls within this range. The range of 2×10^{-12} to 30×10^{-12} m/s reported by Skempton and Henkel in Section 3.5.2 is also similar.

It can be concluded that the range of values of c_v and k for brown London clay measured from remoulded and undisturbed simple shear samples are similar to those measured from undisturbed oedometer samples taken from various sites. Hence, the range of values obtained in this study are typical values for London clay.

7.4.3 London clay (blue)

The values of c_v obtained from the remoulded and undisturbed simple shear samples, shown in Table 6.5, range from 6×10^{-9} to 48×10^{-9} m²/s . The range of values of 7×10^{-9} to 50×10^{-9} m²/s measured by Skempton and Henkel, described in Section 3.5.2, is very close. The values of k obtained, shown in Table 6.5, range from 10×10^{-12} to 63×10^{-12} m/s . The value of 30×10^{-12} m/s measured from samples taken from the same site by BRE, described in Section 4.4.2, is within this range. The range of 2×10^{-12} to 30×10^{-12} m/s reported by Skempton and Henkel in Section 3.5.2 is also similar.

It can be concluded that the range of values of c_v and k for blue London clay measured from remoulded and undisturbed

159

simple shear samples are similar to those measured from
undistorbed oedometer samples taken from various sites. Hence,
the range of values obtained in this study are typical values
for London clay.

7.5 Critical states in shear tests and triaxial tests

7.5.1 Identification of critical and peak states

The concept of critical state has been discussed in
Section 2.5.3. Figures 2.22 to 2.24 show that at critical state
the soil shears at a constant ratio of shear stress to
normal stress and there are no changes in stresses and
specific volume. The variation of stress ratio with shear
strain for all tests reported in this study, except for the
stress probing tests TUB1 and TUL5 , have been plotted in
Figures 7.3 to 7.15. To determine whether the samples sheared
at constant stresses and specific volume the results plotted
in Figures 6.9 to 6.21 were used.

Although in theory the state of a soil shearing at critical
state is constant, in practice, there may be very slight
changes in the state measured due to, for example, inaccuracies
in measurements discussed in Sections 5.3 to 5.6, limitations of
the apparatus discussed in Section 3.3 and dissipation of
excess pore pressures discussed in Appendix E. In this study
a simple shear or shear box sample is considered to have
reached critical state when it satisfies the following
conditions for at least 5 % shear strain before the end of
test :

(1) The ratio $(\tau_v'/\sigma_v')_{cs}$ does not change by more
than 0.02 which corresponds to 1° of the angle
ρ_{cs}' ;

(2) the stress $(\tau_v')_{cs}$ does not change by more than
10 kPa ; and

(3)   the stress $(\sigma_v')_{cs}$ does not change by more than
       20 kPa for constant volume tests or the volumetric
       strain does not change by more than 0.5 % for
       constant σ_v' tests.

In condition (3) the allowance for changes in $(\sigma_v')_{cs}$ is
larger than that for $(\tau_v')_{cs}$ in condition (2) because
$(\sigma_v')_{cs}$ could have been affected by the dissipation of excess
pore pressures. According to Equation (E.7) the dissipation
of an excess pore pressure of 20 kPa will result in a change in
volumetric strain of the order of 0.5 % . Examples of
samples which do not satisfy condition (1) are samples CC5
to CC8 . Figure 7.4(c) shows that for the last 5 % change
in γ the ratio τ_v'/σ_v' for these tests increases by
about 0.03 . An example of a sample which satisfies
condition (1) but not condition (2) is sample UB5 .
Figure 7.7(b) shows that for the last 5 % change in γ
the ratio τ_v'/σ_v' changes by less than 0.02 but
Figure 6.13(c) shows that τ_v' decreases by more than
10 kPa . The peak τ_v'/σ_v' states and critical states for
all simple shear samples and shear box samples are tabulated
in Tables 7.1 to 7.5.

For triaxial tests a sample is considered to have reached
critical state when it satisfies the following conditions for
at least 5 % shear strain before the end of test :

(1)   The ratio $(q'/p')_{cs}$ does not change by more than
       0.04 which corresponds to 1° of the angle ϕ_{cs}' ;

(2)   the stresses q' and u do not change by more than
       10 kPa .

Since all triaxial tests performed were undrained tests no
dissipation of excess pore pressures was allowed. In
addition, it is illustrated in Figures 2.23 and 2.24 that if an
overconsolidated sample reaches critical state its value of
q'/p' will become the same as that for the normally
consolidated samples. For example, samples TCL7 and TCL8

161

are considered not to have reached critical state because although Figures 6.20(d) and (e) and 7.14 show that conditions (1) and (2) are satisfied, Figure 7.14 shows that the final q'/p' ratio of these samples are different to $(q'/p')_{cs}$ for the normally compressed samples TCL6 , TCL9 and TCL10 . The peak q'/p' states and critical states for all triaxial samples are tabulated in Tables 7.6 and 7.7 .

The critical states for the simple shear tests are plotted on the σ_v' , τ_v' plane in Figures 7.16 to 7.19 . The lines joining the critical states are best fit lines for the experimental results. In Figure 7.16 the critical states for remoulded and for reconstituted samples are plotted together and in Figures 7.18 and 7.19 the critical states for brown and blue London clay samples are plotted together. This is because there is very little difference between the remoulded and reconstituted samples and between the brown and blue London clay.

The critical states for constant σ_v' tests and for constant volume tests are plotted separately because even for samples with same OCR and same pre-shearing state the value of ρ_{cs}' obtained for the two different types of tests are distinctly different. For instance, Figures 7.6 and 7.8 show that the normally compressed samples MB1 , ML1 and ML9 which were sheared at constant σ_v' reached critical states with $\tan \rho_{cs}'$ close to 0.26 but the normally compressed samples MB5 and ML5 which were sheared at constant volume reached critical states with $\tan \rho_{cs}'$ close to 0.35 . Further analysis on this will be given in Section 7.5.2.

Conventionally, the results in Figures 7.16 to 7.19 would be interpreted as evidence of the failure of soils governed by the Mohr-Coulomb criterion represented by Equation (2.98) which states that soil has cohesive strength. An example of such an interpretation of results of shear box tests can be seen in Figure 3.31. This conventional interpretation is considered to be incorrect in this study. Instead, it is suggested above that the critical states in Figures 7.16 to 7.19 lie on critical state lines represented by

Equation (2.97) which states that the strength of soil is purely frictional.

Figures 7.16 to 7.19 demonstrate that for remoulded and reconstituted samples different values of ρ_{cs}' are obtained for samples with different OCR and for undisturbed samples different values of ρ_{cs}' are obtained for samples with different pre-shearing states. A theoretical relationship between ρ_{cs}' and K_0 which is a function of OCR has been proposed in Section 2.5.3. A comparison between the predictions of this theoretical relationship and the experimental results will be given in Section 7.5.3. A proposed representation of the critical state line on the σ_v', v plane for simple shear tests has been given in Section 2.5.3. The proposed representation will be compared with experimental results in Section 7.5.3.

The peak q'/p' states and critical states for the triaxial tests are plotted on p', q' plane and on $\ln p'$, v plane in Figures 7.20 and 7.21. Figure 7.20 shows that for each of compression and extension a unique critical state line described by Equations (2.93) and (2.94) exists. In Figure 7.20(a) the values of M for compression and extension are 0.87 and 0.78 respectively. From Equations (2.95a) and (2.95b) the values of ϕ_{cs}' for compression and extension are 22° and 26° respectively. These are close to the values of $\phi_{cs}' = 22°$ for compression and $\phi_{cs}' = 24°$ for extension obtained by Atkinson et al (1984) described in Section 3.5.2. In Figure 7.20(b) the critical states for compression and extension fall close to the same line. The value of Γ is 2.945 and the value of λ is 0.185 which is close to the value of $\lambda = 0.192$ for the normal compression line given in Table 6.2. In Figure 7.21 the critical state lines are those obtained from the reconstituted samples and are plotted as references for the peak states of the undisturbed samples.

In this section, critical states and peak states have been identified for simple shear, shear box and triaxial samples. For simple shear tests the critical state lines on the

163

σ_v' , τ_v' plane are described by Equation (2.97). The values of ρ_{cs}' are dependent on OCR and on whether the sample was sheared under constant σ_v' or constant volume condition. For triaxial tests the results are in agreement with the critical state theory. For each of compression and extension a unique critical state line described by Equations (2.93) and (2.94) exists and the values of the soil parameters M , Γ and λ have been obtained.

7.5.2   Difference between constant σ_v' and constant volume simple shear tests

In section 7.5.1 it is found that the values of ρ_{cs}' obtained from constant σ_v' tests and from constant volume tests are significantly different. Simple shear tests performed on kaolin by Airey (1984) described in Section 3.3.1 showed the same behaviour. It can be deduced from Figures 3.9(b) and (c) that the values of $\tan\rho_{cs}'$ at the sample core for constant σ_v' shearing and constant volume shearing are 0.28 and 0.39 respectively.

It is concluded in Section 3.3.2 that the most suitable method for estimating the stress states of normally compressed clay samples tested in the NGI simple shear apparatus is by using Equation (3.4) with the relationship between k and ϕ_{cs}' as shown in Figure 3.20. For London clay, using $\phi_{cs}' = 22°$ as described in Section 7.5.1 the value of k is given by Figure 3.20 as 0.42 . Substituting k = 0.42 into Equation (3.4) the variation of θ during shearing of the normally compressed remoulded brown London clay samples MB1 and MB5 are plotted in Figure 7.22. The values of θ_{cs} for tests MB1 and MB5 are 33° and 39° respectively.

The values of θ for strain increments in Figure 7.22 were calculated by Equations (2.48) and (2.50). It can be seen that coaxiality does not apply at any stage during shearing in both types of tests and the pattern of behaviour shown in Figure 7.22(a) is similar to that for kaolin obtained by

Borin (1973)   shown in   Figure 3.15.

Using the relationships for the   parameters ϕ_{cs}' , ρ_{cs}' and
θ_{cs} given in   Section 2.3.1 , the Mohr's circles of stress
at critical state for remoulded brown London clay samples
have been plotted in   Figure 7.23 .   The   value   of ϕ_{cs}' is
22° and the values of $(\sigma_v' , \tau_v')_{cs}$ were   taken from
Table 7.2.   In   Section 2.3.1   it   is   stated   that
Equations (2.34) to (2.36b) apply if $K_o < 1$ before shearing and
Equations (2.37) to (2.39b) apply if $K_o > 1$ before shearing.
The   variation of K_o with   OCR   will be   given in
Section 7.5.3.   For London clay samples with OCR equal to
1 and 2 the values of K_o are   0.57 and 0.80
respectively.   Also, Figure 7.22   suggests that $2\theta_{cs}$ was
much less than   90° + ϕ_{cs}' .   Hence, Equation (2.36a)   was
applied for drawing the Mohr's circles in Figure 7.23.   For
samples MB3 and MB7   which have an   OCR equal to 4   the
value of K_o is 1.08 .   For samples with K_o close to 1
it is not entirely certain which set of equations apply
without knowing how the stresses developed during shearing.
For test MB1 ,   Figure 7.23(a) shows that   Equation (2.36a)
gives $\theta_{cs} = 30°$ compared with $\theta_{cs} = 33°$ given by
Equation (3.4) in   Figure 7.22(a).   For   test   MB5 ,
Figure 7.23(b)   shows that   Equation (2.36a)   gives $\theta_{cs} = 40°$
compared with $\theta_{cs} = 39°$ given by Equation (3.4) in
Figure 7.22(b).   Hence, there is a close agreement between
the two methods for estimating the stress state at critical
state.   Figure 7.23 shows that the values of θ_{cs} for the
constant volume   tests are significantly higher than the
values of θ_{cs} for the constant σ_v' tests.   The effect
of θ_{cs} on the value of ρ_{cs}' will be discussed later in
this section.

Using Equations (3.5) and (3.6)   which are based on
Equation (3.4)   the Mohr's circles of stress for tests MB1
and MB5   at $\gamma = 0$,   3   and   24 %   are plotted   in
Figure 7.24.   Both Equation (3.6)   and   Figure 7.24(a)   show
that for constant σ_v' tests the relationship given by
Equation (3.4) predicts that σ_3' remains constant during
shearing.   The   Mohr's   circle   at   critical   state   in

Figure 7.24(a) is close to but does not reach the failure envelope set by $\phi_{cs}' = 22°$. The values of ϕ_{cs}' calculated from the stress states defined by the Mohr's circles for tests MB1 and MB5 are 20° and 22° respectively.

Finally, the theoretical relationships between ρ_{cs}' and θ_{cs} given by Equations (2.35) and (2.38) have been plotted in Figure 7.25 for the particular ϕ_{cs}' value of 22°. Figure 7.25 shows that for samples with pre-shearing $K_o < 1$ the values of ρ_{cs}' increase with θ_{cs} for values of θ_{cs} less than 56°. In Figure 7.23 the values of θ_{cs} for all four Mohr's circles are less than 56°, hence, the constant volume tests which result in higher values of θ_{cs} have higher values of ρ_{cs}'.

In this section, the values of θ_{cs} for constant σ_v' tests and constant volume tests on remoulded brown London clay have been estimated using the two different methods represented by Equation (2.36a) and by Equation (3.4). The values of θ_{cs} for the constant volume tests are significantly higher than for the constant σ_v' tests. According to Equation (2.35) these higher values of θ_{cs} for the constant volume tests are responsible for causing higher values of ρ_{cs}'. It can be concluded that constant σ_v' tests and constant volume tests result in different values of θ_{cs} and hence different values of ρ_{cs}'.

7.5.3   Influence of K_o on critical states

In Section 7.5.1 the critical states for simple shear samples show that the values of ρ_{cs}' are dependent on OCR. The proposed theoretical relationship between ρ_{cs}' and K_o which is a function of OCR is represented by Equation (2.102). Figure 7.26 shows the variation of $\tan \rho_{cs}'$ with K_o according to Equation (2.102) for $\phi_{cs}' = 22°$ for London clay. The maximum K_o value of 2.20 was obtained from Equation (2.103) and the K_o value of 1.33 for $\rho_{cs}' = \phi_{cs}'$ was obtained from Equation (2.104).

166

In order to compare the predictions of Equation (2.102) with experimental results, the variation of K_O with OCR obtained from reconstituted triaxial sample are presented in Figure 7.27. Comparisons between the simple shear and shear box tests results with predictions by Equation (2.102) are shown in Figures 7.28 to 7.31. The values of OCR for the undisturbed samples were calculated from Equation (2.84b). In accordance with the descriptions in Section 6.3.4, the normal compression lines used for the undisturbed samples were the normal compression lines obtained from remoulded samples of the same material tested in the same apparatus. The values of the parameters for the normal compression lines obtained from the remoulded samples and the values of the parameters for the swelling lines defined by the undisturbed samples are tabulated in Table 7.8. The value of σ_{vp}' for each type of undisturbed samples, also tabulated in Table 7.8, is the value of σ_v' at the point of intersection of the normal compression line and the swelling line. Considering the results of the stress path tests on Cowden till performed by Ng (1988) in Table 3.1, the value of ϕ_{cs}' for Cowden till is taken as 31°.

On the whole, the agreement between the predictions by Equation (2.102) and the simple shear test results is good but the results for the shear box tests are very scattered. In Figure 7.30(b) the scatter of the results for the undisturbed London clay samples is relatively large compared with the other results from simple shear tests. This is likely to be due to the relatively large variation in specific volume of the samples which has already been discussed in Sections 7.3.2 and 7.3.3.

In Figures 7.28 and 7.29 the results for remoulded and reconstituted samples show that at OCR = 1 the predictions by Equation (2.102) are closer to the constant σ_v' test results than the constant volume test results. The reason for this is, as described in Section 2.5.3, Equation (2.102) was derived by assuming that the stress increments applied during shearing are pure shear stress increments and that σ_v' remains unchanged. It has been explained in Section 2.4.1

that the application of pure shear stress increments results in the Mohr's circle of stress changing in size but the centre of the Mohr's circle remains unchanged. Figure 7.24 shows that from $\gamma = 0$ to $\gamma = 24 \%$ the changes in the positions of the centres of the Mohr's circles for tests MB1 and MB5 are 36 kPa and 112 kPa respectively. Hence, at OCR = 1 the stress states of the samples sheared at constant σ_v' are much closer to the stress states assumed in deriving Equation (2.102). As OCR increases the stress paths followed by constant σ_v' shearing and by constant volume shearing become closer as illustrated in Figures 2.23(a) and 2.24(a) and Figures 7.28 to 7.30 show that for OCR > 1 the predictions by Equation (2.102) apply equally well for both types of shearing.

The proposed representation of the critical state line on the σ_v', v plane is represented by Equation (2.109). Comparisons between the predictions by Equation (2.109) and the results from simple shear tests on Cowden till and blue London clay are shown in Figure 7.32. In Figures 7.32(a) and (c) the results for constant volume tests on normally compressed samples are not included because, as described in Section 2.5.3 , Equation (2.109) was also derived by assuming that σ_v' remains constant during shearing. Best fit lines are drawn through the critical states for constant σ_v' tests on normally compressed samples to act as critical state lines for samples with OCR = 1 . From these lines the values of λ_s for Cowden till and blue London clay are 0.066 and 0.134 respectively. Both values are very close to the values of λ_s for the corresponding normal compression lines given in Table 6.2. Substituting the values of λ_s and Γ_s for the critical state lines for samples with OCR = 1 into Equation (2.112) gives values of Γ for Cowden till and blue London clay as 1.797 and 2.573 respectively. Using these values of Γ together with Equation (2.109) the critical state lines for samples with OCR > 1 have been plotted.

In Figures 7.32(b) and (d) the values of λ_s for the critical state lines are assumed to be the same as those for the

remoulded samples. Best fit lines are drawn through samples with the lowest OCR and using values of λ_s and Γ_s for these lines values of Γ for Cowden till and blue London clay were obtained as 1.809 and 2.542 respectively. Using these values of Γ together with Equation (2.109) the critical state lines for samples with higher OCR are plotted.

On the whole the agreement between the predictions by Equation (2.109) and the test results is reasonable. It becomes worse as OCR increases, nevertheless, the predicted trend of decreasing Γ_s with increasing OCR is in agreement with experimental results. It is expected that Equation (2.109) gives less accurate predictions than Equation (2.102) since an extra assumption is made in Equation (2.107) when Equation (2.109) was derived.

From the discussions in this section it can be concluded that Equation (2.102) gives a good prediction of the variation of ρ_{cs}' with K_o for simple shear tests. For normally compressed samples the predictions are closer to the constant σ_v' test results than to the constant volume test results. Equation (2.109) gives reasonable predictions of the critical state lines on σ_v', v plane for simple shear samples with various OCR. The accuracies of the predictions decrease with increasing OCR.

7.5.4   Undrained shear strength

The undrained shear strength c_u for triaxial samples is given by Equation (2.96). Comparisons between c_u calculated from Equation (2.96) and results from constant volume simple shear tests for London clay are shown in Figure 7.33. The triaxial test results are based on parameters obtained from the reconstituted blue London clay samples and the simple shear test results include data from remoulded brown and blue London clay samples. From Section 7.5.1 the values of M for compression and extension are 0.87 and 0.78 respectively and the values of Γ and λ for the critical

state line are 2.945 and 0.185 respectively. These values of M , Γ and λ together with values of v_o at different OCR were substituted into Equation (2.96) to obtain the full and broken curves in Figure 7.33. The values of v_o were calculated using Equations (2.73) and (2.74) with values of λ , N_o and κ equal to 0.192 , 3.037 and 0.054 respectively as given in Table 6.2. Also, a value of $p_p' = 277$ kPa corresponding to $\sigma_{vp}' = 388$ kPa was used in calculating v_o since all the simple shear test results plotted in Figure 7.33 are for samples with $\sigma_{vp}' = 388$ kPa . The definition of σ_{vp}' is given in Section 2.5.1 and is illustrated in Figure 2.26. The values of $(\tau_v')_{cs}$ plotted in Figure 7.33(a) were taken from Tables 7.2 and 7.3. Figure 7.33(a) shows that $(\tau_v')_{cs}$ obtained from constant volume simple shear tests are lower than c_u for triaxial compression and extension tests. Theoretical predictions and experimental evidence of c_u for triaxial compression greater than $(\tau_v')_{cs}$ for simple shear have been given by Wroth (1984) and Berre and Bjerrum (1973) respectively.

It has been discussed in Section 2.5.3 that $(\tau_v')_{cs}$ measured from constant volume shearing is related to c_u by Equation (2.113) and so c_u can be calculated from $(\tau_v')_{cs}$, ρ_{cs}' and ϕ_{cs}' as illustrated by Equation (2.114). The value of ϕ_{cs}' is 22° for London clay as described in Section 7.5.1. For London clay samples with OCR equal to 1 and 2 it has been explained in Section 7.5.2 that Equation (2.36a) is suitable for expressing θ_{cs} in terms of ρ_{cs}' and ϕ_{cs}' and hence, Equation (2.114) was applied to calculate c_u for these samples. For the samples with OCR equal to 4 and 8 it was not possible to decide which equation to use to relate θ_{cs} with ρ_{cs}' and ϕ_{cs}' without further information about θ_{cs} . However, three of the samples, ML7 , MB8 and ML8 , have values of ρ_{cs}' slightly greater than 22° and since ρ_{cs}' could not have been greater than ϕ_{cs}' it was assumed that for these samples $\rho_{cs}' = \phi_{cs}'$. As a result, Equation (2.39a) became the same as Equation (2.39b) and was combined with Equation (2.113) to

calculate c_u. The values of c_u for the simple shear tests are plotted in Figure 7.33(b) and are considered to be estimates rather than accurate measurements. It can be seen that the values of c_u for the simple shear tests in Figure 7.33(b) are only very slightly higher than the values of $(\tau_v')_{cs}$ in Figure 7.33(a). The differences in c_u obtained from triaxial tests and simple shear tests are likely to be due to the different intermediate principal stresses σ_2' acting in the two different types of tests. This would have caused the triaxial and simple shear samples to follow different effective stress paths in terms of three-dimensional stress parameters and so reaching different shear stresses at the end of the paths. The effective stress paths followed by simple shear tests in terms of the stress parameters p', q' will be examined in Section 7.6.1.

It can be concluded that $(\tau_v')_{cs}$ measured from constant volume simple shear tests are lower than c_u calculated from Equation (2.96) using triaxial test results. Values of c_u estimated from ϕ_{cs}' together with simple shear parameters $(\tau_v')_{cs}$ and ρ_{cs}' are slightly higher than the corresponding values of $(\tau_v')_{cs}$ but are also lower than c_u calculated from triaxial test results.

7.5.5   Normalised critical states

The reasons for normalising test data has been discussed in Section 2.6 and the theoretical relationships between normalised critical states and K_o are given in Section 2.6.2. The normalised critical states for the Cowden till and blue London clay simple shear samples are plotted in Figures 7.34 to 7.37.

In the σ_v'/σ_{ve}', τ_v'/σ_{ve}' plots, the predicted values of $(\sigma_v'/\sigma_{ve}')_{cs}$ which are represented by the broken lines can, in theory, be calculated from Equation (2.139). However, in practice, the value of λ_s for the normal compression line is very slightly different to the value of λ_s for the

171

critical state line for both Cowden till and blue London clay as already mentioned in Section 7.5.3. Hence, in calculating the predicted values of $(\sigma_v'/\sigma_{ve}')_{cs}$, the λ_s for normal compression line was used to calculate $(\sigma_{ve}')_{cs}$ from Equation (2.136) and the λ_s for critical state line was used to calculate $(\sigma_v')_{cs}$ from Equation (2.109). In the Γ_s, τ_v'/σ_v' plots, the predicted values of Γ_s which are represented by the broken lines were calculated from Equation (2.112) using the value of λ_s for critical state line.

The agreement between the predictions and the data points is reasonable. The accuracies of the predictions of $(\sigma_v'/\sigma_{ve}')_{cs}$ and Γ_s are similar to those in Figure 7.32 since Equation (2.139) is partly derived from Equation (2.109) and Equation (2.112) is part of Equation (2.109).

The normalised peak q'/p' states and normalised critical states of the reconstituted blue London clay triaxial samples are plotted in Figure 7.38. For each of compression and extension tests a critical state point is clearly defined by the normally compressed samples. Comparing Figure 7.38 with Figure 2.25 the behaviour of the London clay samples is in agreement with the critical state theory, except that the overconsolidated samples did not reach critical states.

It can be concluded that Equations (2.139) and (2.112) give reasonable predictions of the normalised critical states for simple shear tests. The accuracies of the predictions tend to decrease with increasing OCR. The normalised critical states of the reconstituted blue London clay triaxial samples give well-defined critical state points for compression and extension and generally behave as the critical state theory predicts.

7.5.6   Summary

By considering the variation of the ratio of shear stress to normal stress with shear strain and the variation of shear

stress, normal stress and specific volume with shear strain, critical states and peak states have been identified for simple shear, shear box and triaxial samples of Cowden till and London clay (brown and blue).

For simple shear tests, the critical states are described by critical state lines represented by Equation (2.97) instead of the conventional Mohr-Coulomb criterion represented by Equation (2.98). For each soil, the values of ρ_{cs}' are dependent on OCR and on whether the sample was sheared under constant σ_v' or constant volume condition. Two different methods, represented by Equation (2.36a) and by Equation (3.4), have been used to estimate θ_{cs}. Both methods give similar estimations and they indicate that θ_{cs} for constant σ_v' tests and θ_{cs} for constant volume tests are different. According to Equation (2.35) this difference in θ_{cs} caused the difference in ρ_{cs}' for the two types of tests. The variation of ρ_{cs}' with OCR for the test results are compared with predictions by the proposed theoretical relationship between ρ_{cs}' and K_o represented by Equation (2.102). In general, the agreement between the predictions by Equation (2.102) and the test results is good. For normally compressed samples the predictions are closer to the constant σ_v' test results than to the constant volume test results. The proposed representation of the critical state line on the σ_v', v plane given by Equation (2.109) is also compared with the test results. The agreement is reasonable but worsens with increasing OCR. The normalised critical states are presented together with the predictions by Equations (2.102), (2.139) and (2.112).

For the triaxial tests on blue London clay, a unique critical state line exists for each of compression and extension. The normalised critical states of the reconstituted samples give well-defined critical state points for compression and extension. In general, the results of the triaxial tests are close to the predictions by the critical state model.

The shear stresses $(\tau_v')_{cs}$ measured from constant volume

simple shear tests are lower than c_u calculated from Equation (2.96) using triaxial test results. Values of c_u estimated from ϕ_{cs}' together with simple shear parameters $(\tau_v')_{cs}$ and ρ_{cs}' are slightly higher than the corresponding values of $(\tau_v')_{cs}$ but are also lower than c_u calculated from triaxial test results.

7.6   State paths for simple shear tests and triaxial tests

7.6.1   Discussion on state paths

The state paths for all simple shear tests are presented in Figures 7.39 to 7.45 and the state paths for all triaxial tests, except for the stress probing tests TUB1 and TUL5, are presented in Figures 7.46 and 7.47. On the $\ln \sigma_v'$, v plots for the undisturbed simple shear samples (Figures 7.41(d) and (e), 7.43(c) and (d) and 7.45(c) and (d)), the normal compression lines are those for remoulded samples of the same material. On the $\ln p'$, v plot for the undisturbed blue London clay triaxial samples (Figure 7.47(b)), the broken line is the normal compression line for the reconstituted samples shown in Figure 7.46(b).

It has been demonstrated in Section 2.4.1 that for simple shear tests and triaxial tests on isotropic elastic materials, elastic shear strain increments are caused by shear stress increments only and elastic volumetric strain increments are caused by normal stress increments only. According to the critical state model, described in Section 2.5, the behaviour of overconsolidated samples are purely elastic before they reach the state boundary surface. Hence, for overconsolidated samples, the stress paths of constant volume simple shear tests on σ_v', τ_v' plane and the stress paths of undrained triaxial tests on p', q' plane are theoretically vertical before yielding if the soil is isotropic. Figures 7.39 to 7.45 show that all stress paths for constant volume simple shear tests are only vertical initially. Therefore, they exhibit anisotropic behaviour with elastic shear strain increments

$\delta\gamma^e$ relating to both shear stress increments $\delta\tau_v'$ and normal stress increments $\delta\sigma_v'$. Figure 7.46(a) shows that the stress paths for the overconsolidated reconstituted blue London clay triaxial samples are close to vertical before they reach the critical state lines and Figure 7.47(a) shows that the stress paths for the undisturbed blue London clay triaxial samples are not vertical.

In order to compare the stress paths for simple shear tests with those for triaxial tests, the overconsolidation ratio OCR used for simple shear tests can be related to the overconsolidation ratio R_p used for triaxial tests by Equation (2.85). For example, using Equation (2.85) together with Figure 7.27(a) Cowden till simple shear samples with OCR = 2, 4 and 8 have R_p = 1.7, 3.0 and 5.3 respectively and using Equation (2.85) together with Figure 7.27(b) blue London clay triaxial samples with R_p = 2 and 4 have OCR = 2.7 and 6.5 respectively. For Cowden till the stress paths for constant volume simple shear tests presented in Figures 7.39 to 7.41 can be compared with the stress paths for triaxial tests on isotropic samples reported by Atkinson et al (1985a) in Figure 3.25. For London clay the state paths for constant volume simple shear tests presented in Figures 7.42 to 7.45 can be compared with the state paths for undrained triaxial tests presented in Figure 7.46. In general, the overall pattern of the state paths for simple shear tests and triaxial tests are similar with decreases in normal stresses when the normally compressed samples were sheared and increases in normal stresses when the heavily overconsolidated samples were sheared. Both normally compressed simple shear samples and normally compressed triaxial samples show small drops in shear stresses before reaching critical states. The stress paths presented in Figure 7.47 and the stress paths obtained by Apted (1977) reproduced in Figure 3.30(a) are both for undrained tests on undisturbed London clay triaxial samples with 100 mm diameter. For tests TUL1 and TUL2 the portions of the paths above the isotropic line have similar shape as those in Figure 3.30(a). The stress paths for the overconsolidated

reconstituted triaxial samples will be compared with those for the undisturbed triaxial samples in the next section.

In Section 7.5.1 it has been mentioned that there is very little difference between the critical states for remoulded and reconstituted samples. Figures 7.39 and 7.40 show that the shape of the state paths for these two types of samples are also very similar. In Figure 7.48 the stress paths for a remoulded simple shear sample and two reconstituted triaxial samples are compared. Samples ML5, TCL1 and TCL6 were all blue London clay samples normally compressed under K_O condition. Sample ML5 was compressed to a pre-shearing effective vertical stress σ_{vo}' of 388 kPa and samples TCL1 and TCL6 were compressed to p_o' of 284 kPa corresponding to σ_{vo}' of 398 kPa so that the pre-shearing stress states of all three samples were similar. Using Equations (3.5) and (3.6) which are based on the relationship represented by Equation (3.4) the values of σ_1' and σ_3' during shearing for test ML5 were calculated. As described in Section 7.5.2 the value of ϕ_{cs}' for London clay was taken as 22° and the value of k was given by Figure 3.20 as 0.42. In order to estimate the general states of stress for test ML5 in terms of the stress invariants p' and q' defined by Equations (2.8) and (2.9), it was necessary to estimate the values of σ_2' also. In Figure 7.48 one estimated stress path for test ML5 was obtained by assuming $\sigma_2' = \sigma_h'$ which is similar to the assumption represented by Equation (2.107) used in deriving Equation (2.109). Another estimated stress path for test ML5 was obtained by assuming $\sigma_2' = \sigma_3'$. The magnitudes of σ_2' relative to σ_1' and σ_3' can be described by the parameter b the definition of which has been given in Section 3.4. In test ML5, for $\sigma_2' = \sigma_h'$ the value of b varied from zero before shearing to 0.42 at critical state compared with b equal to zero for $\sigma_2' = \sigma_3'$. Although the two different assumptions about σ_2' resulted in two different estimated stress paths for the simple shear test, neither of them resembles the triaxial stress paths. The estimated paths for the simple shear test suggest that the sample was slightly extended towards failure but the main

176

cause of failure was the reduction in effective normal stresses.

It has been discussed in Section 3.4 that Henkel and Wade (1966) plotted stress paths for undrained plane strain compression tests and undrained triaxial compression tests on the same soil in terms of σ_{oct}' and τ_{oct}'. Henkel and Wade concluded that with the values of σ_2' taken into consideration by the octahedral stress parameters the shape of the effective stress paths for the undrained compression tests was unique but the paths terminated at different states because at critical state the Mohr-Coulomb criterion which ignored the effects of σ_2' governed. From Figure 7.48 it can be concluded that the effective stress paths for simple shear tests and triaxial tests even when plotted in terms of p' and q' have different shapes. This is likely to be due to the completely different modes of shearing. At critical state both tests ML5 and TCL1 have ϕ_{cs}' of 22° but their stress paths on p', q' plane terminate at different states because the parameter ϕ_{cs}' is independent of σ_2' but the parameters p' and q' take σ_2' into account. Moreover, q_{cs}' for the simple shear test is lower than q_{cs}' for the triaxial compression test and this could be the reason for c_u from simple shear tests lower than c_u from triaxial tests in Section 7.5.4.

In this section, the stress paths of the constant volume simple shear tests on overconsolidated samples suggest that the elastic stress-strain behaviour of the samples before reaching the state boundary surface is anisotropic. Comparisons are made among the state paths for simple shear tests and triaxial tests on remoulded, reconstituted and undisturbed samples. The general patterns of the state paths for simple shear tests and triaxial tests are similar. The stress paths for a simple shear test was plotted in terms of p' and q' using the relationship represented by Equation (3.4) together with assumptions for σ_2'. This suggests that the effective stress paths for simple shear tests and triaxial tests on p', q' plane have different shapes and terminate at different states.

177

7.6.2   Discussion on normalised state paths

The normalised state paths for all simple shear tests are presented in Figures 7.49 to 7.55 and the normalised state paths for all triaxial tests, except for the probing tests, are presented in Figures 7.58 and 7.59. The method for estimating the values of OCR for the undisturbed simple shear samples has been described in Section 7.5.3. For the normalised state paths for remoulded and undisturbed Cowden till and blue London clay simple shear samples the critical state points predicted by Equations (2.102), (2.112) and (2.139), already shown in Figures 7.34 to 7.37, are included for comparison. In Figures 7.49(f) and 7.51(f) the predicted critical state points are further away from the experimental results than as shown before in Figures 7.34(b) and 7.35(b). This is because in Figures 7.49(f) and 7.51(f) the values of $v_{\lambda s}$ for the paths were computed using the λ_s for the normal compression line which is slightly different to the λ_s for the critical state line as already explained in Section 7.5.5. It can be deduced from Figure 2.26 that a small difference in the value of λ_s results in large differences in the values of $v_{\lambda s}$.

For the normally compressed remoulded and reconstituted simple shear samples, those which were sheared under the same condition but with different values of σ_{vo}' give the same normalised state paths. For instance, Figure 7.49(a) shows that samples MC1 and MC9 which were both sheared under constant σ_v' condition but with σ_{vo}' of 388 kPa and 776 kPa respectively have the same normalised stress path as predicted in Section 2.6. When the normalised state paths for constant σ_v' and constant volume tests are plotted together in the figures labelled (c) and (f) in Figures 7.49 to 7.55 the overall pattern of behaviour is the same as shown in Figure 2.25 but the exact shapes of the normalised state paths for constant σ_v' tests are different to those for constant volume tests. For the normally compressed samples, at any value of τ_v'/σ_{ve}' the value of σ_v'/σ_{ve}' for a constant volume test is generally lower than those for a constant σ_v' test. For the overconsolidated samples, the

normalised state paths for the constant $\sigma_v{}'$ tests are much closer to vertical than those for constant volume tests. These differences are likely to be caused by the difference between constant $\sigma_v{}'$ tests and constant volume tests discussed in Section 7.5.2.

The normalised constant v section and the normalised constant $\sigma_v{}'$ section of the Roscoe surface predicted by Modified Cam-clay are given by Equations (2.143) and (2.144). For remoulded Cowden till and remoulded blue London clay the Roscoe surface$_\wedge$ predicted by Modified Cam-clay are plotted together with the experimental results in Figures 7.56 and 7.57. The values of λ_s , N_s and κ_s used were taken from Table 6.2. For remoulded Cowden till the value of tan $\rho_{cs}{}'$ used was the average of the values of tan $\rho_{cs}{}'$ for tests MC1 , MC9 and MC10 given in Table 7.1 and, similarly, for remoulded blue London clay the value of tan $\rho_{cs}{}'$ used was the average of the values of tan $\rho_{cs}{}'$ for tests ML1 , ML5 and ML9 given in Table 7.3. Figure 7.56 shows that for Cowden till Modified Cam-clay gives good predictions but Figure 7.57 shows that for blue London clay the predictions by Modified Cam-clay are different to the experimental results.

Figure 7.58 shows that the normalised state paths for the reconstituted blue London clay triaxial samples have the same pattern as the idealised behaviour given in Figure 2.25. The normally compressed samples which had different pre-shearing states give a unique Roscoe surface for both compression and extension. Figure 7.59 shows that the normalised state paths for the undisturbed blue London clay triaxial samples have similar shape to those of the overconsolidated reconstituted samples in Figure 7.58. A comparison between the normalised paths for the undisturbed samples and those for the reconstituted samples with $R_p = 4$ is made in Figure 7.60. It can be seen that the undisturbed samples have significantly lower peak normalised shear stresses than the reconstituted samples both in compression and extension. This is likely to be due to the presence of fissures in the undisturbed material. The

179

effects of fissures on the testing of undisturbed London clay have been described in Section 3.5.2.

It can be concluded that the overall pattern of the normalised state paths for the simple shear tests is in agreement with the critical state model. The exact shapes of the normalised paths for constant σ_v' tests are different to those for constant volume tests. Therefore, it has not been possible to identify a unique state boundary surface. Modified Cam-clay gives good predictions of the Roscoe surface for remoulded Cowden till but not for remoulded London clay. The overall pattern of the normalised state paths for the triaxial tests is also as predicted by the critical state model. A comparison between the normalised paths for the London clay triaxial samples shows that the undisturbed samples have significantly lower peak normalised shear stresses than the reconstituted samples.

7.7 Stiffnesses determined from simple shear tests and stress path tests

7.7.1 Tangent stiffnesses from simple shear and triaxial tests

The shear stress versus shear strain curves for all simple shear tests and stress path tests have been given in Chapter 6. However, it is difficult to identify any pattern of behaviour at relatively small strains from these curves because they tend to cluster near the origin. The problem is solved by plotting the data using a logarithmic scale for strains as shown in Figures 7.61 to 7.69. In Figure 7.61, at $\gamma < 1.0 \%$, the curves for samples MC1 to MC4 and MC5 to MC8 show that for both constant σ_v' and constant volume simple shear tests the slopes of the curves decrease with increasing OCR. Also, for the normally compressed samples the curves for samples MC9 and MC10 with $\sigma_{vo}' = 776$ kPa have greater slopes than the curves for samples MC1 and MC5 with $\sigma_{vo}' = 388$ kPa . These patterns of behaviour can also be identified in Figures 7.62, 7.64 and 7.66. In

Figures 7.63, 7.65 and 7.67 it is clear that the slopes of the curves for the undisturbed samples increase with σ_{vo}' and therefore decrease with OCR which is in agreement with the behaviour of the remoulded and reconstituted samples described above. In Figure 7.68 the slopes of the curves for the triaxial compression tests TCL1 to TCL5 do not show any clear pattern of behaviour. For the extension tests, at strains before -1.0 % , the curves for TCL6 to TCL8 show that the slopes of the curves decrease with R_p . Also, the slopes of the curves for the normally compressed samples TCL6 , TCL9 and TCL10 are similar.

All tangent stiffnesses presented in this study are tangent stiffnesses calculated by a microcomputer using a program written in BASIC by Woods (1985). A description of the procedure of calculation is also given in Atkinson et al (1986). Basically, to calculate the tangent at a point P on a stress-strain curve, a quadratic function was fitted to the point P and its two neighbouring points using a standard least-squares method. The function was differentiated at all three points and the tangent to point P was taken as the average of the three differentials.

The variation of tangent shear stiffness with shear strain on a logarithmic scale for all simple shear tests and undrained triaxial tests are shown in Figures 7.70 to 7.78. The magnitudes of the shear stiffnesses of the simple shear samples are all below 50 MPa and the magnitudes of the shear stiffnesses of the triaxial samples are all below 100 MPa .

The shear stiffnesses obtained from constant σ_v' simple shear tests are compared with the shear stiffnesses obtained from constant volume simple shear tests in Figures 7.79 to 7.81. A logarithmic scale is used for the values of OCR on the horizontal axes. For the remoulded samples only the results for samples with the same σ_{vp}' of 388 kPa are compared. The definition of σ_{vp}' has been given in Section 2.5.1 and also illustrated in Figure 2.26. It is necessary that the samples compared have similar σ_{vp}' because as each of Figures 7.70, 7.71, 7.73 and 7.75 shows

181

two samples with the same OCR of 1 but with σ_{vp}' at different values of 776 kPa and 388 kPa give different stiffnesses. For the undisturbed samples the method for estimating the values of OCR has been described in Section 7.5.3 . Figures 7.79 to 7.81 illustrate that the shear stiffnesses measured by constant σ_v' and constant volume simple shear tests are the same and that the stiffnesses decrease with increasing OCR . Comparing among Figures 7.79 to 7.81 shows that at the same OCR and γ the shear stiffnesses for all three soils are similar.

For an isotropic elastic material the elastic shear moduli for triaxial tests and simple shear tests are defined in Equations (2.53) and (2.56) respectively. As discussed in Section 2.5.5 , for constant volume simple shear loading $G_{us} = G_s'$ and, similarly, for undrained triaxial loading $G_u = G'$. Therefore, Equation (2.53) shows that G_u is one third of the tangent shear stiffness parameter $dq'/d\mathcal{E}_s^e$ and Equation (2.56) shows that G_{us} is equal to the tangent shear stiffness parameter $d(\tau_v')/d(\gamma^e)$. Based on these definitions, the shear moduli for constant volume simple shear tests and undrained triaxial tests on blue London clay are compared in Figure 7.82. A logarithmic scale is used for the values of OCR and it has been discussed in Section 7.6.1 that the triaxial samples TCL2 and TCL7 with $R_p = 2$ had OCR = 2.7 and the samples TCL3 and TCL8 with $R_p = 4$ had OCR = 6.5 . The value of σ_{vp}' for samples ML5 to ML8 was 388 kPa and the value of p_p' for samples TCL1 to TCL3 and TCL6 to TCL8 was 284 kPa corresponding to σ_{vp}' of 398 kPa so that the values of σ_{vp}' for the simple shear and triaxial samples were similar. The relationship between the simple shear strain parameter γ and the shear strain invariant $\mathcal{E}_s$ has been given in Equation (2.46). For constant volume simple shear tests Equation (2.46) shows that $\mathcal{E}_s$ is equal to $(\sqrt{3}/3)\gamma$. Hence, as indicated in Figure 7.82, for γ values of 0.1 , 0.2 and 0.5 % the corresponding values of $\mathcal{E}_s$ are 0.06 , 0.12 , and 0.29 % respectively.

Figure 7.82(a) shows that the shear moduli G_u for samples TCL2 and TCL3 with OCR = 2.7 and 6.5 respectively have similar values as the interpolated shear moduli G_{us} for the simple shear samples, but G_u for sample TCL1 with OCR = 1 are lower than G_{us}. Figure 7.82(b) shows that G_u for sample TCL6 with OCR = 1 are similar to G_{us}, but G_u for samples TCL7 and TCL8 with OCR = 2.7 and 6.5 respectively are lower than the interpolated values of G_{us}. The orders of magnitude of G_u and G_{us} are similar and are both within 20 MPa.

In Section 3.5.2 results of undrained compression tests on two undisturbed London clay triaxial samples with 98 mm diameter obtained by Jardine et al (1984) showed that at ε_a = 0.1 %, E_u/p_0' are 198 and 228. It has been shown in Section 2.5.5 that for an isotropic elastic material $G_{us} = (1/3)E_u$ for simple shear tests and it can be shown similarly that $G_u = (1/3)E_u$ for triaxial tests. Applying the latter relationship the values of E_u/p_0' at ε_a = 0.1 % obtained by Jardine et al correspond to G_u/p_0' of 66 and 76. Earlier in this section it has been discussed that G_u is one third of $dq'/d\varepsilon_s^e$. Hence, it can be deduced from Figure 7.78 that for samples TUL1 and TUL2, which were undisturbed blue London clay triaxial samples with 100 mm diameter tested in undrained compression, G_u at ε_s = 0.1 % are 10 and 13 MPa respectively. These values of G_u also lie within the order of magnitude of 20 MPa for the G_u and G_{us} values in Figure 7.82. Using the values of p_0' given in Table 6.10 and since for undrained triaxial tests $\varepsilon_a = \varepsilon_s$, G_u/p_0' at ε_a = 0.1 % for tests TUL1 and TUL2 are 60 and 52 respectively which are close to the values obtained by Jardine et al.

In this section the variation of shear stress with shear strain on a logarithmic scale and the variation of tangent shear stiffness with shear strain on a logarithmic scale have been plotted for all simple shear and triaxial tests. These plots show that for simple shear tests the tangent shear stiffnesses decrease with increasing OCR and that for two

samples with the same OCR of 1 the sample with higher $\sigma_{vo}{}'$ has greater stiffnesses. No clear pattern of behaviour was identified for the triaxial compression tests but the stiffnesses for the extension tests decrease with R_p . For the simple shear tests, the stiffnesses measured by constant $\sigma_v{}'$ shearing are the same as the stiffnesses measured by constant volume shearing. At the same OCR and shear strain the stiffnesses of Cowden till, brown London clay and blue London clay are similar. For London clay the shear moduli G_u and G_{us} have similar orders of magnitude.

, ᐟ

7.7.2   Tangent stiffnesses from probing tests

The q' versus ε_s curves for probing tests TUB1 and TUL5 have been given in Figure 6.24 which shows that all the curves are linear except the curve for the undrained probe AC of test TUL5 . The variation of shear stress with shear strain on a logarithmic scale are shown in Figures 7.83 and 7.84.

Since the undisturbed London clay samples are heavily overconsolidated, theoretically the strains caused by the probes are purely elastic as stated in Section 2.5.5. As elastic strains are fully recoverable on unloading the states of the sample at the beginning of each probe should be the same and unaffected by previous probing. This was the reason for adopting the test procedure which used just one sample for various probes. It can be seen from Figure 5.17 that in test TUB1 the last probe O'P' has the same stress path as the second probe O'C' and it can be seen from Figure 5.18 that in test TUL5 the last probe A'S' has the same stress path as the third probe A'F' . The purpose of carrying out probes O'P' and A'S' was to compare the stiffnesses measured at the end of a test with the stiffnesses for the same probe measured at an early stage of the test. The differences in these stiffnesses will serve as indications of the amount of disturbance caused by probing and, hence, whether the testing procedure is acceptable.

Furthermore, Figure 5.17 shows that before each probe started from state O' the stress path would have travelled at least 25 kPa along a path in the same direction as the probe. Also, Figure 5.18 shows that before each probe started from state A' the stress path would have travelled at least 50 kPa along a path in the same direction as the probe. These were precautions taken to eliminate threshold effects which have been studied by Richardson (1988). In both tests the length of each path travelled before reaching the starting state was at least 25 % of the p_o' value of the probe as recommended by Richardson.

The tangent stiffnesses measured from the probing tests are given in Figures 7.85 and 7.86. Since the $q' - \varepsilon_s$ curves for all the drained probes, shown in Figure 6.24, are linear the tangent stiffnesses for these probes are constants. For probes O'C' and O'P' of test TUB1 , Figure 7.85(b) shows that the difference in bulk stiffness is 1 MPa while the bulk stiffnesses for all probes range from 5 to 15 MPa . Figure 7.85(d) shows that the difference in the stiffness parameter $dp'/d\varepsilon_s$ is 5 MPa . For probes A'F' and A'S' of test TUL5 , Figure 7.86(a) shows that the difference in shear stiffness is 2 MPa while the shear stiffnesses for all probes range from 13 to 36 MPa . Figure 7.86(c) shows that the difference in the stiffness parameter $dq'/d\varepsilon_v$ is 9 MPa . These differences in stiffnesses are considered to be small compared with the ranges of values measured for all probes and the test procedure followed is considered to be acceptable.

The stress-strain behaviours of isotropic and anisotropic elastic material have been described in Section 2.4.1. It has been explained that the relationships between increments of stress and strain for isotropic material are decoupled whereas those for anisotropic material are coupled. For the undisturbed London clay samples, Figure 6.22(a) shows that for the constant q' probes O'B' and O'C' the shear strains ε_s are not equal to zero and Figures 6.23(e) and (g) show that for the constant q' probes A'L' and A'M'

the strains ε_s are also non-zero. Figure 6.22(f) shows that for the constant p' probes O'H' and O'J' the volumetric strain ε_v are not equal to zero and Figures 6.23(b) and (d) show that for the constant p' probes A'E' and A'F' the strains ε_v are also non-zero. Hence, the material was anisotropic.

Since London clay was formed by deposition as described in Section 4.3.2 the material is likely to be cross-anisotropic as suggested in Section 2.4.1. The stress-strain behaviour of a cross-anisotropic elastic material are given by Equations (2.61a) and (2.61b) with the parameters A^e to D^e as shown in Appendix A. Equation (A.2) shows that theoretically B^e is equal to C^e. It can be deduced from Equation (2.61a) that A^e is equal to $1/(dq'/d\varepsilon_s^e)$ for a constant p' probe and B^e is equal to $1/(dp'/d\varepsilon_s^e)$ for a constant q' probe. Similarly, it can be deduced from Equation (2.61b) that C^e is equal to $1/(dq'/d\varepsilon_v^e)$ for a constant p' probe and D^e is equal to $1/(dp'/d\varepsilon_v^e)$ for a constant q' probe. Hence, values of A^e to D^e for tests TUB1 and TUL5 can be obtained from Figures 7.85 and 7.86. For the drained probes, since the tangent stiffnesses are constants the parameters A^e to D^e are also constants. Figure 7.85(d) shows that B^e obtained from probes O'B' and O'C' are both 0.040 MPa^{-1} and Figure 7.85(c) shows that C^e obtained from probes O'H' and O'J' are 0.048 MPa^{-1} and 0.042 MPa^{-1} respectively. Figure 7.86(d) shows that B^e obtained from probes A'L' and A'M' are both 0.020 MPa^{-1} and Figure 7.86(c) shows that C^e obtained from probes A'E' and A'F' are 0.017 MPa^{-1} and 0.024 MPa^{-1} respectively. Therefore, in each of tests TUB1 and TUL5 the values of B^e and C^e obtained are very close as predicted by theory.

For the probes which were neither constant q' nor constant p' probes, a comparison is made in Figures 7.87 to 7.90 between strains ε_s and ε_v measured experimentally and strains predicted by Equations (2.61a) and (2.61b). Each

predicted shear strain ε_s was calculated from Equation (2.61a) using the value of A^e obtained from the adjacent constant p' probes and the value of B^e obtained from the adjacent constant q' probe. Similarly, each predicted volumetric strain ε_v was calculated from Equation (2.61b) using the value of C^e obtained from the adjacent constant p' probe and the value of D^e obtained from the adjacent constant q' probe. For example, for probe O'L' in Figure 7.87(a) the adjacent constant p' probe was O'H' and the value of A^e given by O'H' can be deduced from Figure 7.85(a) as $1/(34)$ MPa^{-1}. The constant q' probe adjacent to O'L' was O'C' and the value of B^e given by O'C' can be deduced from Figure 7.85(d) as $1/(25)$ MPa^{-1}. For probe O'L' the values of $\delta q'$ and $\delta p'$ have been shown in Figure 5.17 as -28 and 28 kPa respectively. Substituting these values of A^e, $\delta q'$, B^e and $\delta p'$ into Equation (2.61a) gave the predicted $\delta \varepsilon_s^e$ of 0.030 % plotted in Figure 7.87(a). Figures 7.87 to 7.90 demonstrate that for undisturbed London clay the elastic parameters A^e to D^e measured from constant q' and constant p' paths can be used to give good predictions of the elastic strains caused by other paths in other directions.

It can be concluded that for drained loading inside the state boundary surface the elastic stress-strain behaviour of undisturbed London clay is linear and anisotropic. It has been demonstrated that following the testing procedure described in Section 5.12 a single sample can be used to give acceptable test data for more than one probe in a test. The elastic parameters A^e to D^e of Equations (2.61a) and (2.61b) have been obtained from the constant q' and constant p' probes and the experimental results agree with the theory that B^e is equal to C^e. Equations (2.61a) and (2.61b) together with the measured values of A^e to D^e gave good predictions of the elastic shear and volumetric strains caused by the different probes in different directions.

7.7.3   Normalised tangent stiffnesses from simple shear and triaxial tests

The variation of normalised tangent shear stiffness with shear strain on a logarithmic scale for the simple shear tests and undrained triaxial tests are shown in Figures 7.91 to 7.99. The magnitudes of the normalised shear stiffnesses of the simple shear samples are all below 110 and the magnitudes of the normalised shear stiffnesses of the triaxial samples are all below 220 . It has been shown in Section 2.6.4 that for constant σ_v' and constant volume simple shear tests, the variation of normalised tangent shear stiffness $d\tau_v'/(v\sigma_v'd\gamma)$ with the multiple of specific volume and shear strain $v\gamma$ is the same for normally compressed samples with any pre-shearing state. By analogy, it can be shown that for both constant p' and undrained triaxial tests, the variation of $dq'/(vp'd\epsilon_s)$ with $v\epsilon_s$ is the same for normally compressed samples with any pre-shearing state. For constant σ_v' simple shear tests on normally compressed samples, Figure 7.91(a) shows that the normalised stiffnesses for sample MC1 with σ_{vo}' of 388 kPa are the same as the normalised stiffnesses for sample MC9 with σ_{vo}' of 776 kPa . For constant volume simple shear tests on normally compressed samples, Figure 7.91(b) shows that the normalised stiffnesses for sample MC5 with σ_{vo}' of 388 kPa are the same as the normalised stiffnesses for sample MC10 with σ_{vo}' of 776 kPa . Similar experimental evidence can be seen in Figures 7.92(a), 7.94(a), 7.96(a) and (b).   For undrained triaxial tests on normally compressed samples, Figure 7.98 shows that in compression samples TCL1 , TCL4 and TCL5 which had different pre-shearing states have the same normalised stiffnesses and in extension samples TCL6 , TCL9 and TCL10 which had different pre-shearing states also have the same normalised stiffnesses.

The normalised shear stiffnesses obtained from constant σ_v' simple shear tests are compared with the normalised shear stiffnesses obtained from constant volume simple shear tests in Figures 7.100 to 7.102.   A logarithmic scale is used for the values of OCR on the horizontal axes.   The method for

estimating the values of OCR for the undisturbed samples has been described in Section 7.5.3. Figures 7.100 to 7.102 illustrate that the normalised shear stiffnesses measured by constant σ_v' and constant volume simple shear tests are the same and that the normalised stiffnesses increase with OCR. The remoulded samples of each material show that at OCR = 1 the same normalised shear stiffnesses are obtained irrespective of pre-shearing state and whether the sample was sheared under constant σ_v' or constant volume condition. Comparing among Figures 7.100 to 7.102 shows that at the same OCR and γ the normalised shear stiffnesses of Cowden till are higher than those of London clay and the normalised shear stiffnesses of brown and blue London clay are similar.

For the undrained triaxial tests the variation of normalised shear stiffnesses with R_p is shown in Figure 7.103. In compression, the normalised stiffnesses increase with R_p and in extension, the normalised stiffnesses decrease with R_p.

The definitions of the shear modulus for undrained triaxial tests G_u and the shear modulus for constant volume simple shear tests G_{us} have been given in Section 7.7.1. A comparison of the normalised shear moduli for undrained triaxial tests and constant volume simple shear tests on blue London clay is shown in Figure 7.104. A logarithmic scale is used for the values of OCR. The correspondence between the values of the shear strain parameters γ and ε_s have been discussed in Section 7.7.1. Figure 7.104(a) shows that the normalised shear moduli $G_u/(vp')$ for samples TCL2 and TCL3 have similar values as the interpolated normalised shear moduli $G_{us}/(v\sigma_v')$ for the simple shear tests, but $G_u/(vp')$ for sample TCL1 are lower than $G_{us}/(v\sigma_v')$. Figure 7.104(b) shows that $G_u/(vp')$ for sample TCL6 are similar to $G_{us}/(v\sigma_v')$, but $G_u/(vp')$ for samples TCL7 and TCL8 are lower than the interpolated values of $G_{us}/(v\sigma_v')$. The orders of magnitude of $G_u/(vp')$ and $G_{us}/(v\sigma_v')$ are similar and are both within 60.

It has been described in Section 3.5.1 that Ng (1988) performed undrained compression tests on K_o compressed

189

reconstituted Cowden till triaxial samples with 38 mm diameter at different overconsolidation ratios. The results showed that at ε_s = 0.06 % , $dq'/(vp'd\varepsilon_s)$ ranged from 40 to 195 corresponding to $G_u/(vp')$ of 13 to 65 . Figure 7.100(a) shows that for the constant volume simple shear tests on remoulded Cowden till, at γ = 0.1 % which corresponds to ε_s = 0.06 % , $d\tau_v'/(v\sigma_v'd\gamma)$ which corresponds to $G_{us}/(v\sigma_v')$ range from 28 to 59 . Therefore, the orders of magnitude of $G_u/(vp')$ and $G_{us}/(v\sigma_v')$ for Cowden till are similar.

In this section the variation of normalised tangent shear stiffnesses with shear strain on a logarithmic scale for simple shear tests and triaxial tests have been presented. The magnitudes of the normalised shear stiffnesses of the simple shear samples and triaxial samples are within 110 and 220 respectively. It is demonstrated that, for constant σ_v' and constant volume simple shear tests and for undrained triaxial tests, as theory predicts, the normalised tangent shear stiffnesses of the normally compressed samples are independent of their pre-shearing states. For simple shear tests the normalised stiffnesses increase with OCR and normalised stiffnesses measured from constant σ_v' shearing are the same as those measured from constant volume shearing. At the same OCR and shear strain the normalised stiffnesses of Cowden till are higher than those of London clay and the normalised stiffnesses of brown and blue London clay are similar. For undrained triaxial tests, the normalised stiffnesses increase with R_p in compression and decrease with R_p in extension. For both London clay and Cowden till, the normalised shear moduli $G_u/(vp')$ and $G_{us}/(v\sigma_v')$ have similar orders of magnitude.

7.7.4   Normalised tangent stiffnesses from probing tests

The normalised tangent shear stiffnesses for probing tests TUB1 and TUL5 and the normalised tangent bulk stiffnesses for the constant q' probes of the two tests are plotted in Figures 7.105 and 7.106 respectively. The purpose of these plots is to compare the normalised stiffnesses for the

corresponding probes of the two tests. All the normalised tangent stiffnesses shown in Figures 7.105 and 7.106, apart from the normalised shear stiffnesses for probes O'L' and O'M' , are close to constant over the strains caused by the probes. Figure 7.105 shows that the normalised shear stiffnesses for the probes of test TUB1 which had lower effective stresses are higher than the normalised shear stiffnesses for the corresponding probes of test TUL5 which had higher effective stresses. Figure 7.106 shows that similar normalised bulk stiffnesses were obtained for all four constant q' probes which were along the swelling lines. It can be deduced from Equation (2.124) that for an isotropic material the normalised tangent bulk stiffness for a state path along the swelling line is equal to $1/\kappa$. The average of the normalised bulk stiffnesses shown in Figure 7.106 is 33 giving an estimated value for κ of 0.030 which is of the same order of magnitude as the values shown in Table 6.2.

It can be concluded that normalised tangent stiffnesses for the drained probes are constant and the normalised shear stiffnesses for the probes with lower effective stresses are higher than the normalised shear stiffnesses for the corresponding probes which had higher effective stresses. The normalised bulk stiffnesses for the constant q' probes which were paths along the swelling line are similar and give a reasonable estimate of κ .

7.7.5   Summary

For simple shear tests, plots of tangent shear stiffness against shear strain on a logarithmic scale show that the stiffnesses decrease with OCR and increase with pre-shearing stresses. The tangent shear stiffnesses obtained from constant σ_v' shearing are the same as those obtained from constant volume shearing. For undrained triaxial extension tests, the tangent shear stiffnesses decrease with R_p . For London clay, the shear moduli for undrained triaxial

tests G_u have the same order of magnitude as the shear moduli for constant volume simple shear tests G_{us} .

Results of the probing tests show that for drained loading inside the state boundary surface the elastic stress-strain behaviour of undisturbed London clay are linear and anisotropic. The elastic parameters A^e to D^e of Equations (2.61a) and (2.61b) have been measured from the constant q' and constant p' probes. Using these measured values of A^e to D^e the elastic shear strains and elastic volumetric strains caused by drained probes in any direction and within the state boundary surface can be predicted.

Experimental results agree with theoretical prediction that for normally compressed simple shear and triaxial samples the variation of normalised tangent shear stiffness with shear strain is independent of pre-shearing state. For simple shear tests, the normalised shear stiffnesses increase with OCR and the normalised shear stiffnesses measured from constant σ_v' shearing were the same as those measured from constant volume shearing. At the same OCR and shear strain the normalised stiffnesses of Cowden till are higher than those of London clay and the normalised stiffnesses of brown and blue London clay are similar. For undrained triaxial tests, the normalised stiffnesses increase with R_p in compression and decrease with R_p in extension. For both London clay and Cowden till the normalised shear moduli for undrained triaxial tests $G_u/(vp')$ have the same order of magnitude as the normalised shear moduli for constant volume simple shear tests $G_{us}/(v\sigma_v')$.

The normalised tangent stiffnesses for the drained probes are constants and the normalised shear stiffnesses for the probes at lower effective stresses are higher than the normalised shear stiffnesses for the corresponding probes at higher effective stresses.

8.1   Conclusions for one-dimensional compression and consolidation

During one-dimensional compression and swelling the behaviours of Cowden till and London clay are governed by Equations (2.75) and (2.76) for simple shear tests and by analogous equations for shear box and triaxial tests. The values of the parameters in these equations measured from remoulded, reconstituted and undisturbed simple shear and shear box samples are similar. The normal compression lines obtained from samples prepared by the different methods and compressed in the different equipment tend to converge with increasing effective stresses.

For both Cowden till and London clay the values of the coefficient of consolidation c_v and the values of the coefficient of permeability k measured from remoulded and undisturbed simple shear samples are similar to those measured from undisturbed oedometer samples.

8.2   Conclusions for critical states

For simple shear tests, the critical states on the σ_v' , τ_v' plane are described by critical state lines represented by Equation (2.97). The value of ρ_{cs}' is dependent on whether the sample was sheared under constant σ_v' or constant volume condition and on the pre-shearing value of OCR. The values of the angle of rotation of principal stresses θ_{cs} for constant volume shearing are significantly higher than that for constant σ_v' shearing. The geometry of the Mohr's circle of stress shows that the higher values of θ_{cs} caused the higher values of ρ_{cs}' . A theoretical relationship between ρ_{cs}' and the pre-shearing value of K_o which is a function of OCR has been proposed. This proposed relationship, represented by

Equation (2.102), gives good predictions of the experimental results. For normally compressed samples the relationship is better suited for constant σ_v' shearing than for constant volume shearing. The proposed representation of the critical state line on the σ_v', v plane, represented by Equation (2.109), agrees reasonably well with the experimental data. Using relationships based on Equations (2.102) and (2.109) the normalised critical states can also be predicted.

For triaxial tests, the reconstituted London clay samples behaved as critical state theory predicts. In each of compression and extension loading a unique critical state line described by Equations (2.93) and (2.94) exists and the values of the critical state constants M , Γ and λ have been obtained. When normalised the critical states become a critical state point for each of compression and extension.

The shear stresses $(\tau_v')_{cs}$ measured from constant volume simple shear tests are lower than c_u calculated from Equation (2.96) using triaxial test results. Values of c_u estimated from ϕ_{cs}' together with simple shear parameters $(\tau_v')_{cs}$ and ρ_{cs}' are slightly higher than the corresponding values of $(\tau_v')_{cs}$ but are also lower than c_u calculated from triaxial test results.

8.3   Conclusions for state paths

The general patterns of the state paths obtained from simple shear tests and triaxial tests are similar. The stress path for a simple shear test was plotted in terms of p' and q' using the relationship represented by Equation (3.4) together with assumptions for σ_2' . This suggests that the effective stress paths for simple shear tests and triaxial tests when plotted together on p' , q' plane have different shapes and reach different states at critical state.

The overall pattern of the normalised state paths for simple

shear tests and triaxial tests are in agreement with the critical state model. For simple shear tests, the exact shapes of the normalised paths for constant σ_v' tests are different to those for constant volume tests. Therefore, it has not been possible to identify a unique state boundary surface. Modified Cam-clay gives good predictions of the Roscoe surface for remoulded Cowden till but not for remoulded London clay. For triaxial tests on London clay, the undisturbed samples have significantly lower peak normalised shear stresses than the reconstituted samples.

8.4   Conclusions for stiffnesses

For simple shear tests, the tangent shear stiffnesses for Cowden till and London clay decrease with OCR and increase with pre-shearing stresses. The tangent shear stiffnesses obtained from constant σ_v' shearing are the same as those obtained from constant volume shearing. For undrained triaxial extension tests, the tangent shear stiffnesses decrease with R_p. For London clay, the shear moduli for undrained triaxial tests G_u and the shear moduli for constant volume simple shear tests G_{us}, based on definitions given by Equations (2.53) and (2.56) respectively, have the same order of magnitude.

For drained loading inside the state boundary surface, the elastic stress-strain behaviour of undisturbed London clay is linear and anisotropic. Using Equations (2.61a) and (2.61b), with the elastic parameters A^e to D^e measured by constant q' and constant ·p' stress paths, the elastic shear strains and elastic volumetric strains caused by drained stress paths in any direction can be predicted.

Experimental results agree with theoretical predictions that for normally compressed simple shear and triaxial samples the variation of normalised tangent shear stiffness with shear strain is independent of pre-shearing state. For simple shear tests, the normalised shear stiffnesses increase with

OCR and the normalised shear stiffnesses measured from constant σ_v' shearing are the same as those measured from constant volume shearing. At the same OCR and shear strain the normalised stiffnesses of Cowden till are higher than those of London clay. For undrained triaxial tests, the normalised shear stiffnesses increase with R_p in compression and decrease with R_p in extension. For both London clay and Cowden till, the normalised shear moduli for undrained triaxial tests $G_u/(vp')$ have the same order of magnitude as the normalised shear moduli for constant volume simple shear tests $G_{us}/(v\sigma_v')$.

For drained loading inside the state boundary surface, the normalised tangent shear stiffnesses and normalised tangent bulk stiffnesses are constants for each path. The normalised shear stiffnesses decrease with increasing pre-loading effective stresses.

8.5   Practical implications of conclusions

Because of the problems with the simple shear apparatus described in Section 3.3 , simple shear tests are not as widely used to obtain parameters for design as triaxial tests. The conclusions in Sections 8.1 to 8.4 show that simple shear tests can be used to measure stiffnesses but not strengths of soils. Section 8.1 shows that results of one-dimensional compression and consolidation measured from simple shear tests can be treated as oedometer test results. Sections 8.2 and 8.3 show that the effective stress strength parameters ρ_{cs}' and Γ_s from simple shear tests are not soil constants but are dependent on the overconsolidation ratio of the soil and the drainage conditions during loading. Also, the shear stresses $(\tau_v')_{cs}$ obtained from constant volume simple shear tests are different to the undrained shear strengths obtained from triaxial tests. Hence, the simple shear parameters ρ_{cs}' , Γ_s and $(\tau_v')_{cs}$ cannot be used as strength parameters for a soil except for the special case when strengths along the horizontal plane are

required. Section 8.4 shows that the stiffnesses obtained from simple shear tests and triaxial tests have the same orders of magnitude. Moreover, the trends of behaviour of the stiffness parameters for both types of tests are affected by similar factors including overconsolidation ratio and current state of the soil. Therefore, the practical applications of the stiffnesses measured from simple shear tests are expected to be similar to triaxial tests.

8.6 Recommendations for further work

The results of this study show that for simple shear tests the pre-shearing value of OCR has important effects on the critical state and stiffness parameters measured. Since most of the overconsolidated remoulded simple shear samples tested were normally compressed to σ_{vp}' of 388 kPa before swelling, a suggestion for further work is to perform more series of tests on remoulded samples with different values of σ_{vp}'.

The analyses of the simple shear test results in this study have concentrated mainly on critical states rather than peak τ_v'/σ_v' states. More tests on remoulded samples with a wider and more comprehensive range of OCR values are needed to study the state boundary surface for overconsolidated samples.

Further understanding of the behaviour of clays in simple shear with reference to the critical state model will require measuring the complete stress states of samples with different OCR values. Data from such measurements can lead to improvements for Equations (2.102) and (2.109) which describe the effects of OCR on critical states. Also, with the complete stress states known, the stress paths for simple shear tests and triaxial tests can be compared on the p' , q' plane and the stiffness parameters for the two types of test can be compared directly.

197

APPENDIX A   Expressions for anisotropic elastic parameters

The elastic parameters A^e to D^e of Equations (2.61a) and (2.61b) have been given by Clinton (1987) as

$$A^e = \frac{2}{9}\left[\frac{2(1+2\nu_{vh}')}{E_v'} + \frac{1-\nu_{hh}'}{E_h'}\right] \tag{A.1}$$

$$B^e = C^e = \frac{2}{3}\left(\frac{1-\nu_{vh}'}{E_v'} + \frac{\nu_{hh}'-1}{E_h'}\right) \tag{A.2}$$

$$D^e = \frac{1-4\nu_{vh}'}{E_v'} + \frac{2(1-\nu_{hh}')}{E_h'} \tag{A.3}$$

where the elastic parameters E_v', E_h', ν_{vh}', ν_{hh}' and G_{vh}' are as defined in Section 2.4.1.

However, only the two parameters E_v' and ν_{vh}' can be expressed in terms of A^e, B^e and D^e as

$$E_v' = \frac{9}{9A^e + 6B^e + D^e} \tag{A.4}$$

$$\nu_{vh}' = \frac{9(3A^e + B^e)}{2(9A^e + 6B^e + D^e)} - 1 \tag{A.5}$$

The parameters E_h' and ν_{hh}' cannot be expressed in terms of A^e, B^e and D^e separately, but only as

$$\frac{1-\nu_{hh}'}{E_h'} = \frac{9A^e - 12B^e + 4D^e}{18} \tag{A.6}$$

(a)   Expressions for the parameters A_s to D_s

For the Roscoe surface, substituting Equations (2.130) and (2.131) into Equations (2.70) and (2.71) and rearranging, the parameters A_s to D_s in Equations (2.149) and (2.150) can be obtained as

$$A_s = \frac{(\lambda_s - \kappa_s)(4\,\eta_s'^2)}{(\tan^2\rho_{cs}' - \eta_s'^2)(\tan^2\rho_{cs}' + \eta_s'^2)} + \mu_s'\,\kappa_s \qquad (B.1)$$

$$B_s = C_s = \frac{(\lambda_s - \kappa_s)(2\,\eta_s')}{\tan^2\rho_{cs}' + \eta_s'^2} \qquad (B.2)$$

$$D_s = \frac{(\lambda_s - \kappa_s)(\tan^2\rho_{cs}' - \eta_s'^2)}{\tan^2\rho_{cs}' + \eta_s'^2} + \kappa_s \qquad (B.3)$$

where μ_s' is as defined in Equation (2.127).

For the Hvorslev surface, substituting Equations (2.132) and (2.133) into Equations (2.70) and (2.71) and rearranging, the parameters A_s to D_s in Equations (2.149) and (2.150) can be obtained as

$$A_s = \mu_s'\,\kappa_s - \frac{\lambda_s}{(\eta_s' - h_s)[(\kappa_s/\lambda_s)(\eta_s' - h_s) + h_s]} \qquad (B.4)$$

$$B_s = C_s = \frac{\lambda_s}{(\eta_s' - h_s)} \qquad (B.5)$$

$$D_s = \kappa_s - \frac{\lambda_s}{(\eta_s' - h_s)}\left[\left(\frac{\kappa_s}{\lambda_s}\right)(\eta_s' - h_s) + h_s\right] \qquad (B.6)$$

(b)   Derivation of the relationship between $\delta\eta_s'$ and $v\,\delta\gamma$ for

constant volume tests on normally consolidated samples

Although the critical state model and the normalising of test data have been described mostly in terms of simple shear parameters, the derivation here will be given in terms of the more familiar triaxial parameters so that it can be followed more easily. The same procedures are applicable for simple shear tests.

The Roscoe surface in the Modified Cam-clay model is

$$v = \Gamma - \lambda \ln p' - (\lambda - \kappa) \ln \left(\frac{M^2 + \eta'^2}{2M^2} \right) \tag{B.7}$$

Differentiating and dividing by v ,

$$\delta\varepsilon_v = -\frac{\delta v}{v} = \left[\frac{\lambda}{vp'} \right] \delta p' + \left[\frac{(\lambda - \kappa)}{v} \left(\frac{2\,\eta'}{M^2 + \eta'^2} \right) \right] \delta\eta' \tag{B.8}$$

The elastic volumetric strains are given by

$$\delta\varepsilon_v^e = \frac{\kappa}{vp'} \, \delta p' \tag{B.9}$$

Subtracting $\delta\varepsilon_v^e$ from $\delta\varepsilon_v$,

$$\delta\varepsilon_v^p = \left[\frac{(\lambda - \kappa)}{vp'} \right] \delta p' + \left[\frac{(\lambda - \kappa)}{v} \left(\frac{2\,\eta'}{M^2 + \eta'^2} \right) \right] \delta\eta' \tag{B.10}$$

Multiplying Equation (B.10) by the flow parameter $2\eta'/(M^2 - \eta'^2)$,

$$\delta\varepsilon_s^p = \left[\frac{(\lambda - \kappa)(2\,\eta')}{vp'(M^2 - \eta'^2)} \right] \delta p' + \left[\frac{(\lambda - \kappa)(4\,\eta'^2)}{v(M^2 + \eta'^2)(M^2 - \eta'^2)} \right] \delta\eta' \tag{B.11}$$

The elastic shear strains are given by

$$\delta \varepsilon_s^e = \frac{\mu'\kappa}{vp'} \, \delta q' \qquad (B.12)$$

where

$$\mu' = K'/(3G') \qquad (B.13)$$

Adding $\delta \varepsilon_s^e$ to $\delta \varepsilon_s^p$,

$$v \, \delta \varepsilon_s = \left[\mu'\kappa \right] \frac{\delta q'}{p'} + \left[\frac{(\lambda - \kappa)(2\eta')}{(M^2 - \eta'^2)} \right] \frac{\delta p'}{p'} + \left[\frac{(\lambda - \kappa)(4\eta'^2)}{(M^2 + \eta'^2)(M^2 - \eta'^2)} \right] \delta \eta' \qquad (B.14)$$

To obtain a relationship between $\delta p'/p'$ and $\delta \eta'$, using Equation (B.8), for $\delta \varepsilon_v = 0$,

$$\frac{\delta p'}{p'} = -\left[\frac{(\lambda - \kappa)(2\eta')}{\lambda(M^2 + \eta'^2)} \right] \delta \eta' \qquad (B.15)$$

To obtain a relationship between $\delta q'/p'$ and $\delta \eta'$, using Equations (2.71), (2.130) and (2.131) in terms of triaxial parameters, for $\delta \varepsilon_v = 0$,

$$\frac{\delta q'}{p'} = -\left[\frac{\lambda(M^2 - \eta'^2) + 2\kappa \eta'^2}{(\lambda - \kappa)(2\eta')} \right] \frac{\delta p'}{p'} \qquad (B.16)$$

Substituting Equation (B.15) into Equation (B.16) gives

$$\frac{\delta q'}{p'} = \left[\frac{\lambda(M^2 - \eta'^2) + 2\kappa \eta'^2}{\lambda(M^2 + \eta'^2)} \right] \delta \eta' \qquad (B.17)$$

Substituting Equations (B.15) and (B.17) into Equation (B.14) and rearranging,

$$v \; \delta\mathcal{E}_s = \left\{ \frac{\mu'\mathcal{K}(M^2-\eta'^2)[\lambda(M^2-\eta'^2)+2\mathcal{K}\eta'^2] + \mathcal{K}(\lambda-\mathcal{K})(4\eta'^2)}{\lambda(M^2+\eta'^2)(M^2-\eta'^2)} \right\} \delta\eta' \qquad (B.18)$$

An analogous equation can be written for simple shear tests.

APPENDIX C   Estimation of inaccuracy in volumetric strain due to deformation of reinforced membrane of simple shear apparatus

The reinforced membrane is considered here as a thin ring with diameter d , thickness t and height h as shown in Figure C.1 .   If the internal stress is uniformly distributed and has a value of σ_r , then the stresses acting on a diametric cross-section are as shown in Figure C.1(a) where σ_t is the tangential stress in the ring.   To satisfy equilibrium of forces,

$$2 \; h \; t \; \sigma_t = h \; d \; \sigma_r \qquad (C.1)$$

For a change of internal stress from σ_r to $\sigma_r + \delta\sigma_r$, Equation (C.1) becomes

$$2 \; h \; t \; (\sigma_t + \delta\sigma_t) = h \; d \; (\sigma_r + \delta\sigma_r)$$

giving $$\delta\sigma_t = \delta\sigma_r \; d \; / \; (2 \; t) \qquad (C.2)$$

Assuming the ring deforms elastically,

$$\delta\mathcal{E}_t = \delta\sigma_t \; / \; E \qquad (C.3)$$

where $\delta\mathcal{E}_t$ is the tangential strain increment and E is the Young's modulus of the ring.   But,

$$\delta\mathcal{E}_t = \frac{\delta(2\pi r)}{2\pi r} = \frac{\delta r}{r} = \delta\mathcal{E}_r \qquad (C.4)$$

where $r = d/2$ and $\delta\varepsilon_r$ is the radial strain increment. Combining Equations (C.2) to (C.4),

$$\delta\varepsilon_r = \delta\sigma_r \, d \, / \, (2 \, t \, E) \qquad\qquad (C.5)$$

The thickness and the Young's modulus of the reinforcement wire of the standard reinforced membrane are given in Section 5.3.1 as 0.15 mm and 152×10^3 MPa respectively. Using these values as t and E of the ring, for every 100 kPa change of internal stress, the radial strain increment is given by Equation (C.5) as 0.018 % . This will give rise to an error of 0.036 % in the volumetric strain measurement.

Since the radial stress acting on the membrane varied for each individual test, the inaccuracies involved were test dependent. The maximum change in vertical stress that occurred during shearing in any of the tests performed was about 400 kPa. By taking half of this value i.e. 200 kPa as the maximum change in radial stress, the resulting error in volumetric strain can be expected to be 0.07 % . For tests with less changes in normal stresses the errors involved were smaller.

APPENDIX D   Effect of pins on shear strain and slips in simple shear tests

The effect of the pins on the uniformity of strains was investigated by Airey (1984) using radiographic techniques. The radiographs indicated that the uniformity of strains was affected by the pins to varying degrees depending on the test procedure for shearing, stage of shearing and the part of the sample considered. In general, the pins inhibit shear strains over most of their height but the rest of the sample strained approximately uniformly. No reliable method for estimating the error involved in the measurement of shear strains was recommended.

If it is assumed that the pins prevented any shear strains from developing over a certain distance from the horizontal boundaries, then the effect would be to reduce the sample height as illustrated in Figure D.1 . Figure D.2 shows how a typical shear stress τ_v' versus shear strain γ curve would be affected by reductions of effective sample height. It seems that the effects are significant only at large values of γ .

Slips which occurred in some of the tests might have affected mainly the shapes of the $\tau_v' - \gamma$ curves obtained. In the beginning of the study it was not certain what caused the slips. One possible method for estimating the inaccuracies introduced by slipping is to choose a test which was affected by slip and repeat the test until no slip occurs to compare the results.

Later, it was found that, during setting up, by pushing the pedestal firmly towards the clamping device at the base of the apparatus in the direction of the applied horizontal load, the number of slips appeared to be greatly reduced. So, it is possible that most slips which occurred in the earlier tests were due to movement of the pedestal to take up slacks between itself and the clamping device.

APPENDIX E   Excess pore pressures in simple shear samples during shearing

In all simple shear tests performed, drainage was allowed all the time and no back pressure was applied. Therefore, if the pore pressure in the sample was allowed to come to equilibrium the steady-state pore pressure was zero. During shearing, changes of total stresses applied resulted in changes of pore pressures and, hence, excess pore pressures in the samples. The magnitudes of these excess pore pressures depended on the rates at which pore pressures were generated and the rates at which pore pressures dissipated. The rates at which pore pressures were generated were controlled by the

rate of shearing used and the rates at which pore pressures dissipated were controlled by the consolidation properties of the soils and the drainage condition.

Although slower rates of shearing would give rise to smaller excess pore pressures, it was necessary to have a rate of shearing that would allow the tests to be completed in a reasonable time. The purpose of this appendix is to demonstrate that the rate of shearing used was slow enough to allow the excess pore pressures to dissipate so that the remaining excess pore pressures were within acceptable limits. Three methods, one theoretical and two experimental, were used to assess the excess pore pressures and their effects on the tests performed.

Method 1

This is a theoretical calculation based on an approach proposed by Atkinson (1984b). The routine methods for calculating loading rates given by Bishop and Henkel (1962) are not used here because they may lead to unnecessarily slow rates for tests in which stress-strain curves are required.

For a simple shear test in which no dissipation of pore pressure is allowed, the change of pore pressure is related to changes in total stresses by an equation of the form

$$\delta u = \delta \sigma_v + \alpha_s \, \delta \tau_v \qquad (E.1)$$

where α_s is an empirical parameter. For a test in which drainage is allowed, if the total stress increments $\delta \sigma_v$ and $\delta \tau_v$ were applied suddenly, the excess pore pressures generated will be

$$\bar{u} = (1 - U_t)(\delta \sigma_v + \alpha_s \, \delta \tau_v) \qquad (E.2)$$

where U_t is the degree of dissipation which varies with elapsed time t after the stress increments have been applied. The rate at

which the excess pore pressures dissipate is given by Bishop and Henkel as

$$t = \frac{\mu\, t_1}{1 - U_t} \qquad\qquad (E.3)$$

where μ depends only on the drainage conditions and t_1 may be obtained from the results of one-dimensional consolidation using the $\sqrt{}$(time) curve fitting method described in Section 2.5.2. Eliminating $(1 - U_t)$ from Equations (E.2) and (E.3)

$$\bar{u} = \frac{\mu\, t_1}{t} (\delta\sigma_v + \alpha_s\, \delta\tau_v) \qquad\qquad (E.4)$$

If the value of α_s for each increment of total stresses could be determined, then Equation (E.4) can be used to obtain the variation of the magnitudes of the excess pore pressures with time for each increment of total stresses.

Figure E.1 shows how α_s can be determined for three different types of shearing on three normally consolidated samples with the same pre-shearing states. Figure E.1(a) shows the total stress path AB and effective stress path AC of a sample sheared undrained with no dissipation of pore pressures allowed. Since $\delta\sigma_v = 0$, Equation (E.1) gives

$$\alpha_s = \delta u / \delta\tau_v \qquad\qquad (E.5)$$

Figure E.1(b) shows the stress paths for a constant volume test with drainage allowed and zero pore pressure all the time. For this test the total stress path AC coincides with the effective stress path which is also the same as the effective stress path for an undrained test. Since $\delta u = 0$, Equation (E.1) gives

$$\alpha_s = - \delta\sigma_v / \delta\tau_v \qquad\qquad (E.6)$$

Figure E.1(c) shows the stress paths for a constant σ_v' test with

drainage allowed and zero pore pressure all the time. For this test
the total stress path AD coincides with the effective stress path.
Because $\delta u = \delta\sigma_v = 0$, the value of α_s cannot be determined from
Equation (E.1). It is assumed that during shearing if the test
condition was suddenly changed at any point E from constant σ_v' to
undrained condition, the effective stress increment corresponding to
the total stress increment EF would become EG . The direction of
increment EG would be the same as that of increment HJ of the
effective stress path AC for undrained shearing. Furthermore,
as shown in Figure E.1(c), states J , G and F have the same
stress ratio and states H and E have the same stress
ratio. Since the effective stress path for undrained shearing
coincides with the total and effective stress paths for constant
volume shearing, the effective stress increment HJ can be
considered as a total stress increment for constant volume
shearing. Hence, the value of α_s for the total stress
increment EF is the same as that for the total stress
increment HJ which is given by Equation (E.6). Therefore,
values of α_s for increments of total stress along the total
stress path of a constant σ_v' test can be determined from the
total stress path of a constant volume test performed on a
sample with the same pre-shearing state.

Method 2

This method requires the carrying out of a separate experiment. In
Figure E.2(a), AB represents the true effective stress path on
$(\sigma_v-\bar{u}),\tau_v'$ plane for a normally consolidated sample sheared under
supposedly constant σ_v' condition. The path is slightly curved
instead of vertical because of the excess pore pressure $\bar{u}$ which are
not measured. If shearing is suddenly stopped at point B and the
sample allowed to come to equilibrium, the excess pore pressures
will dissipate and consolidation will take place. Also, the shear
stress will drop resulting in path BC. Figure E.2(b) shows the
corresponding path A'B'C' on $\ln(\sigma_v-\bar{u}),v$ plane. Assuming that
the drop in shear stress has no effect on the excess pore pressures
and assuming B'C' is parallel to the normal compression line,

$$\delta v \ / \ \delta \ln(\sigma_{vo} - \bar{u}) = \lambda_s$$

But, $\qquad\qquad \delta \ln(\sigma_{vo} - \bar{u}) = - \ \delta \bar{u} \ / \ (\sigma_{vo} - \bar{u})$

so, $\qquad\qquad \delta \bar{u} = - \ \delta v(\sigma_{vo} - \bar{u}) \ / \ \lambda_s$

and approximating $(\sigma_{vo} - \bar{u})$ to σ_{vo} ,

$$\delta \bar{u} = - \ \frac{\delta v \ \sigma_{vo}}{\lambda_s} \qquad\qquad\qquad (E.7)$$

Equation (E.7) gives an estimation of the excess pore pressure in the sample at B .

Method 3

This method involves the shearing of samples with the same pre-shearing state and OCR at different rates. At the same shear strain γ , samples sheared at faster rates will have greater excess pore pressures and lower effective vertical stresses σ_v' . Hence, the effects of the excess pore pressures can be studied by comparing the results plotted against γ .

Estimation of excess pore pressures in test UB9 using method 1

Figure E.3 shows the variation of total shear stress τ_v with elapsed time after the start of shearing for constant σ_v' test UB9 . The total vertical stress σ_v remained constant all the time so that $\delta\sigma_v$ was always zero. Because the test was strain controlled the rate at which τ_v changed varied throughout the test.

The curve in Figure E.3 is approximated to a series of step increments separated by one hour intervals. Equation (E.4) is used to calculate the excess pore pressures due to each increment of τ_v .

The value of μ is 0.42 for drainage from both ends. Results of one-dimensional consolidation with U_t plotted against $\sqrt{t}$ is shown in Figure E.4. Using the $\sqrt{(time)}$ curve fitting method the value of t_1 is 0.8 hr . As already described, the values of α_s for each increment of $\delta\tau_v$ can be determined from the total stress path of the corresponding constant volume test. Figure E.5 shows the total stress path of test UB9 and the total stress path of the corresponding constant volume test UB10. The stress paths were divided into the increments defined in Figure E.3. For each increment along the total stress path of the constant volume test, the value of α_s was obtained according to Equation (E.6).

The excess pore pressures due to each $\delta\tau_v$ increment at hourly intervals of elapsed time from the start of shearing were calculated and tabulated in Table E.1. The accumulated excess pore pressures due to different increments of $\delta\tau_v$ were then added together to give the excess pore pressures in the sample.

Estimation of excess pore pressures in test UB9 using method 2

A sample, UB9A , of the same material as sample UB9 was prepared and sheared using the same procedures as for sample UB9 . After shearing for $2\frac{1}{2}$ hr , shearing was suddenly stopped and changes in readings of proving rings and dial gauges that followed were recorded. The sample was left overnight for it to reach equilibrium.

After shearing was stopped, the shear stress τ_v decreased from 167 kPa to 125 kPa and the sample consolidated due to the dissipation of excess pore pressures. The variation of U_t with $\sqrt{t}$ is shown in Figure E.6. The specific volume of the sample changed from 1.768 to 1.765.

For this test, $\sigma_{vo} = 776$ kPa and $\lambda_s = 0.139$ for remoulded samples of the same material. Applying Equation (E.7), the excess pore pressure $\bar{u}$ at the point when shearing was suddenly stopped was 16.7 kPa.

Remarks

Using Method 1 the excess pore pressures in sample UB9 at 2 and 3 hr after start of shearing were estimated to be 17.1 and 26.4 kPa respectively. By interpolation, the excess pore pressure at $2\frac{1}{2}$ hr after start of shearing was 21.8 kPa . Using Method 2 the excess pore pressure in sample UB9A at $2\frac{1}{2}$ hr after start of shearing was estimated to be 16.7 kPa. The difference is not large and could be due to Equation (E.3) used in Method 1 being conservative or the assumption in Method 2 that the drop in shear stress had no effect on the excess pore pressures was incorrect.

The order of magnitude of the excess pore pressures estimated by either method was considered to be acceptable. Test UB9 was one of the tests performed at the highest σ_v' of 776 kPa so that the excess pore pressures in this test was expected to be among the worst. Excess pore pressures in the other tests on London clay should be less.

Estimation of excess pore pressures in test MC9 using method 1

Figure E.7 shows the variation of total shear stress τ_v with elapsed time after the start of shearing for the constant σ_v' test MC9 . The curve is approximated to a series of step increments separated by one hour intervals. The value of μ is 0.42 and results of one-dimensional consolidation shown in Figure E.8 gives $t_1 = 0.3$ hr . The value of α_s for each increment of $\delta\tau_v$ defined in Figure E.7 were obtained from the total stress paths for tests MC9 and MC10 shown in Figure E.9.

The excess pore pressures due to each $\delta\tau_v$ increment at hourly intervals of elapsed time from the start of shearing were calculated and tabulated in Table E.2. The accumulated excess pore pressures due to various increments of $\delta\tau_v$ were added together to give the excess pore pressures in the sample.

210

Remarks

The order of magnitude of the excess pore pressures estimated was considered to be acceptable. Since test MC9 was one of the tests performed at the highest σ_v' of 776 kPa , other tests on Cowden till were expected to have less excess pore pressures.

The effects of excess pore pressures in test MB1 observed by Method 3

The pre-shearing state of the normally compressed remoulded brown London clay sample MB1 which was sheared at constant σ_v' is given in Table 6.7. It has been stated in Section 5.10.3 that all samples were sheared at a rate of 0.52 mm/hr . A remoulded brown London clay sample, called MB1A , with the same pre-shearing state and OCR as sample MB1 was prepared. Sample MB1A was also sheared under constant σ_v' condition but at a slower rate of 0.12 mm/hr . The only difference between test MB1 and MB1A was the different rates of shearing used. The results obtained from these two tests are compared in Figure E.10. Since the data were recorded manually, during the slower test MB1A no data was recorded overnight. This is indicated by the broken line sections of the curves. Figure E.10(a) shows that the maximum difference in shear stress τ_v' between the two curves is 5 kPa and at γ = 22 % the difference in τ_v' is 3 kPa . Figure E.10(b) shows that at γ = 22 % the difference in ε_v is 0.4 % .

The comparison shows that even though sample MB1A was sheared at a rate over 4 times as slow as the rate used for sample MB1 , the differences in the shear stresses and volumetric strains measured are small. It can be concluded that the effects of excess pore pressures on samples sheared at 0.52 mm/hr are acceptably small.

References

Agarwal, K.B. (1967)   "The influence of size and orientation of samples on the strength of London clay", Ph.D. thesis, Imperial College, University of London.

Airey, D.W. (1980)   "Soils in the circular simple shear apparatus", M.Phil. thesis, University of Cambridge.

Airey, D.W. (1984)   "Clays in circular simple shear apparatus", Ph.D. thesis, University of Cambridge.

Apted, J.P. (1977)   "Effects of weathering on some geotechnical properties of London clay", Ph.D. thesis, Imperial College, University of London.

Arthur, J.R.F., Dunstan, T., Al-Ani, Q.A.J.L. and Assadi, A. (1977) "Plastic deformation and failure in granular media", Geotechnique, Vol. 27, No. 1, p. 53-74.

Arthur,J.R.F., Chua, K.S., Dunstan, T. and Rodriguez del C., J.I. (1980)   "Principal stress rotation : a missing parameter", Proc. ASCE, Vol. 106, No. GT4, p. 419-432.

Atkinson, J.H. (1973)   "The deformation of undisturbed London clay", Ph.D. thesis, Imperial College, University of London.

Atkinson, J.H. (1981)   "Foundations and slopes", McGraw-Hill, London.

Atkinson, J.H. (1984a)   "Some procedures for normalising soil test results", Geotechnical Engineering Research Centre, The City University, Internal Report GE/84/3.

Atkinson, J.H. (1984b)   "Rate of loading in drained and undrained stress path and triaxial tests", Geotechnical Engineering Research Centre, The City University, Internal Report GE/84/1.

Atkinson, J.H. and Bransby, P.L. (1978) "The mechanics of soils", McGraw-Hill, London.

Atkinson, J.H. and Clinton, D.B. (1984) "Stress path tests on 100 mm diameter samples", Geotechnical Engineering Research Centre, The City University, Internal Report GE/84/8.

Atkinson, J.H. and Richardson, D. (1987) "The effect of local drainage in shear zones on the undrained strength of overconsolidated clay", Geotechnique, Vol. 37, No. 3, p. 393-403.

Atkinson, J.H., Evans, J.S. and Scott, C.R. (1983) "Stress path testing equipment, Spectra system — operating manual", Geotechnical Engineering Research Centre, The City University, Internal Report GE/83/1.

Atkinson, J.H., Evans, J.S. and Richardson, D. (1984) "Effects of stress path and stress history on the stiffness of reconstituted London clay", Geotechnical Engineering Research Centre, The City University, Internal Report GE/84/9.

Atkinson, J.H., Lewin, P.I. and Ng, C.L. (1985a) "Undrained strength and overconsolidation of a clay till", Proc. Int. Conf. on construction in glacial tills and boulder clays, Edinburgh, p. 49-54.

Atkinson, J.H., Evans, J.S. and Scott, C.R. (1985b) "Developments in microcomputer controlled stress path testing equipment for measurement of soil parameters", Ground Engineering, Vol. 18, No. 1, p. 15-22.

Atkinson, J.H., Richardson, D. and Woods, R.I. (1986) "Technical note on the determination of tangent stiffness parameters from soil test data", Computers and Geotechnics, Vol. 2, p.131-140.

Atkinson, J.H., Richardson, D. and Robinson, P.J. (1987) "Compression and extension of K_o normally consolidated kaolin clay", Journal of Geotechnical Engineering, ASCE,

Vol. 113, No. 12, p. 1468-1482.

Bassett, R.H. (1967)   "The behaviour of granular materials in the simple shear apparatus", Ph.D. thesis, University of Cambridge.

Berre, T. and Bjerrum, L. (1973)   "Shear strength of normally consolidated clays", Proc. 8th ICSMFE, Moscow, Vol. 1.1, p. 39-49.

Bishop, A.W. and Henkel, D.J. (1962)   "The measurement of soil properties in the triaxial test", Edward Arnold, London.

Bishop, A.W. and Wesley, L.D. (1975)   "A hydraulic triaxial apparatus for controlled stress path testing", Geotechnique, Vol. 25, No. 4, p. 657-670.

Bjerrum, L. and Landva, A. (1966)   "Direct simple shear tests on a Norwegian quick clay", Geotechnique, Vol. 16, No. 1, p. 1-20.

Borin, D.L. (1973)   "The behaviour of saturated kaolin in the simple shear apparatus", Ph.D. thesis, University of Cambridge.

Bransby, P.L. (1973)   "Cambridge contact stress transducers", Department of Engineering, University of Cambridge, Internal Report CUED/C-SOILS/LN2.

Bromhead, E.N. (1979)   "A simple ring shear apparatus", Ground Engineering, Vol. 12, No. 5, p. 40-44.

Brooker, E.W. and Ireland, H.O. (1965)   "Earth pressures at rest related to stress history", Canadian Geotechnical Journal, Vol. 2, No. 1, p. 1-15.

Budhu, M. (1979)   "Simple shear deformation of sands", Ph.D. thesis, University of Cambridge.

Budhu, M. and Britto, A. (1987)   "Numerical analysis of soils

in simple shear devices", Soils and Foundations, Vol. 27, No. 2, p. 31-41.

Budhu, M. and Wood, D.M. (1979) "A study of the simple shear test", Department of Engineering, University of Cambridge, Report submitted to BRE.

Burnett, A.D. (1974) "The modification and application of the quantitative x-ray diffraction method of Schultz (1964) to the mineralogical study of London clay samples", J. Soil Science, Vol. 25, p. 179-188.

Burnett, A.D. and Fookes, P.G. (1974) "A regional engineering geological study of the London clay in the London and Hampshire basins", Quarterly Journal of Engineering Geology, Vol. 7, p. 257-295.

Catt, J.A. and Madgett, P.A. (1981) "The work of W.S. Bisat on the Yorkshire coast", The Quaternary in Britain, Pergamon Press, p.119-136.

Clinton, D.B. (1986) "User manual for 'TRIAX' and 'TRIAX.+'", Geotechnical Engineering Research Centre, The City University, Internal Report GE/86/14.

Clinton, D.B. (1987) "The determination of soil parameters for design from stress path tests", Ph.D. thesis, Geotechnical Engineering Reseach Centre, The City University, London.

Cole, E.R. (1967) "The behaviour of soils in the simple shear apparatus", Ph.D. thesis, University of Cambridge.

Cornforth, D.H. (1964) "Some experiments on the influence of strain conditions on the strength of sand", Geotechnique, Vol. 14, No. 2, p. 143-167.

Costa Filho, L.M. (1980) "A laboratory investigation of the small strain behaviour of London clay", Ph.D. thesis, Imperial College, University of London.

De Josselin de Jong, G. (1972) "Stress-strain behaviour of soils", Proc. Roscoe Memorial Symp., Foulis, Cambridge, p. 258-261.

Derbyshire, E., Foster, D., Love, M.A. and Edge, M.J. (1985) "Pleistocene lithostratigraphy of N.E. England, a sedimentological approach to the Holderness sequence", Correlation of Quaternary Chronology, Geo Books Ltd.

Drescher, A., Budhu, M. and Wood, D.M. (1978) "On the determination of the stress state in the simple shear apparatus", Department of Engineering, University of Cambridge, Internal Report CUED/C-SOILS TR43.

Duncan, J.M. and Dunlop, P. (1969) "Behaviour of soils in simple shear tests", Proc. 7th ICSMFE, Mexico, Vol. 1, p. 101-109.

Duncan, J.M. and Seed, H.B. (1966) "Strength variation along failure surfaces in clay", Proc. ASCE, Vol. 92, No. SM6, p. 81-104.

Dyvik, R. and Zimmie, T.F. (1983) "Lateral stress measurements during static and cyclic direct simple shear testing", Norwegian Geotechnical Institute, Oslo, Publication No. 149.

Dyvik, R., Zimmie, T.F. and Floess, C.H.L. (1981) "Lateral stress measurements in direct simple shear device", Proc. Symp. on laboratory shear strength of soil, ASTM, STP 740, p. 191-206.

Gallagher, K.A. (1983) "Site investigation and soil properties at Cowden", Report by BRE, private communication.

Gens,A. and Hight, D.W. (1979) "The laboratory measurement of design parameters for a glacial till", Proc. 7th European Conf., Brighton, Vol. 2, p. 57-66.

Geonor (1968) "Description and instructions for use of direct simple shear apparatus model h-12", Geonor A/S, Oslo.

216

Gunn, M.J. and Britto, A.M. (1984) "CRISP - User's and programmer's guide", Department of Engineering, University of Cambridge.

Hambly, E.C. and Roscoe, K.H. (1969) "Observations and predictions of stresses and strains during plane strain of 'wet' clays ", Proc. 7th ICSMFE, Mexico, Vol. 1, p. 173-181.

Head, K.H. (1982) "Manual of soil laboratory testing", Pentech Press, London, Vol. 2.

Henkel, D.J. and Wade, N.H. (1966) "Plane strain tests on a saturated remoulded clay", Proc. ASCE, Vol. 92, No. SM6, p. 67-80.

Hight, D.W., Gens, A. and Symes, M.J. (1983) "The development of a new hollow cylinder apparatus for investigating the effects of principal stress rotation in soils", Geotechnique, Vol. 33, No. 4, p. 355-383.

Houlsby, G.T. and Wroth, C.P. (1980) "Strain and displacement discontinuities in soil", Proc. ASCE, Vol. 106, No. EM4, p. 753-771.

Jardine, R.J., Symes, M.J. and Burland, J.B. (1984) "The measurement of soil stiffness in the triaxial apparatus", Geotechnique, Vol. 34, No. 3, p. 323-340.

Kjellman, W. (1951) "Testing the shear strength of clays in Sweden", Geotechnique, Vol. 2, No. 3, p. 225-232.

Ladd, C.C. and Edgers, L. (1972) "Consolidated-undrained direct simple shear tests on saturated clays", Department of Civil Engineering, Massachusetts Institute of Technology, Internal Report R72-82.

Ladd, C.C., Foott, R., Ishihara, K., Schlosser, F. and Poulos, H.G. (1977) "Stress-deformation and strength characteristics", State-of-the-art report, Proc. 9th ICSMFE, Tokyo, Vol. 2, p. 421-494.

Lade, P.V. and Duncan, J.M. (1973) "Cubical triaxial tests on cohesionless soil", Proc. ASCE, Vol. 99, No. SM10, p. 793-812.

Lau, W.H.W. (1985) "Report on progress of first year research", Geotechnical Engineering Research Centre, The City University, Internal Report.

Leussink, H. and Wittke, W. (1963) "Difference in triaxial and plane strain shear strength", ASTM, Special Technical Publication, No. 361, p. 77-89.

Lewin, P.I. and Powell, J.J.M. (1985) "Patterns of stress-strain behaviour for a clay till", Proc. 11th ICSMFE, San Francisco, Vol. 2, p. 553-556.

Lucks, A.S., Christian, J.T., Brandow, G.E. and Høeg, K. (1972) "Stress conditions in NGI simple shear test", Proc. ASCE, No. SM1, p. 155-160.

Marsland, A. (1971a) "The shear strength of stiff fissured clays", Proc. Roscoe Memorial Symp., University of Cambridge, p. 59-68.

Marsland, A. (1971b) "Laboratory and in-situ measurements of the deformation moduli of London clay", Proc. Symp. on the interaction of structures and foundations, The Midland Soil Mechanics and Foundation Engineering Society, Birmingham, p. 7-17.

Marsland, A. and Powell, J.J.M. (1985) "Field and laboratory investigations of the clay tills at the Building Research Establishment test site at Cowden Holderness", Proc. Int. Conf. on construction in glacial tills and boulder clays, Edinburgh, p. 147-168.

Marsland, A. and Randolph, M. (1977) "Comparisons of the results from pressuremeter tests and large in-situ plate tests in London clay", Geotechnique, Vol. 27, No. 2, p. 217-243.

Naylor, D.J., Pande, G.N., Simpson, B. and Tabb, R. (1981) "Finite elements in geotechnical engineering", Pineridge Press, Swansea.

Ng, C.L. (1988) "The stress-strain behaviour of Cowden till", Ph.D. thesis in preparation, Geotechnical Engineering Research Centre, The City University, London.

Ochiai, H. (1975) "The behaviour of sands in direct shear tests", Journal of JSSMFE, Vol. 15, No. 4, p. 93-100 (in Japanese).

Oda, M. and Konishi, J. (1974) "Rotation of principal stresses in granular material during simple shear", Soils and Foundations, Vol. 14, No. 4, p. 39-53.

Parry, R.G.H. and Swain, C.W. (1977) "A study of skin friction on piles in stiff clay", Ground Engineering, Vol. 10, No. 8, p. 33-37.

Powell, J.J.M. (1988) Information on the automatic data logging system used by BRE for standard shear box tests, private communication.

Powell, J.J.M. and Uglow, I.M. (1985) "A comparison of Menard, self-boring and push-in pressuremeter tests in a stiff clay till", Proc. Int. Conf. on offshore site investigations, London, p. 201-217.

Powell, J.J.M. and Uglow, I.M. (1986) "Dilatometer testing in stiff overconsolidated clays", Proc. 39th Canadian Geotechnical Conf. on in-situ testing and field behaviour, Ottawa.

Powell, J.J.M., Marsland, A. and Al-Khafagi, A.N. (1983) "Pressuremeter testing of glacial clay tills", Proc. Int. Symp. on in-situ testing, Paris, Vol. 2, p. 373-378.

Prevost, J.H. and Høeg, K. (1976) "Re-analysis of simple shear soil testing", Canadian Geotechnical Journal, Vol. 13, No. 4, p. 418-429.

Randolph, M.F. and Wroth, C.P. (1981) "Application of the failure state in undrained simple shear to the shaft capacity of driven piles", Geotechnique, Vol. 31, No. 1, p. 143-157.

Reades, D.W. and Green, G.E. (1974) "Discussion on cubical triaxial tests on cohesionless soil", Proc. ASCE, Vol. 100, No. GT9, p. 1065-1067.

Richardson, D. (1984a) "The importance of natural strains in soil mechanics", Geotechnical Engineering Research Centre, The City University, Internal Report GE/84/23.

Richardson, D. (1984b) "Effects of stress path on the strength and stiffness near retaining walls", Geotechnical Engineering Research Centre, The City University, Internal Report GE/84/4.

Richardson, D. (1988) "Investigations of threshold effects in soil deformations", Ph.D. thesis, Geotechnical Engineering Research Centre, The City University, London.

Roscoe, K.H. (1953) "An apparatus for the application of simple shear to soil samples", Proc. 3rd ICSMFE, Vol. 1, p. 186-191.

Roscoe, K.H. and Burland, J.B. (1968) "On the generalised stress-strain behaviour of 'wet' clay", Engineering Plasticity, Cambridge University Press, Cambridge, p. 535-609.

St. John, H.J. (1975) "Field and theoretical studies of the behaviour of ground around deep excavations in London clay", Ph.D. thesis, University of Cambridge.

Sandroni, S.S. (1977) "The undrained strength of London clay in total and effective stress terms", Ph.D. thesis, Imperial College, University of London.

Schmertmann, J.M. (1953) "Estimating the time-consolidation behaviour of clay from laboratory test results", Proc. ASCE, Separate No. 311.

Schofield, A.N. and Wroth, C.P. (1968) "Critical state soil mechanics", McGraw-Hill, London.

Sherlock, R.L. (1962) "British regional geology - London and the Thames Valley", Geological Survey, 3rd edition, H.M.S.O.

Simpson, B., O'Riordan, N.J. and Croft, D.D. (1979) "A computer model for the analysis of ground movements in London clay", Geotechnique, Vol. 29, No. 2, p. 149-175.

Skempton, A.W. (1961) "Horizontal stresses in an overconsolidated Eocene clay", Proc. 5th ICSMFE, Paris, Vol. 1, p. 351-358.

Skempton, A.W. and Henkel, D.J. (1957) "Tests on London clay from deep borings at Paddington, Victoria and South Bank", 4th ICSMFE, London, Vol. 1, p. 100-106.

Som, N.N. (1968) "The effect of stress path on the deformation and consolidation of London clay", Ph.D. thesis, Imperial College, University of London.

Sowa, V.A. (1963) "A comparison of the effects of isotropic and anisotropic consolidation on the shear behaviour of a clay", thesis presented to University of London in partial fulfilment of the requirements for Ph.D. degree.

Soydemir, C. (1976) "Strength anisotropy observed through simple shear tests", Norwegian Geotechnical Institute, Oslo, Laurits Bjerrum Memorial Vol., p. 99-113.

Straw, A. and Clayton, K.M. (1979) "Eastern and Central England (geomorphology of British Isles)", Cambridge University Press, Chapter 3, p. 21-45.

Stroud, M.A. (1971) "The behaviour of sand at low stress levels in the simple shear apparatus", Ph.D. thesis, University of Cambridge.

Taylor, D.W. (1948) "Fundamentals of soil mechanics", Wiley, New York.

Terzaghi, K. (1936) "The shearing resistance of saturated soil and the angle between the planes of shear", Proc. 1st ICSMFE, Harvard, Vol. 1, p. 54-56.

Vaid, Y.P. and Campanella, R.G. (1974) "Triaxial and plane strain behaviour of natural clay", Proc. ASCE, Vol. 100, No. GT3, p. 207-224.

Webb, D.L. (1966) "The mechanical properties of undisturbed London clay and Pierre shale", Ph.D. thesis, Imperial College, University of London.

Wesley, L.D. (1975) "Influence of stress path and anisotropy on the behaviour of a soft alluvial clay", Ph.D. thesis, University of London.

West, R.G. (1968) . "Pleistocene geology and biology with special reference to the British Isles", Longmans.

Windle, D. and Wroth, C.P. (1977) "In-situ measurement of the properties of stiff clays", Proc. 9th ICSMFE, Tokyo, Vol. 1, p. 347-352.

Wood, D.M., Drescher, A. and Budhu, M. (1980) "On the determination of the stress state in the simple shear apparatus", Geotechnical Testing Journal, ASTM, Vol. 2, No. 4, p. 211-221.

Woods, R.I. (1985) "Evaluation of soil stiffness from triaxial test data", Geotechnical Engineering Research Centre, The City University, Internal Report GE/85/12.

Wroth, C.P. (1984) "The interpretation of in-situ soil tests", Geotechnique, Vol. 34, No. 4, p. 449-489.

Wroth, C.P. (1987) "The behaviour of normally consolidated clay as observed in undrained direct shear tests", Geotechnique, Vol. 37, No. 1, p. 37-43.

(a)

Sample type	Pre-shearing compression and swelling (Isotropic or K_o)	λ	κ	N
Remoulded	Isotropic	0.077	0.015	1.915
Reconstituted	Isotropic	0.093	0.015	2.000
Reconstituted	K_o	0.093	0.015	1.990

(b)

Sample type	Isotropic or K_o	Compression				Extension			
		M	ϕ'_{cs}	λ	Γ	M	ϕ'_{cs}	λ	Γ
Remoulded	Isotropic	1.1	28°	0.077	1.885	0.8	27°	0.077	1.894
Reconstituted	Isotropic	1.2	30°	0.090	1.936	0.9	32°	0.093	1.942
Reconstituted	K_o	1.2	30°	0.093	1.936	0.9	32°	0.093	1.931

Table 3.1   Critical state parameters for Cowden till
(after Ng, 1988)

Reference	Site	γ (kN/m³)	PL	LL	clay fraction by weight (%)	Activity	G_s
Skempton (1961)	Bradwell	18.9	30	95	52	1.25	2.75
Webb (1966)	Ashford Common	20.1	27	68	50	0.82	2.76
Som (1968)	Oxford Circus	20.0	27	63	48	0.75	2.68
Som (1968)	High Ongar	19.3	27	68	48	0.86	2.71
Argarwal (1967)	Wraysbury	19.1	28	74	57	0.80	2.68
Apted (1977)	South Ockendon	18.8	30	78	56	0.85	2.72
Apted (1977)	Broakoak	18.8	30	83	64	0.84	2.72

Table 3.2   Summary of classification test results for London clay

Sources of inaccuracies	Vertical stress σ_v' (kPa)	Horizontal stress τ_v' (kPa)	Volumetric strain ε_v (%)	Shear strain γ (%)
Hysteresis	± 2	± 2	-	-
Friction	± 2	± 1	-	-
Shear stiffness of membrane	-	± 2	-	-
Radial defor -mation of mem -brane	-	-	± 0.07	-
Effect of pins	-	-	± 0.01	uncertain
Overall	± 4	± 5	± 0.08	uncertain

Table 5.1   Summary of estimated maximum values for inaccuracies in NGI simple shear apparatus

	Deviator stress $(\sigma_a - \sigma_r)$	Pore & cell pressures u and σ_r	Axial strain ε_a	Volumetric strain ε_v
Working range	±700kPa	0-1000kPa	0-25%	0-44%
Transducer output (mV)	±20	0-100	0-40	0-40
Analogue in -put channel range (mV)	±20	±160	±40	±40
Resolution	0.04kPa	0.10kPa	0.002%	0.003%

Table 5.2   Resolutions of measurements obtained by stress path testing equipment for samples with 38 mm diameter

Sources of inaccuracies	Deviator stress $(\sigma_a-\sigma_r)$ (kPa)	Pore & cell pressures u and σ_r (kPa)	Axial strain ε_a (%)	Volumetric strain ε_v (%)
Hysteresis	± 1.5	± 0.5	± 0.01	*
Drift	± 1.0	± 0.5	0	± 0.02
Noise	± 1.0	± 1.0	± 0.01	± 0.01
Overall	± 3.5	± 2.0	± 0.02	± 0.03

*   See Section 5.4.2

Table 5.3   Typical values of inaccuracies of measurements obtained by stress path testing equipment for samples with 38 mm diameter

	Deviator stress $(\sigma_a-\sigma_r)$ (kPa)	Pore & cell pressures u and σ_r (kPa)	Axial strain ε_a (%)	Volumetric strain ε_v (%)
Resolution	0.8	0.8	0.027	0.008
Inaccuracies:-				
Hysteresis	± 1.5	± 0.5	± 0.01	± 0.01
Drift	± 1.0	± 0.1	± 0.01	± 0.01
Noise	± 0.5	± 0.1	0	0
Overall inaccuracies	± 3.0	± 0.7	± 0.02	± 0.02

Table 5.4   Resolutions and typical values of inaccuracies of measurements obtained by stress path testing equipment for samples with 100 mm diameter

Soil	Test no.	Borehole no.	Sample tube no.	Depth below ground level (m)
Cowden till	UC1-UC8	S100	8	8.1 - 8.8
	UC9-UC12	S100	12	11.6 - 12.2
	BUC3-BUC6	1	4	6.3 - 6.5
	BUC7&BUC8	1	5	7.1 - 7.2
London clay (brown)	UB1-UB10	596/100	8	5.0 - 5.6
	TUB1	-	2	6.1 - 6.7
	BUB9-BUB15	1	9	5.7 - 6.1
	BUB16	1	10	6.4
	BUB18-BUB24 (excluding BUB21)	1	12	7.7 - 8.0
London clay (blue)	UL1-UL7	596/101	2	9.7 - 10.3
	UL8&UL9	596/101	4	11.1 - 11.7
	UL10	596/101	5	11.7 - 12.1
	TUL1	1	1.	9.0 - 9.6
	TUL2	-	4	11.2 - 11.8
	TUL3	1	2	9.8 - 10.4
	TUL4	-	3	10.5 - 11.1
	TUL5	596/100	13	8.1 - 8.5

Table 5.5   Borehole numbers, sample tube numbers and depths of undisturbed samples

Sample no.	Sequence and values of vertical stresses applied (kPa)
MC1 CC1 ML1 MB1	388
MC2 CC2 ML2 MB2	388 194
MC3 CC3 ML3 MB3	388 97
MC4 CC4 ML4 MB4	388 49
MC5 CC5 ML5 MB5	388
MC6 CC6 ML6 MB6	388 194
MC7 CC7 ML7 MB7	388 97
MC8 CC8 ML8 MB8	388 49
MC9 MC10 CC9 ML9 ML10	39 97 194 291 388 582 776
MB9	97 194 291 388 582 776
CC10	39 97 194 291 388 582 776 388 194 97 49
MB10	97 194 291 388 582 776 582 388 194 97 49
UC1 UC5 UL1 UL5	388
UC2 UC6 UL2 UL6	194
UC3 UC7 UL3 UL7	97
UB7	97
UC4 UC8 UL4 UL8	49
UB4 UB8	49
UB1 UB5	39 97 194 291 388
UB2	39 97 194
UB3	39 97
UB6	97 194
UC9	97 194 388 582
UL9 UB9	39 97 194 291 388 582 776
UC10 UB10	97 194 388 582 776
UL10	776
UC11	582
UC12	388 776

Table 5.6   Sequence and values of vertical stresses applied on simple shear samples during one-dimensional compression

Soil	γ (kN/m³)	w (%)	PL	LL	PI	clay fraction by weight (%)	A	G_s
Cowden till	21.5	14.9	16	34	18	33	0.55	2.66
London clay (brown)	19.1	29.6	32	72	40	64	0.63	2.75
London clay (blue)	19.7	26.0	26	71	45	59	0.76	2.75

Table 6.1   Results of classification tests

Soil	Sample type	Simple shear			Shear box			Triaxial		
		λ_s	N_s	κ_s	λ_b	N_b	κ_b	λ	N_o	κ
Cowden till	Remoulded	0.071	1.897	0.010	0.083	1.993	–	–	–	–
	Reconsti-tuted	0.085	2.024	0.011	–	–	–	–	–	–
	Undistur-bed	–	–	0.020	–	–	0.045	–	–	–
London clay (brown)	Remoulded	0.139	2.745	0.037	0.150	2.834	0.040	–	–	–
	Undistur-bed	–	–	0.061	–	–	0.073	–	–	–
London clay (blue)	Remoulded	0.135	2.675	0.030	–	–	–	–	–	–
	Reconsti-tuted	–	–	–	–	–	–	0.192	3.037	0.054
	Undistur-bed	–	–	0.043	–	–	–	–	–	–

Table   6.2   Summary of one-dimensional compression and swelling parameters

Sample		Change in σ_v' (kPa)	m_v ($\times 10^{-3}$ m^2/kN)	t_1 (min)	c_v ($\times 10^{-9}$ m^2/s)	k ($\times 10^{-12}$ m/s)
no.	type					
MC9		39 to 97	0.44	9	110	472
MC9		97 to 194	0.29	9	104	294
MC9		194 to 291	0.18	25	35	63
MC9		291 to 388	0.11	36	24	25
MC9		388 to 582	0.12	16	52	62
MC9		582 to 776	0.067	25	32	21
MC10	Remoulded	39 to 97	0.42	9	113	464
MC10		97 to 194	0.24	9	107	256
MC10		194 to 291	0.16	25	37	56
MC10		291 to 388	0.14	36	25	35
MC10		388 to 582	0.11	16	54	59
MC10		582 to 776	0.078	25	33	25
UC9		97 to 194	0.056	4	269	149
UC9		194 to 388	0.060	4	266	157
UC10	Undistur -bed	97 to 194	0.056	4	265	146
UC10		194 to 388	0.060	4	262	154
UC10		388 to 582	0.043	9	114	48

Table 6.3   Results of one-dimensional consolidation for Cowden
till simple shear samples

Sample		Change in σ_v' (kPa)	m_v ($\times 10^{-3}$ m²/kN)	t_1 (min)	c_v ($\times 10^{-9}$ m²/s)	k ($\times 10^{-12}$ m/s)
no.	type					
MB9		97 to 194	0.26	36	30	74
MB9		194 to 291	0.21	64	16	33
MB9		291 to 388	0.18	100	9.6	17
MB9		388 to 582	0.16	81	12	18
MB9	Remoulded	582 to 776	0.10	144	6.0	6.1
MB10		291 to 388	0.19	121	7.3	14
MB10		388 to 582	0.17	81	11	18
MB10		582 to 776	0.11	121	6.6	7.3
MB10		776 to 582	0.020	25	30	5.9
UB1		39 to 97	0.12	36	30	37
UB1		97 to 194	0.20	49	22	43
UB1		194 to 291	0.13	64	16	21
UB1		291 to 388	0.11	81	12	14
UB2		39 to 97	0.12	49	22	26
UB2		97 to 194	0.15	49	22	32
UB3		39 to 97	0.16	36	31	50
UB5		39 to 97	0.13	36	29	37
UB5	Undistur	97 to 194	0.17	49	21	35
UB5	-bed	194 to 291	0.13	64	15	19
UB5		291 to 388	0.099	64	15	15
UB9		39 to 97	0.12	36	31	37
UB9		97 to 194	0.17	36	30	49
UB9		194 to 291	0.13	49	21	26
UB9		291 to 388	0.093	49	21	19
UB9		388 to 582	0.083	49	20	17
UB9		582 to 776	0.065	64	15	9.5

Table 6.4   Results of one-dimensional consolidation for London clay (brown) simple shear samples

Sample		Change in σ_v' (kPa)	m_v ($\times 10^{-3}$ m²/kN)	t_1 (min)	c_v ($\times 10^{-9}$ m²/s)	k ($\times 10^{-12}$ m/s)
no.	type					
ML2	Remoulded	291 to 388	0.20	144	6.1	12
ML3	Remoulded	291 to 388	0.18	121	7.4	13
UL9		39 to 97	0.13	25	48	63
UL9		97 to 194	0.17	36	33	53
UL9	Undistur -bed	194 to 291	0.12	64	18	21
UL9		291 to 388	0.10	64	17	17
UL9		388 to 582	0.073	49	22	16
UL9		582 to 776	0.062	64	17	10

Table 6.5   Results of one-dimensional consolidation for London clay (blue) simple shear samples

Sample		States before shearing			Type of shearing
no.	type	σ'_{vo} (kPa)	v_o	OCR	
MC1		388	1.474	1	
MC2		194	1.480	2	
MC3		97	1.486	4	Constant σ'_v
MC4		49	1.493	8	
MC5	Remoulded	388	1.474	1	
MC6		194	1.480	2	
MC7		97	1.486	4	Constant volume
MC8		49	1.493	8	
MC9		776	1.425	1	Constant σ'_v
MC10		776	1.425	1	Constant volume
CC1		388	1.517	1	
CC2		194	1.523	2	Constant σ'_v
CC3		97	1.532	4	
CC4		49	1.539	8	
CC5	Reconstituted	388	1.517	1	
CC6		194	1.523	2	Constant volume
CC7		97	1.532	4	
CC8		49	1.539	8	
CC9		776	1.458	1	Constant σ'_v
CC10		49	1.488	16	Constant σ'_v
UC1		388	1.430	.	
UC2		194	1.444		Constant σ'_v
UC3		97	1.458		
UC4		49	1.471		
UC5		388	1.430		
UC6	Undisturbed	194	1.444		Constant volume
UC7		97	1.458		
UC8		49	1.471		
UC9		582	1.422		Constant σ'_v
UC10		776	1.416		Constant σ'_v
UC11		582	1.422		Constant volume
UC12		776	1.416		Constant volume

Table 6.6   Summary of states before shearing and type of shearing for Cowden till simple shear samples

Soil	Sample		States before shearing			Type of shearing
	no.	type	σ_{vo}' (kPa)	v_o	OCR	
London clay (brown)	MB1		388	1.916	1	
	MB2		194	1.940	2	Constant σ_v'
	MB3		97	1.966	4	
	MB4		49	1.991	8	
	MB5	Remoulded	388	1.916	1	
	MB6		194	1.940	2	Constant volume
	MB7		97	1.966	4	
	MB8		49	1.991	8	
	MB9		776	1.820	1	Constant σ_v'
	MB10		49	1.930	16	Constant volume
	UB1		388	1.818		
	UB2		194	1.858		Constant σ_v'
	UB3		97	1.903		
	MB4		49	1.945		
	UB5	Undistur -bed	388	1.818		
	UB6		194	1.858		Constant volume
	UB7		97	1.903		
	UB8		49	1.945		
	UB9		776	1.775		Constant σ_v'
	UB10		776	1.775		Constant volume
London clay (blue)	ML1		388	1.870	1	
	ML2		194	1.886	2	Constant σ_v'
	ML3		97	1.907	4	
	ML4		49	1.927	8	
	ML5	Remoulded	388	1.870	1	
	ML6		194	1.886	.2	Constant volume
	ML7		97	1.907	4	
	ML8		49	1.927	8	
	ML9		776	1.777	1	Constant σ_v'
	ML10		776	1.777	1	Constant volume
	UL1		388	1.761		
	UL2		194	1.790		Constant σ_v'
	UL3		97	1.821		
	UL4		49	1.851		
	UL5	Undistur -bed	388	1.761		
	UL6		194	1.790		Constant volume
	UL7		97	1.821		
	UL8		49	1.851		
	UL9		776	1.731		Constant σ_v'
	UL10		776	1.731		Constant volume

Table 6.7   Summary of states before shearing and type of shearing for London clay simple shear samples

Soil	Sample		States before shearing		
	no.	type	σ'_{vo} (kPa)	v_o	OCR
Cowden till	BUC3	Undisturbed	100	1.538	
	BUC4		300	1.488	
	BUC5		400	1.475	
	BUC6		500	1.465	
	BUC7		50	1.569	
	BUC8		209	1.505	
	BMC25	Remoulded	50	1.660	1
	BMC26		100	1.611	1
	BMC27		204	1.552	1
	BMC28		400	1.496	1
London clay (brown)	BUB9	Undisturbed	100	1.956	
	BUB10		300	1.876	
	BUB11		200	1.905	
	BUB12		400	1.855	
	BUB13		50	2.006	
	BUB14		400	1.855	
	BUB15		50	2.006	
	BUB16		200	1.905	
	BUB18		200	1.905	
	BUB19		100	1.956	
	BUB20		300	1.876	
	BUB22		400	1.855	
	BUB23		200	1.905	
	BUB24		400	1.855	
	BMB1	Remoulded	205	2.036	1
	BMB2	Remoulded	413	1.930	1
	BMB3	Remoulded	802	1.831	1

Table 6.8   Summary of states before shearing for Cowden
             till and London clay (brown) shear box samples

| Sample no. | States before shearing | | | | Type of loading |
	p_0' (kPa)	q_0' (kPa)	v_0	R_p	
TCL1	284	173	1.952	1	
TCL2	146	16	1.988	2	
TCL3	73	-26	2.025	4	compression
TCL4	380	230	1.896	1	
TCL5	445	270	1.866	1	
TCL6	284	173	1.952	1	
TCL7	136	5	1.992	2	
TCL8	73	-26	2.025	4	extension
TCL9	370	225	1.902	1	
TCL10	420	254	1.877	1	

Table 6.9   Summary of states before undrained shearing of 38 mm reconstituted triaxial samples of London clay (blue)

| Sample no. | States before shearing | | | Type of loading |
	p_0' (kPa)	q_0' (kPa)	v_0	
TUL1	167	-100	1.787	compression
TUL2	250	-150	1.795	compression
TUL3	167	-100	1.791	extension
TUL4	250	-150	1.809	extension

Table 6.10   Summary of states before undrained shearing of 100 mm undisturbed triaxial samples of London clay (blue)

Soil	Sample no.	Probe	States before probing			Drained or Undrained
			p_o' (kPa)	q_o' (kPa)	v_o	
London clay (brown)	TUB1	O'B'	100	0	1.872	Drained
		O'C'	100	0	1.884	
		O'E'	100	0	1.880	
		O'F'	100	0	1.886	
		O'H'	100	0	1.883	
		O'J'	100	0	1.886	
		O'L'	100	0	1.887	
		O'M'	100	0	1.886	
		O'P'	100	0	1.890	
London clay (blue)	TUL5	A C	213	0	1.809	Undrained
		A'E'	200	0	1.812	Drained
		A'F'	200	0	1.812	
		A'H'	200	0	1.812	
		A'J'	200	0	1.817	
		A'L'	200	0	1.812	
		A'M'	200	0	1.821	
		A'P'	200	0	1.812	
		A'Q'	200	0	1.820	
		A'S'	200	0	1.814	

Table 6.11   Summary of states before probing for 100 mm
undisturbed triaxial samples of London clay

Sample		Peak (τ_v'/σ_v') states			Critical states		
no.	type	$(\tau_v')_p$ (kPa)	$(\sigma_v')_p$ (kPa)	v_p	$(\tau_v')_{cs}$ (kPa)	$(\sigma_v')_{cs}$ (kPa)	v_{cs}
MC1		–	–	–	158	387	1.425
MC2		–	–	–	86	200	1.467
MC3		–	–	–	50	99	1.498
MC4		34	51	1.505	32	51	1.517
MC5	Remoulded	–	–	–	–	–	–
MC6		–	––	–	–	–	–
MC7		–	–	–	65	133	1.486
MC8		–	–	–	54	107	1.494
MC9		–	–	–	281	770	1.382
MC10		–	–	–	171	397	1.422
CC1		–	–	–	141	383	1.457
CC2		–	–	–	84	198	1.510
CC3		–	–	–	51	100	1.549
CC4		38	50	1.550	32	50	1.562
CC5	Reconsti	–	–	–	–	–	–
CC6	-tuted	–	–	–	–	–	–
CC7		–	–	–	–	–	–
CC8		–	–	–	–	–	–
CC9		–	–	–	266	770	1.404
CC10		40	51	1.502	33	51	1.512
UC1		–	–	–	176	387	1.416
UC2		–	–	–	106	198	1.450
UC3		57	97	1.460	55	97	1.458
UC4		36	51	1.481	33	51	1.482
UC5		–	–	–	–	–	–
UC6	Undistur	–	–	–	116	216	1.444
UC7	-bed	–	–	–	75	129	1.458
UC8		–	–	–	46	74	1.471
UC9		–	–	–	241	578	1.402
UC10		–	–	–	295	773	1.390
UC11		–	–	–	–	–	–
UC12		–	–	–	–	–	–

Table 7.1   Peak and critical states for simple shear tests on Cowden till

Sample		Peak $(\mathcal{T}_v'/\sigma_v')$ states			Critical states		
no.	type	$(\mathcal{T}_v')_p$ (kPa)	$(\sigma_v')_p$ (kPa)	v_p	$(\mathcal{T}_v')_{cs}$ (kPa)	$(\sigma_v')_{cs}$ (kPa)	v_{cs}
MB1	Remoulded	–	–	–	103	380	1.875
MB2		77	201	1.943	57	201	1.929
MB3		57	103	1.972	32	103	1.973
MB4		40	53	1.997	24	53	2.008
MB5		–	–	–	71	205	1.914
MB6		–	–	–	52	155	1.939
MB7		60	139	1.966	39	108	1.966
MB8		40	76	1.991	28	62	1.991
MB9		–	–	–	–	–	–
MB10		49	90	1.930	35	84	1.930
UB1	Undistur -bed	–	–	–	111	387	1.788
UB2		84	196	1.854	71	196	1.853
UB3		–	–	–	53	98	1.903
UB4		43	54	1.951	–	–	–
UB5		127	310	1.817	–	–	–
UB6		98	184	1.858	–	–	–
UB7		68	116	1.903	56	112	1.903
UB8		45	72	1.945	37	70	1.945
UB9		241	772	1.768	–	–	–
UB10		–	–	–	–	–	–

Table 7.2   Peak and critical states for simple shear tests on London clay (brown)

no.	type	$(\tau_v')_p$ (kPa)	$(\sigma_v')_p$ (kPa)	v_p	$(\tau_v')_{cs}$ (kPa)	$(\sigma_v')_{cs}$ (kPa)	v_{cs}
		Peak (τ_v'/σ_v') states			Critical states		
ML1		–	–	–	103	381	1.822
ML2		74	200	1.888	62	200	1.874
ML3		56	103	1.915	37	103	1.915
ML4		41	51	1.937	–	–	–
ML5	Remoulded	–	–	–	72	201	1.868
ML6		–	–	–	64	176	1.886
ML7		–	–	–	45	108	1.907
ML8		45	89	1.927	34	74	1.927
ML9		–	–	–	192	770	1.727
ML10		–	–	–	–	–	–
UL1		–	–	–	152	387	1.746
UL2		–	–	–	90	196	1.791
UL3		70	99	1.826	–	–	–
UL4		45	52	1.862	35	52	1.873
UL5	Undistur -bed	–	–	–	123	284	1.760
UL6		111	222	1.790	–	–	–
UL7		71	133	1.821	60	119	1.821
UL8		48	84	1.851	44	97	1.851
UL9		–	–	–	206	774	1.678
UL10		–	–	–	–	–	–

Table 7.3   Peak and critical states for simple shear tests on London clay (blue)

Sample		Peak (τ_v'/σ_v') states			Critical states		
no.	type	$(\tau_v')_p$ (kPa)	$(\sigma_v')_p$ (kPa)	v_p	$(\tau_v')_{cs}$ (kPa)	$(\sigma_v')_{cs}$ (kPa)	v_{cs}
BUC3		65	103	1.530	55	115	1.528
BUC4		-	-	-	157	365	1.469
BUC5	Undistur -bed	-	-	-	254	498	1.456
BUC6		-	-	-	325	617	1.440
BUC7		49	52	1.562	41	62	1.571
BUC8		-	-	-	-	-	-
BMC25		35	52	1.639	38	61	1.632
BMC26	Remoulded	-	-	-	71	123	1.579
BMC27		-	-	-	132	246	1.518
BMC28		-	-	-	243	489	1.464

Table 7.4   Peak and critical states for shear box tests on Cowden till

Sample		Peak (τ_v'/σ_v') states			Critical states		
no.	type	$(\tau_v')_p$ (kPa)	$(\sigma_v')_p$ (kPa)	v_p	$(\tau_v')_{cs}$ (kPa)	$(\sigma_v')_{cs}$ (kPa)	v_{cs}
BUB9		78	104	1.945	–	–	–
BUB10		143	312	1.844	–	–	–
BUB11		112	209	1.878	87	247	1.865
BUB12		207	420	1.824	–	–	–
BUB13		46	51	1.968	–	–	–
BUB14		175	415	1.833	117	494	1.818
BUB15	Undistur -bed	46	51	2.005	44	62	2.009
BUB16		98	205	1.898	57	250	1.896
BUB18		112	205	1.891	–	–	–
BUB19		85	103	1.943	50	122	1.942
BUB20		170	315	1.846	–	–	–
BUB22		176	414	1.839	121	498	1.834
BUB23		113	206	1.896	76	248	1.896
BUB24		215	418	1.841	144	494	1.832
BMB1	Remoulded	–	–	–	56	221	2.005
BMB2	Remoulded	–	–	–	101	442	1.905
BMB3	Remoulded	–	–	–	171	858	1.809

Table 7.5   Peak and critical states for shear box tests on London clay (brown)

Sample no.	Peak q′/p′ states			Critical states		
	q'_{peak} (kPa)	p'_{peak} (kPa)	v_{peak}	q'_{cs} (kPa)	p'_{cs} (kPa)	v_{cs}
TCL1	–	–	–	192	217	1.952
TCL2	195	177	1.988	–	–	–
TCL3	118	92	2.025	–	–	–
TCL4	–	–	–	256	299	1.896
TCL5	–	–	–	295	345	1.866
TCL6	–	–	–	-167	202	1.952
TCL7	-148	160	1.992	–	–	–
TCL8	-106	110	2.025	–	–	–
TCL9	–	–	–	-208	274	1.902
TCL10	–	–	–	-236	316	1.877

Table 7.6   Peak and critical states for stress path tests on 38 mm reconstituted London clay (blue) samples

Sample no.	Peak q′/p′ states		
	q'_{peak} (kPa)	p'_{peak} (kPa)	v_{peak}
TUL1	152	158	1.787
TUL2	171	196	1.795
TUL3	-159	203	1.791
TUL4	-205	278	1.809

Table 7.7   Peak states for stress path tests on 100 mm undisturbed London clay (blue) samples

Soil	Test	Normal compression lines from remoulded samples				Swelling lines from undisturbed samples				σ'_{vp} (kPa)
		λ_s	N_s	λ_b	N_b	κ_s	$v_{\kappa s}$	κ_b	$v_{\kappa b}$	
Cowden till	Simple shear	0.071	1.897	–	–	0.020	1.549	–	–	919
	Shear box	–	–	0.083	1.993	–	–	0.045	1.745	683
London clay (brown)	Simple shear	0.139	2.745	–	–	0.061	2.181	–	–	1381
	Shear box	–	–	0.150	2.834	–	–	0.073	2.292	1140
London clay (blue)	Simple shear	0.135	2.675	–	–	0.043	2.017	–	–	1277

Table 7.8   Estimation of σ'_{vp} values for undisturbed simple shear and shear box samples

$\delta\tau_v$	α_s	Elapsed time after start of shearing (hr)									
		1	2	3	4	5	6	7	8	9	10
①	0	0	0	0	0	0	0	0	0	0	0
②	0.4		17.1	5.7	3.4	2.4	1.9	1.5	1.3	1.1	1.0
③	0.6			20.7	7.2	4.3	3.1	2.4	1.9	1.6	1.4
④	0.9				26.7	8.9	5.3	3.8	2.9	2.4	2.0
⑤	1.8					17.8	5.9	3.5	2.5	1.9	1.6
⑥	-1.3						4.3	1.4	0.8	0.6	0.4
⑦	-1.3							8.5	2.8	1.7	1.2
⑧	-1.3								12.8	4.3	2.5
⑨	-1.3									12.8	4.3
⑩	-1.3										8.5
$\bar{u}$ (kPa)		0	17.1	26.4	37.3	33.4	20.5	21.1	25.0	26.4	22.9

Table E.1   Excess pore pressures in simple shear sample UB9 during shearing

$\delta\tau_v$	α_s	Elapsed time after start of shearing (hr)									
		1	2	3	4	5	6	7	8	9	10
①	0.4	8.1	2.7	1.6	1.1	0.9	0.7	0.6	0.5	0.4	0.4
②	1.5		21.6	7.2	4.3	3.0	2.4	1.9	1.6	1.4	1.2
③	2.0			19.2	6.4	3.8	2.7	2.1	1.7	1.4	1.2
④	2.4				17.2	5.7	3.4	2.4	1.9	1.5	1.3
⑤	2.6					15.6	5.2	3.1	2.2	1.7	1.4
⑥	2.6						9.3	3.1	1.8	1.3	1.0
⑦	3.0							10.8	3.6	2.1	1.5
⑧	3.0								3.6	1.2	0.7
⑨	3.0									3.6	1.2
⑩	3.0										0
$\bar{u}$ (kPa)		8.1	24.3	28.0	29.0	29.0	23.7	24.0	16.9	14.6	9.9

Table E.2   Excess pore pressures in simple shear sample MC9 during shearing
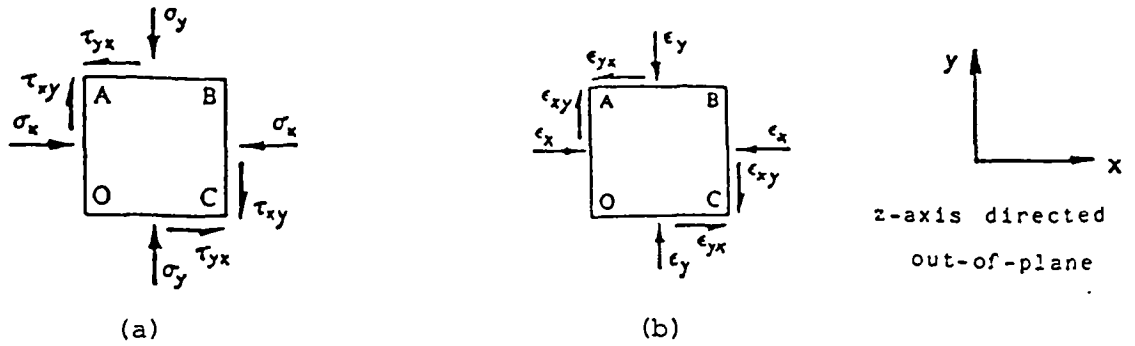
Figure 2.1   Two-dimensional stresses and strains
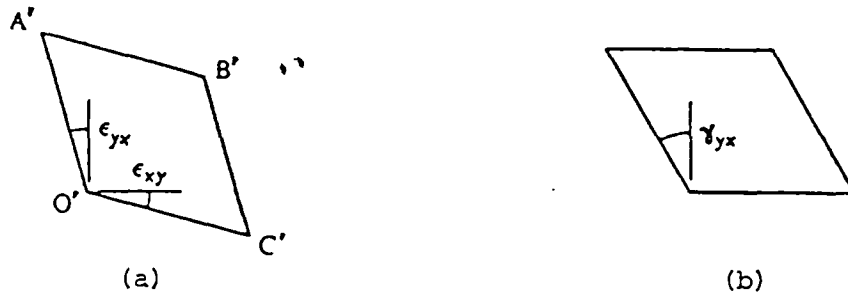
Figure 2.2   Pure shear strain and engineer's shear strain
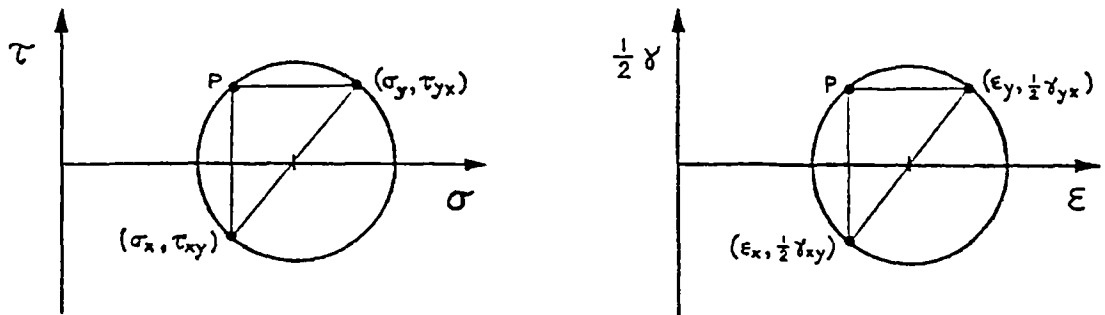
Figure 2.3   Mohr's circles of stress and strain
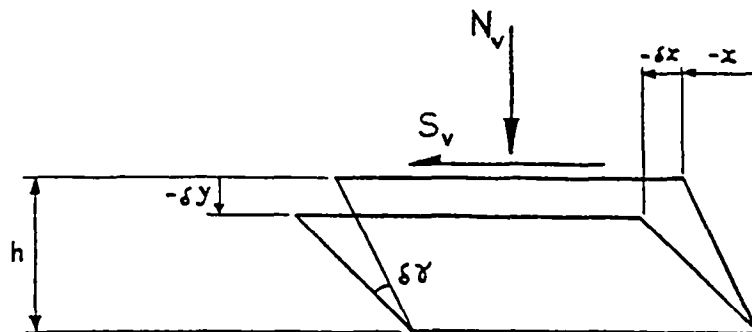
Figure 2.4   External loads, boundary displacements and increment
of simple shear strain
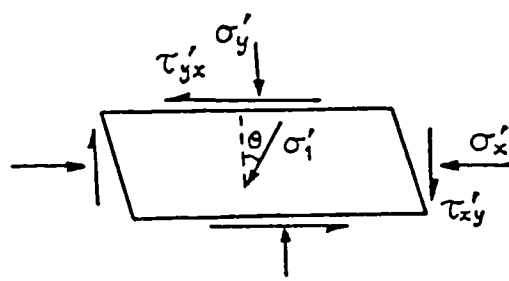
Figure 2.5   Stresses in simple shear sample
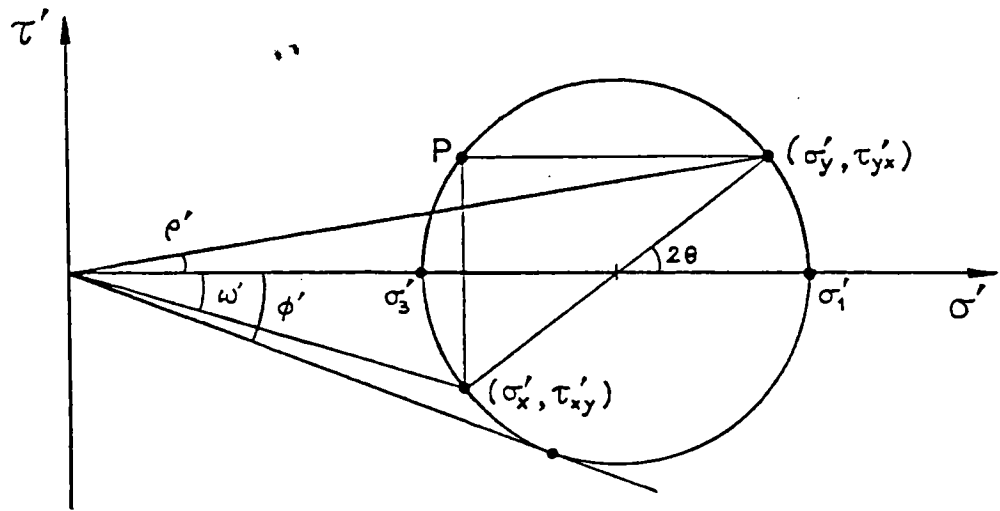
Figure 2.6   Mohr's circle of stress for simple shear sample
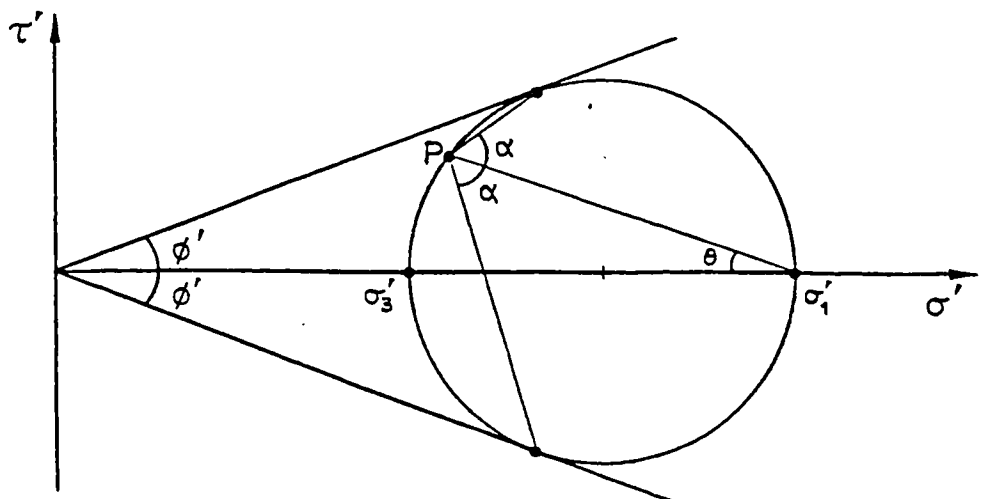
Figure 2.7   Planes subjected to maximum stress ratio
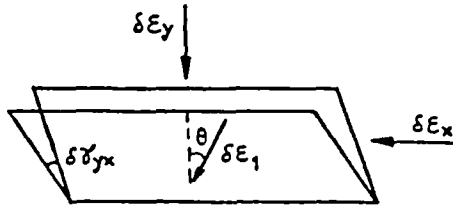
Figure 2.8   Strain increments of simple shear sample
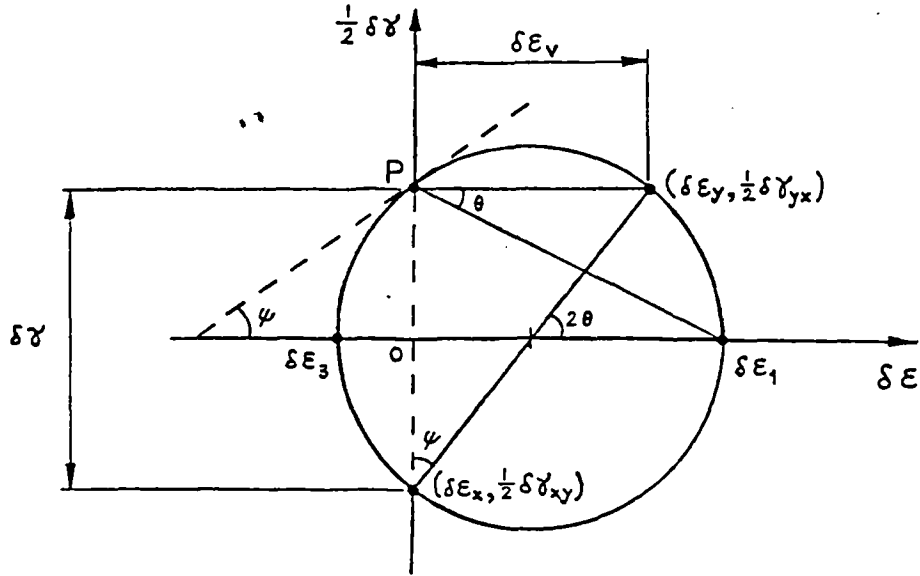
(a)   compression
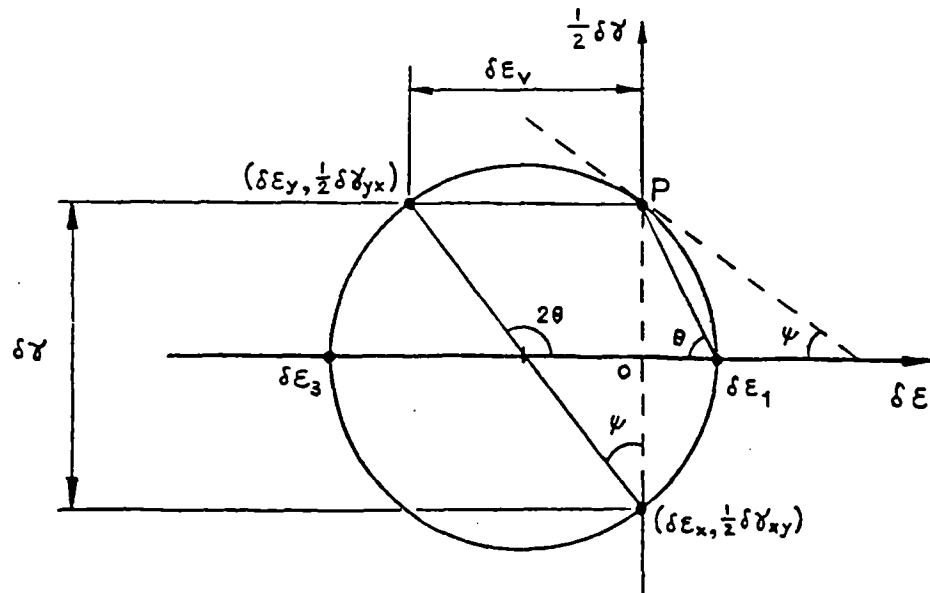
(b)   dilation

Figure 2.9   Mohr's circles of strain increment for simple shear sample
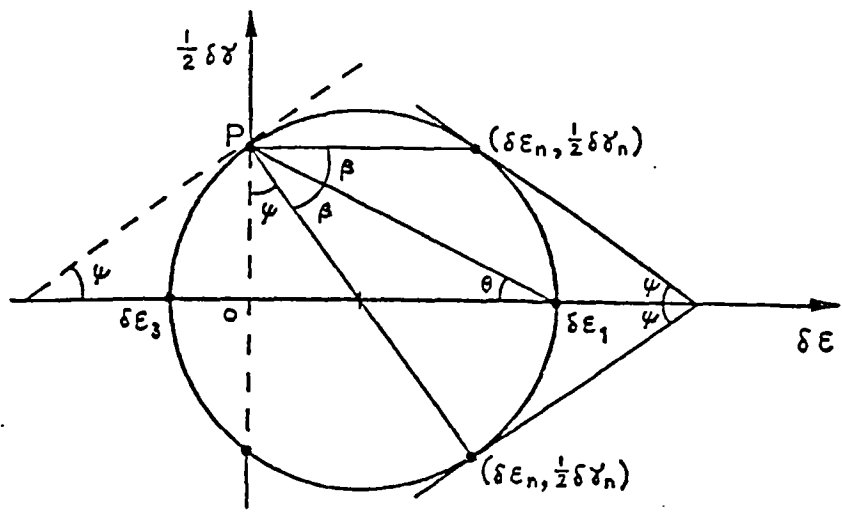
Figure 2.10 Directions of zero strain increment
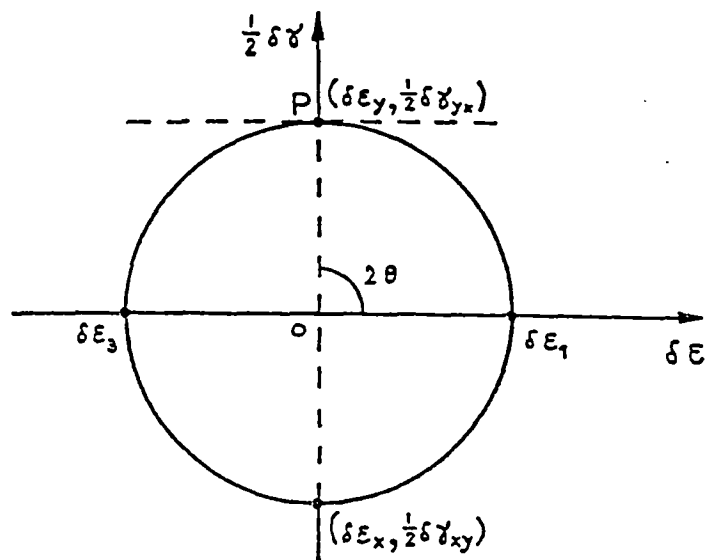
Figure 2.11 Mohr's circle of strain increment for constant volume shearing
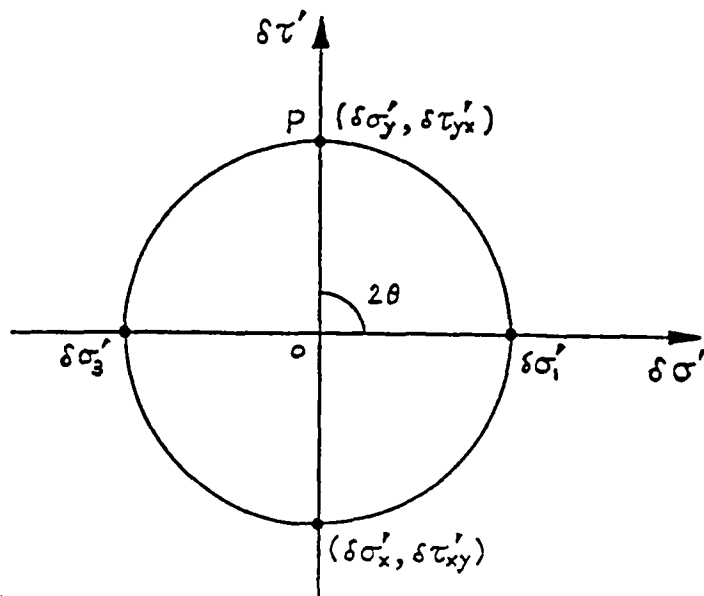
Figure 2.12 Mohr's circle of stress increment for an isotropic elastic simple shear sample
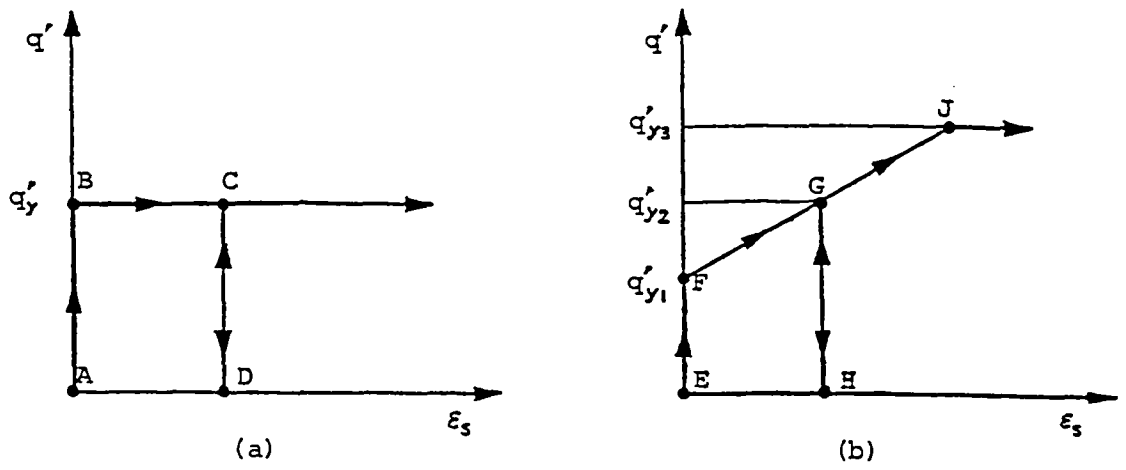
Figure 2.13 Examples of stress-strain behaviour of purely plastic soils
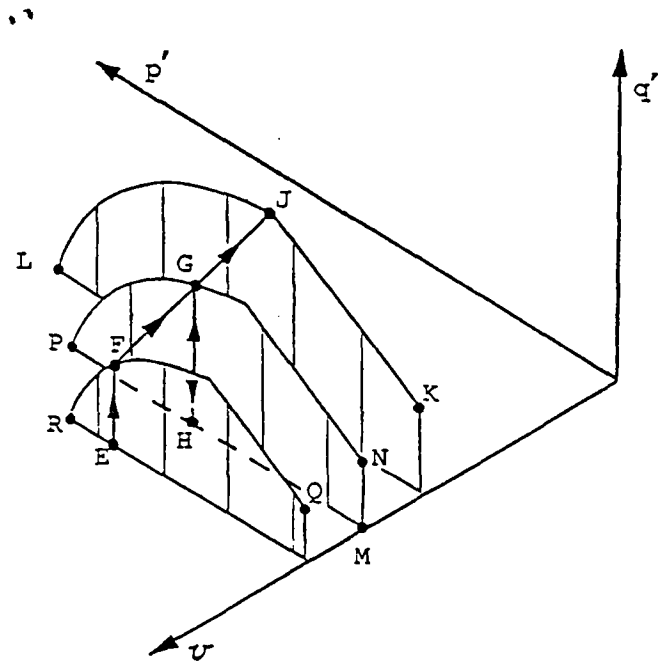
Figure 2.14 Yield curves at different specific volumes for a purely plastic soil
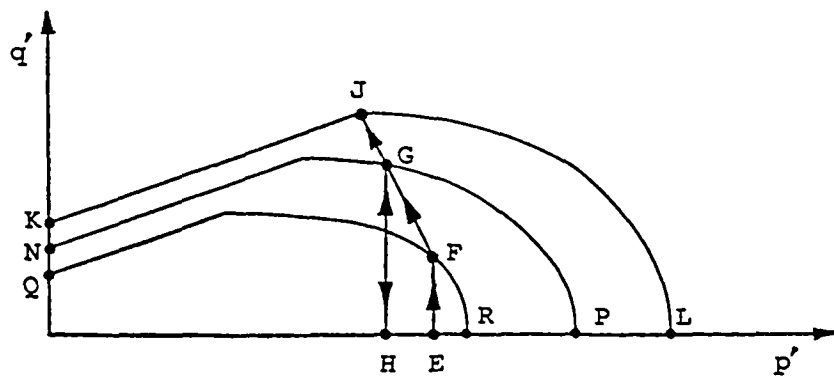
Figure 2.15 Projection of yield curves on p',q' plane
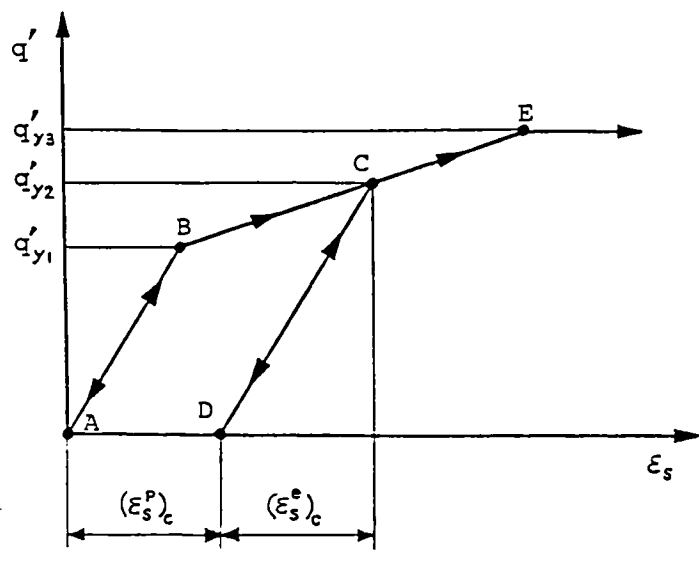
Figure   2.16   Example of stress-strain behaviour of
                   an elasto-plastic soil
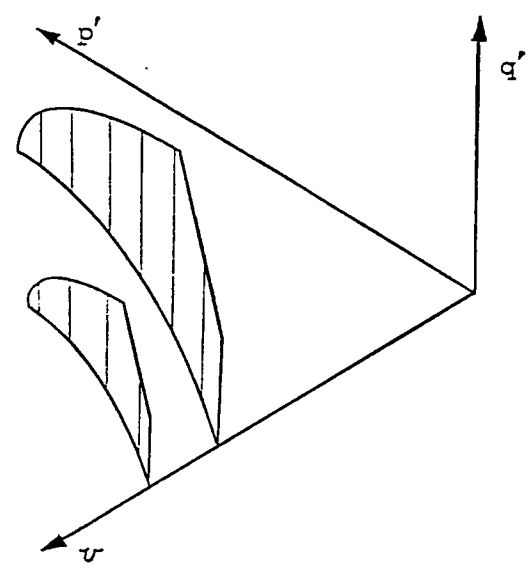
Figure   2.17   Elastic walls of an elasto-plastic soil
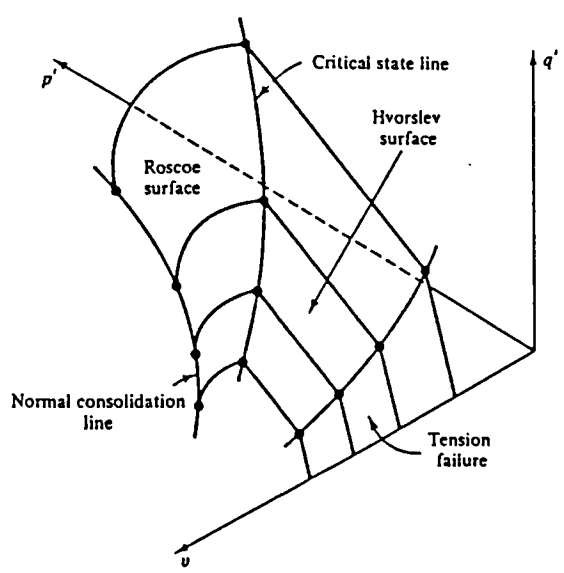
Figure   2.18   The complete state boundary surface
                   (after Atkinson and Bransby, 1978)
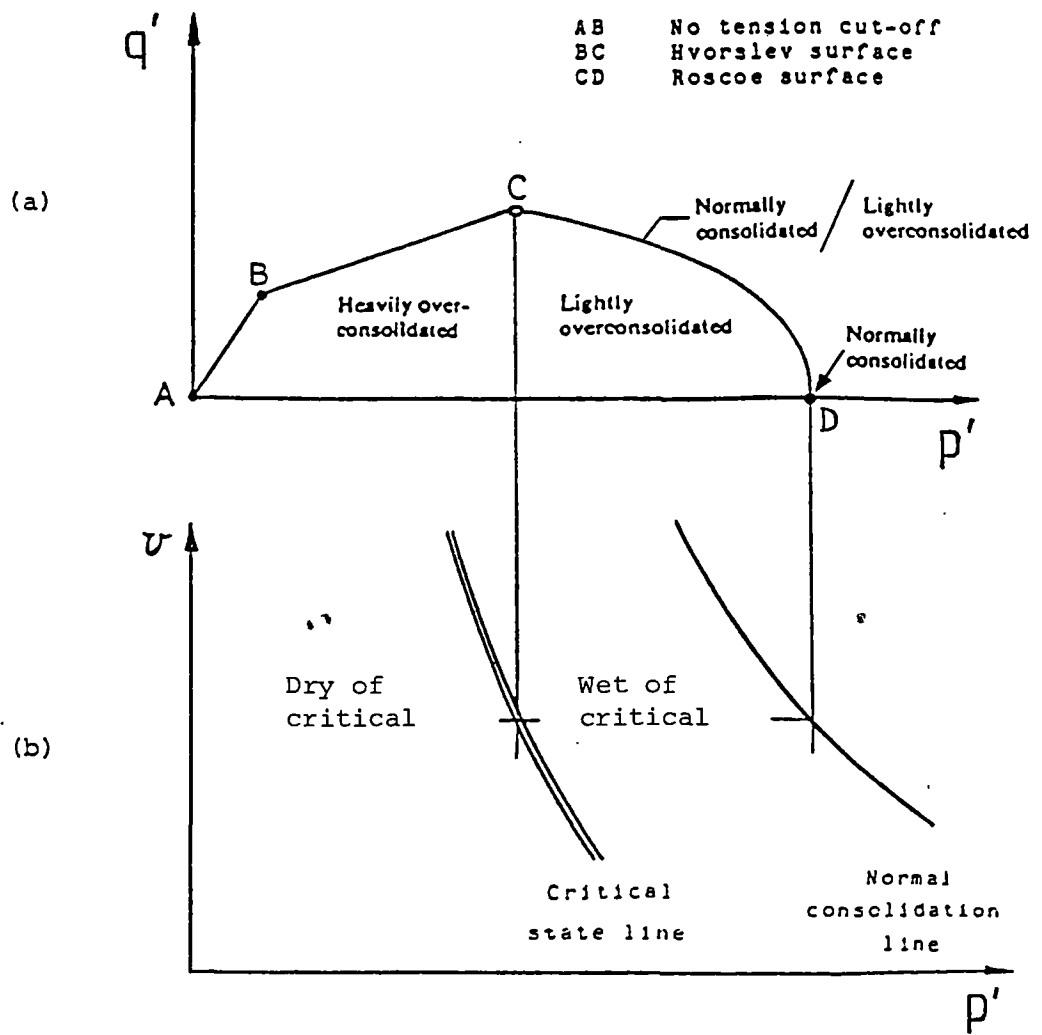
Figure 2.19   (a) Constant volume section of state boundary surface
and (b) wet side and dry side of critical
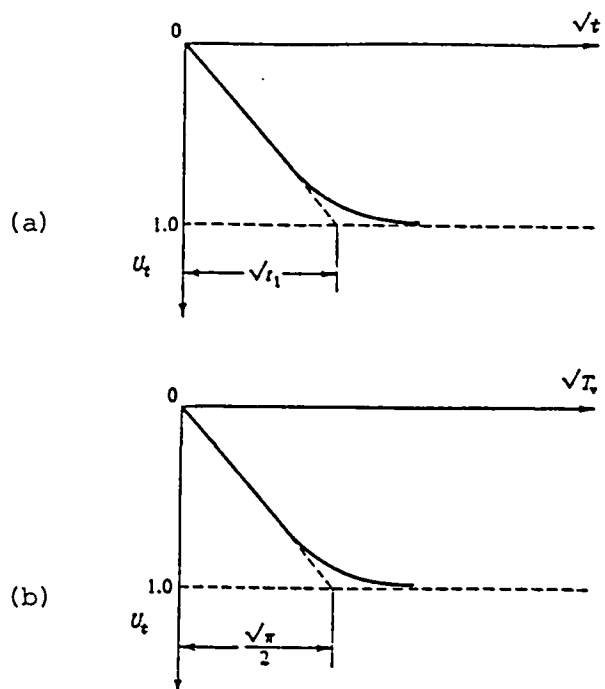
Figure 2.20   The √(time) curve fitting method
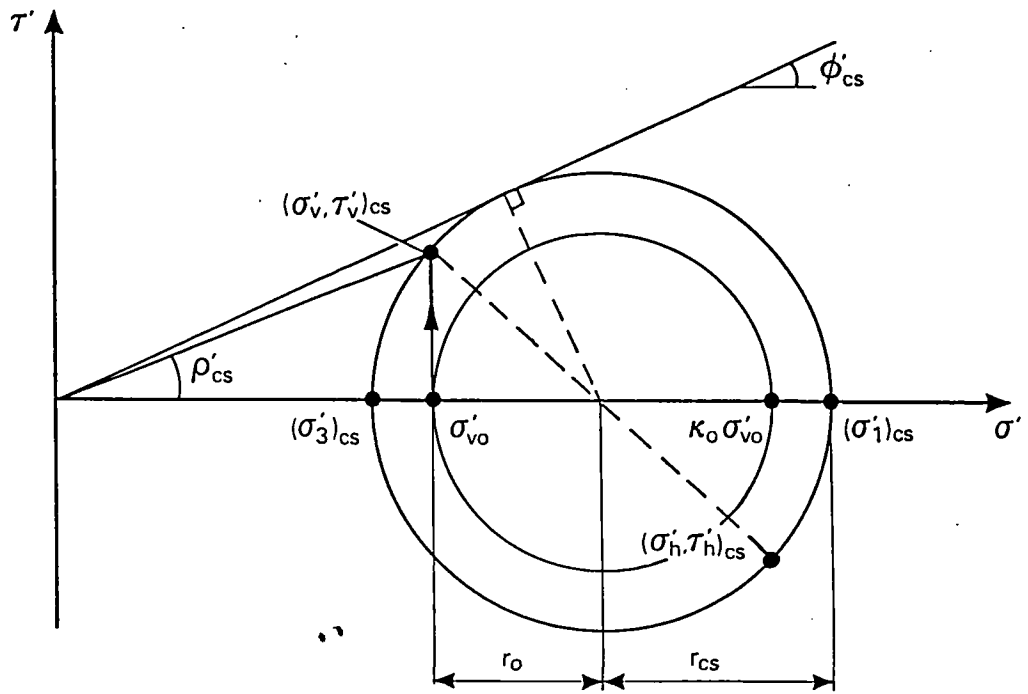
Figure 2.21 Influence of K_0 on ρ'_{cs} for simple shear tests
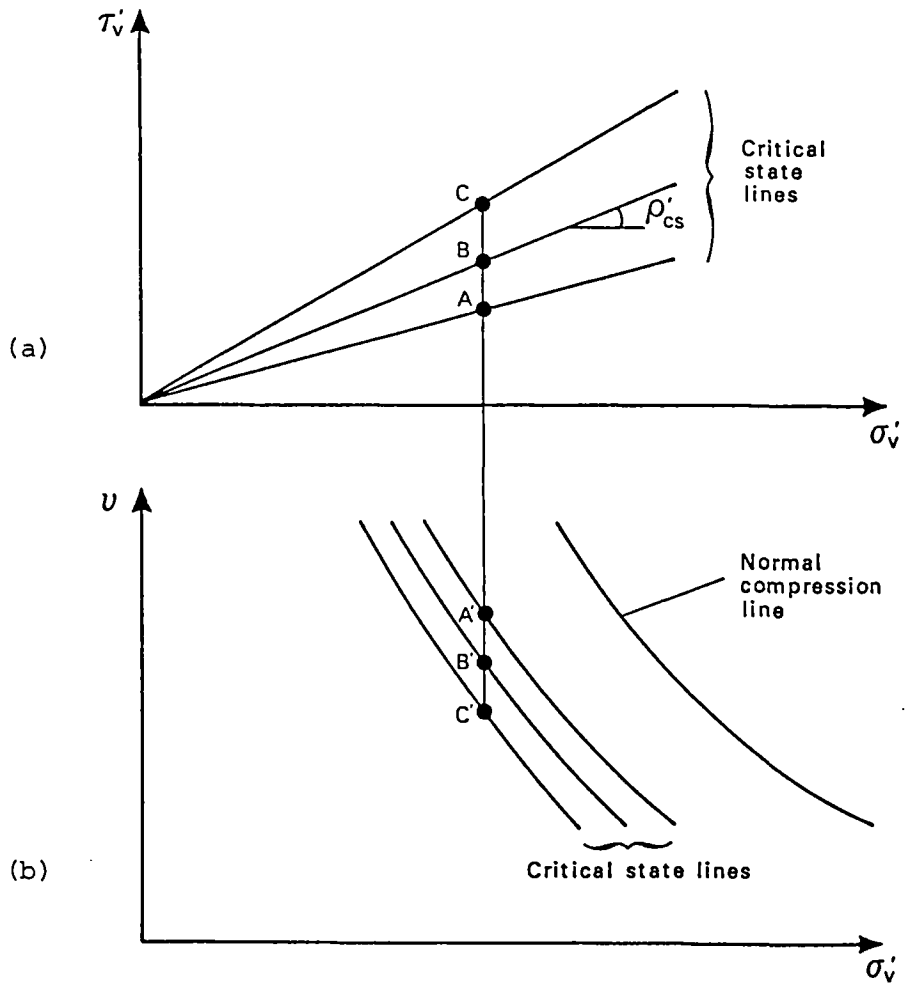
Figure 2.22 Critical state lines for simple shear tests
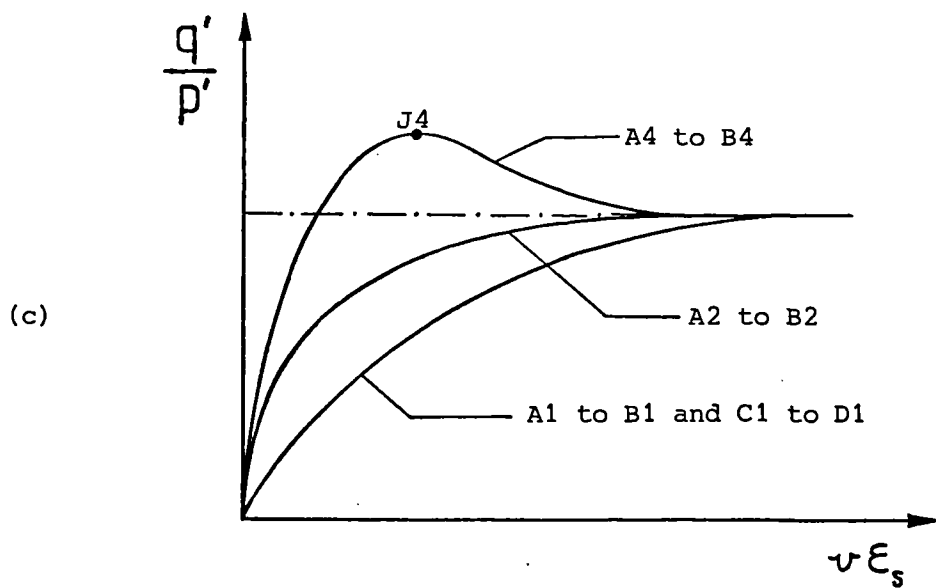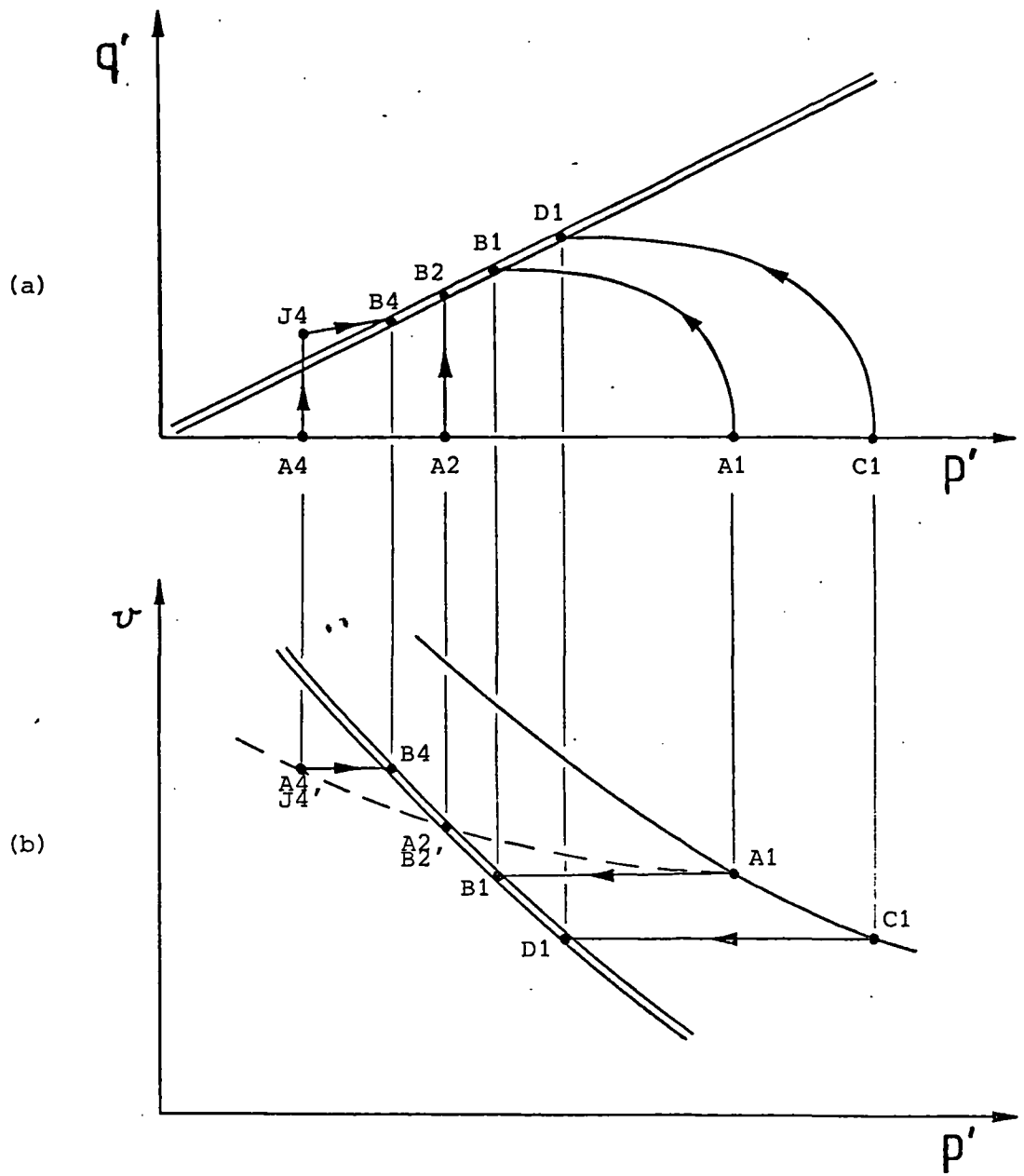
Figure 2.23   Idealised behaviour of soil in undrained
                triaxial compression tests
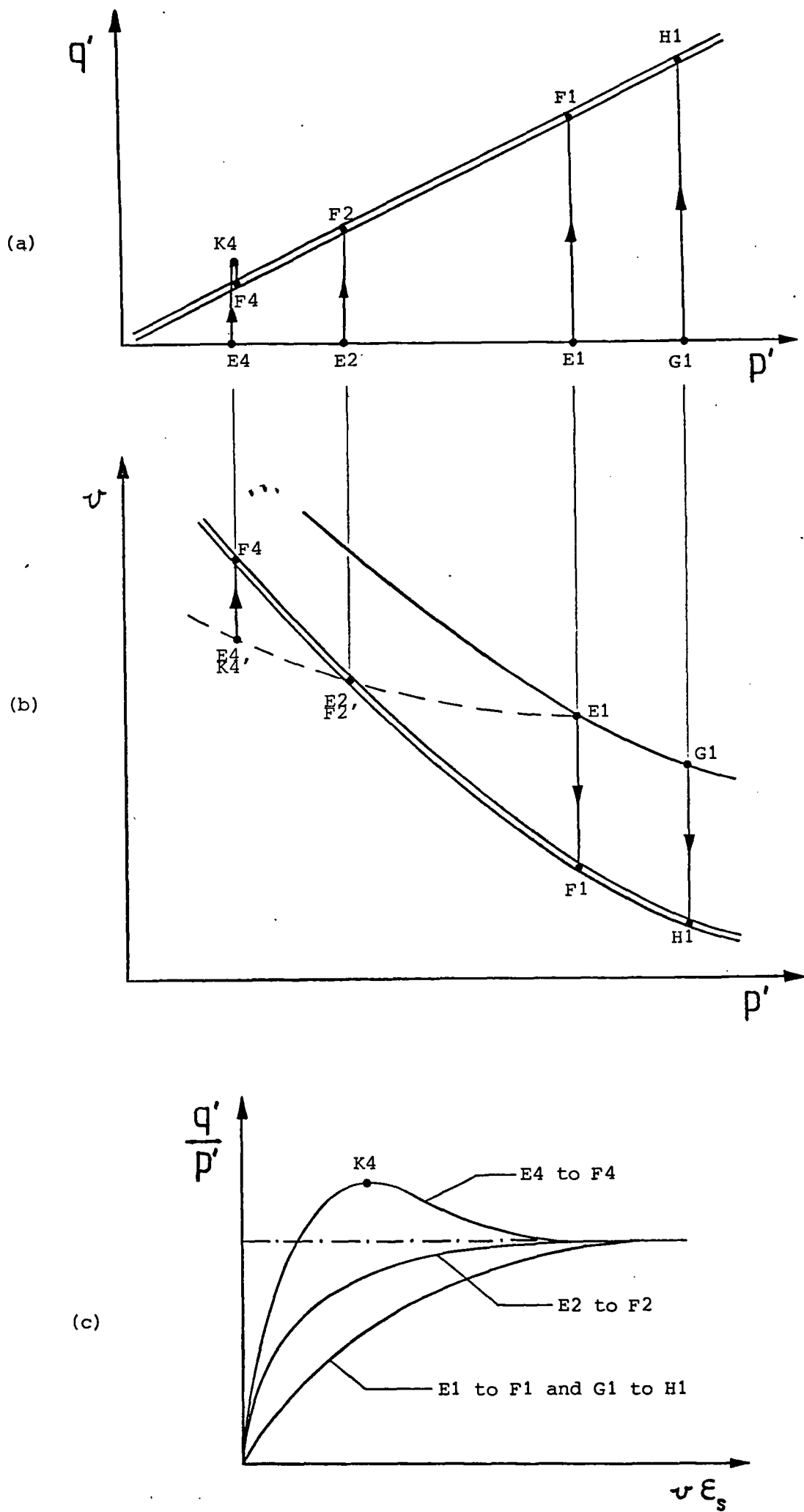
Figure 2.24   Idealised behaviour of soil in constant p'
triaxial compression tests

(a)

(b)
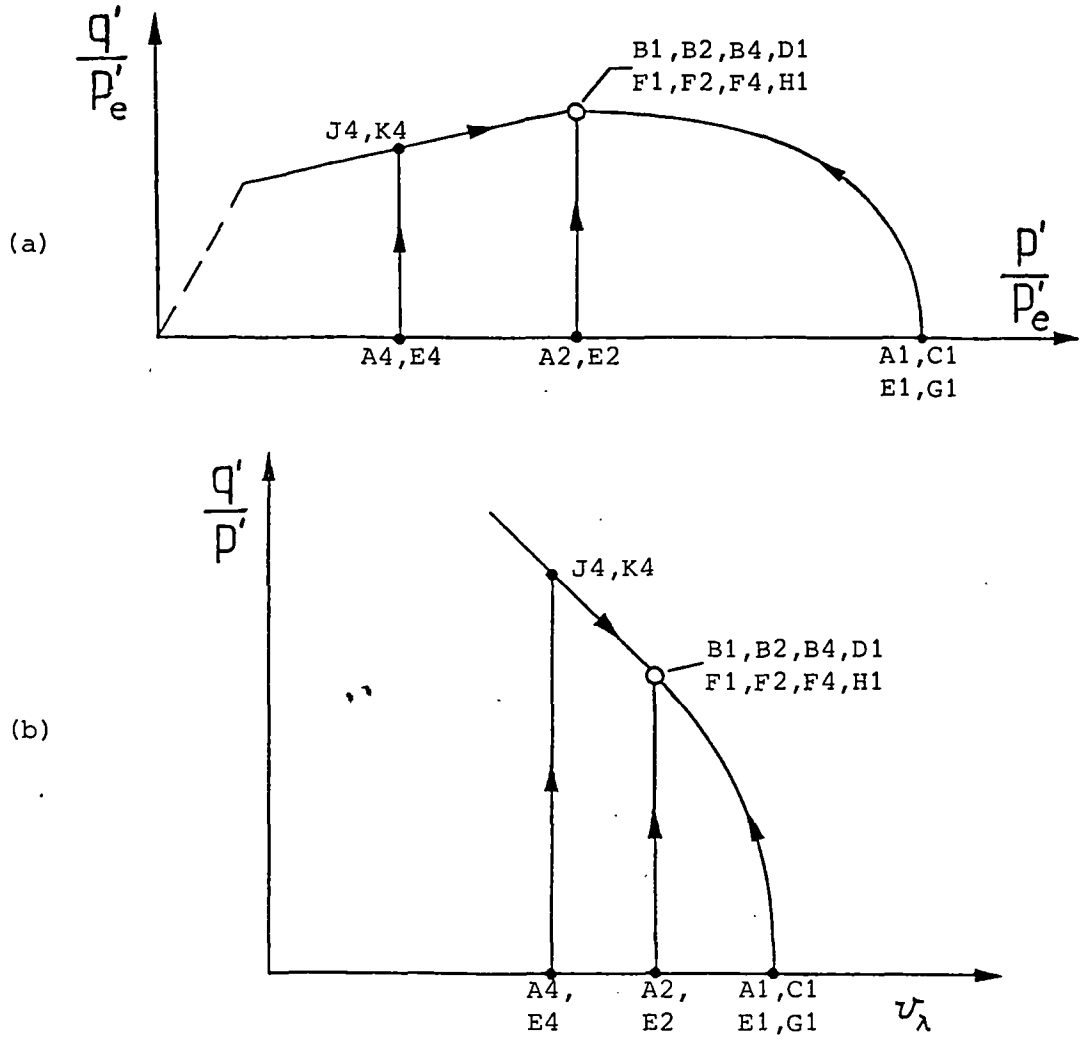
Figure   2.25   Ideal normalised behaviour of soil in
                   triaxial compression tests

NCL = normal consolidation line
CSL = critical state line
SL = swelling line
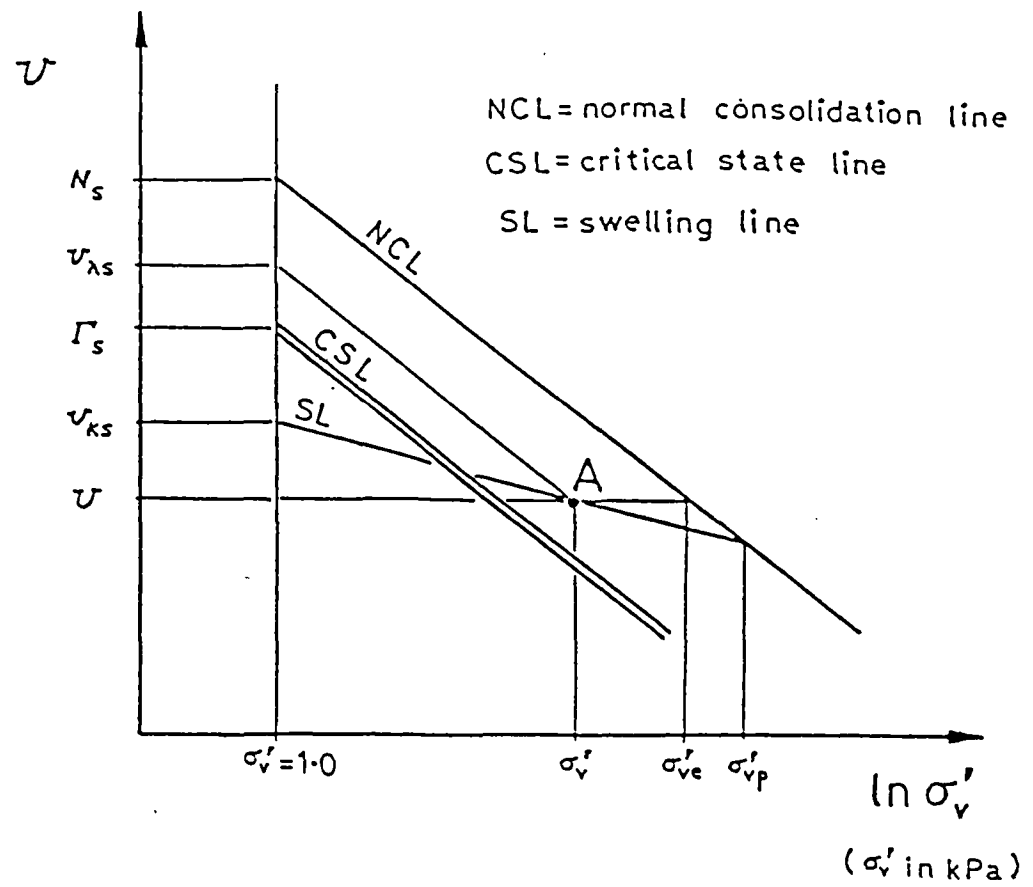
Figure   2.26   Normalising parameters for simple shear tests
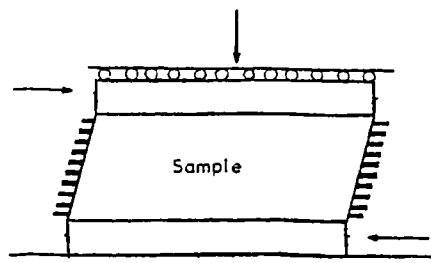
(a) SGI (Kjellman,1951)
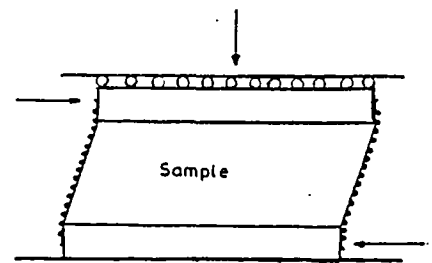
(b) NGI (Bjerrum and Landva,1966)
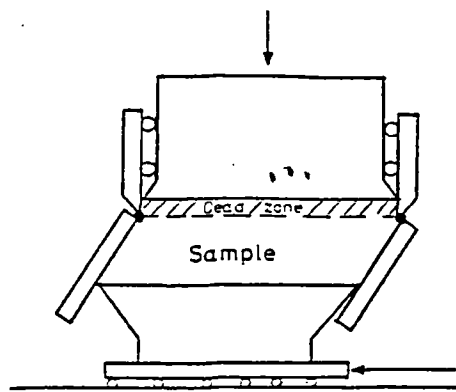
(c) Cambridge (Roscoe,1953)
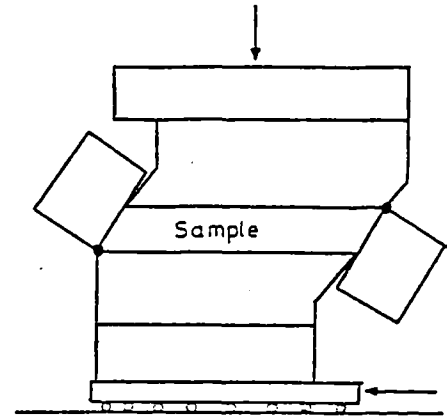
(d) Cambridge (Bassett, 1967)

Figure 3.1   Basic designs of simple shear apparatus
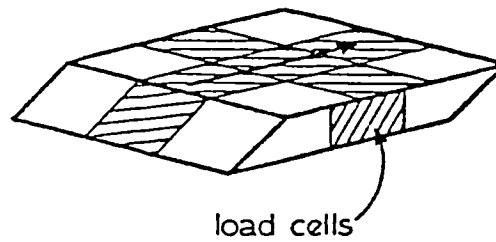
load cells

Figure 3.2   Arrangement of load cells in Cambridge simple shear apparatus (after Wood et al,1980)

shear stress τ_{yx}'

simple shear sample
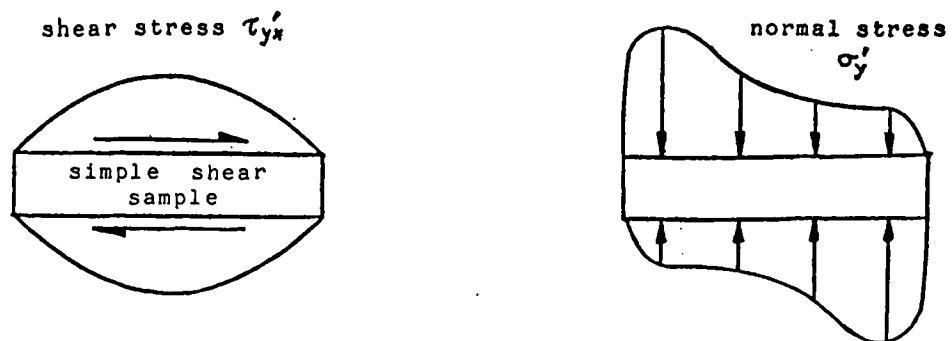
normal stress σ_y'

Figure 3.3   Pattern of non-uniform stress distribution due to lack of complementary shear stress τ_{xy}'
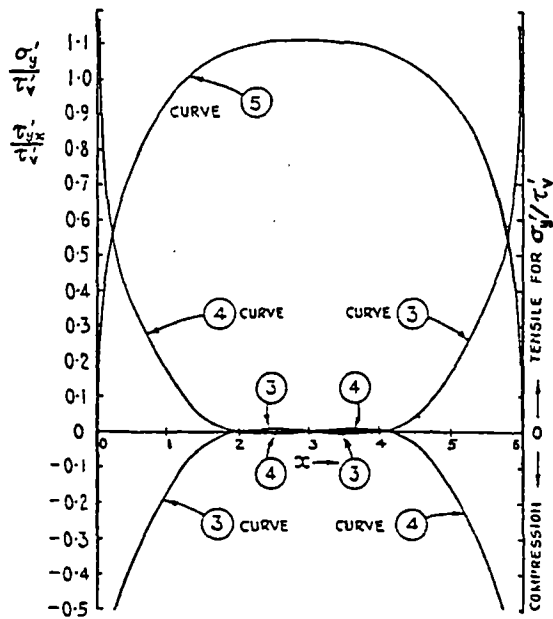
Curve (3): normal stresses for top boundary.

Curve (4): normal stresses for bottom boundary.

Curve (5): shear stresses for top and bottom boundaries.
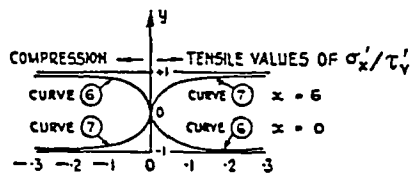
Curves (6) and (7): normal stresses for ends of sample.

Figure   3.4   Stress distributions on simple shear sample
                 calculated by mathematical analyses
                 (after Roscoe, 1953)
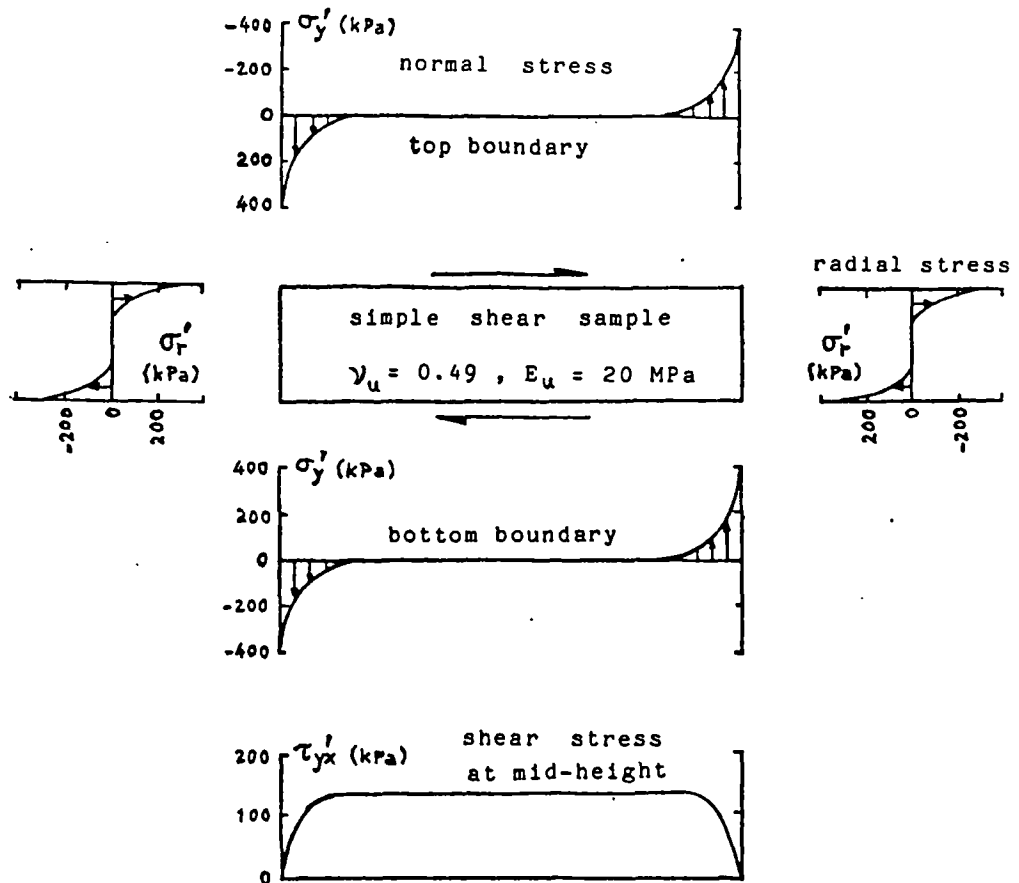
Figure   3.5   Stress distributions on simple shear sample
                 calculated by finite element analyses
                 (After Lucks et al, 1972)
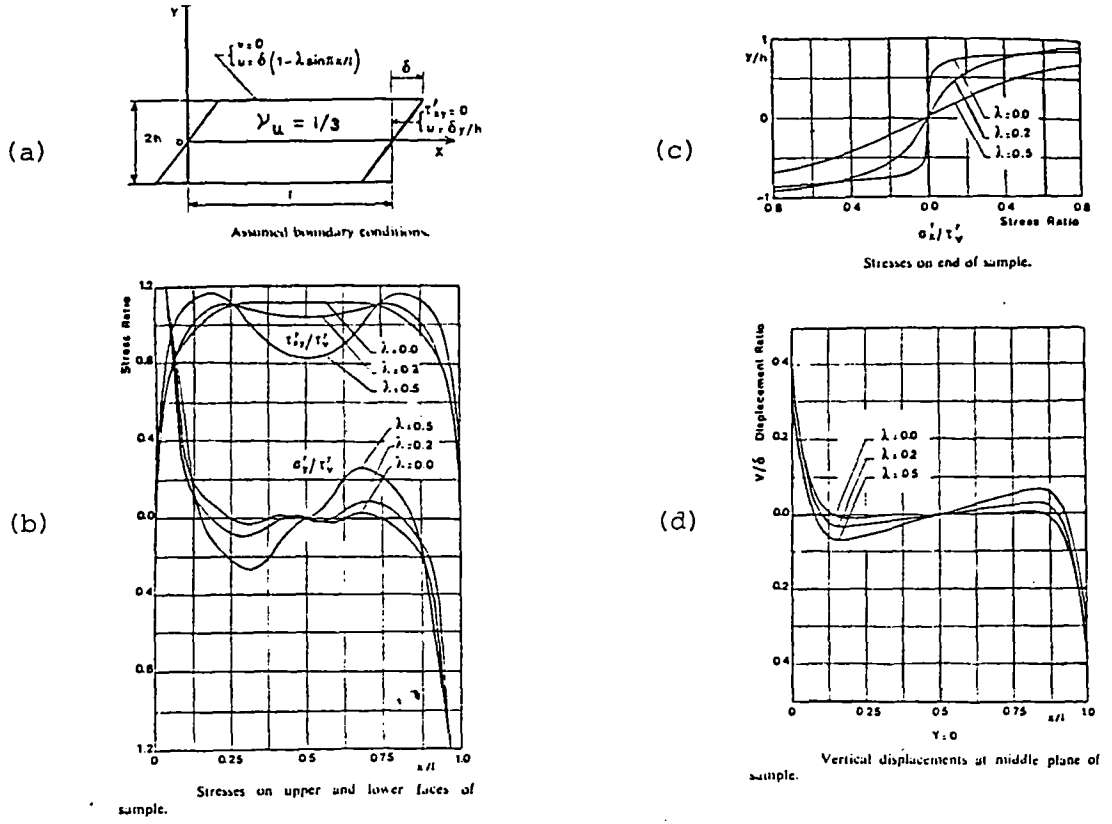
Figure 3.6   Effects of slippage (after Prevost and Høeg,1976)
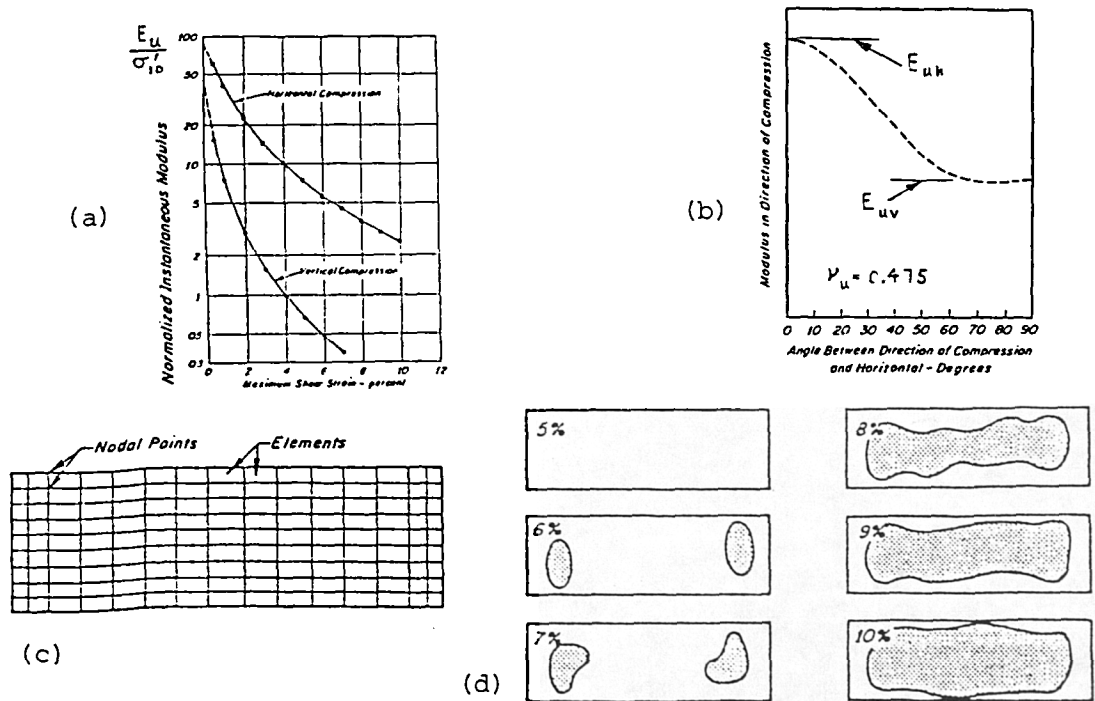
Figure 3.7   Finite element analyses (after Duncan and Dunlop,1969)

(a) Principal third   (b) Central third   (c) Sample core
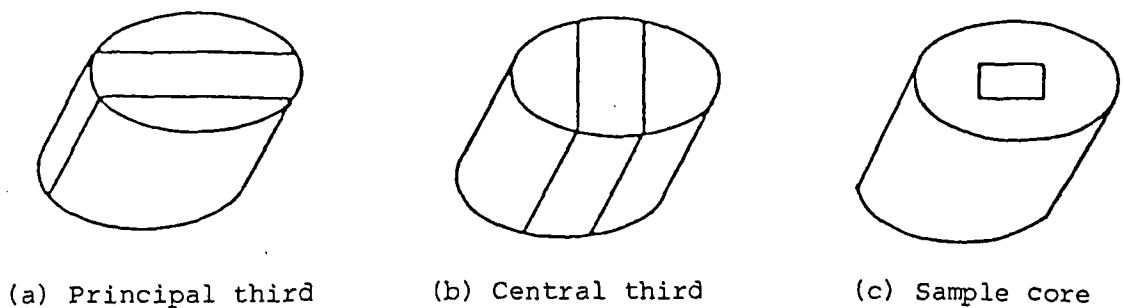
Figure 3.8   Three areas of a simple shear sample

$\gamma = 0$

$\gamma = 10 \%$

$\gamma = 20 \%$

σ_y' (kPa)

σ_y' (kPa)

τ_{yx}' (kPa)

τ_{yx}' (kPa)

τ_{yx}' (kPa)

σ_y' (kPa)
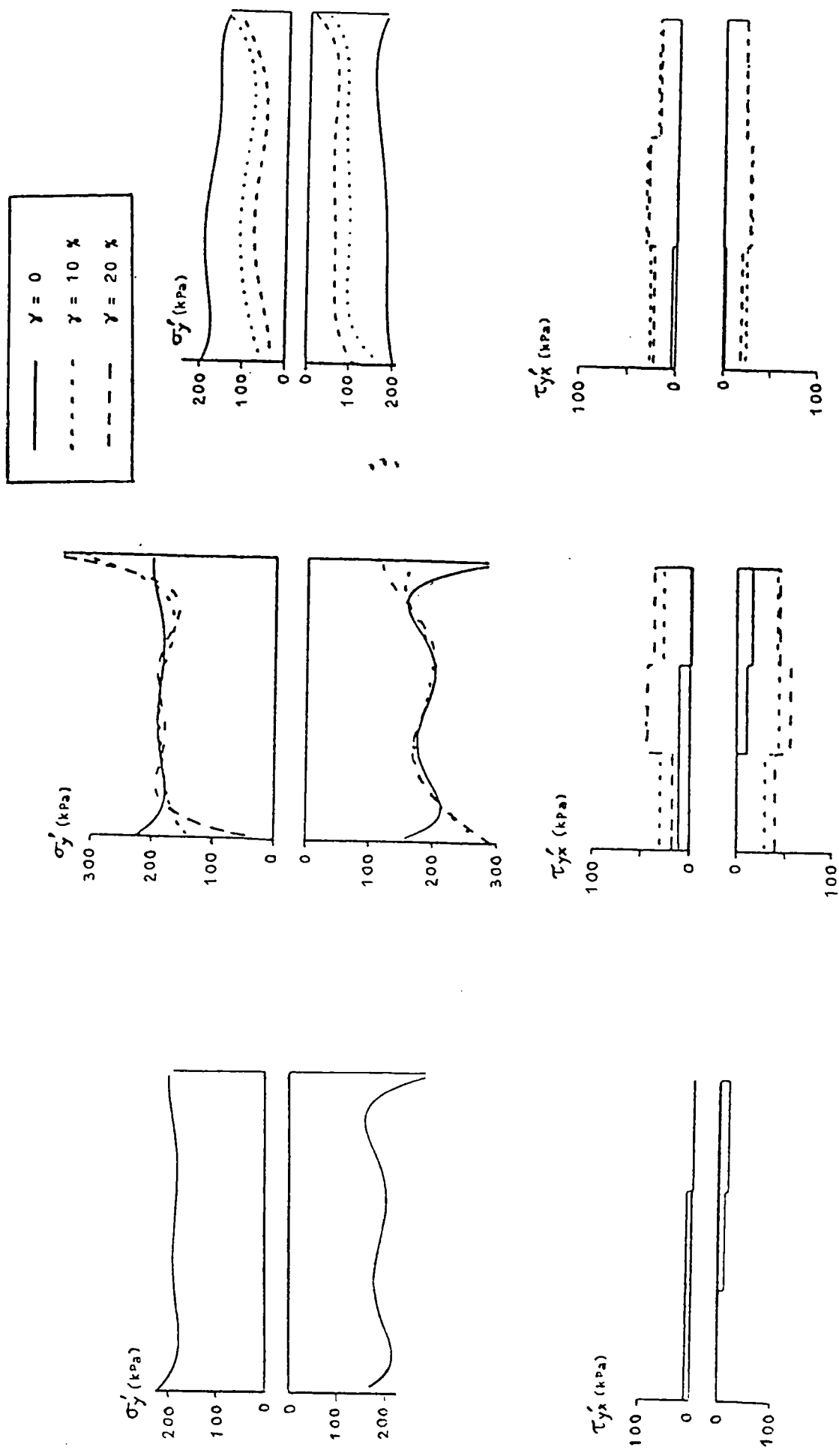
(a) after one-dimensional compression

(b) constant σ_v' shearing

(c) constant volume shearing

Figure 3.9   Stress distributions on the principal third of normally compressed kaolin samples (Airey,1984)
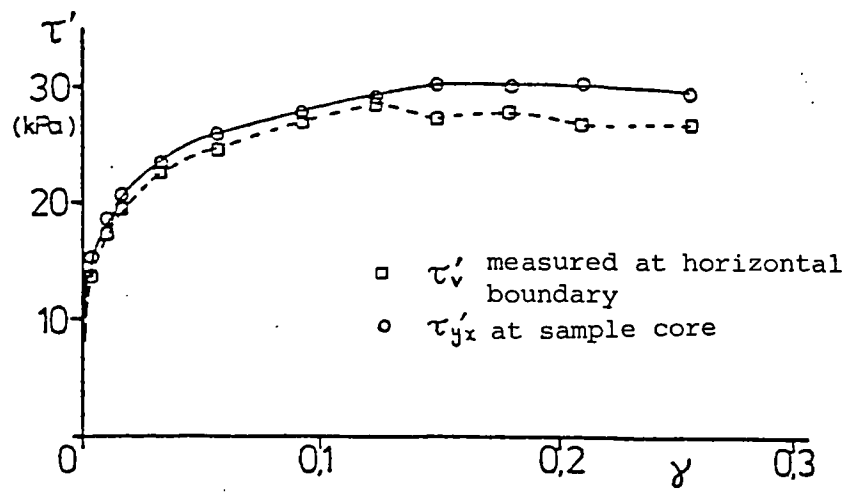
Figure 3.10   Comparison of average and sample core shear
                 stresses in a constant σ_v' test (Airey,1984)
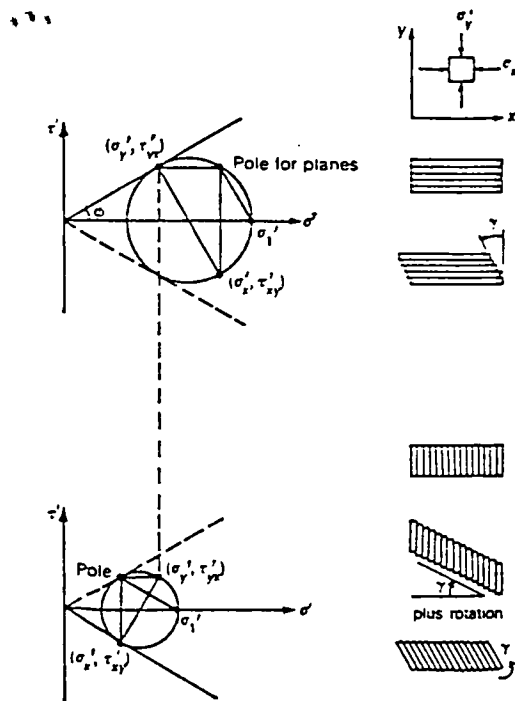
Figure 3.11   Possible modes of failure in simple shear
                 proposed by De Josselin de Jong (1972)
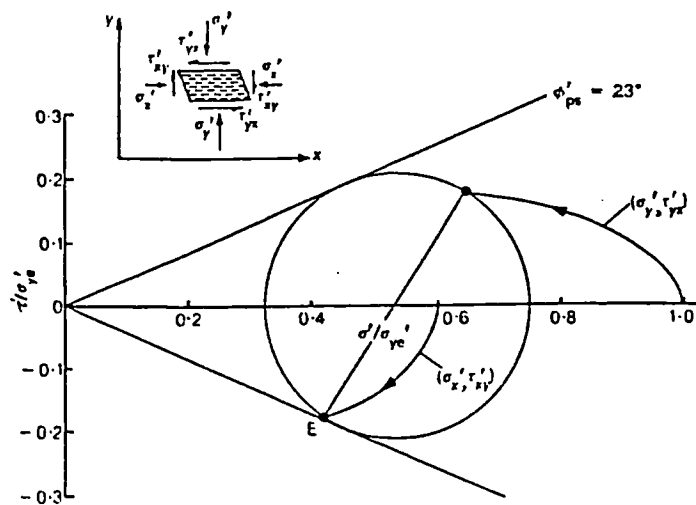
Figure 3.12   Results of an undrained simple shear test on
                 normally compressed kaolin (Borin,1973)
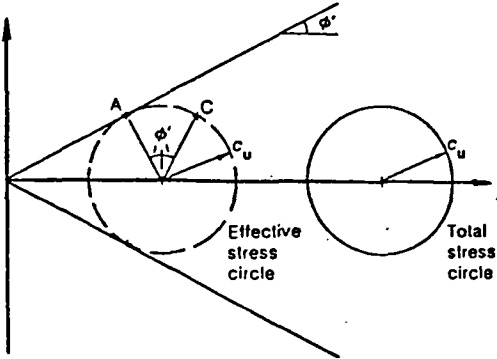
Figure   3.13   Possible stress state at failure in simple shear
                suggested by Ladd and Edgers (1972)
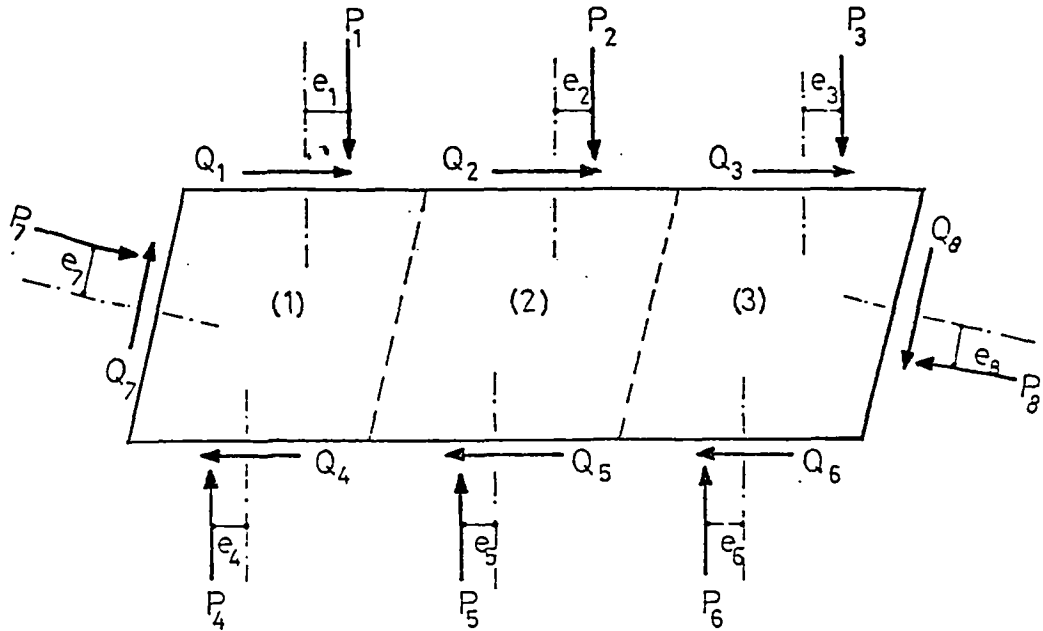
Figure   3.14   Load cell measurements from the principal third
                of a Cambridge simple shear sample (after Budhu
                and Wood, 1979)
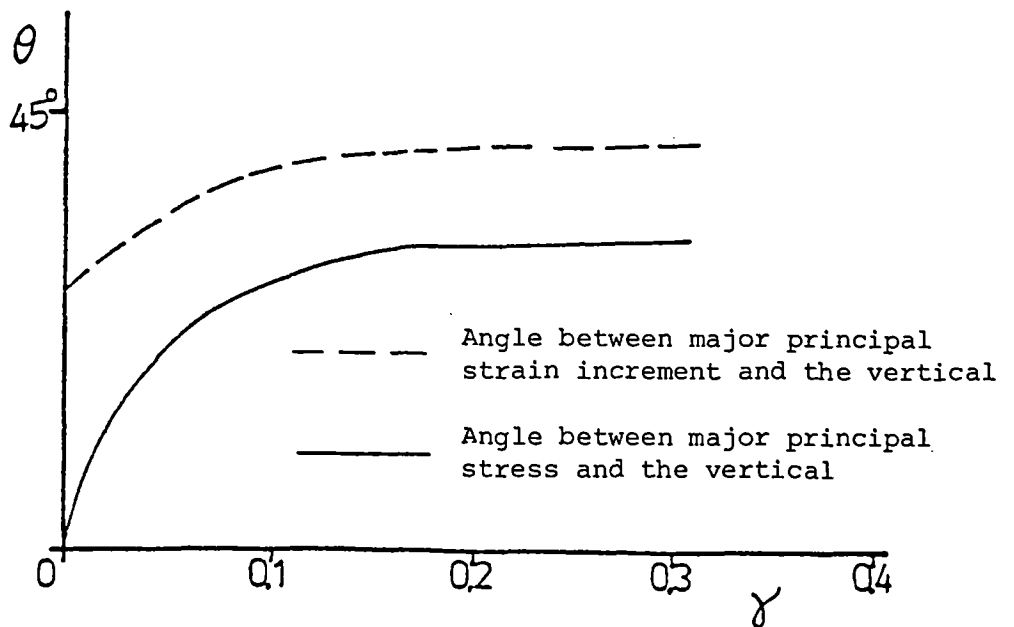
Figure   3.15   Rotations of principal axes of stress and strain
                increment for a simple shear test on kaolin
                (after Borin,1973)
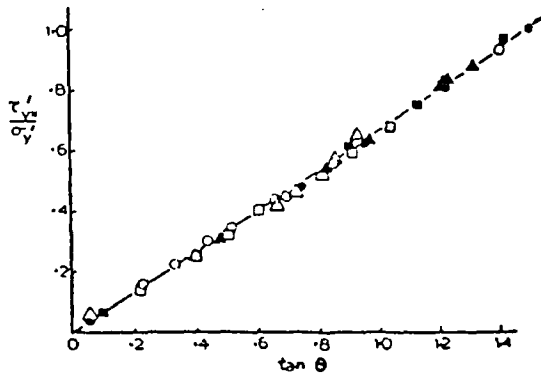
(a) Leighton Buzzard sand
(Wood et al,1980)
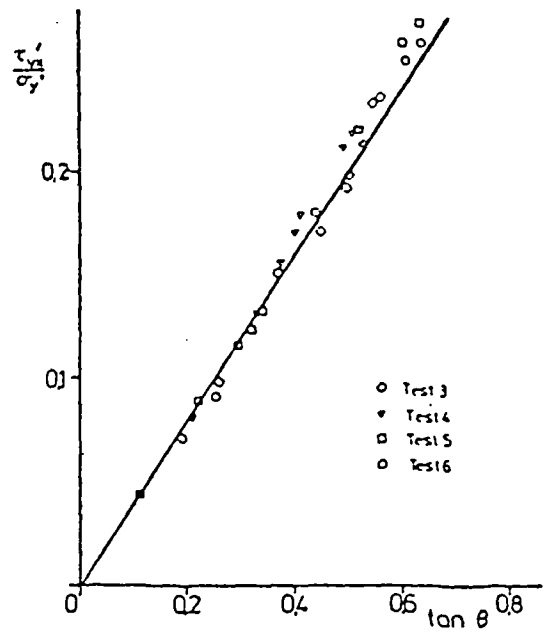
(b) Spestone kaolin (Borin,1973)

Figure 3.16 Relation between stress ratio and rotation of principal stress axes
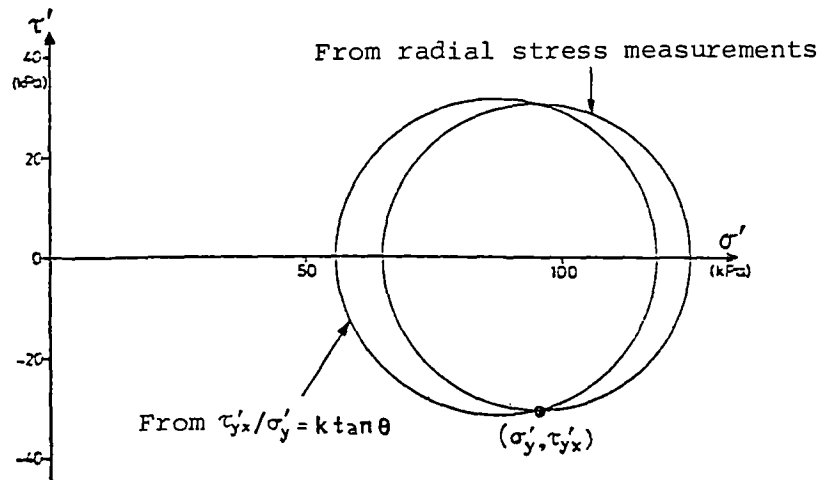
Figure 3.17 Comparison of Mohr's circles of stress at failure constructed using two different methods (Airey,1984)
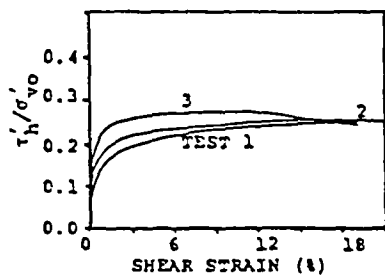
Test 1 — Gulf of Mexico clay

Test 2 — Gulf of Alaska clay

Test 3 — Pacific Illite
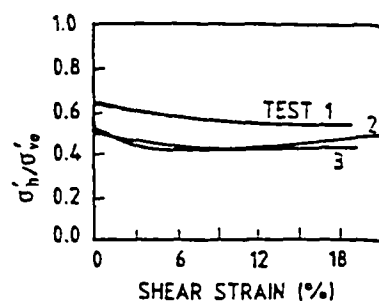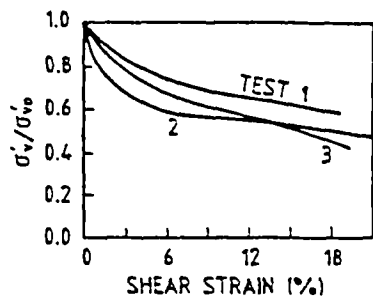
Figure 3.18 Basic test data obtained using NGI simple shear apparatus with radial stress measurements (Dyvik and Zimmie,1983)
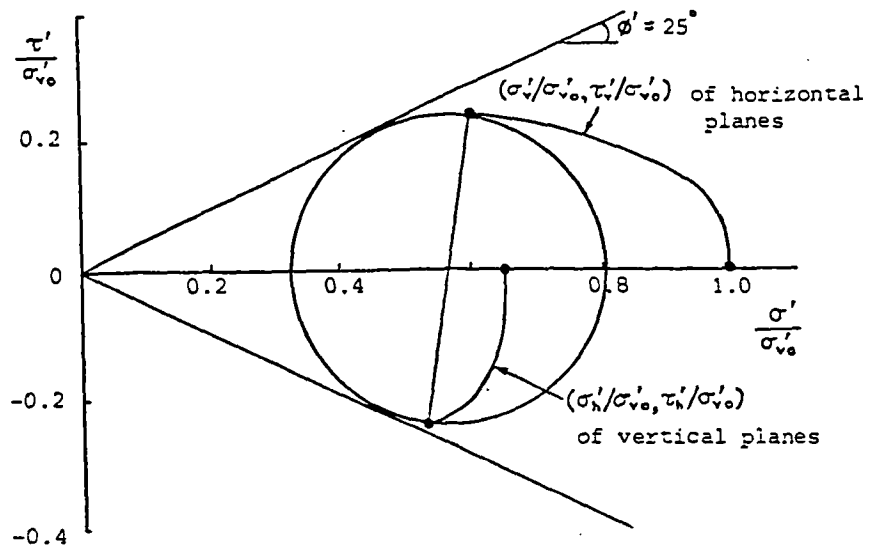
(a) Test 1 — Gulf of Mexico clay
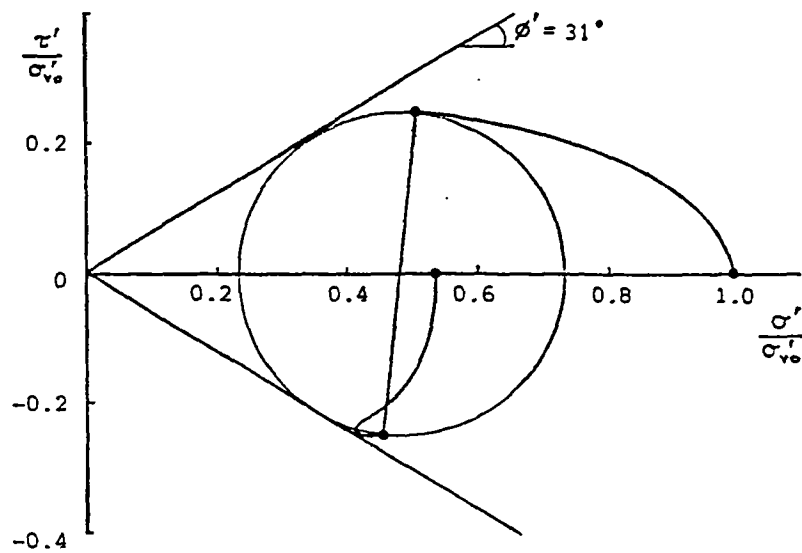
(b) Test 2 — Gulf of Alaska clay
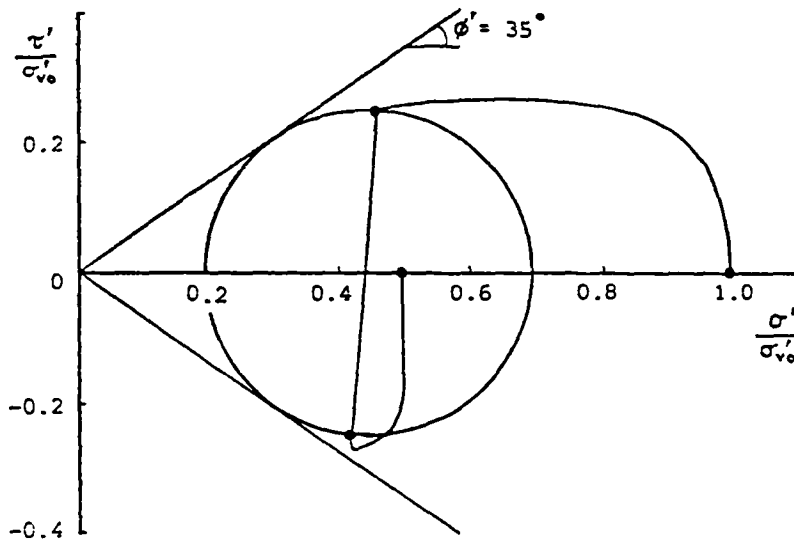
(c) Test 3 — Pacific Illite

Figure 3.19   Effective stress paths and Mohr's circles of
                stress plotted using data shown in Figure 3.18
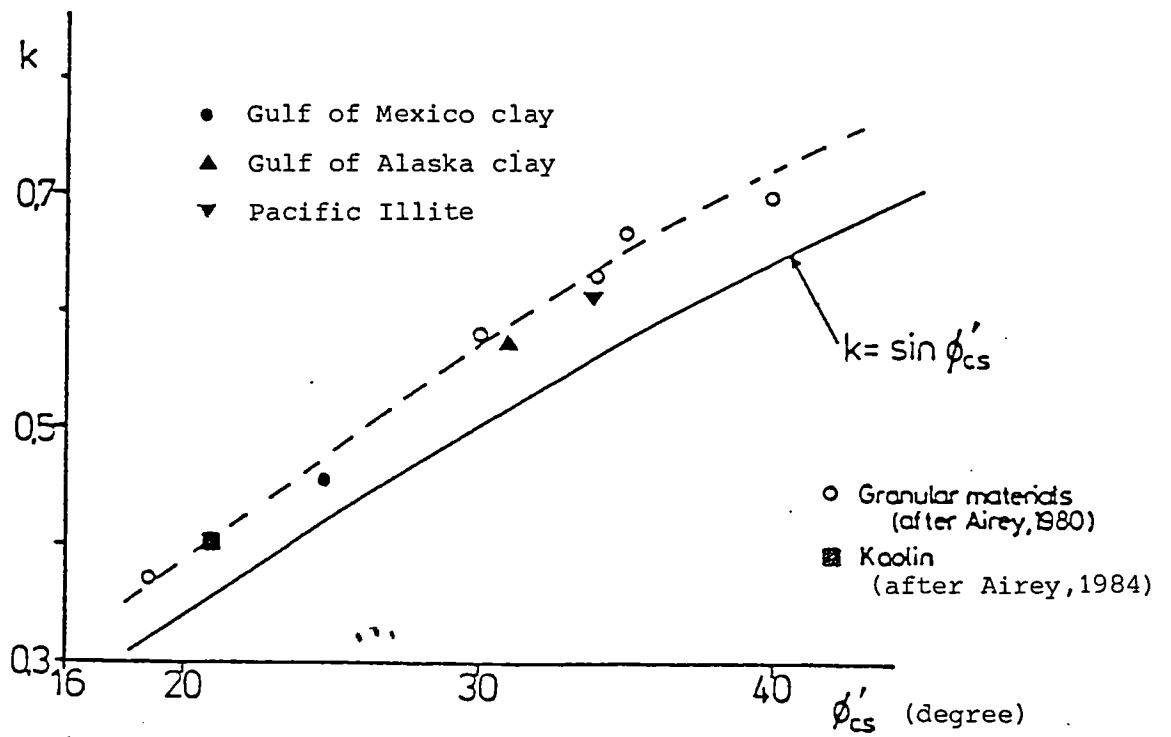
Figure   3.20   Relation between k and critical state friction angle
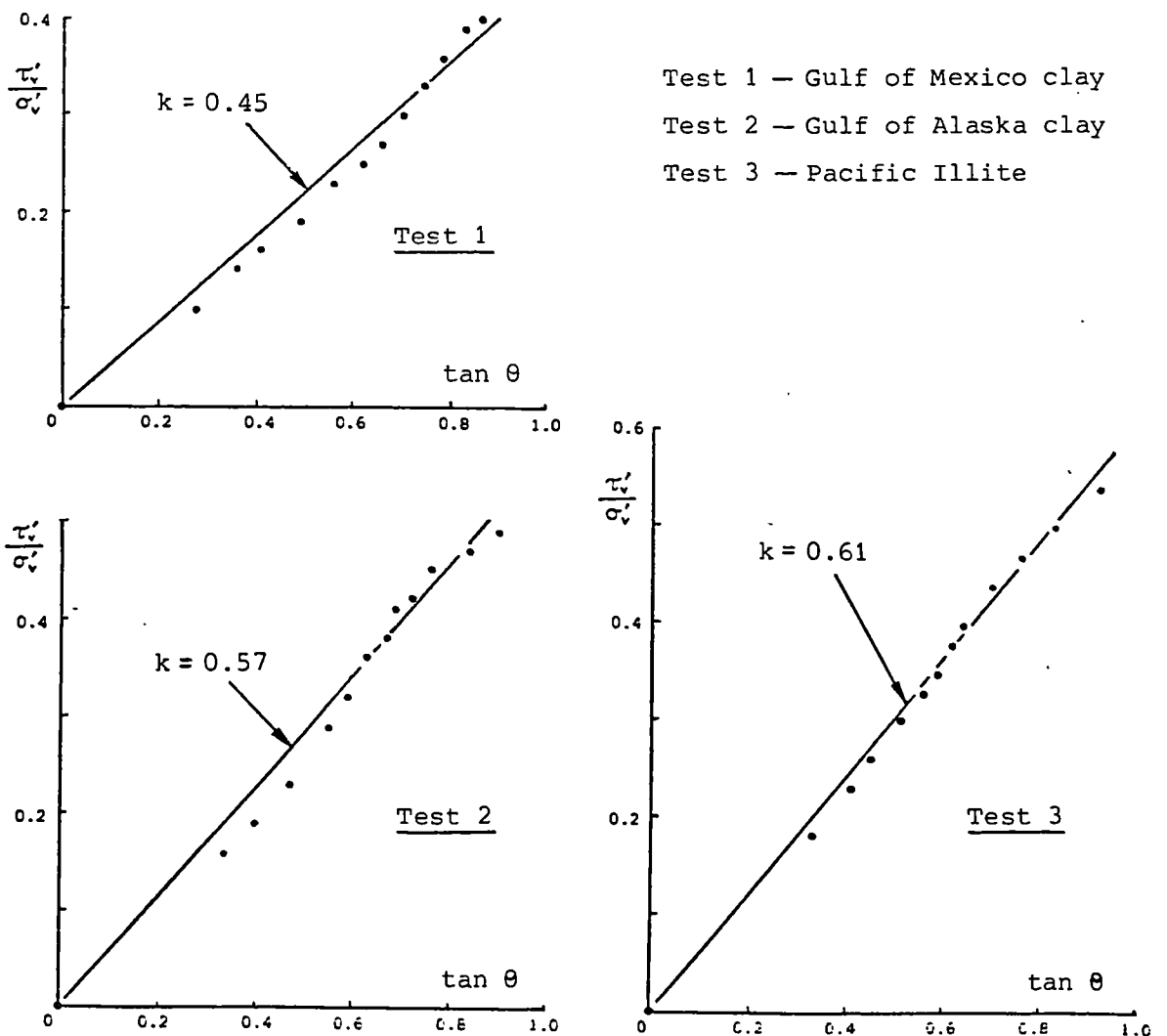
Figure   3.21   Relation between stress ratio and rotation of principal
stress axes plotted using data shown in Figure 3.18

(a)

(b)

(c)
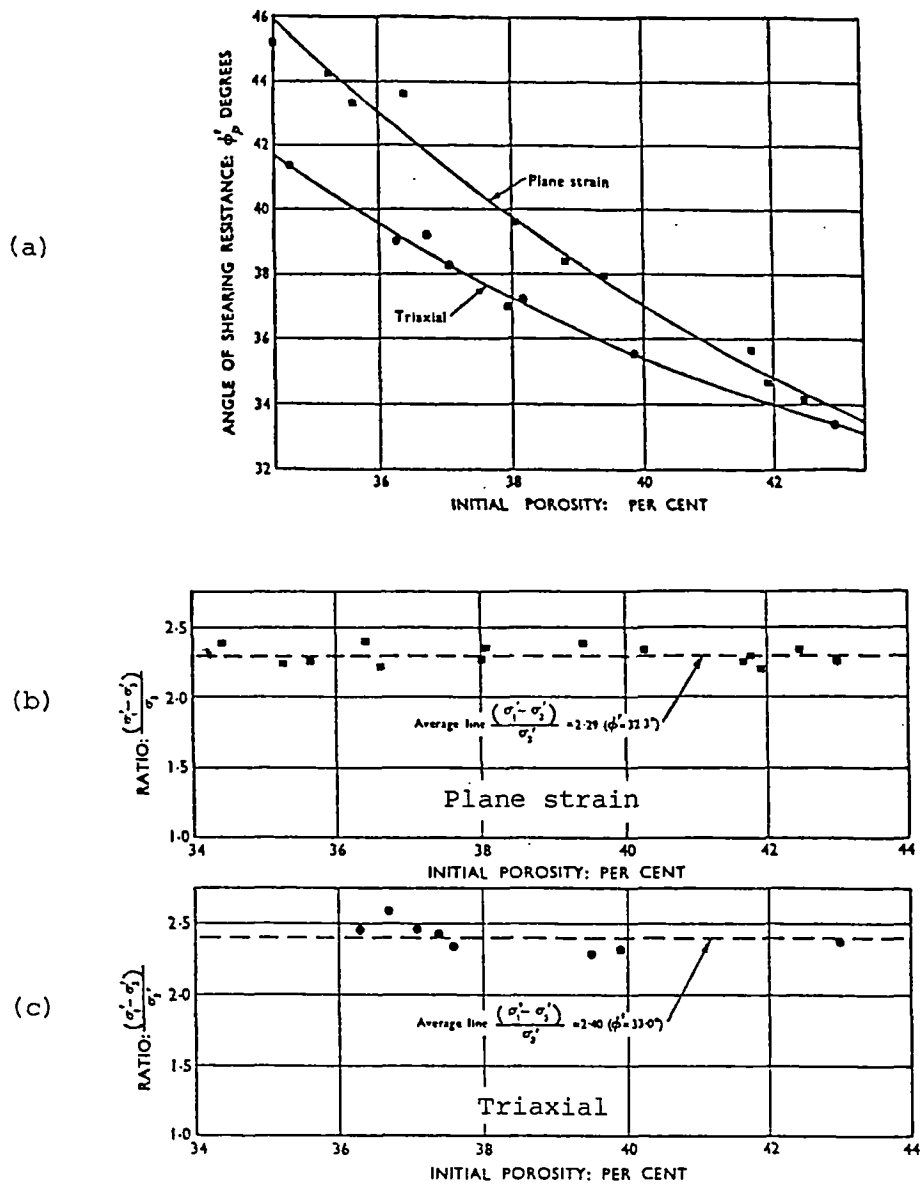
Figure 3.22 Comparison of triaxial test and plane strain test results for Brasted sand (after Cornforth,1964)
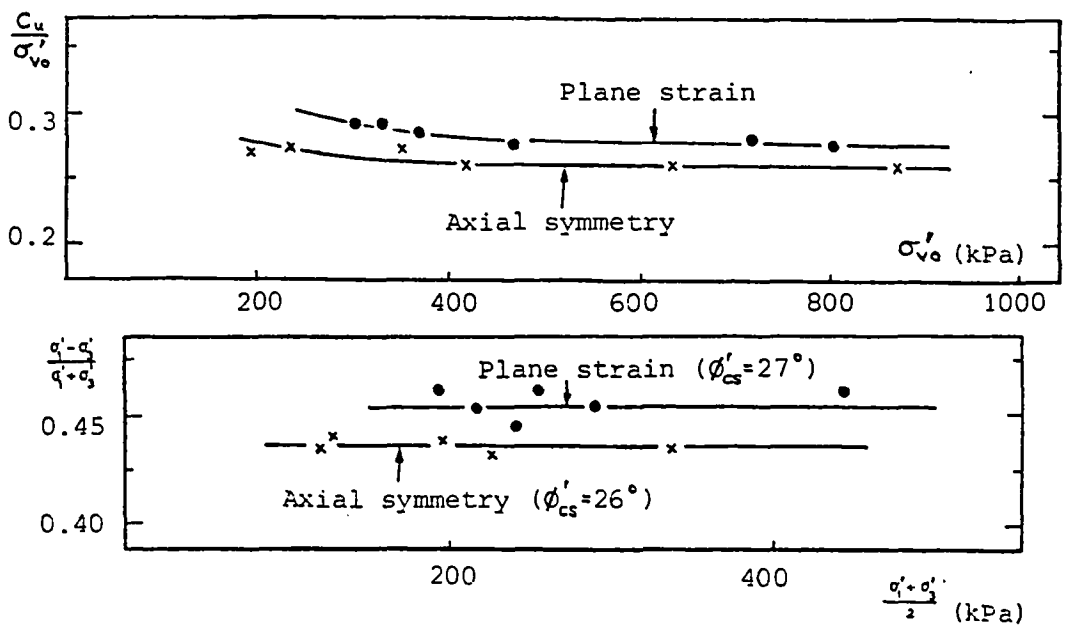
Figure 3.23 Comparison of triaxial test and plane strain test results for Weald clay (after Henkel and Wade,1966)
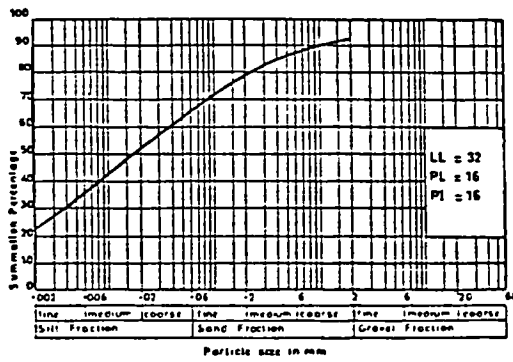
(a)
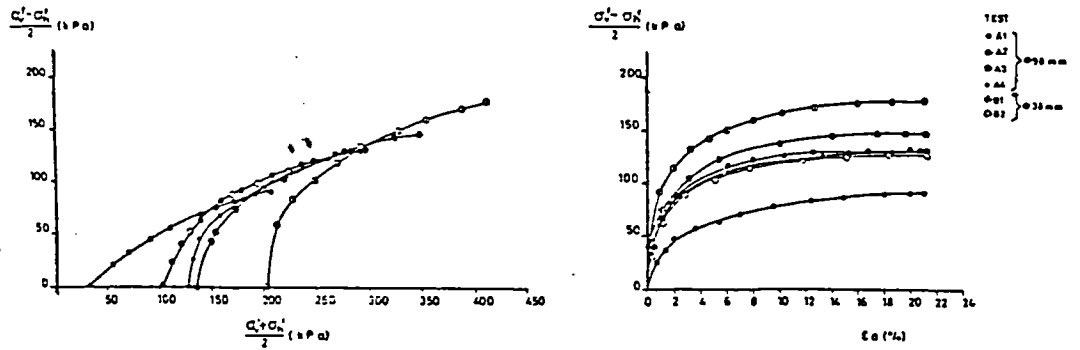
(b)

Figure   3.24   Test results on Cowden till (after Gens and
                     Hight, 1979)
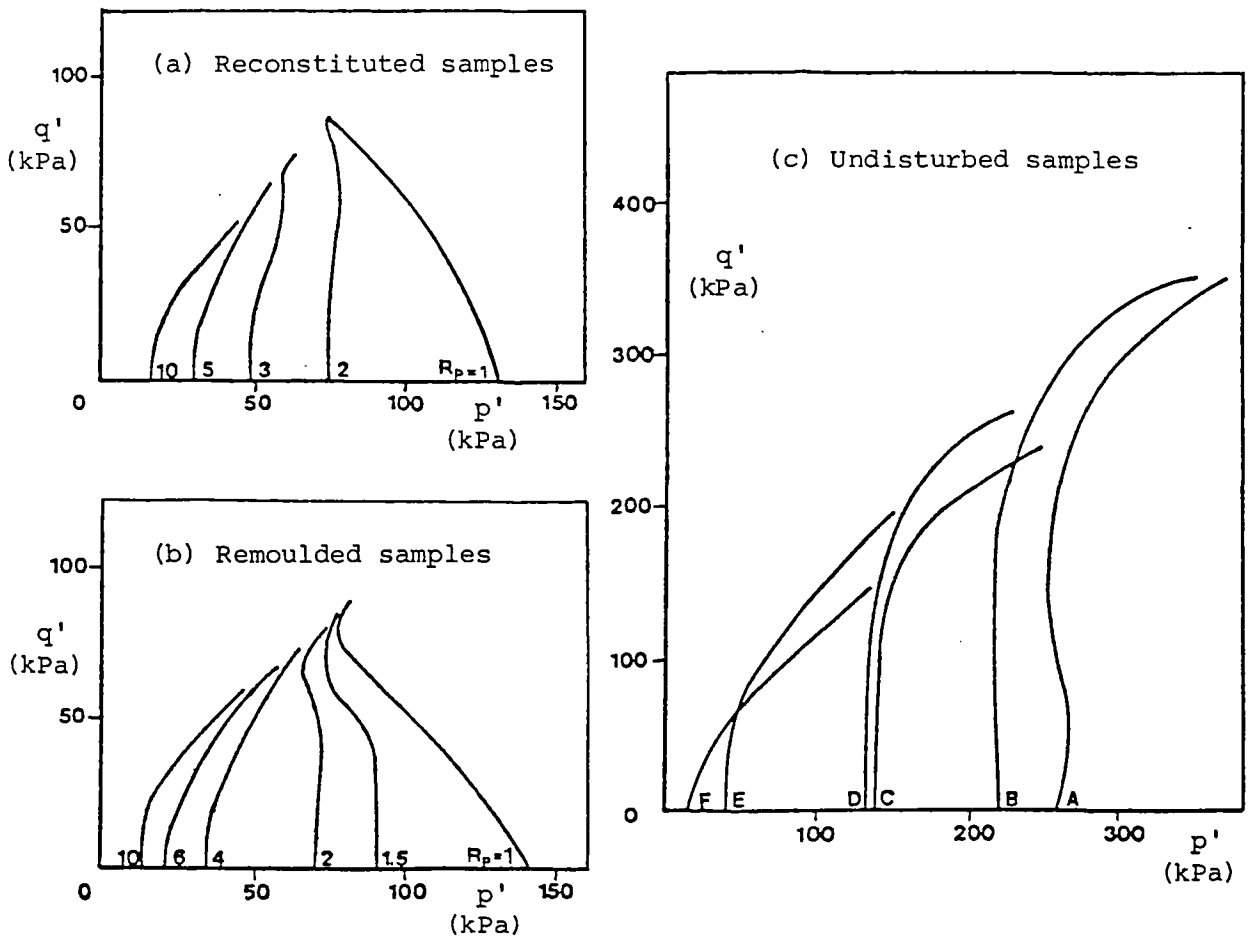
Figure   3.25   Effective stress paths for undrained triaxial tests
                     on Cowden till (after Atkinson et al, 1985 a)
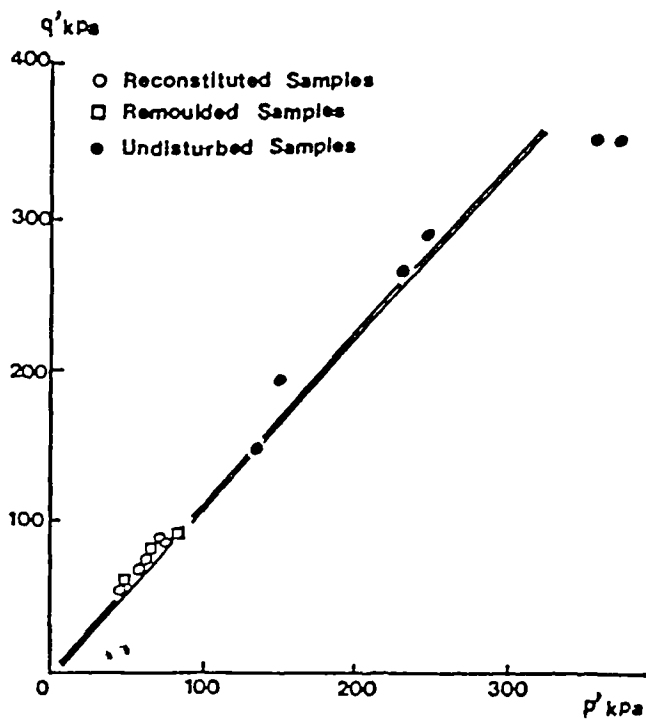
Figure 3.26 Critical states for reconstituted and remoulded samples
and end states for undisturbed samples of Cowden till
(after Atkinson et al, 1985 a)
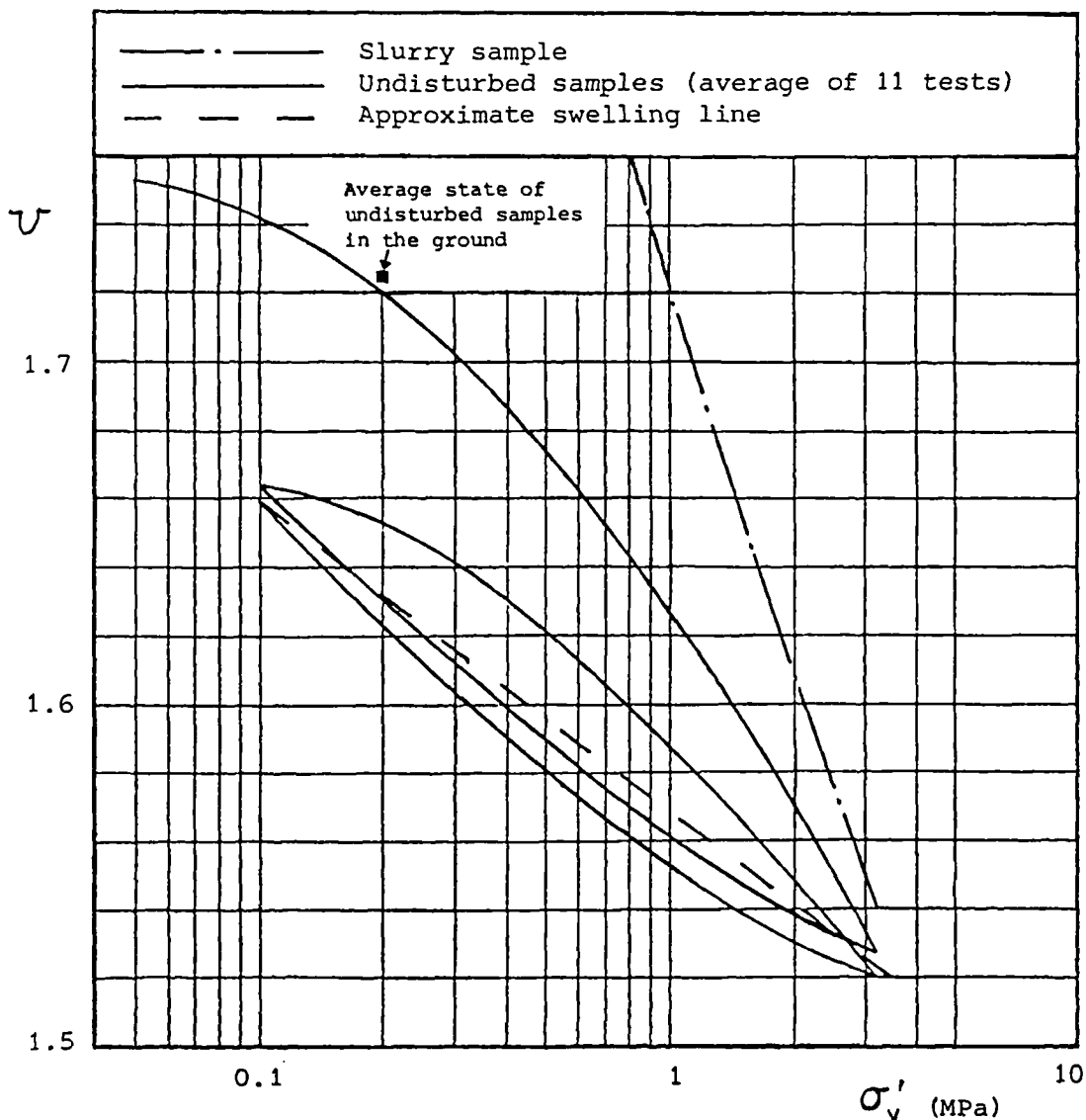
Figure 3.27 Results of oedometer tests on London clay (Som, 1968)
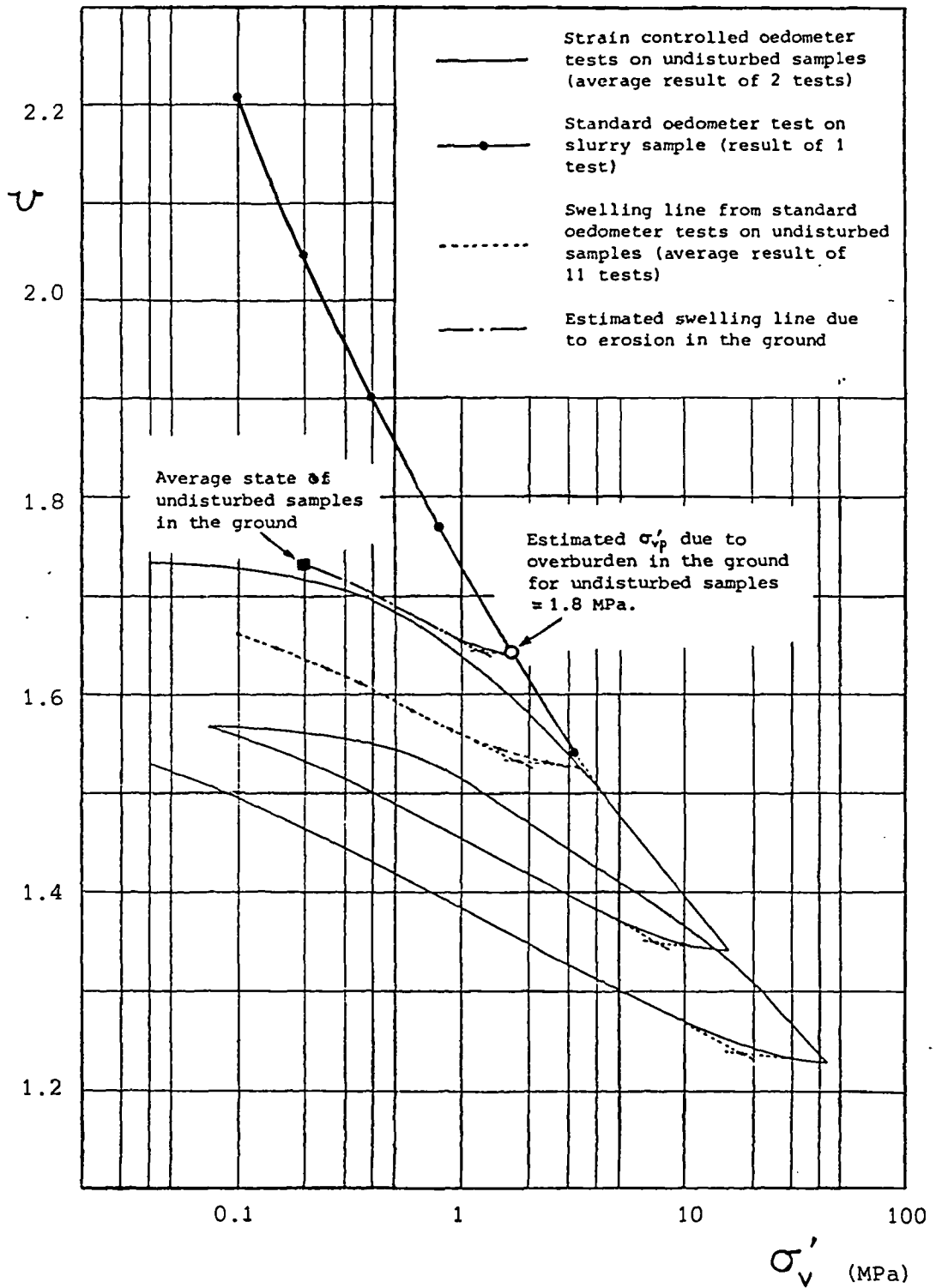
Figure 3.28   Estimation of maximum previous effective vertical
stress σ_{vp}' due to overburden in the ground for
undisturbed samples (after Som, 1968)
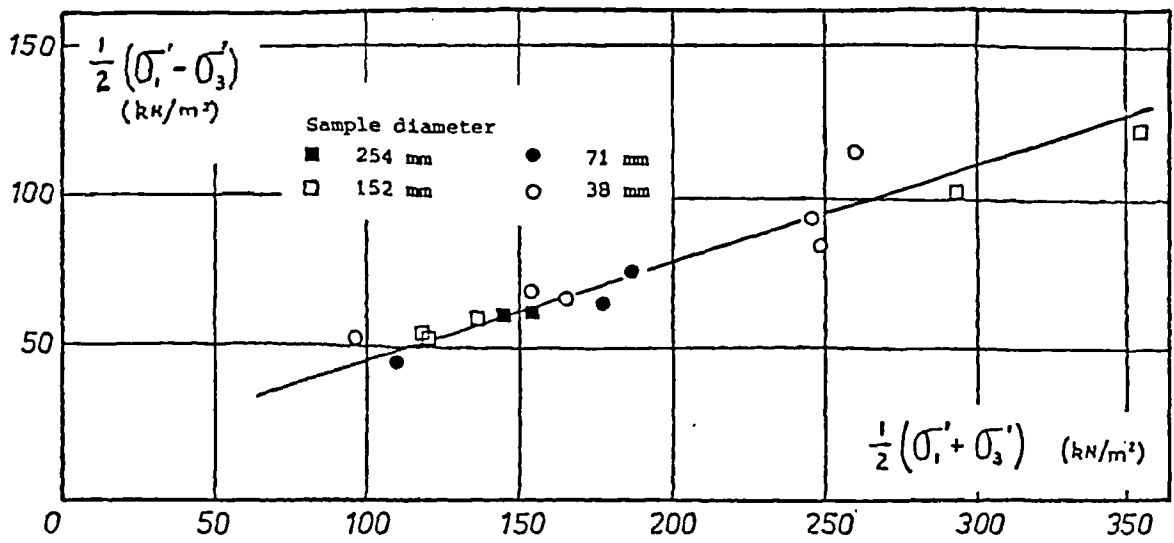
Figure   3.29   Stress states at peak deviator stress for undisturbed
                 London clay (after Sandroni, 1977)
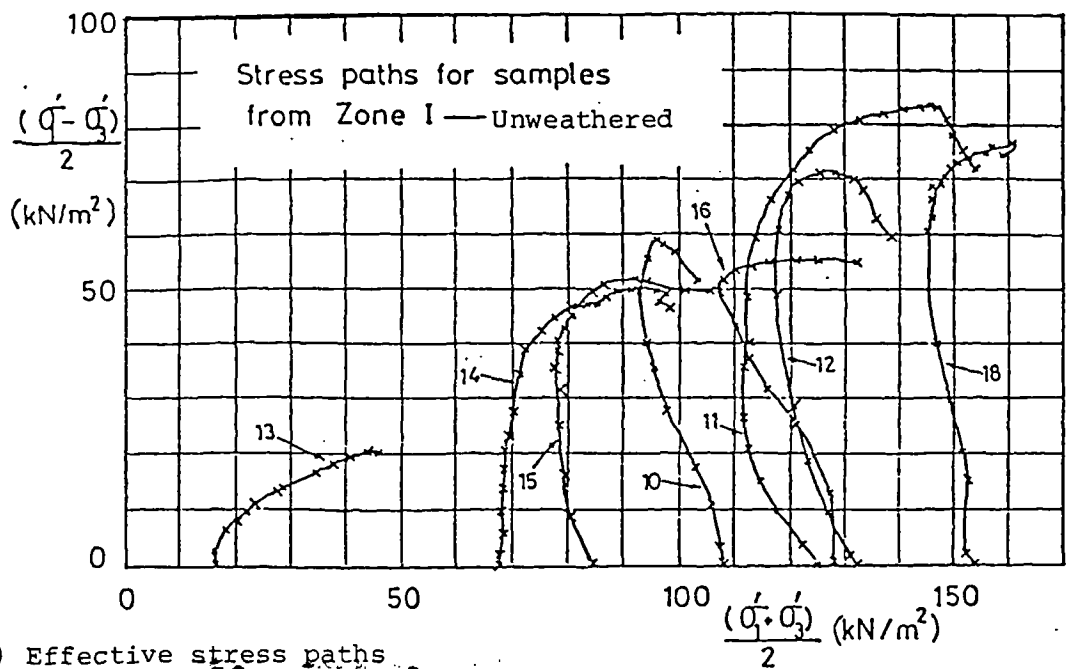
(a) Effective stress paths
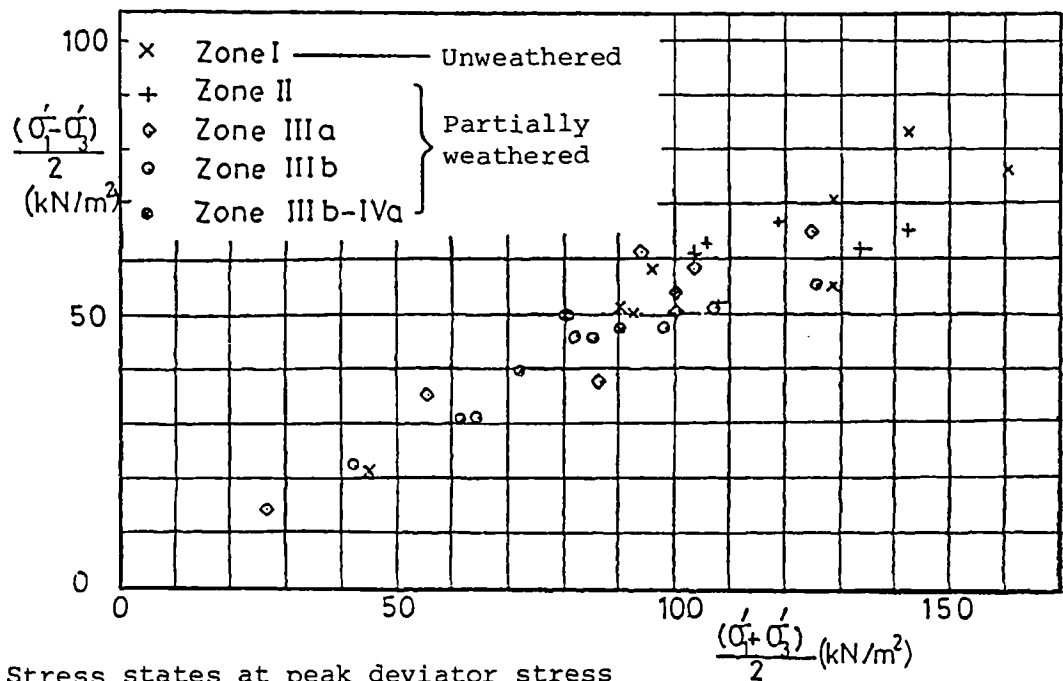
(b) Stress states at peak deviator stress

Figure   3.30   Test results on undisturbed London clay (after Apted, 1977)
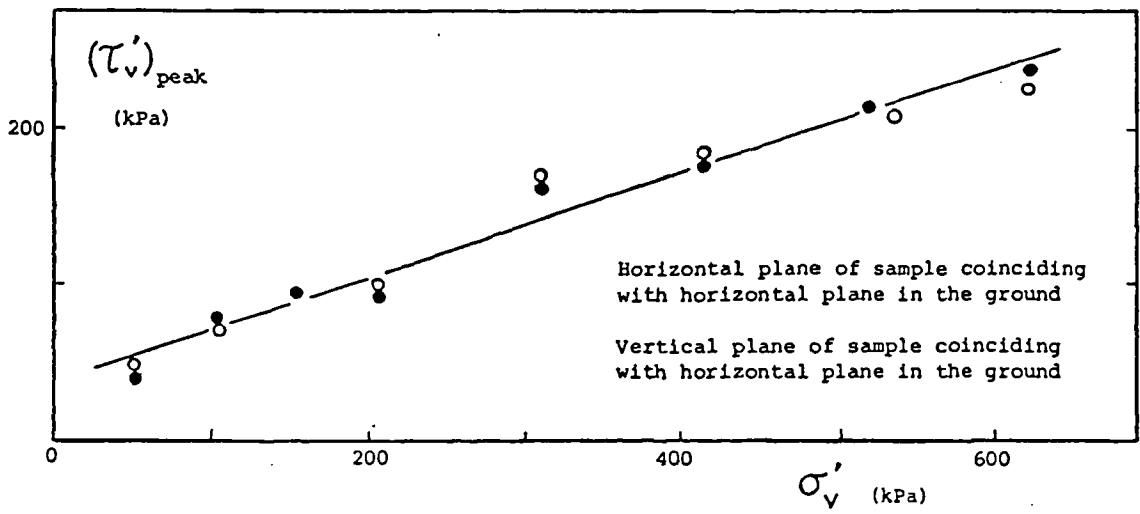
Figure 3.31 Results of standard shear box tests on undisturbed London clay (after Agarwal, 1967)
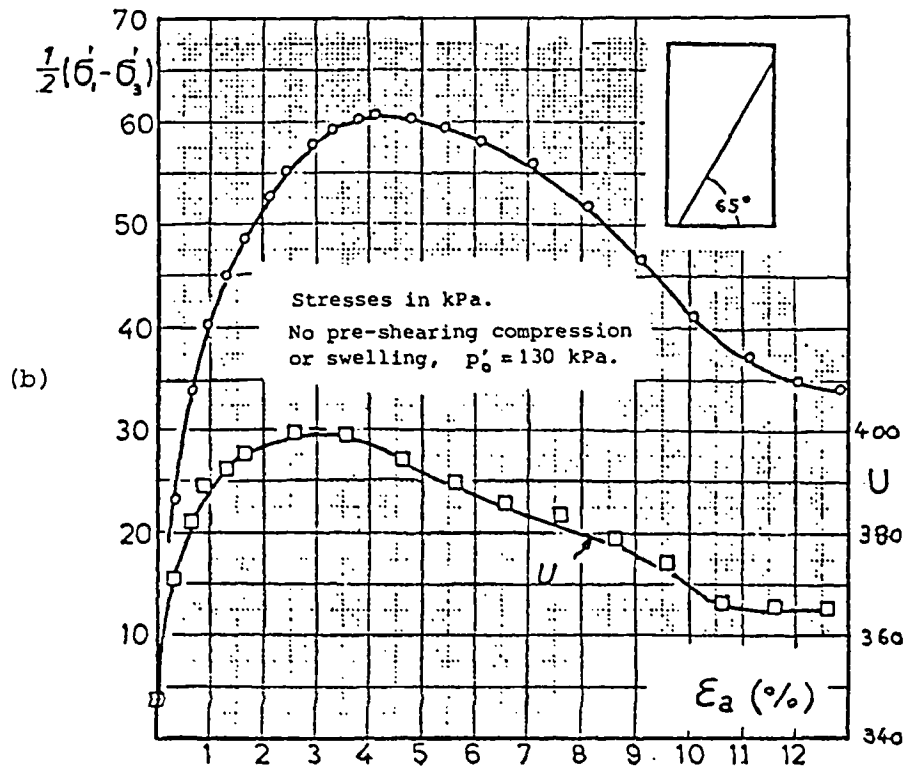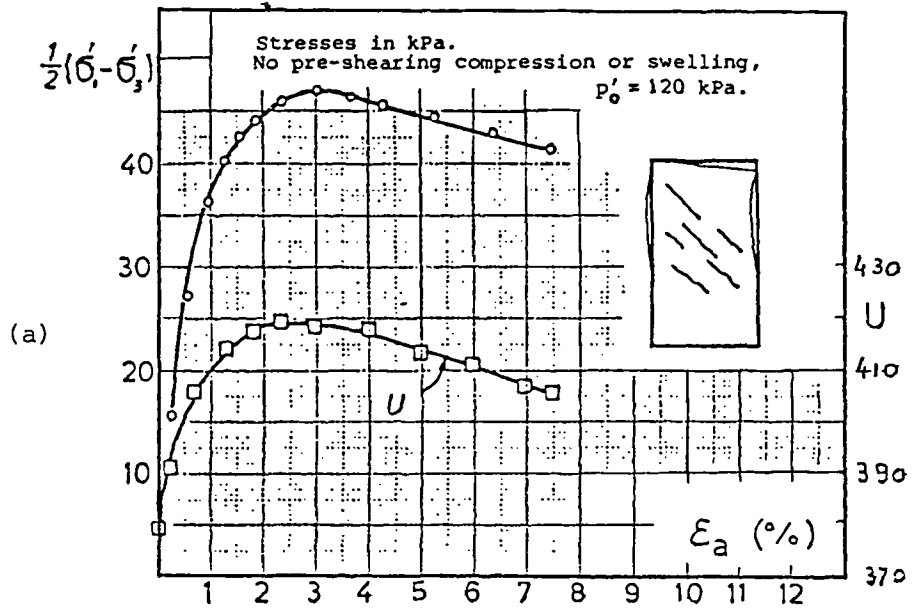
Figure 3.32 Stress-strain curves for undrained triaxial tests on undisturbed London clay (after Sandroni, 1977)
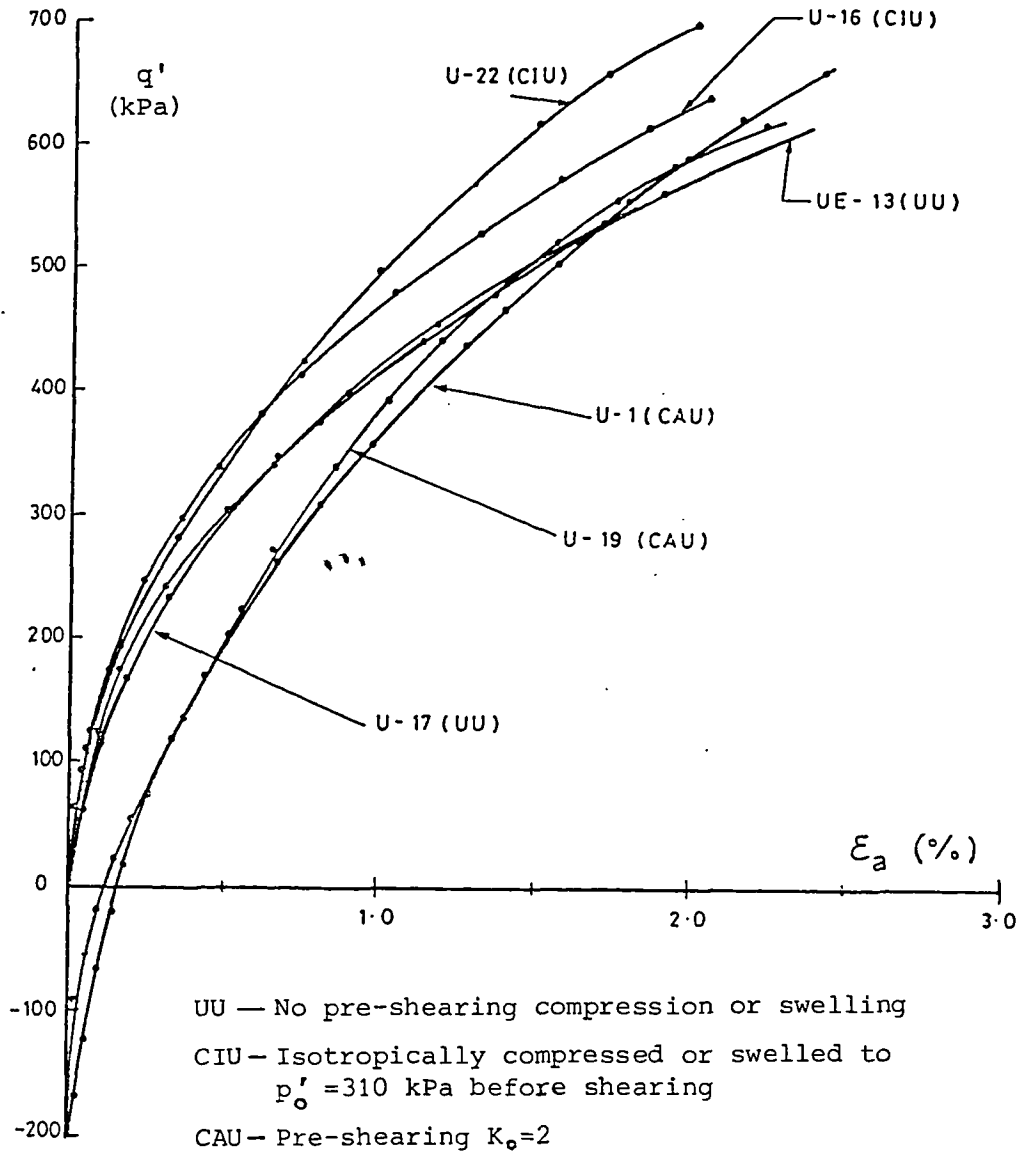
Figure 3.33   Stress-strain curves for undrained triaxial
tests on undisturbed London clay
(after Costa Filho, 1980)

Ordnance Survey   Scale 1:50,000
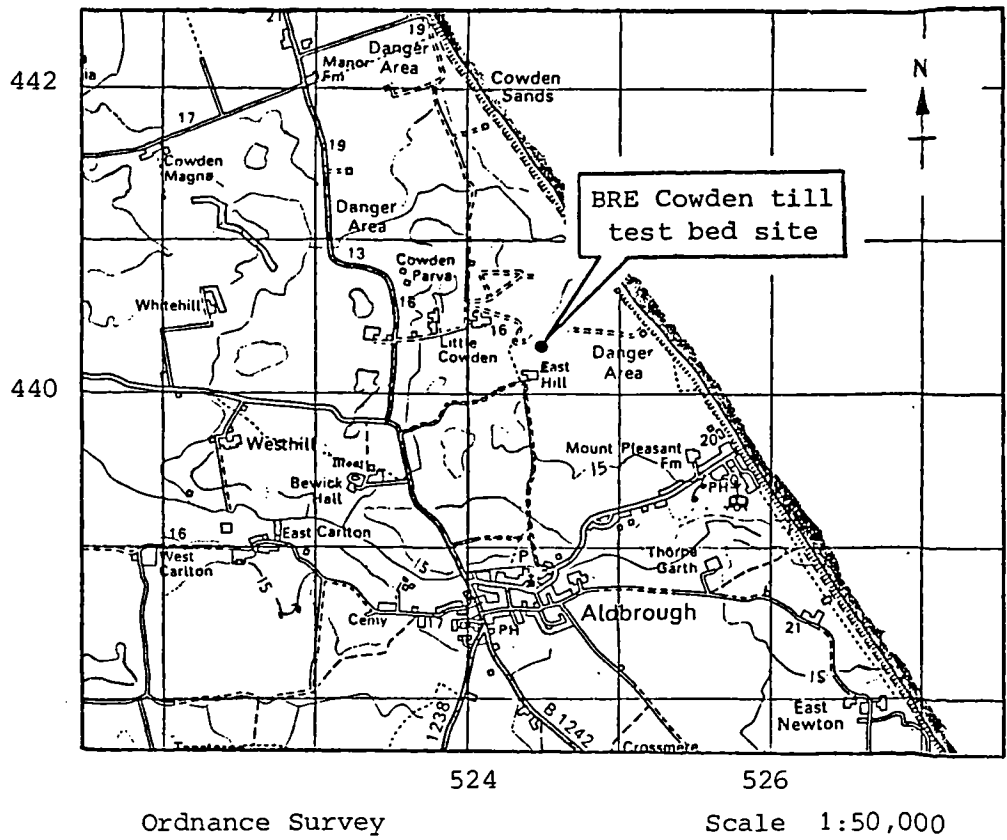
Figure 4.1   Location of BRE Cowden till test bed site

Ordnance Survey   Scale 1:50,000
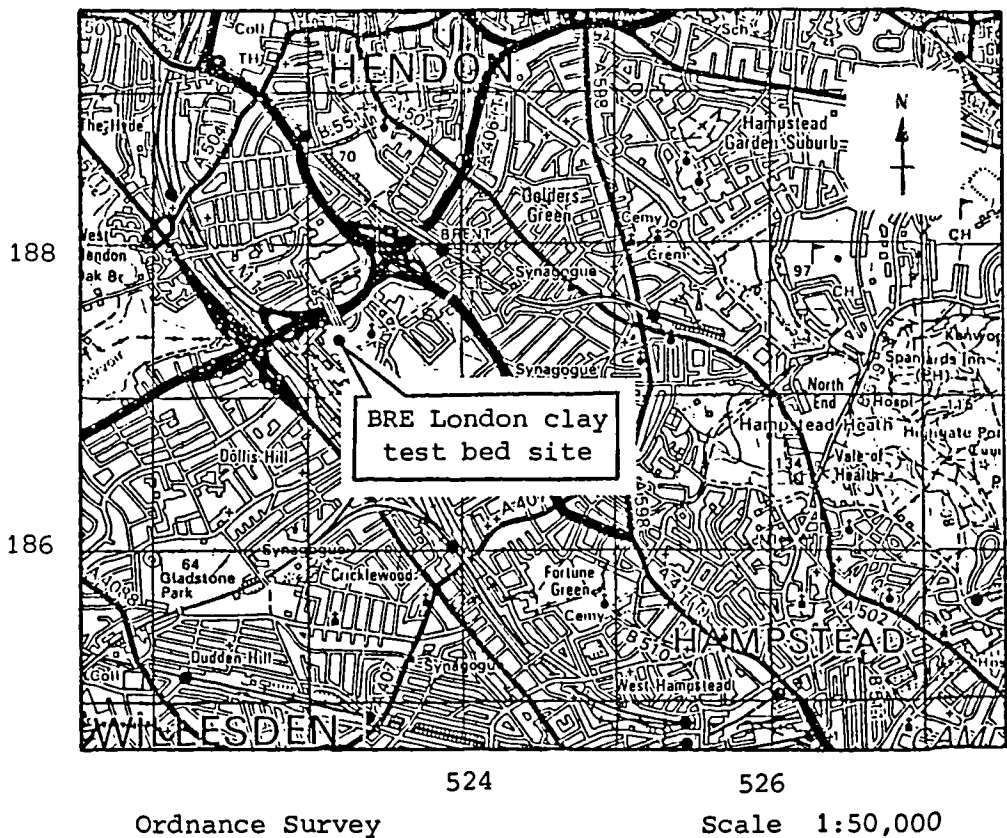
Figure 4.2   Location of BRE London clay test bed site
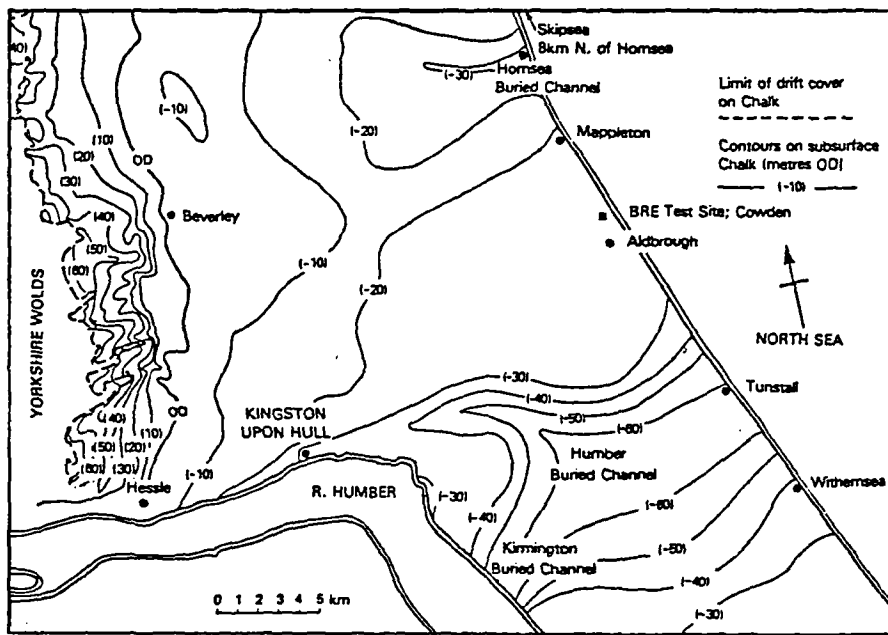
Figure   4.3'ᵎ   Surface contours of chalk at Cowden
            (after Marsland and Powell,1985)
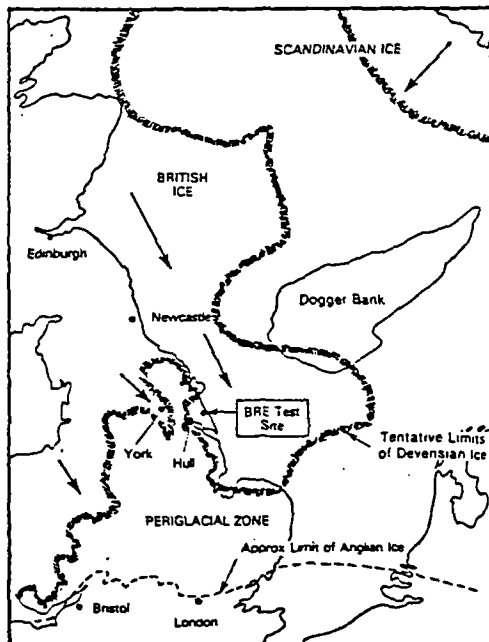
Figure   4.4

Possible extent of
Quaternary ice sheets
(after Marsland and
Powell,1985)
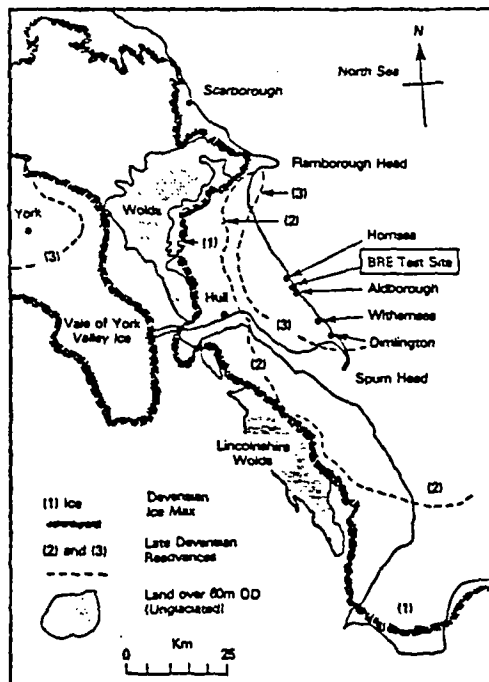
Figure   4.5

Possible extent of glacial
advances during the
Devensian (after Marsland
and Powell,1985)

Scale 1:633,600

Figure 4.6 Regional goelogy of the London basin (after Som,1968)

Legend:

Eocene
- Bagshot Series
- London Clay
- Woolwich and Reading Beds

Cretaceous
- Chalk
- Upper Greensand and Gault
- Lower Greensand
- Weald Clay
- Hastings Beds
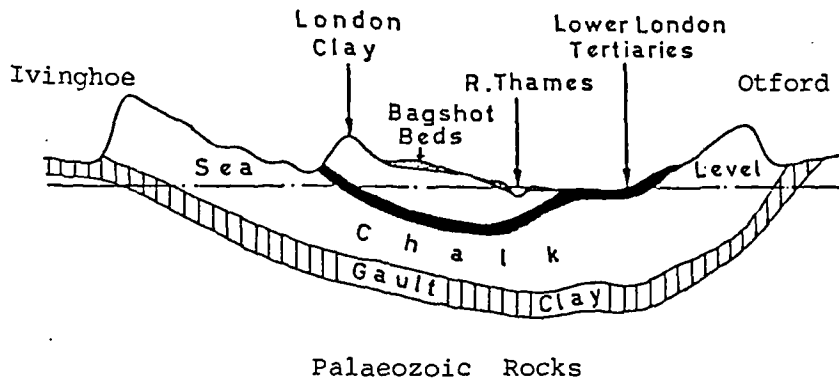
Horizontal scale   1:633,600   Vertical scale   1:12,000

Figure   4.7   Cross-section through the London basin
                (after Sherlock,1962)
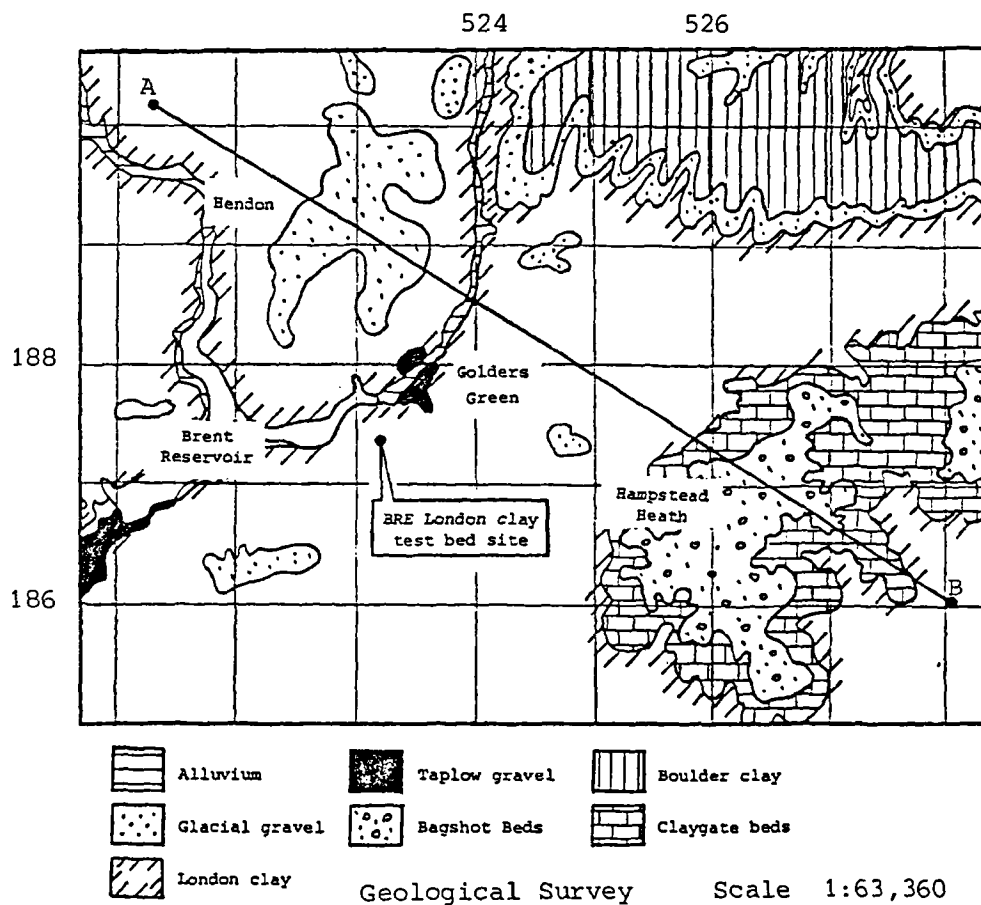
Figure   4.8   Geology of the Brent area
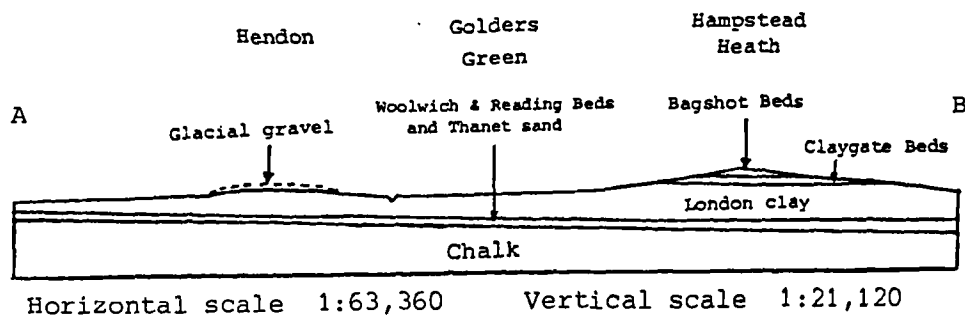
Horizontal scale   1:63,360   Vertical scale   1:21,120

Figure   4.9   Cross-section through the Brent area
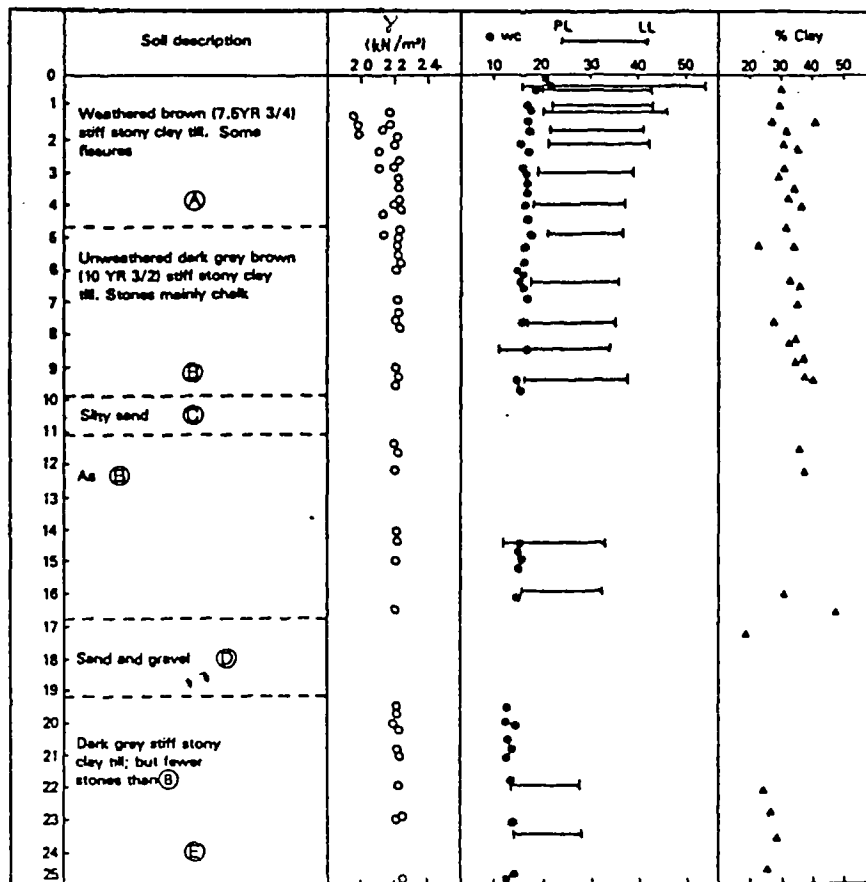
Figure 4.10 Typical soil profile at Cowden till test bed site (after Marsland and Powell,1985)
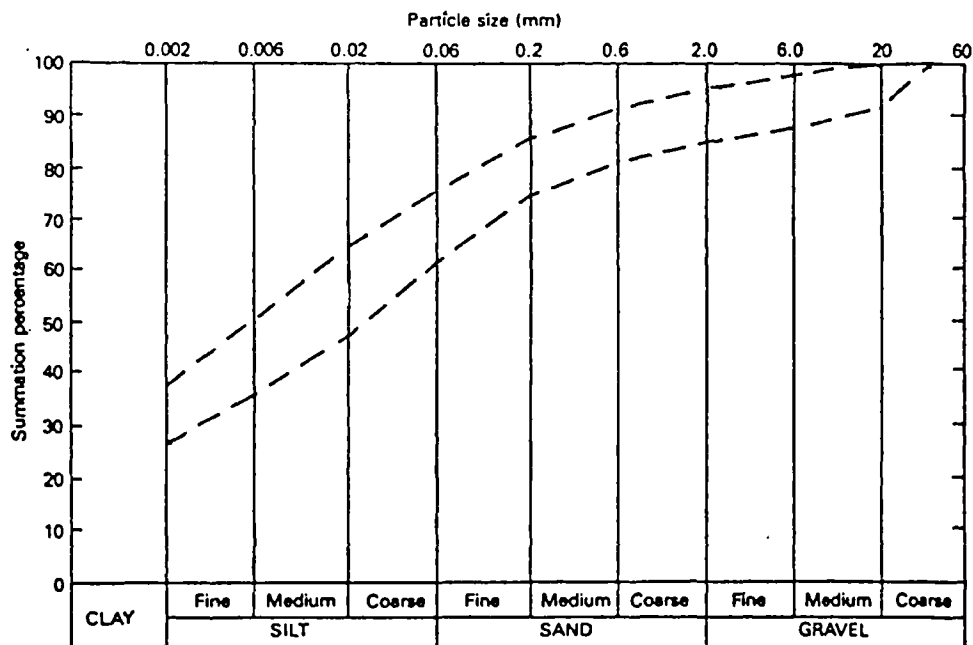
— — — — Envelope for results of eight particle size distribution tests performed by BRE

Figure 4.11 Particle size distribution of Cowden till
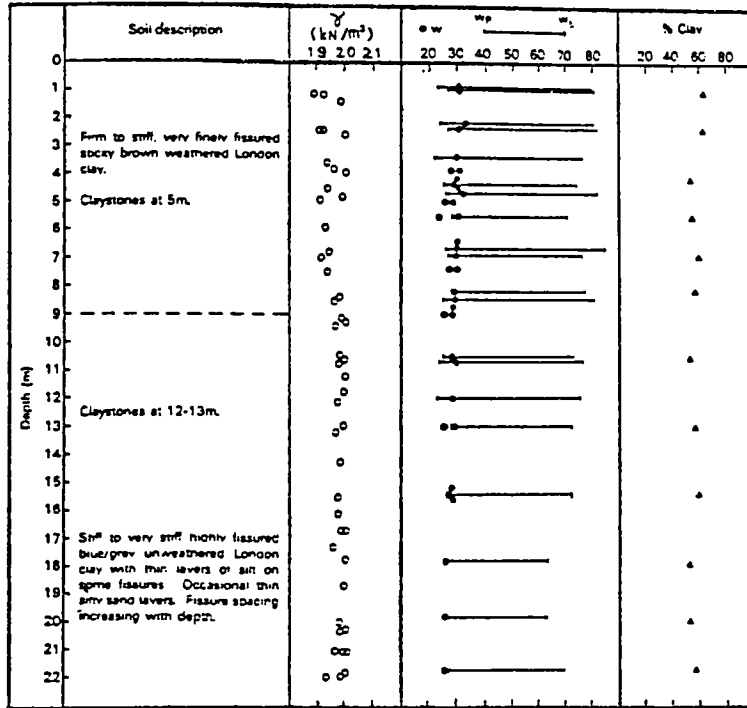
Figure 4.12   Typical soil profile at London clay
                test bed site (after Powell and
                Uglow,1986)
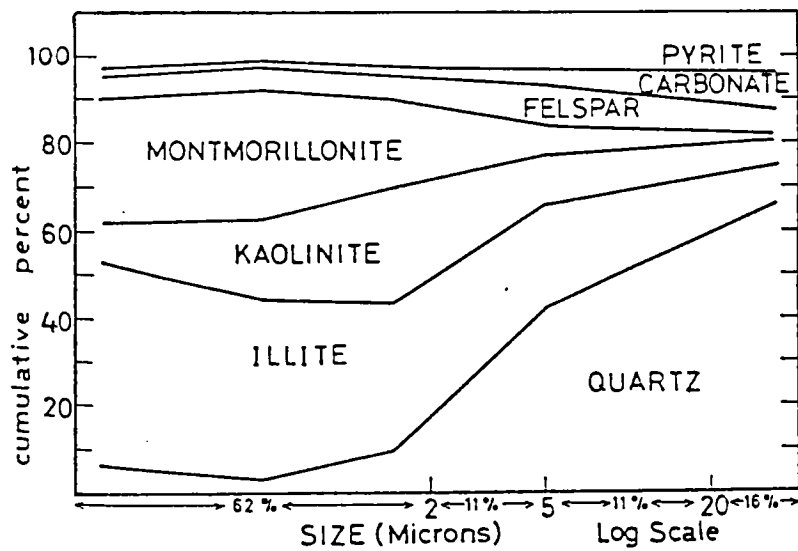
Figure 4.13   Typical mineralogy of London clay
                (after Burnett and Fookes,1974)
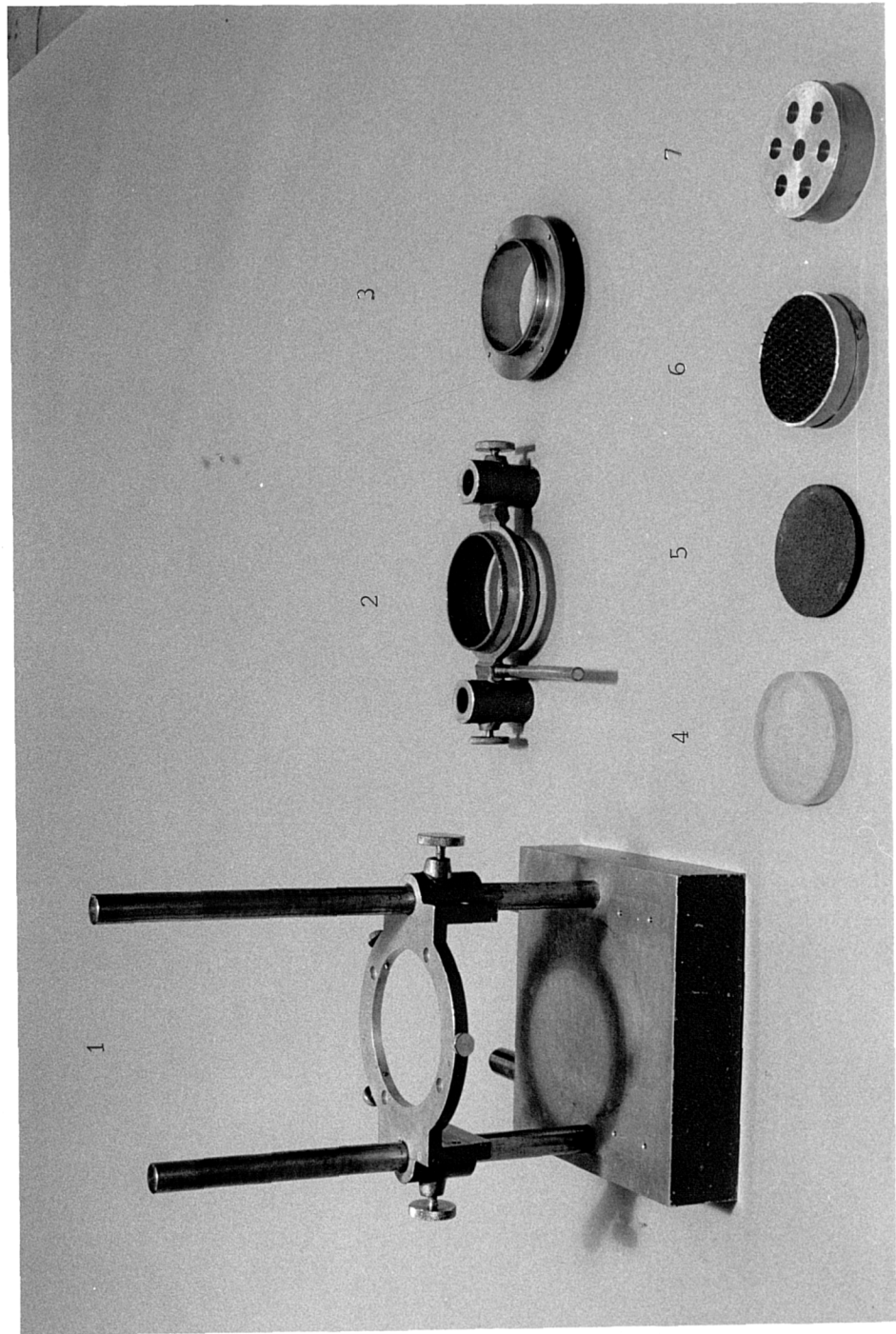
Figure 5.1   Equipment for preparing and setting up
simple shear samples
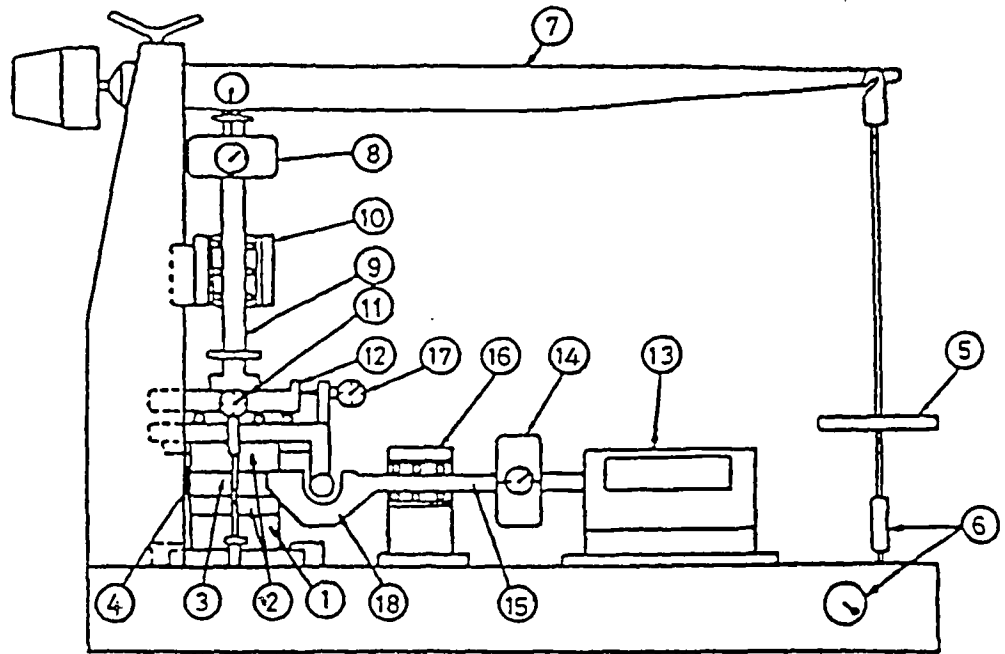
1	pedestal	7	lever arm	13 drive unit
2	filter holders	8	proving ring	14 proving ring
3	soil sample	9	piston	15 piston
4	reinforced membrane	10	bearing	16 bearing
5	loading plate	11	dial gauge	17 dial gauge
6	adjusting mechanism	12	sliding box	18 connection fork

Figure 5.2   NGI simple shear apparatus
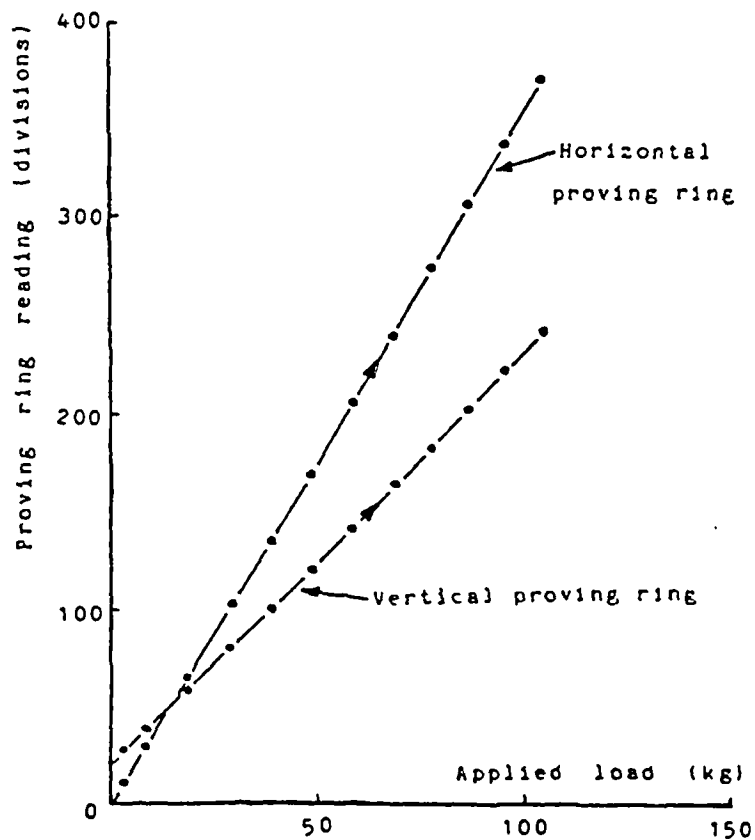
Figure 5.3   Calibration curves for proving rings
of NGI simple shear apparatus
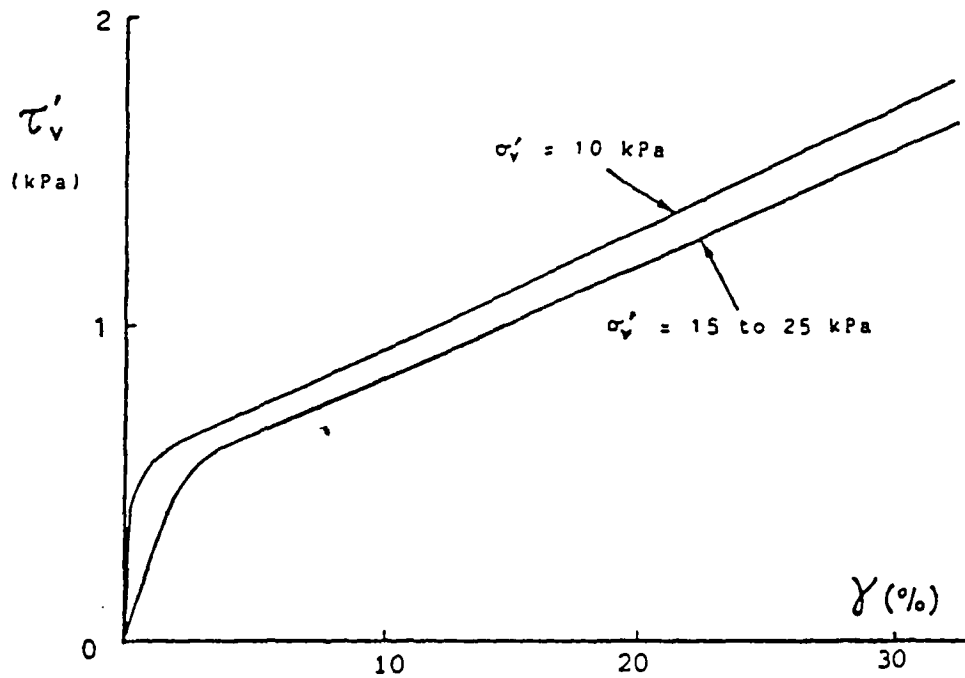
Figure 5.4   Shear resistance of reinforced membrane
of NGI simple shear apparatus
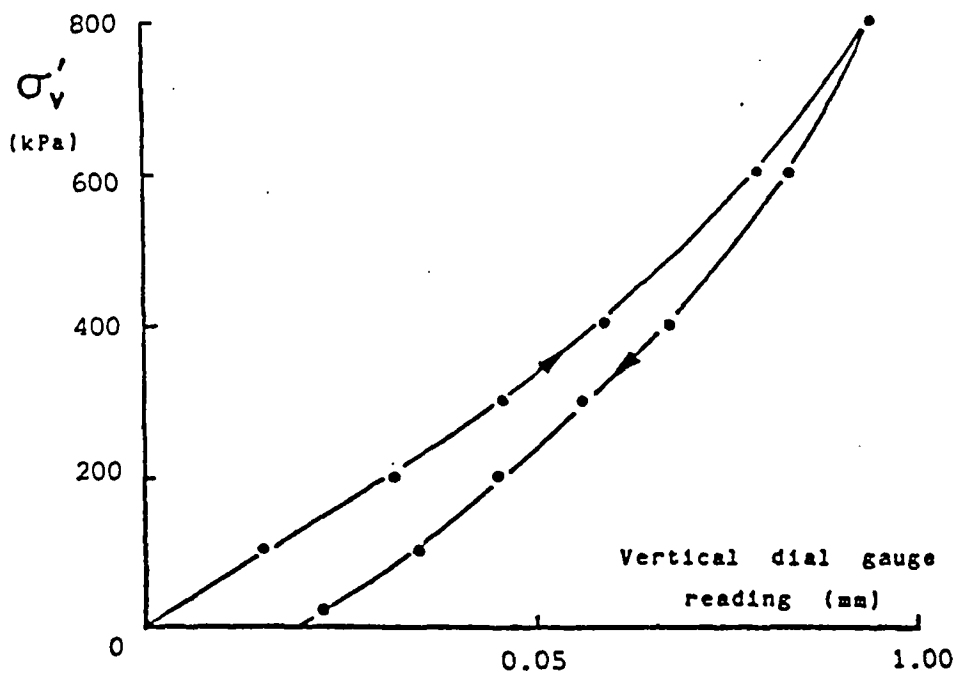
Figure 5.5   Compliance of vertical loading system
of NGI simple shear apparatus
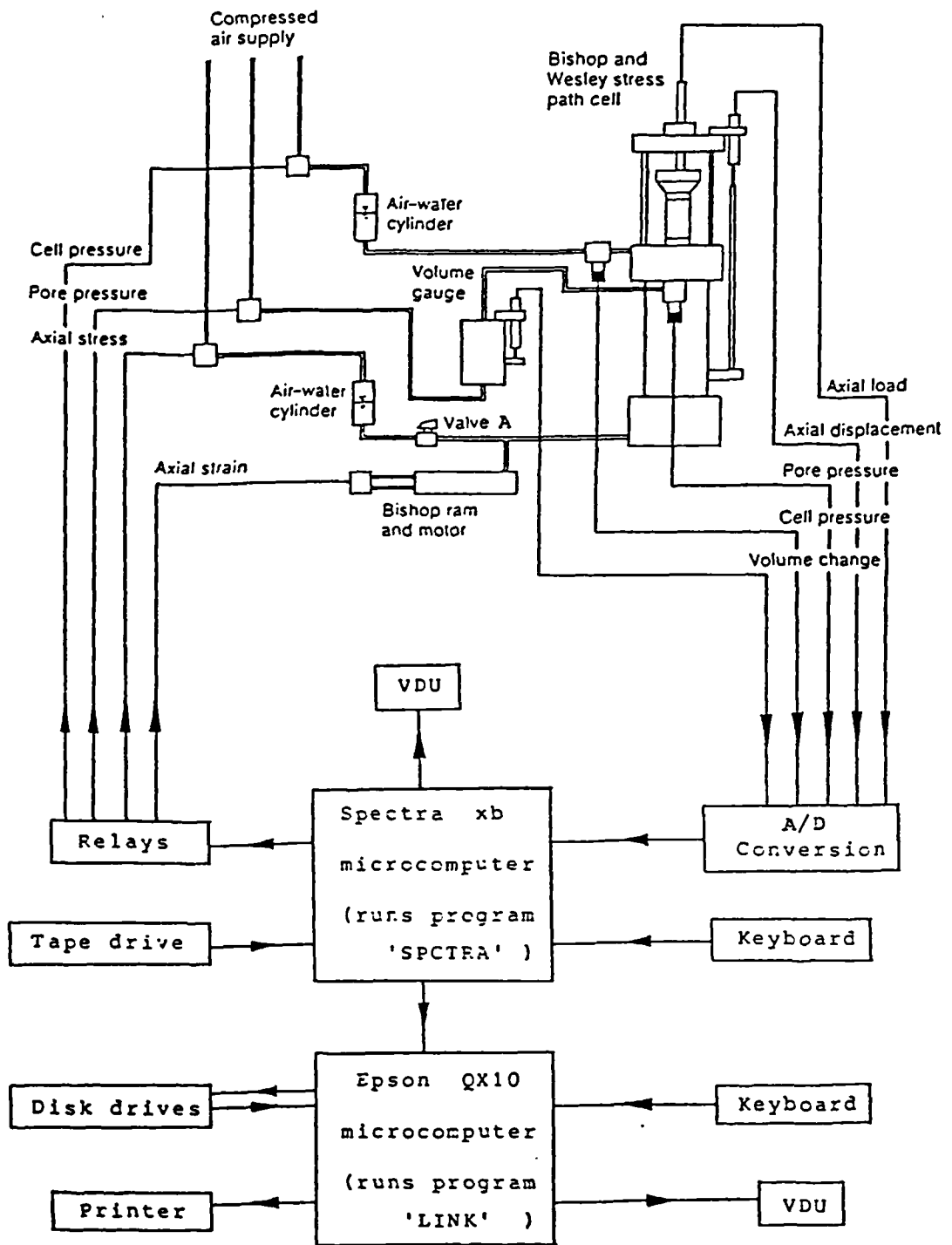
Figure 5.6 Diagrammatic layout of Spectra system
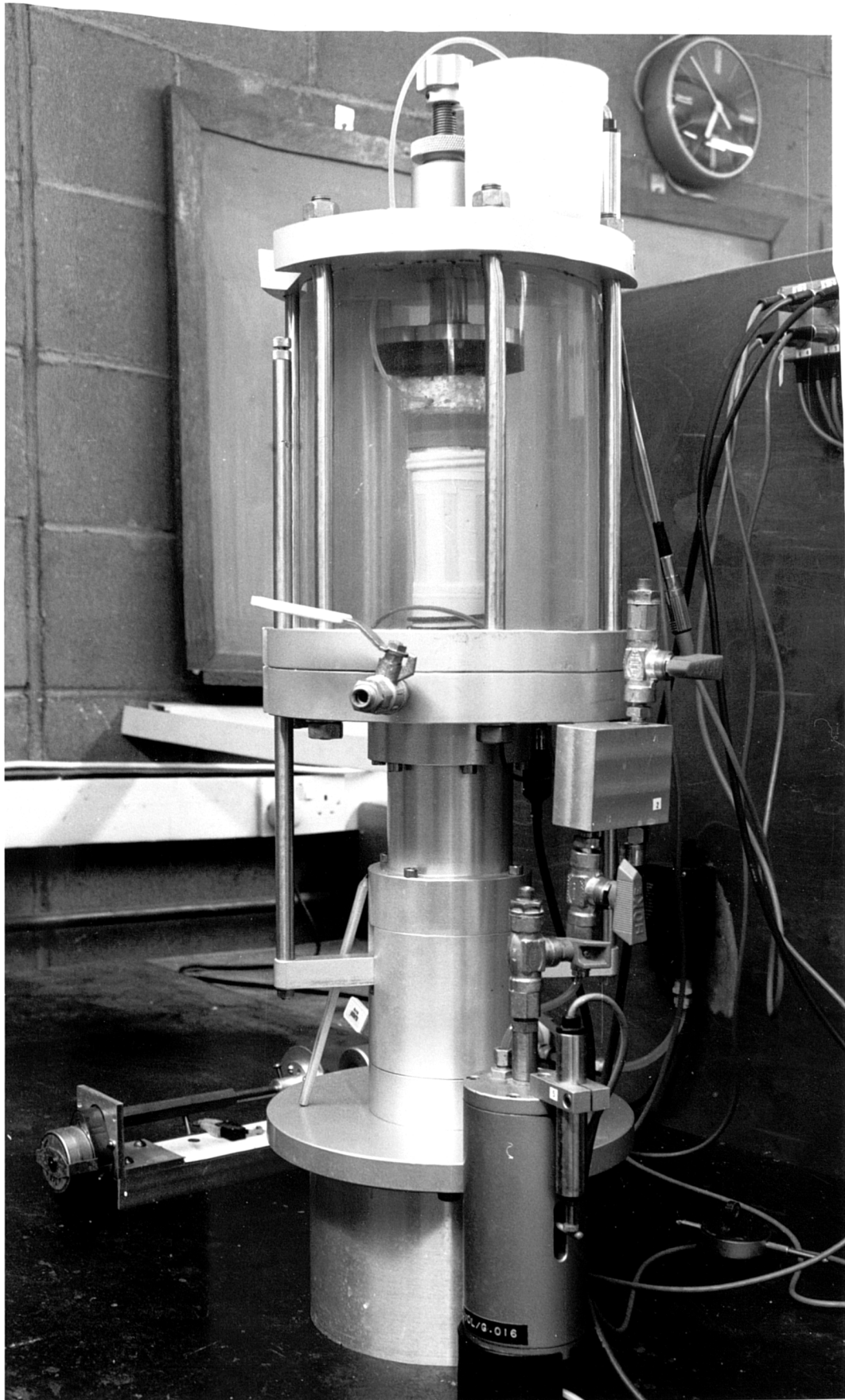
Figure 5.7   Bishop and Wesley hydraulic stress path cell
              for samples with 38 mm diameter
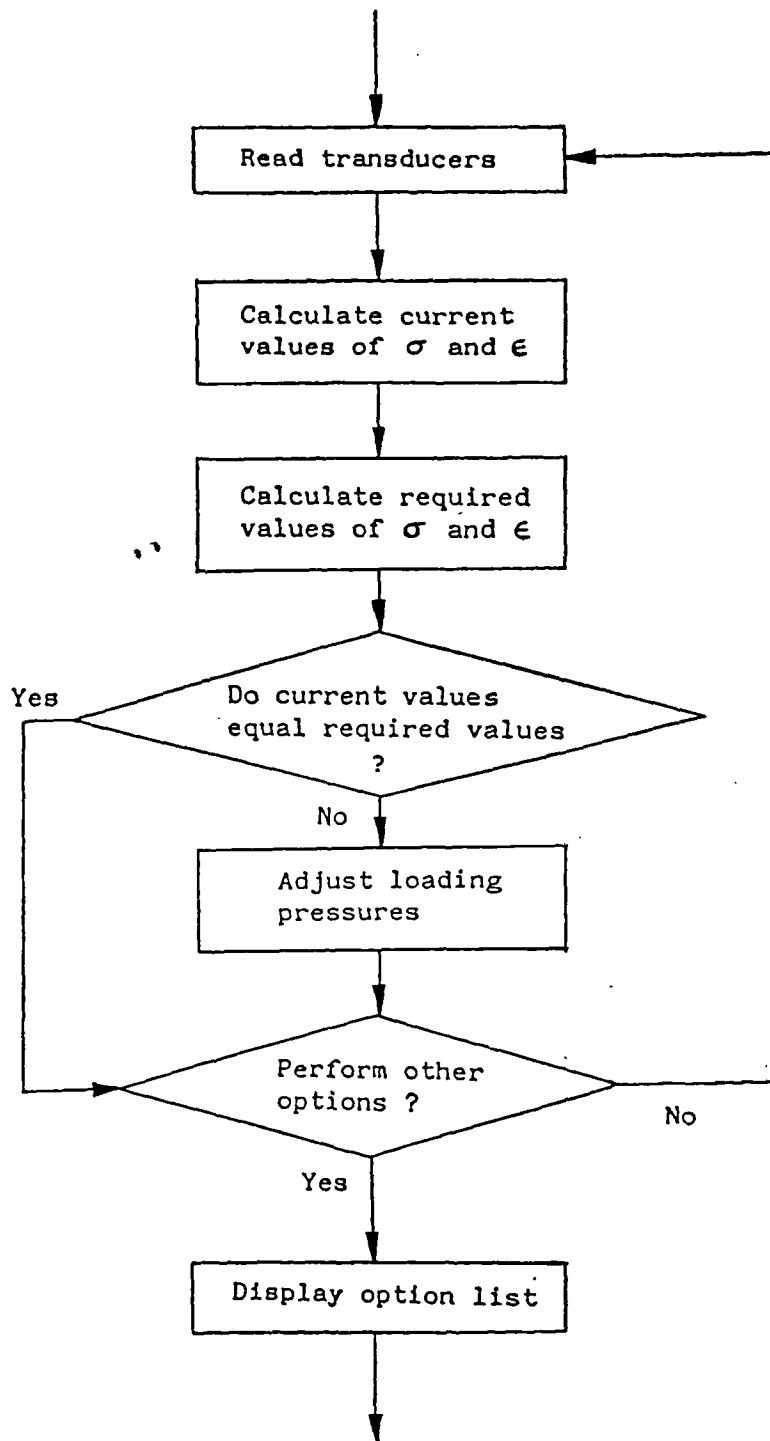
Figure 5.8   Main feed-back control loop of 'SPCTRA' program (after Atkinson et al, 1985b)

=O= valve

water
container

Bishop ram

A

B   D   E

C

digital
pressure
indicator

pore
pressure
transducer

cell
pressure
transducer
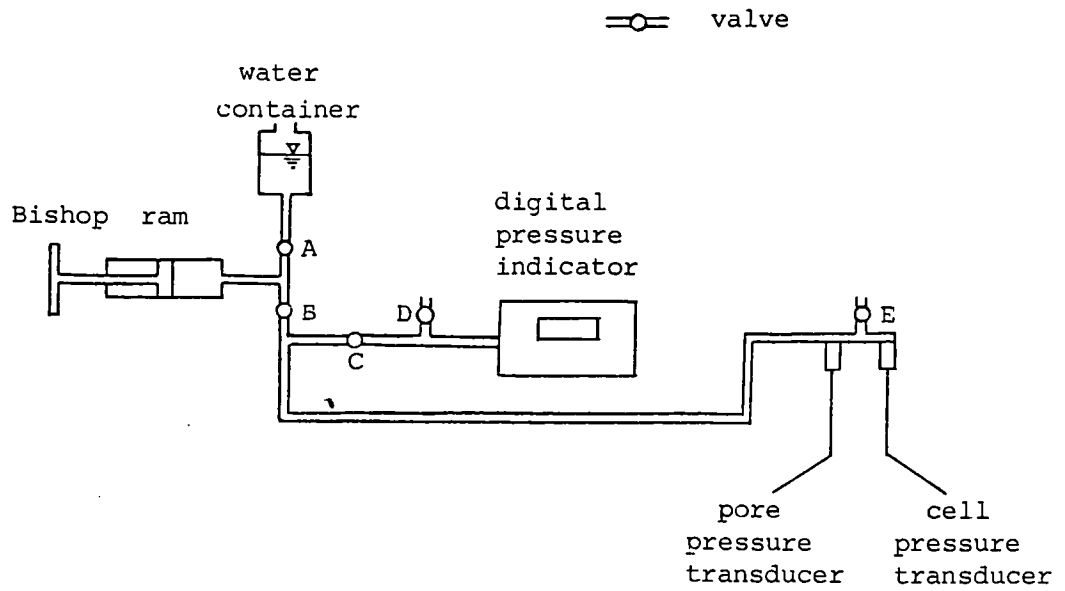
Figure 5.9   Calibration of pressure transducers for stress
path testing

displacement
transducer

micrometer

mounting block
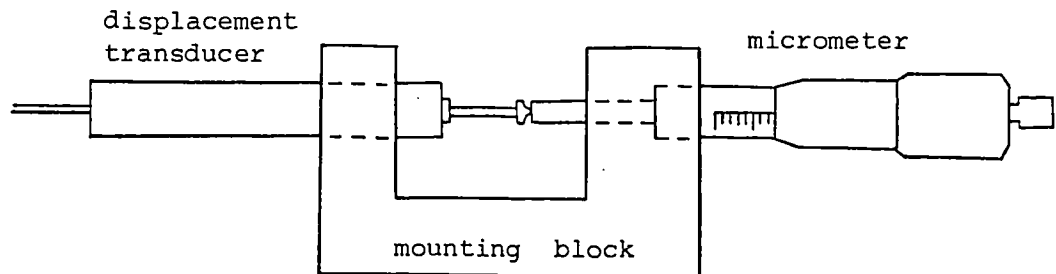
Figure 5.10   Calibration of axial displacement transducer
for stress path testing

B   Bishop ram
L   LVDT
M   Manostat
P   Load cell
S   Stepper motor
T   Pressure transducer
V   Volume gauge

valve A

P

L

V

M M B M
S S S S

Relays

VDU

A/D

Microcomputer

Disc Drive   Keyboard   Printer
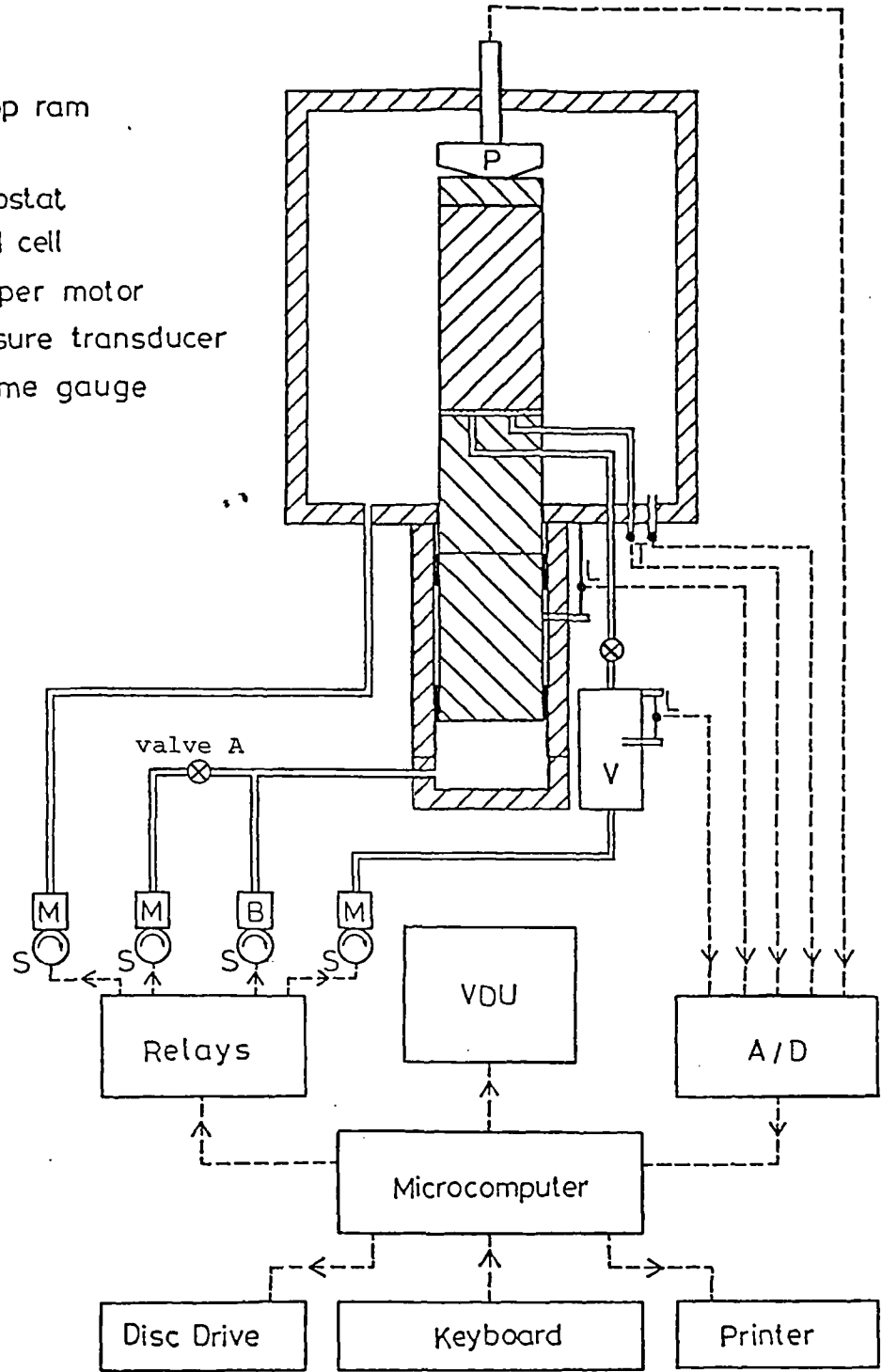
Figure   5.11   Diagrammatic layout of stress path testing
                  equipment for samples with 100 mm diameter
                  (after Atkinson and Clinton, 1984)

LOAD
CELL

PRESSURE
VESSEL

TENSION
BARS
(3 No.)

PEDESTAL

BELLOFRAM
SEAL

LINEAR
BEARING

SCALE 1:5
APPROX.

BELLOFRAM
SEAL

PRESSURE
CHAMBER
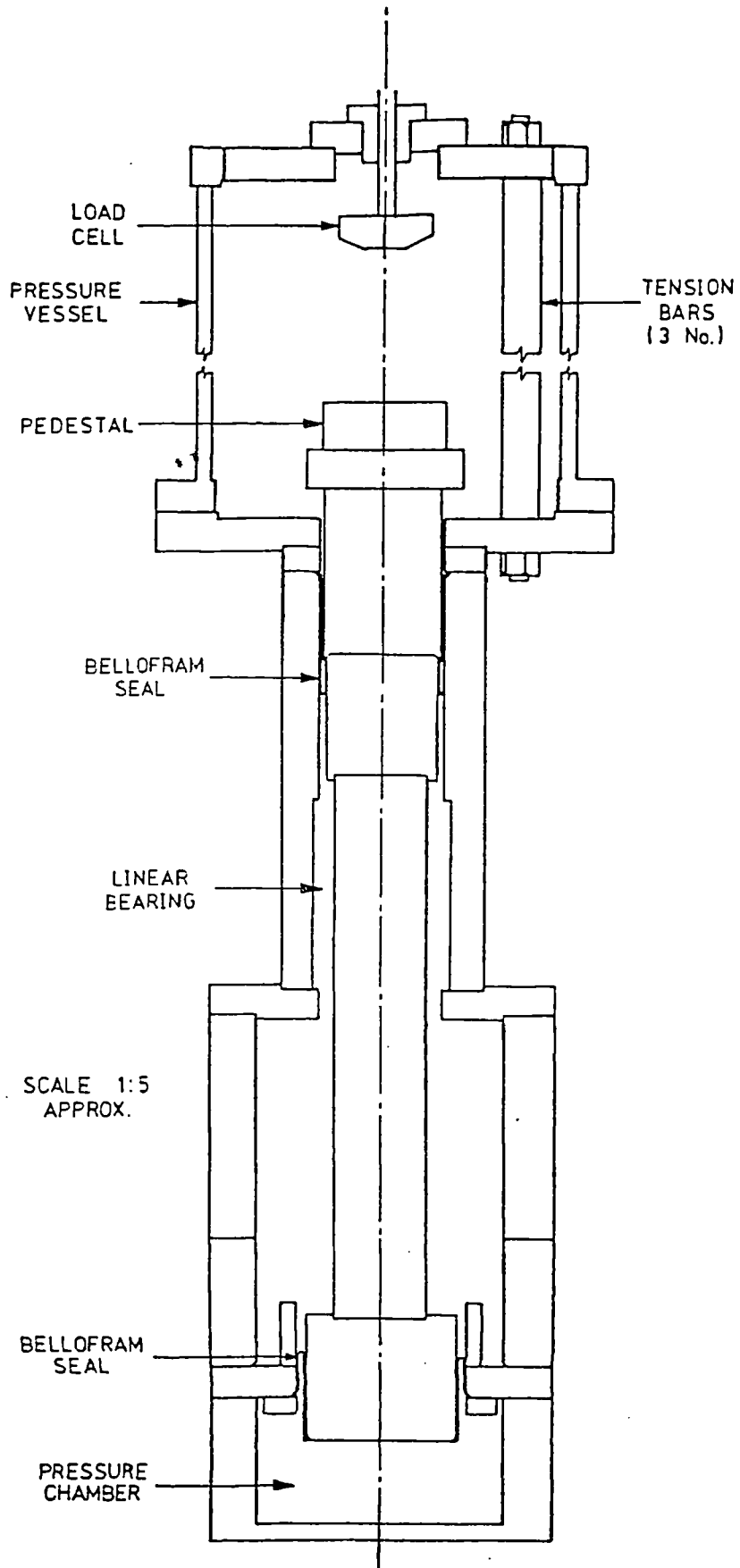
Figure 5.12   Diagrammatic layout of hydraulic stress path
                cell for samples with 100 mm diameter (after
                Clinton, 1987)
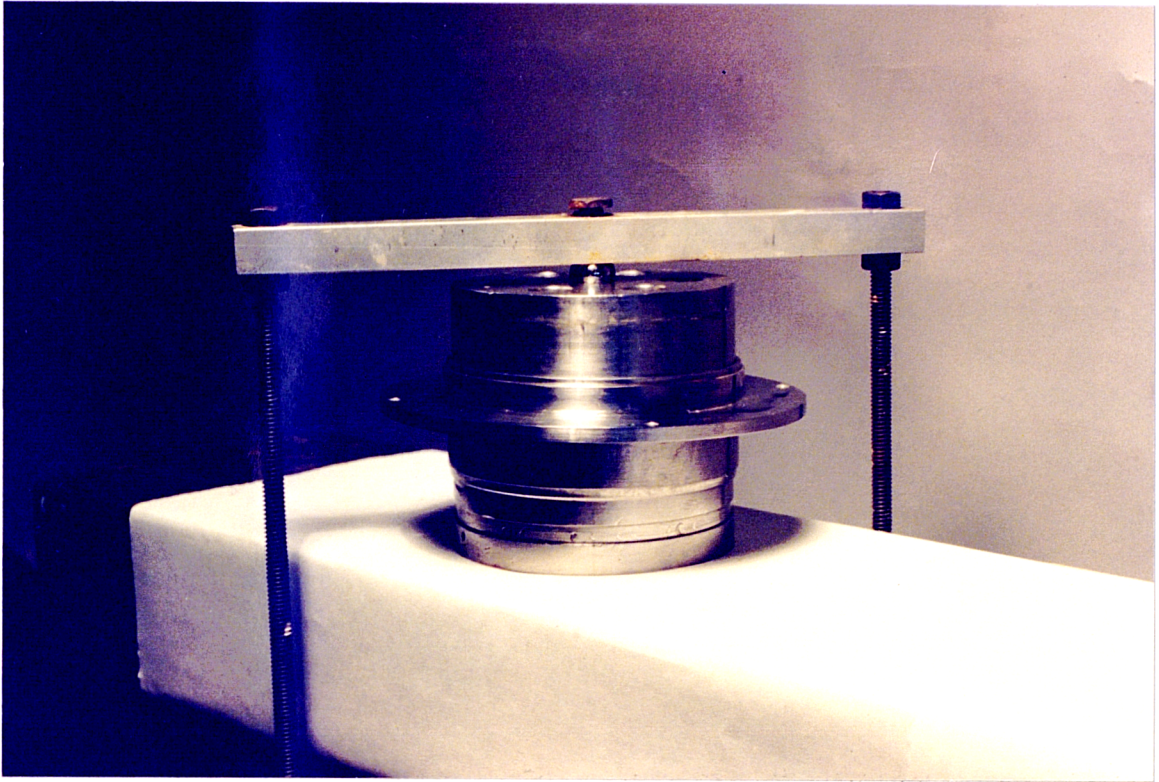
Figure 5.13   Preparation of reconstituted Cowden till simple
shear sample
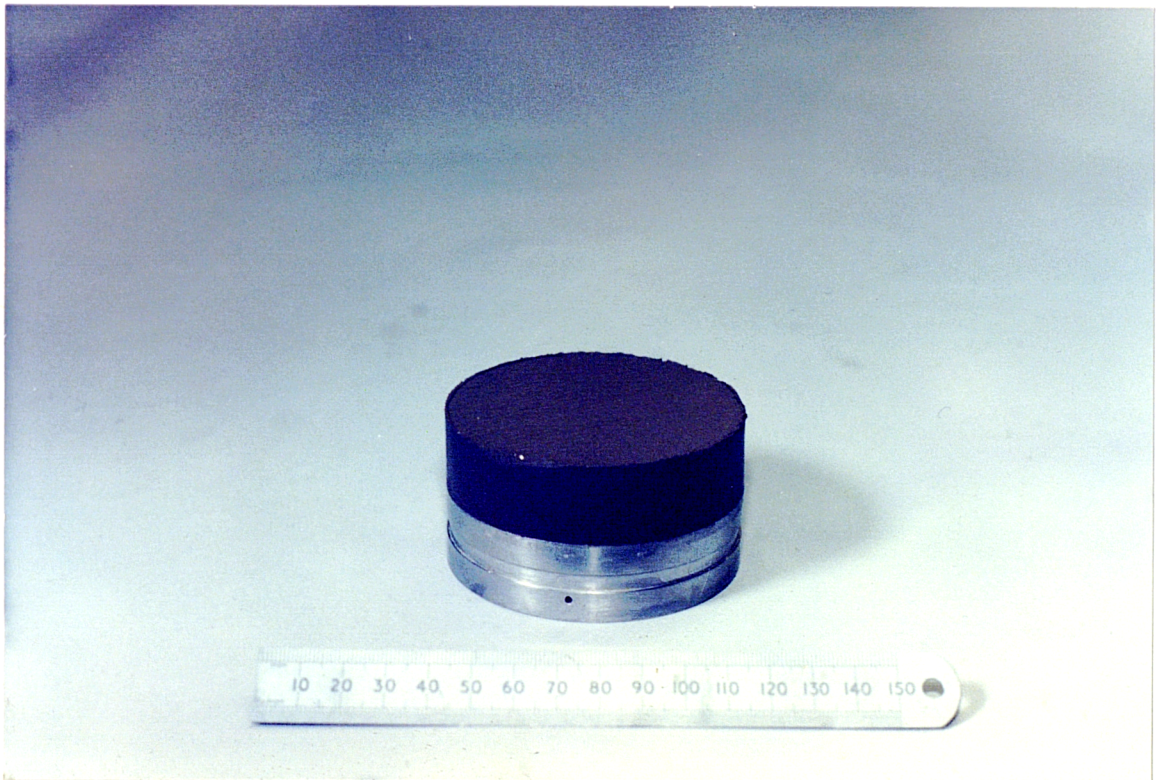
Figure 5.14   Reconstituted Cowden till simple shear sample
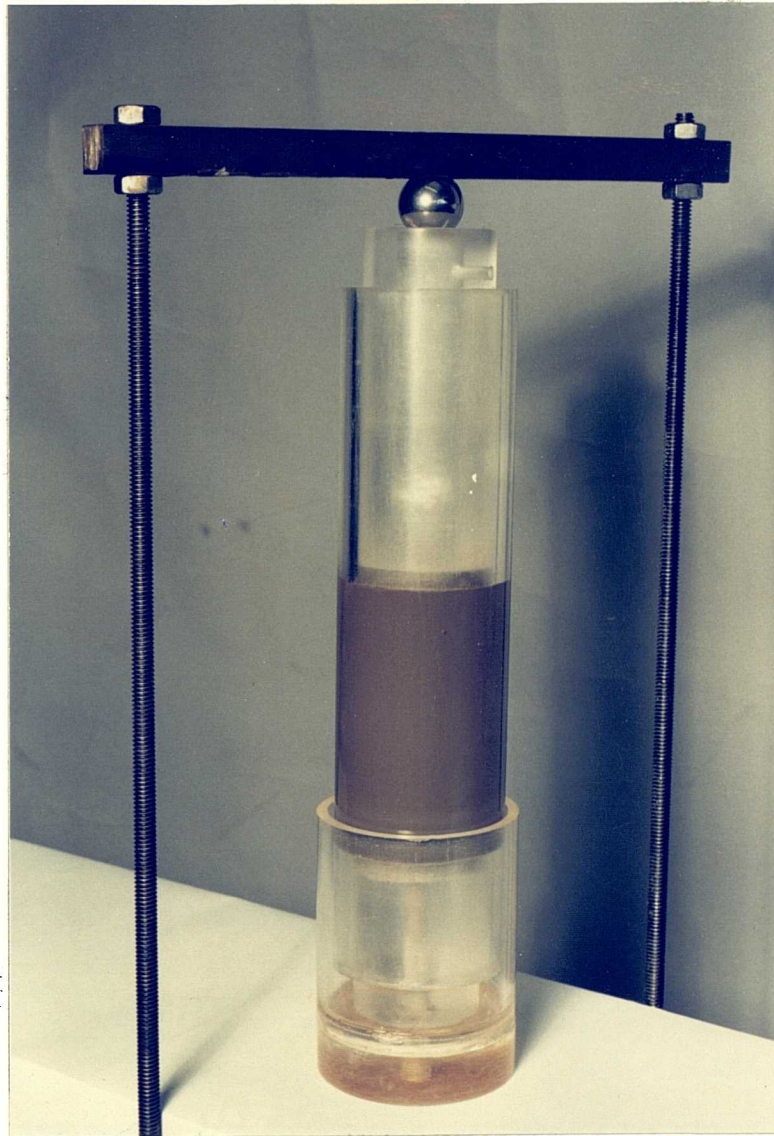
Figure 5.15   Preparation of reconstituted London clay
                (blue) triaxial sample with 38 mm diameter

Test no.	Pre-shearing effective stress path
TUL1 & TUL3	Isotropic to A at 2 kPa/hr and then A to B at 1 kPa/hr
TUL2 & TUL4	Isotropic to C at 2 kPa/hr and then C to D at 1 kPa/hr
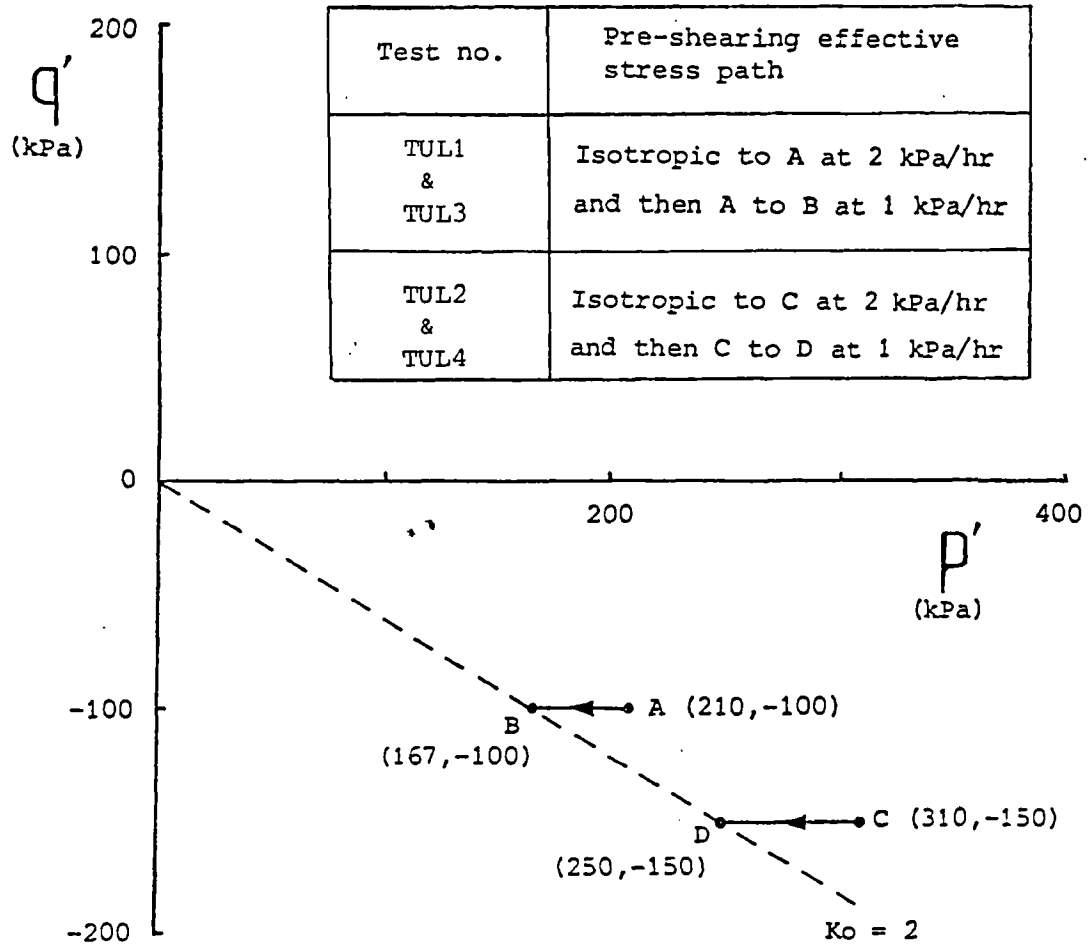
Figure 5.16   Pre-shearing effective stress paths specified for stress path tests on undisturbed London clay (blue) samples with 100 mm diameter
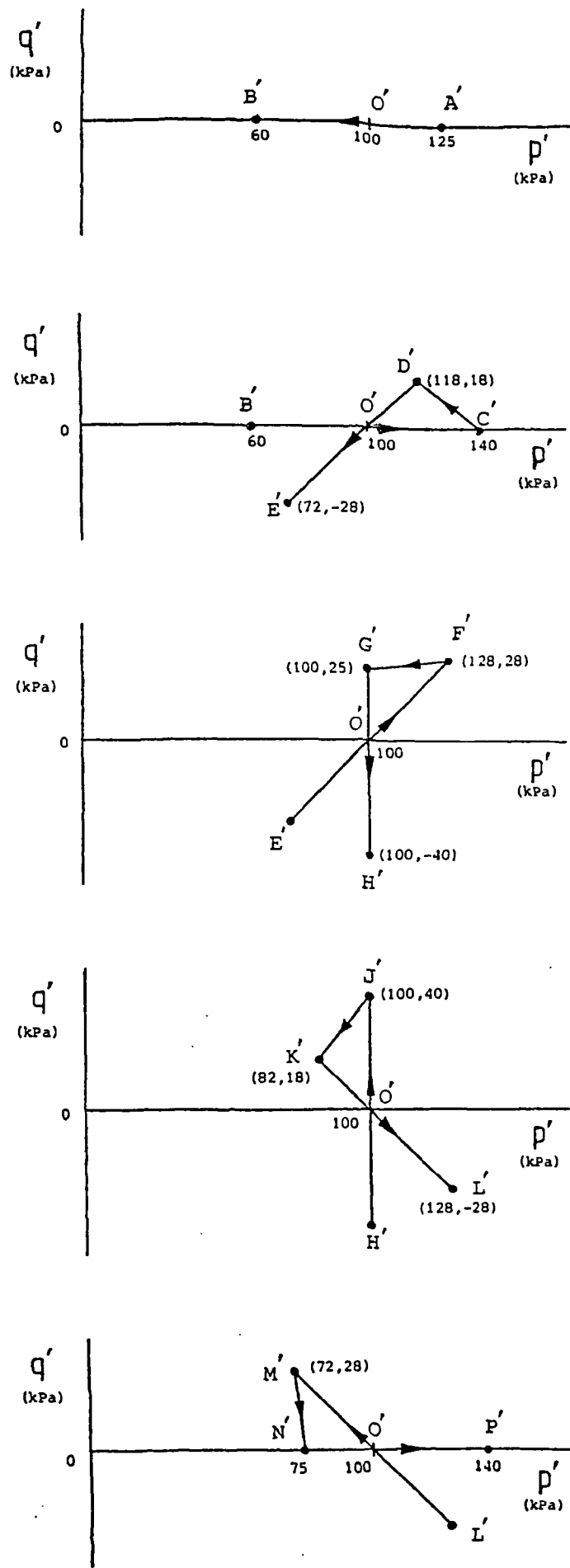
Stress path	Rate of loading along stress path (kPa/hr)	Stopping time at the end of stress path (hr)
A'-B'	1	8
B'-C'	1	16
C'-D'	2.9	12
D'-E'	1	8
E'-F'	1	15
F'-G'	2.9	13
G'-H'	1	27
H'-J'	1	16
J'-K'	2.9	13
K'-L'	1	9
L'-M'	1	6
M'-N'	2.9	10
N'-P'	1	7

Figure 5.17   Specified effective stress paths and specified rates of loading for stress probing test TUB1
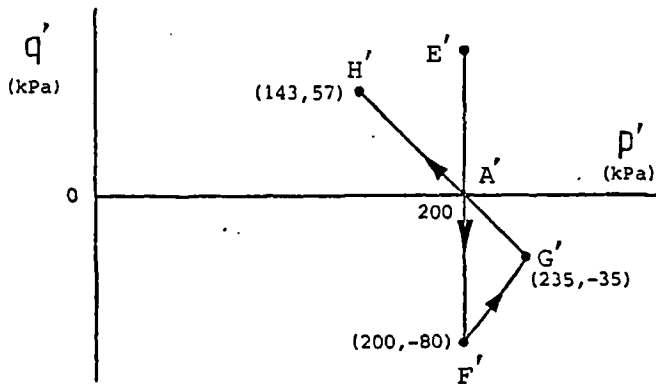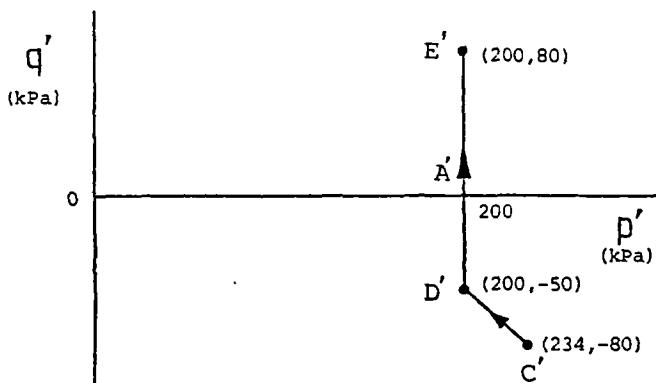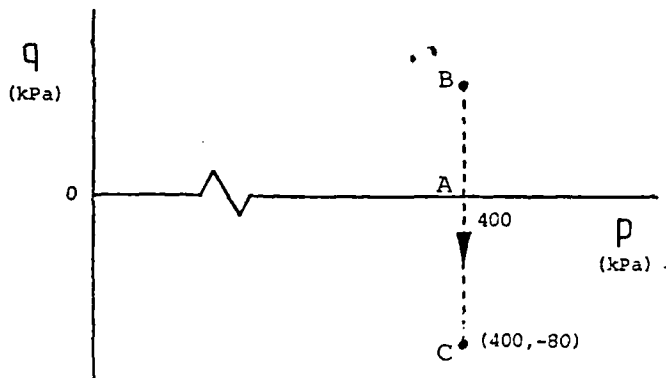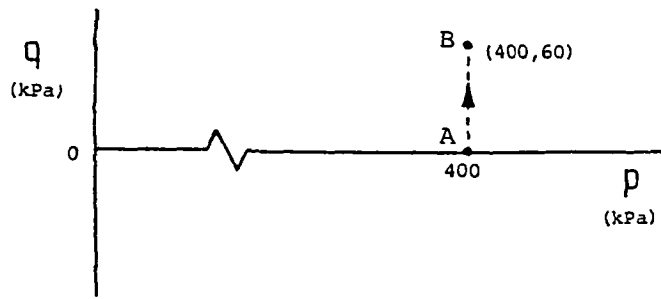
Stress path	Rate of loading along stress path (kPa/hr)	Stopping time at the end of stress path (hr)
A-B	3	5
B-C	3	45
C'-D'	3	36
D'-E'	1	35
E'-F'	1	33
F'-G'	3	9
G'-H'	1	8

(a)

Figure 5.18   Specified total and effective stress paths and specified rates of loading for stress probing test TUL5
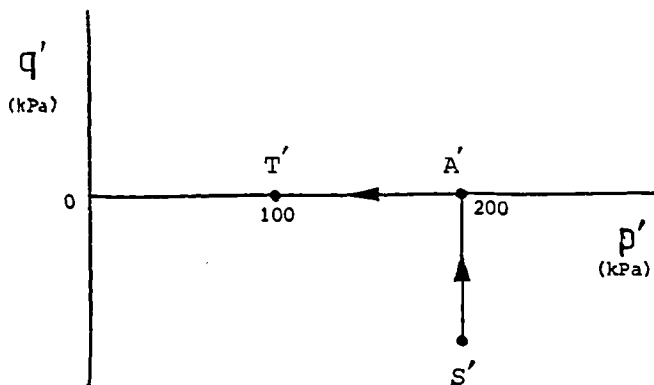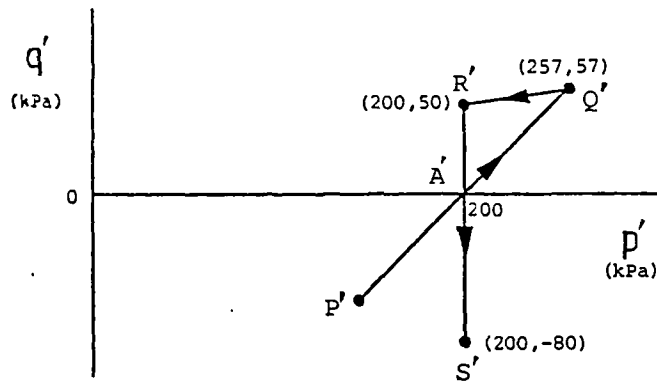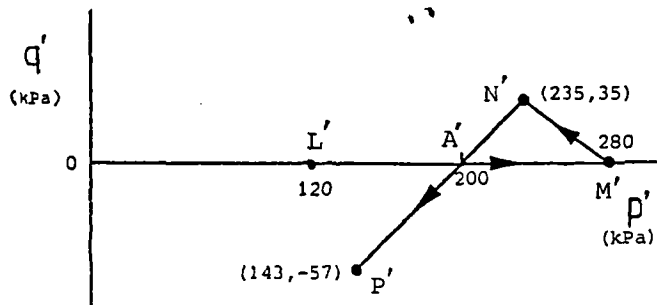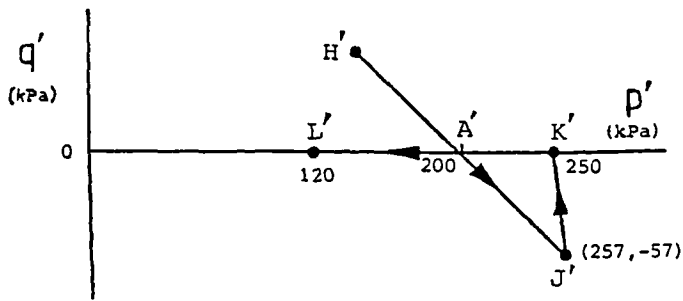
Stress path	Rate of loading along stress path (kPa/hr)	Stopping time at the end of stress path (hr)
H'–J'	1	15
J'–K'	2.9	15
K'–L'	1	40
L'–M'	1	50
M'–N'	2.9	8
N'–P'	1	14
P'–Q'	1	30
Q'–R'	2.9	24
R'–S'	1	40
S'–A'	1	20
A'–T'	2	20

(b)

Figure 5.18 continued

Particle size (mm)
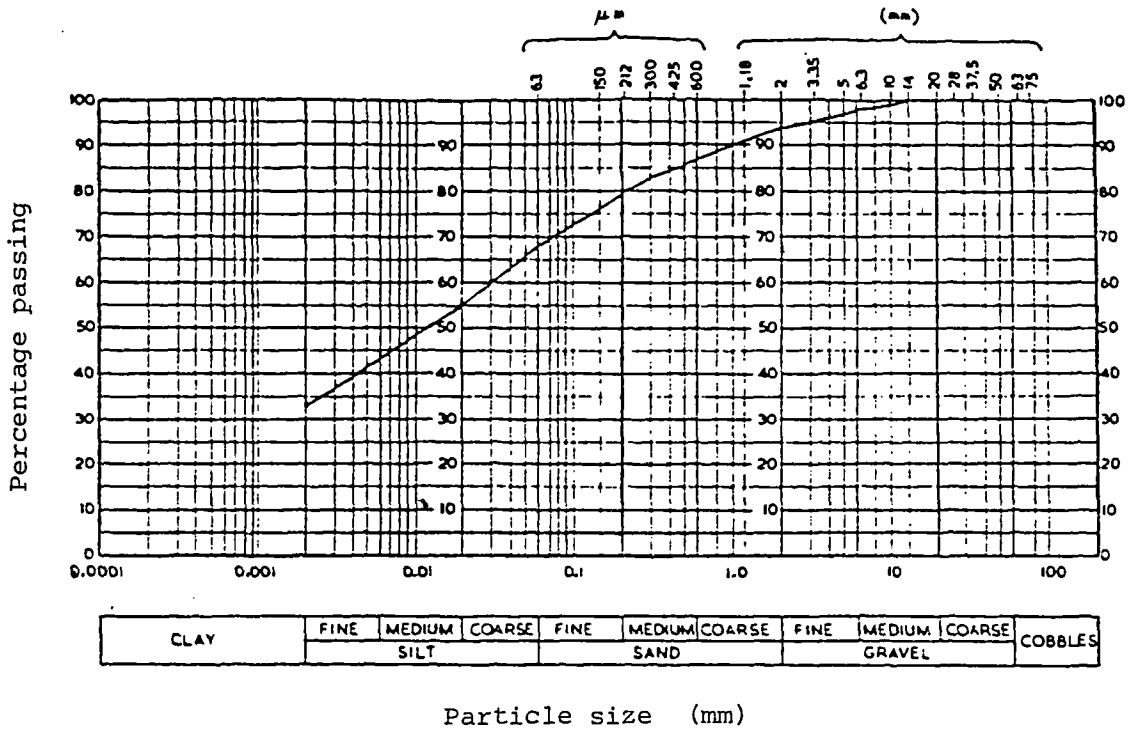
(a) Cowden till
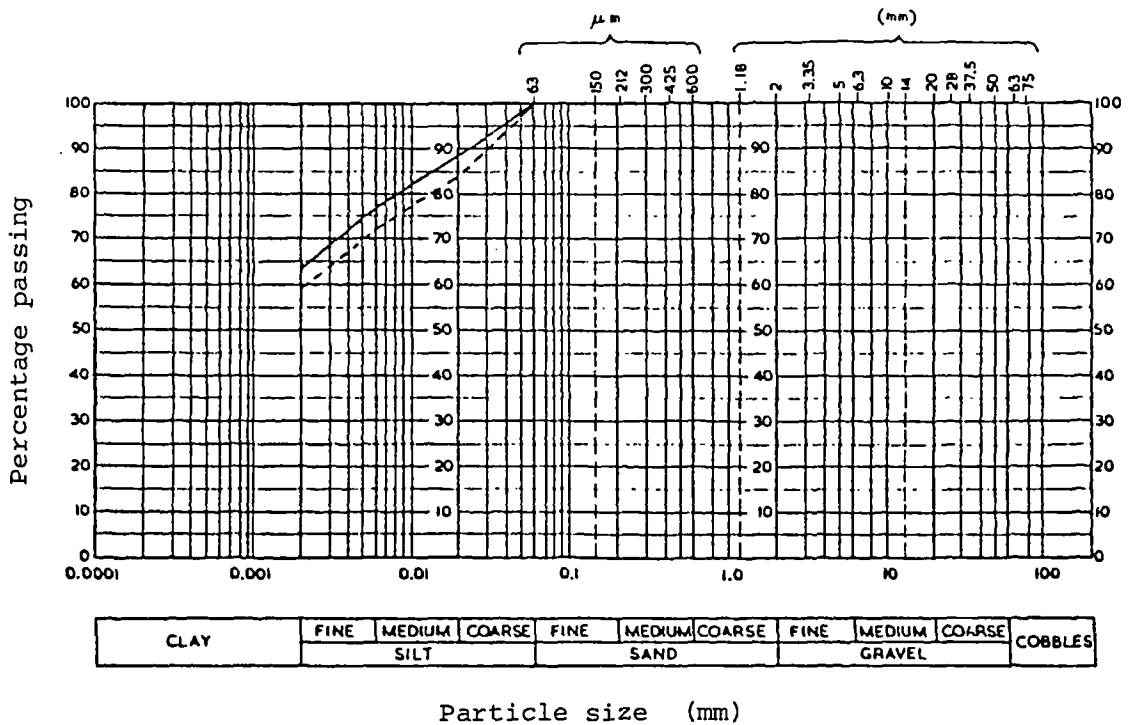
Particle size (mm)

—————— London clay (brown)

- - - - - London clay (blue)

(b) London clay

Figure 6.1 Results of particle size distribution tests
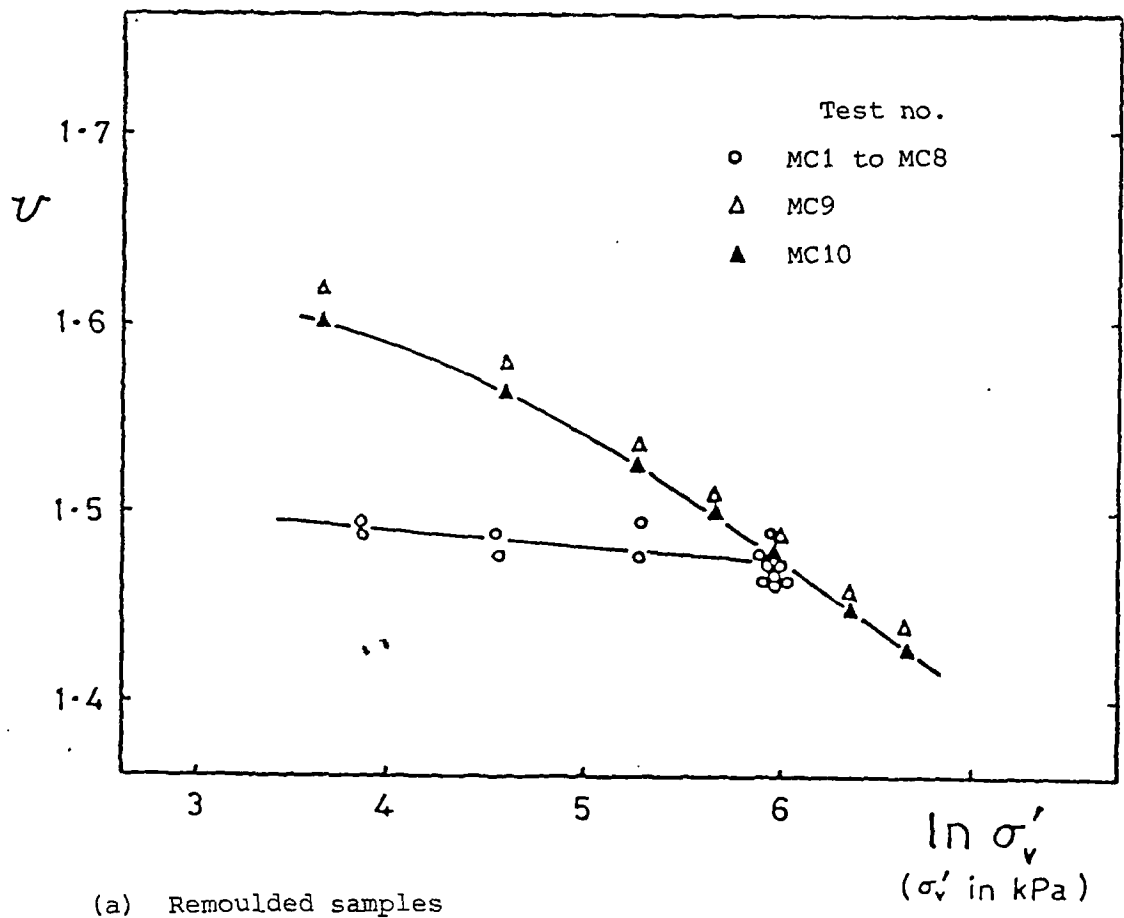
(a) Remoulded samples
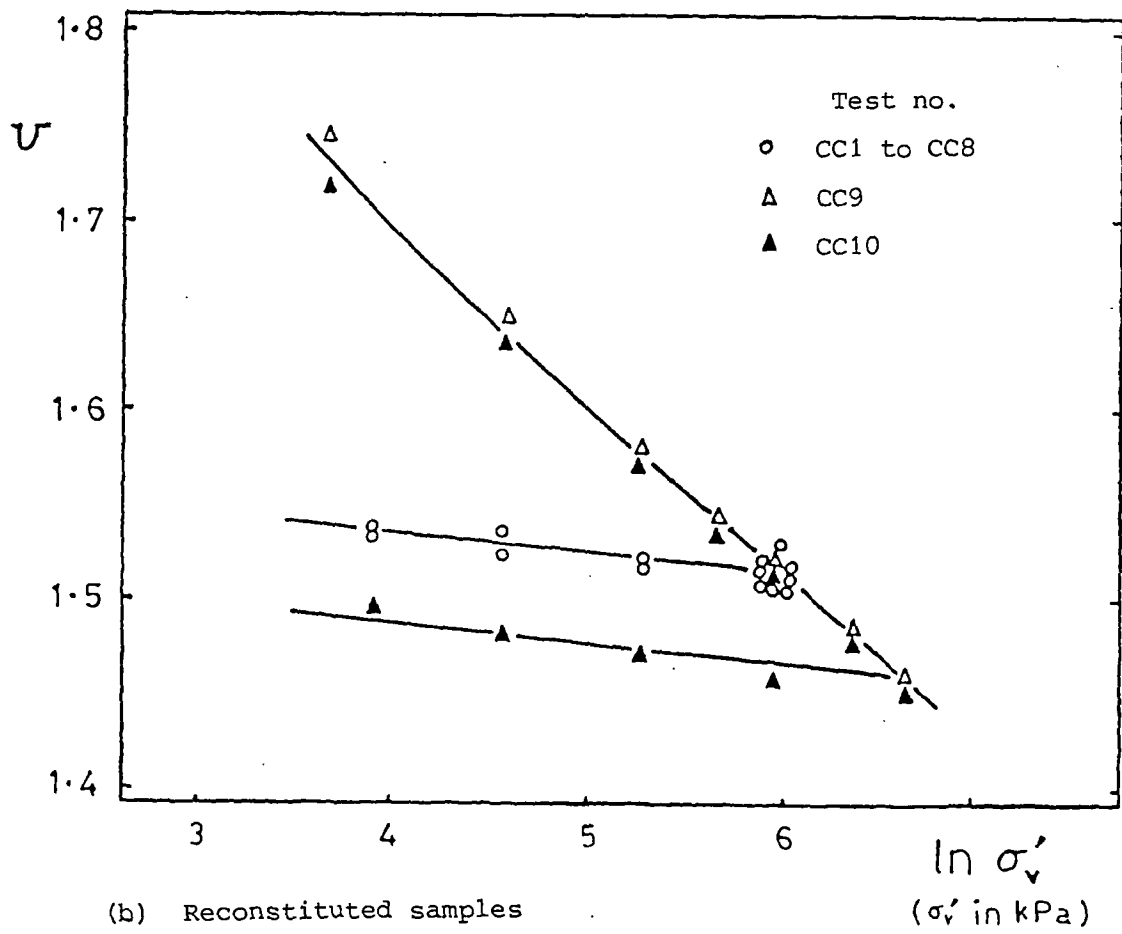
(b) Reconstituted samples

Figure 6.2   Results of one-dimensional compression from Cowden
               till simple shear samples
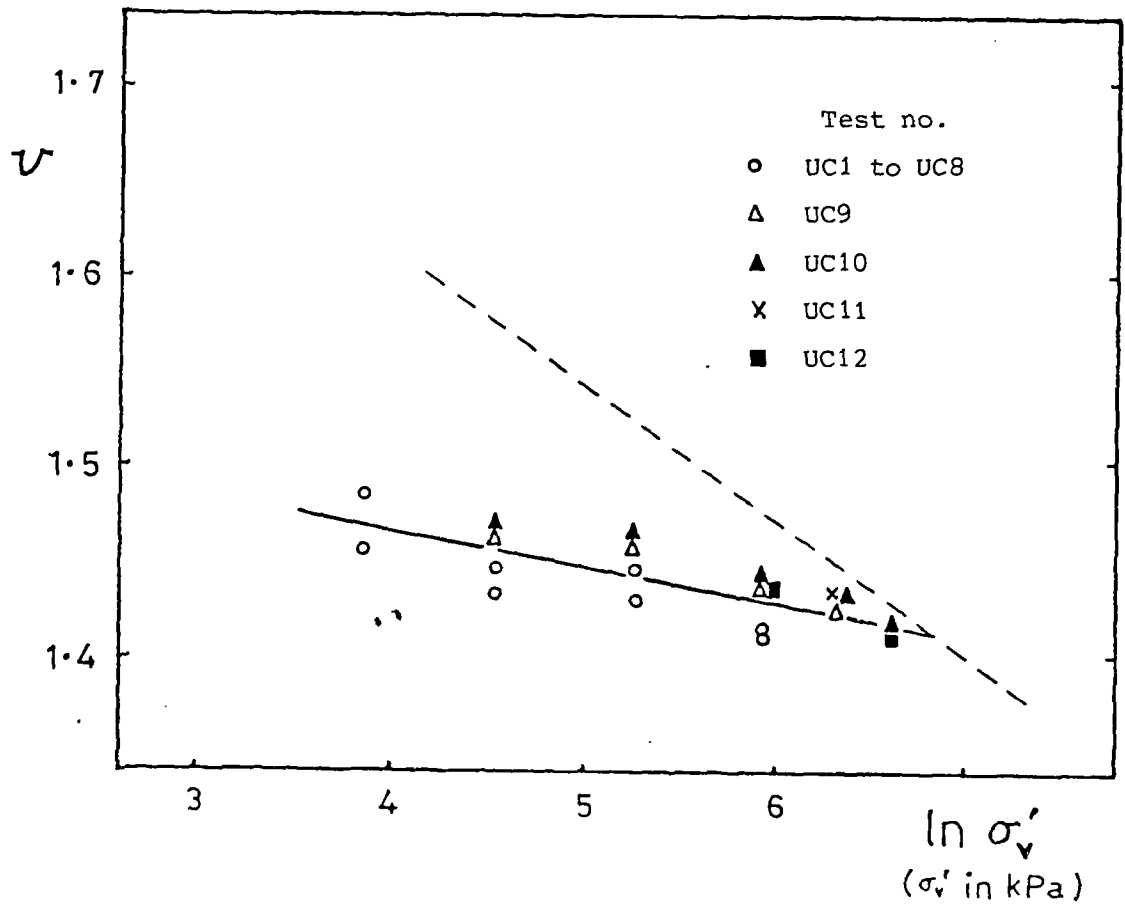
(c)   Undisturbed samples

Figure 6.2 continued

(a) Remoulded samples

(b) Undisturbed samples
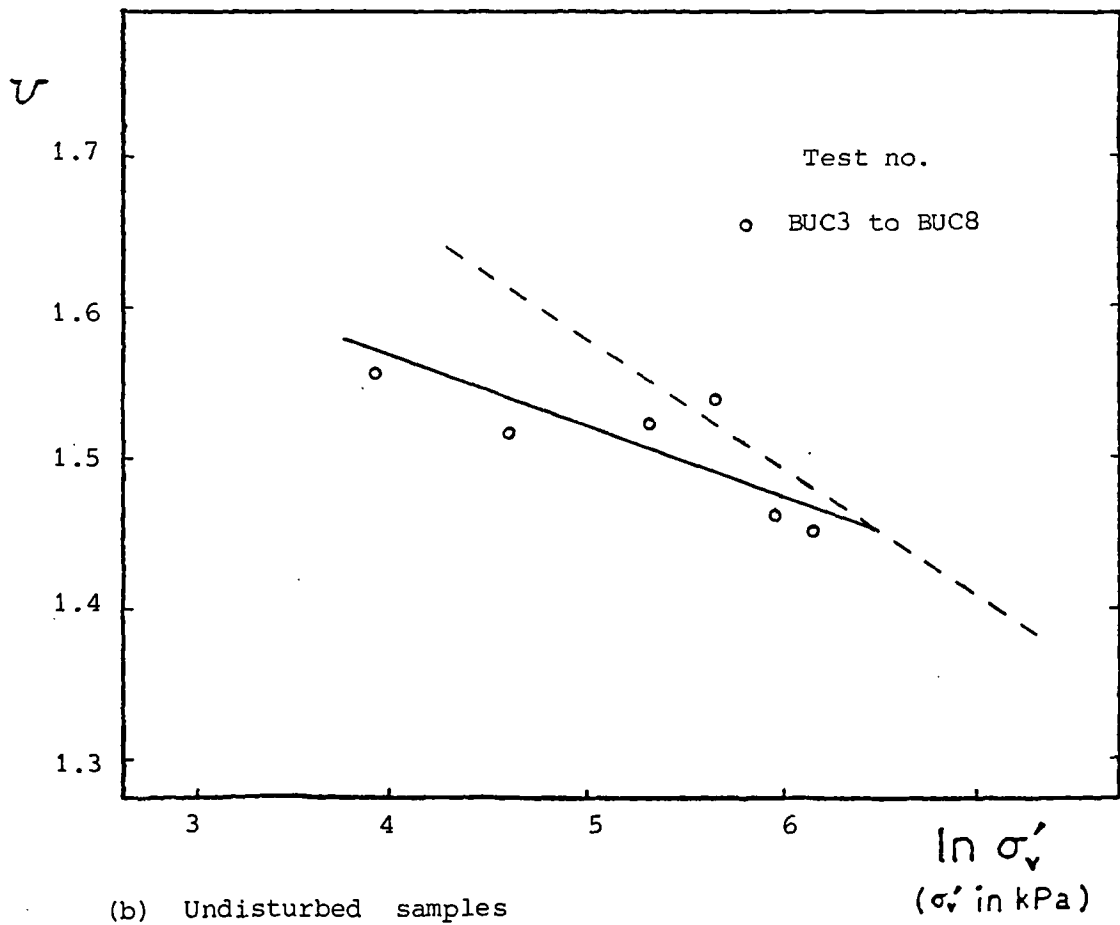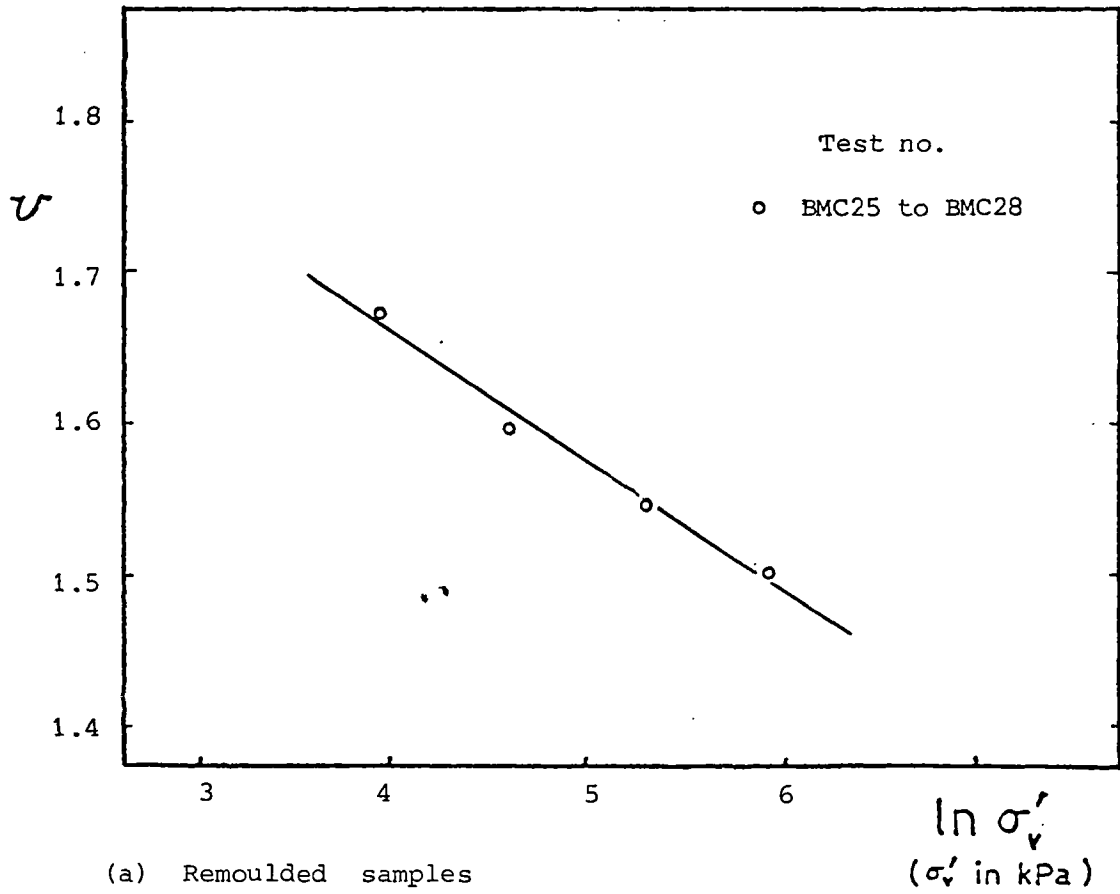
Figure 6.3 Results of one-dimensional compression from Cowden till shear box samples
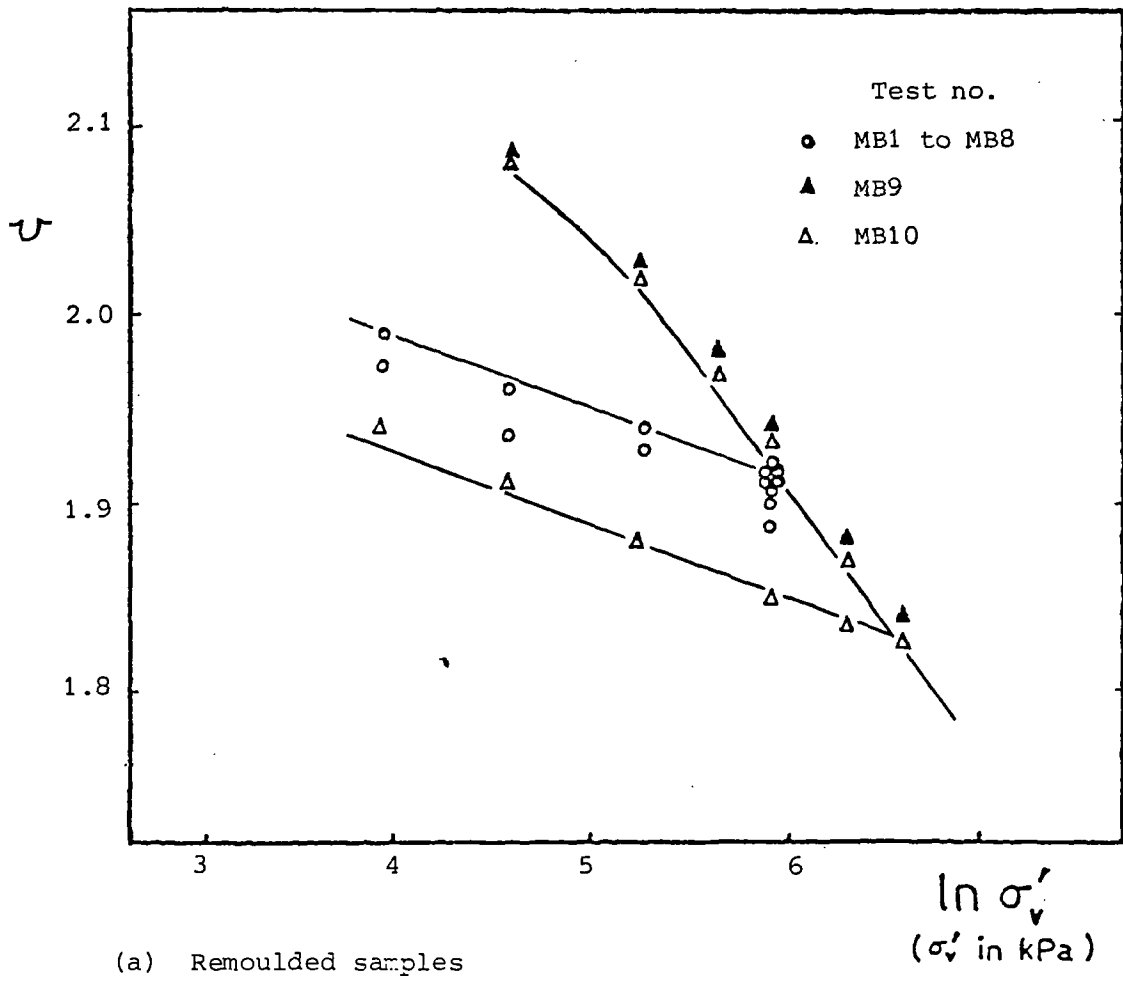
(a) Remoulded samples
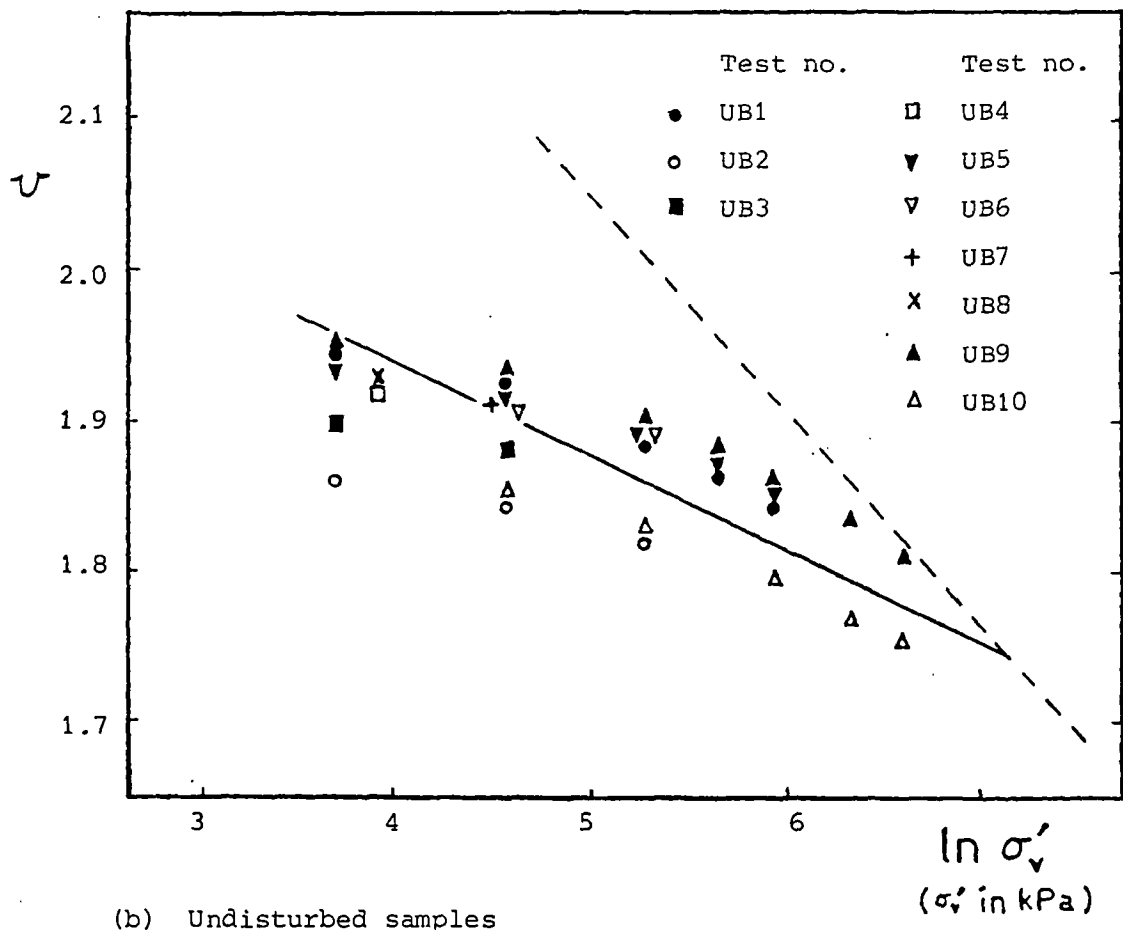
(b) Undisturbed samples

Figure 6.4   Results of one-dimensional compression from London clay (brown) simple shear samples
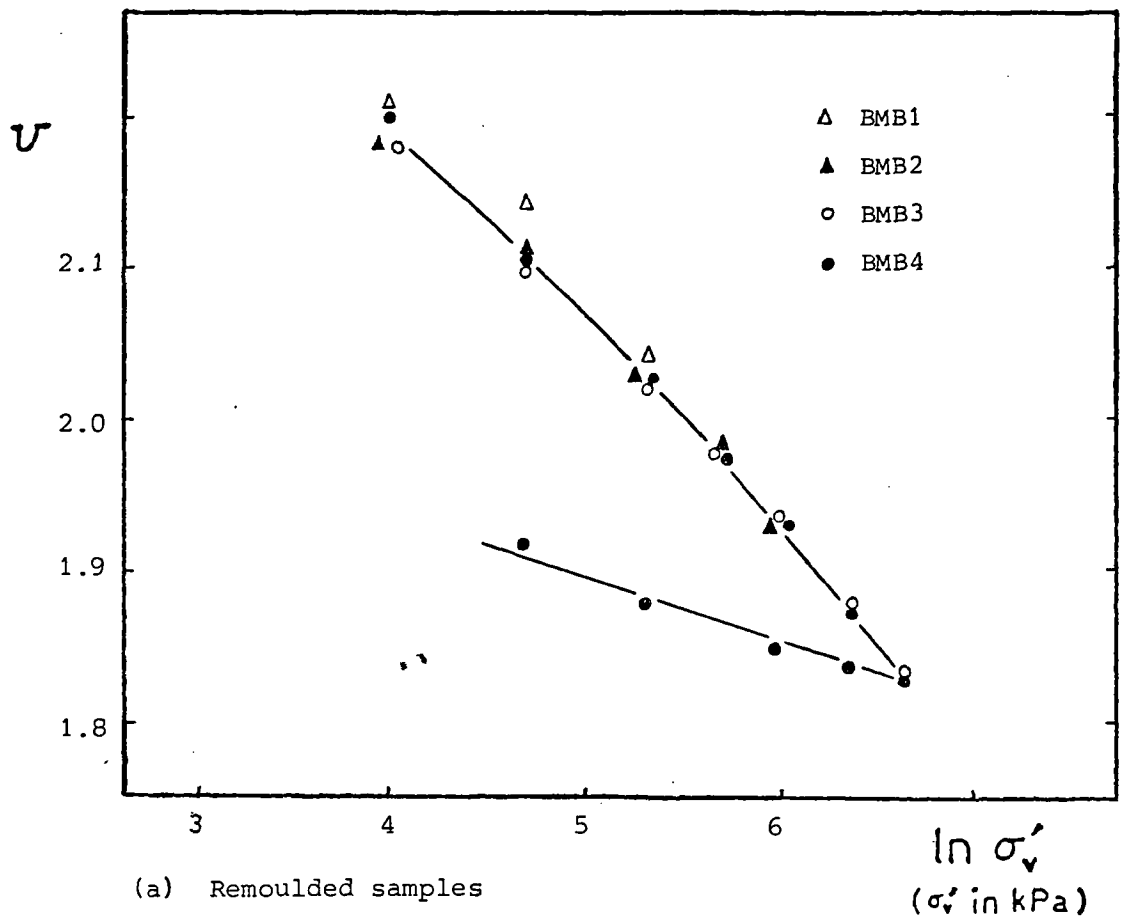
(a)   Remoulded samples
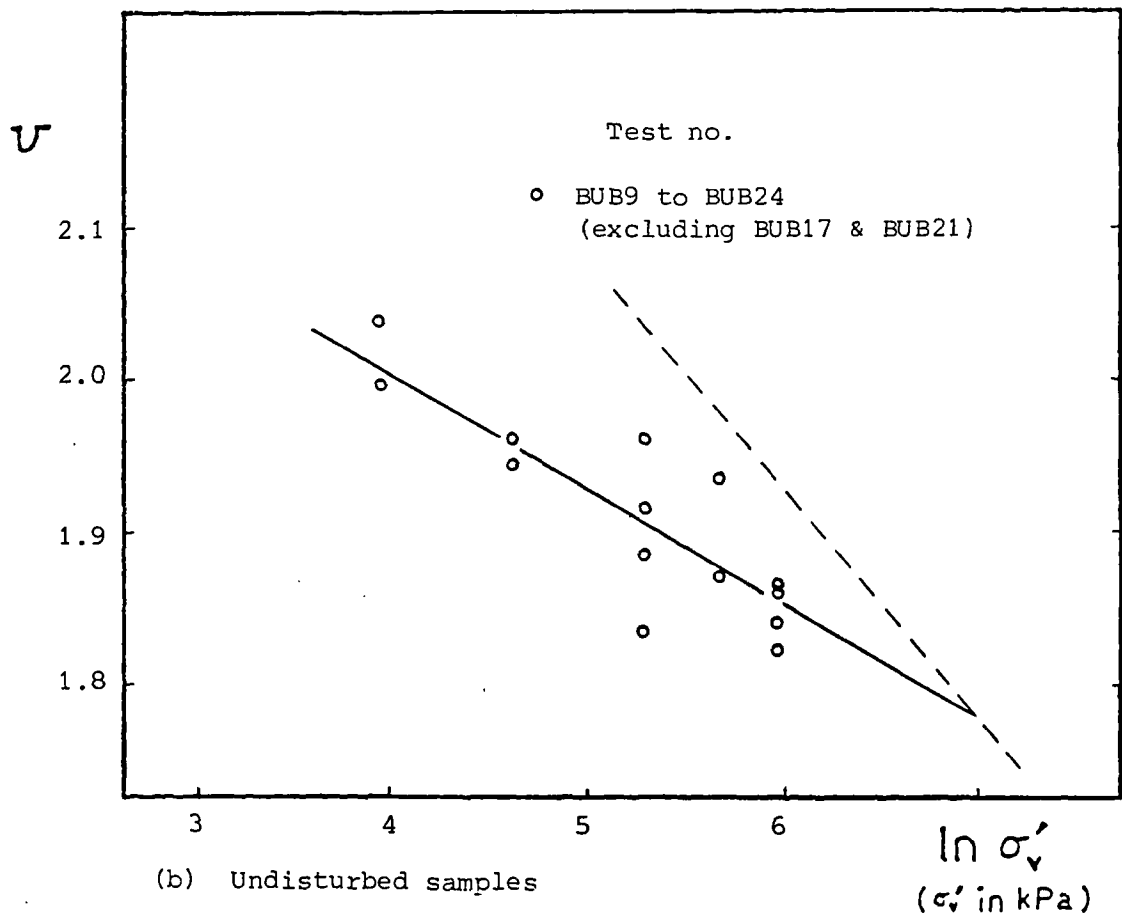
(b)   Undisturbed samples

Figure   6.5   Results of one-dimensional compression from London
                 clay (brown) shear box samples
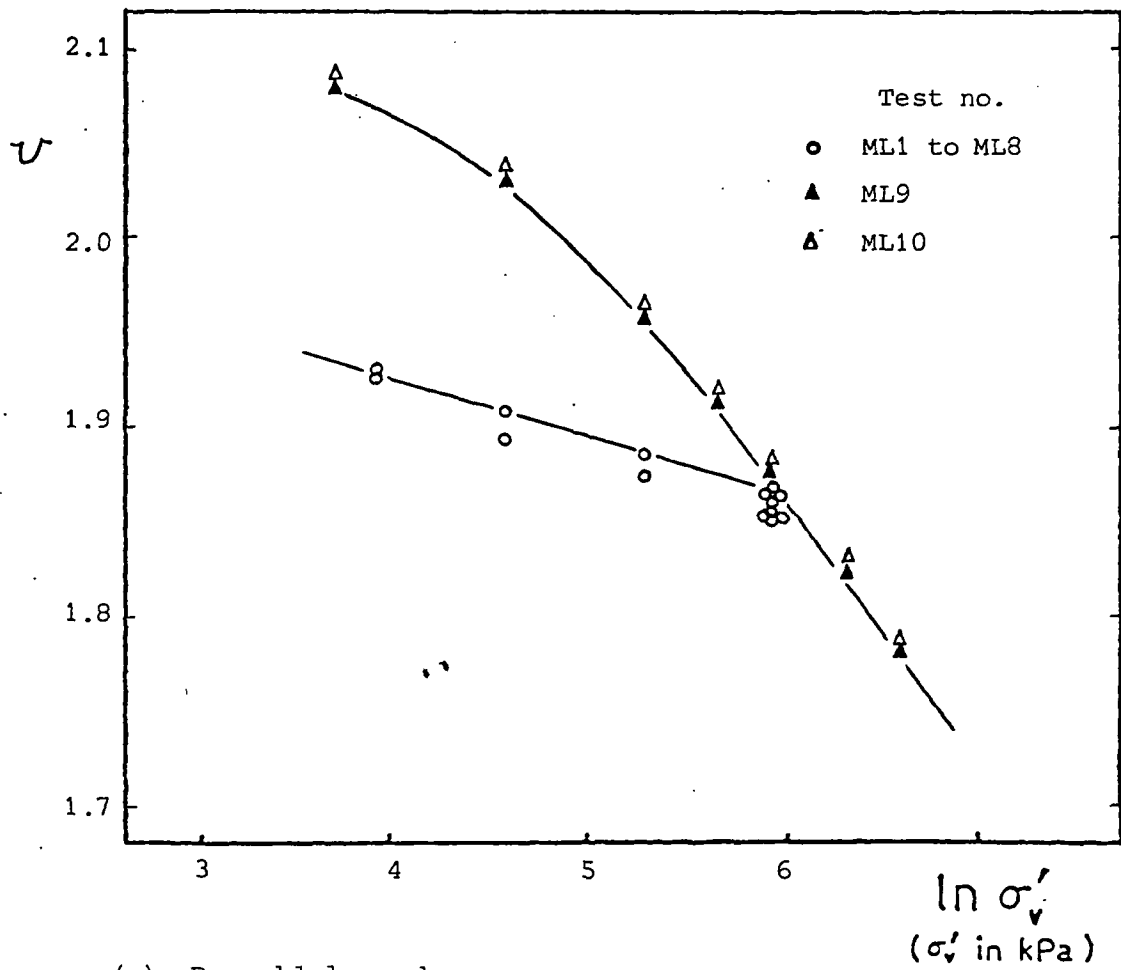
(a) Remoulded samples
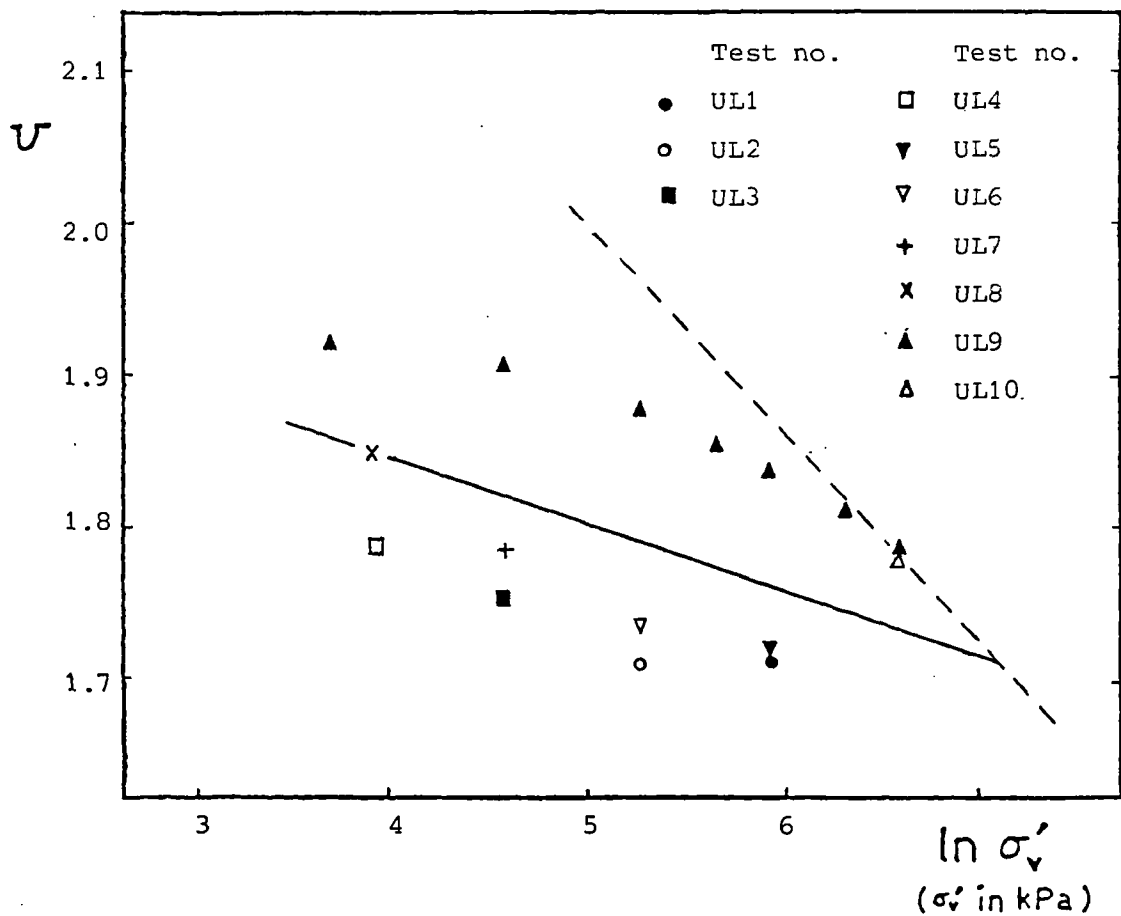
(b) Undisturbed samples

Figure 6.6   Results of one-dimensional compression from London
                clay (blue) simple shear samples
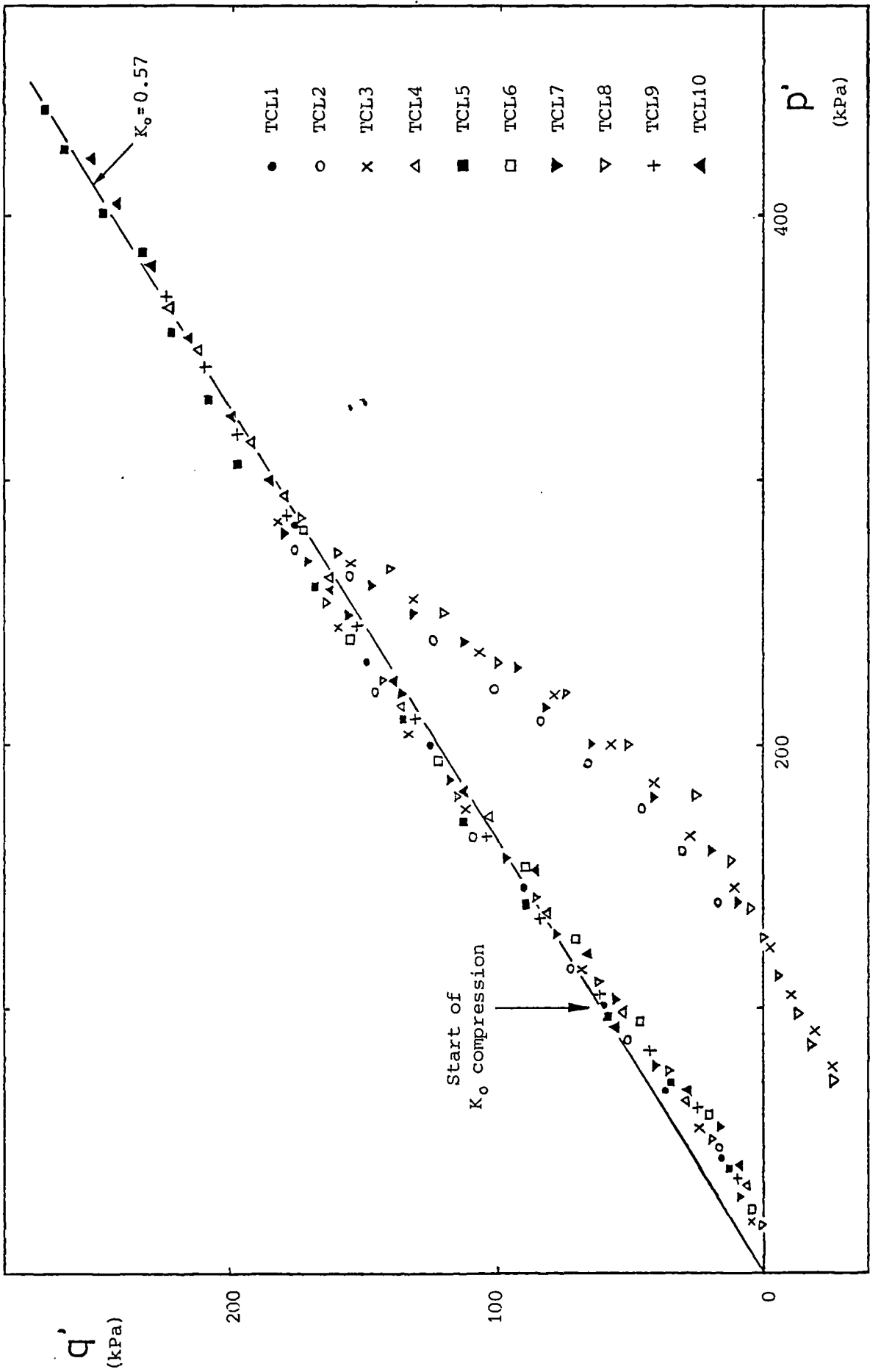
(a)

Figure 6.7   Results of one-dimensional compression from 38 mm
                 reconstituted London clay (blue) triaxial samples

Figure 6.7 continued

√time (√min)

0

20   40   60

0.2 ┤ Test UC9

σ'$_v$ increased from 194
to 388 kPa.

0.4

(a) Cowden
     till

0.6

0.8

U$_t$

1.0

√time (√min)

0

20   40   60

0.2 ┤ Test UL9

σ'$_v$ increased from 582
to 776 kPa.

0.4

(b) London
     clay
     (blue)

0.6

0.8

U$_t$

1.0
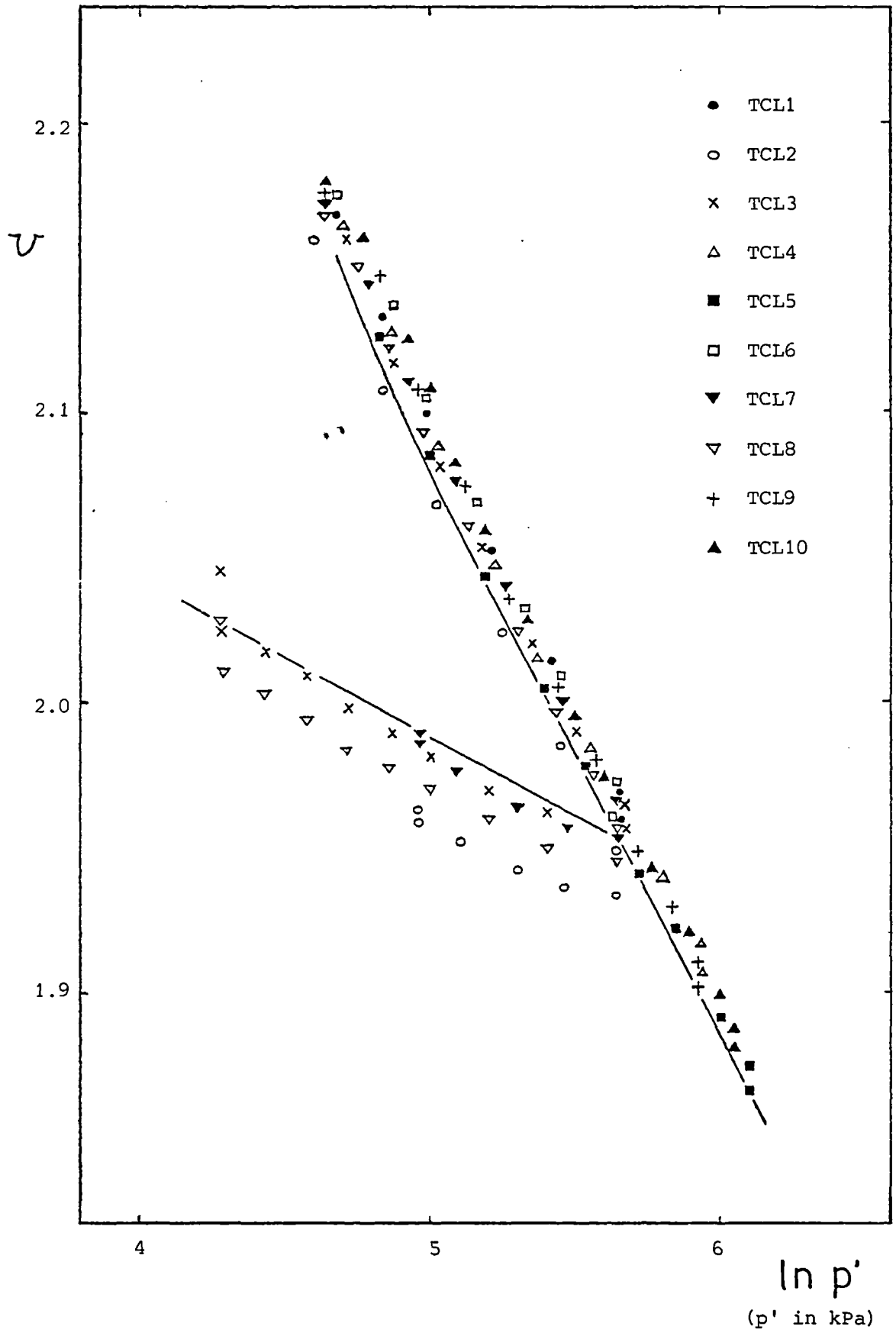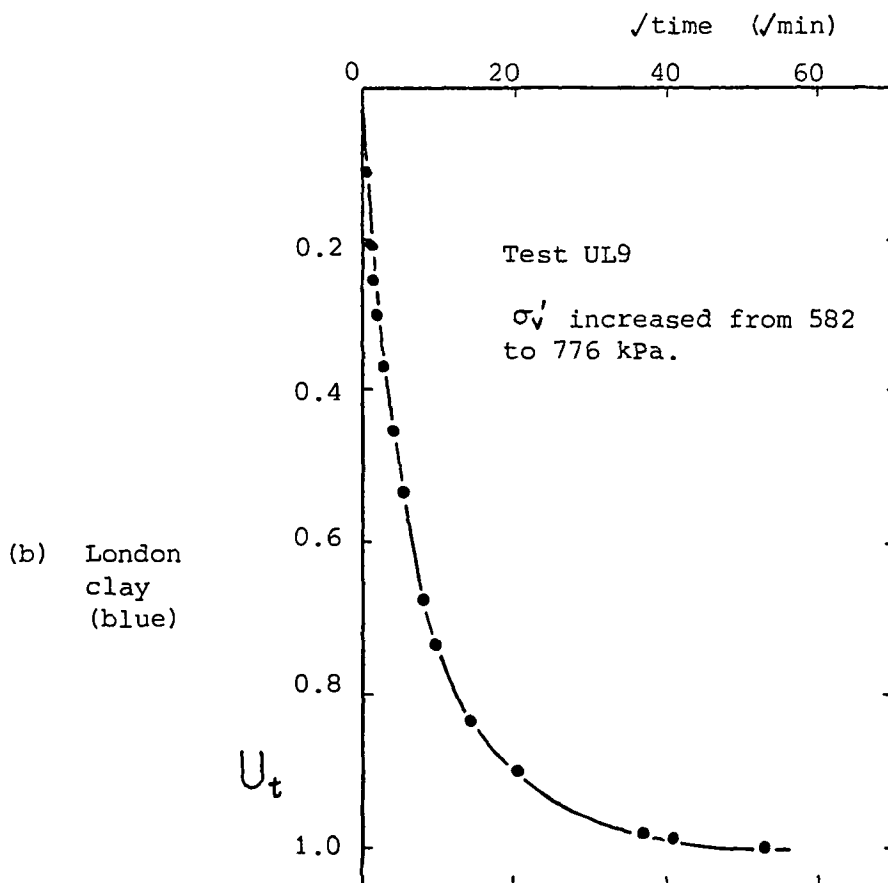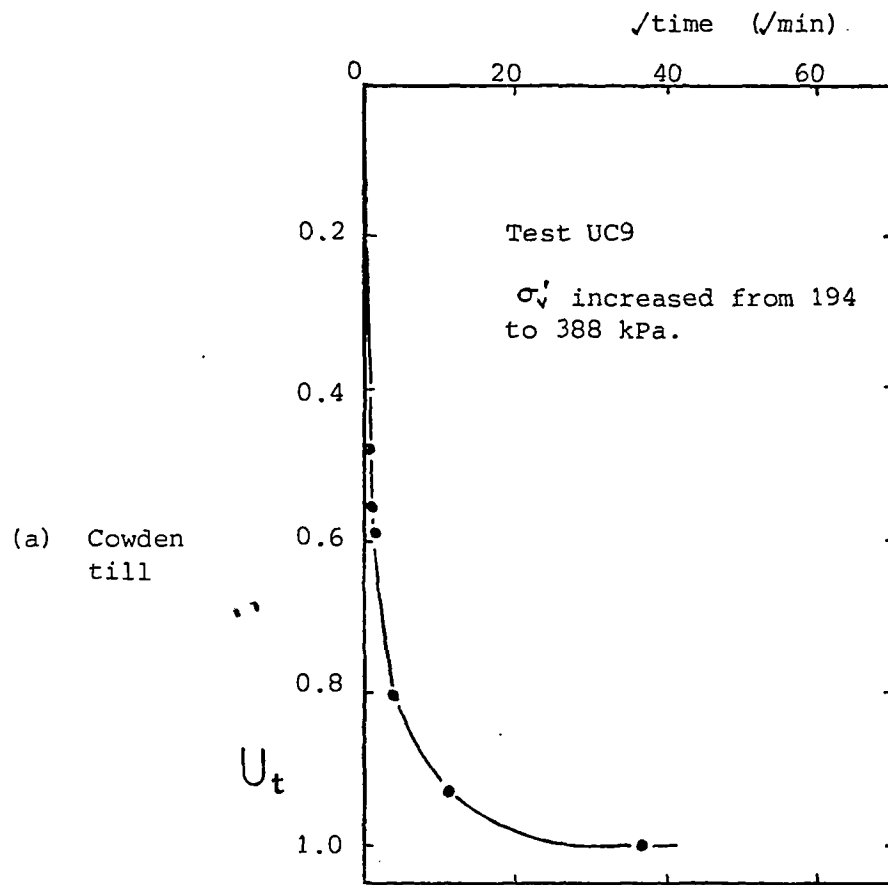
Figure 6.8   Results of one-dimensional consolidation from
                 simple shear samples
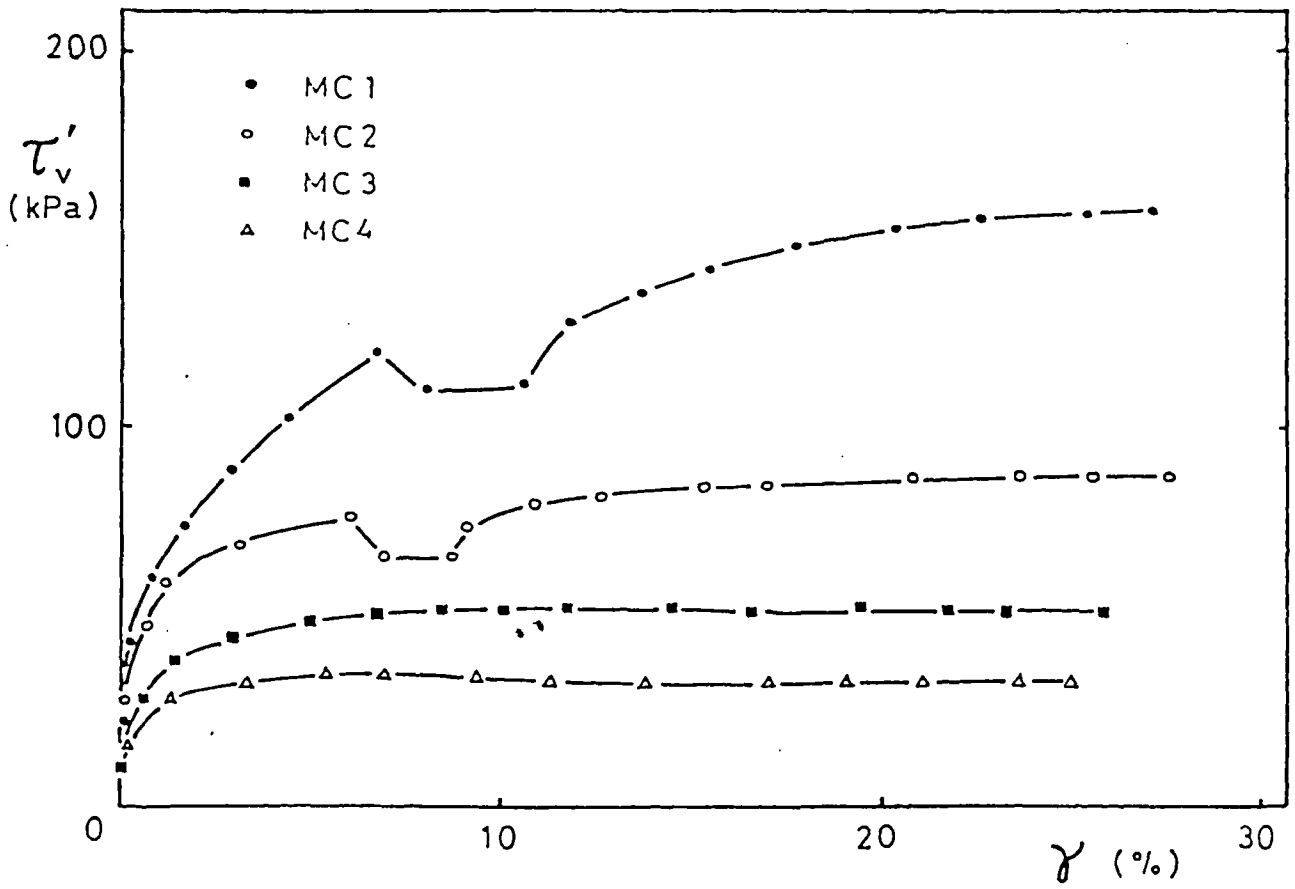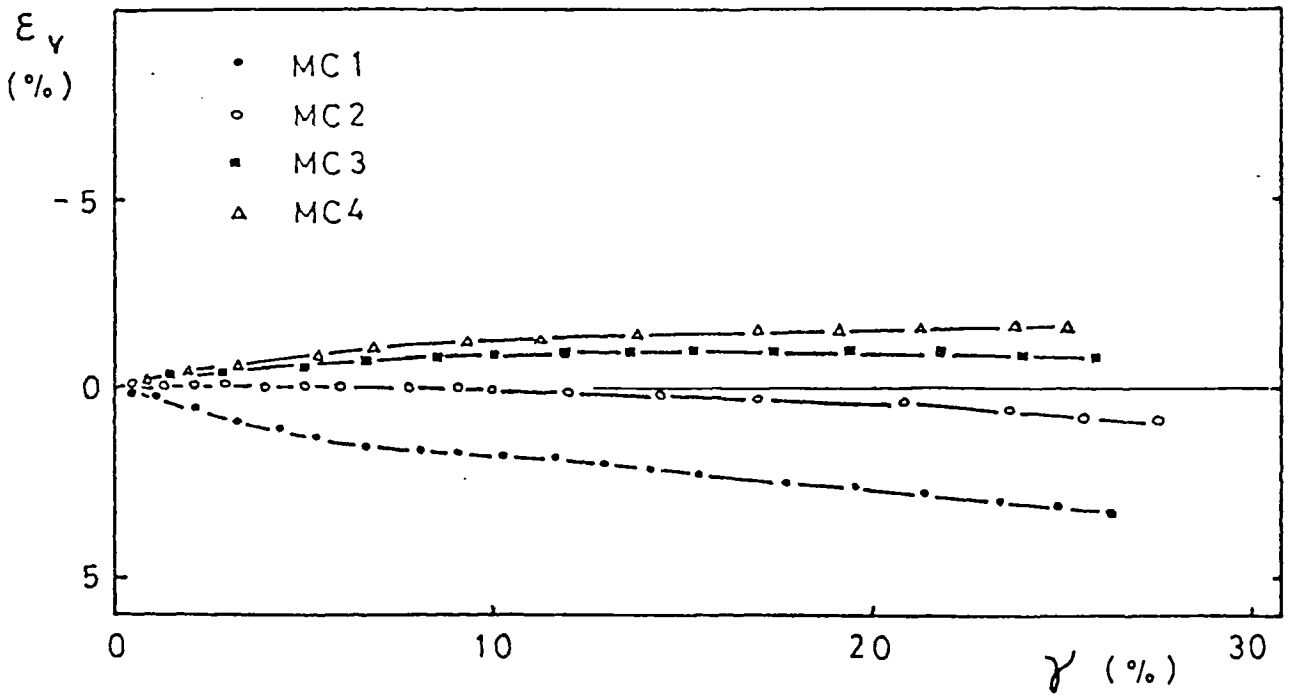
Figure   6.9   Results of shearing from remoulded Cowden till simple
                  shear samples
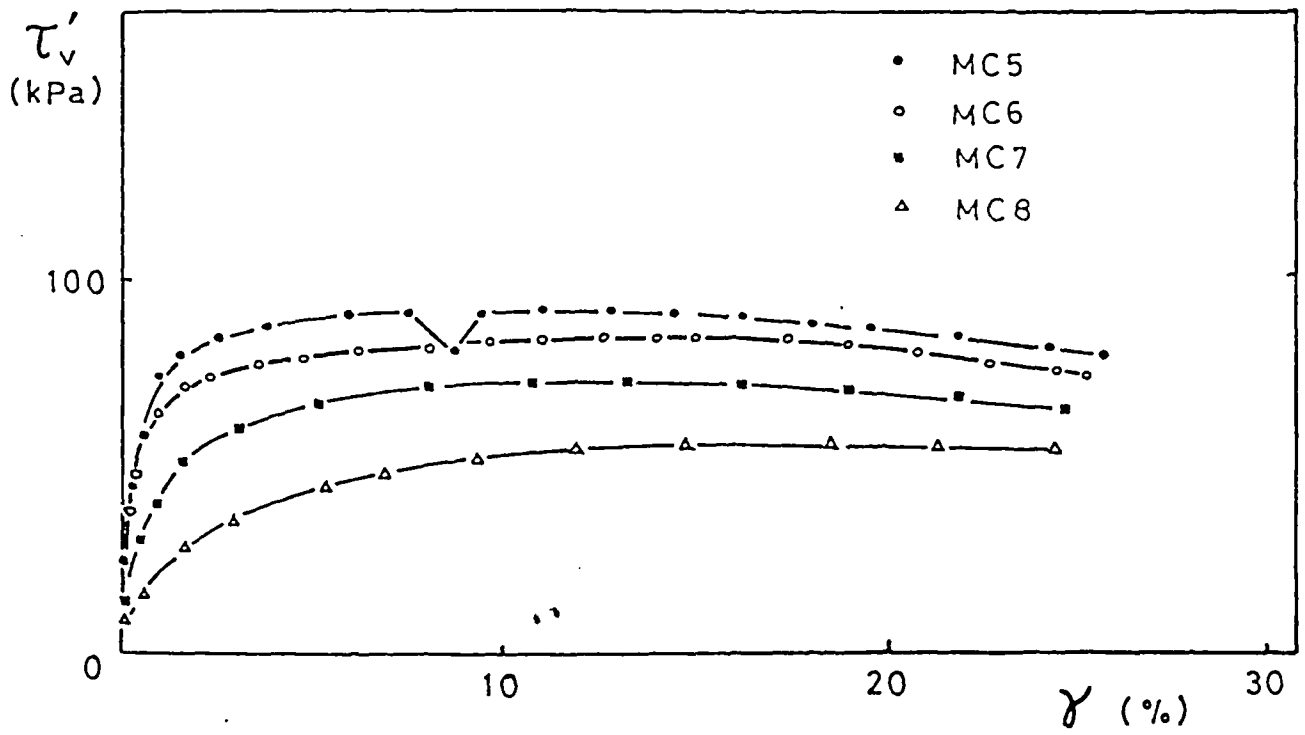
(c)
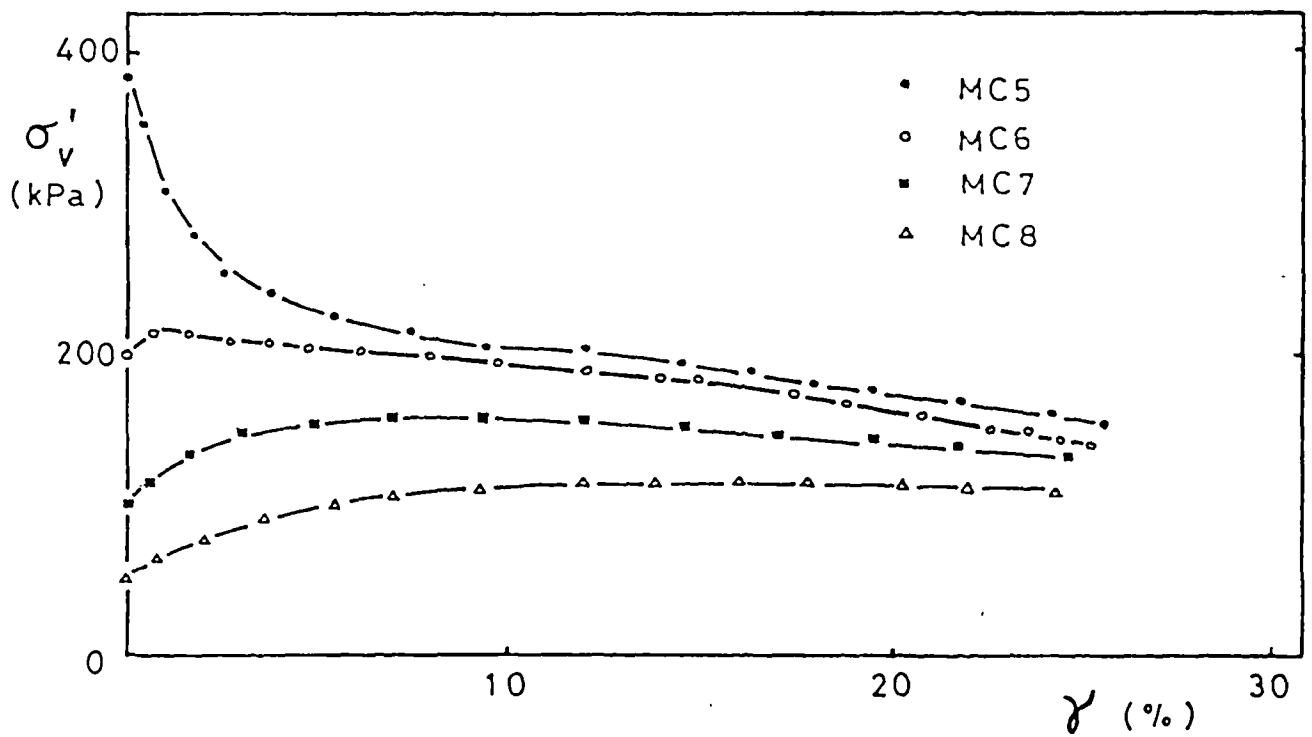
(d)

Figure 6.9 continued
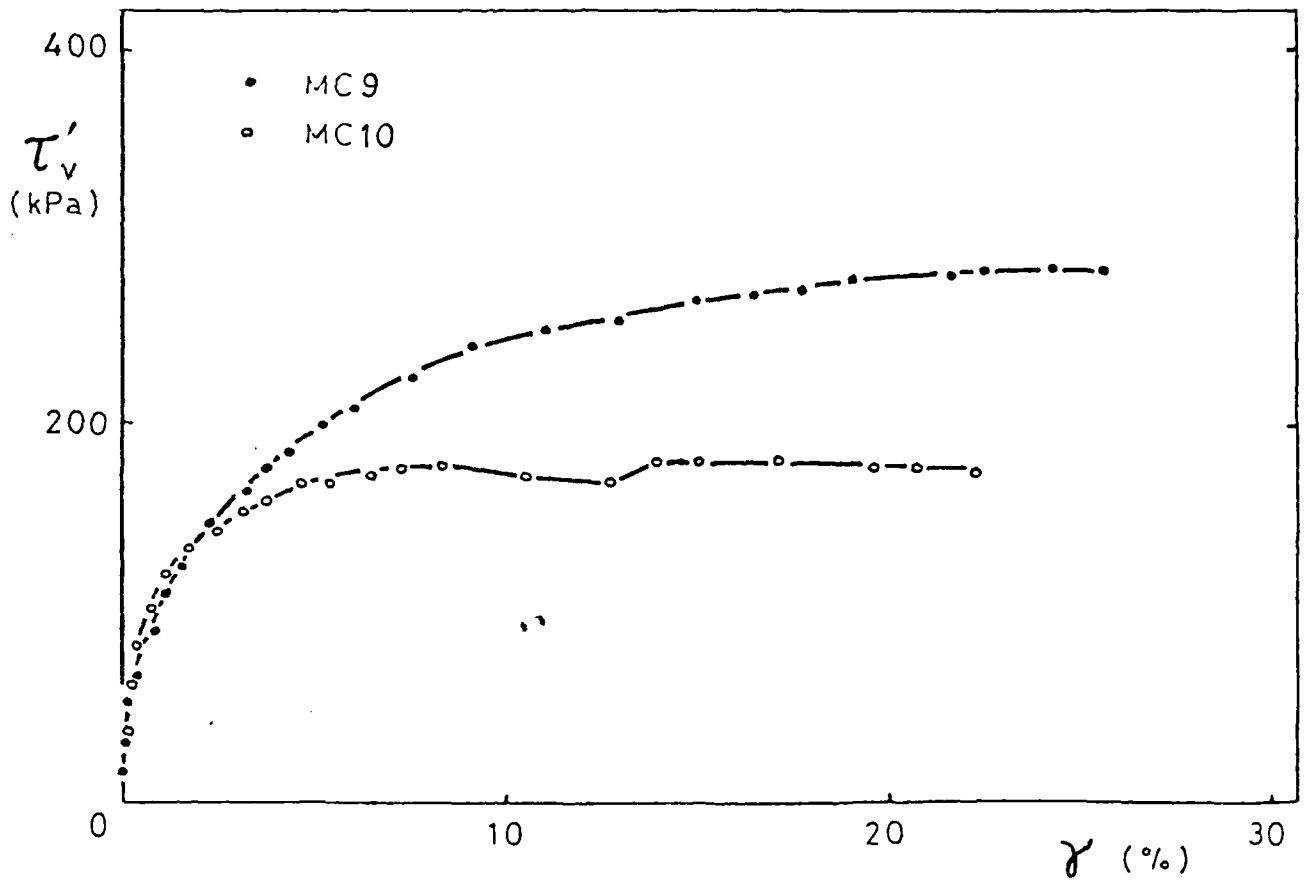
(e)
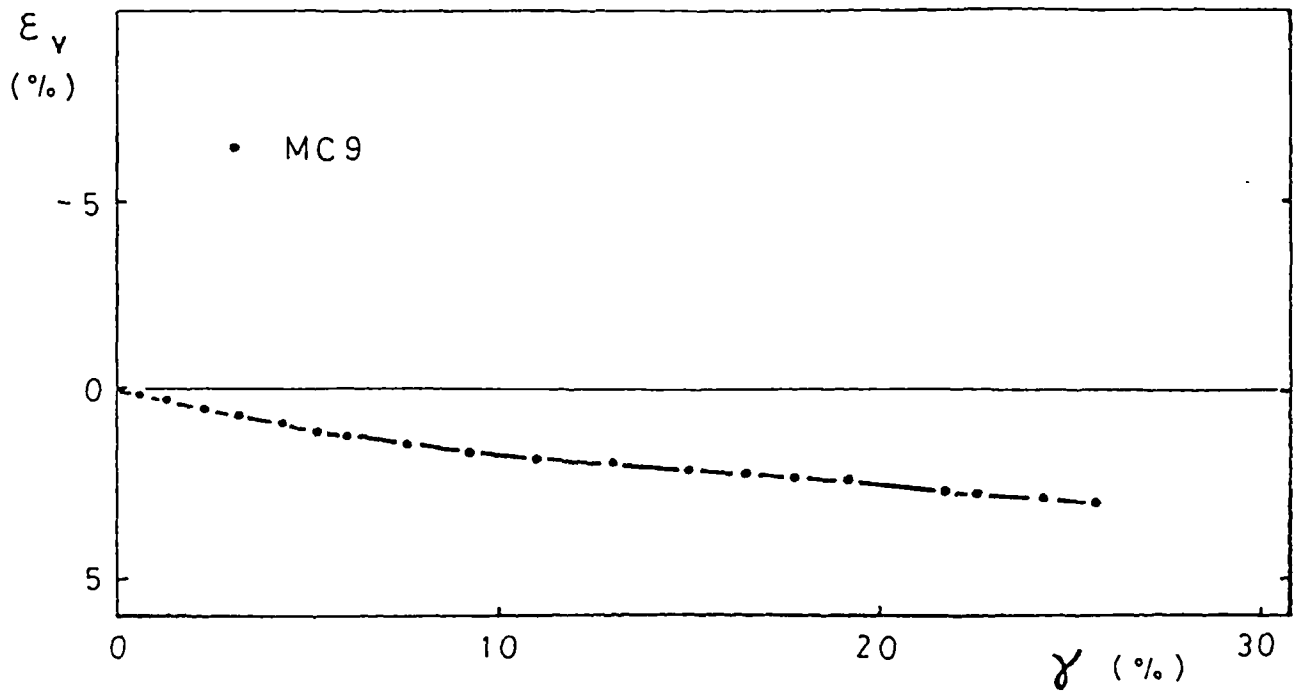
(f)

Figure 6.9 continued
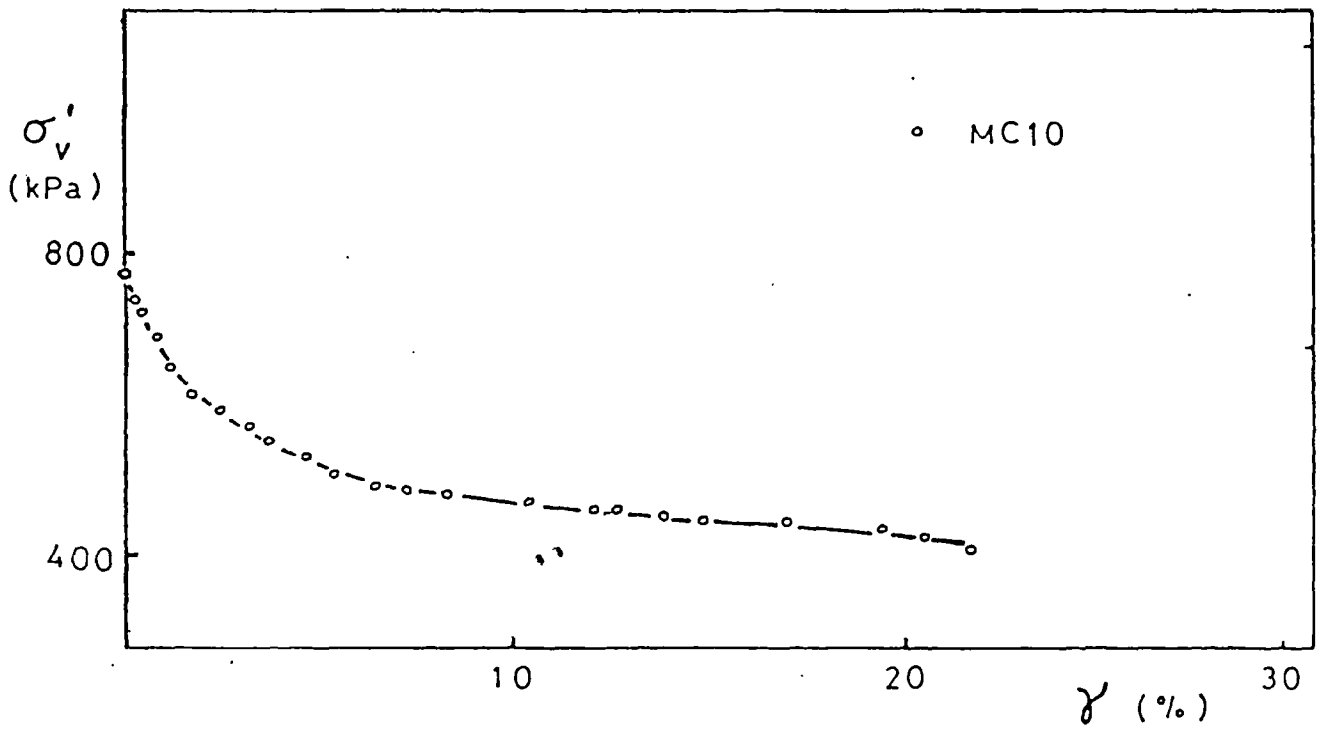
(g)

Figure 6.9 continued
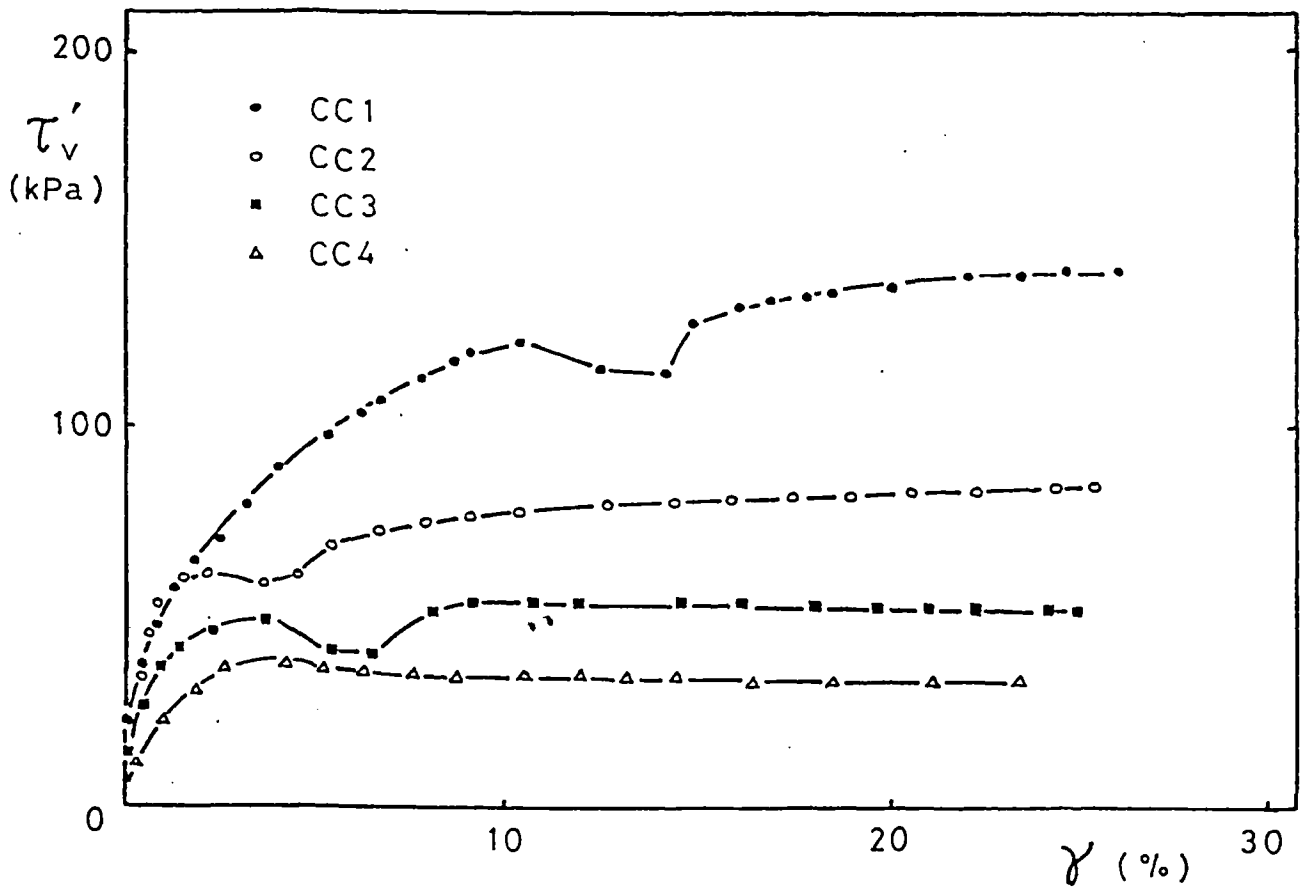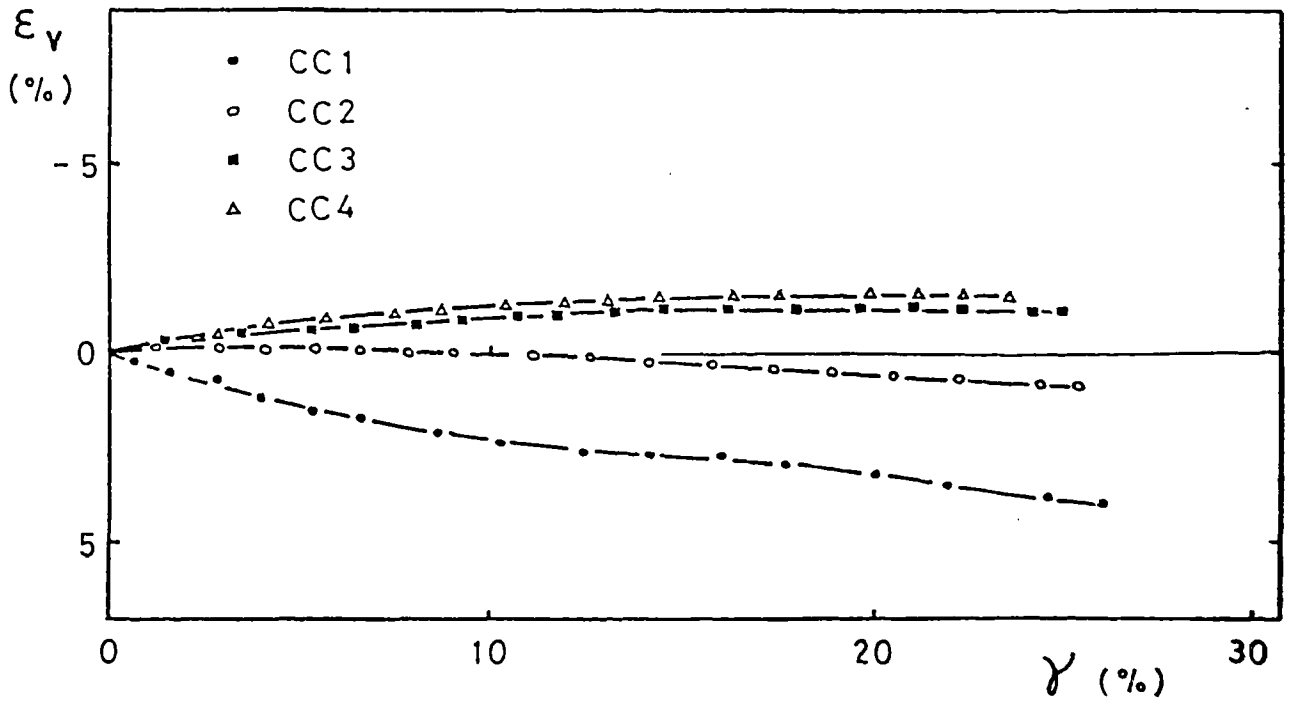
Figure   6.10   Results of shearing from reconstituted Cowden till simple
                     shear samples
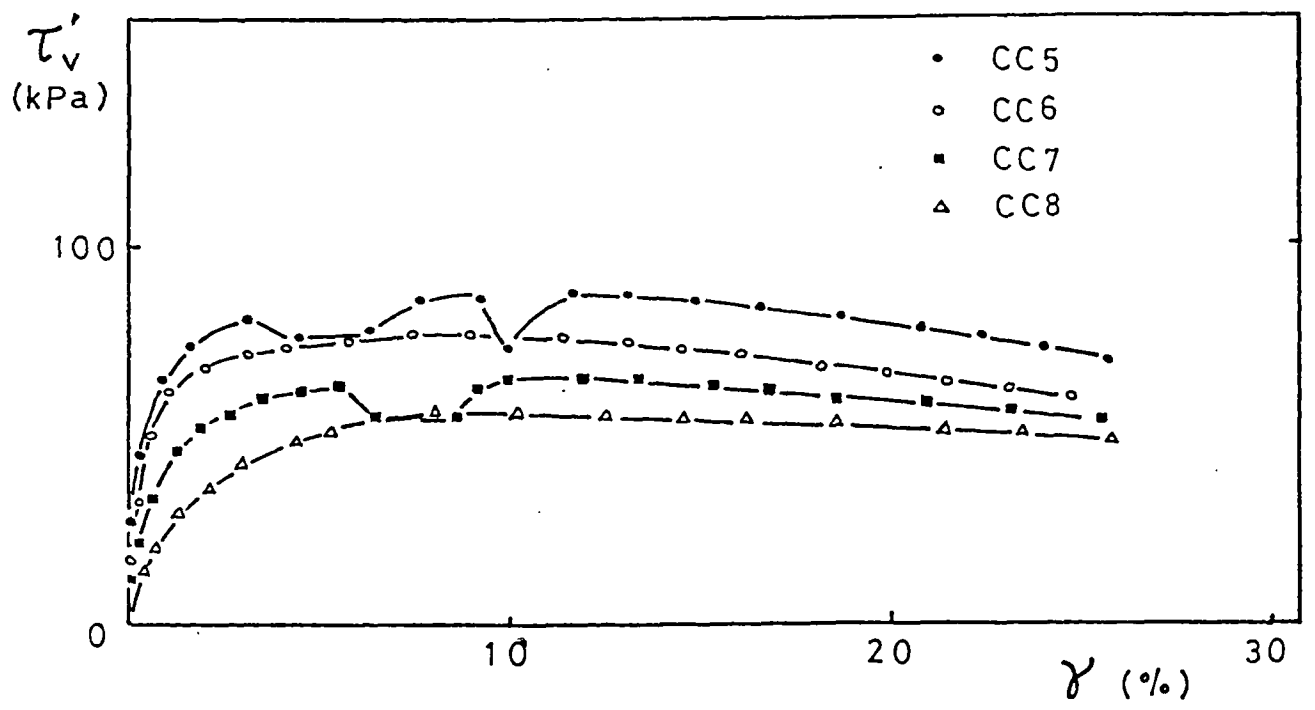
(c)
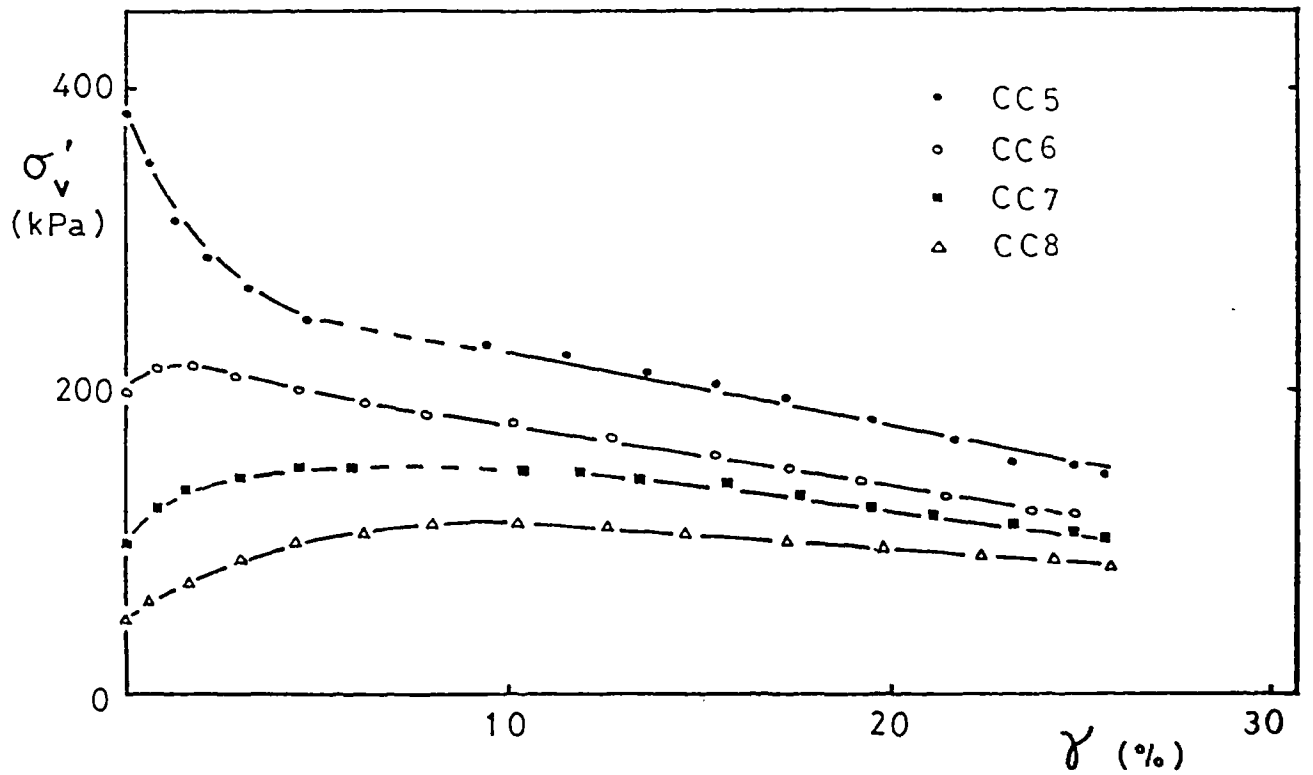
(d)

Figure 6.10 continued

(e)

(f)

(g)
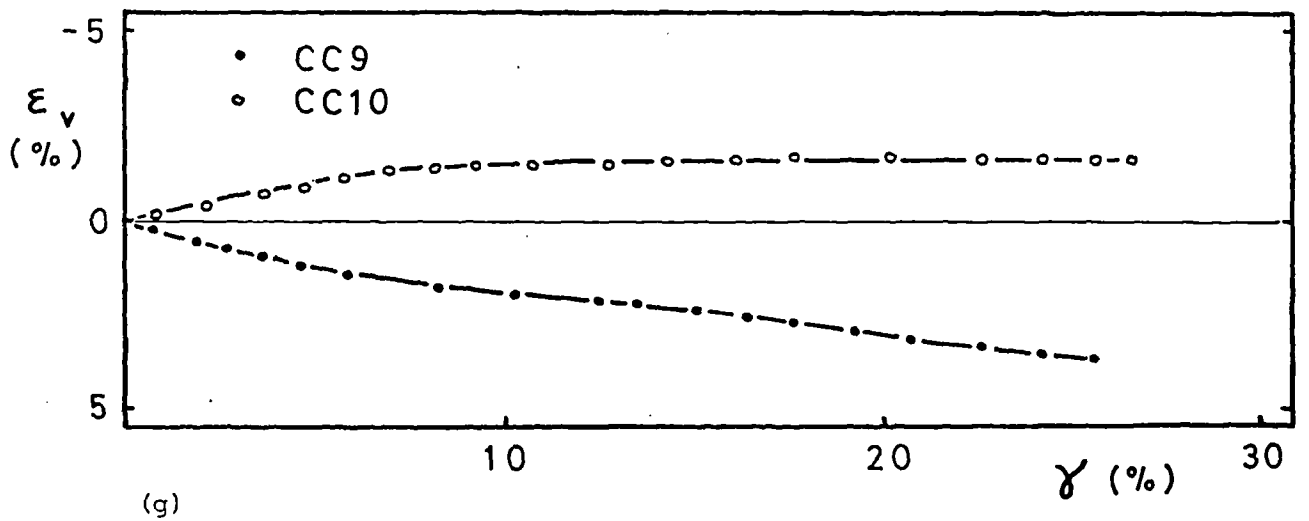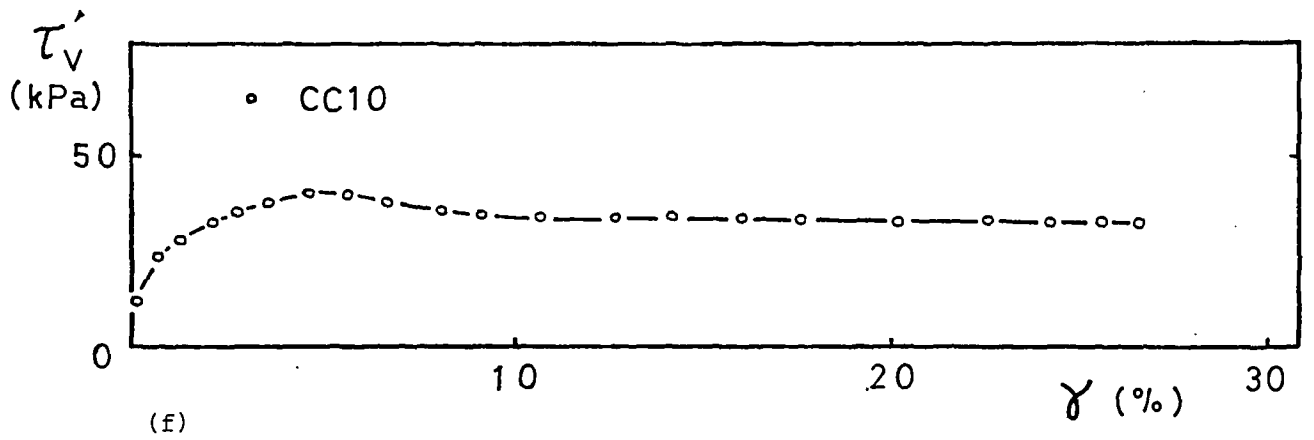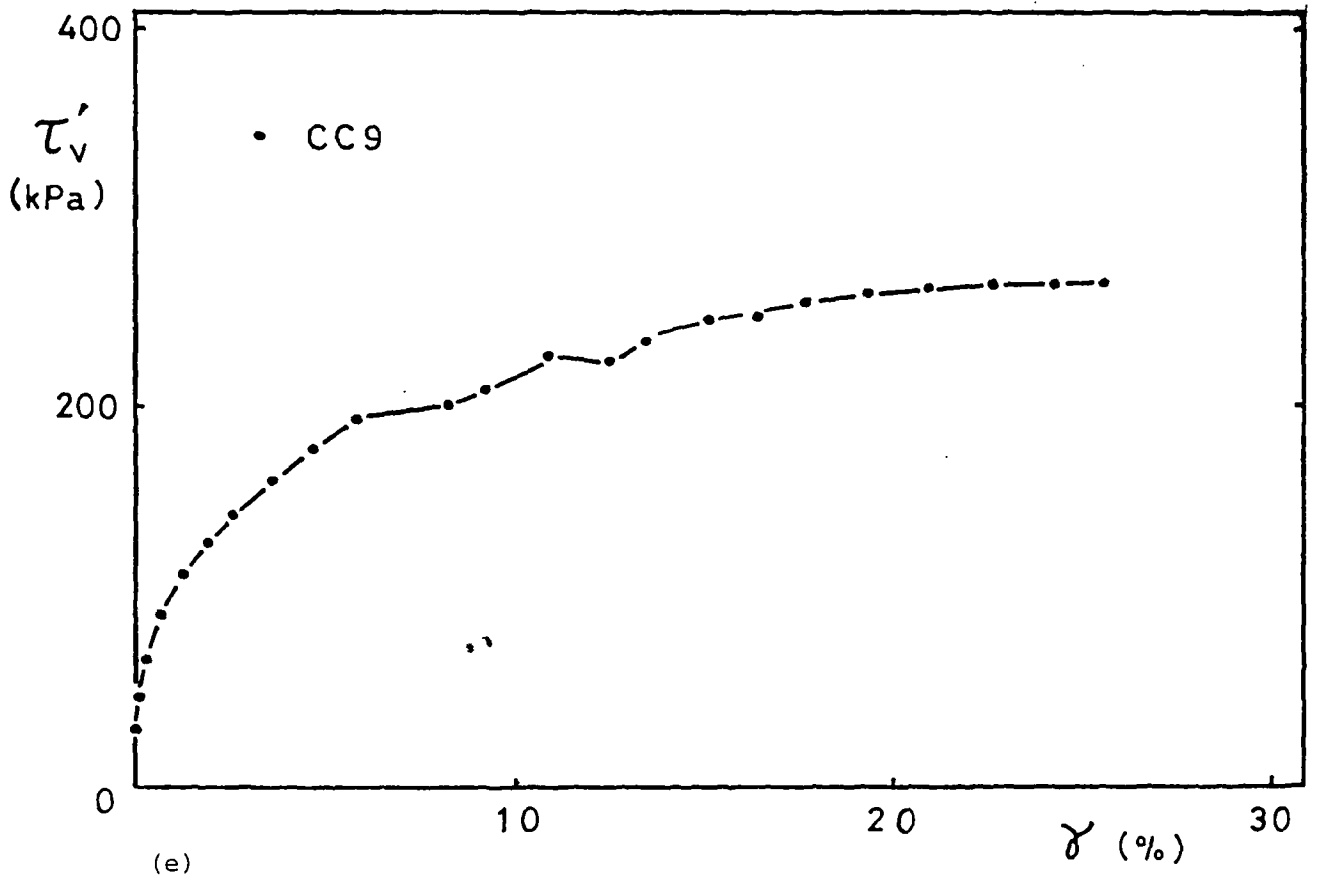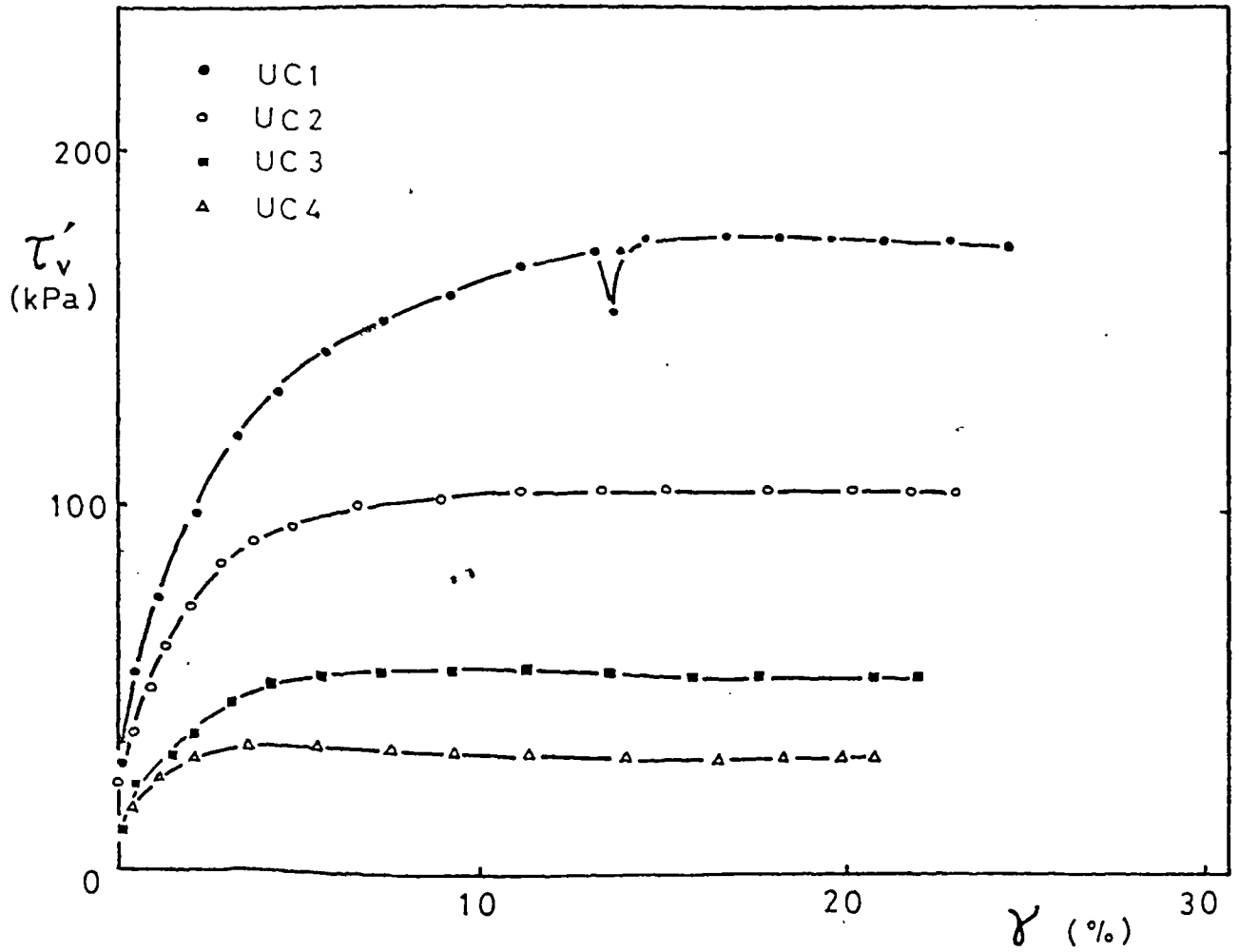
Figure 6.10 continued
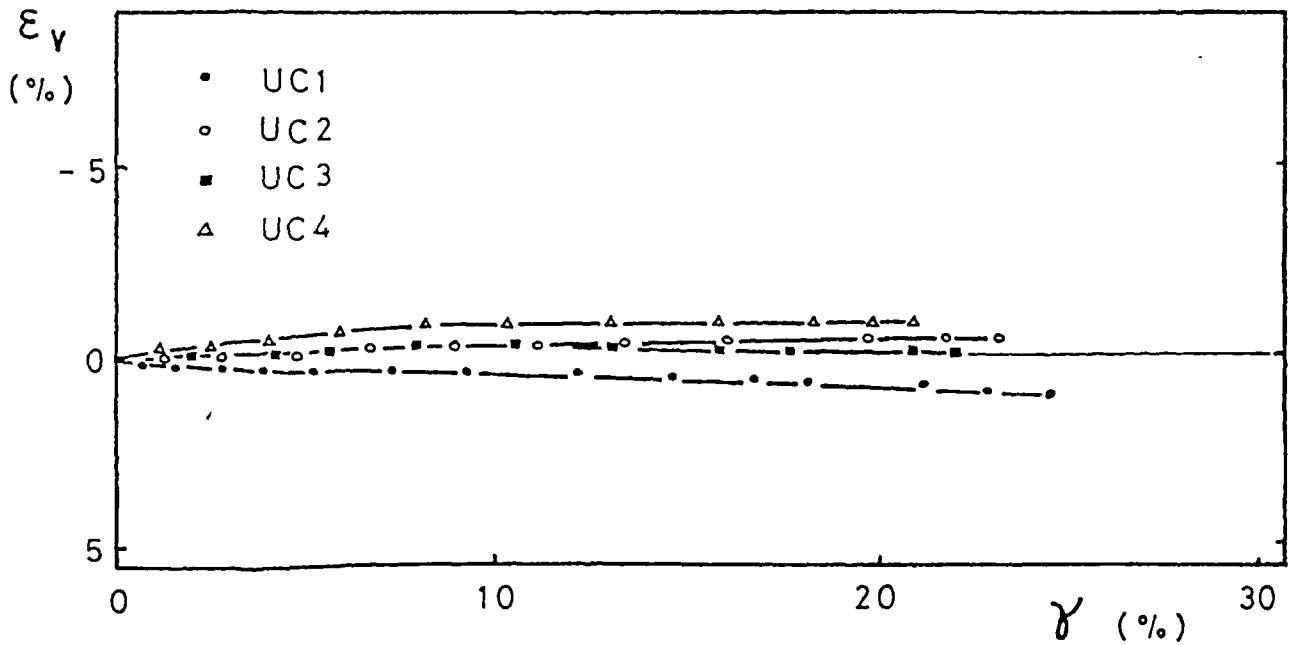
Figure 6.11 Results of shearing from undisturbed Cowden till simple shear samples

(c)
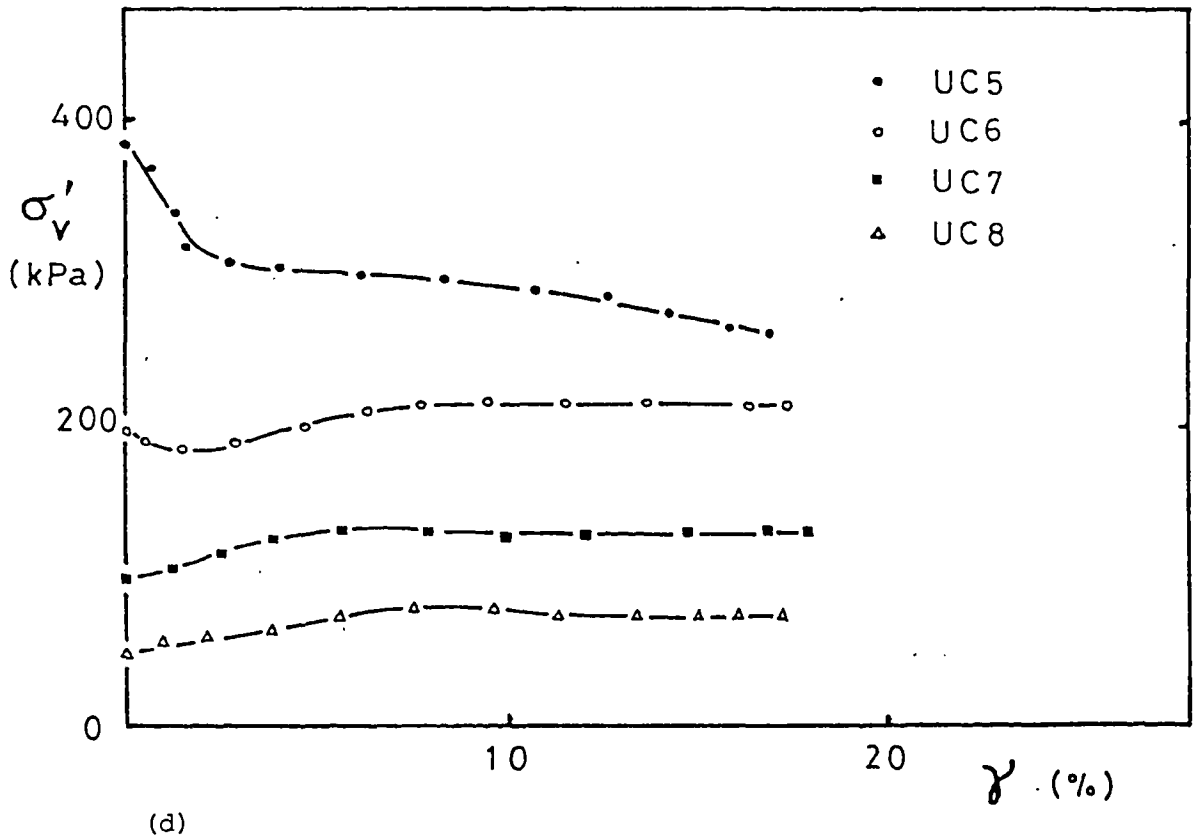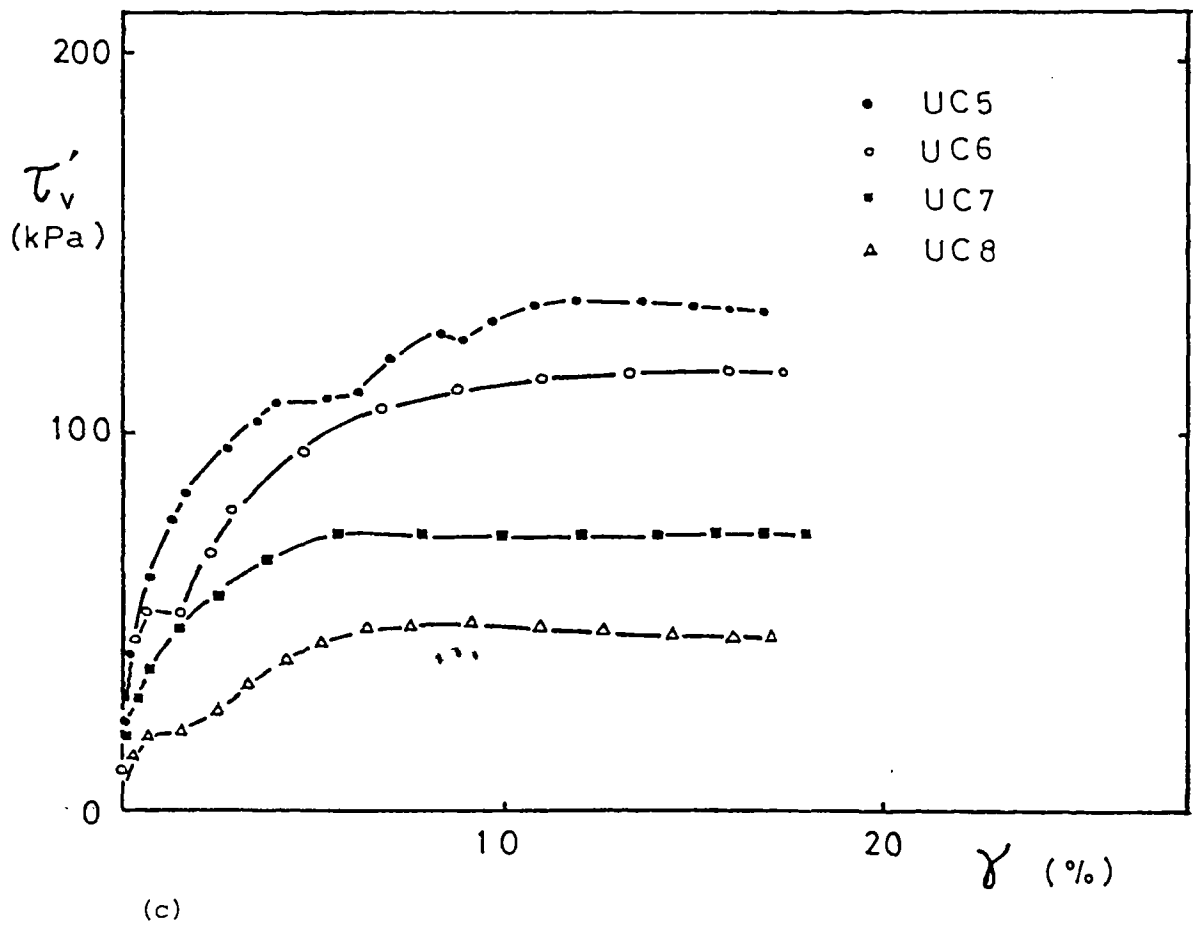
(d)

Figure 6.11 continued

(e)

(f)

Figure 6.11 continued

(g)

(h)
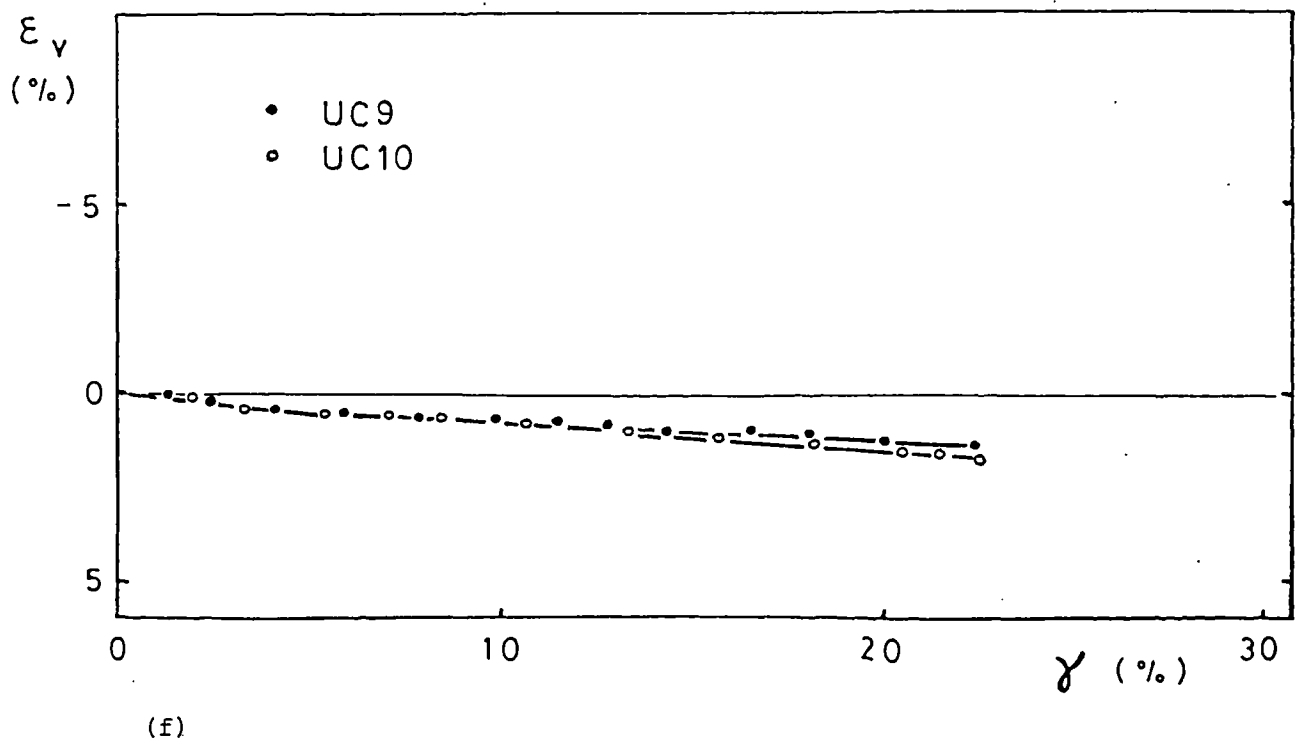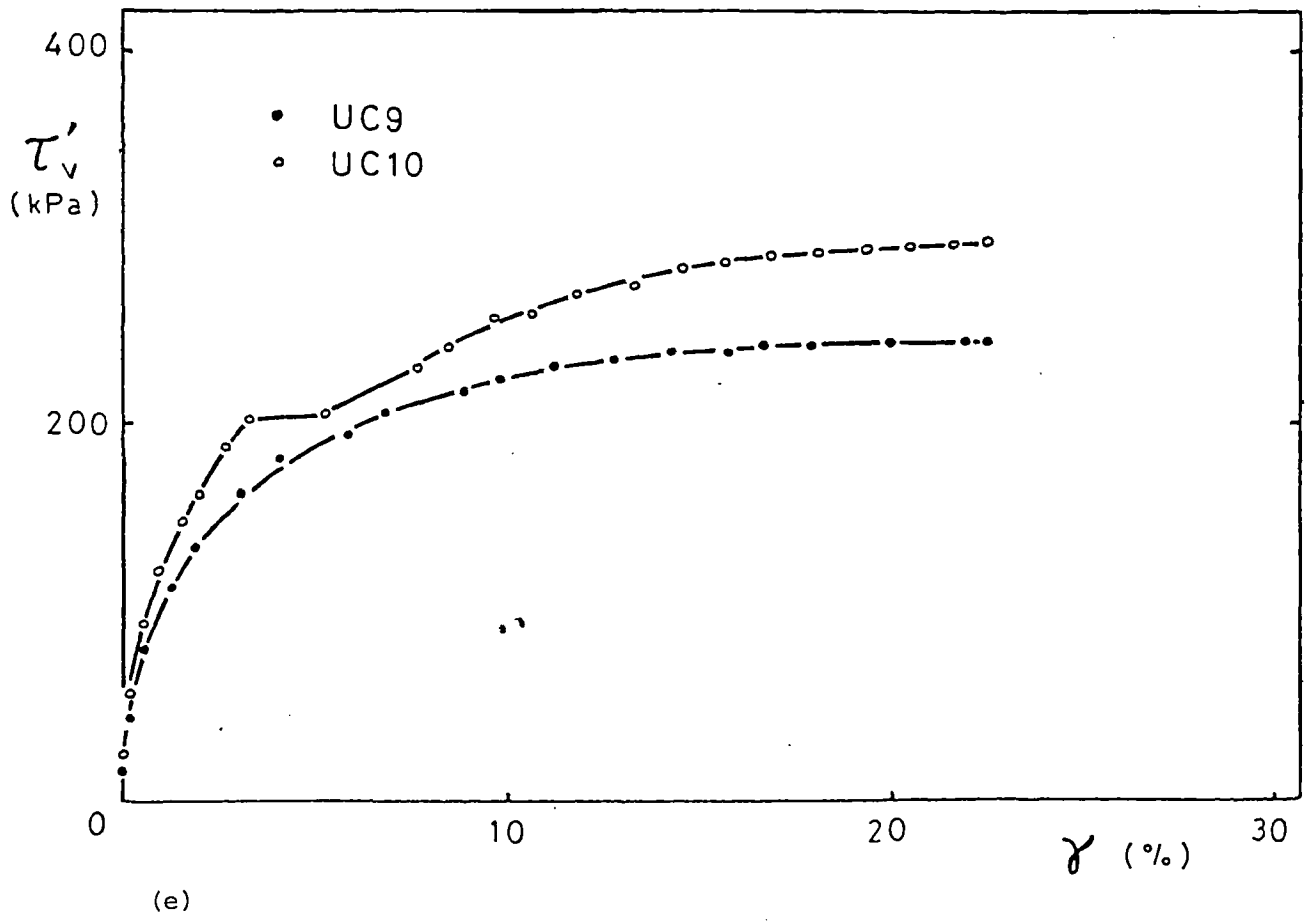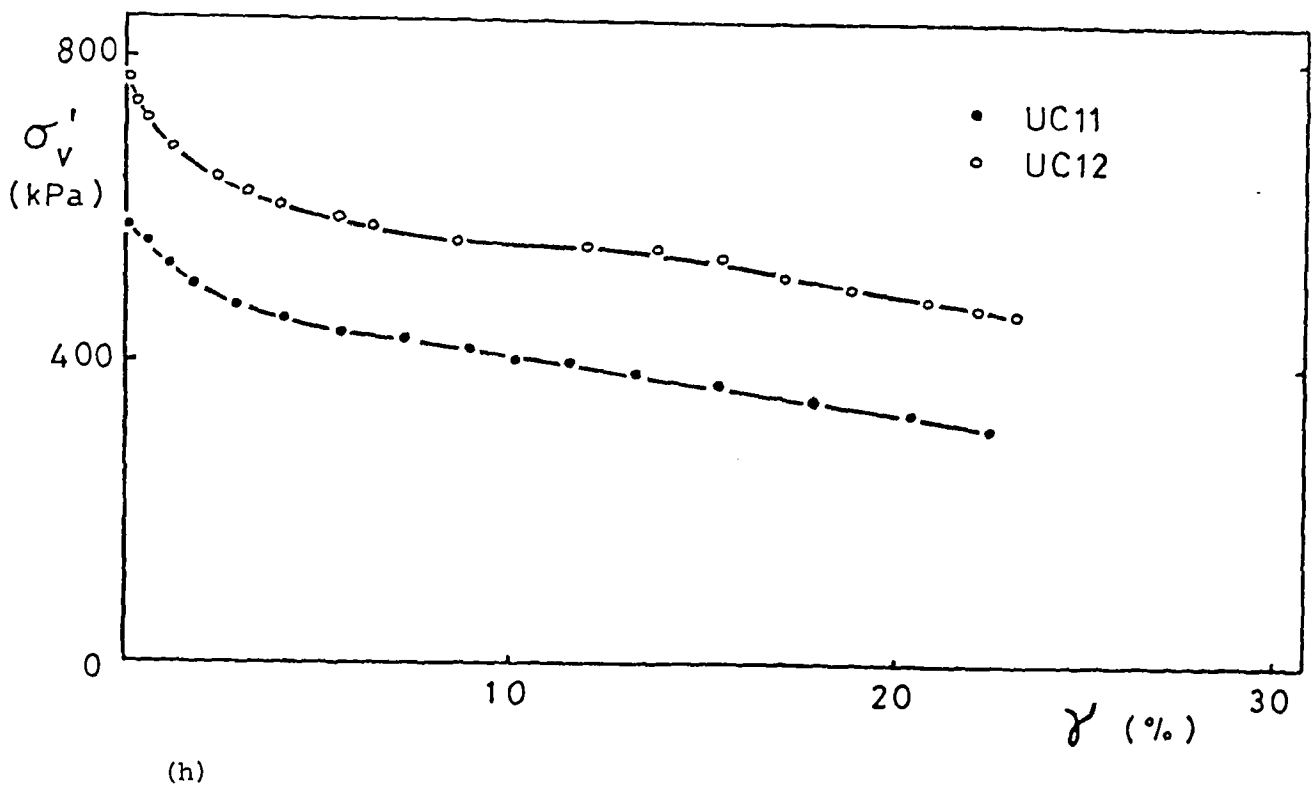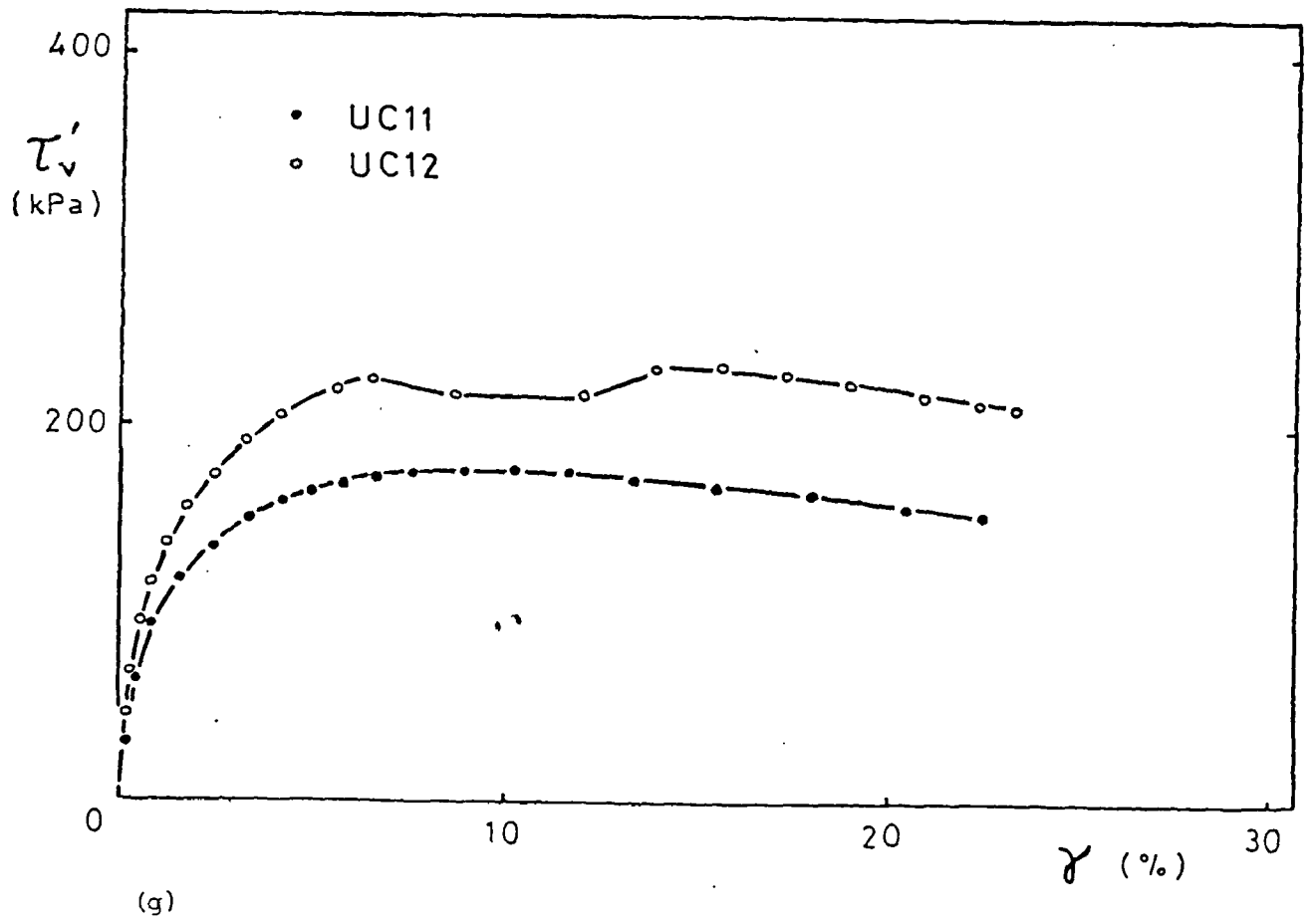
Figure 6.11 continued
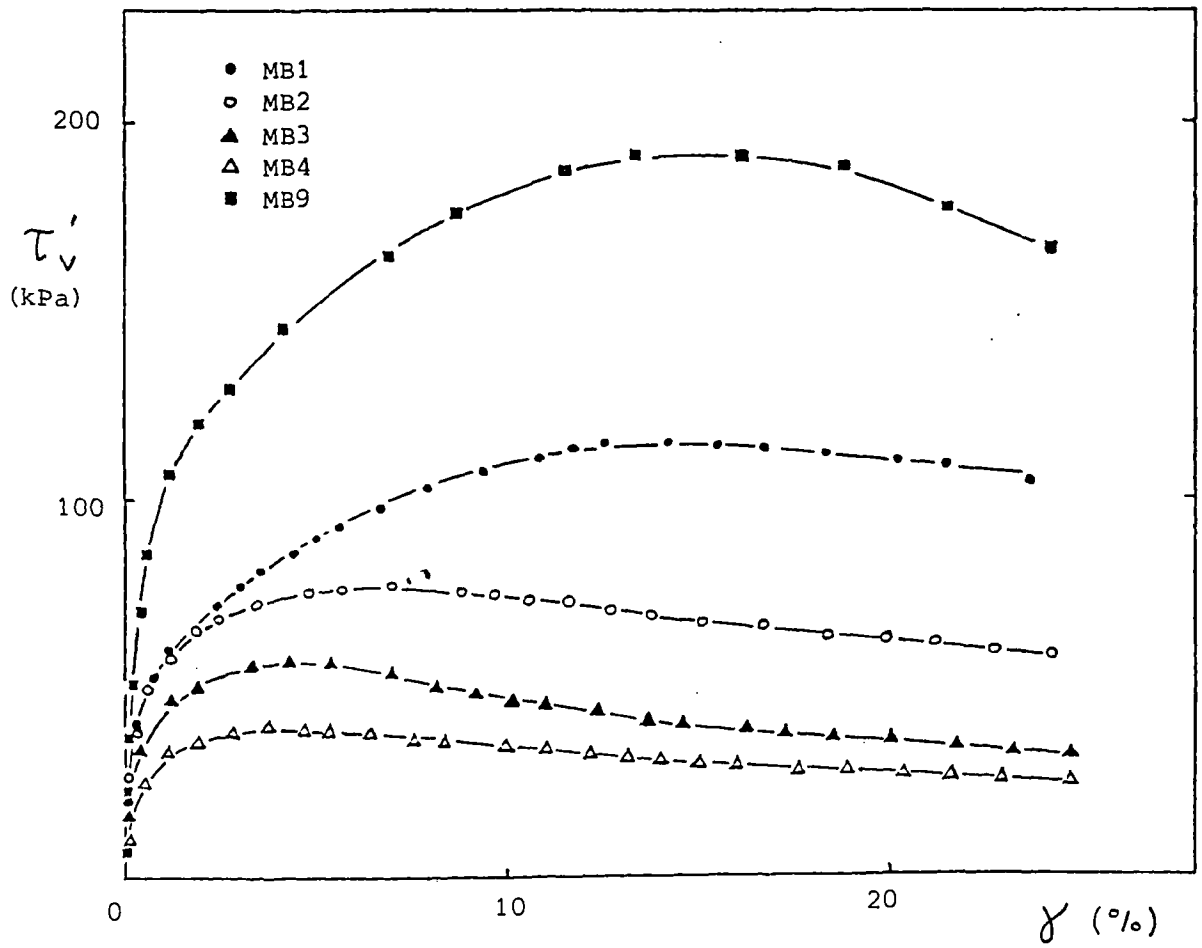
(a)
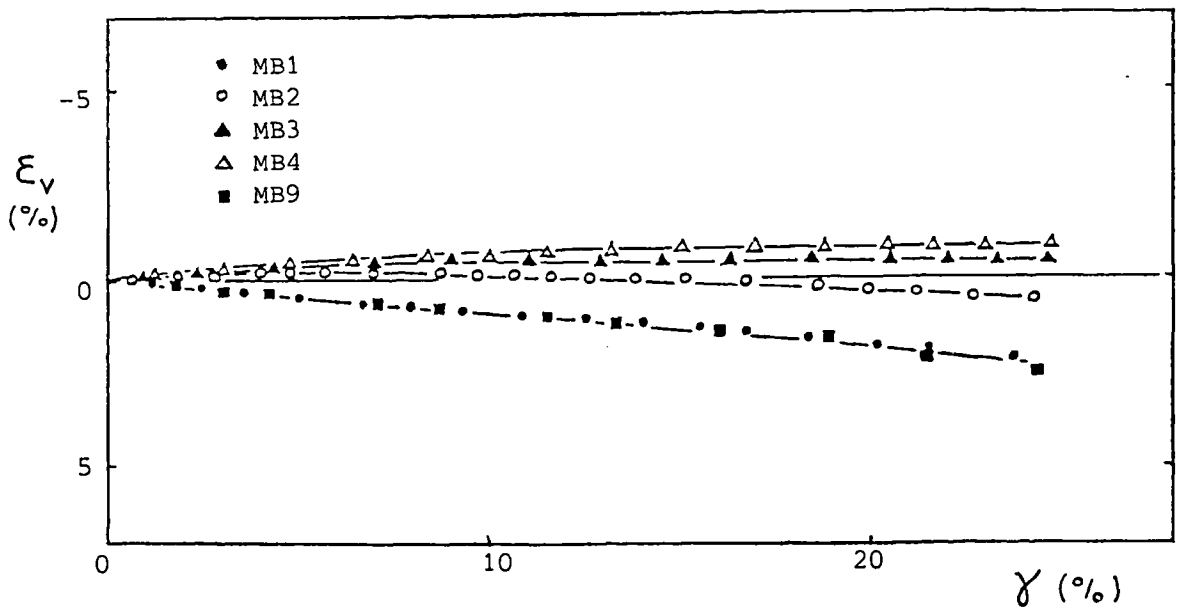
(b)

Figure 6.12   Results of shearing from remoulded London clay (brown)
simple shear samples
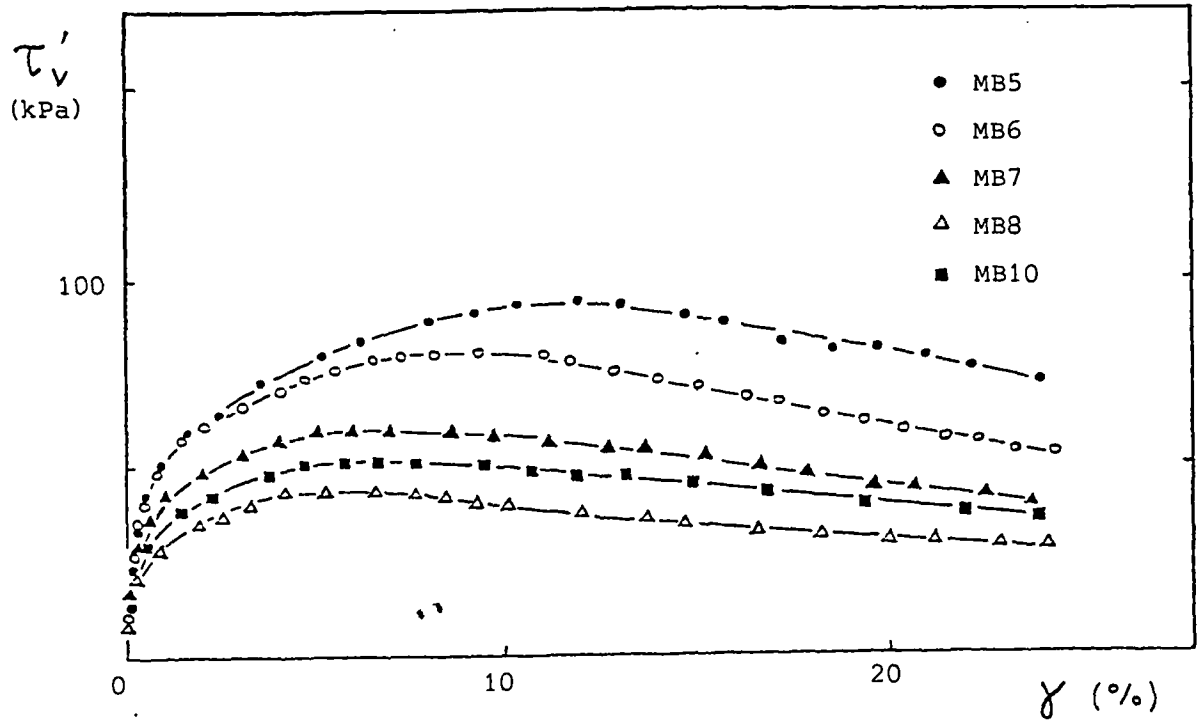
(c)
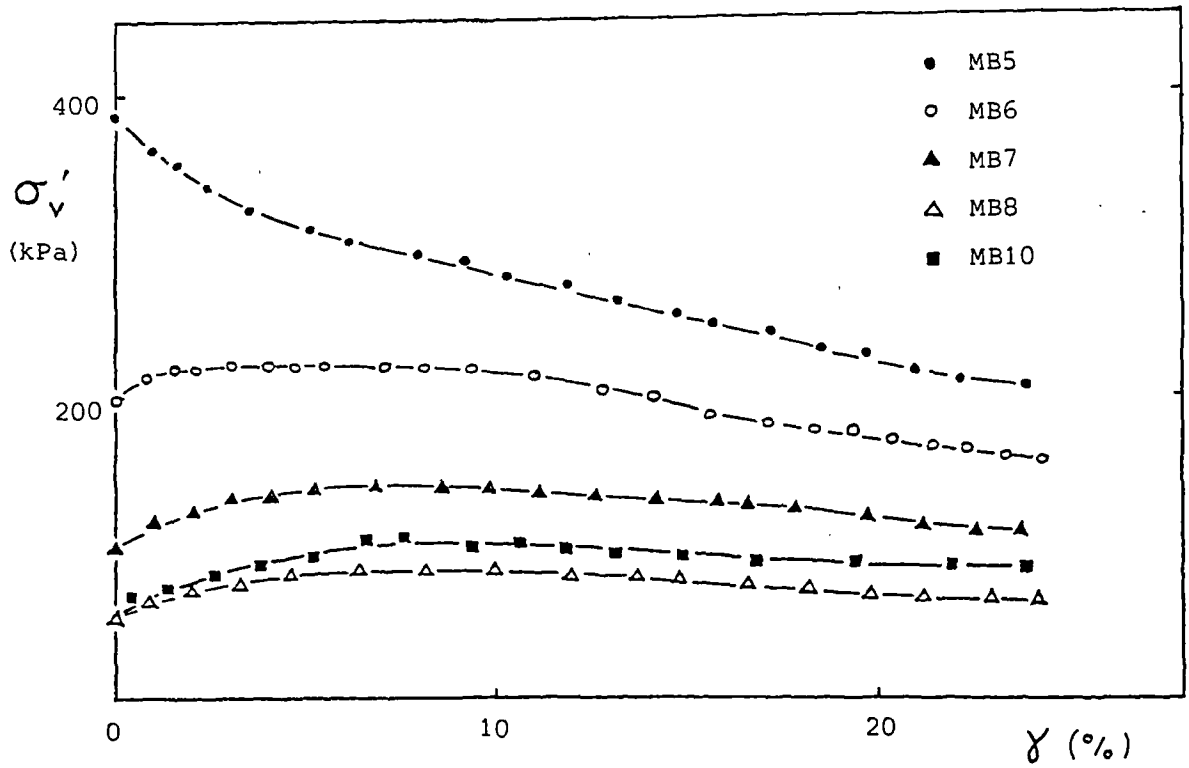
(d)

Figure 6.12 continued
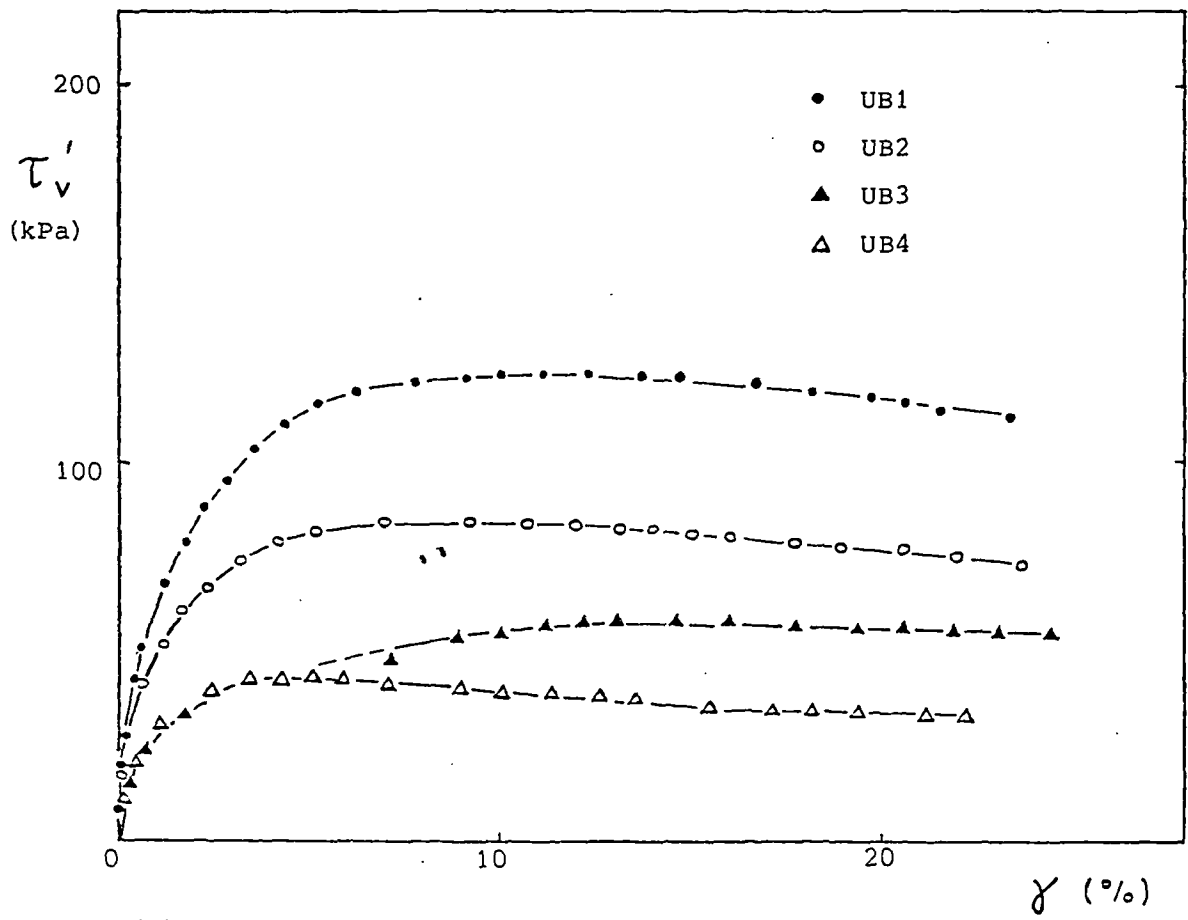
(a)
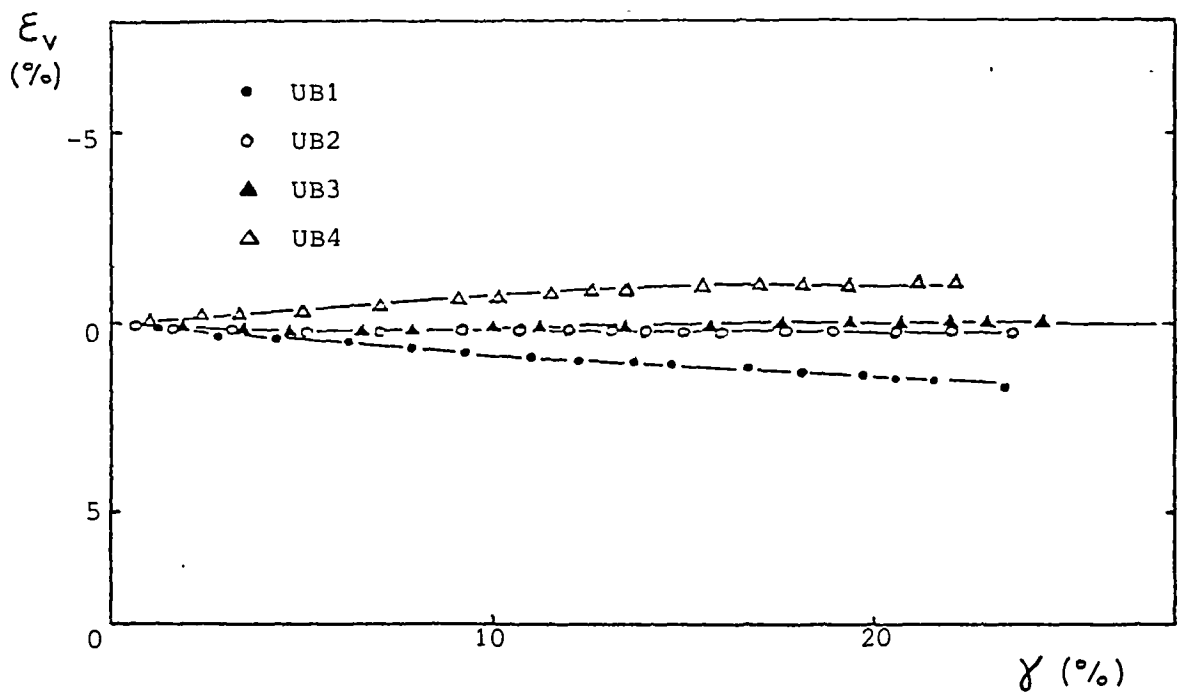
(b)

Figure 6.13   Results of shearing from undisturbed London clay
                (brown) simple shear samples
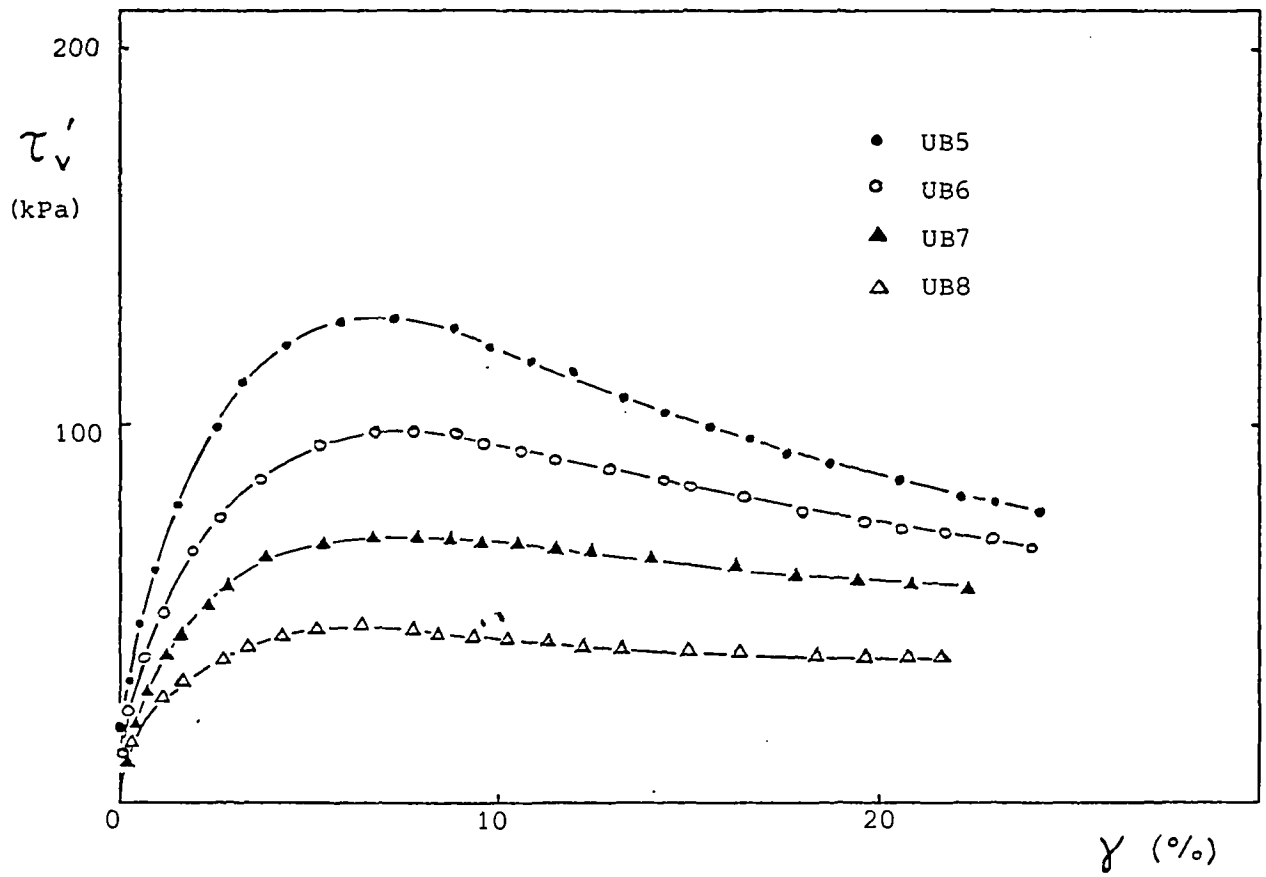
(c)

(d)
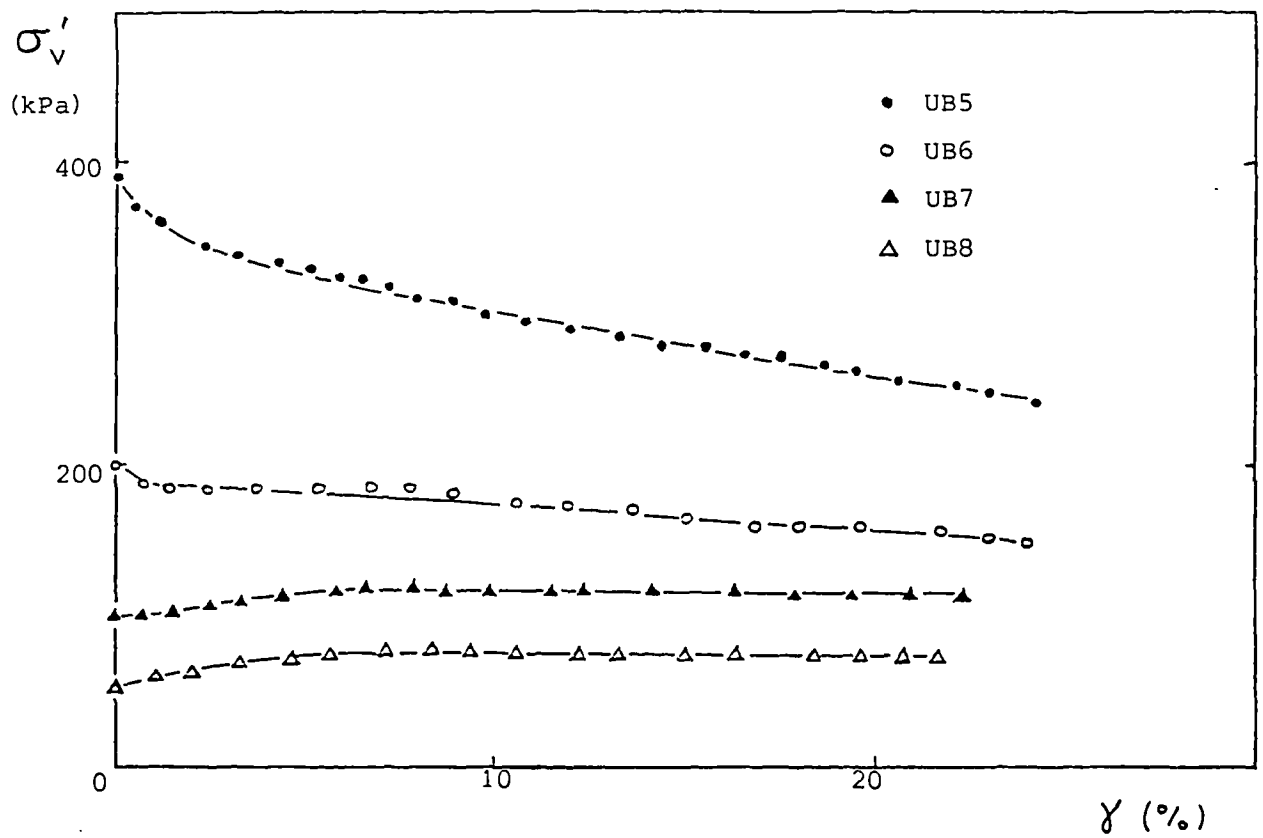
Figure 6.13 continued
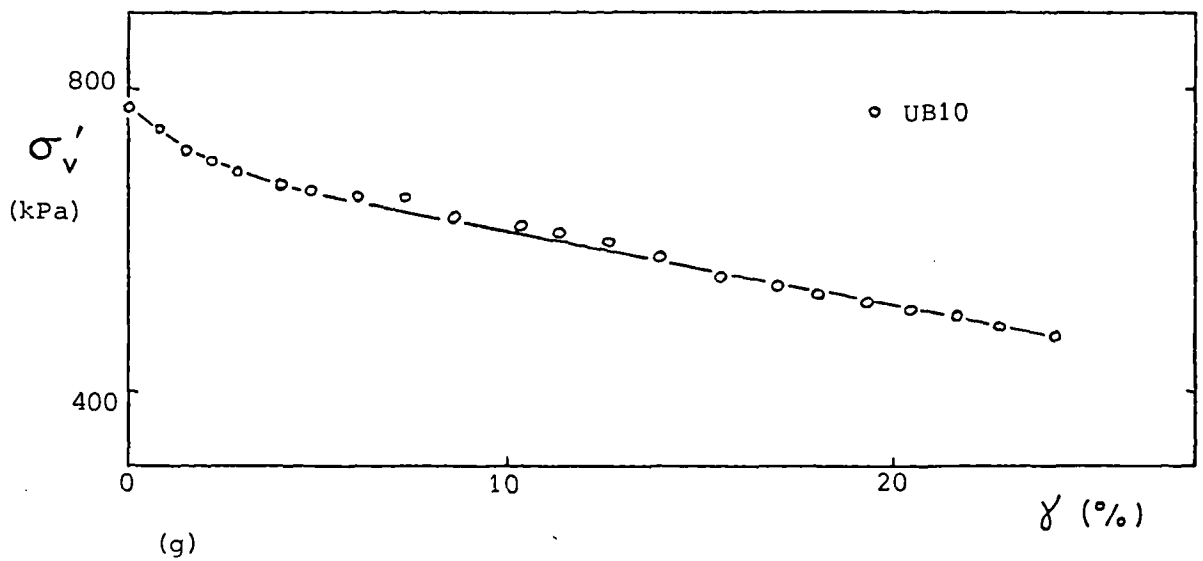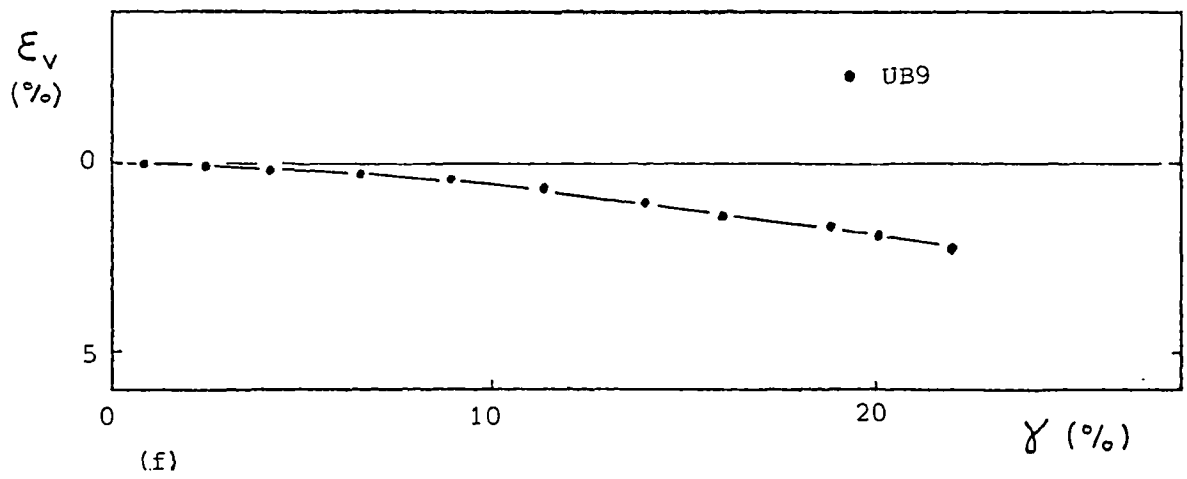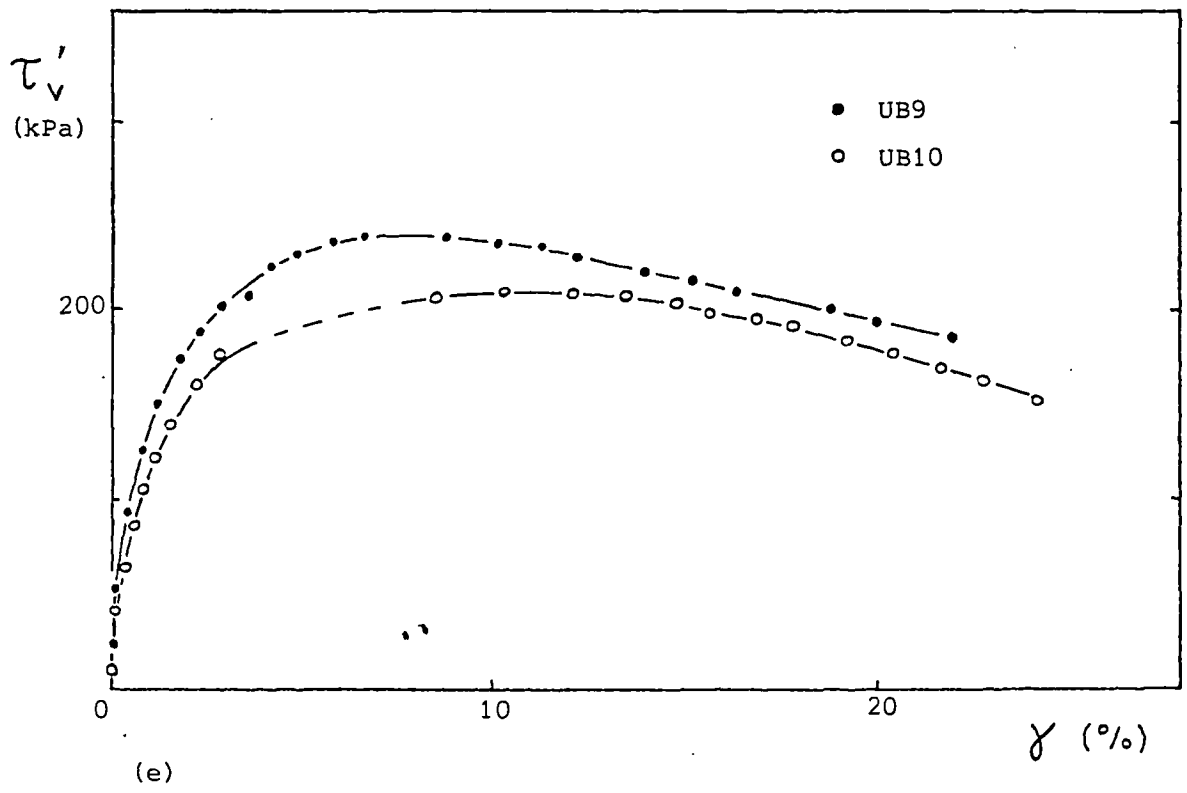
Figure 6.13 continued
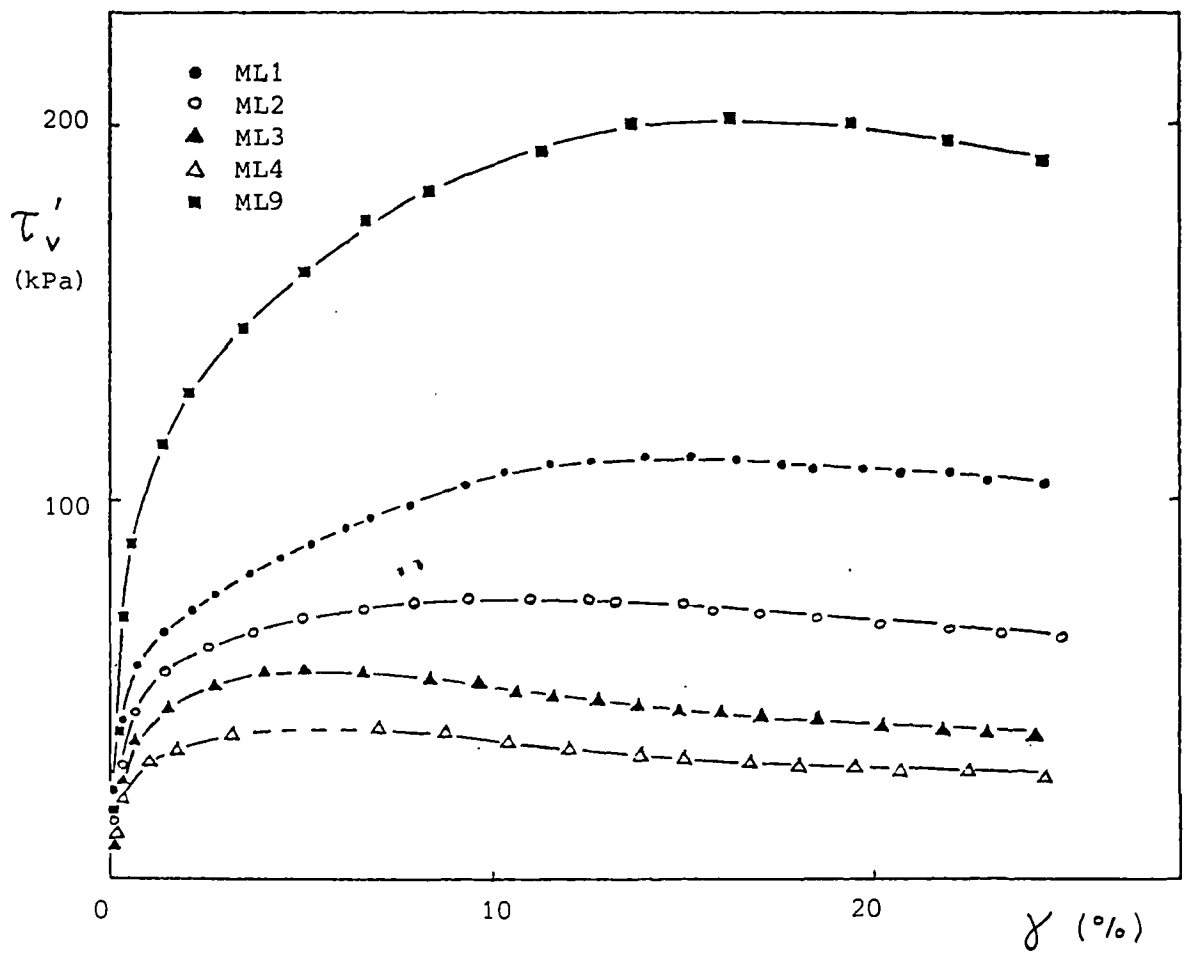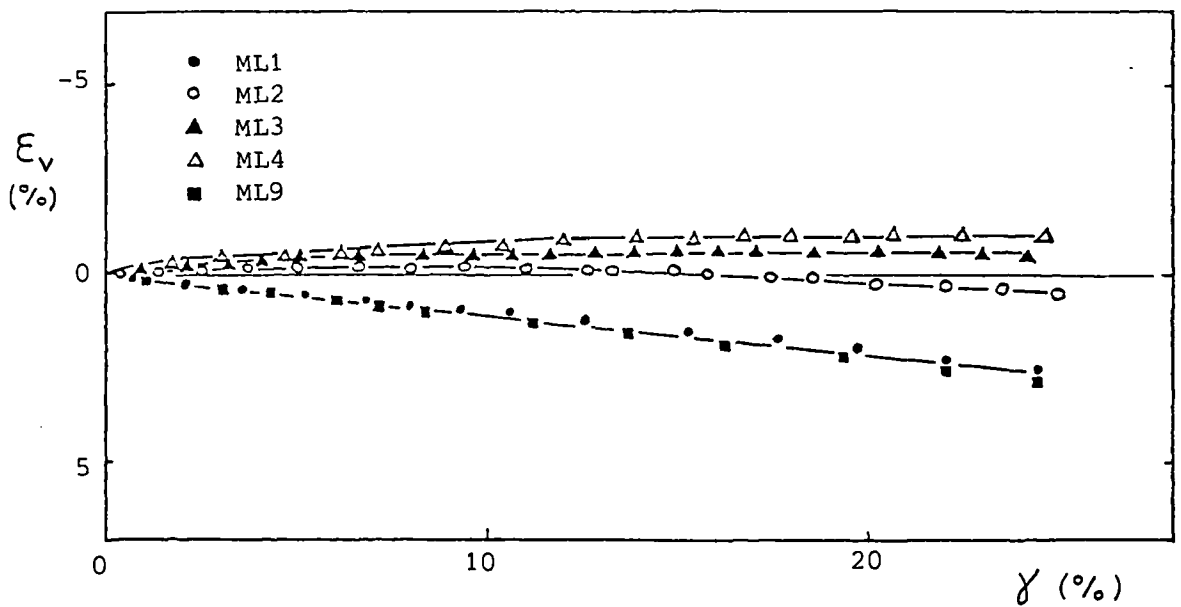
Figure 6.14 Results of shearing from remoulded London clay (blue)
simple shear samples
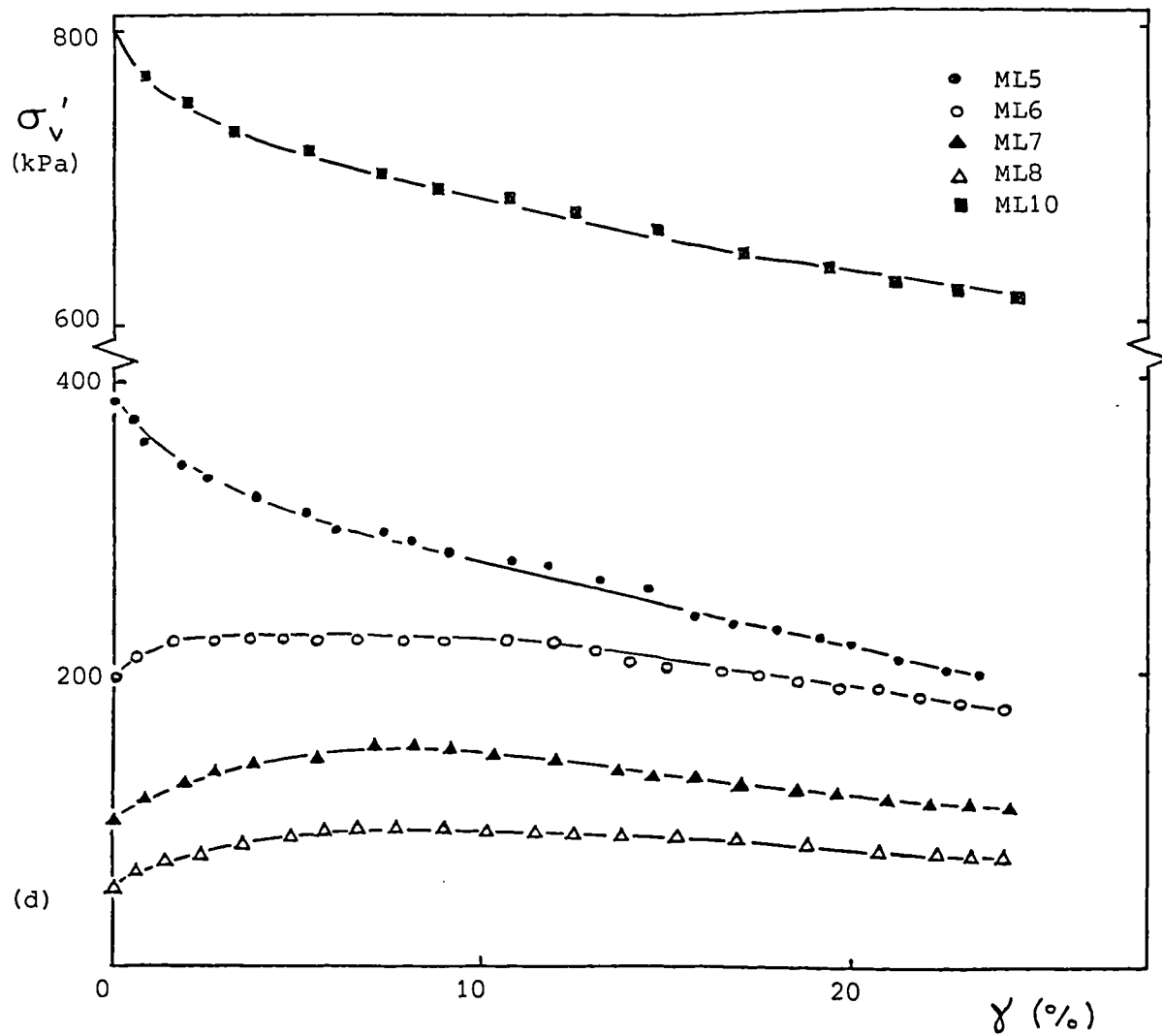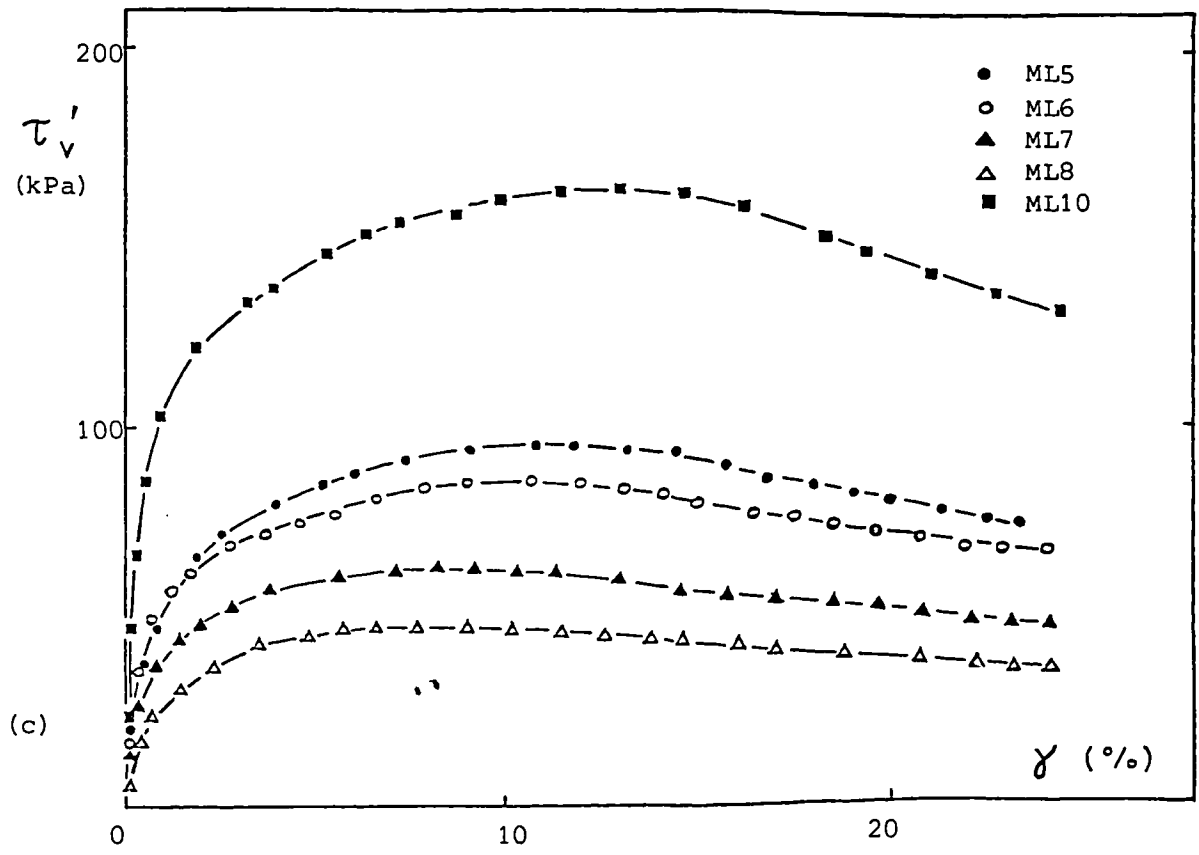
Figure 6.14 continued

(a)

(b)
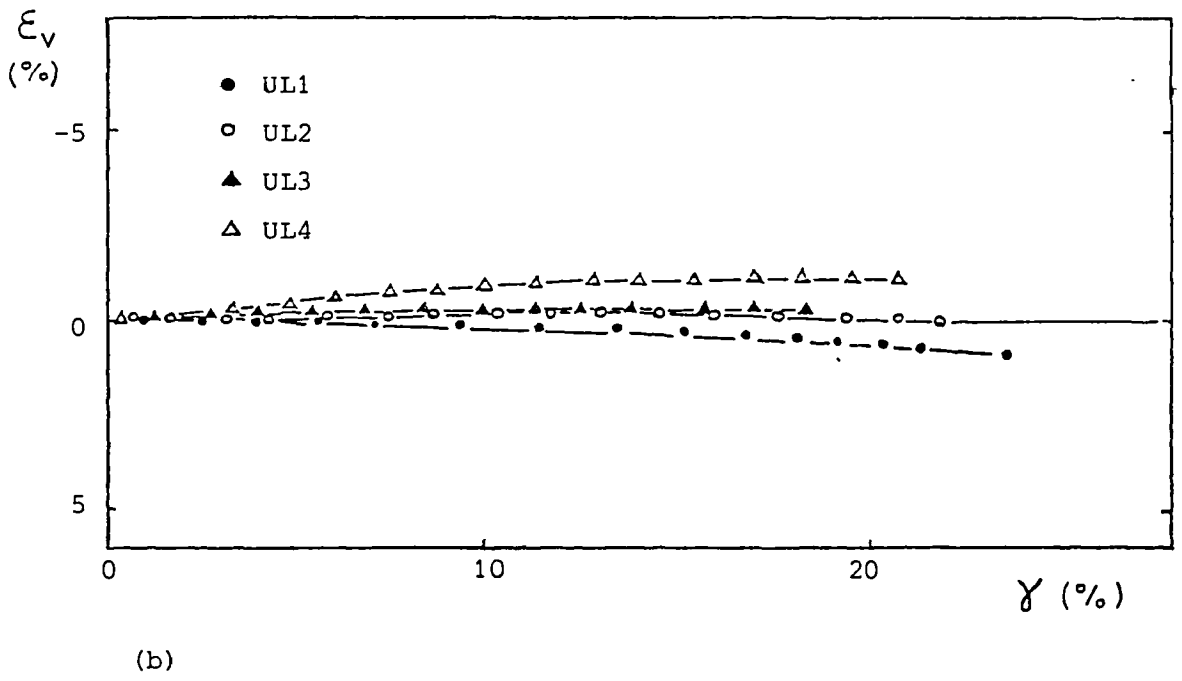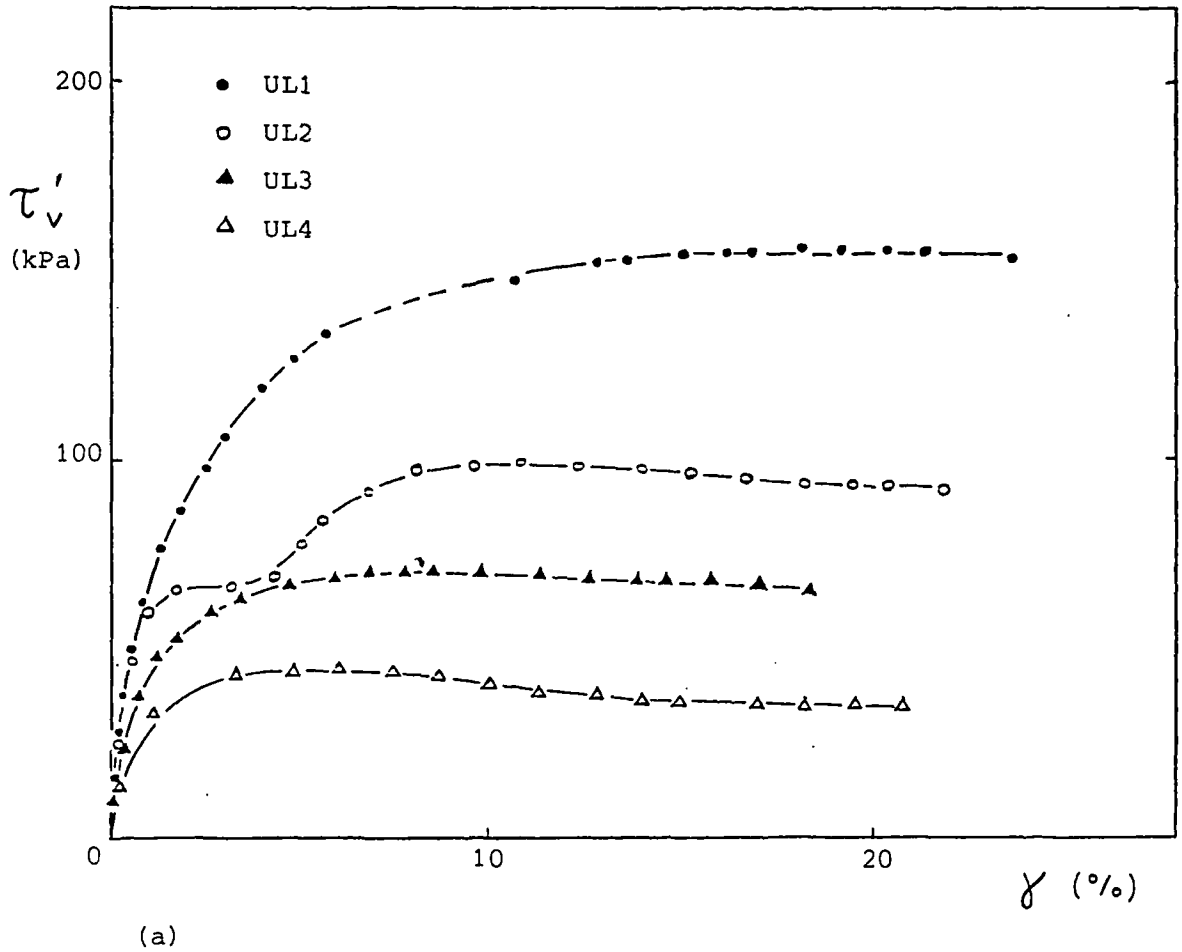
Figure 6.15   Results of shearing from undisturbed London clay (blue) simple shear samples

(c)

(d)
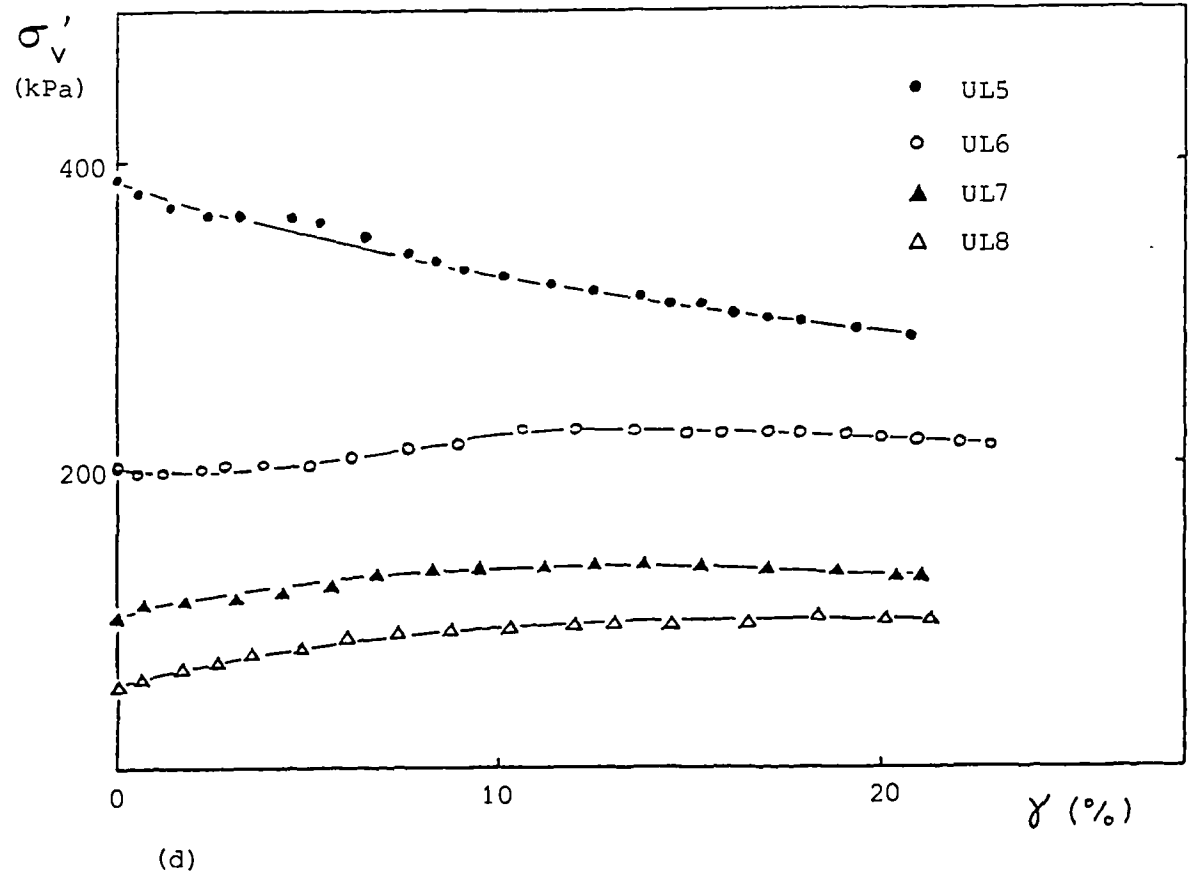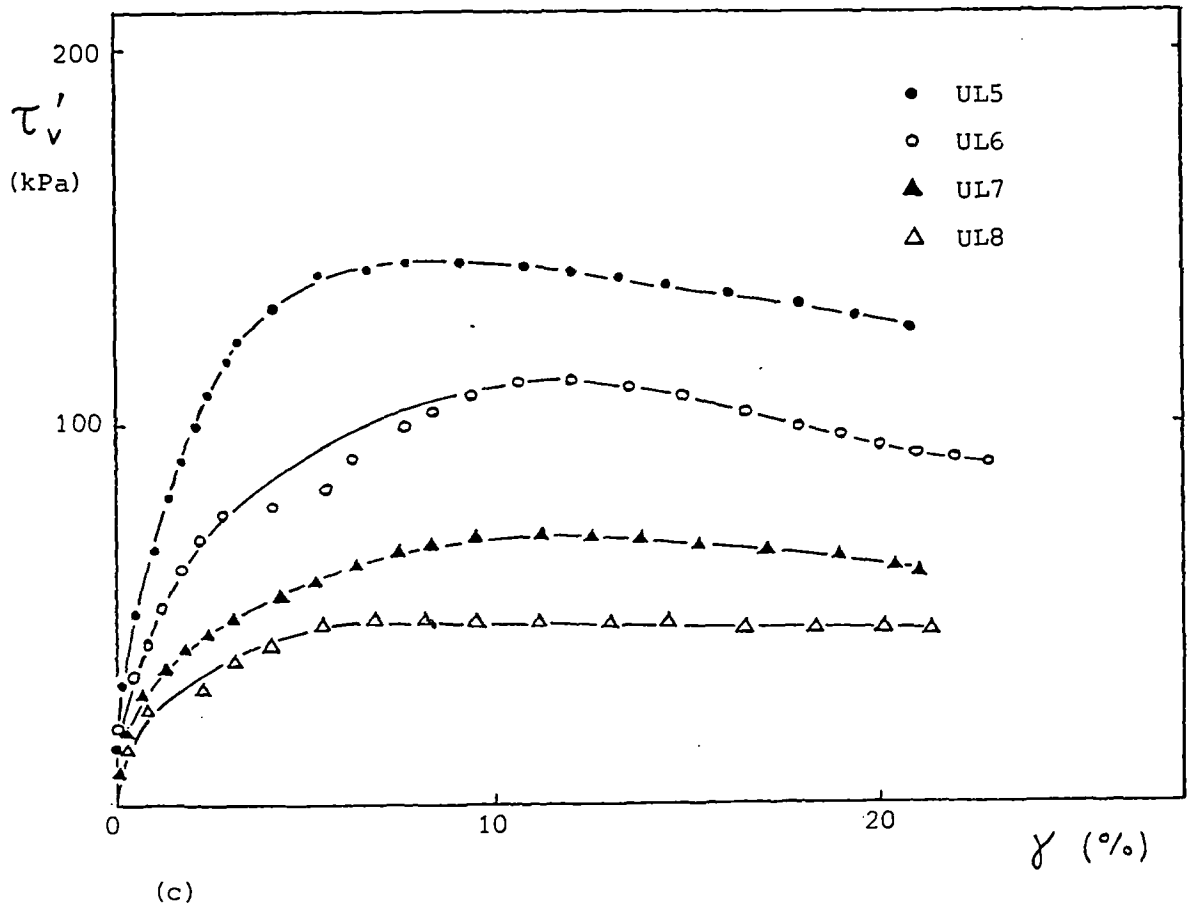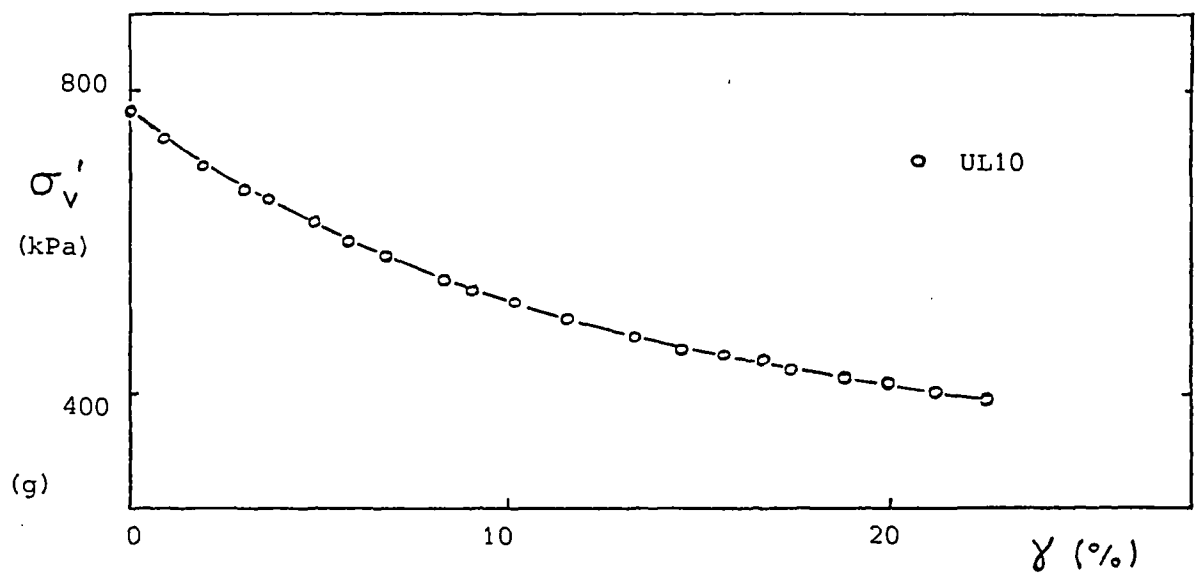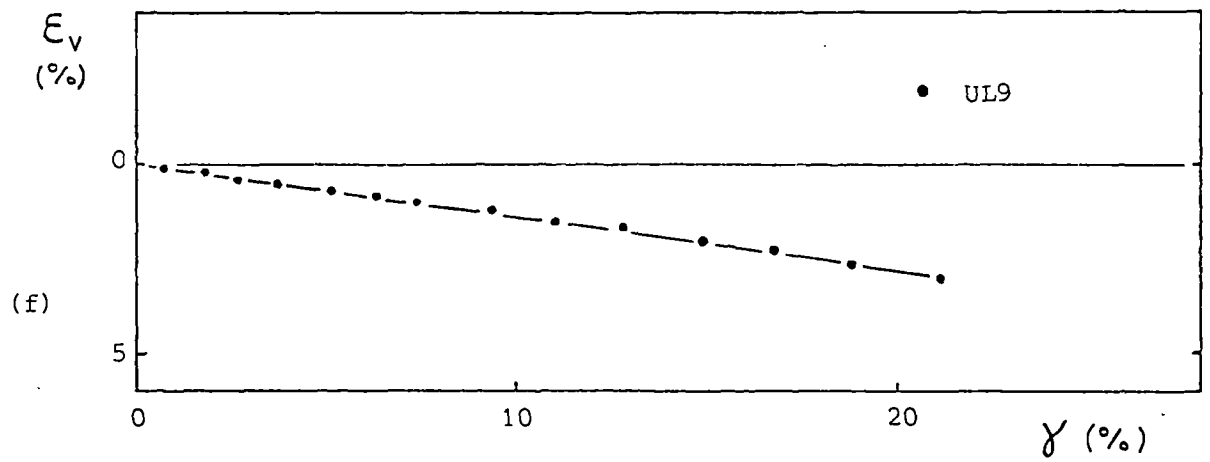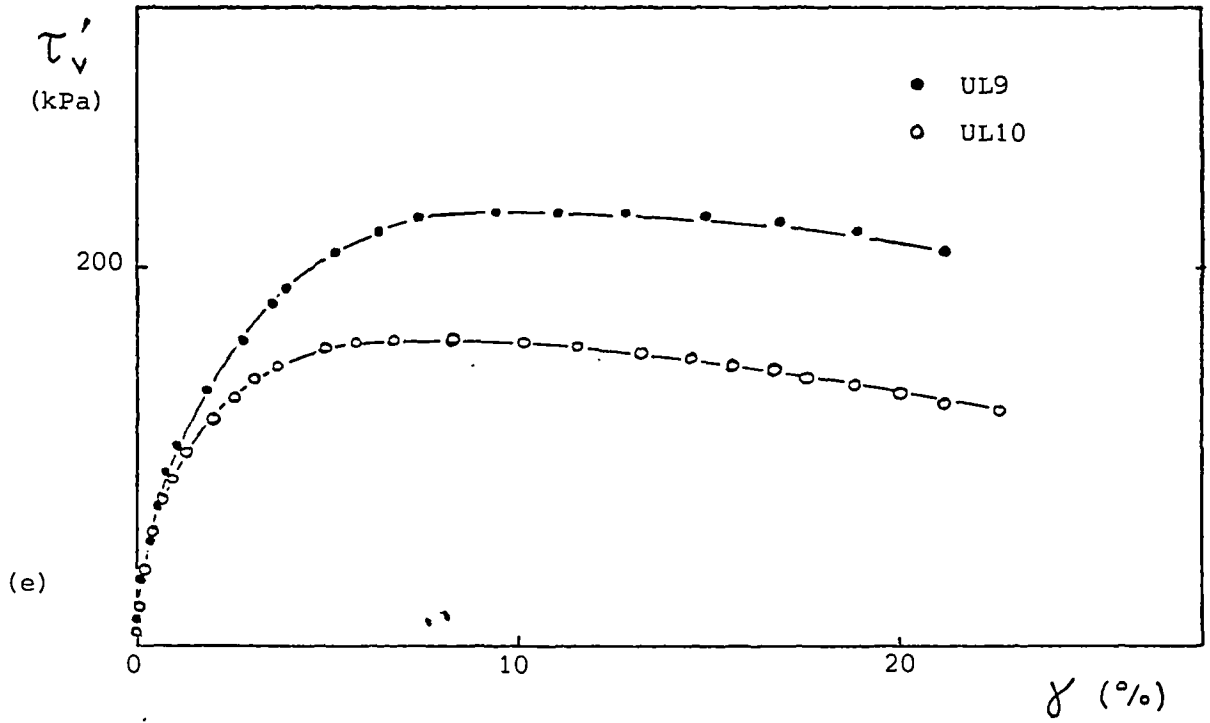
Figure 6.15 continued

Figure 6.15 continued

(a)

(b)
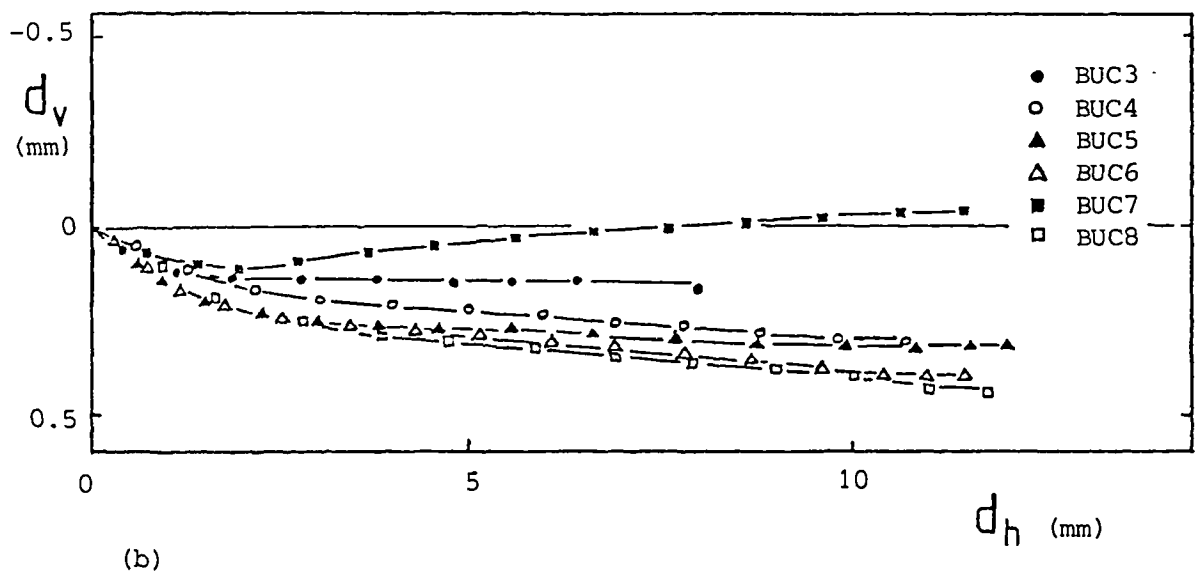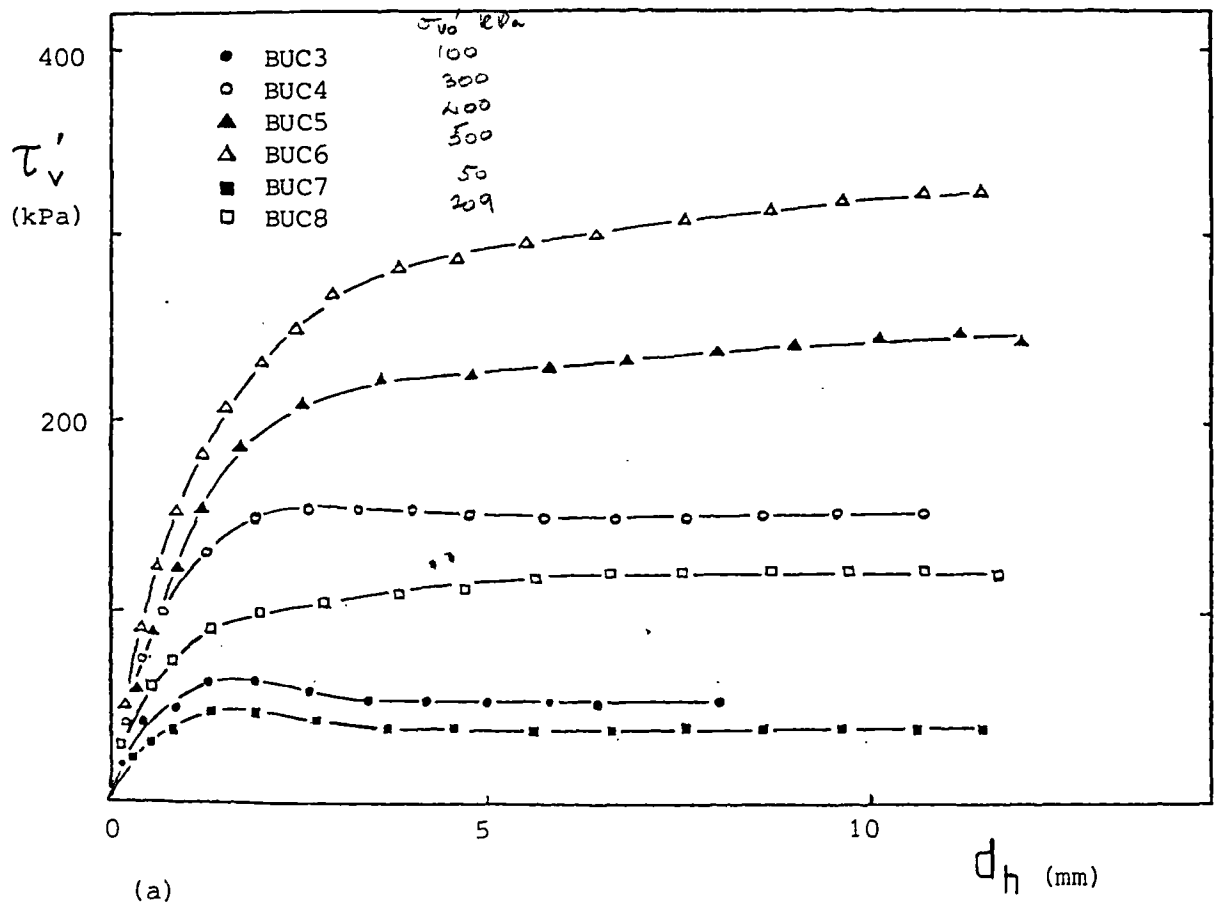
Figure 6.16   Results of shearing from undisturbed Cowden till shear box samples
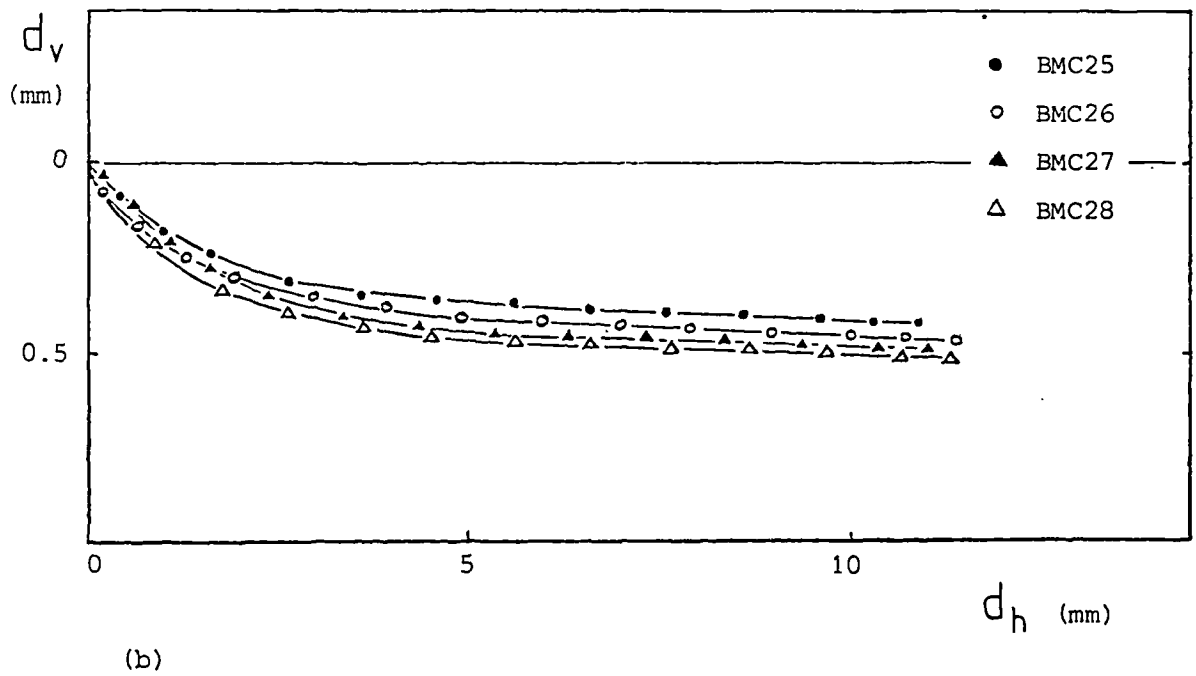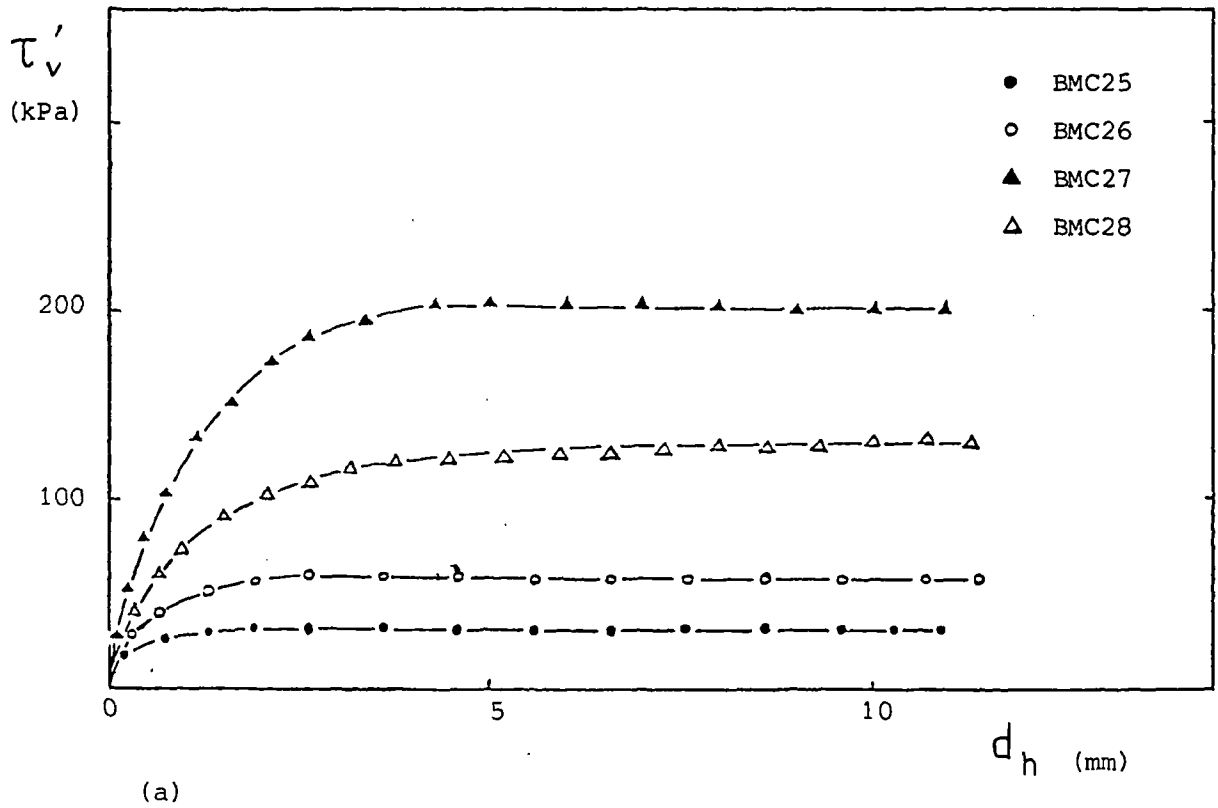
Figure 6.17   Results of shearing from remoulded Cowden till
                 shear box samples
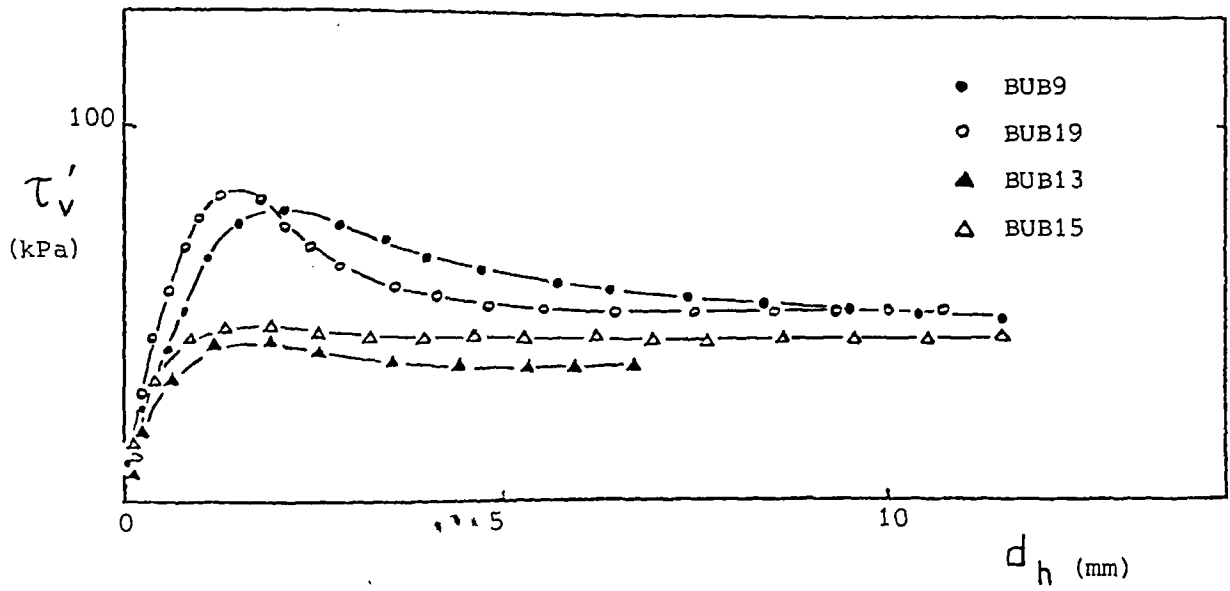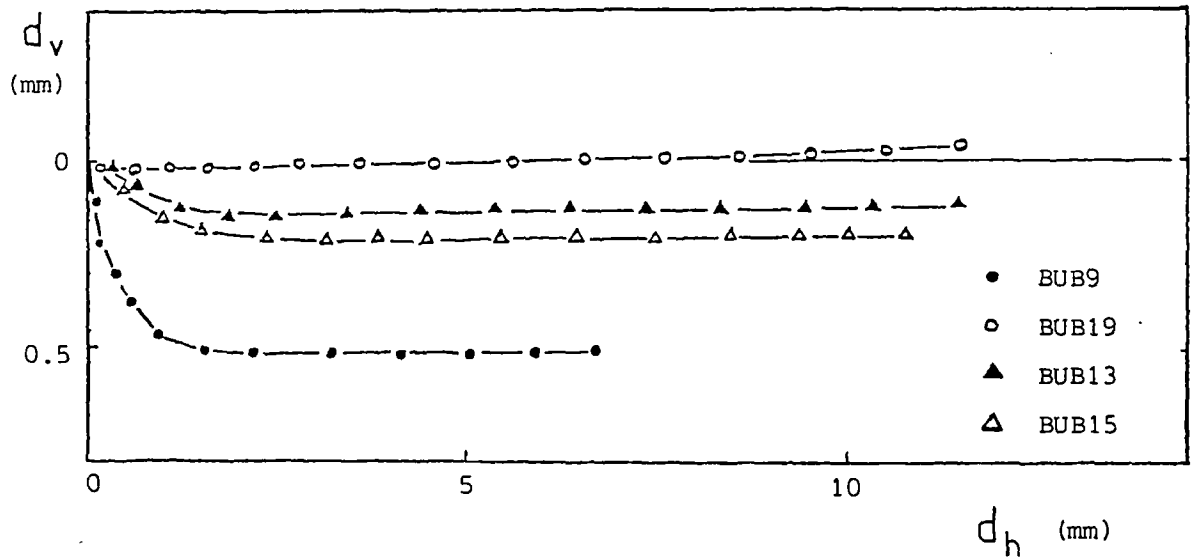
Figure 6.18   Results of shearing from undisturbed London clay
                 (brown) shear box samples
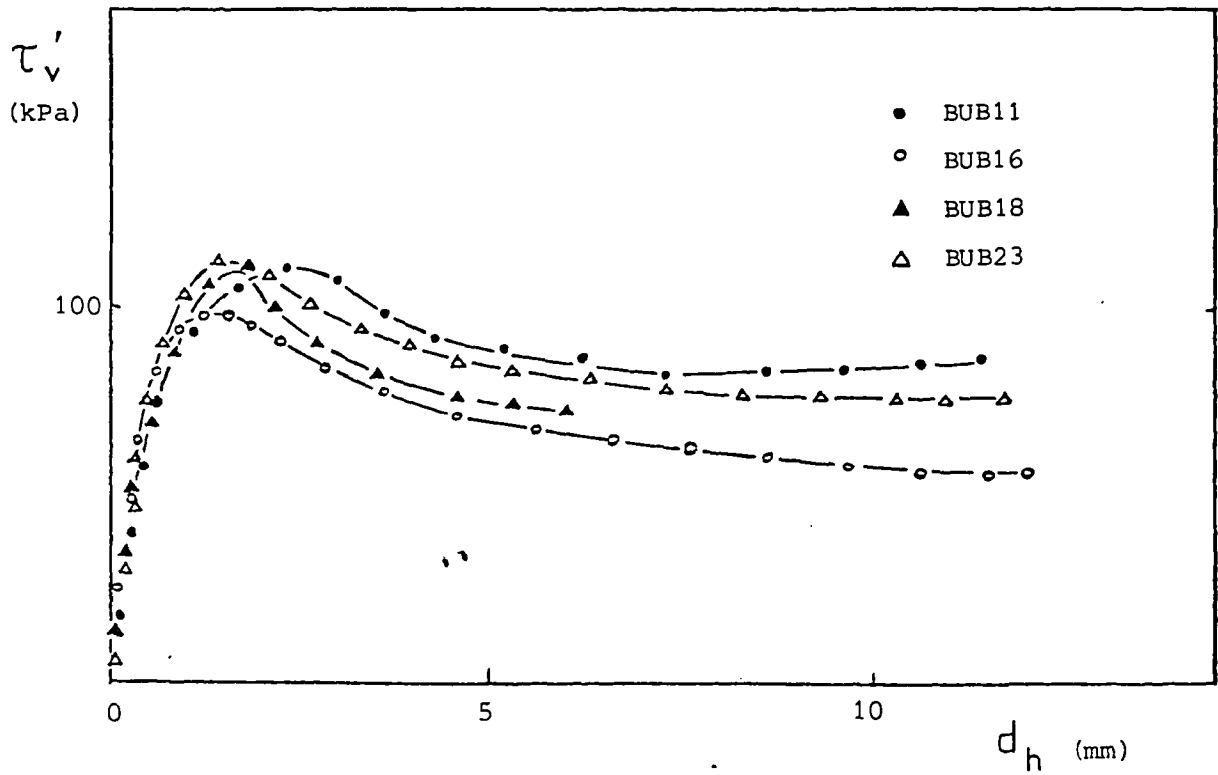
(c)
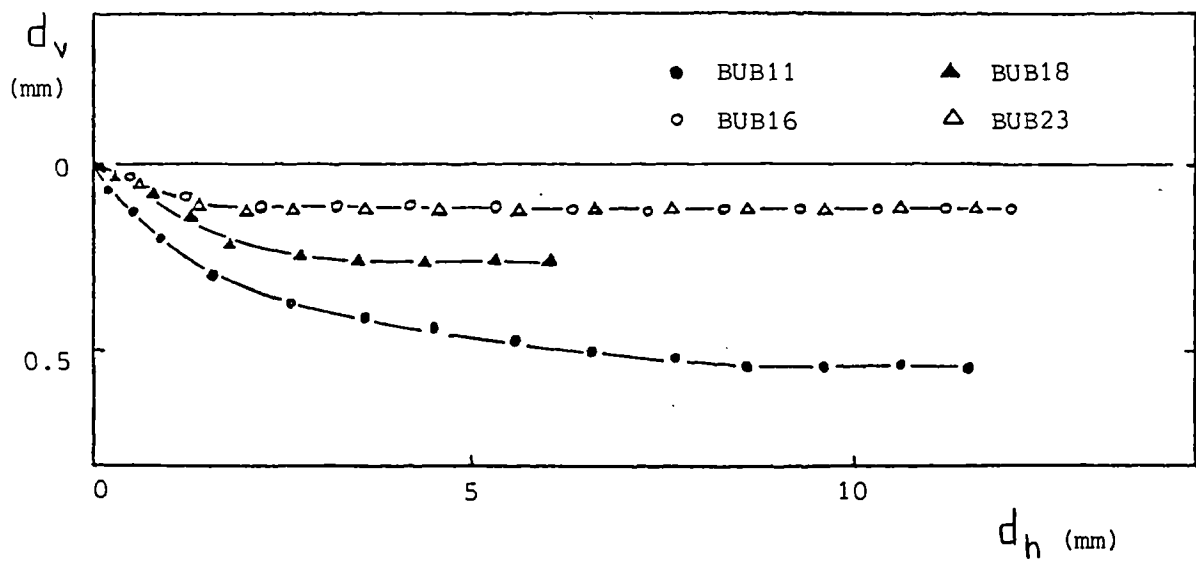
(d)

Figure 6.18 continued
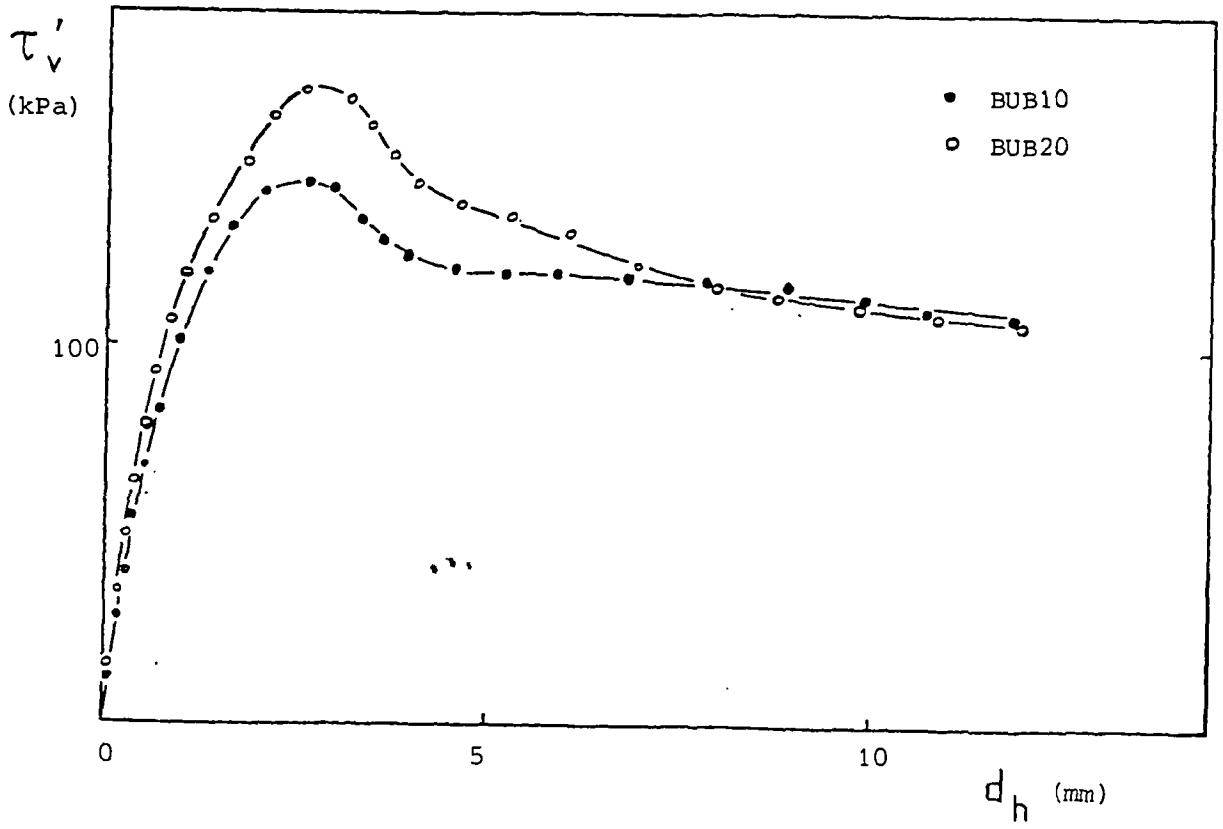
(e)
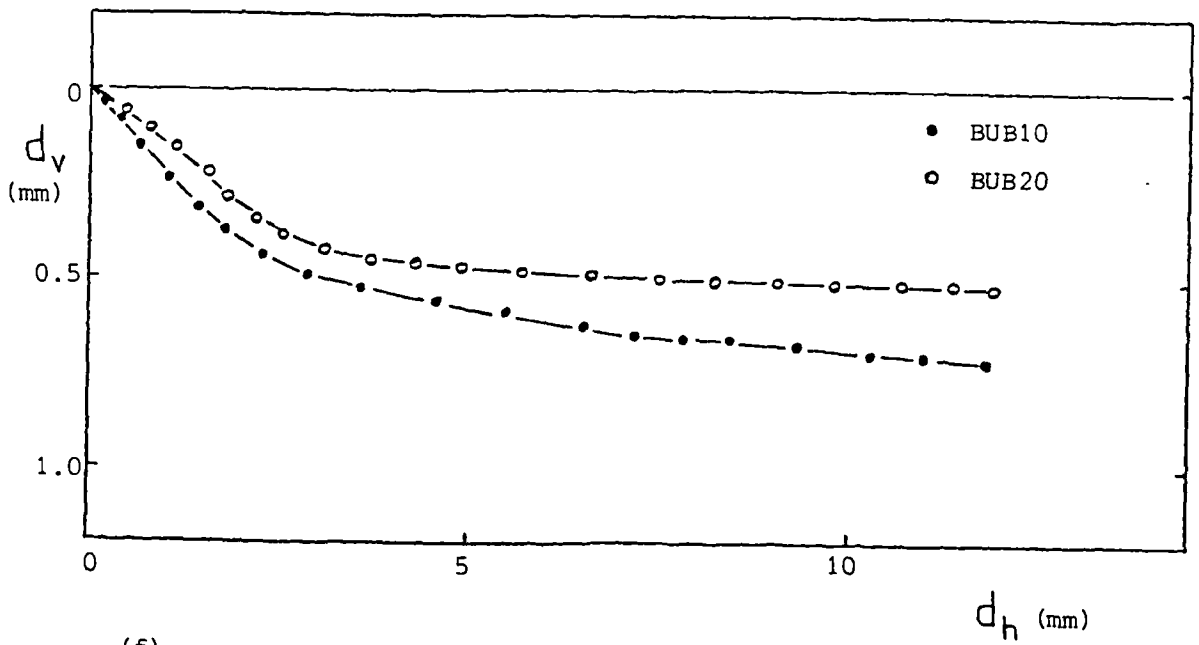
(f)

Figure 6.18 continued

(g)

(h)

Figure 6.18 continued

(a)

(b)
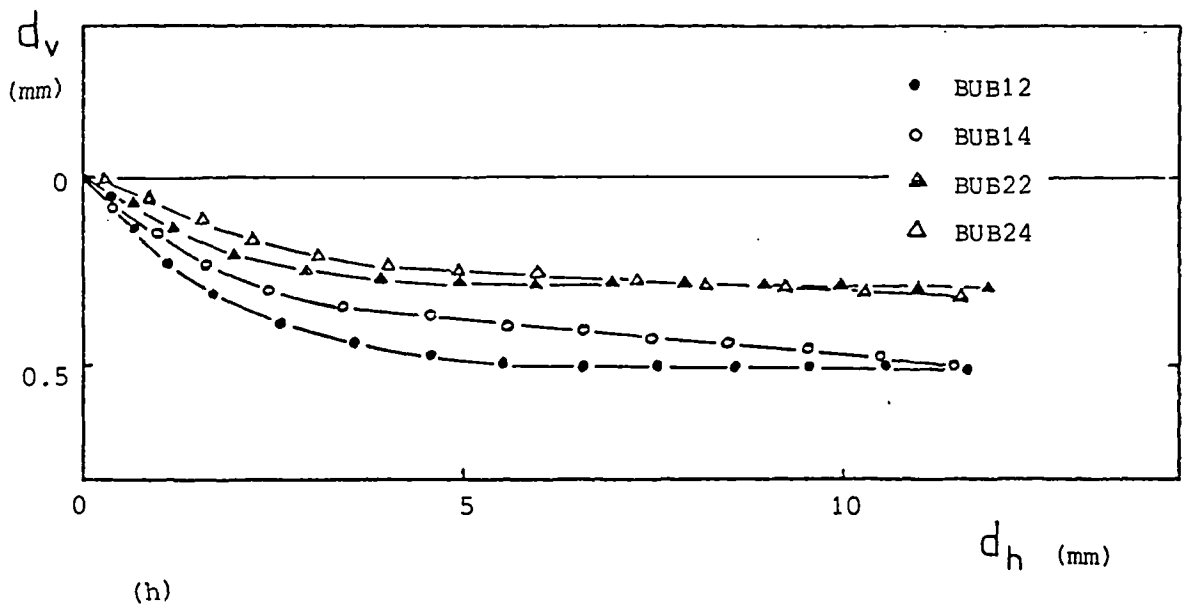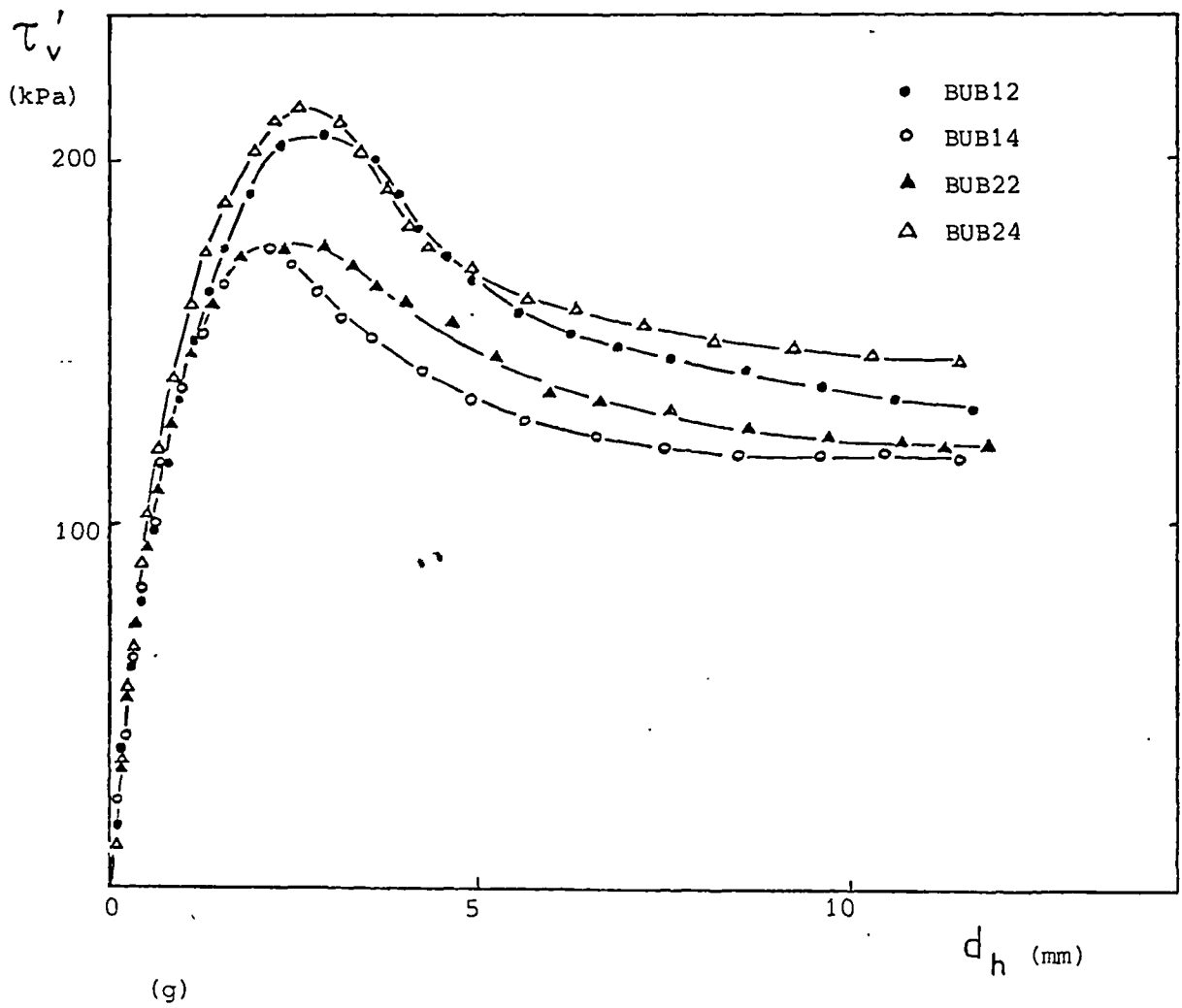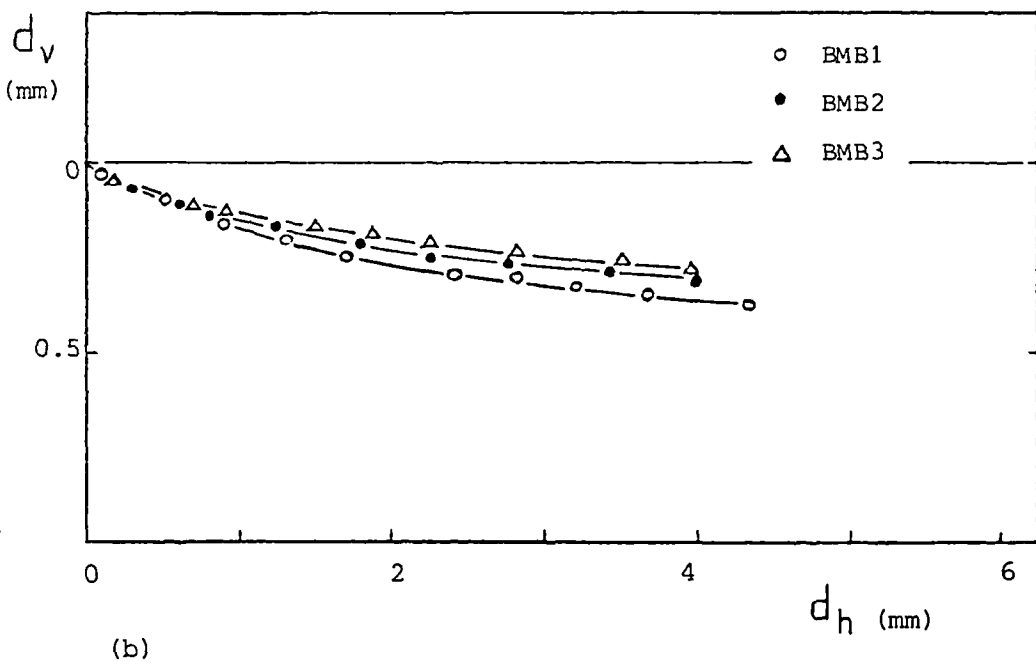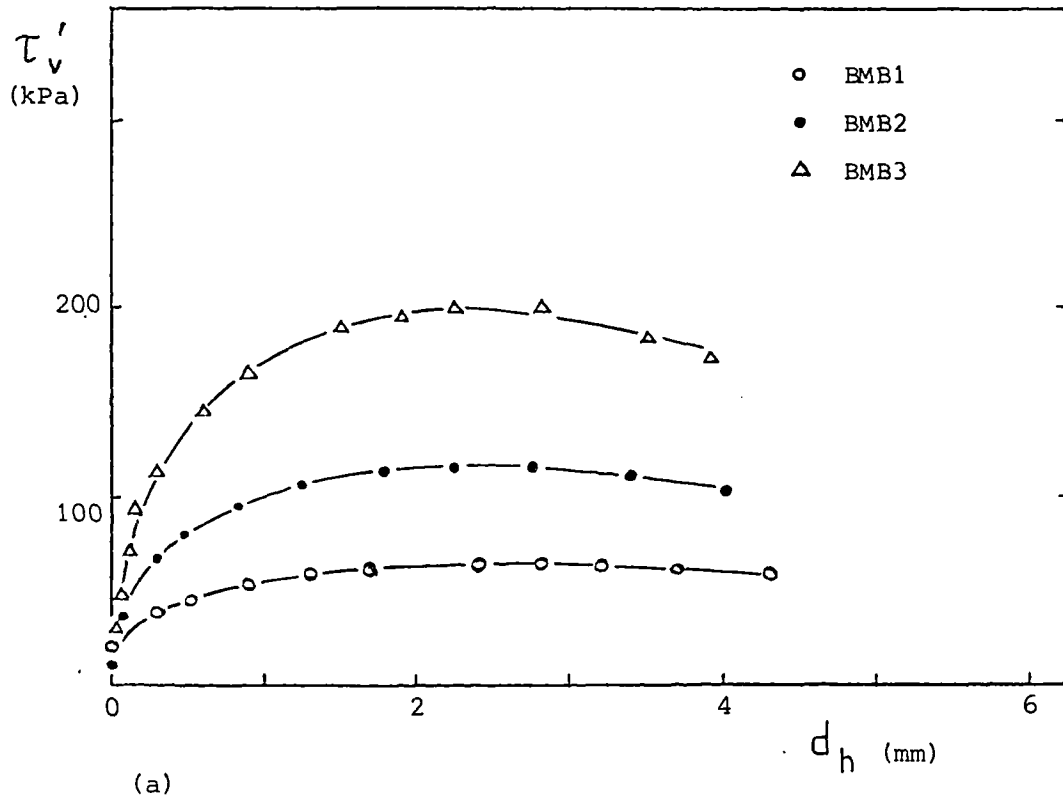
Figure 6.19   Results of shearing from remoulded London clay
(brown) shear box samples
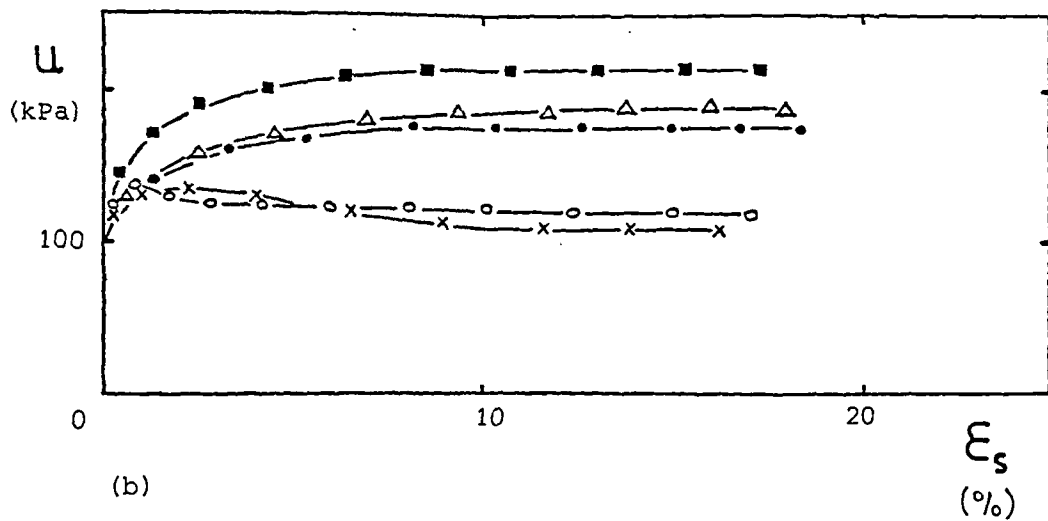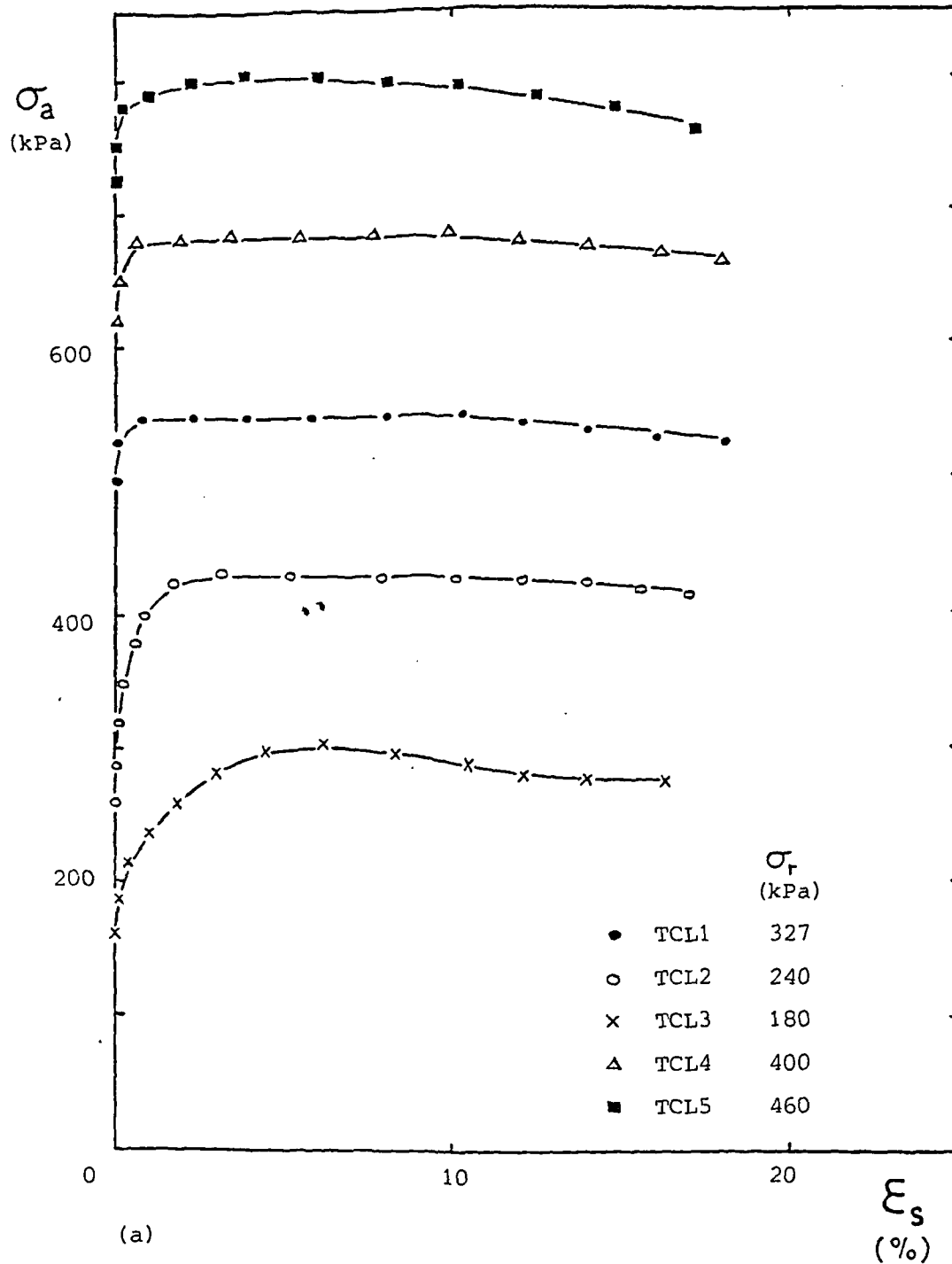
Figure 6.20   Results of shearing from 38 mm reconstituted London clay (blue) triaxial samples
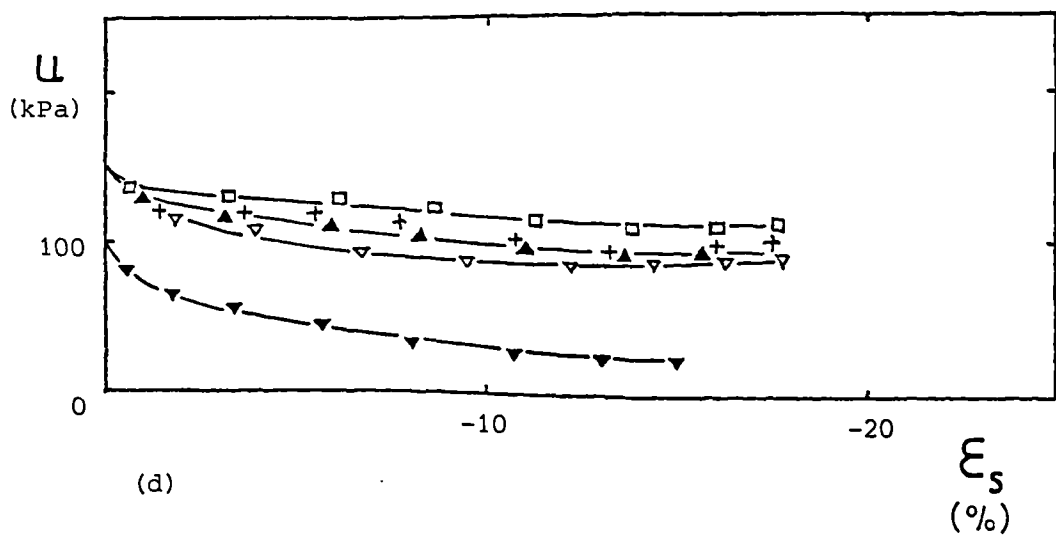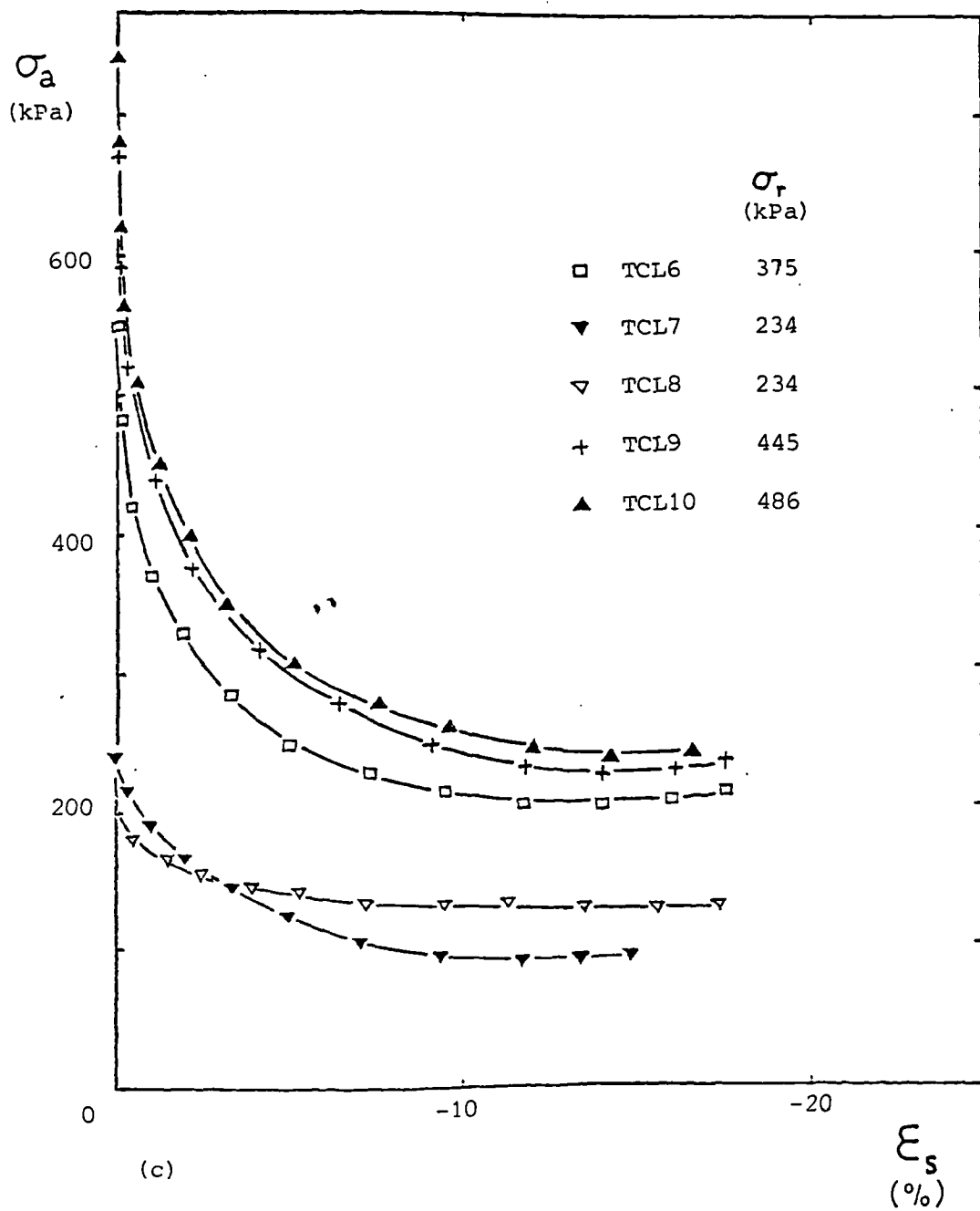
Figure 6.20 continued
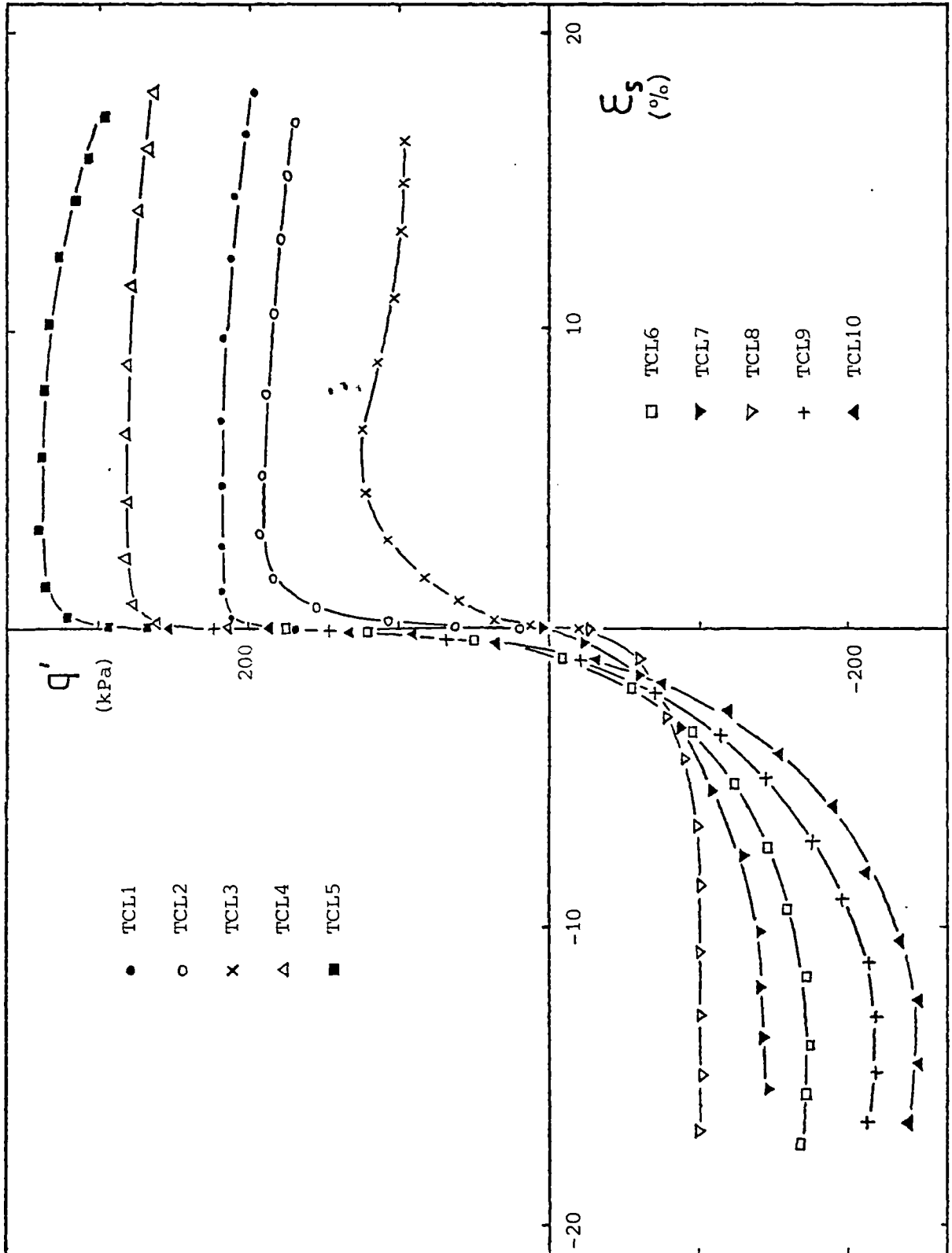
(e)

Figure 6.20 continued

(a)

(b)
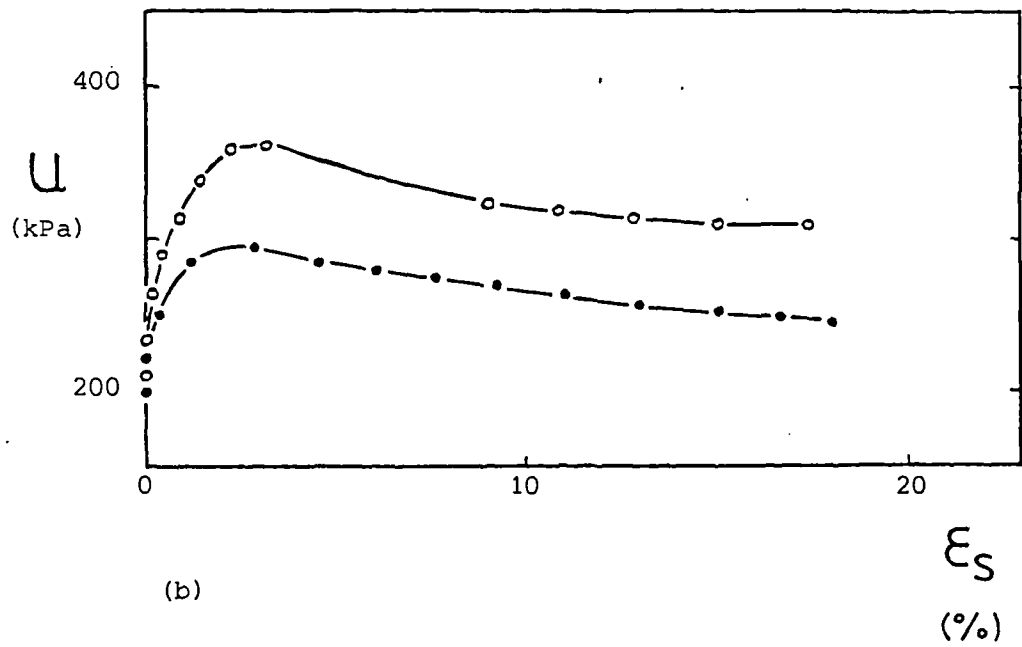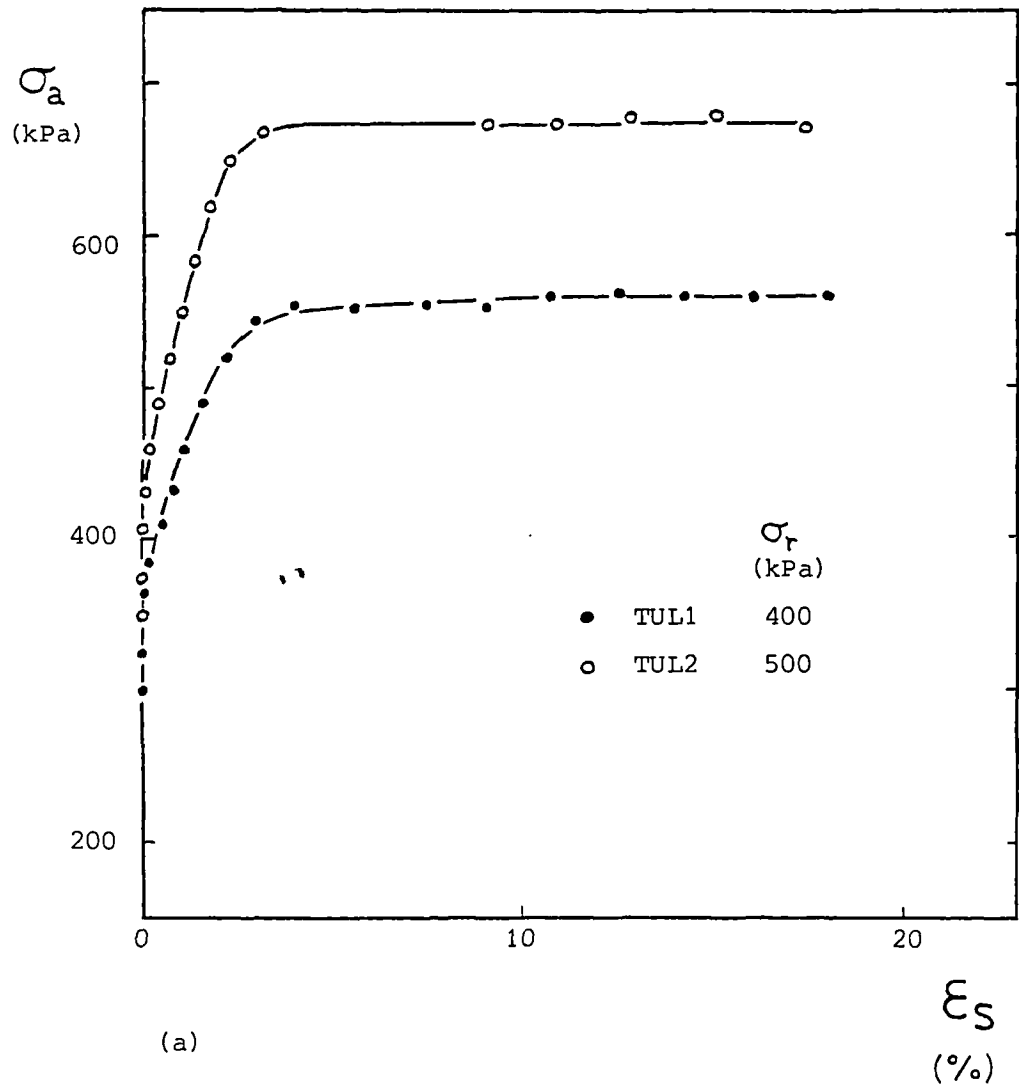
Figure 6.21   Results of shearing from 100 mm undisturbed London clay (blue) triaxial samples

(c)

(d)
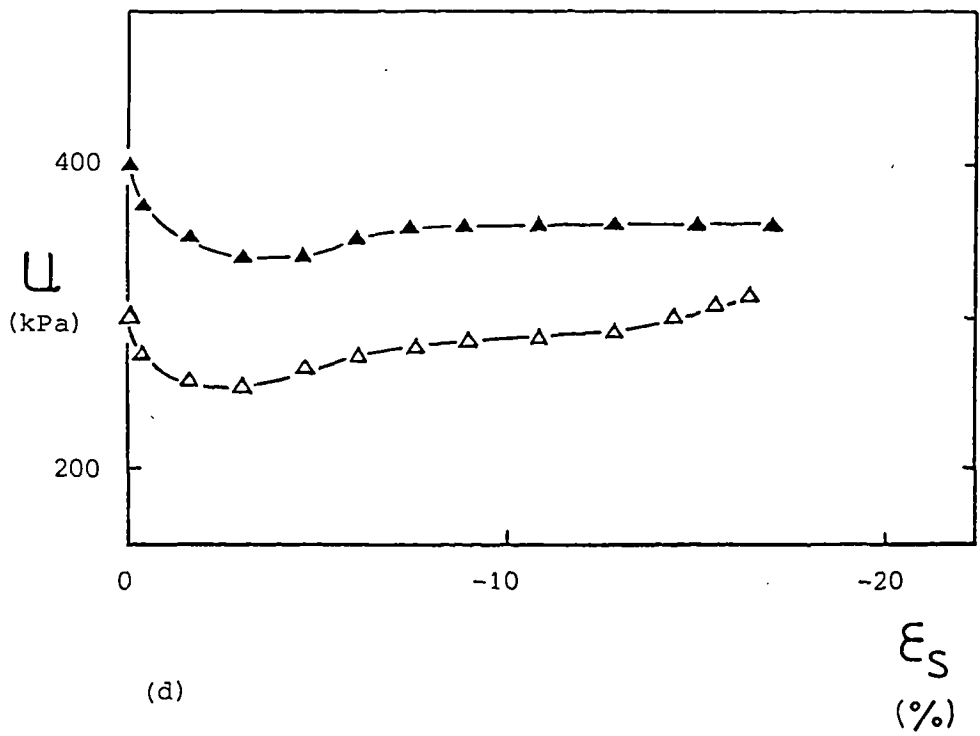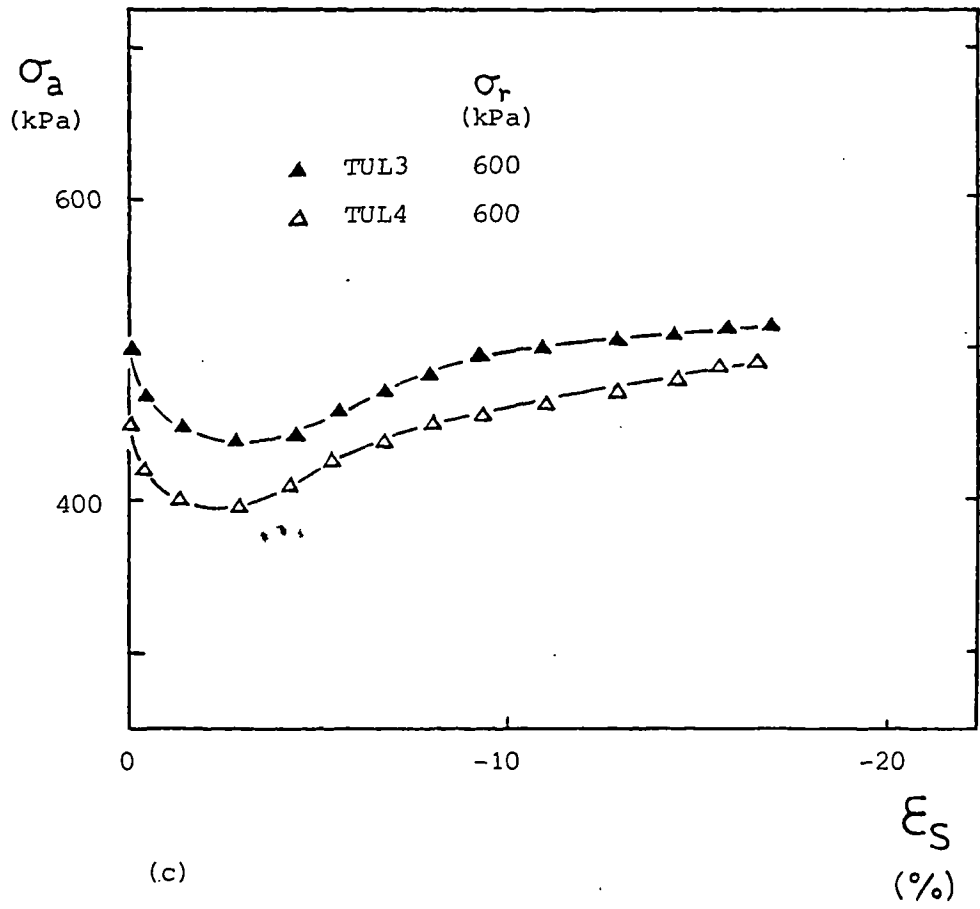
Figure 6.21 continued
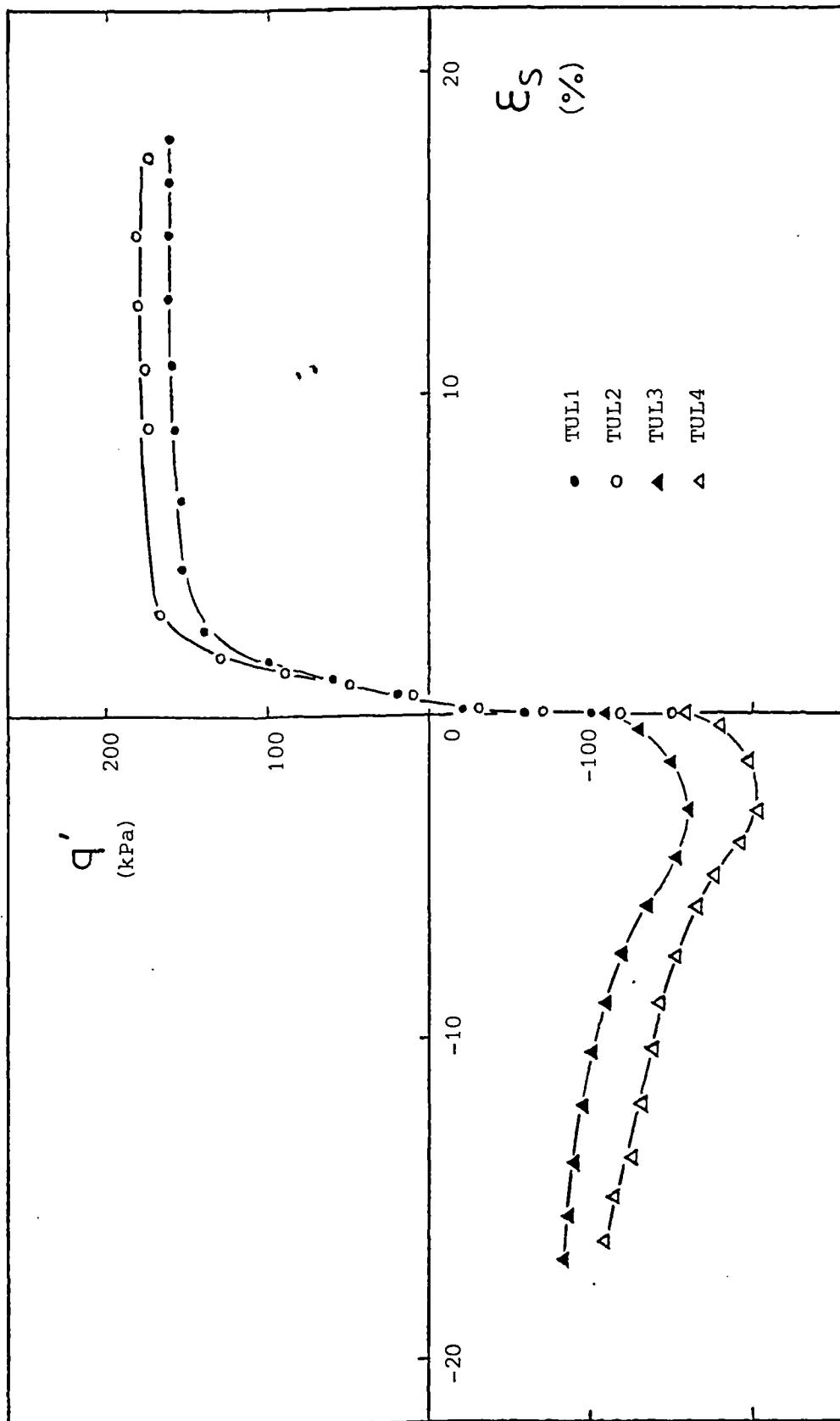
(e)

Figure 6.21 continued
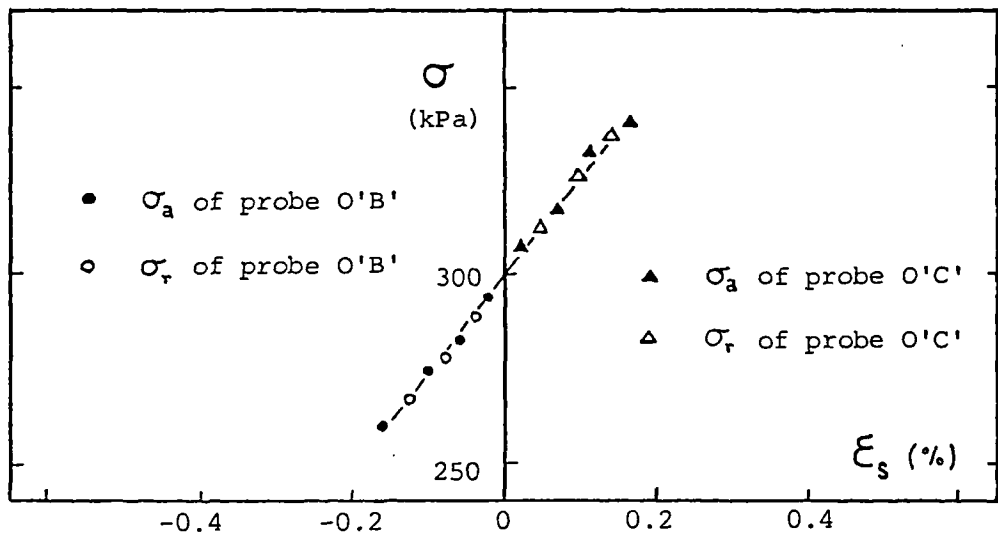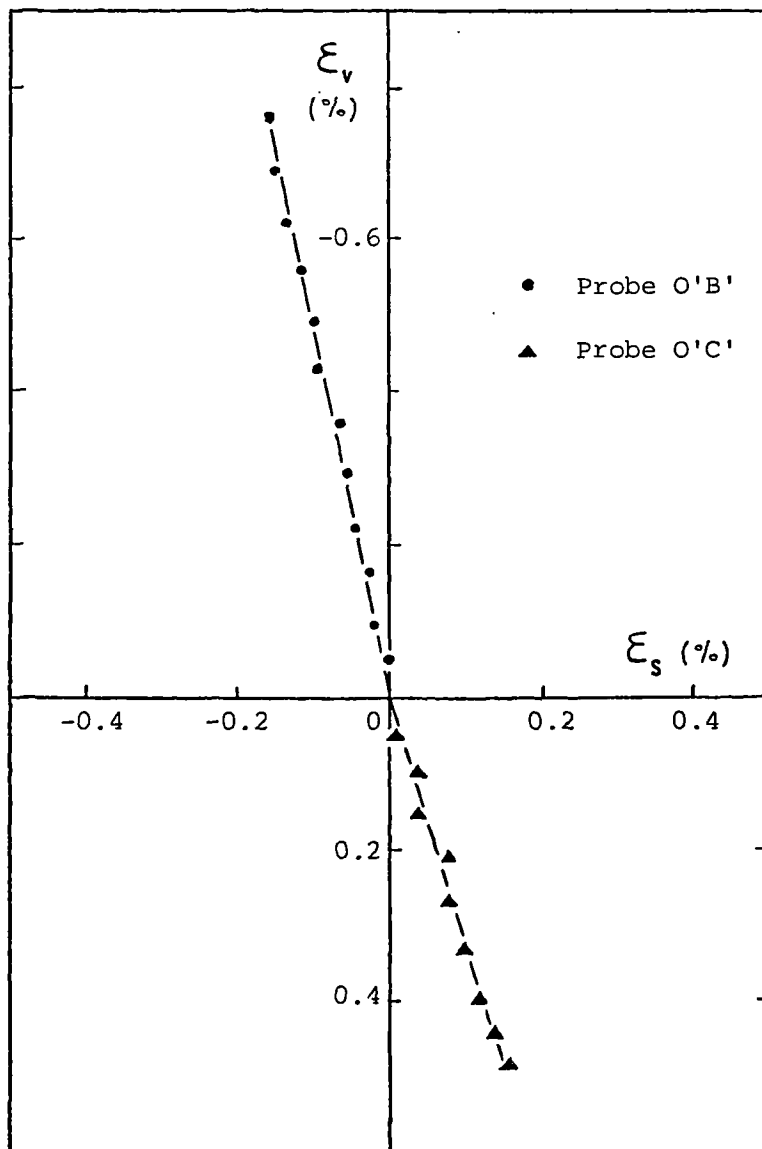
Figure 6.22 Results of stress probing from 100 mm undisturbed London clay (brown) triaxial sample TUB1
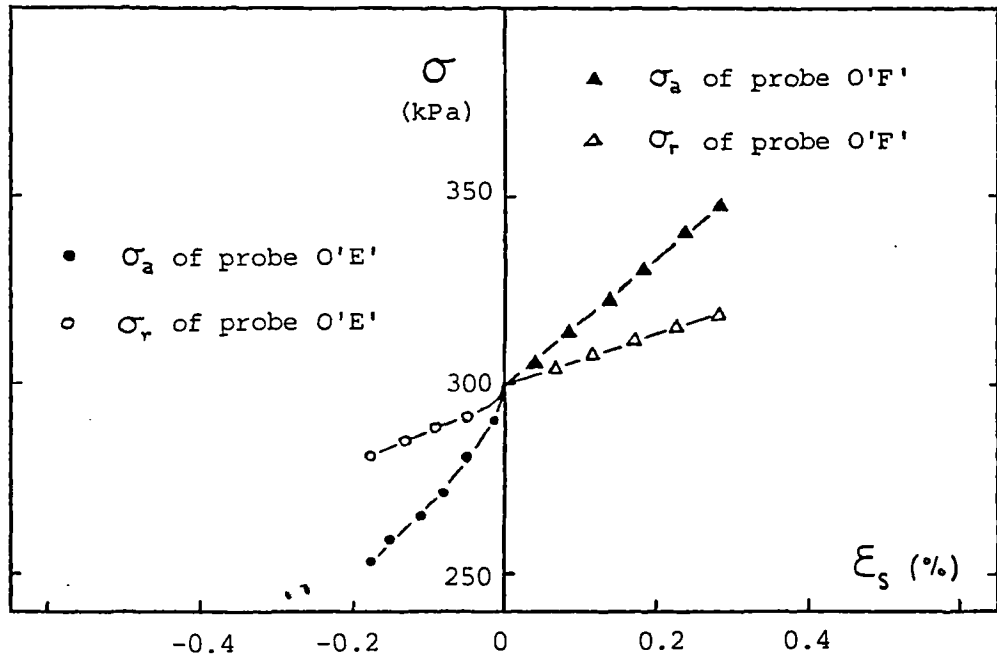
(c)
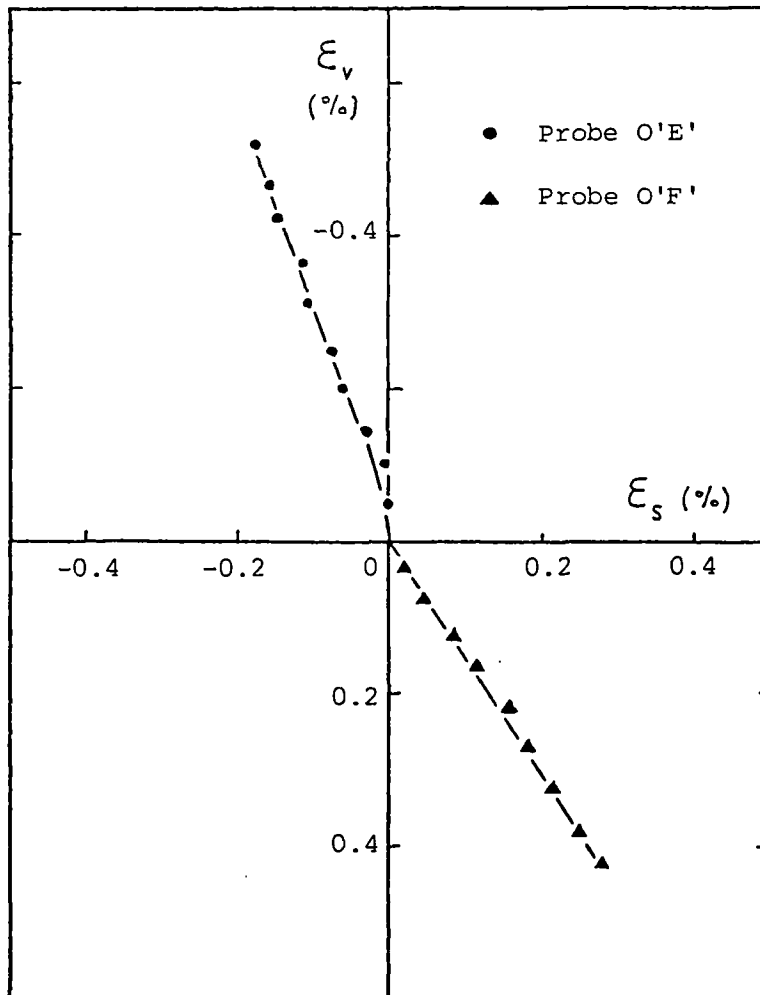
(d)

Figure 6.22 continued
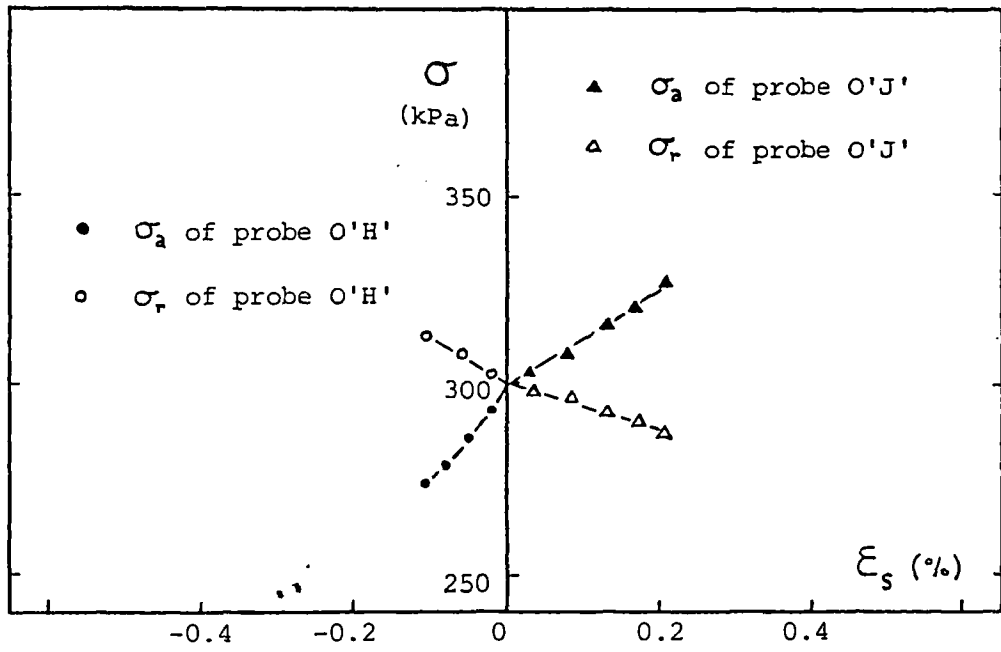
(e)
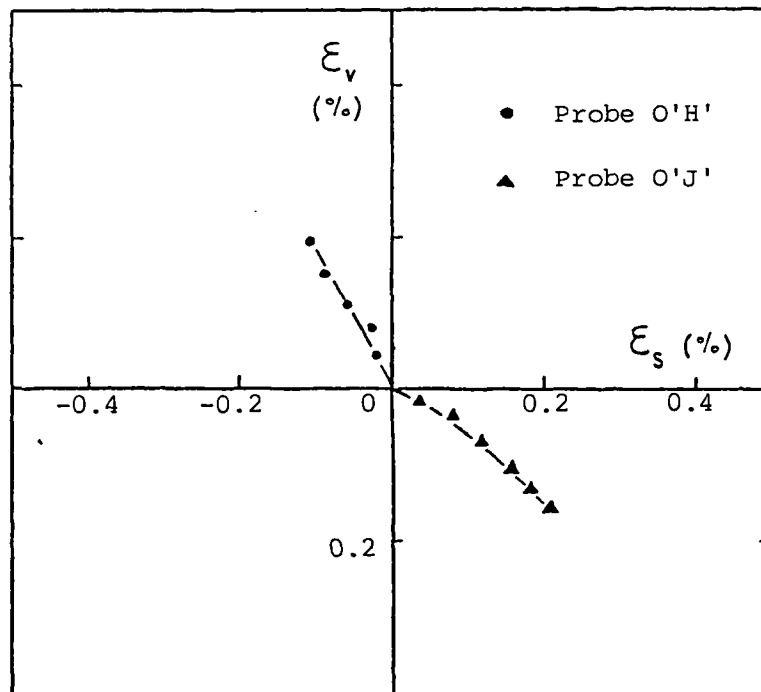
(f)

Figure 6.22 continued
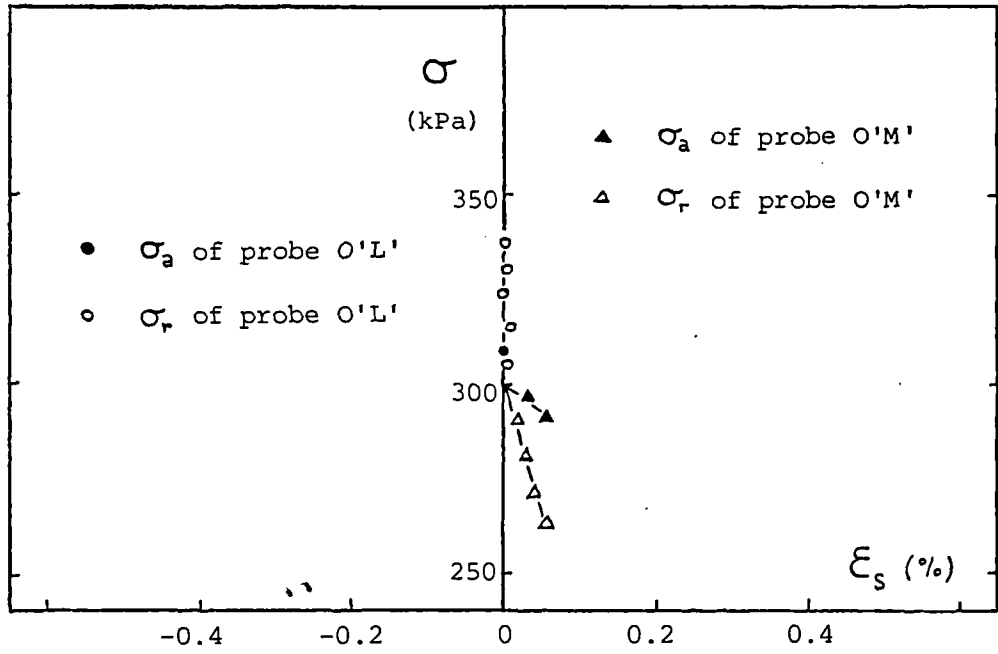
(g)
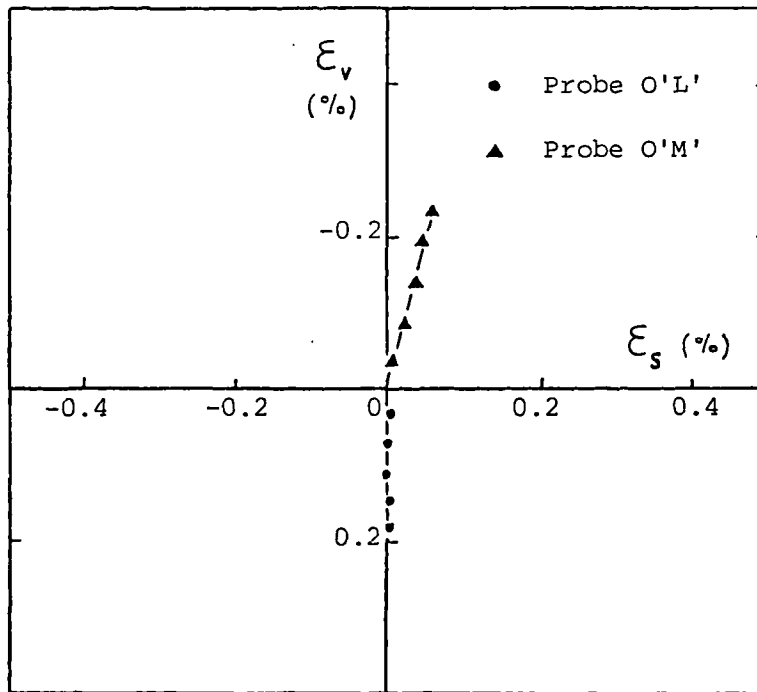
(h)

Figure 6.22 continued

(i)

(j)
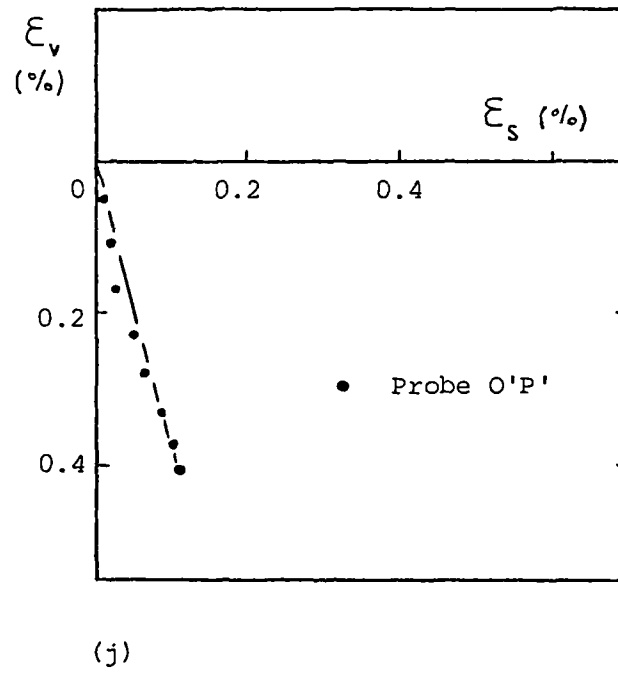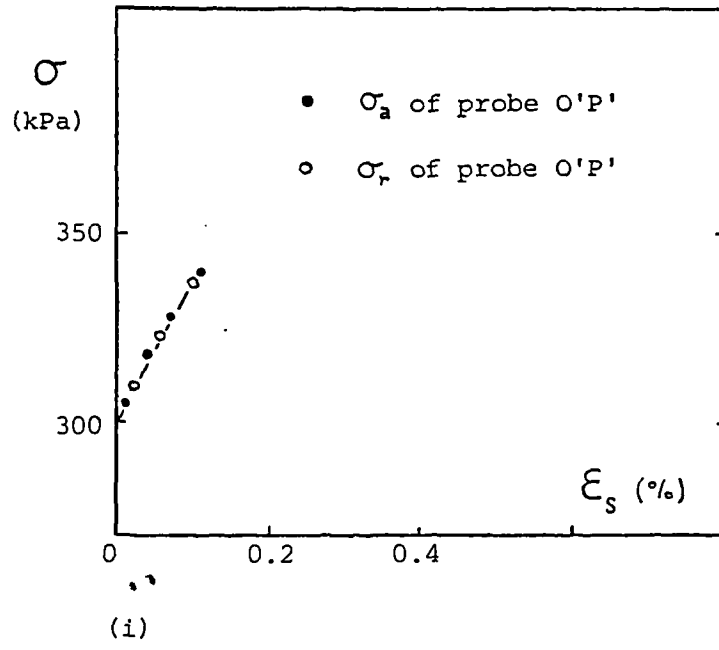
Figure 6.22 continued
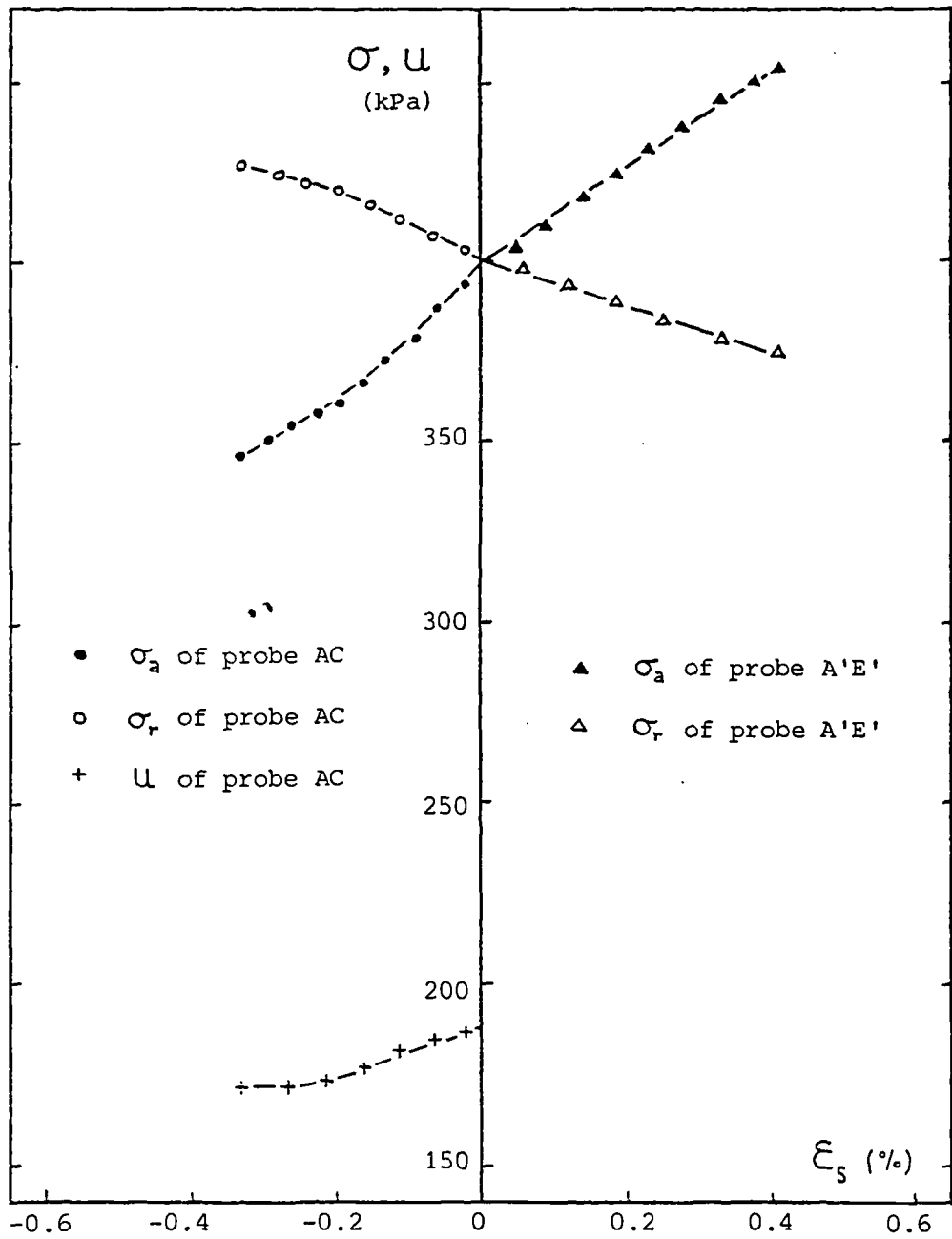
(a)
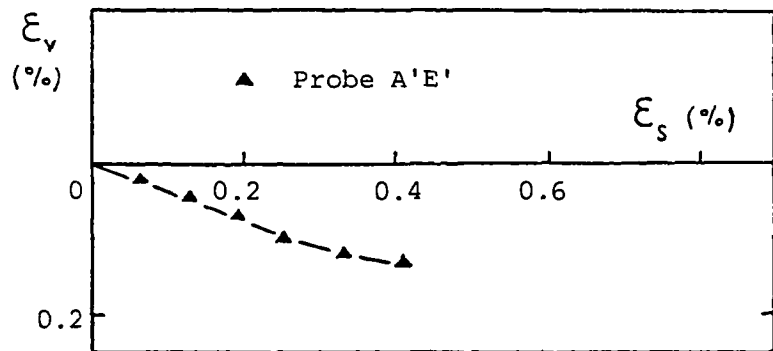
(b)

Figure 6.23   Results of stress probing from 100 mm undisturbed
                London clay (blue) triaxial sample TUL5
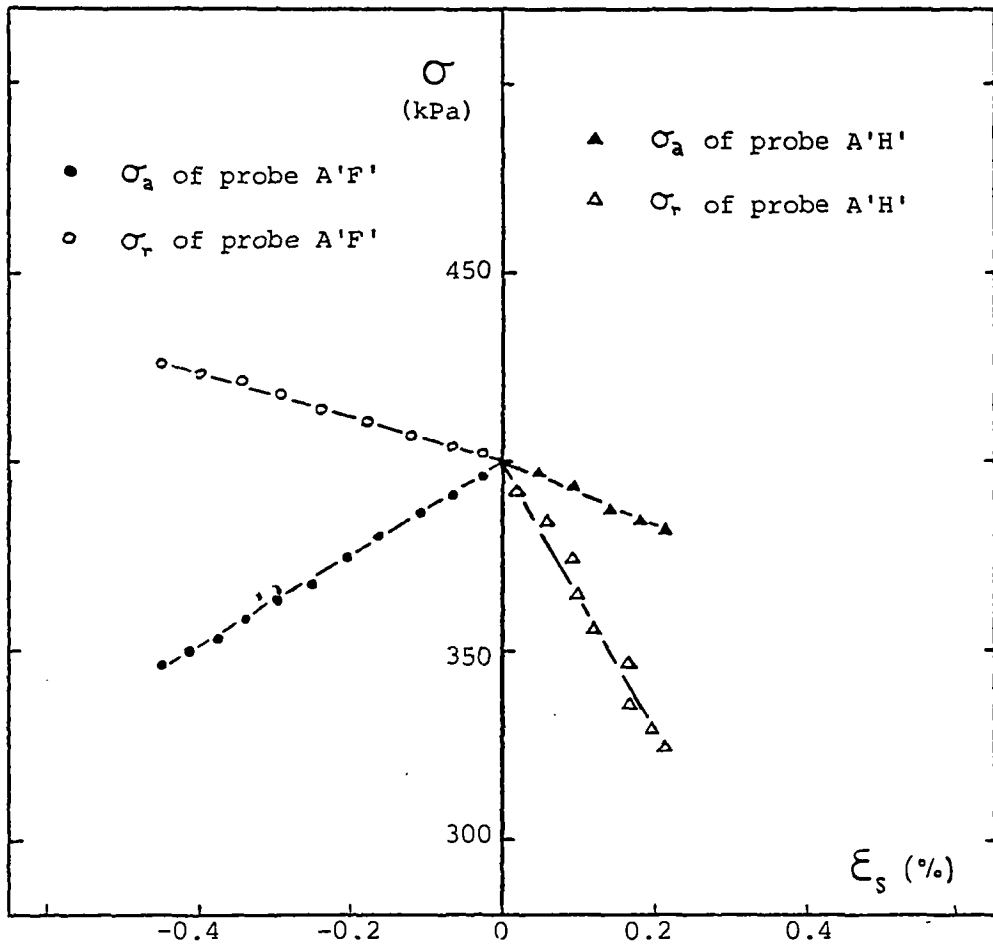
(c)
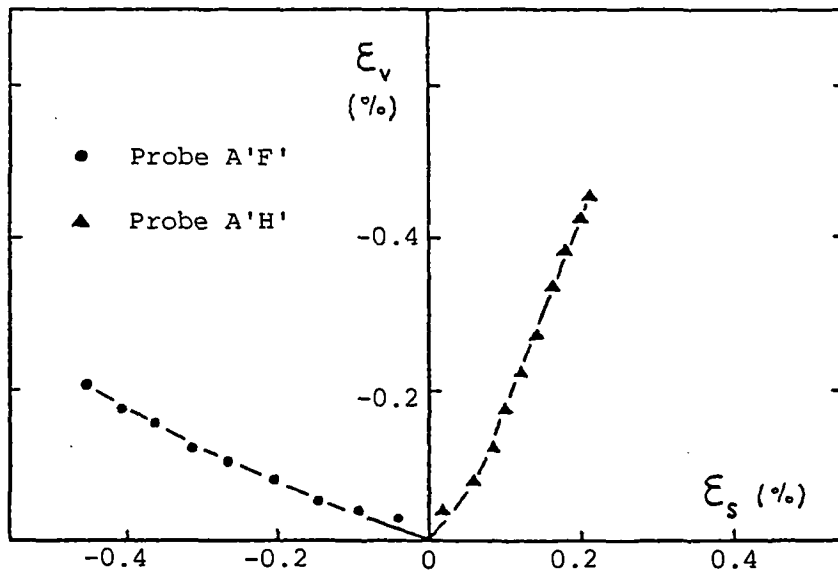
(d)

Figure 6.23 continued
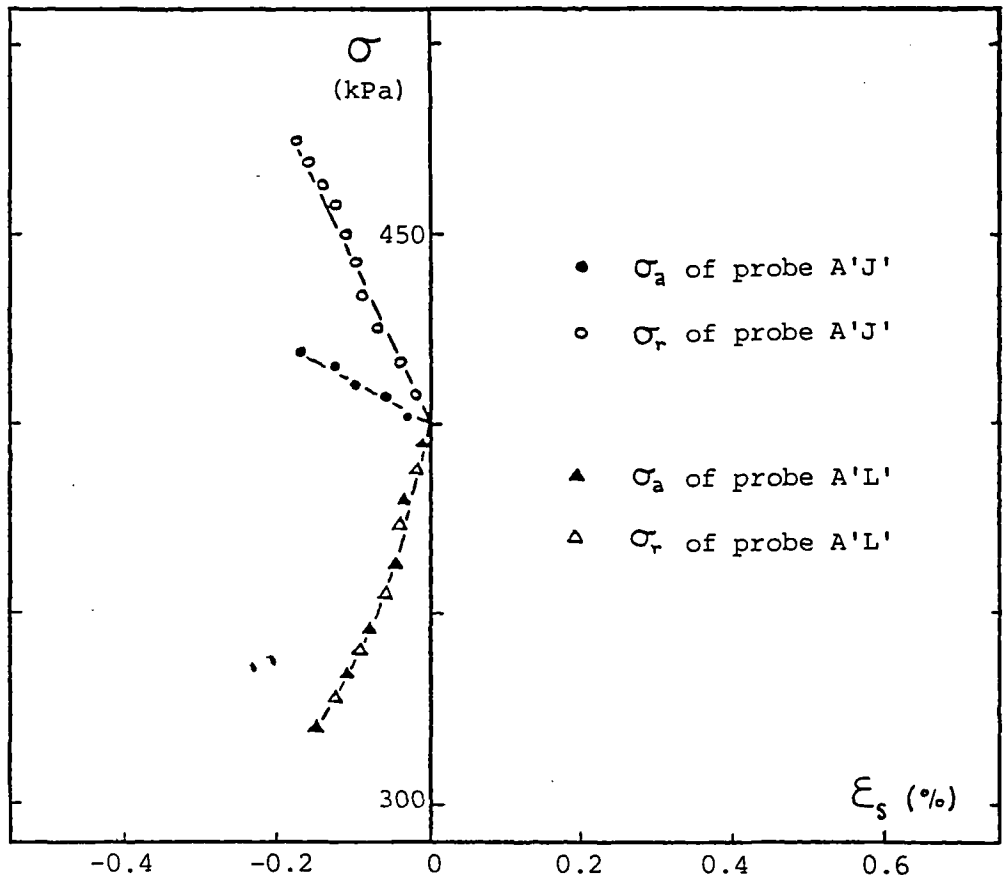
(e)
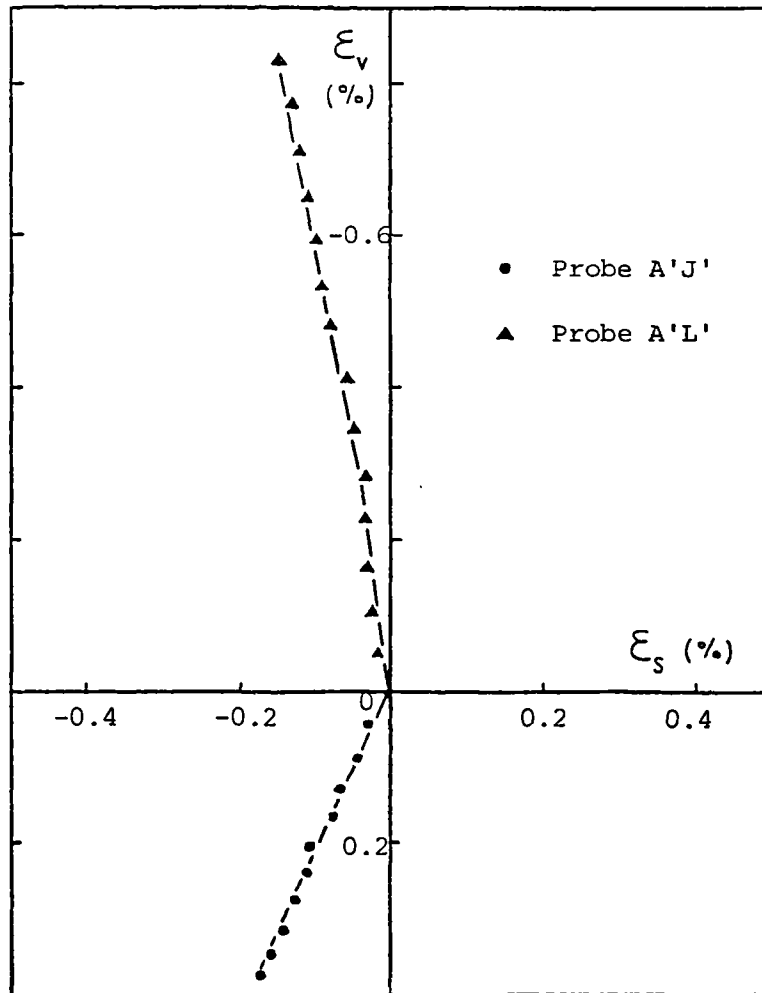
(f)

Figure 6.23 continued

(g)

(h)
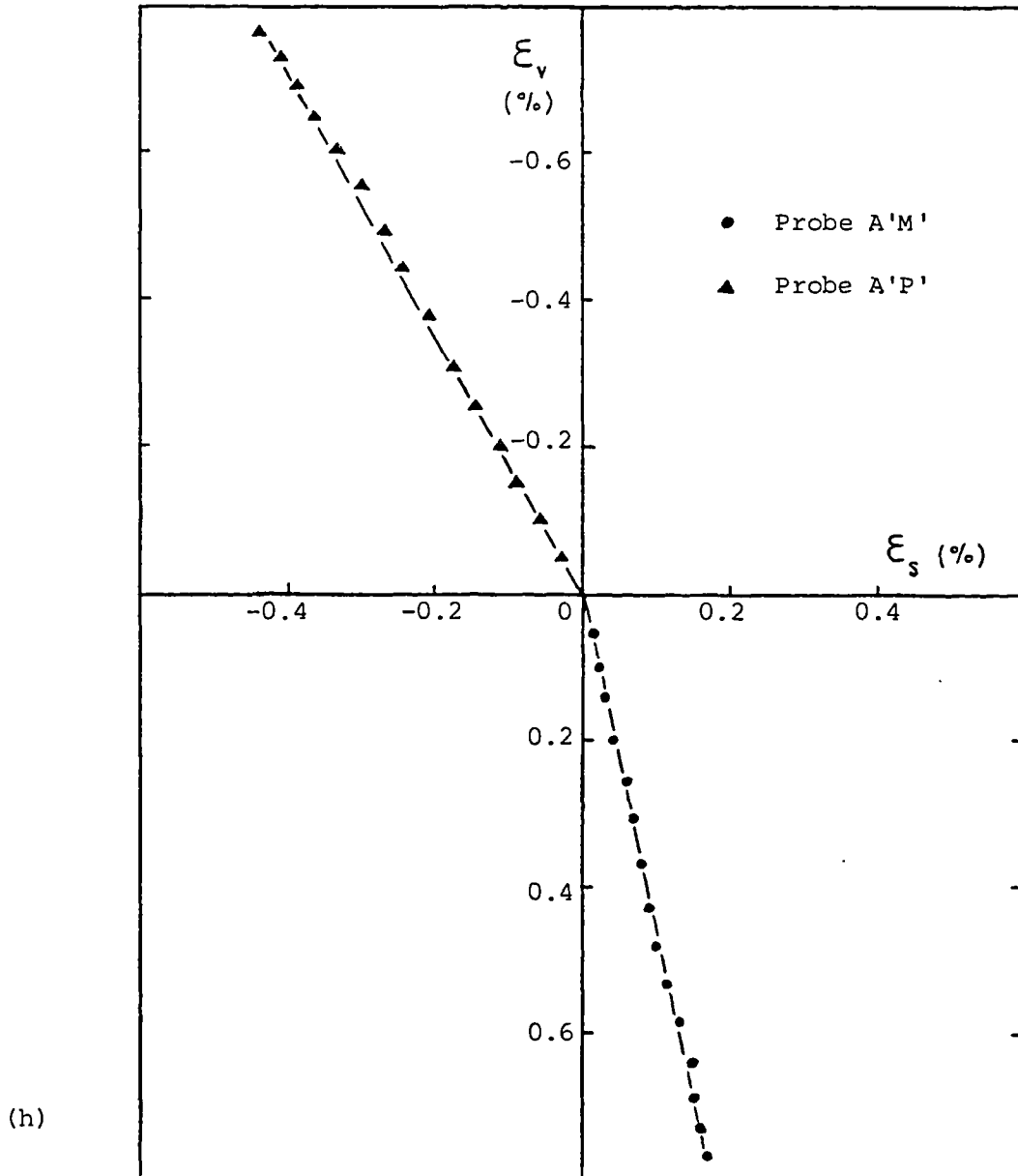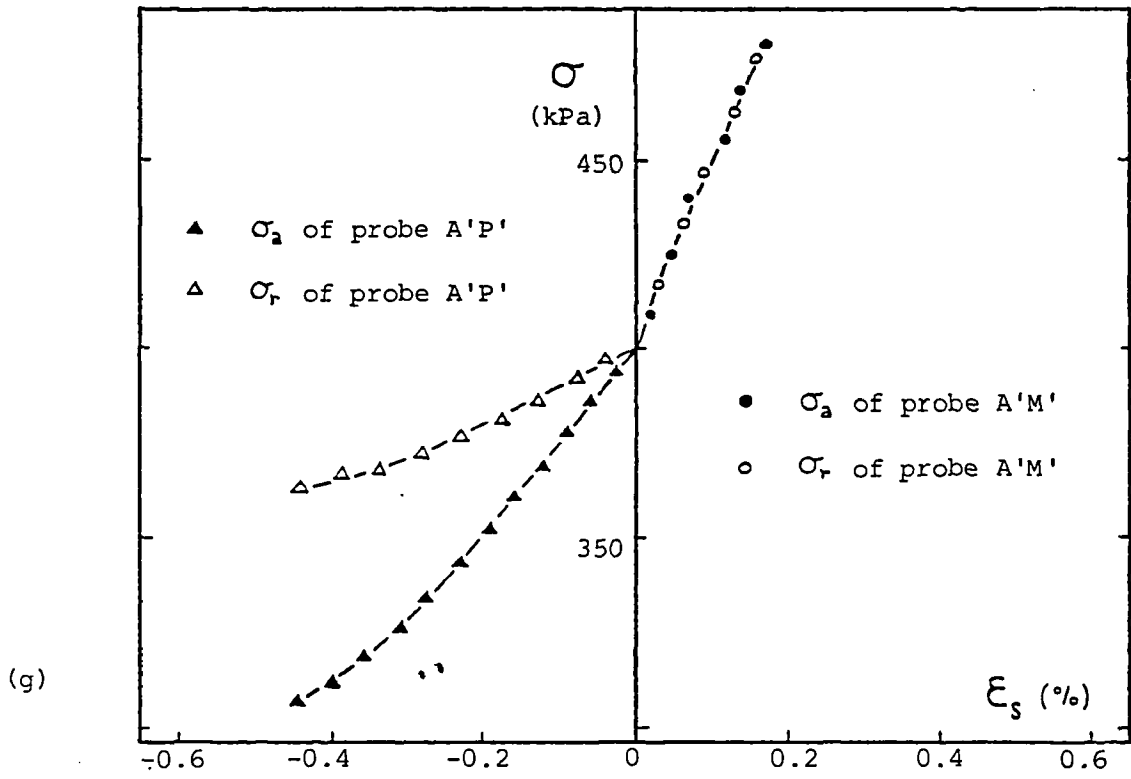
Figure 6.23 continued
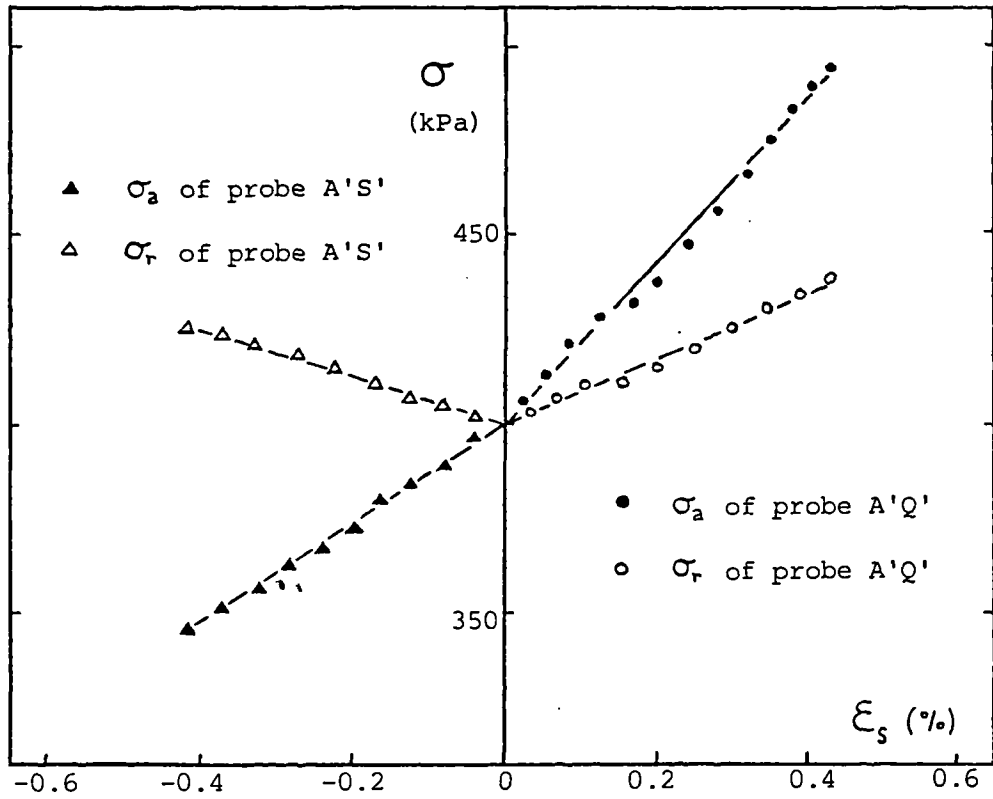
(i)
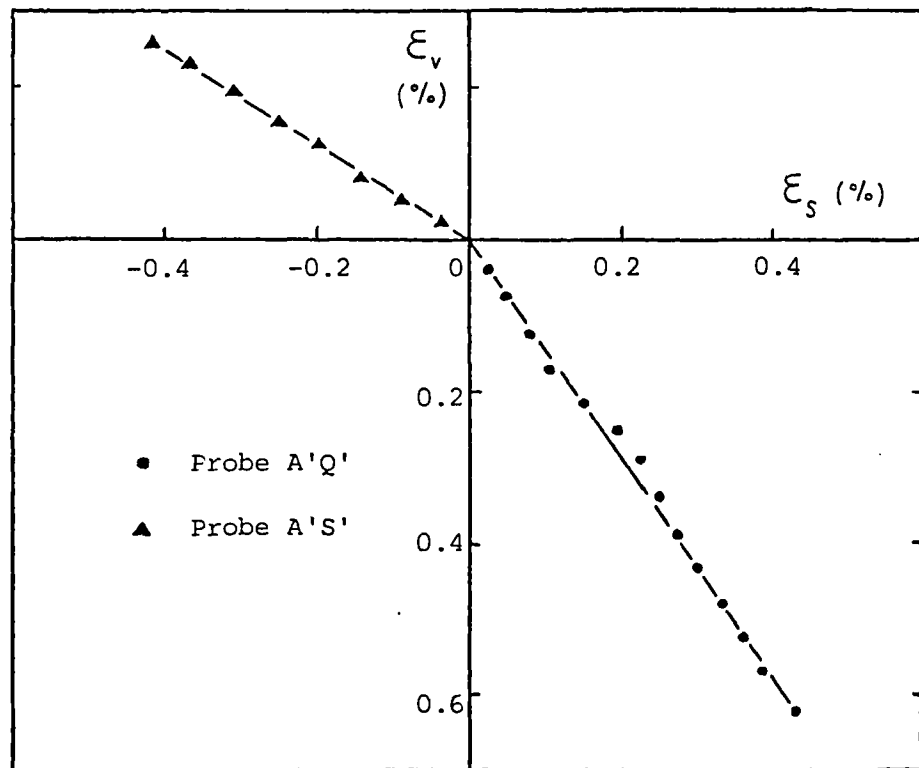
(j)

Figure 6.23 continued
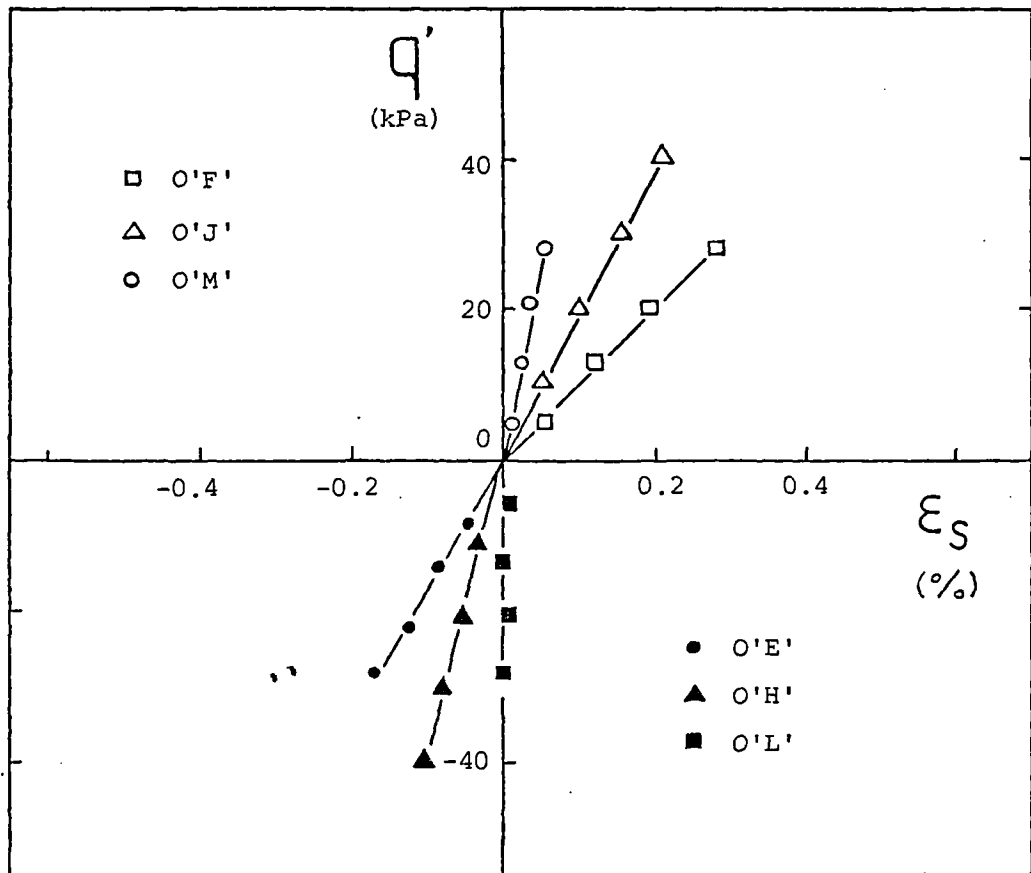
(a) Test TUB1
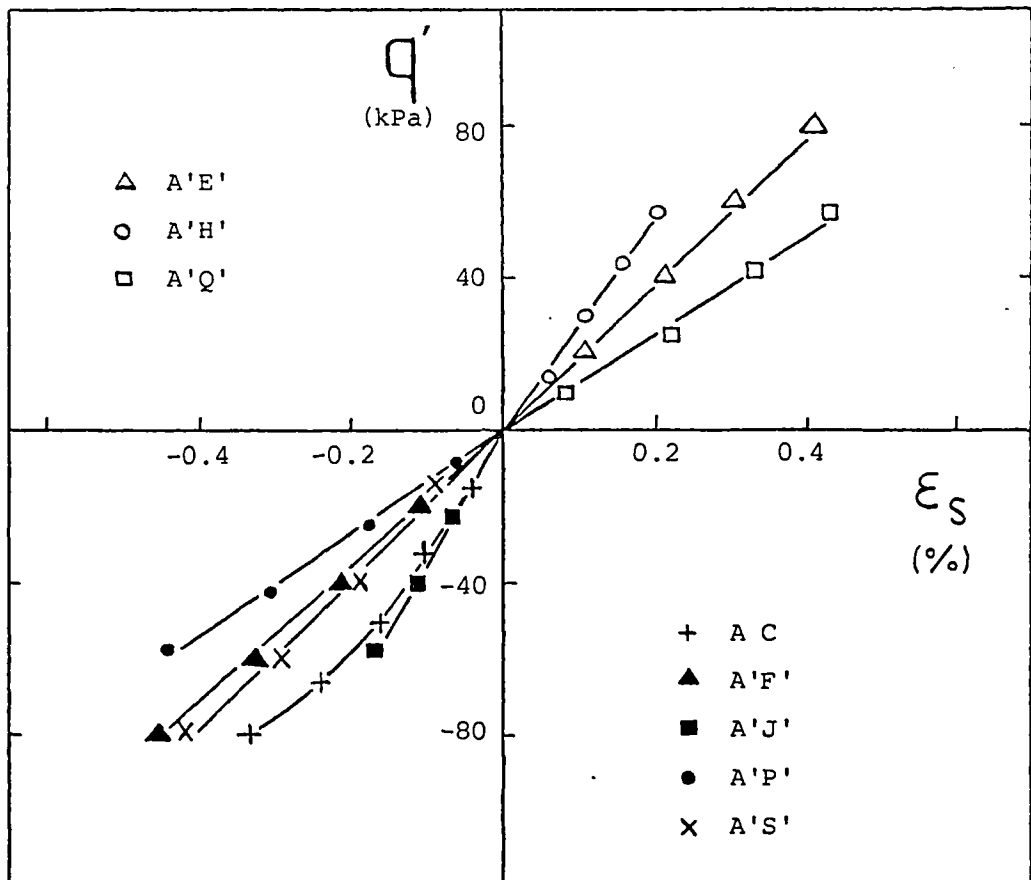
(b) Test TUL5

Figure 6.24   Shear stress versus shear strain curves for probing
                tests on 100 mm undisturbed London clay triaxial
                samples

Particle size (mm)

——————— Results of tests from this study

—·—·— Gens and Hight (1979)

— — — Envelope for results of eight tests performed by BRE
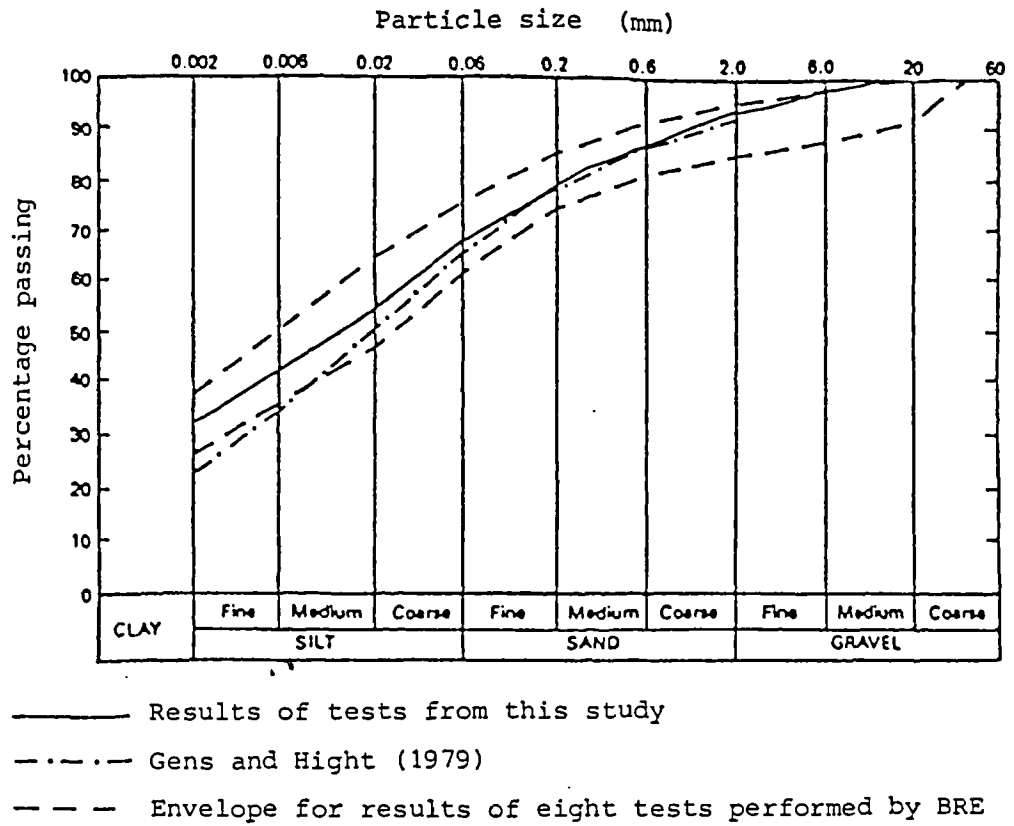
Figure 7.1   Comparison of results from particle size distribution
              tests

——————— Remoulded, simple shear

— — — Reconstituted, simple shear

—·—·— Remoulded, shear box
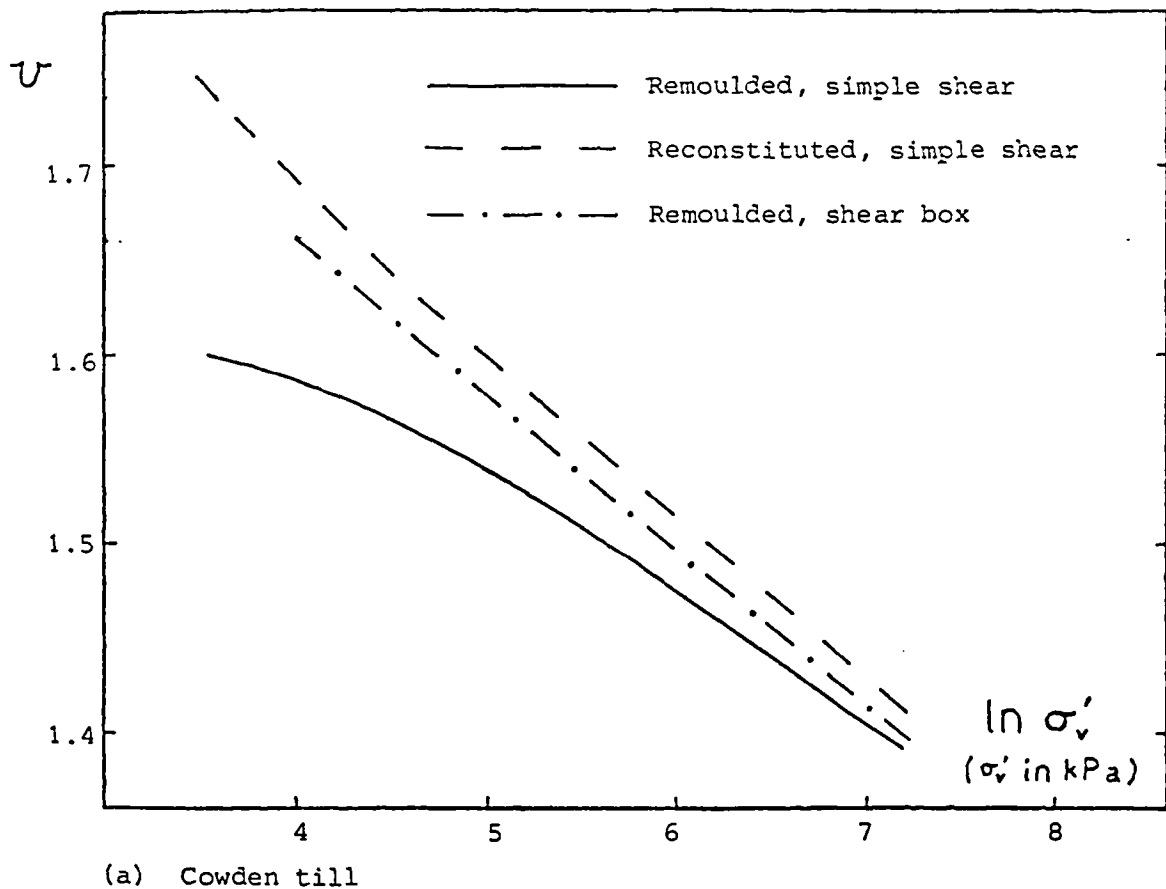
(a) Cowden till

Figure 7.2   Comparison of results for one-dimensional compression
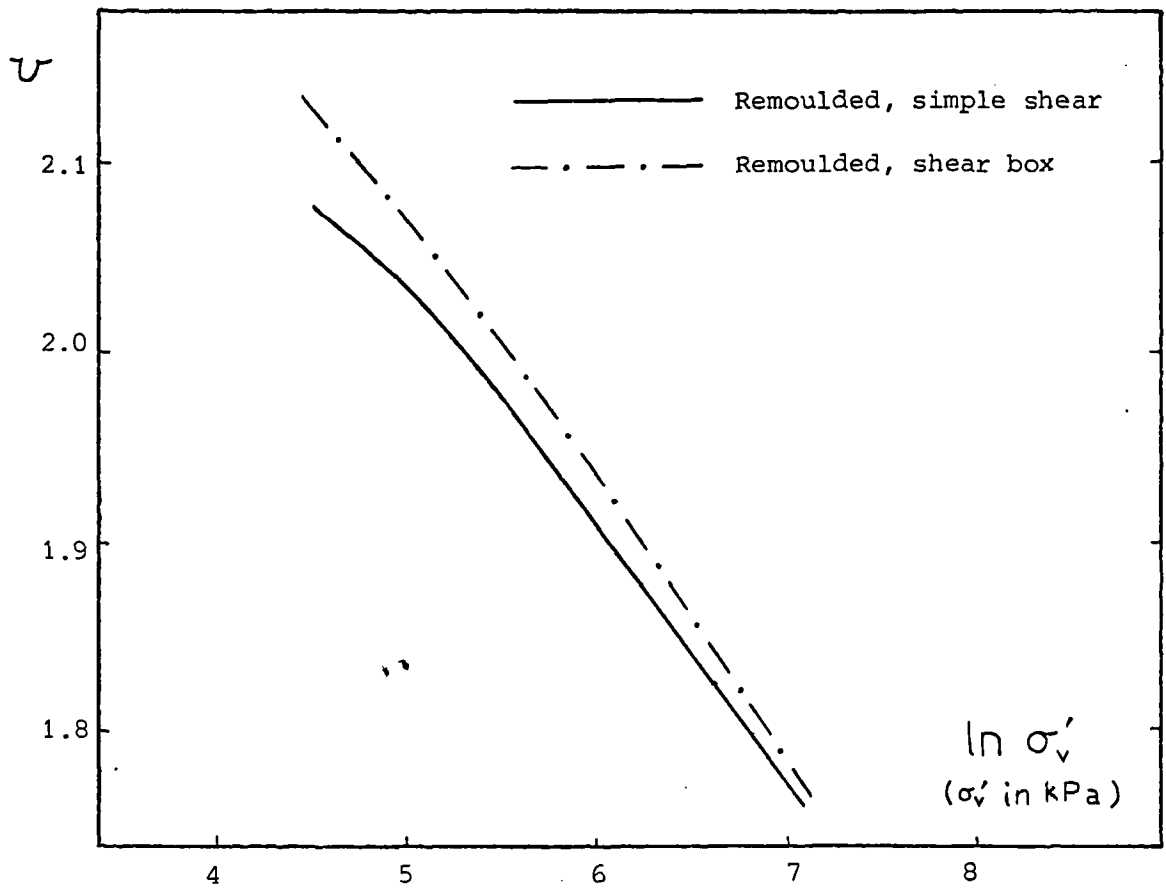
(b)   London clay (brown)
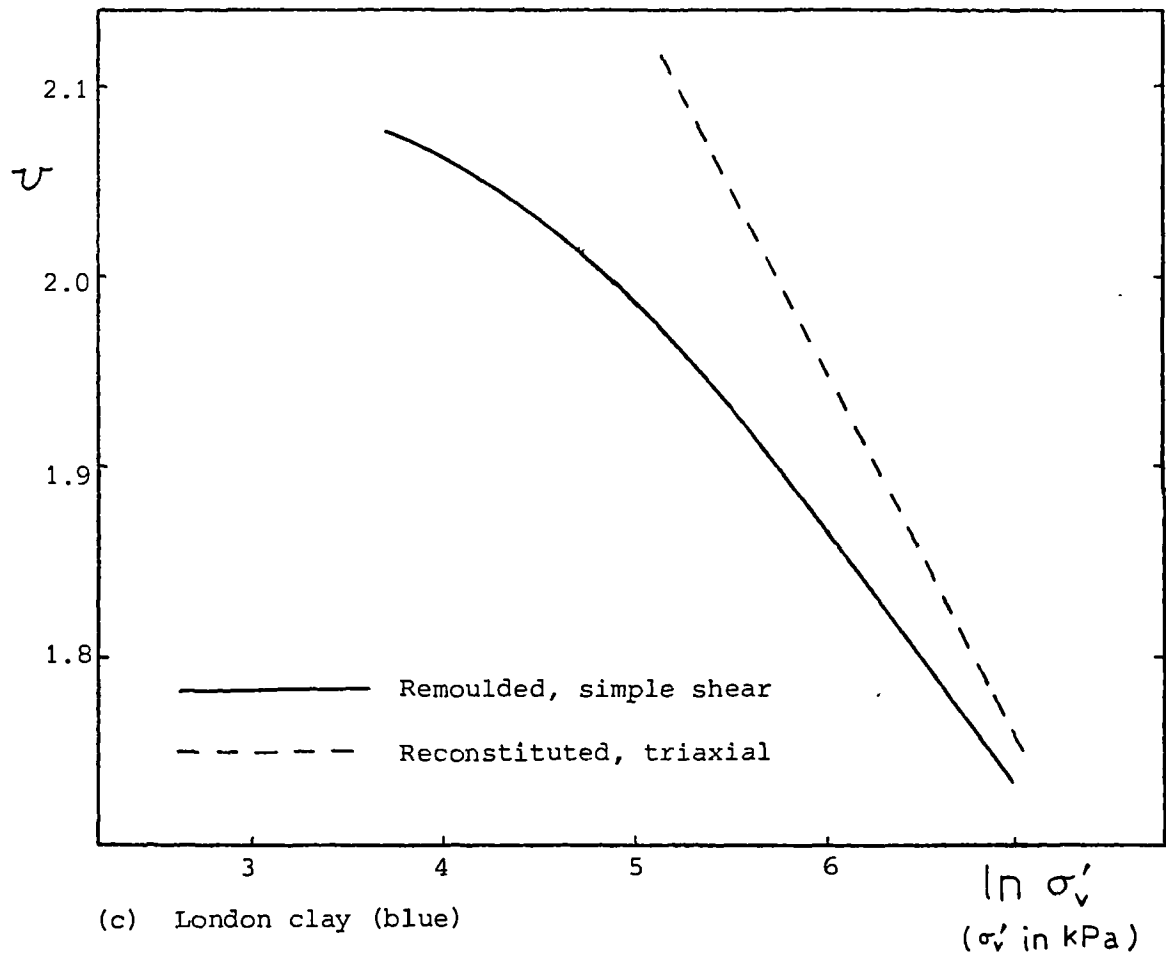
(c)   London clay (blue)

Figure 7.2 continued
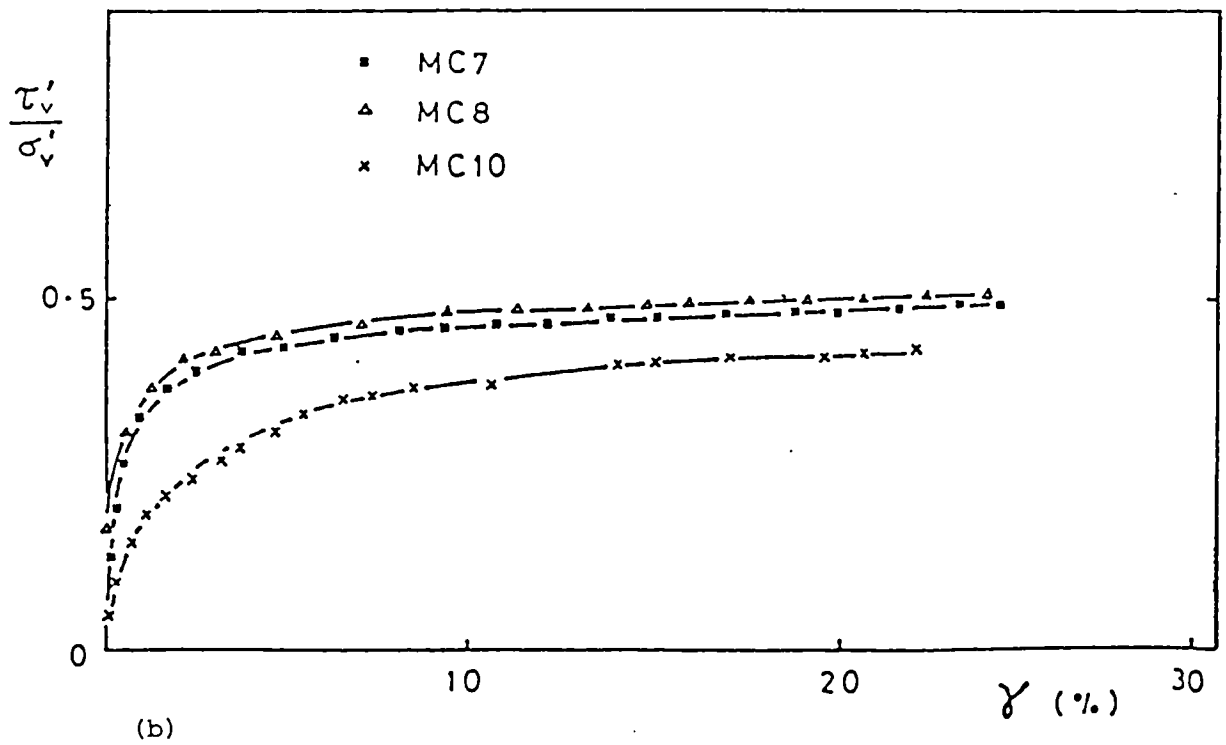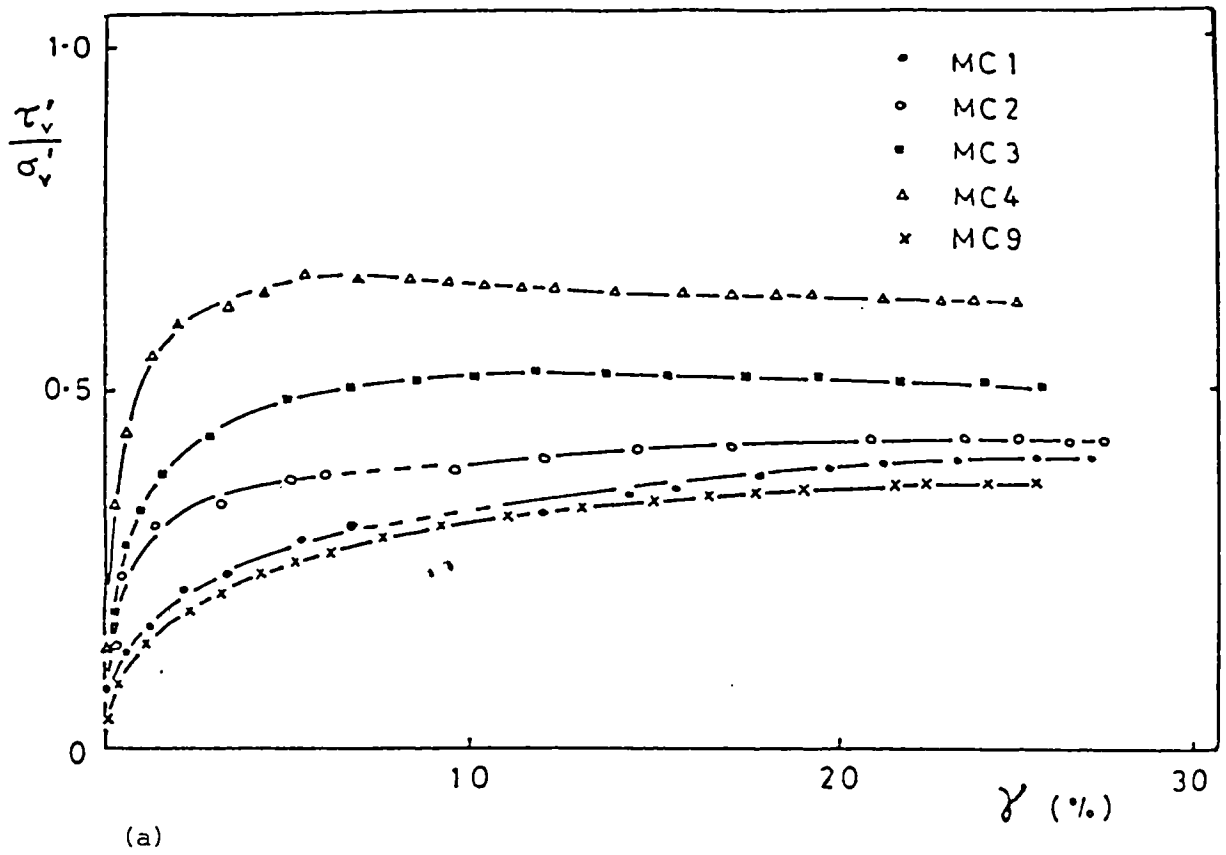
Figure 7.3   Variation of stress ratio with shear strain for
remoulded Cowden till simple shear samples
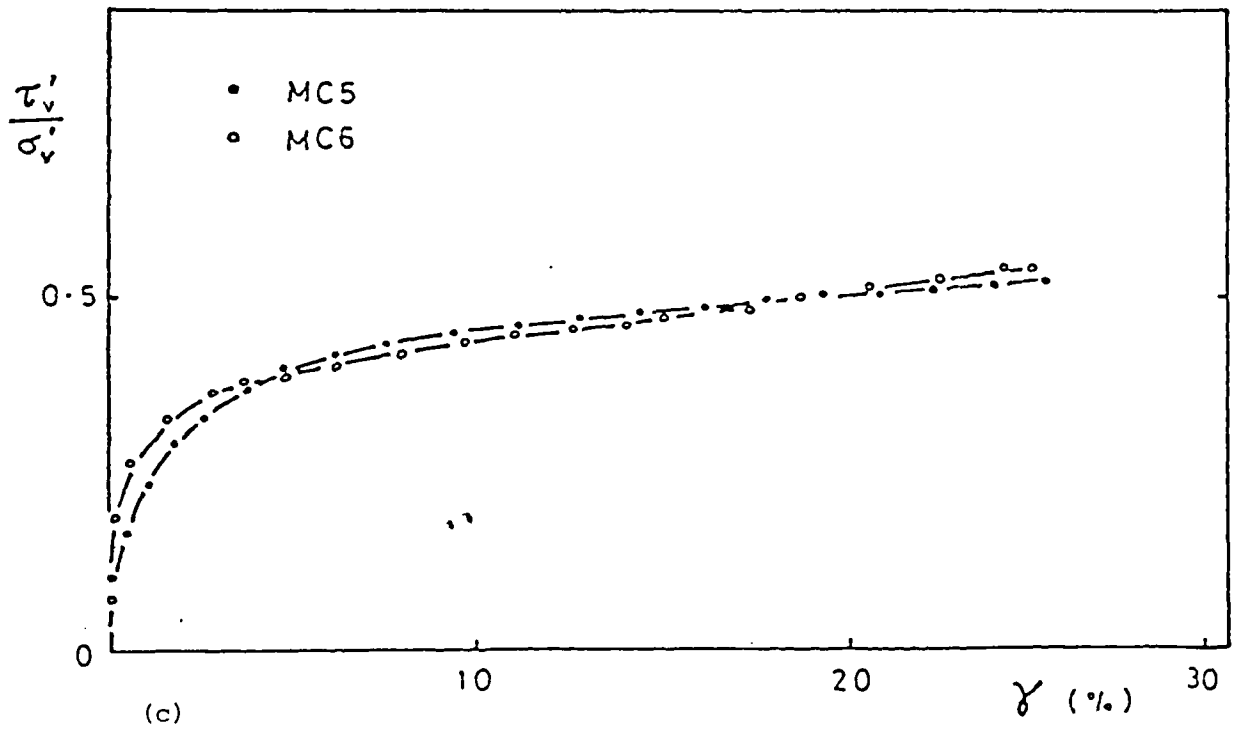
Figure 7.3 continued
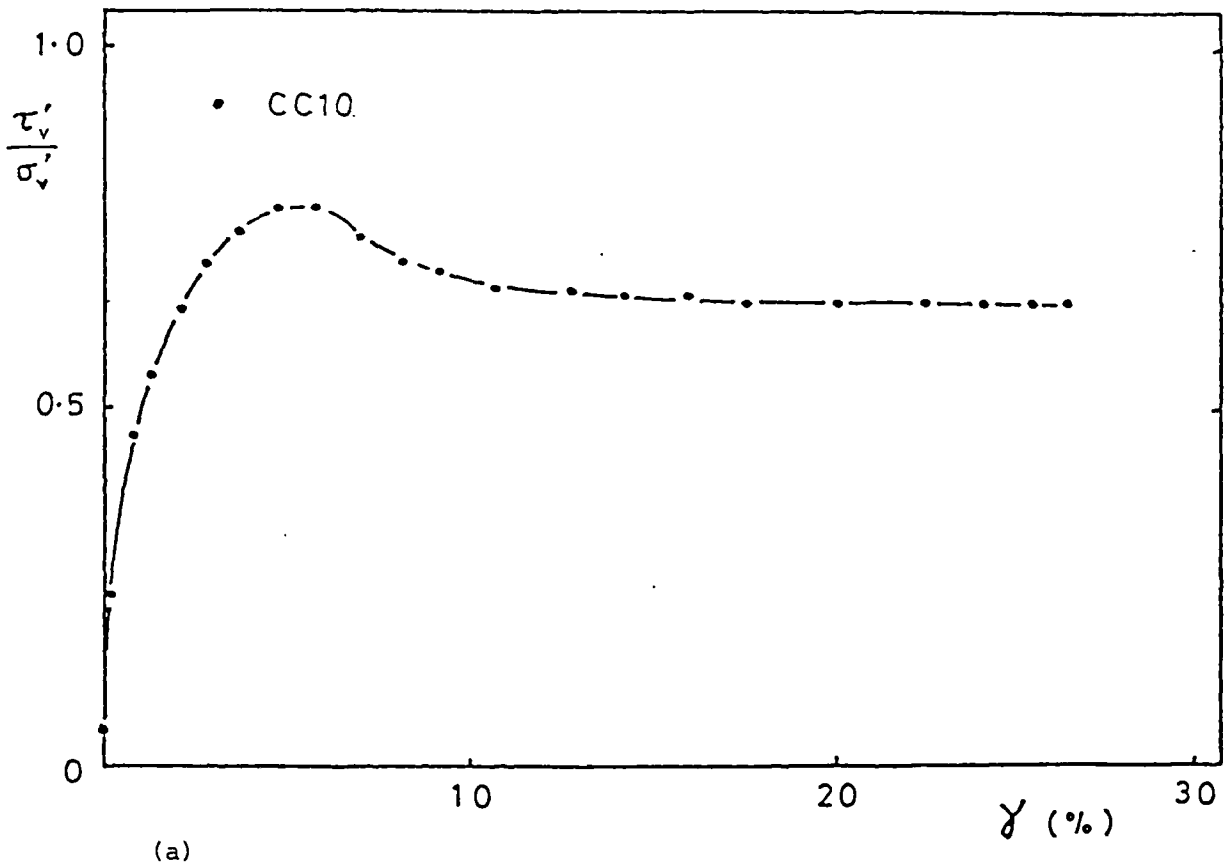
Figure 7.4   Variation of stress ratio with shear strain for
reconstituted Cowden till simple shear samples

(b)

(c)
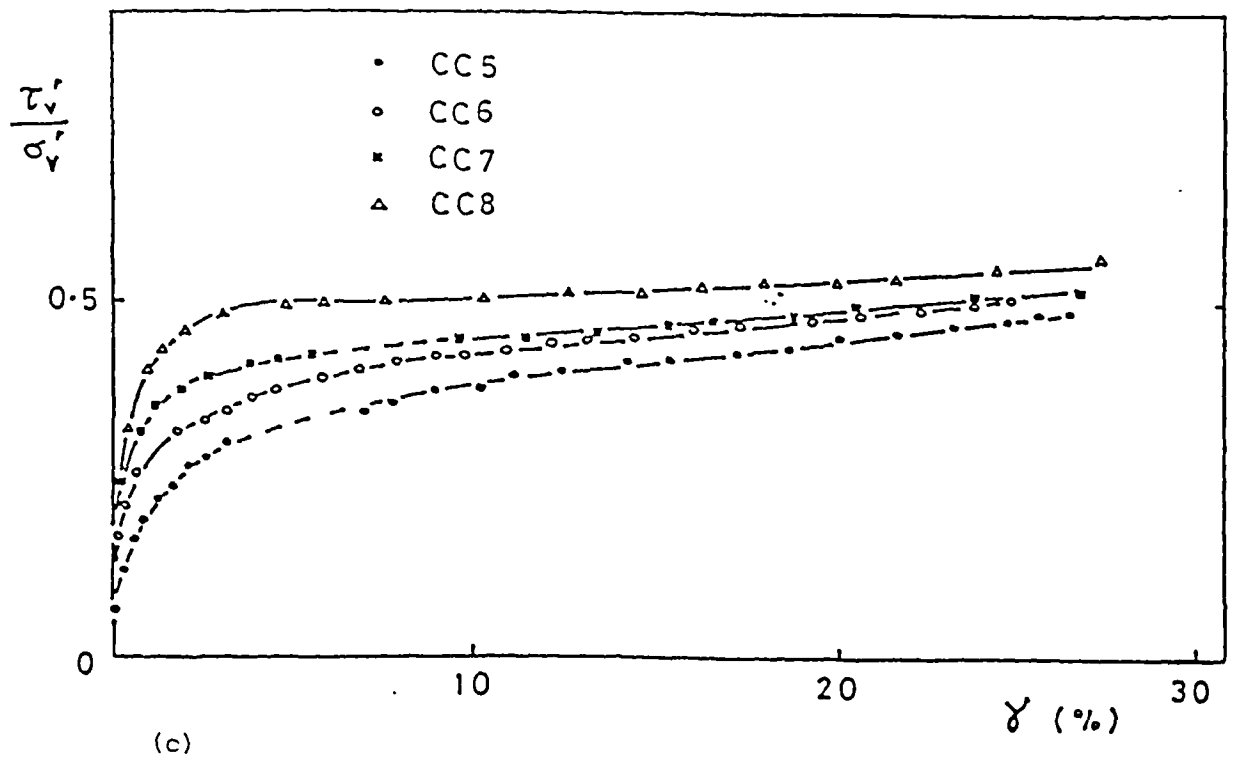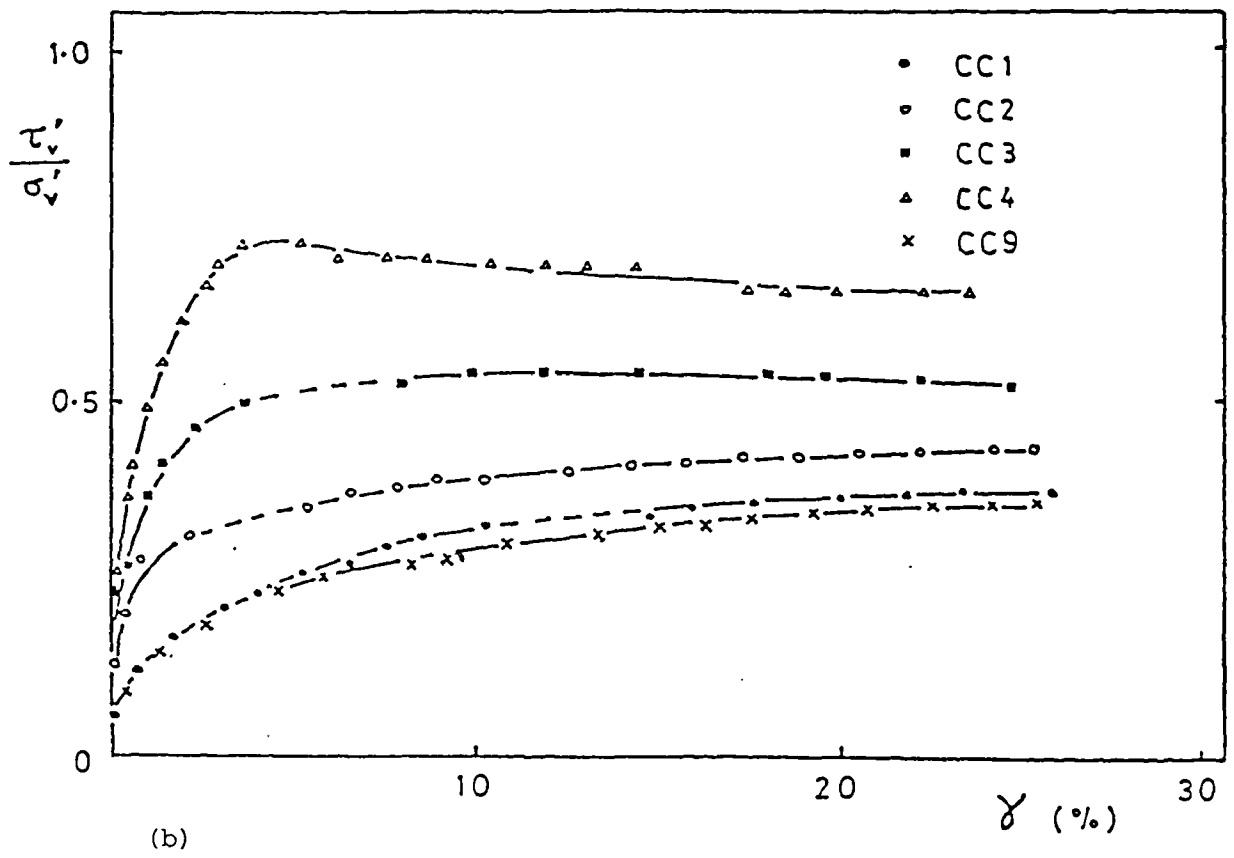
Figure 7.4 continued
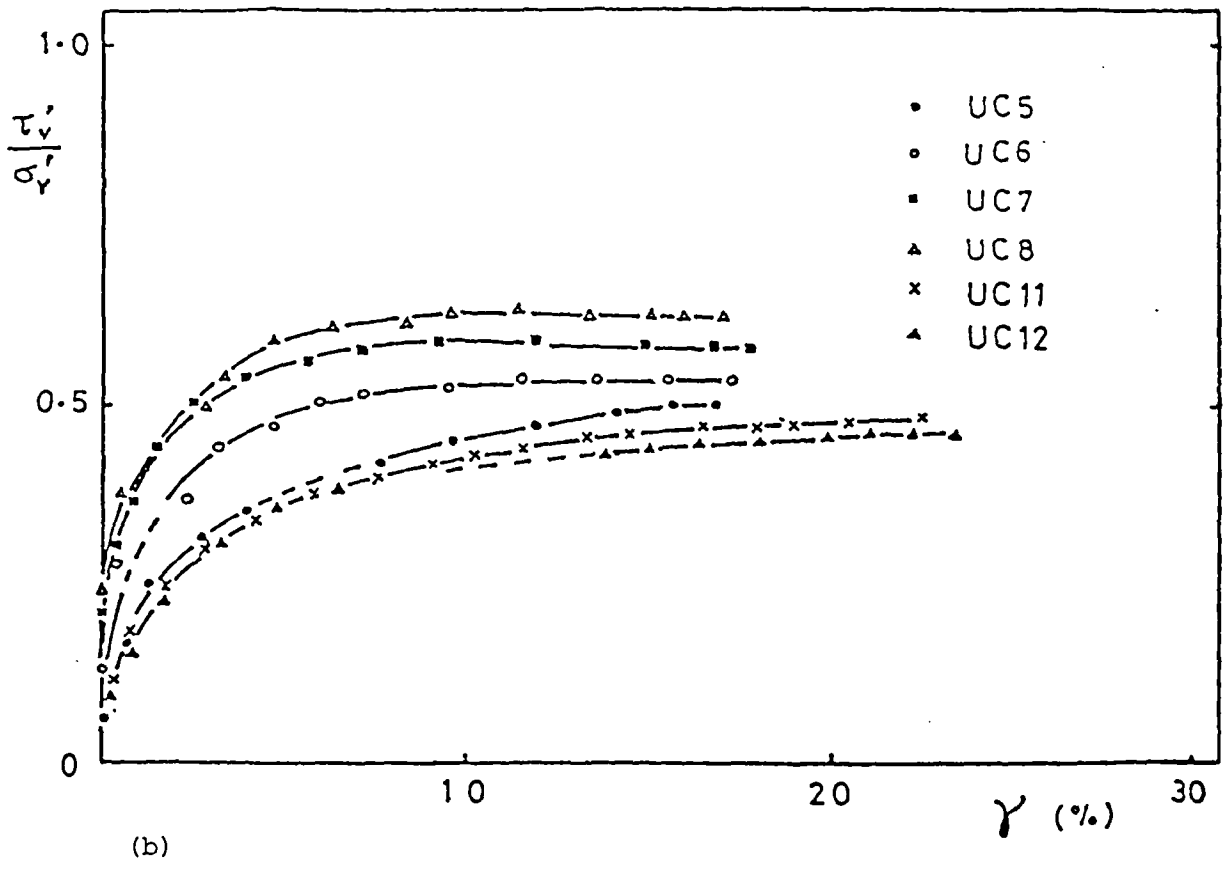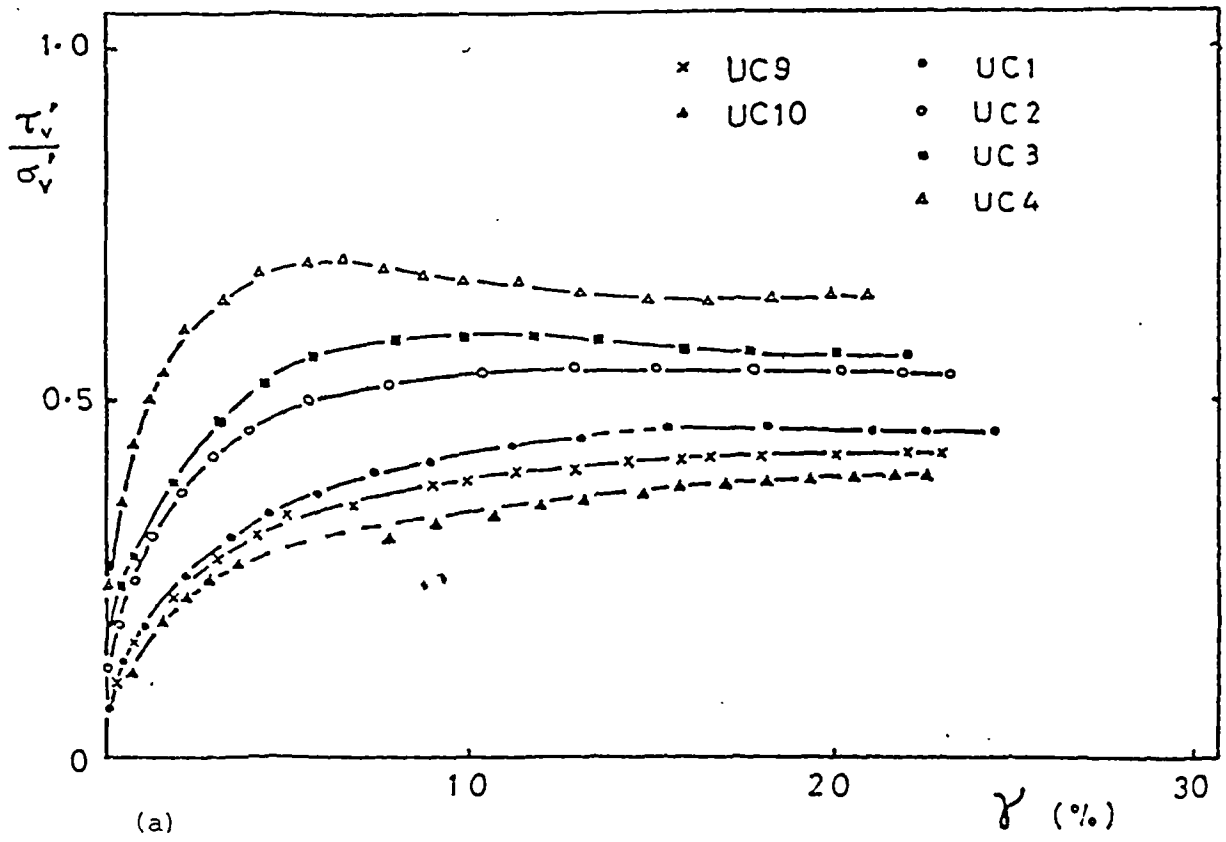
Figure 7.5   Variation of stress ratio with shear strain for
undisturbed Cowden till simple shear samples
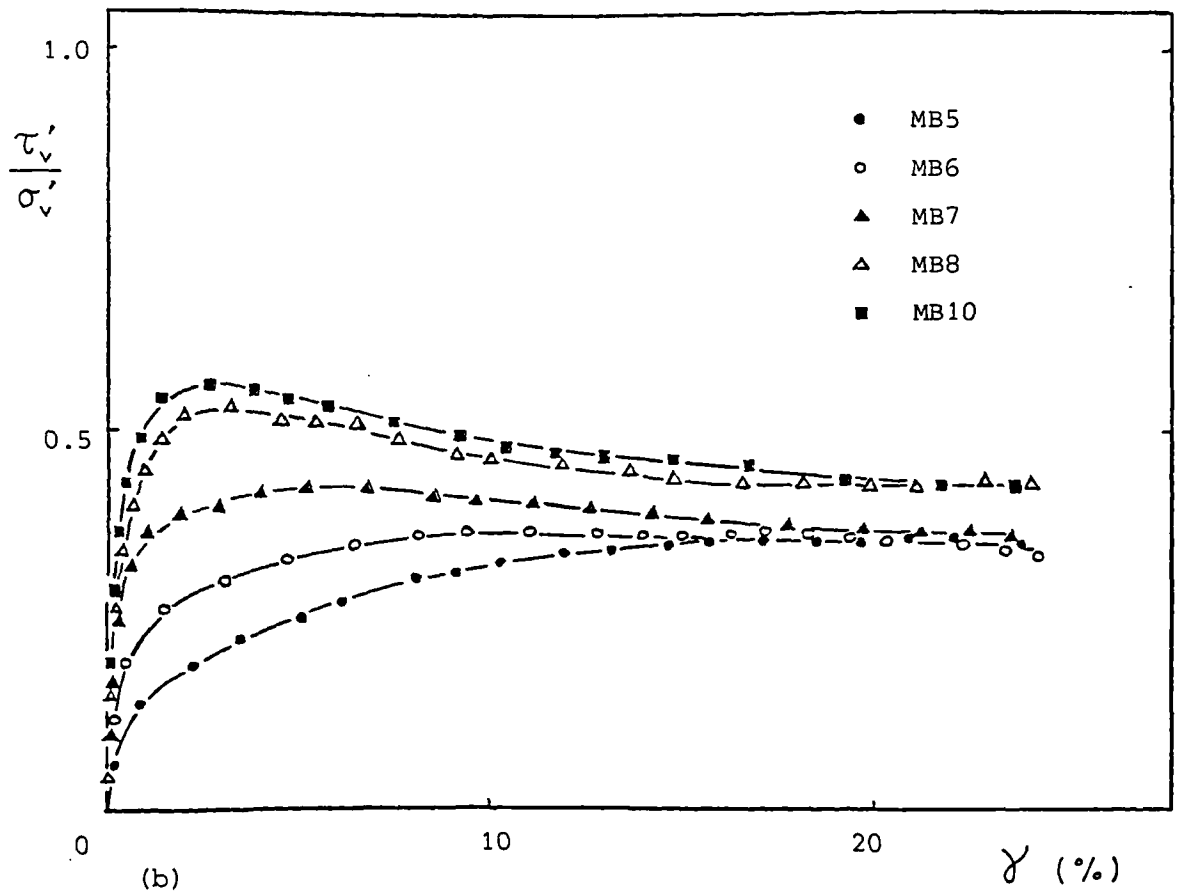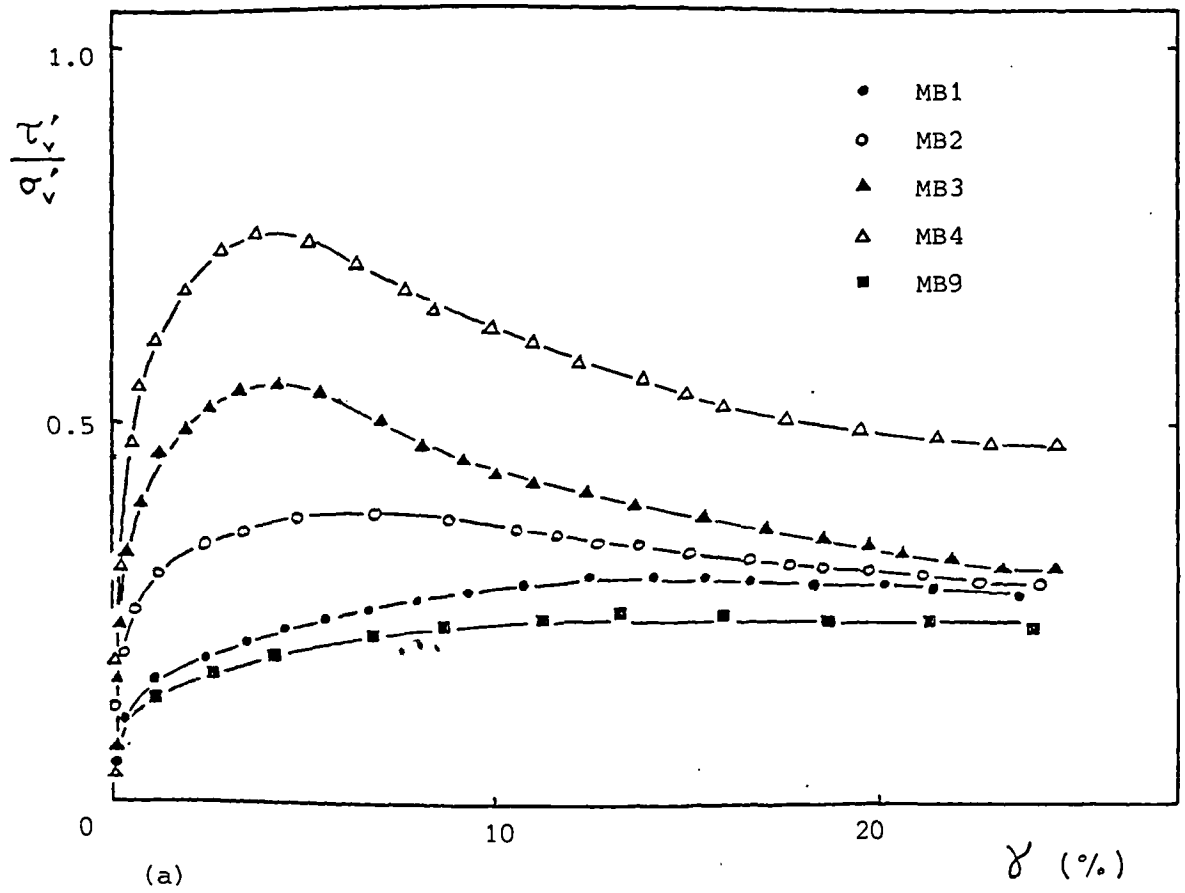
Figure 7.6   Variation of stress ratio with shear strain for
            remoulded London clay (brown) simple shear samples
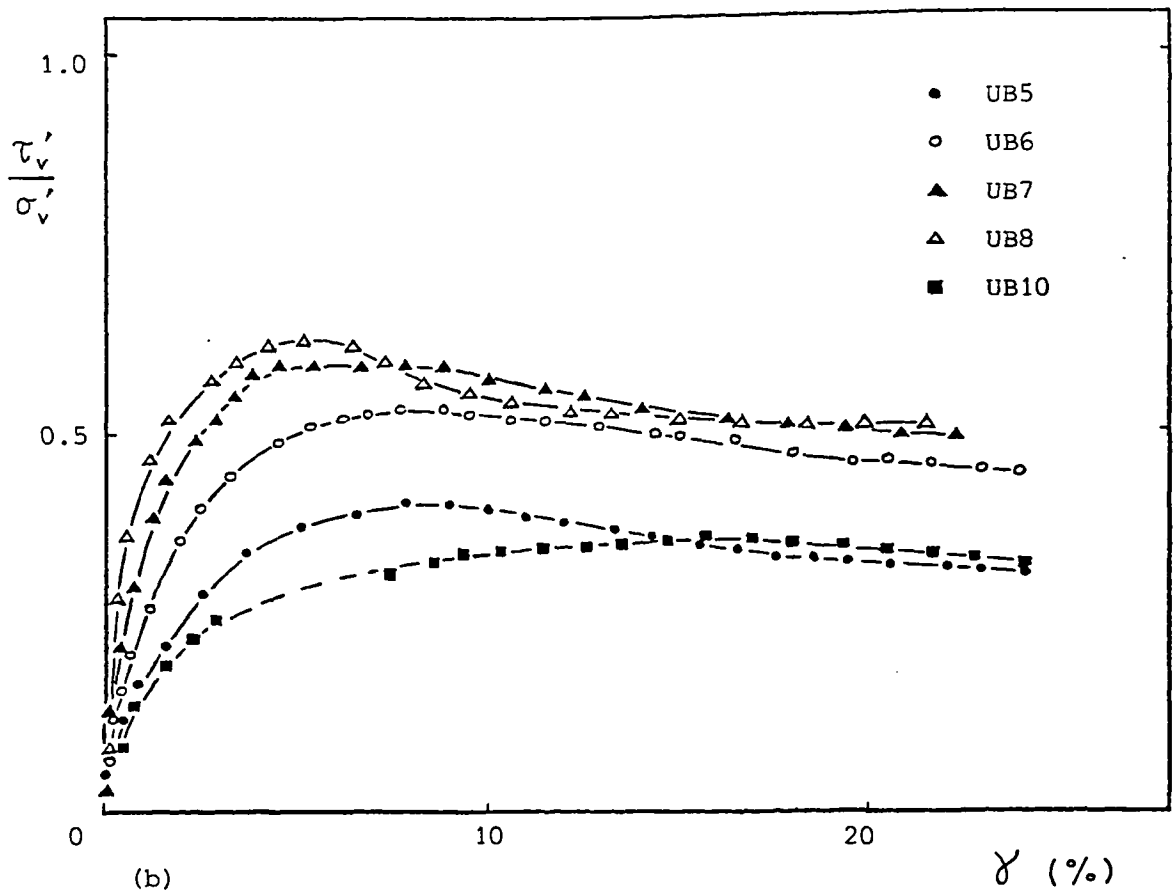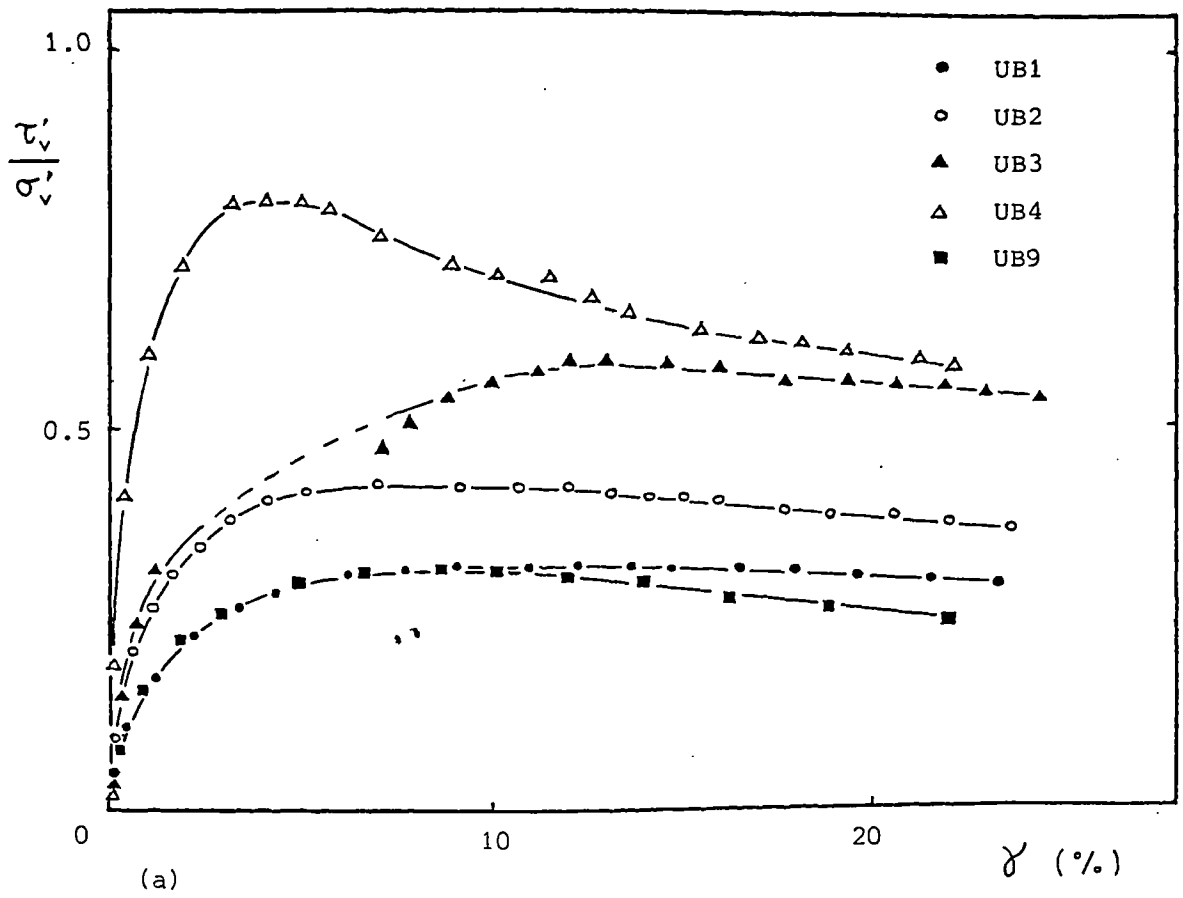
Figure 7.7 Variation of stress ratio with shear strain for undisturbed London clay (brown) simple shear samples
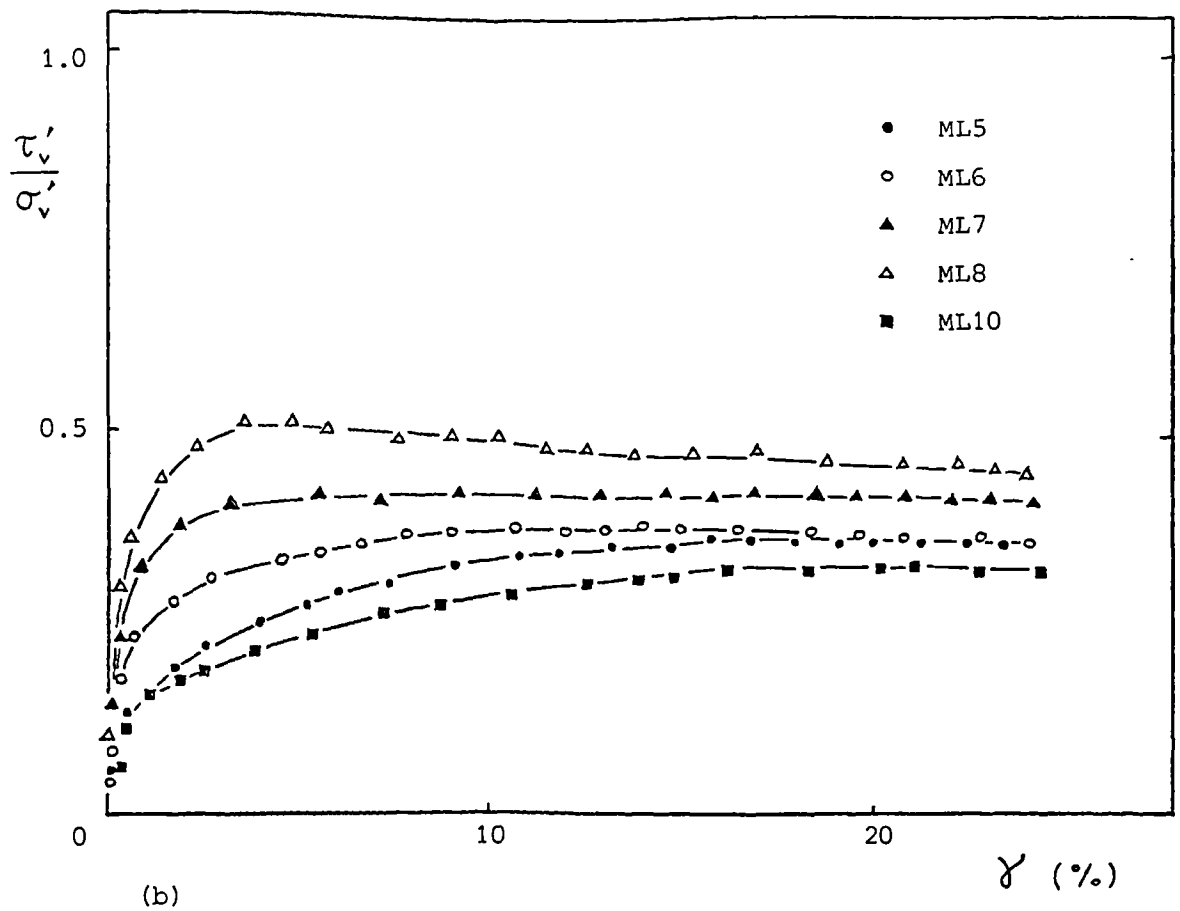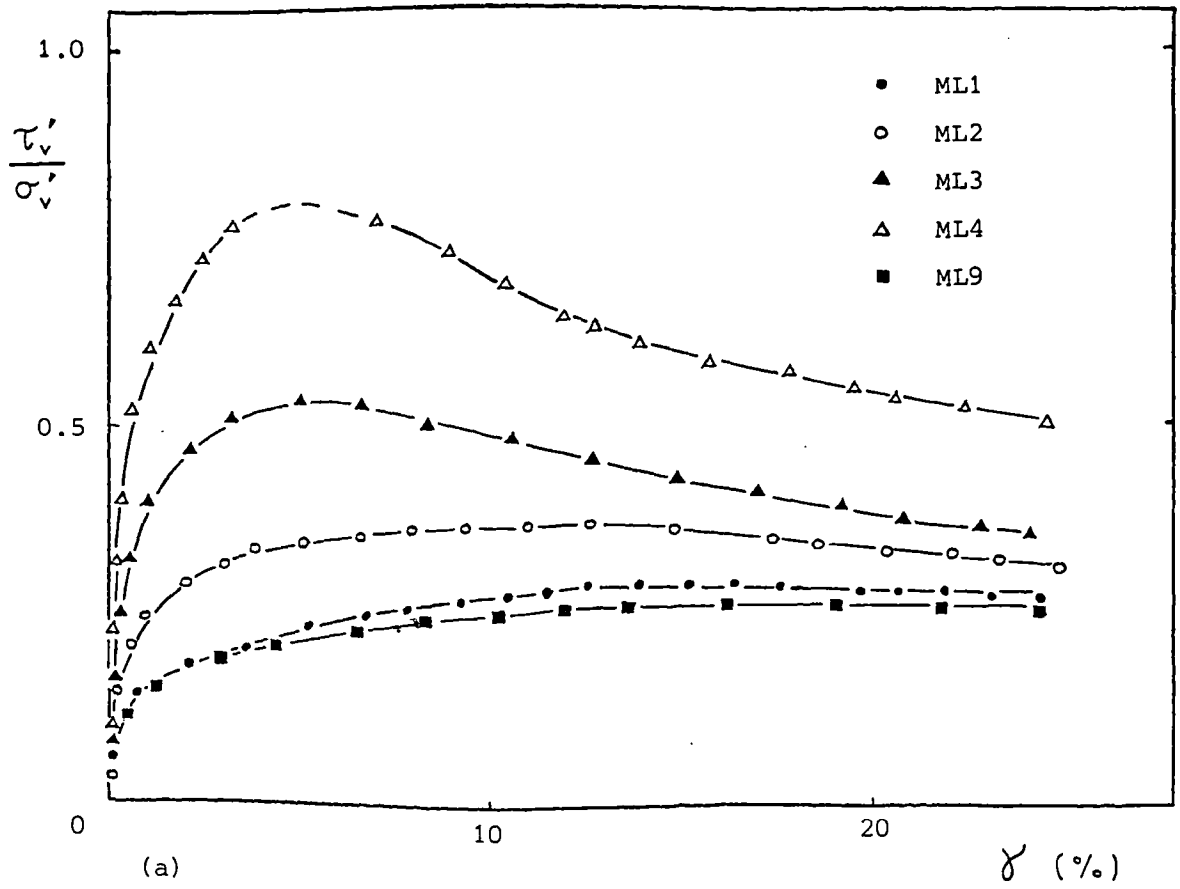
Figure 7.8   Variation of stress ratio with shear strain for
remoulded London clay (blue) simple shear samples
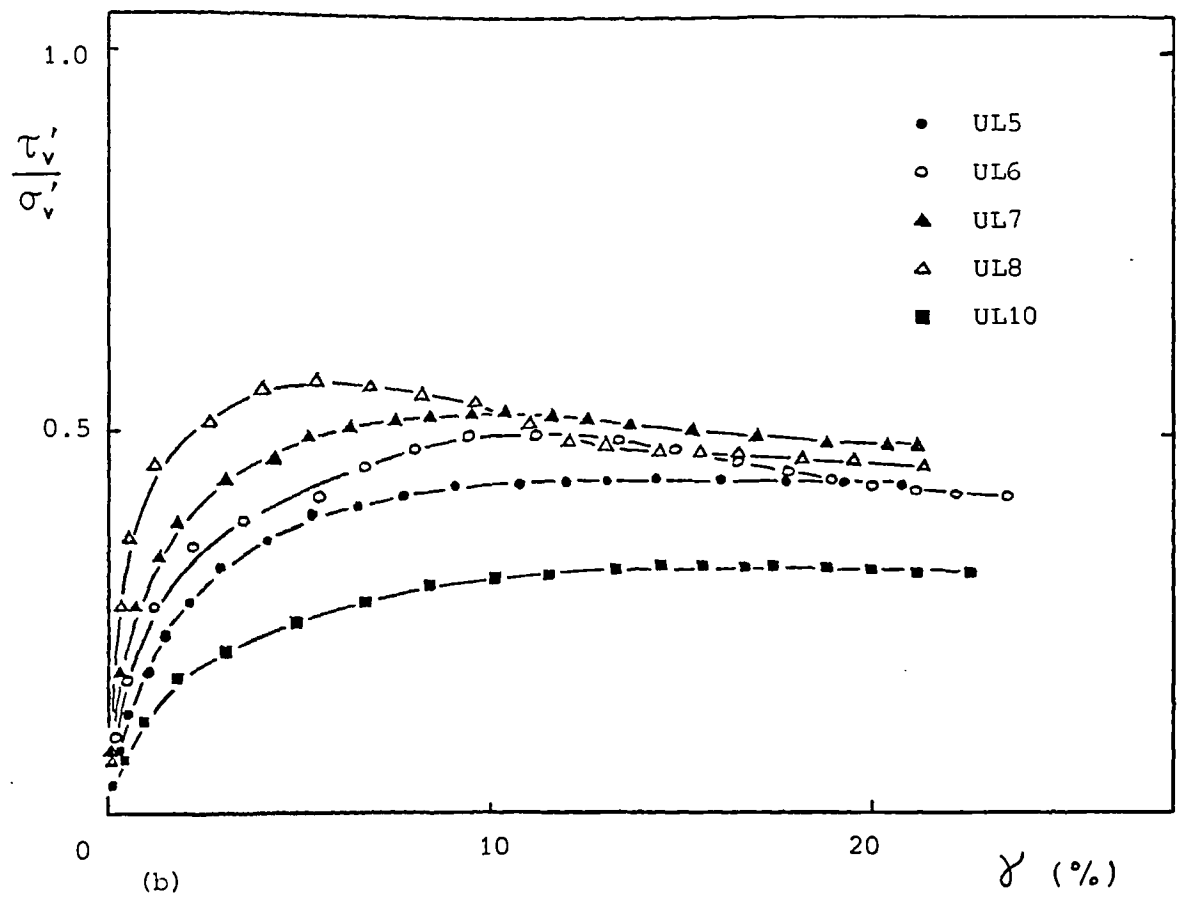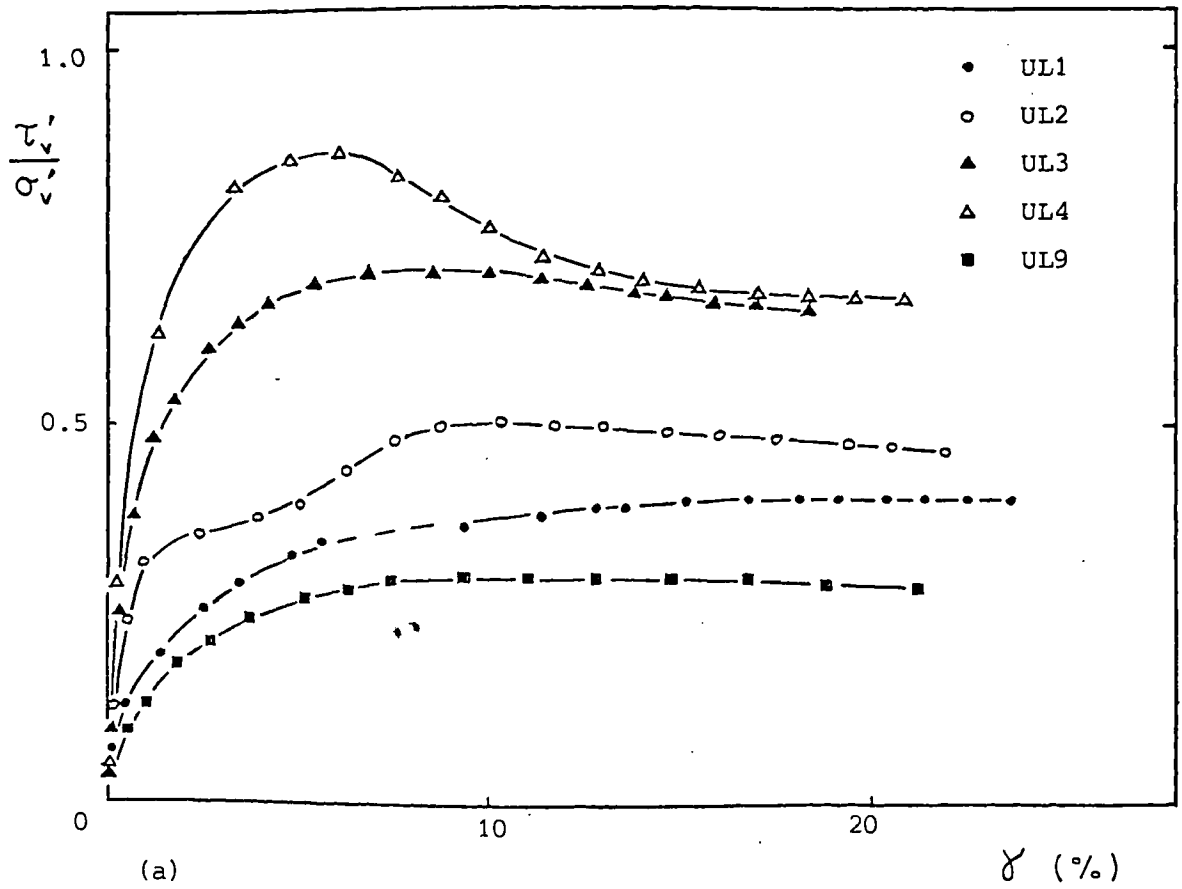
Figure 7.9 Variation of stress ratio with shear strain for undisturbed London clay (blue) simple shear samples
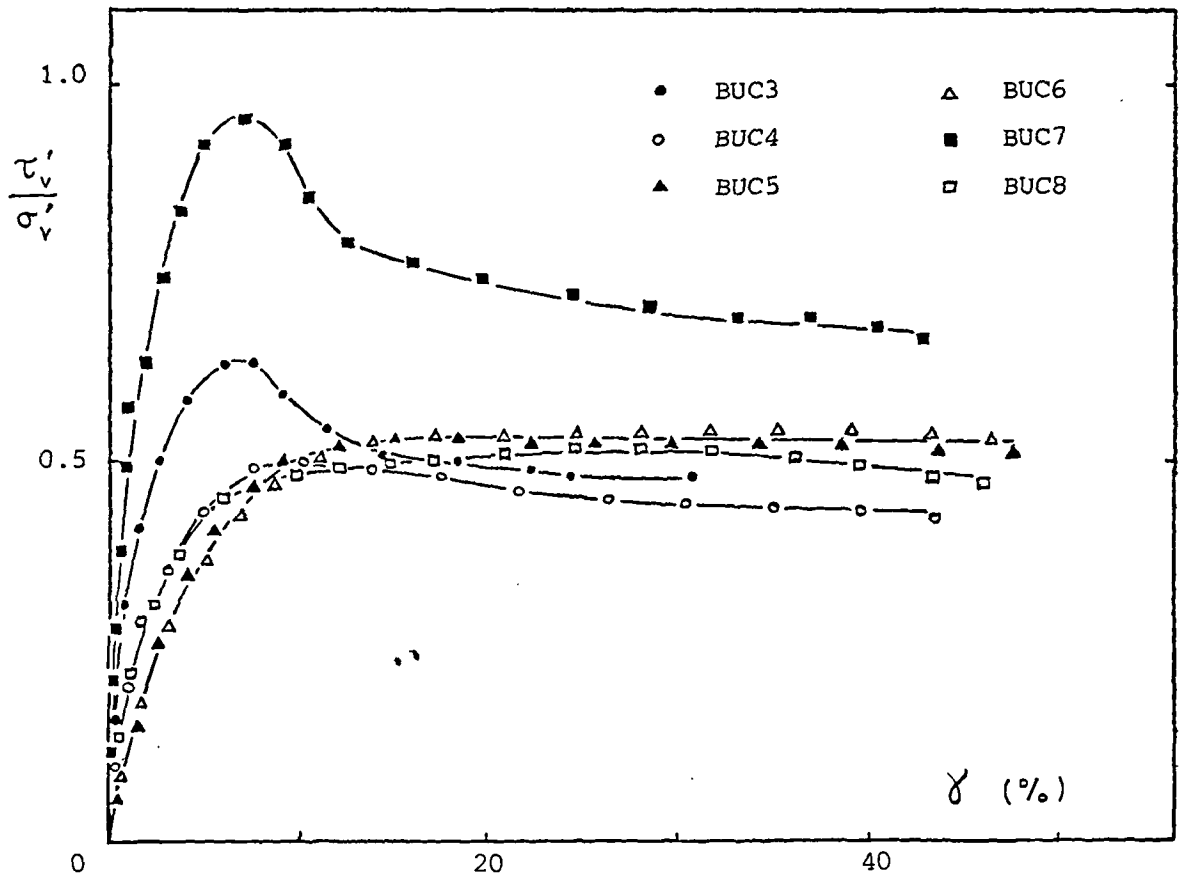
Figure 7.10   Variation of stress ratio with shear strain for undisturbed Cowden till shear box samples
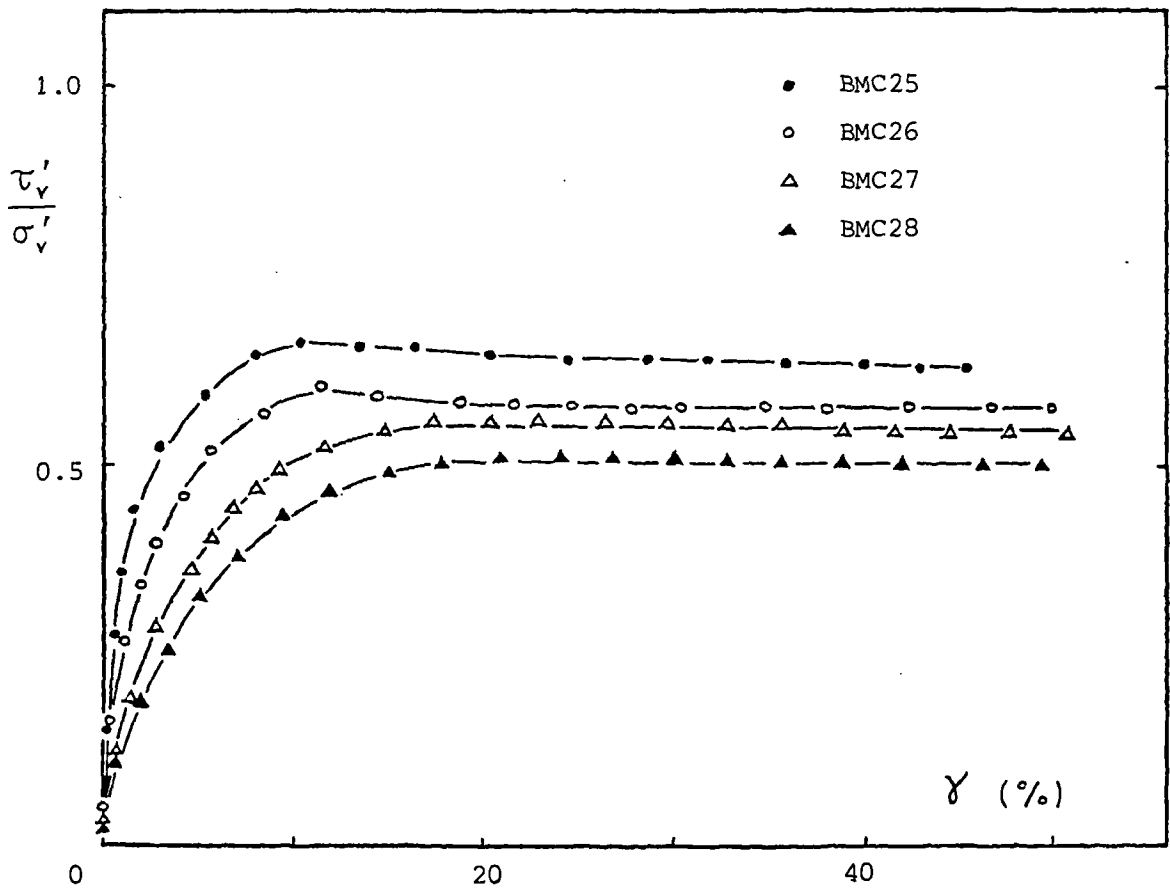
Figure 7.11   Variation of stress ratio with shear strain for remoulded Cowden till shear box samples
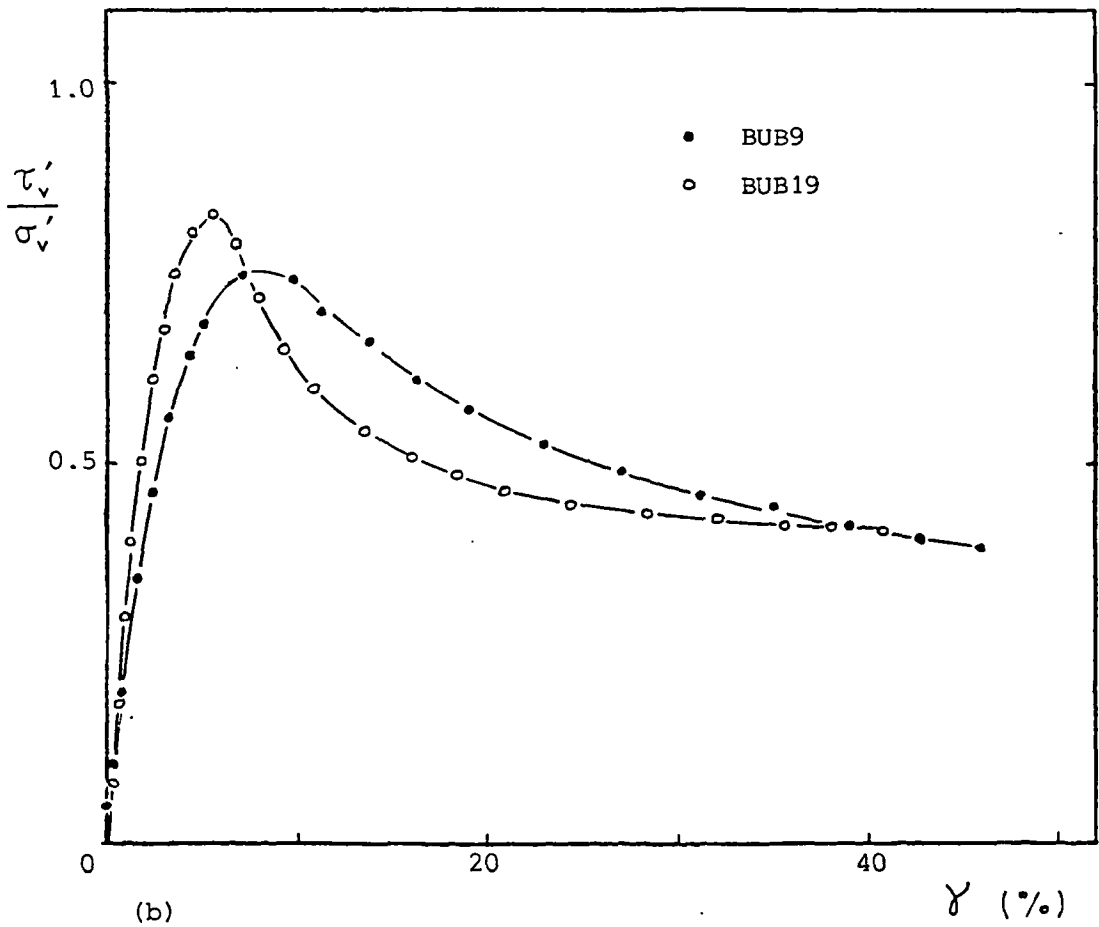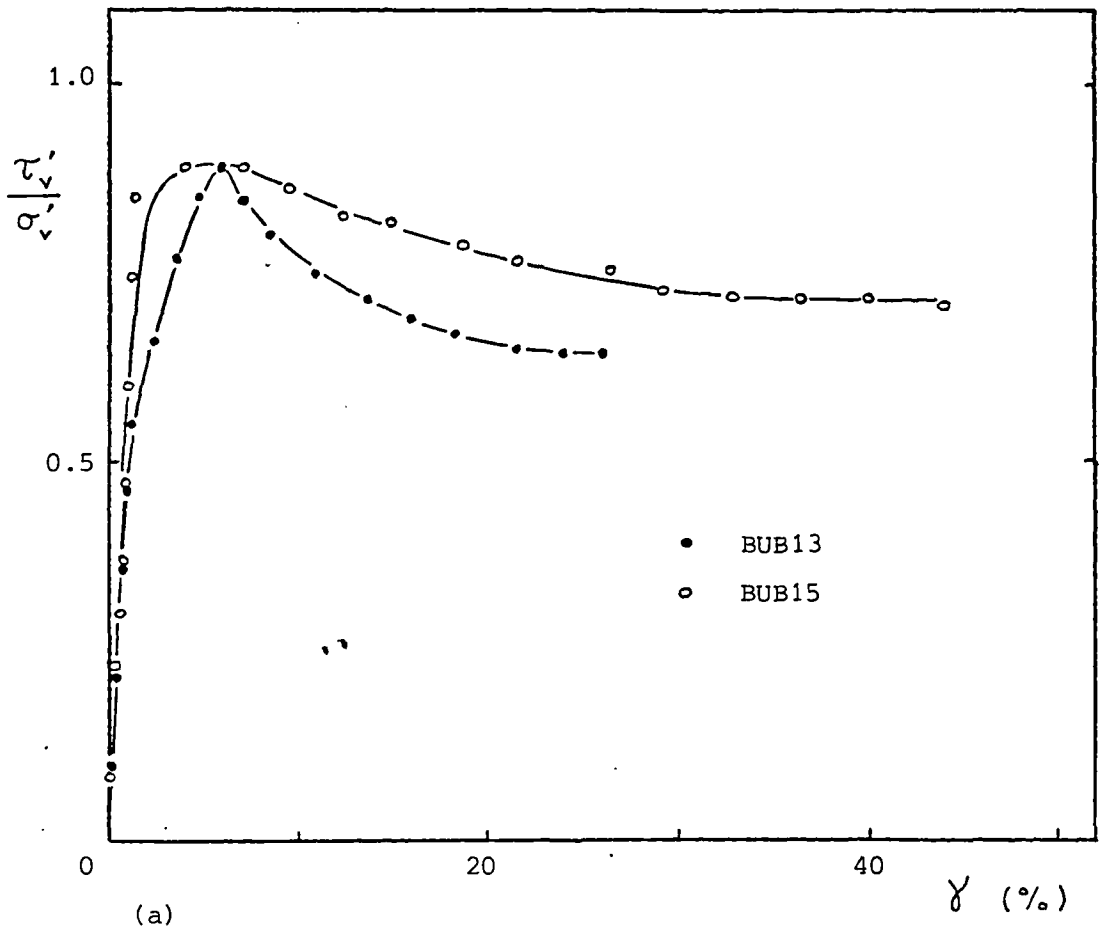
Figure 7.12   Variation of stress ratio with shear strain for
undisturbed London clay (brown) shear box samples

(c)

(d)
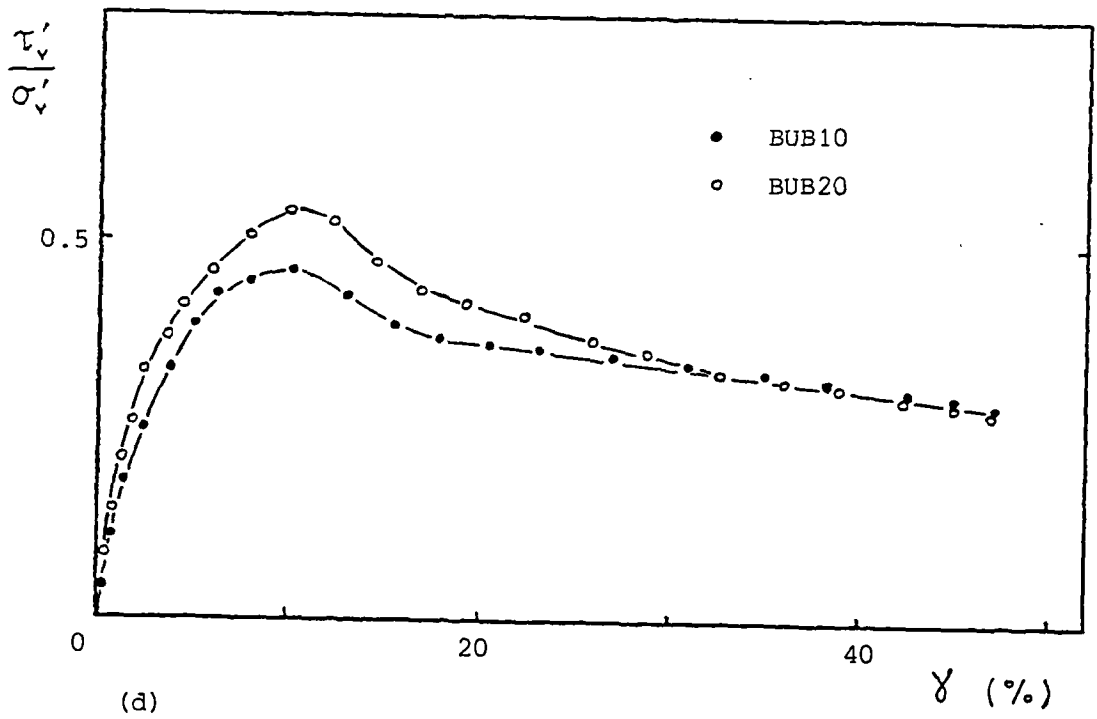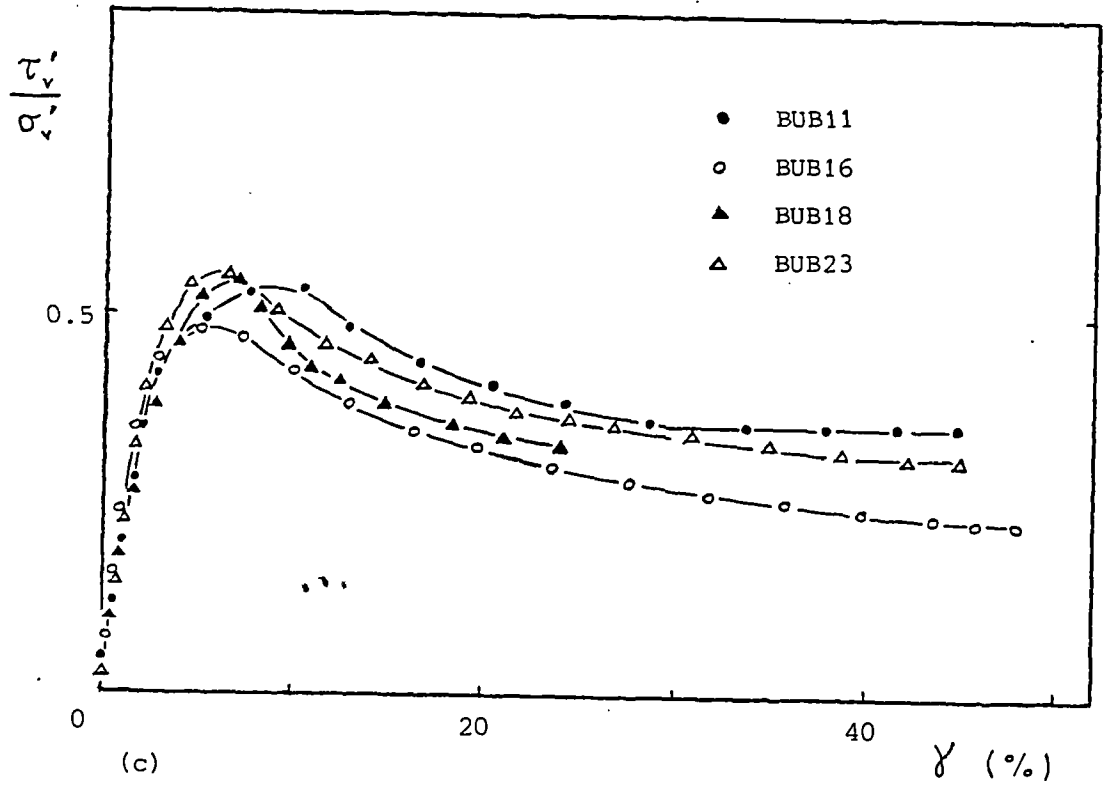
Figure 7.12 continued
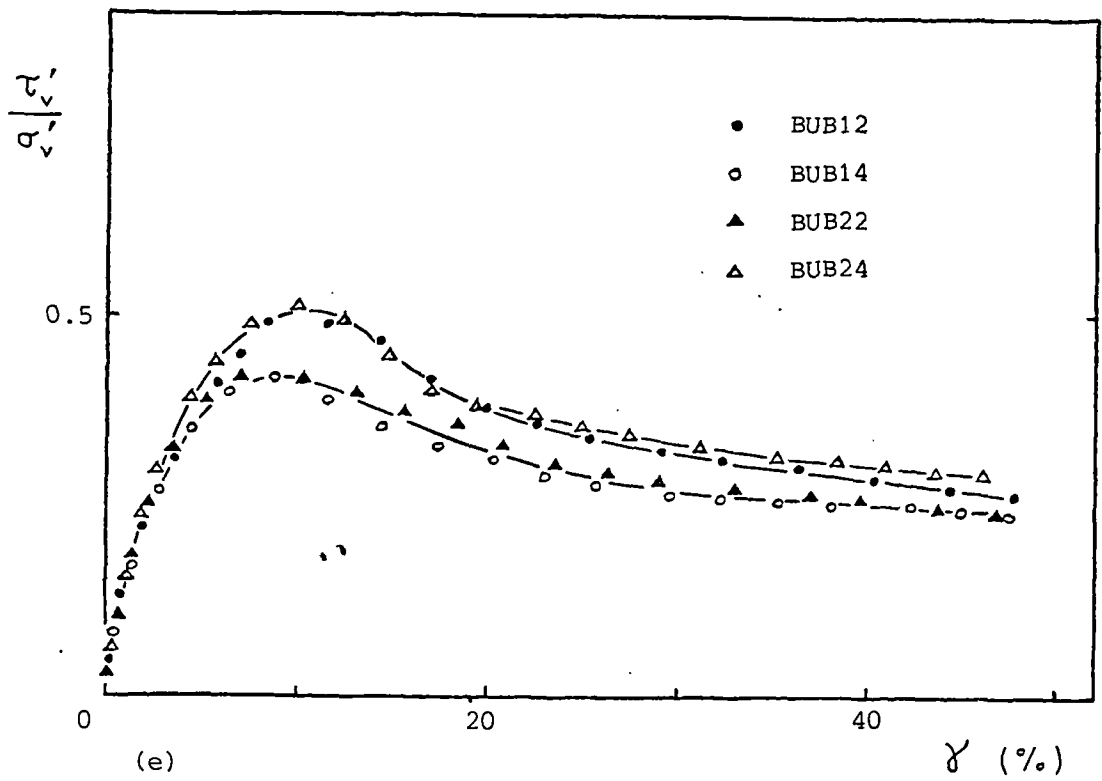
Figure 7.12 continued
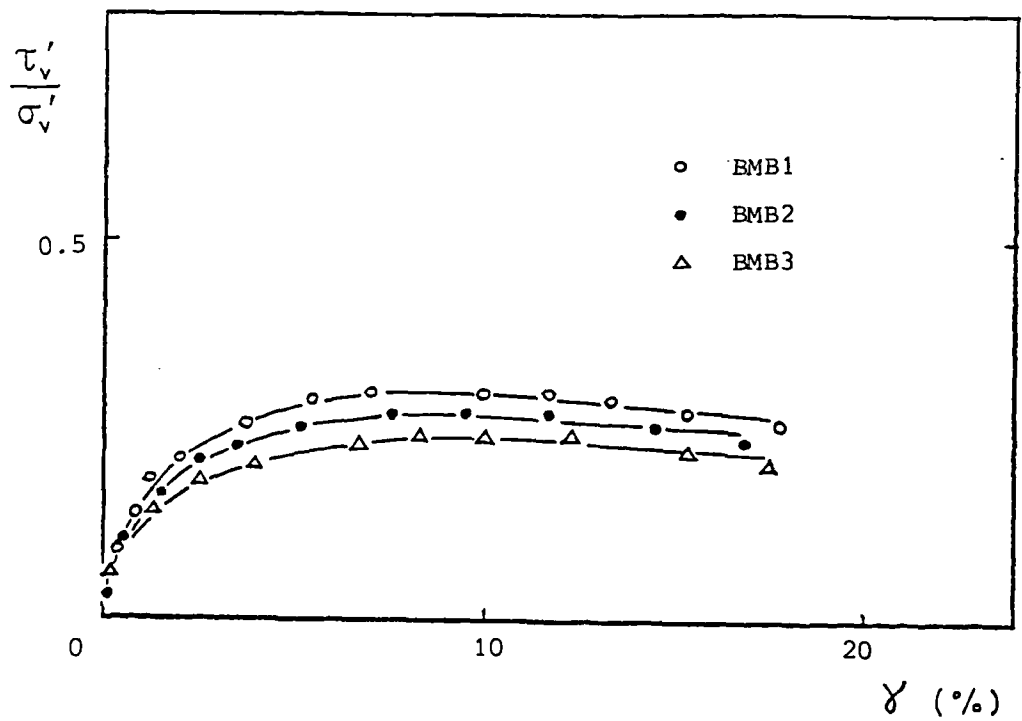
Figure 7.13   Variation of stress ratio with shear strain for
remoulded London clay (brown) shear box samples
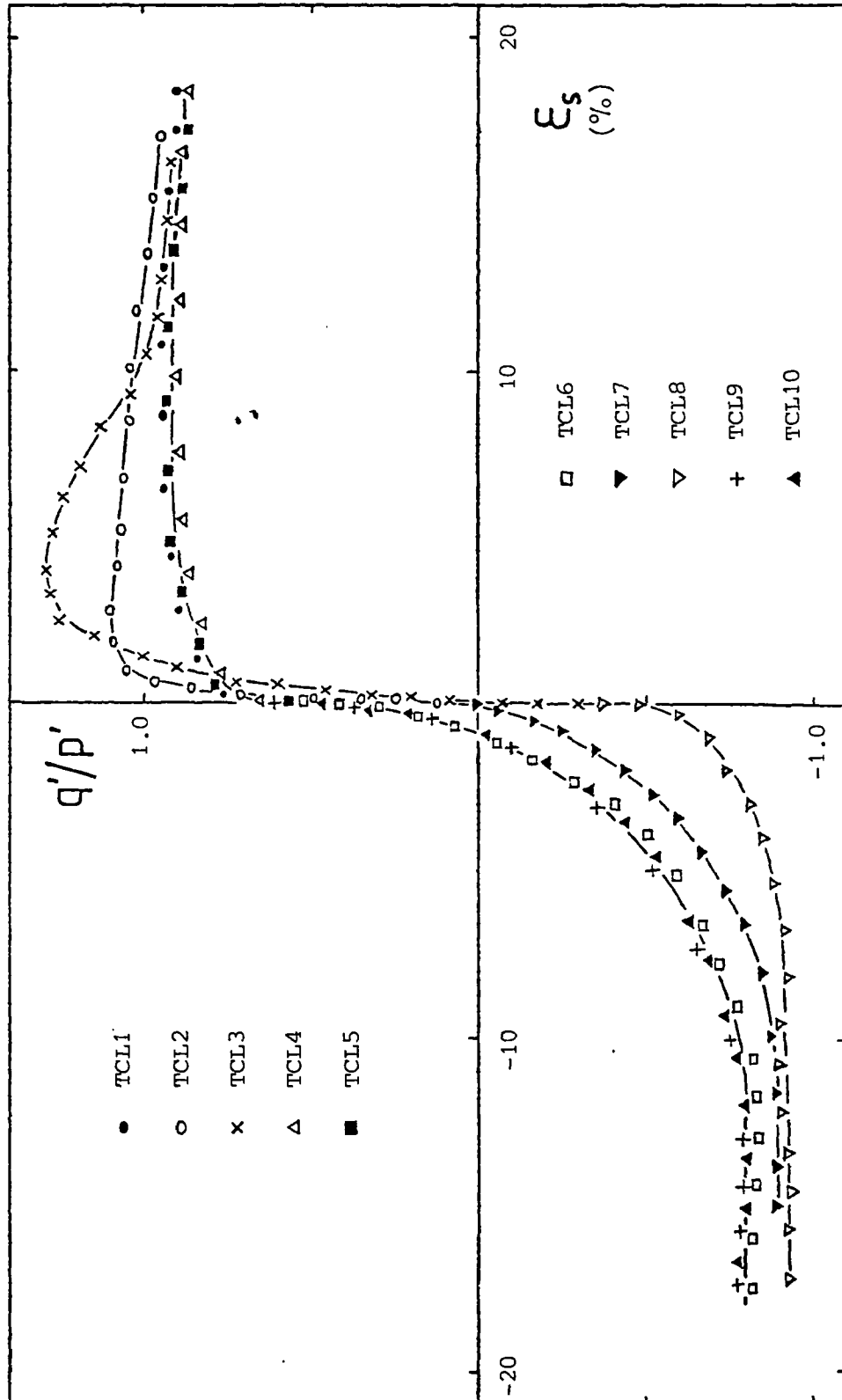
Figure 7.14   Variation of stress ratio with shear strain for
38 mm reconstituted London clay (blue) triaxial
samples
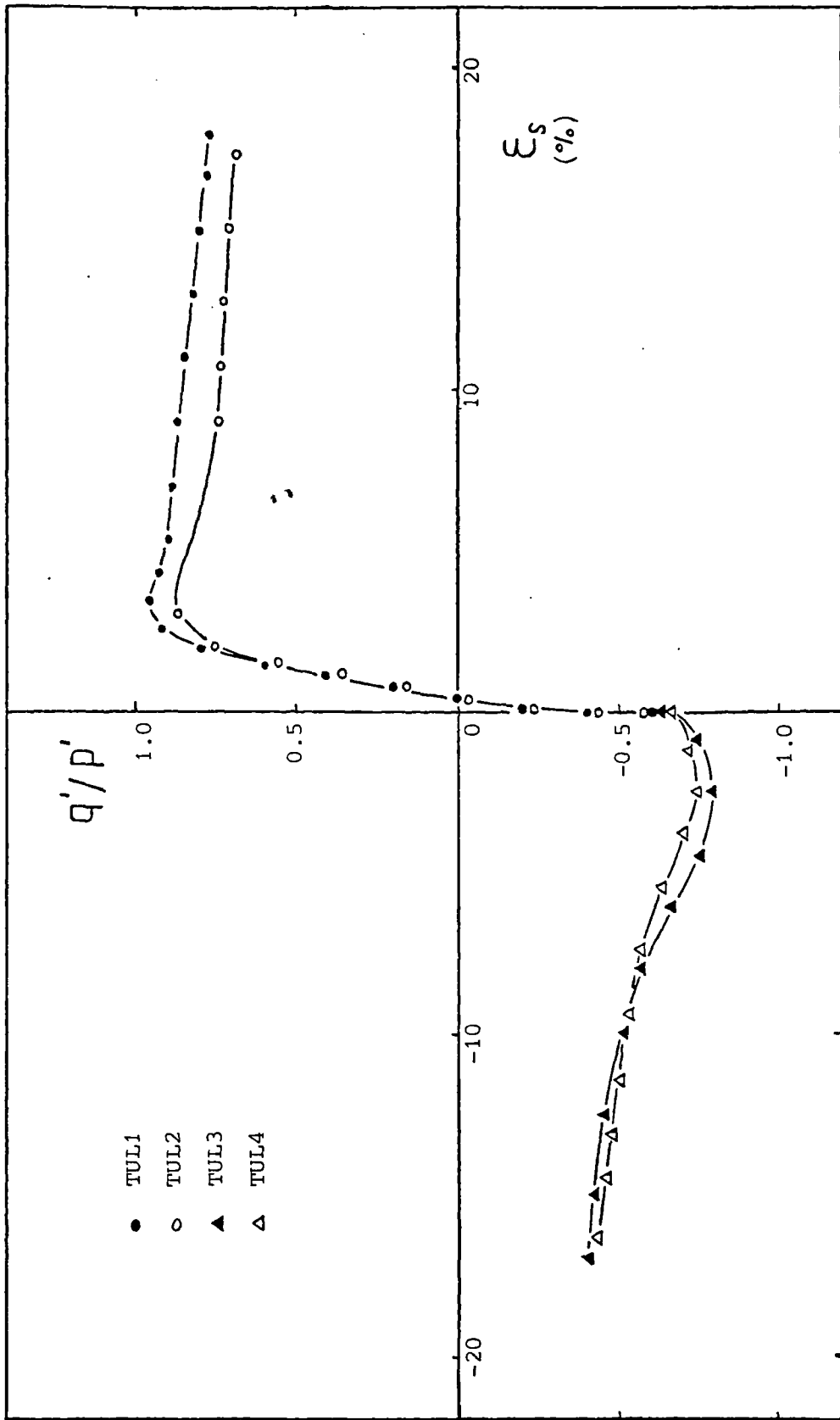
Figure 7.15   Variation of stress ratio with shear strain
for 100 mm undisturbed London clay (blue)
triaxial samples
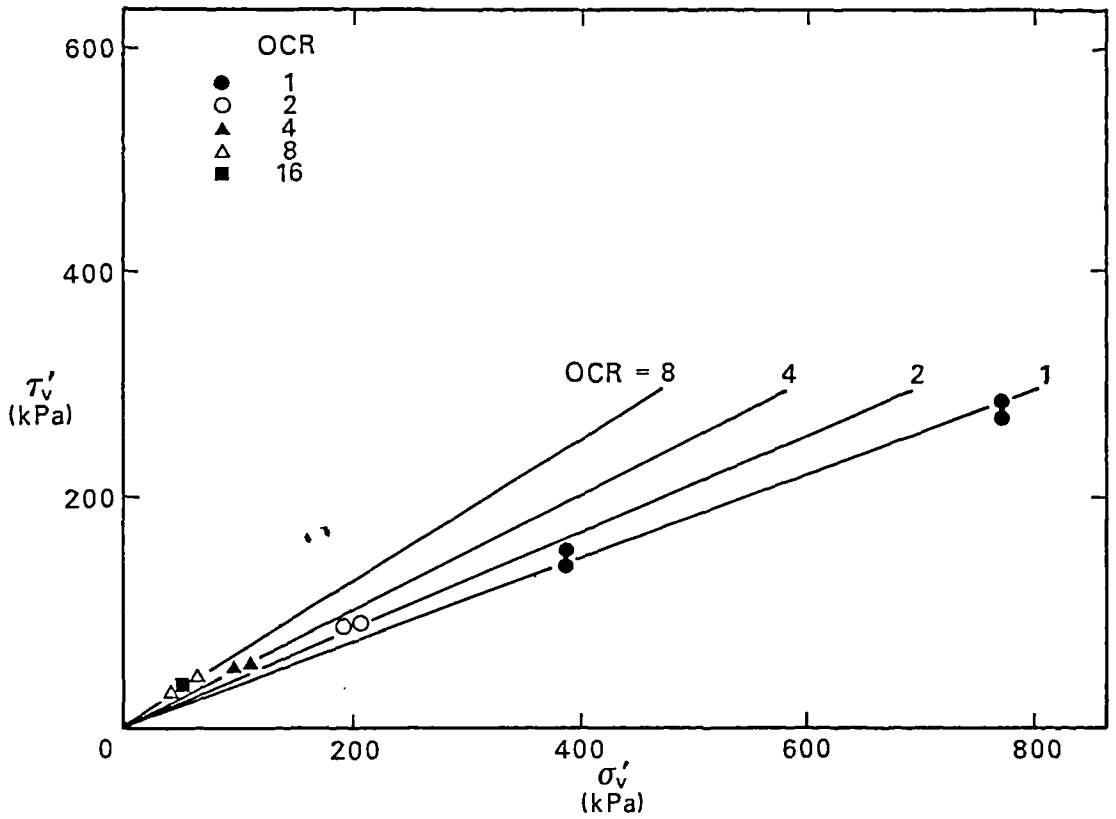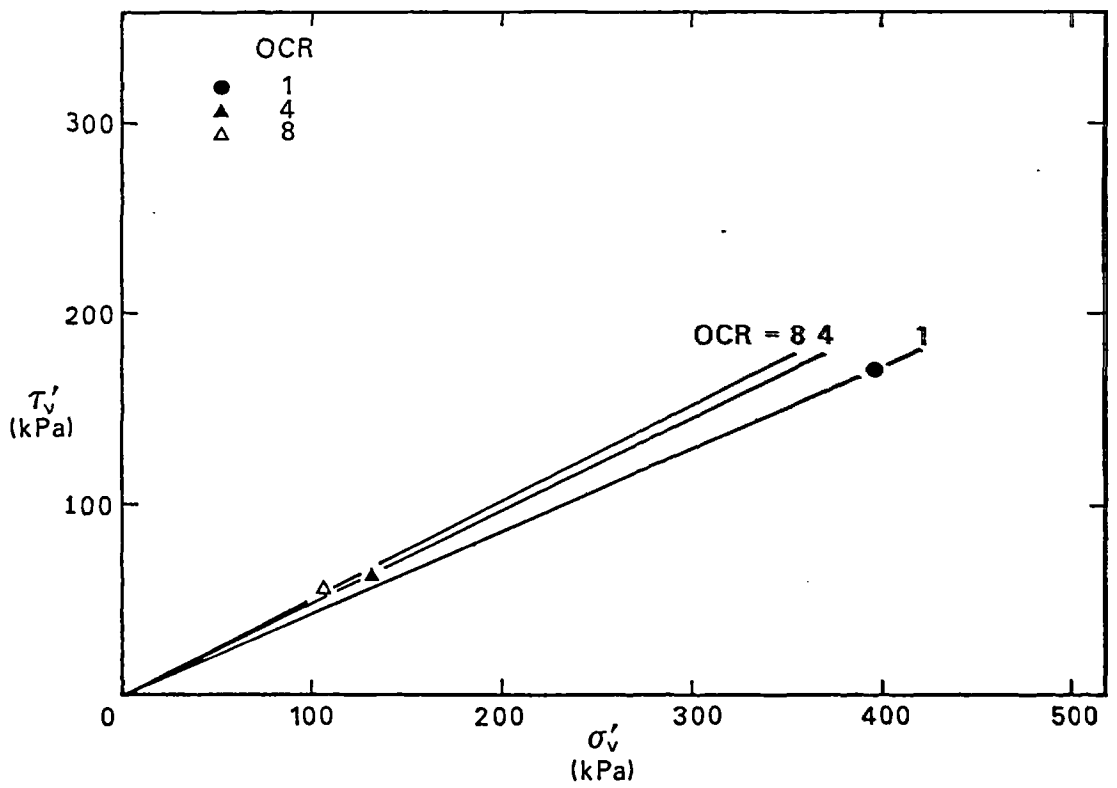
(a) constant σ_v' tests

(b) constant volume tests

Figure 7.16   Critical states for simple shear tests on remoulded
and reconstituted Cowden till
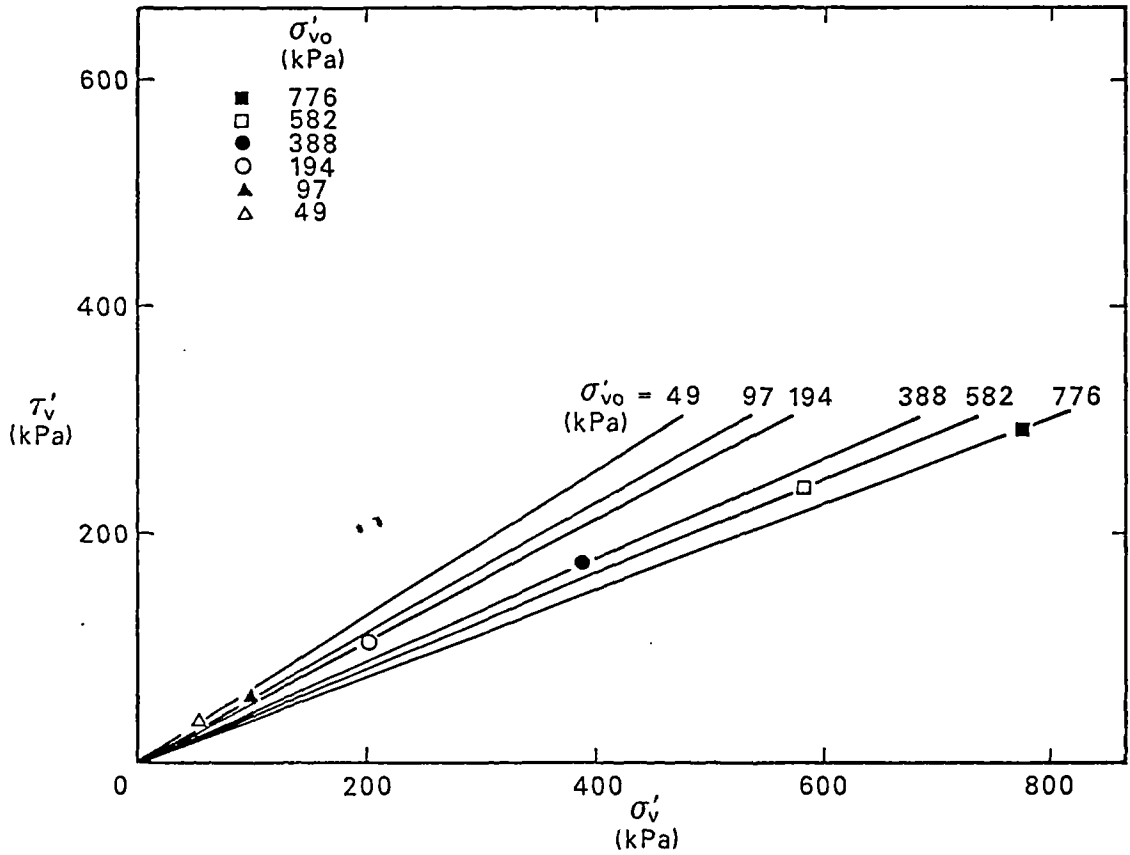
(a) constant σ_v' tests
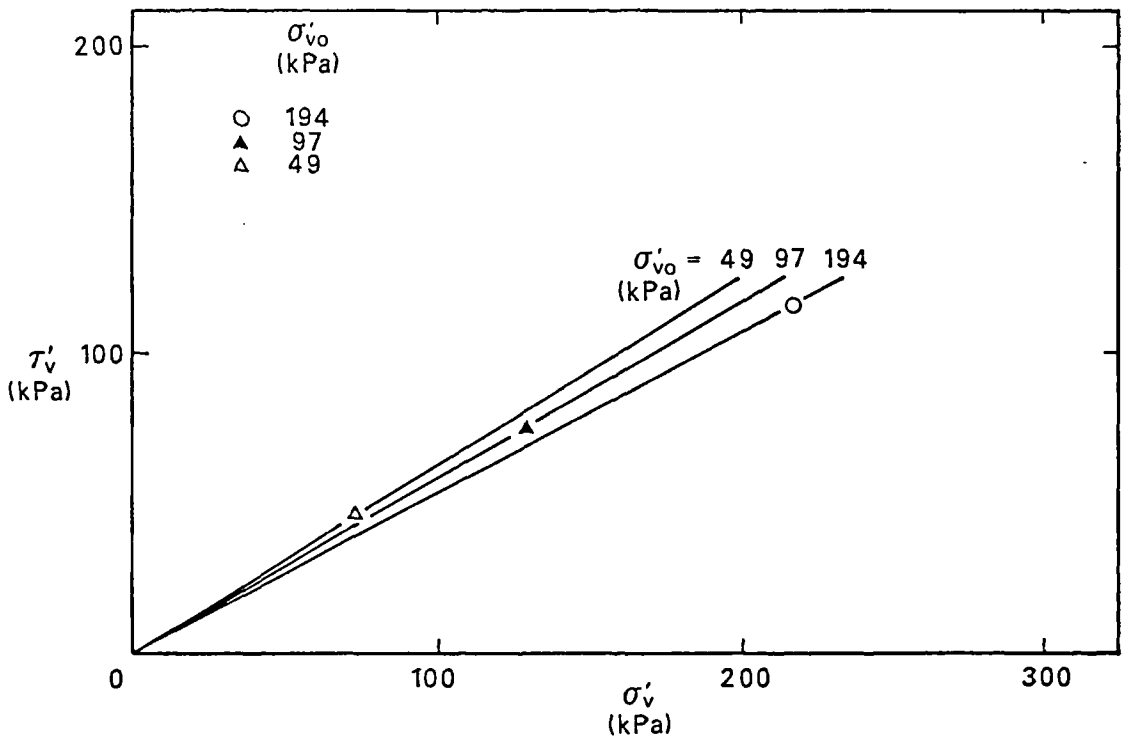
(b) constant volume tests

Figure 7.17   Critical states for simple shear tests on undisturbed
                 Cowden till
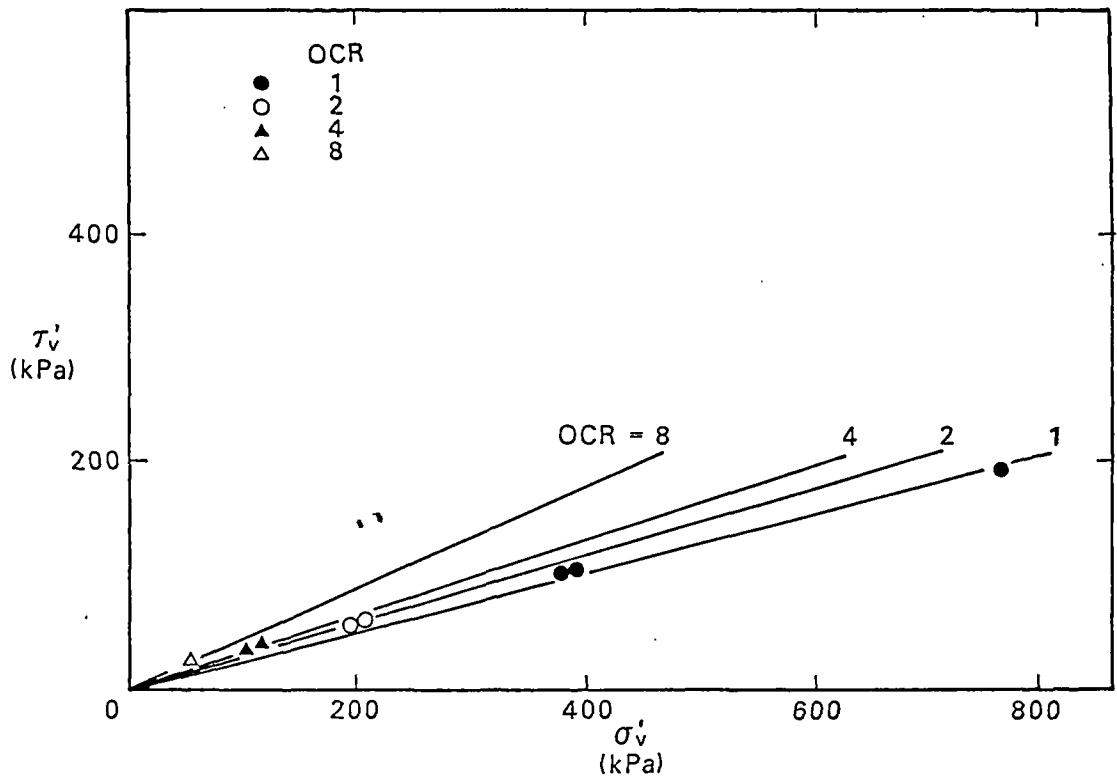
(a) constant σ_v' tests
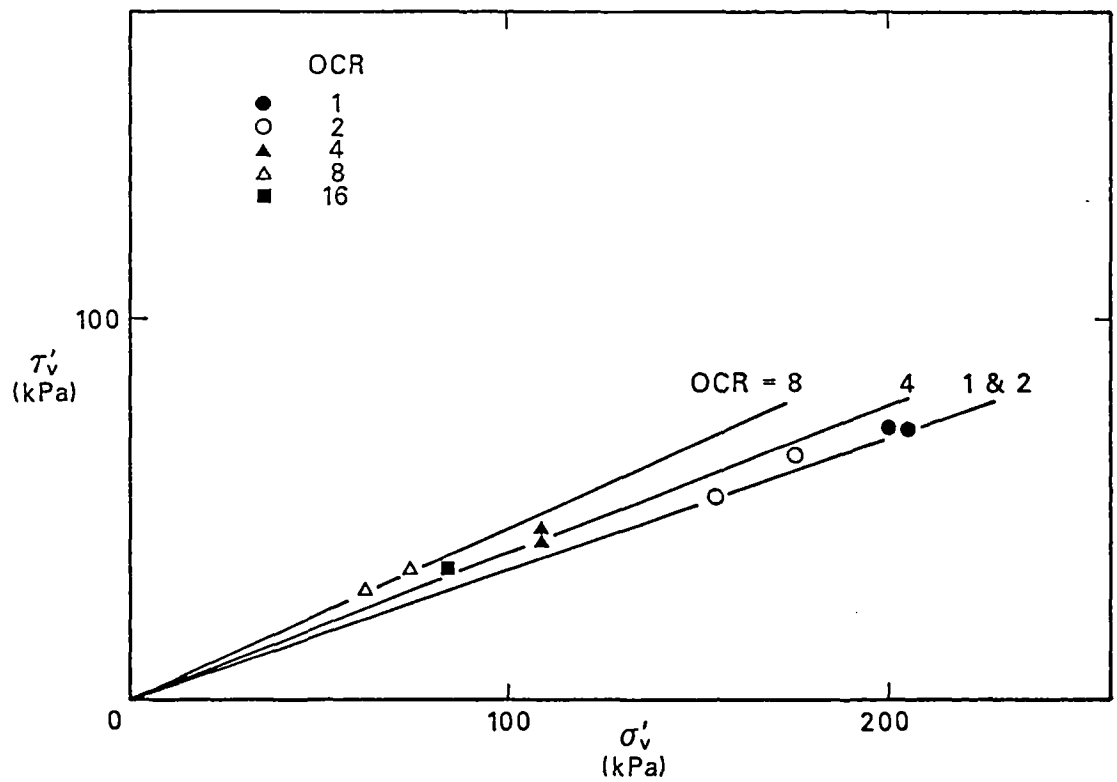
(b) constant volume tests

Figure 7.18   Critical states for simple shear tests on remoulded
London clay (brown and blue)
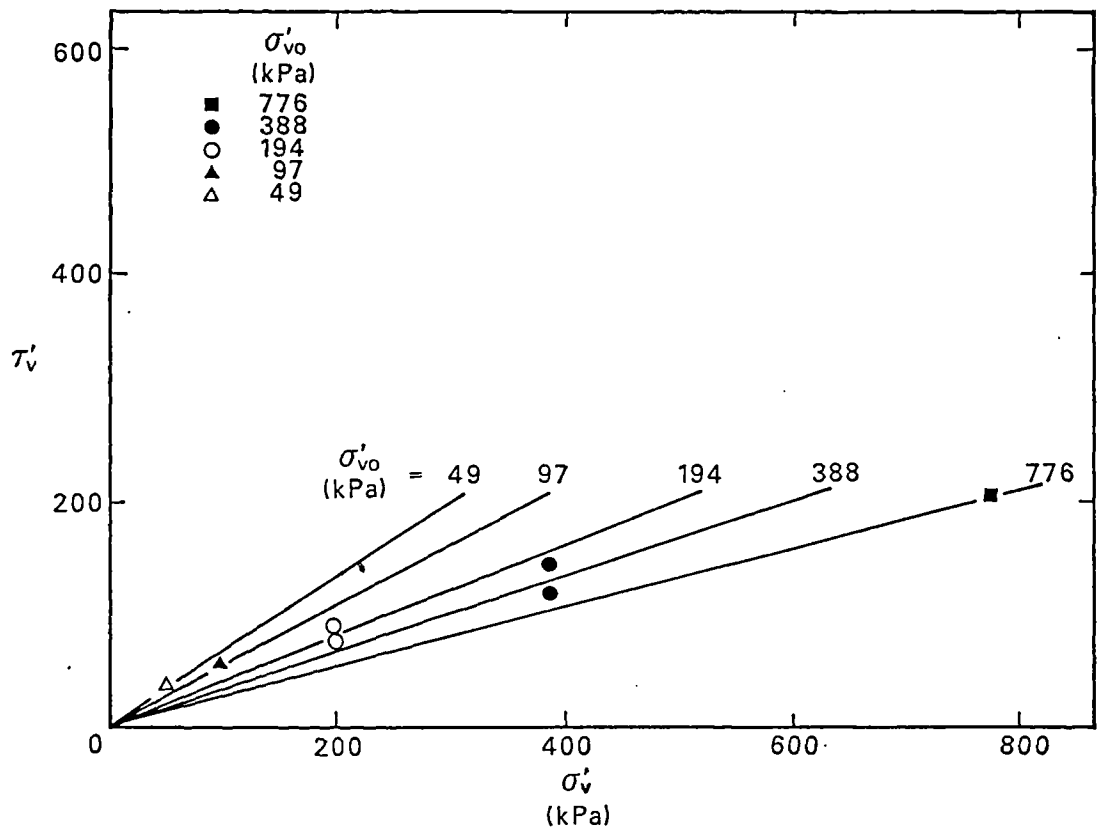
(a)   constant σ_v' tests
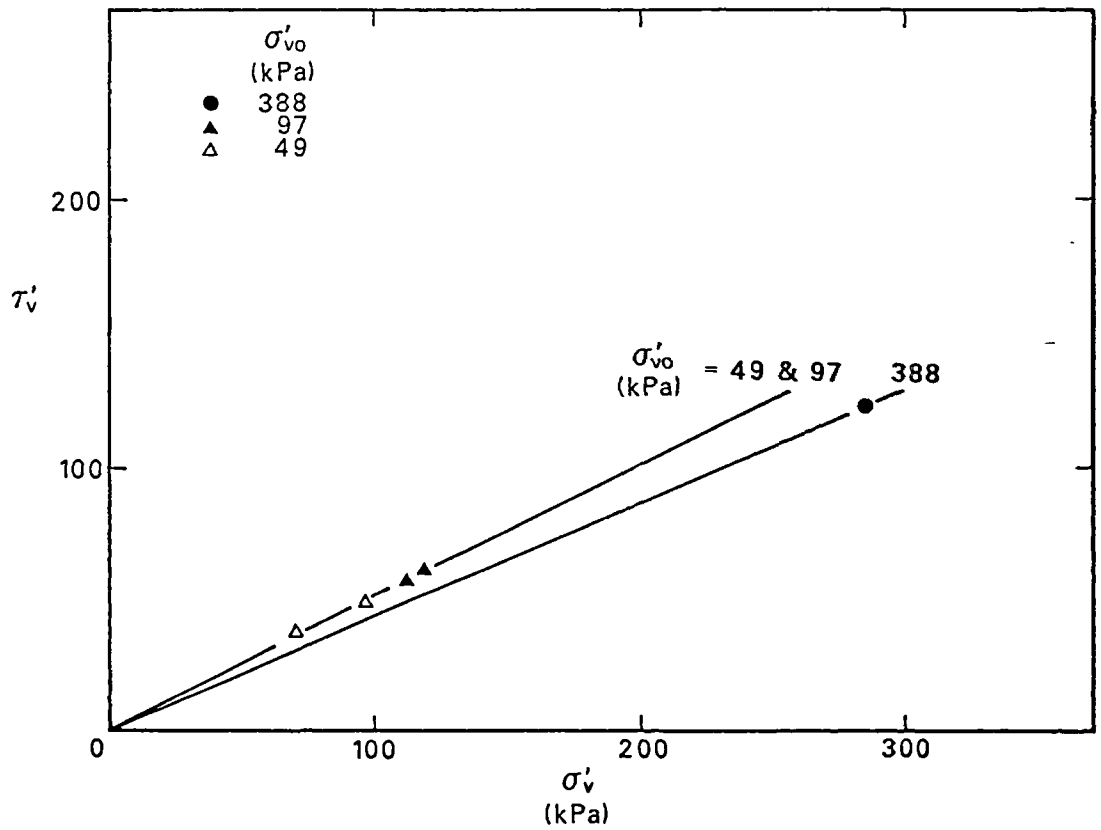
(b)   constant volume tests

Figure 7.19   Critical states for simple shear tests on undisturbed London clay (brown and blue)
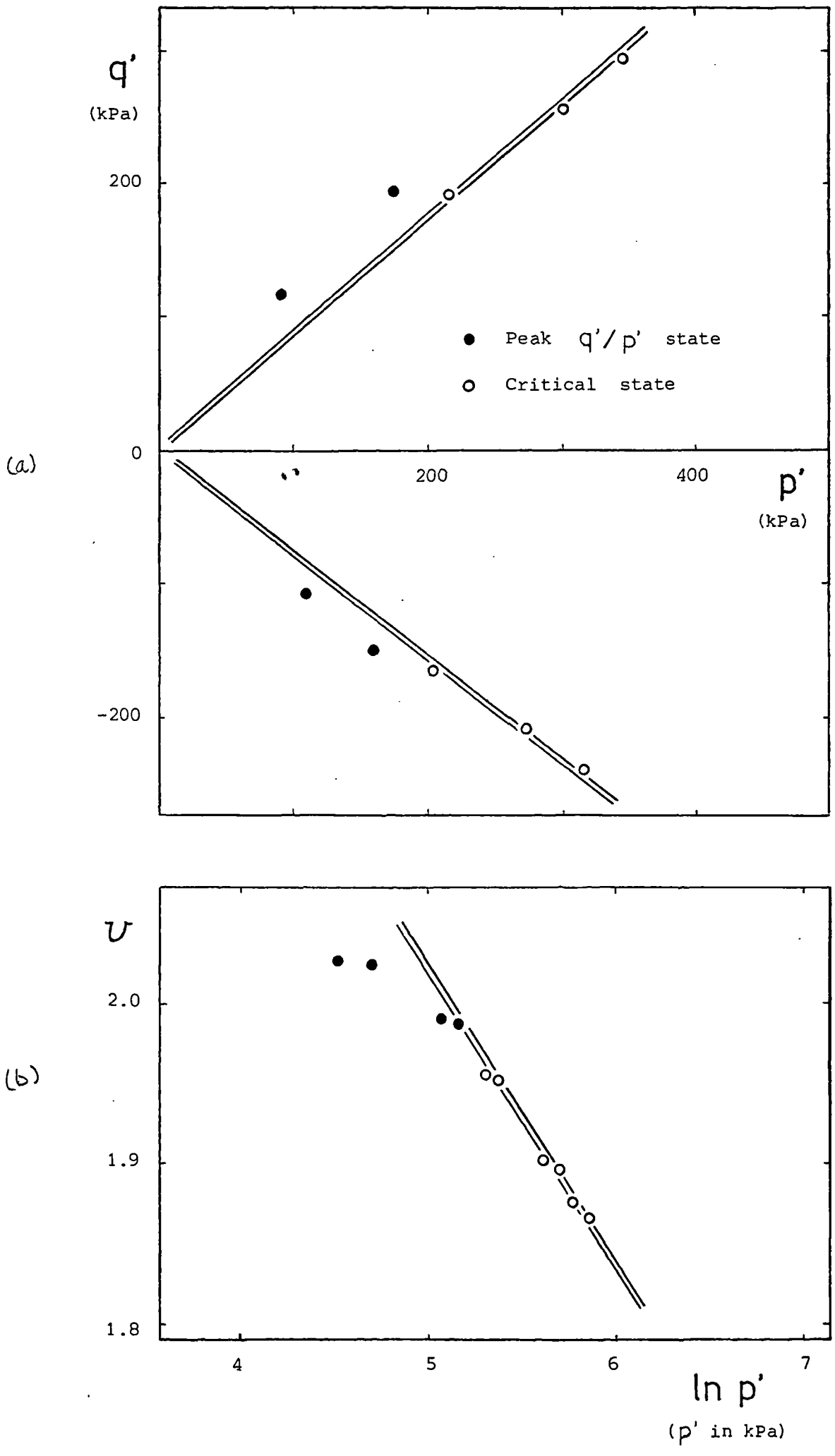
Figure 7.20   Critical and peak states for 38 mm reconstituted
               London clay (blue) triaxial samples
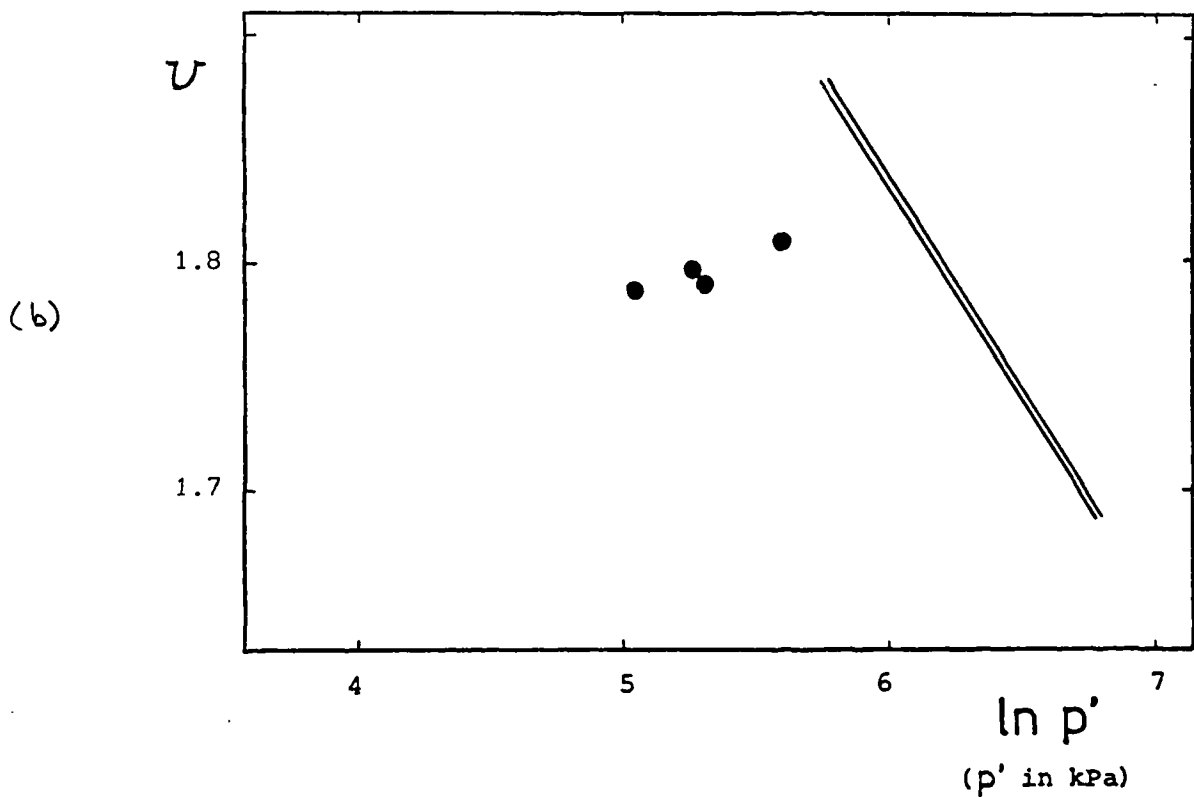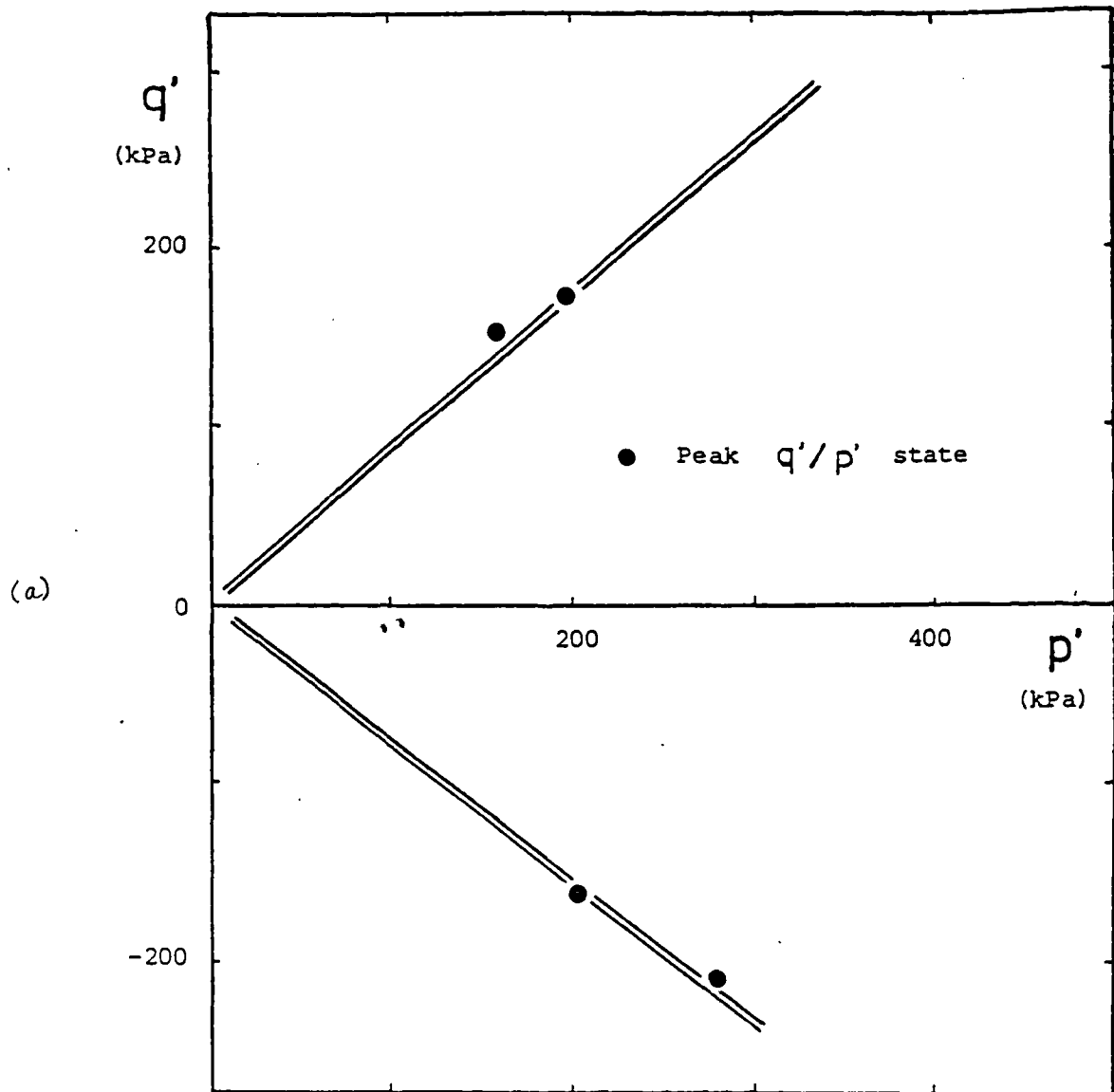
Figure 7.21   Peak states for 100 mm undisturbed London clay
               (blue) triaxial samples
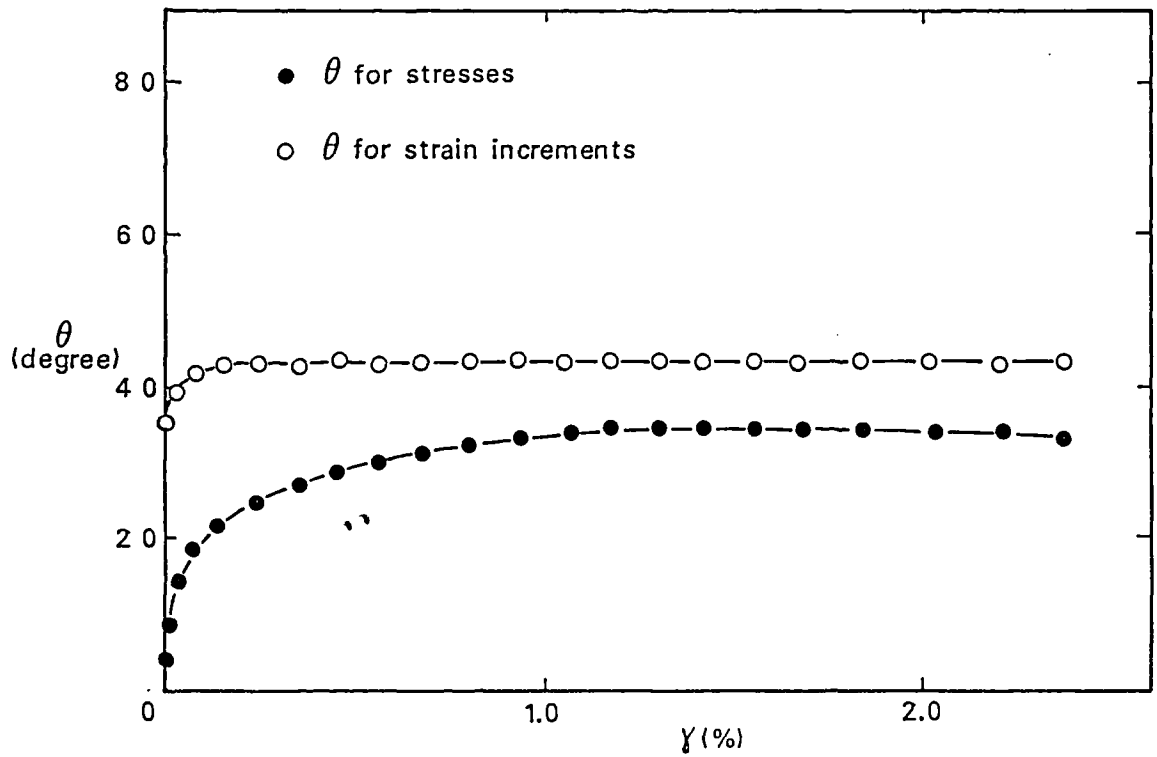
(a)   constant σ_v' test MB1
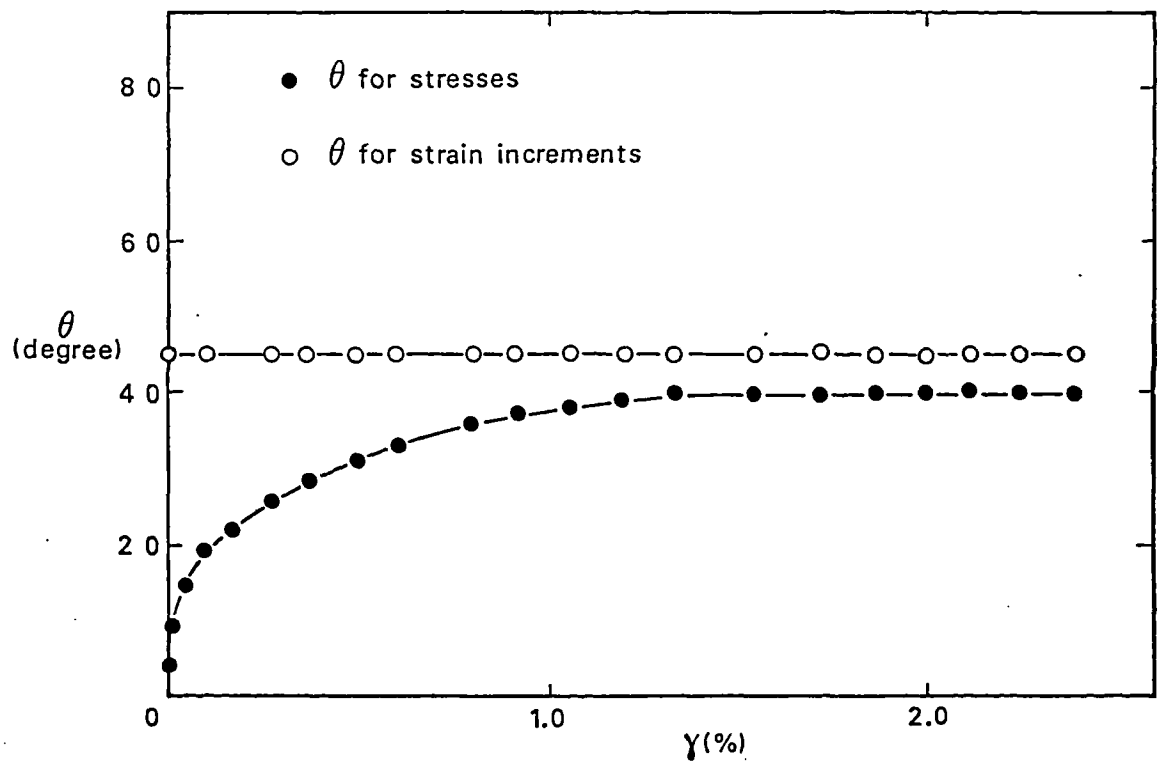
(b)   constant volume test MB5

Figure 7.22   Variation of angle of rotation for principal stresses
and principal strain increments in simple shear tests
on normally compressed remoulded London clay (brown)
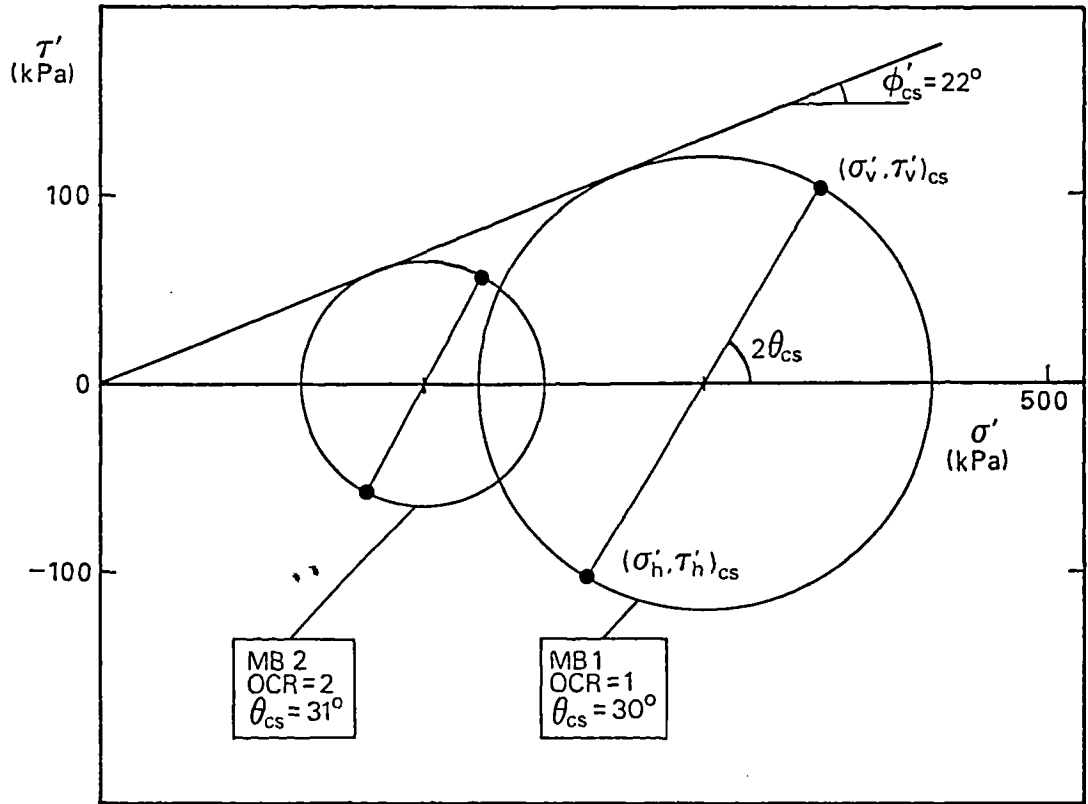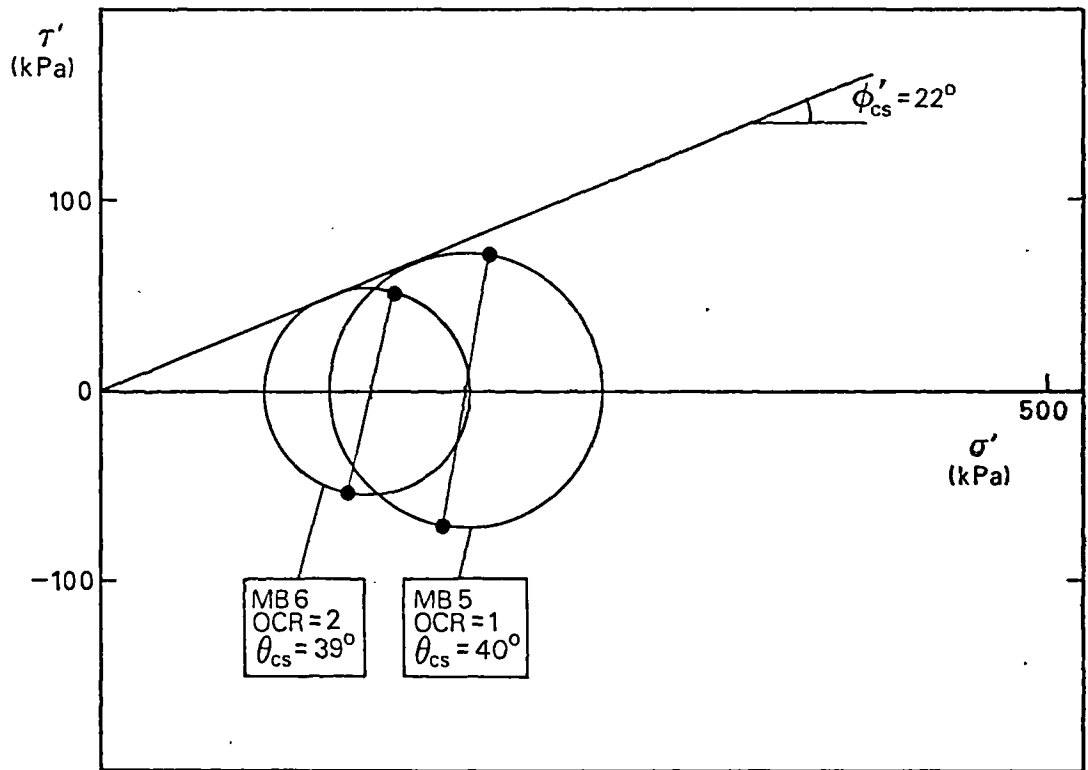
(a)   constant σ_v' tests

(b)   constant volume tests

Figure 7.23   Critical state Mohr's circles of stress for simple
shear tests on remoulded London clay (brown)
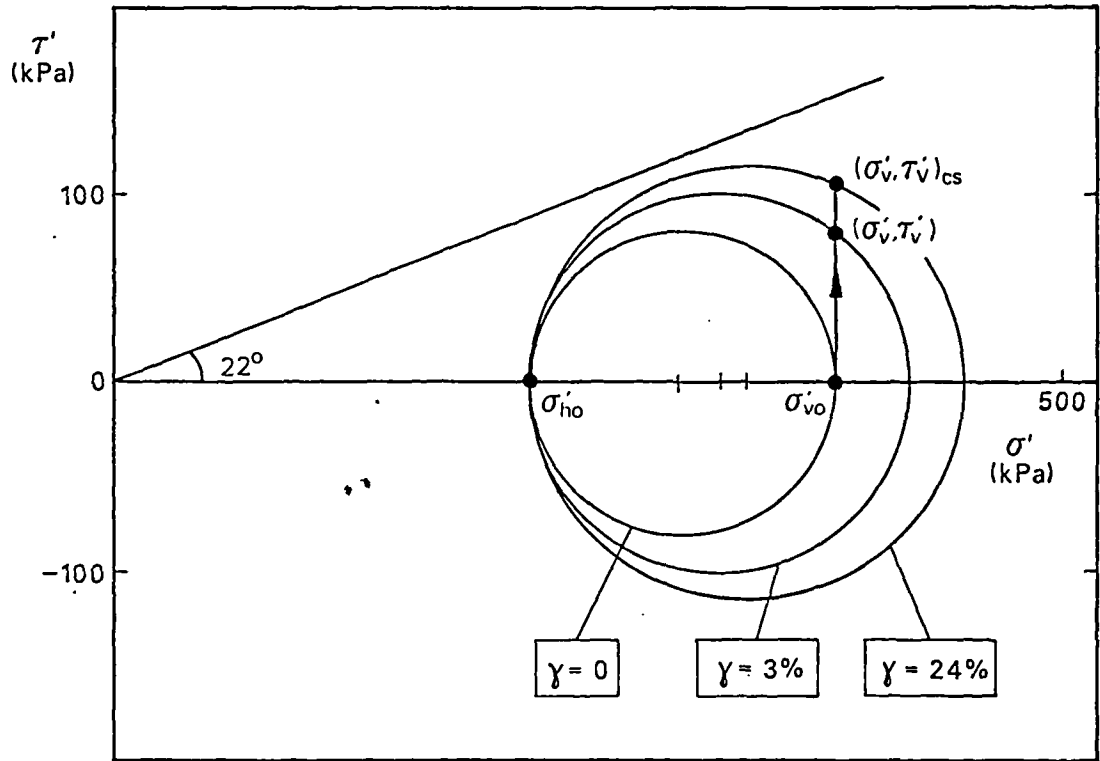
(a) constant σ_v' test MB1
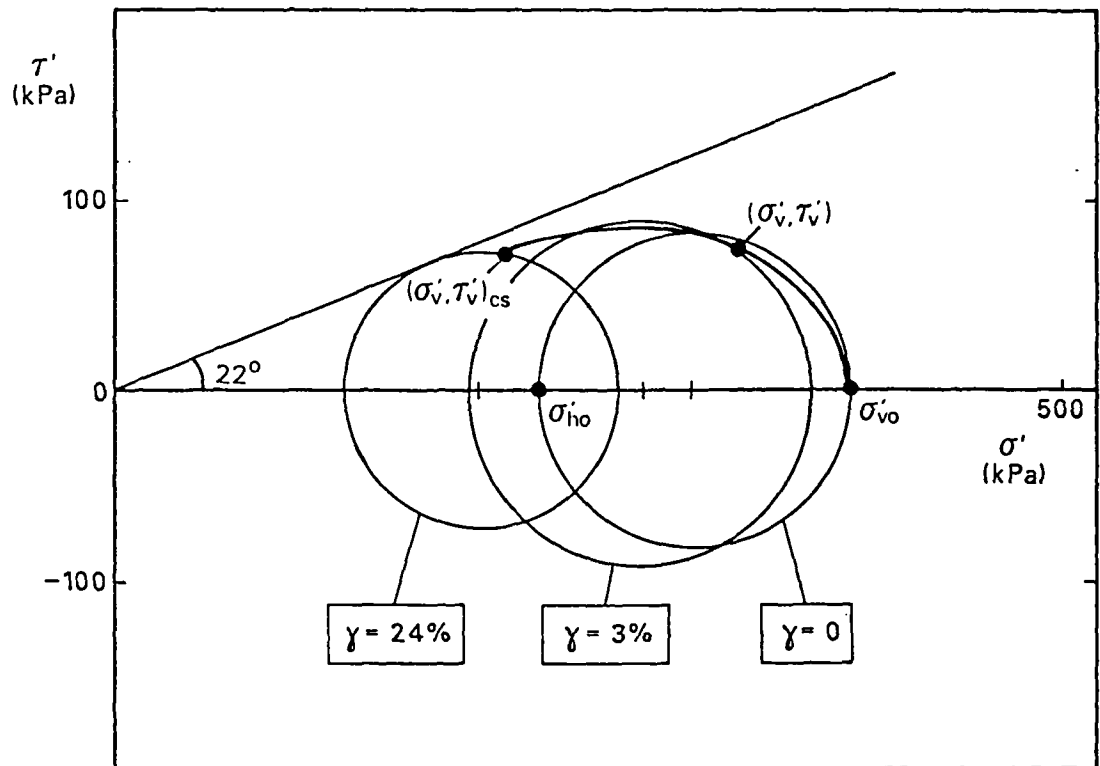
(b) constant volume test MB5

Figure 7.24   Development of Mohr's circles of stress in simple shear tests on normally compressed remoulded London clay (brown)
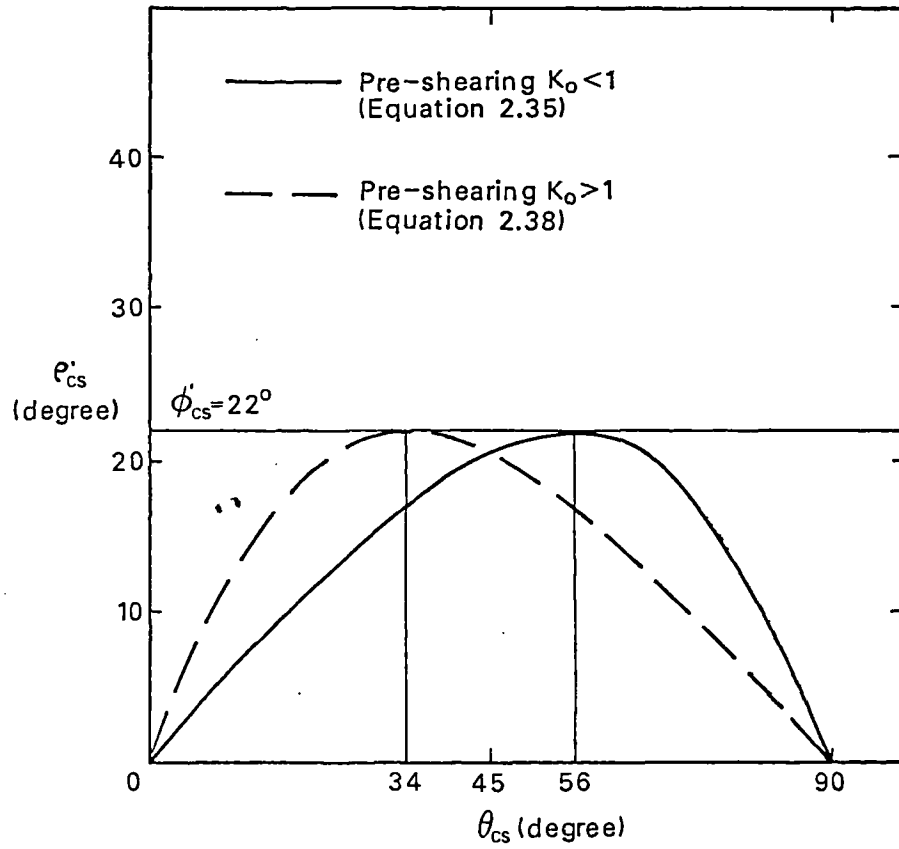
Figure 7.25   Relationships among ϕ_{cs}' , ρ_{cs}' and θ_{cs}
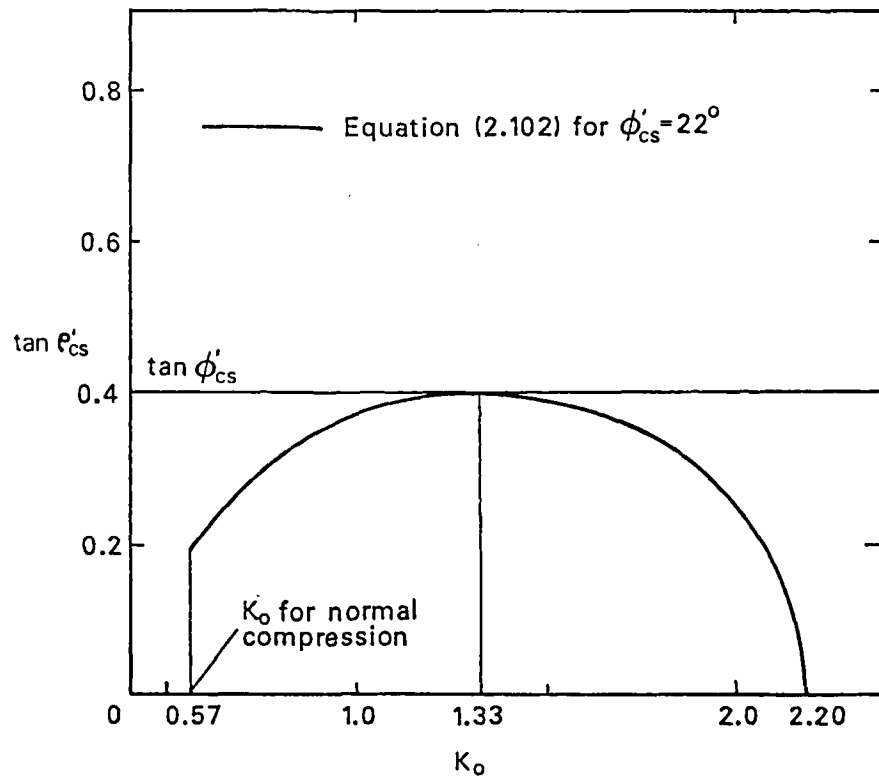
Figure 7.26   Relationship among ϕ_{cs}' , ρ_{cs}' and K_o
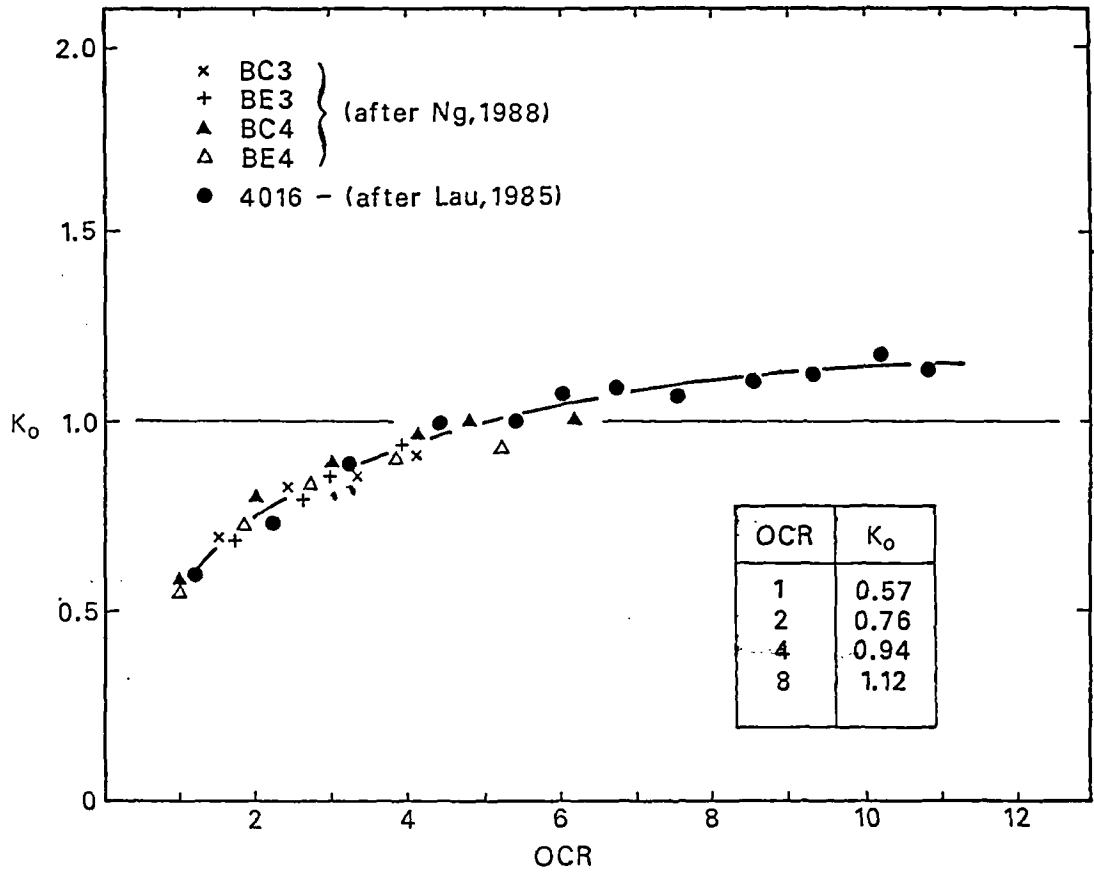
(a) Cowden till
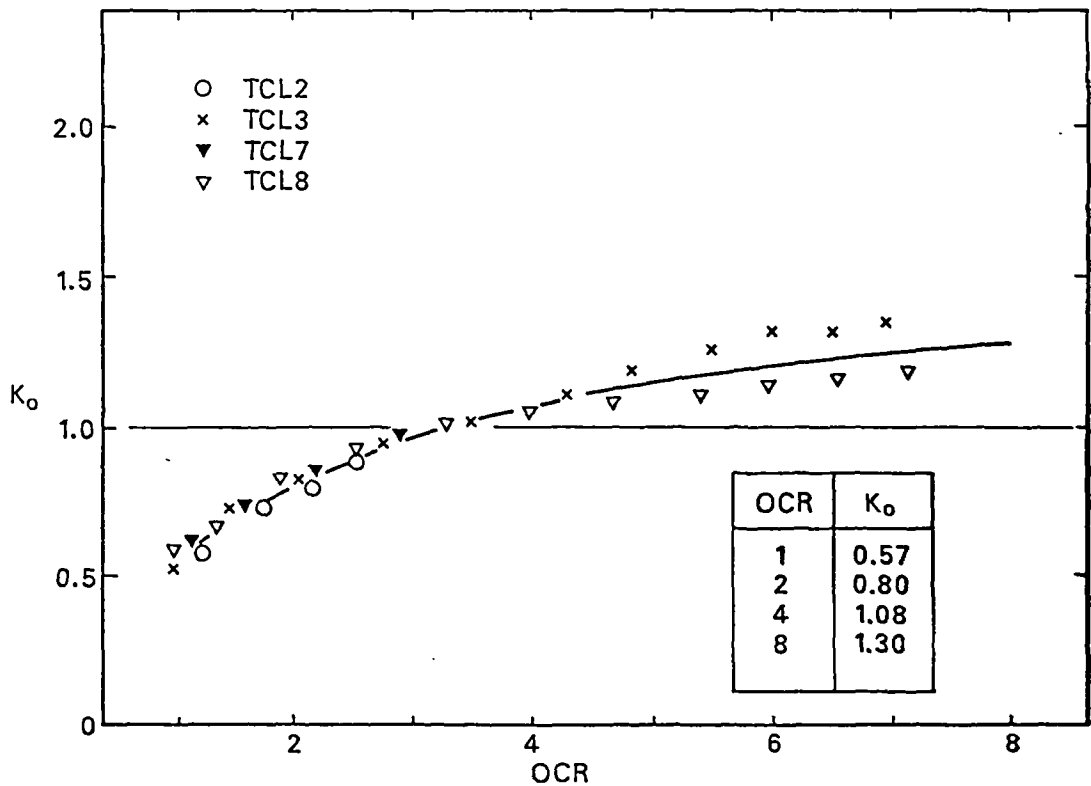
(b) London clay (blue)

Figure 7.27 Variation of K_o with OCR measured from 38 mm reconstituted triaxial samples
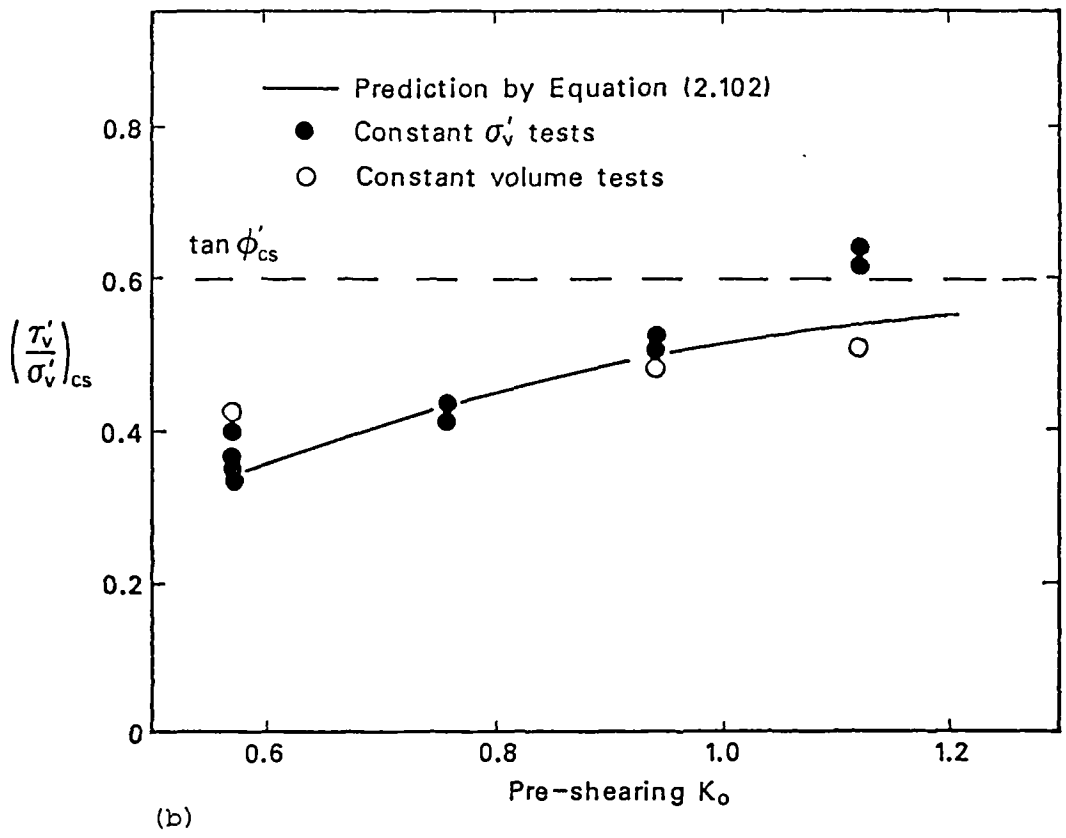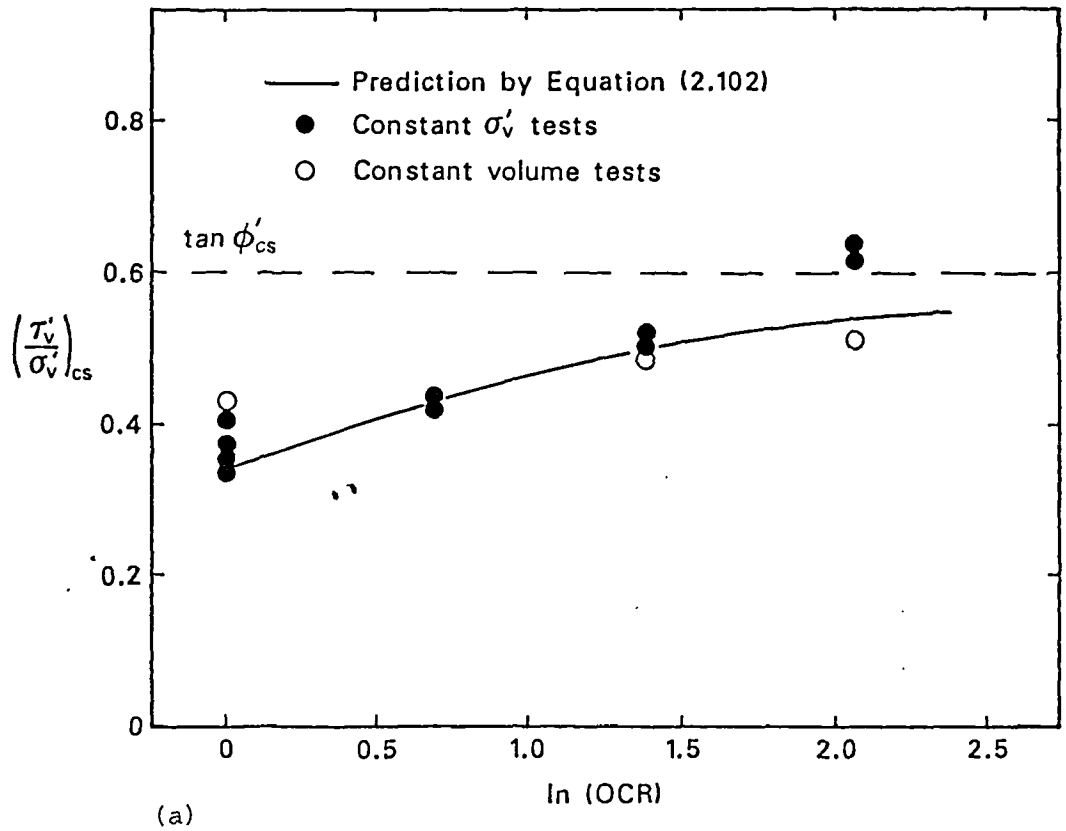
Figure 7.28   Variation of (τ_v' / σ_v')$_{cs}$ with OCR and K_o for remoulded and reconstituted simple shear samples of Cowden till
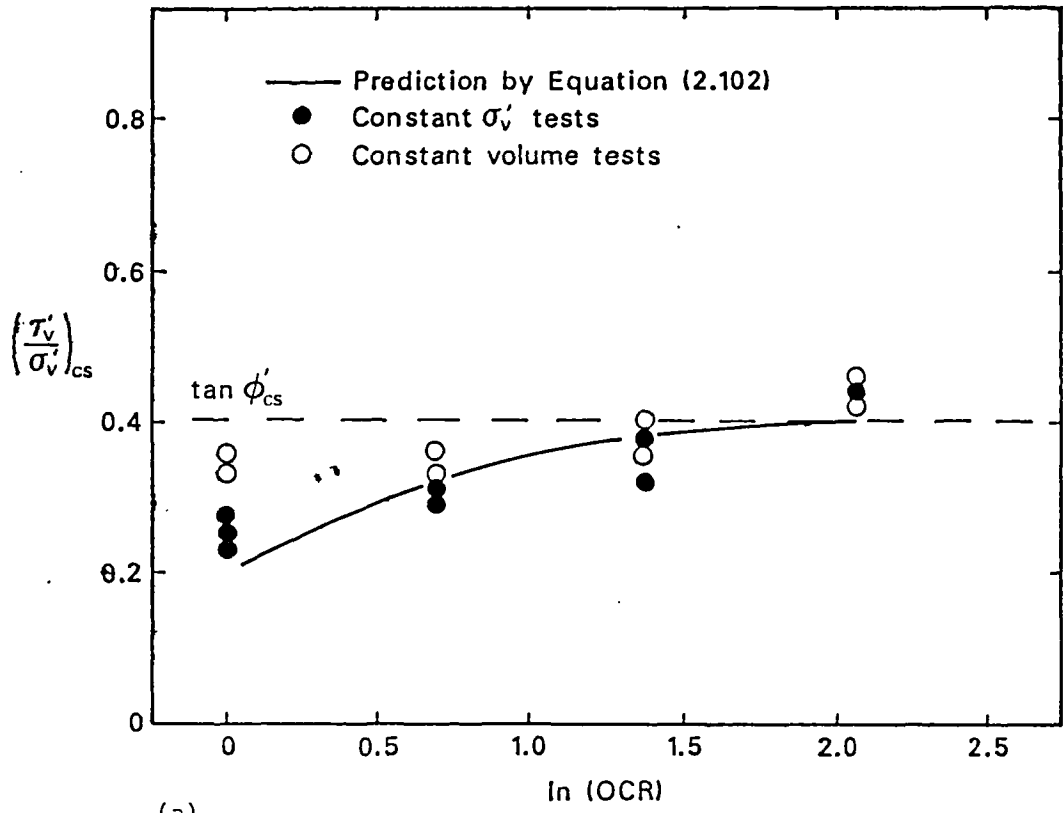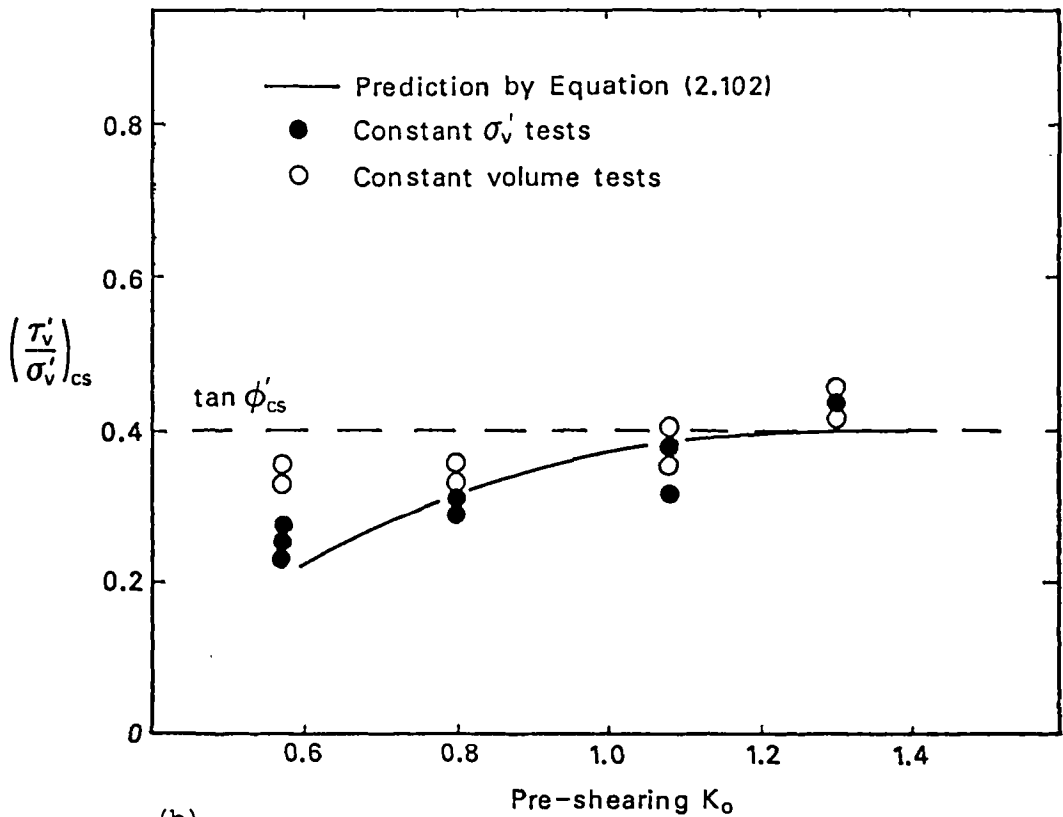
Figure 7.29   Variation of $(\tau_v' / \sigma_v')_{cs}$ with OCR and K_o for remoulded simple shear samples of London clay (brown and blue)
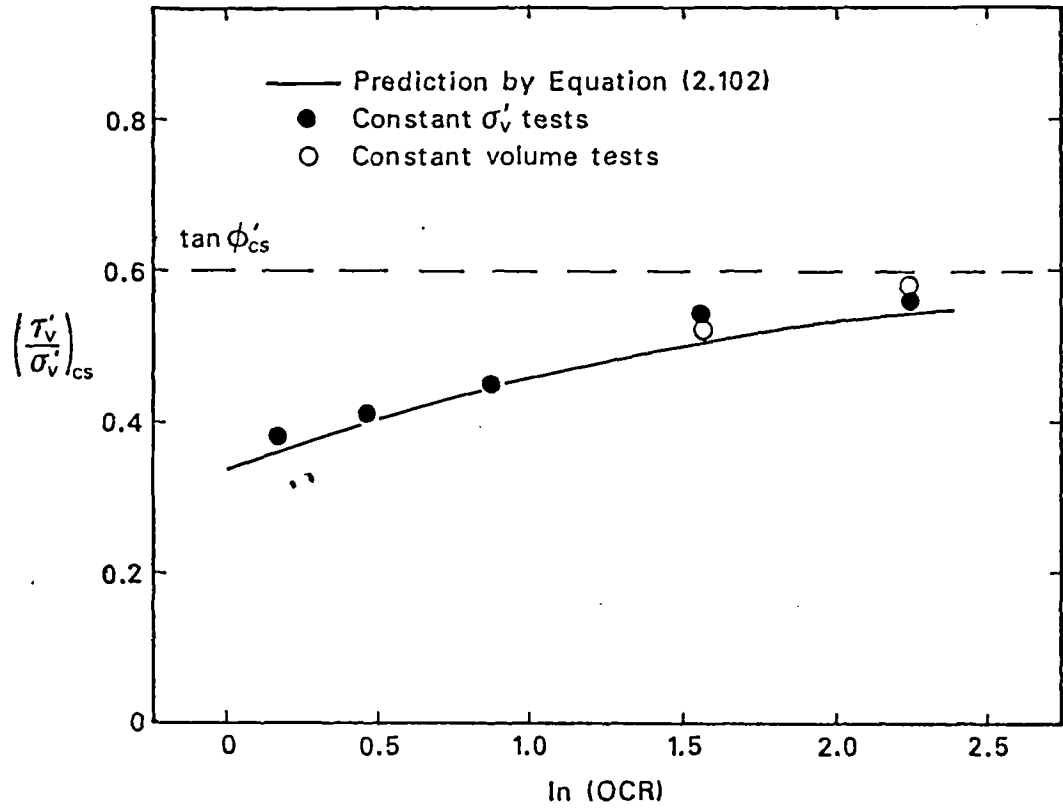
(a) Cowden till
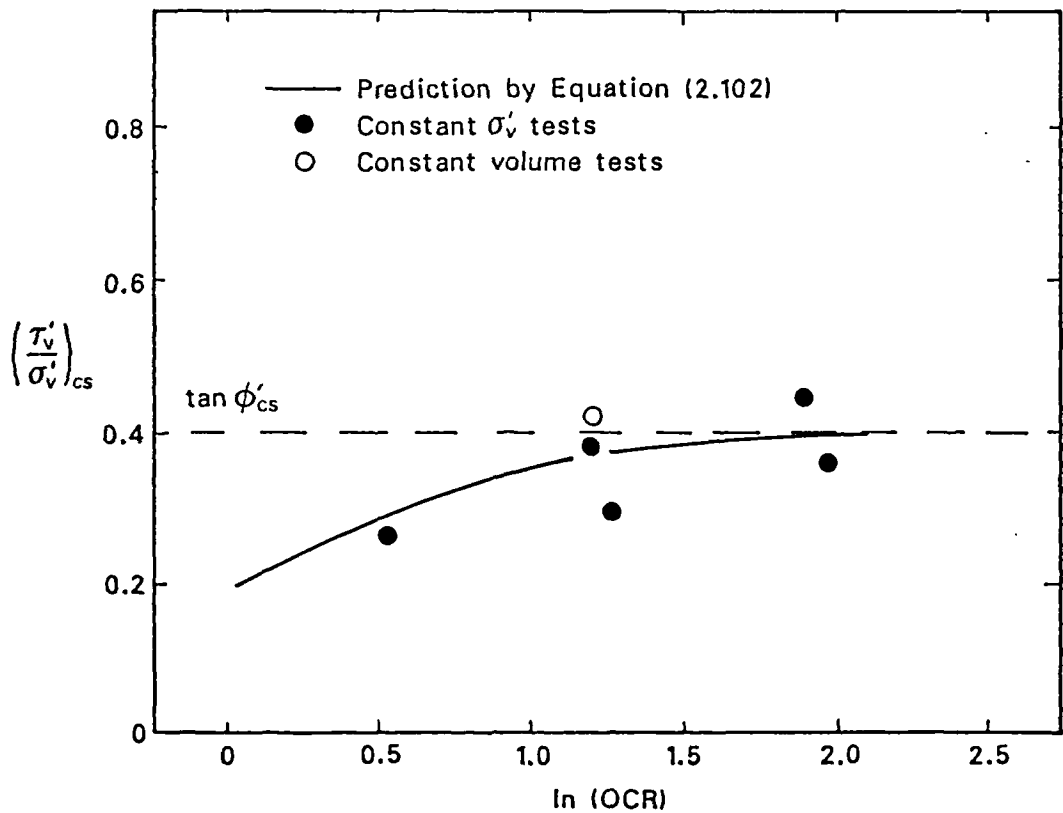
(b) London clay (brown and blue)

Figure 7.30   Variation of $(\tau_v' / \sigma_v')_{cs}$ with OCR for undisturbed simple shear samples
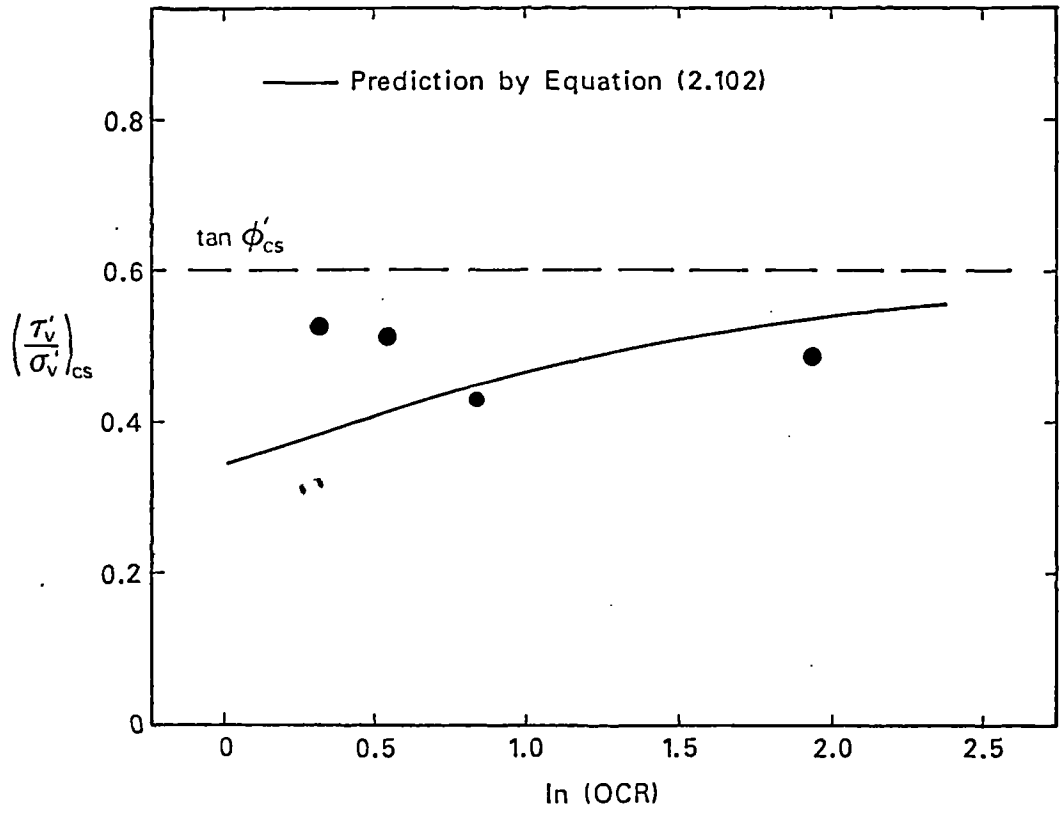
(a) Cowden till
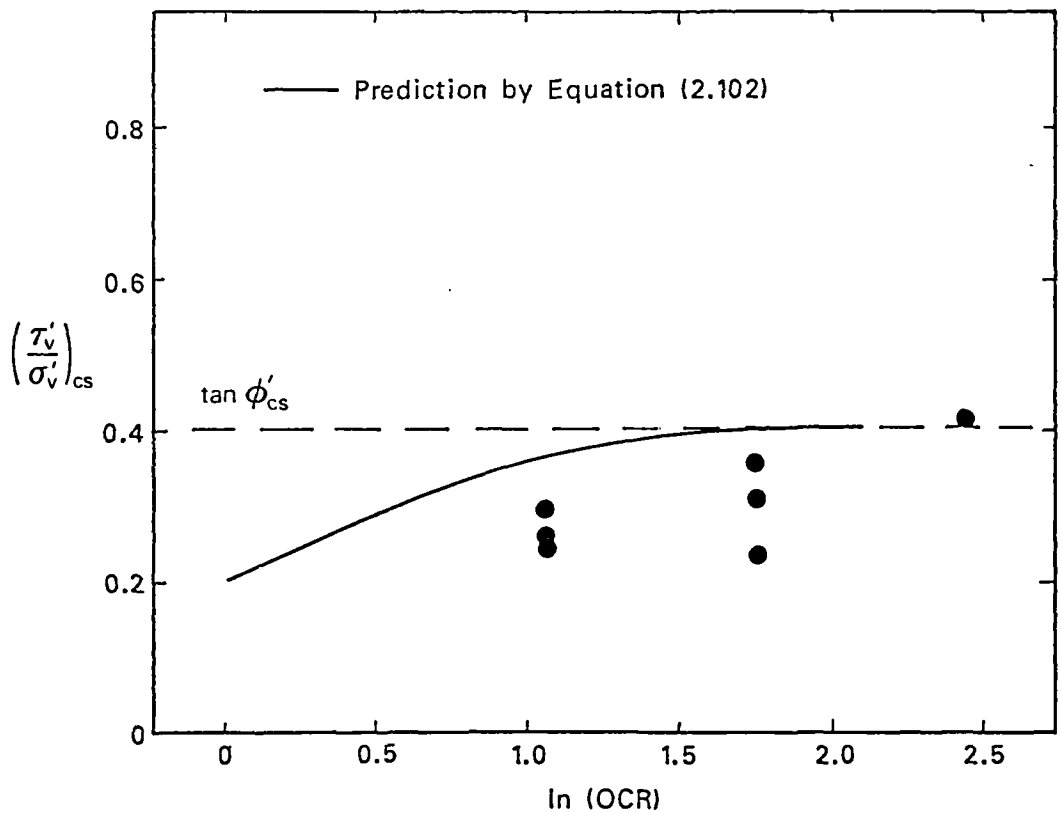
(b) London clay (brown and blue)

Figure 7.31   Variation of (τ_v' / σ_v')$_{cs}$ with OCR for undisturbed shear box samples
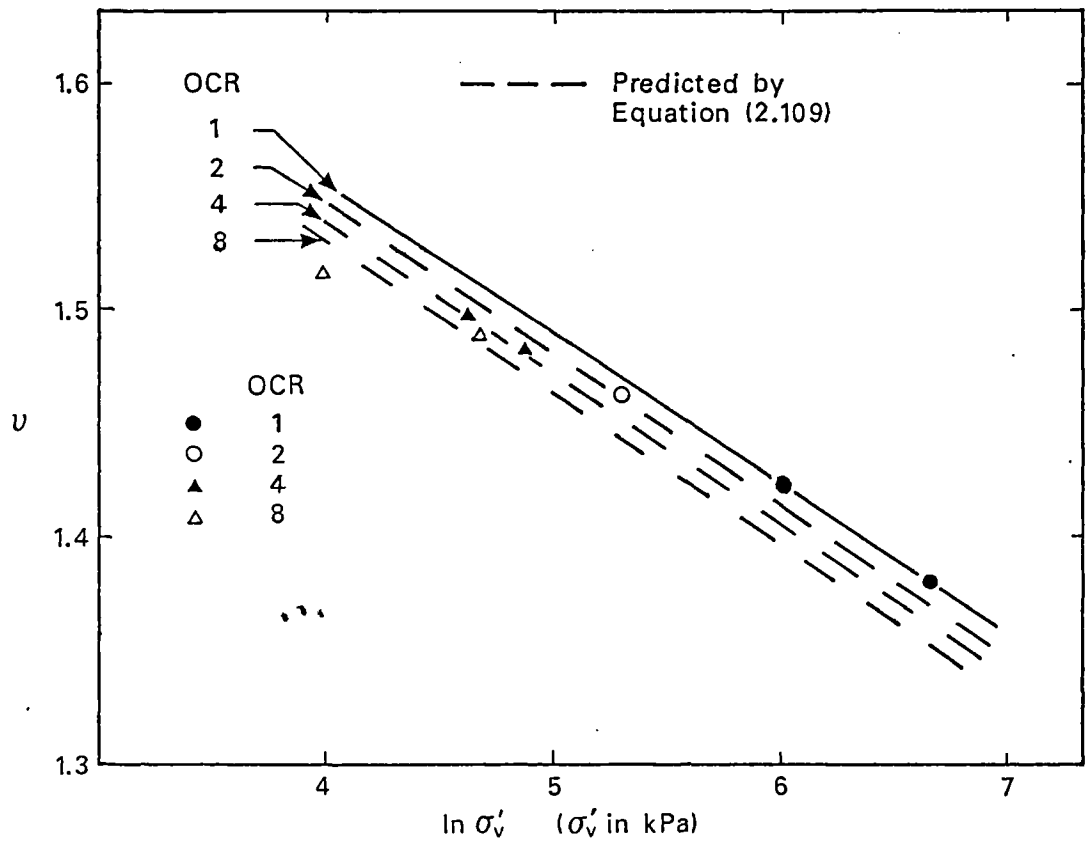
(a) Remoulded Cowden till
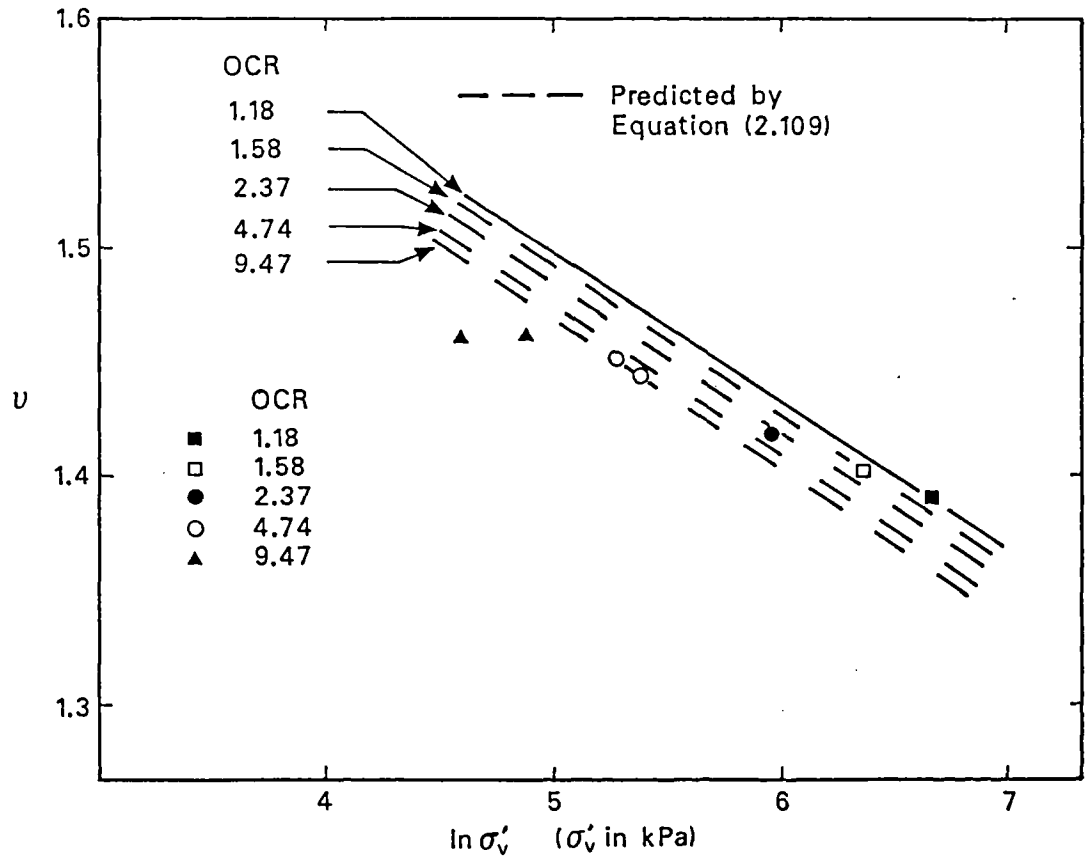
(b) Undisturbed Cowden till

Figure 7.32 Variation of critical state lines with OCR for simple shear samples
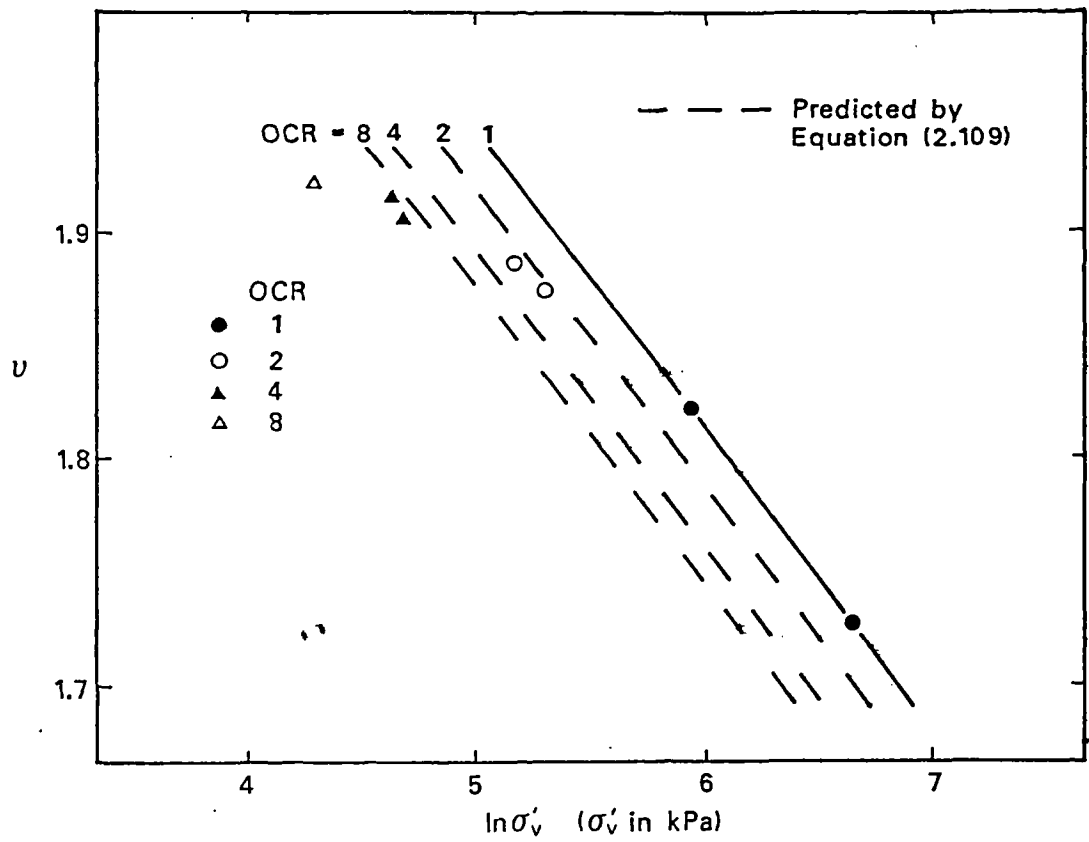
(c) Remoulded London clay (blue)

(d) Undisturbed London clay (blue)

Figure 7.32 continued
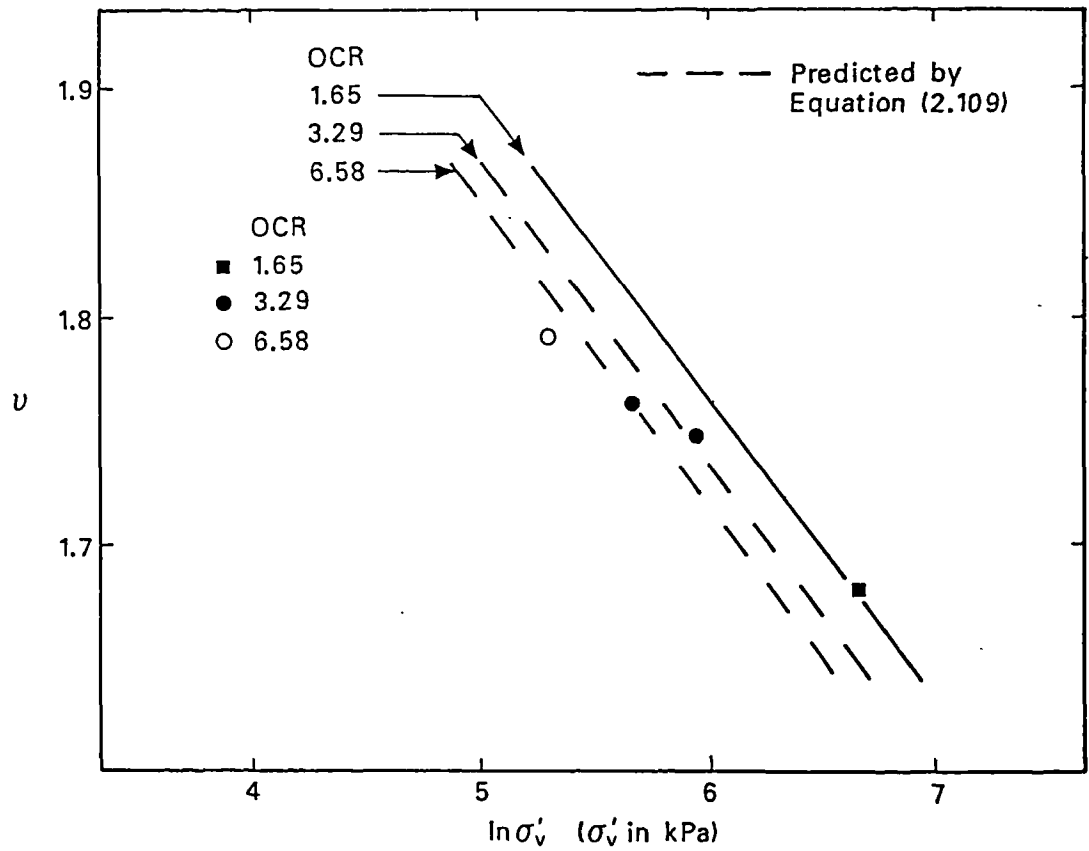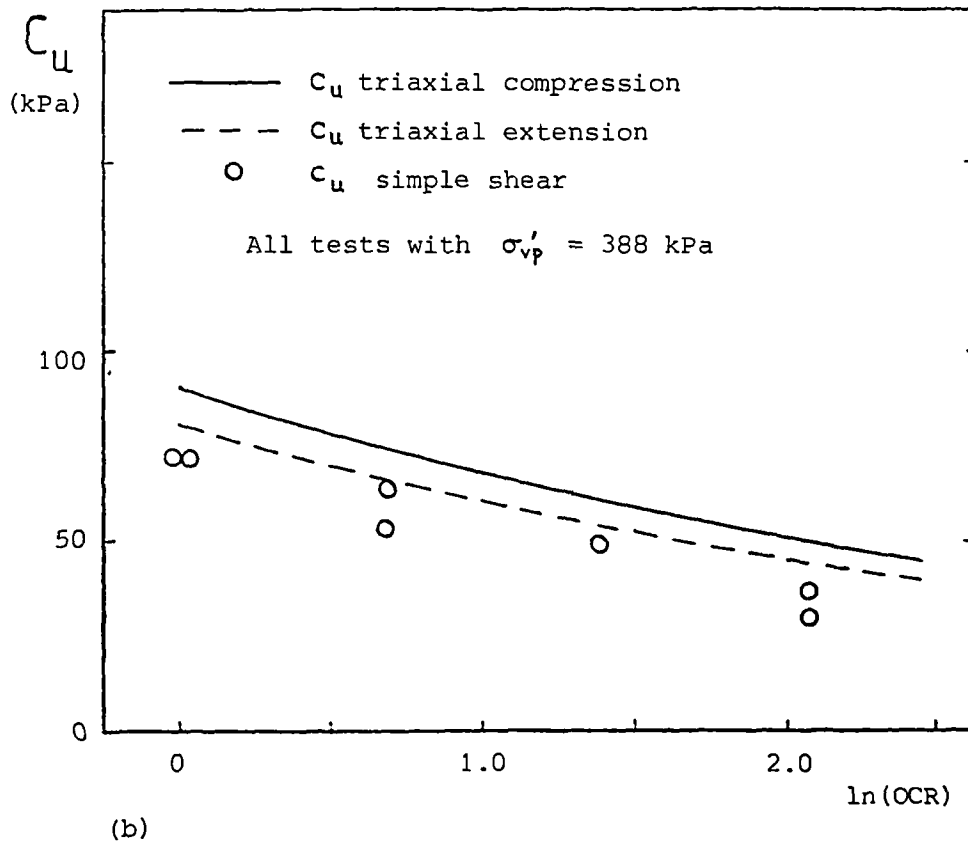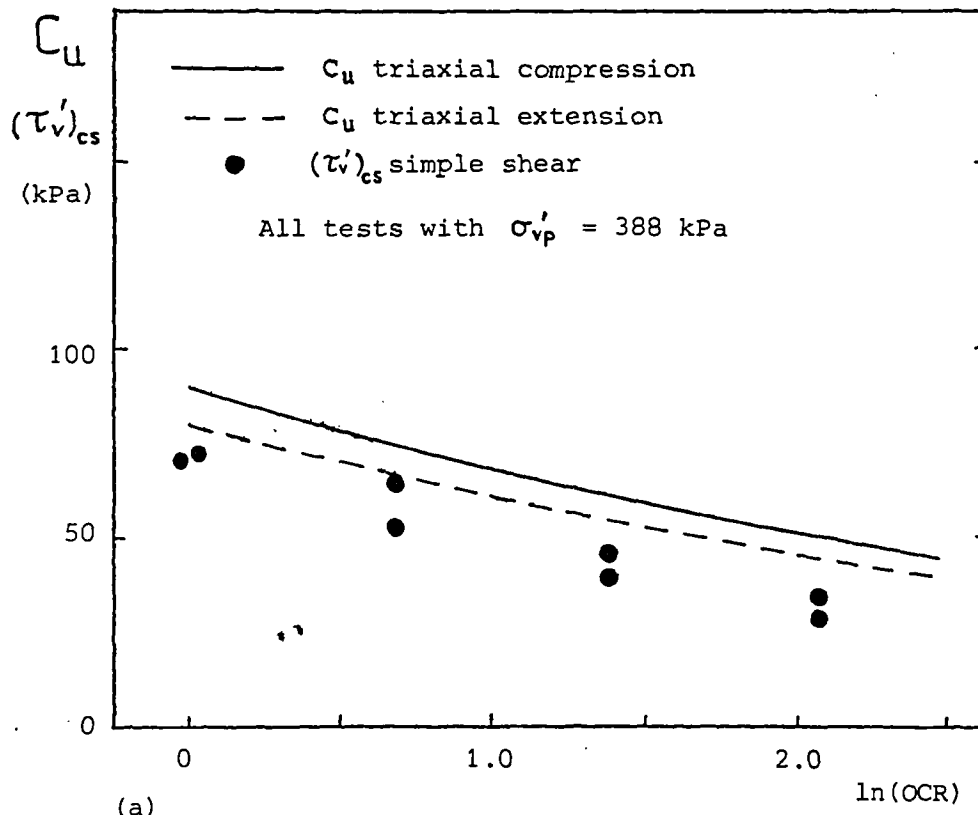
Figure 7.33   Comparisons of $(\tau_v')_{cs}$ and C_u from simple shear tests with C_u from triaxial tests for London clay

(a)

(b)
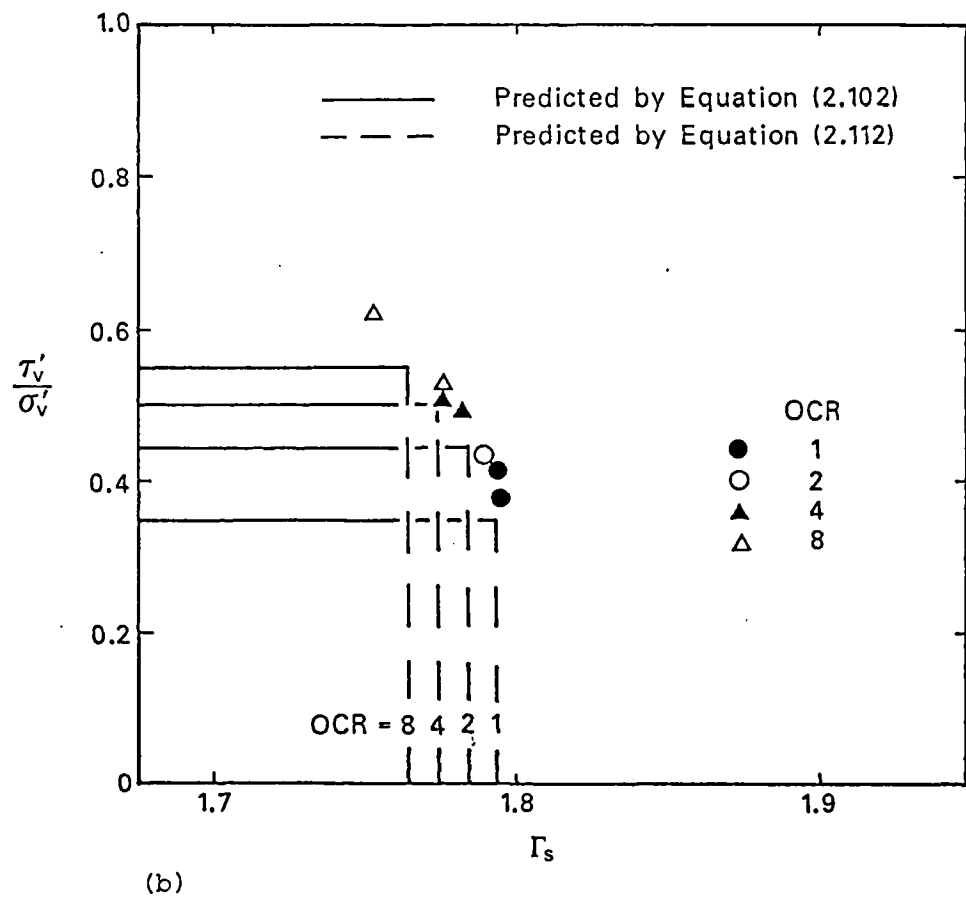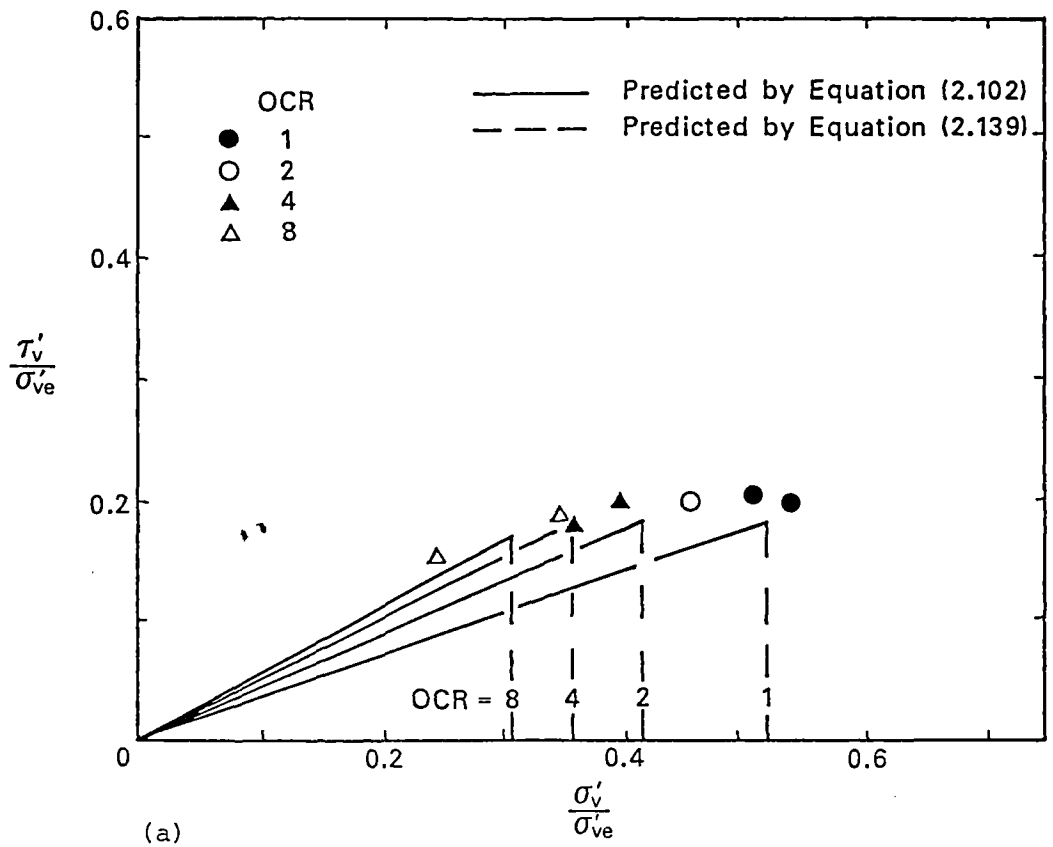
Figure 7.34   Normalised critical states for simple shear tests on remoulded Cowden till
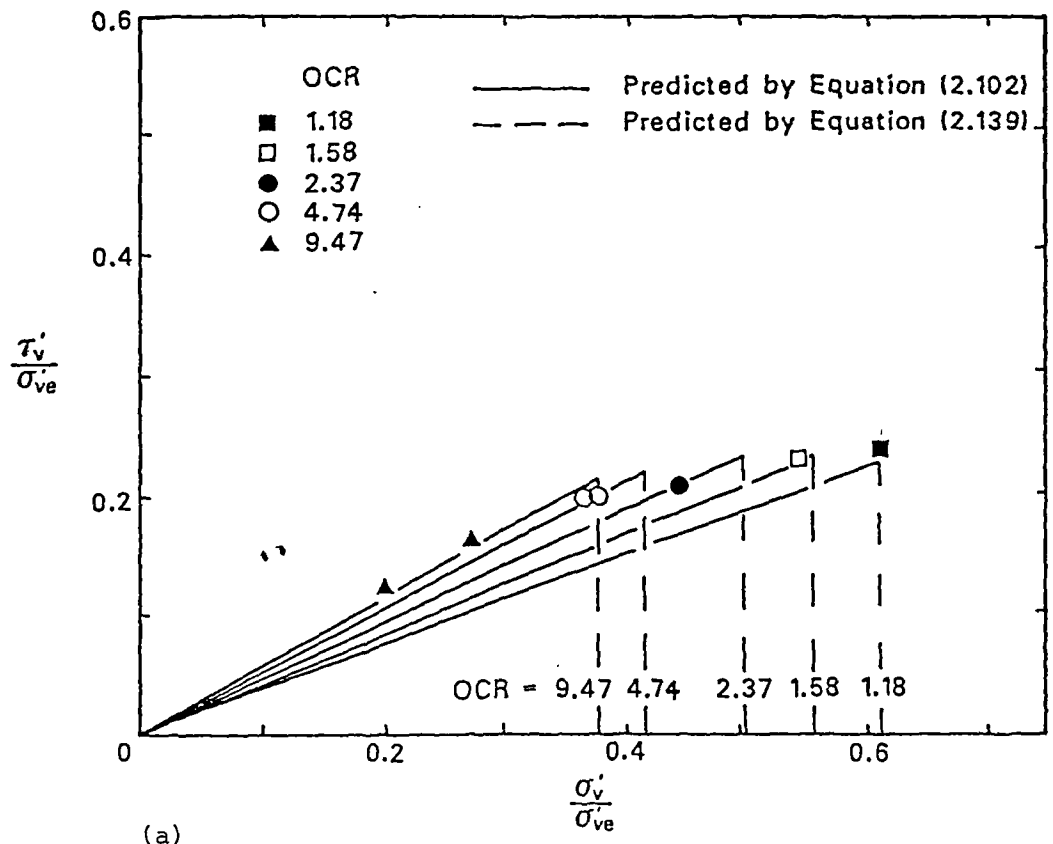
(a)
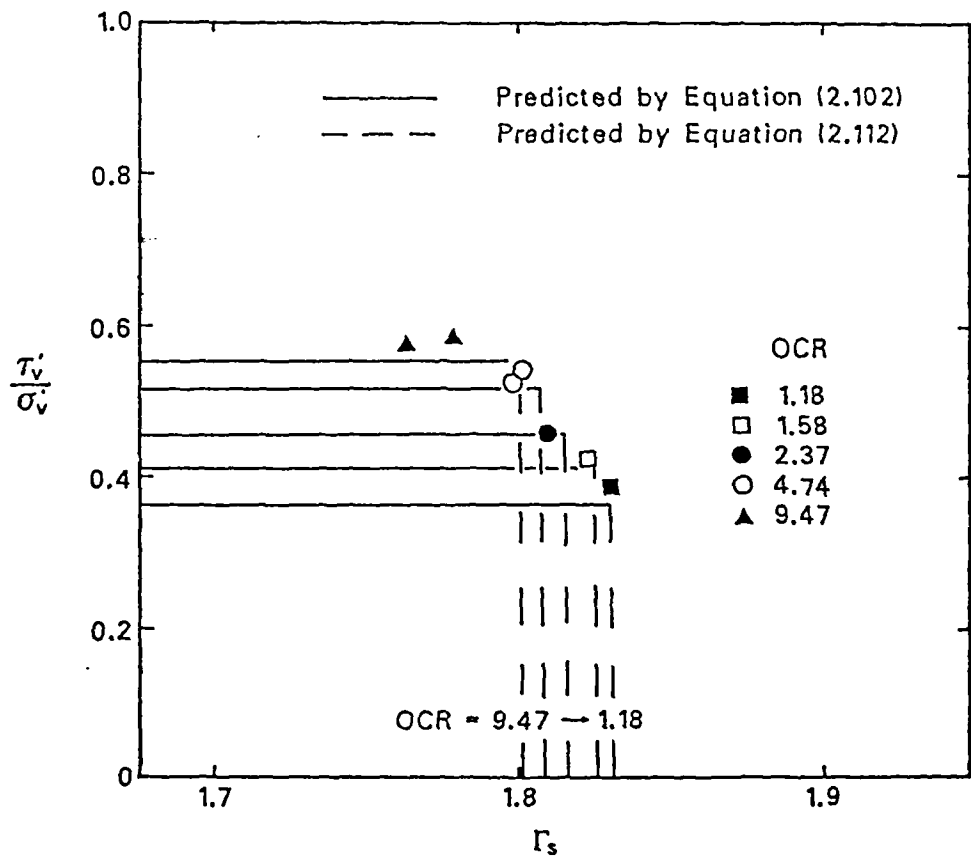
(b)

Figure 7.35   Normalised critical states for simple shear tests on undisturbed Cowden till
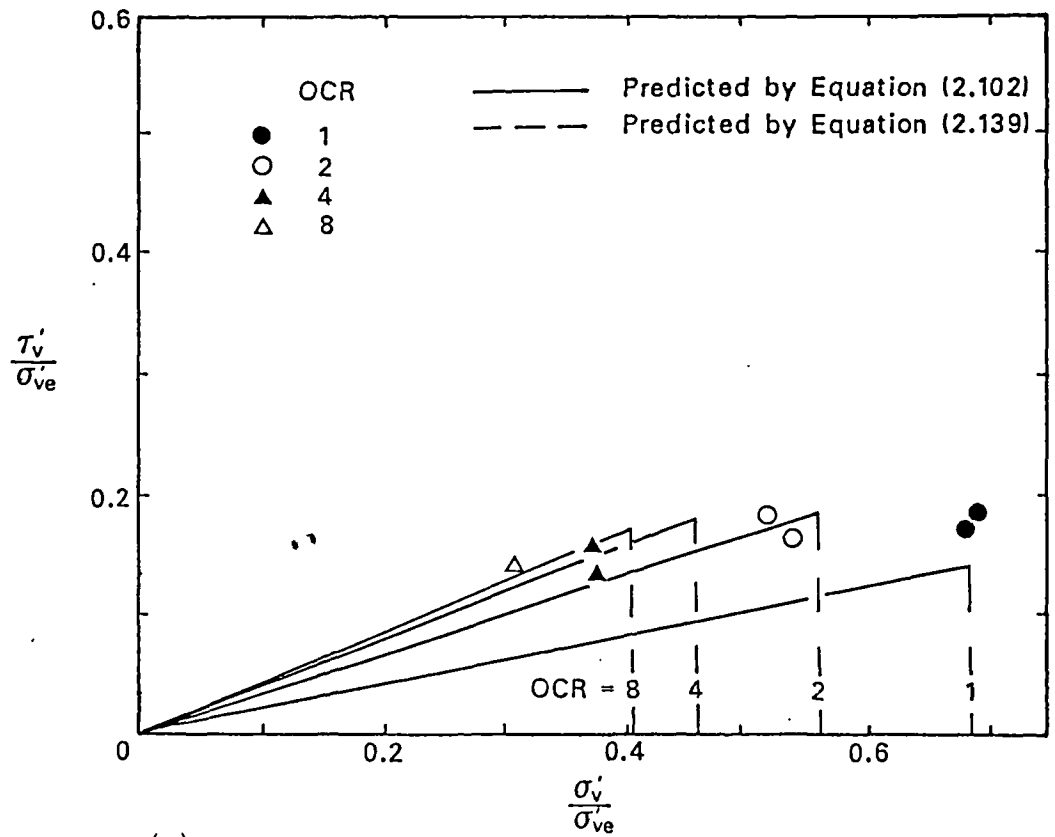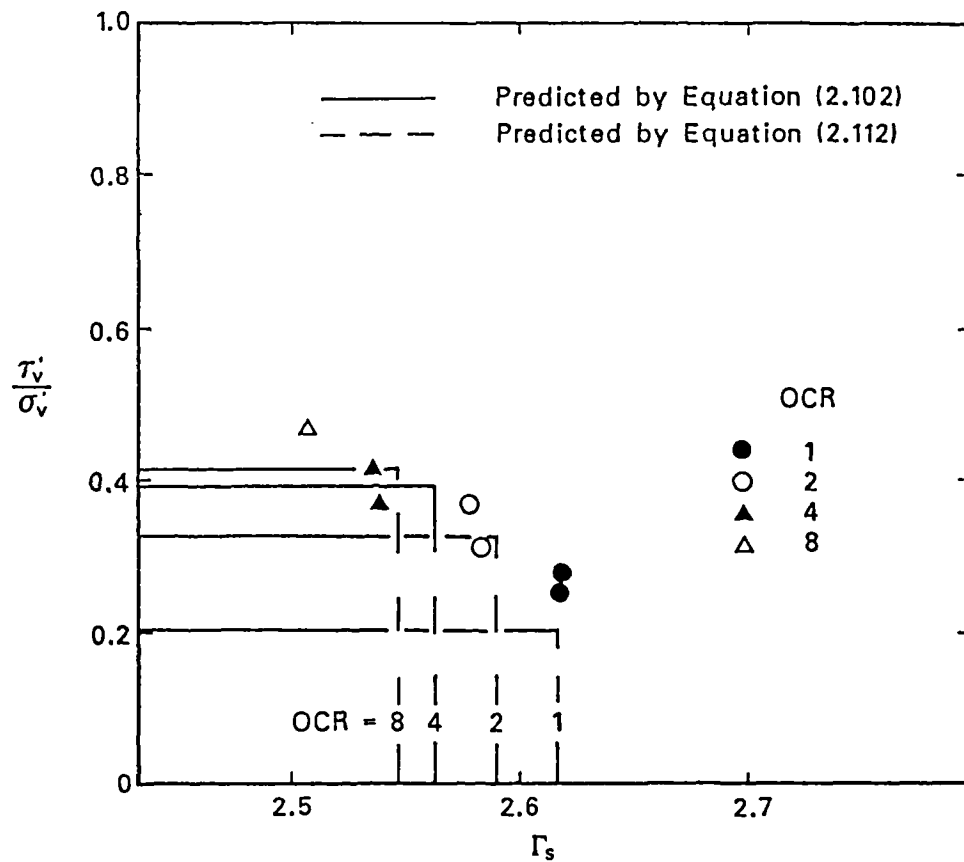
Figure 7.36   Normalised critical states for simple shear tests
on remoulded London clay (blue)
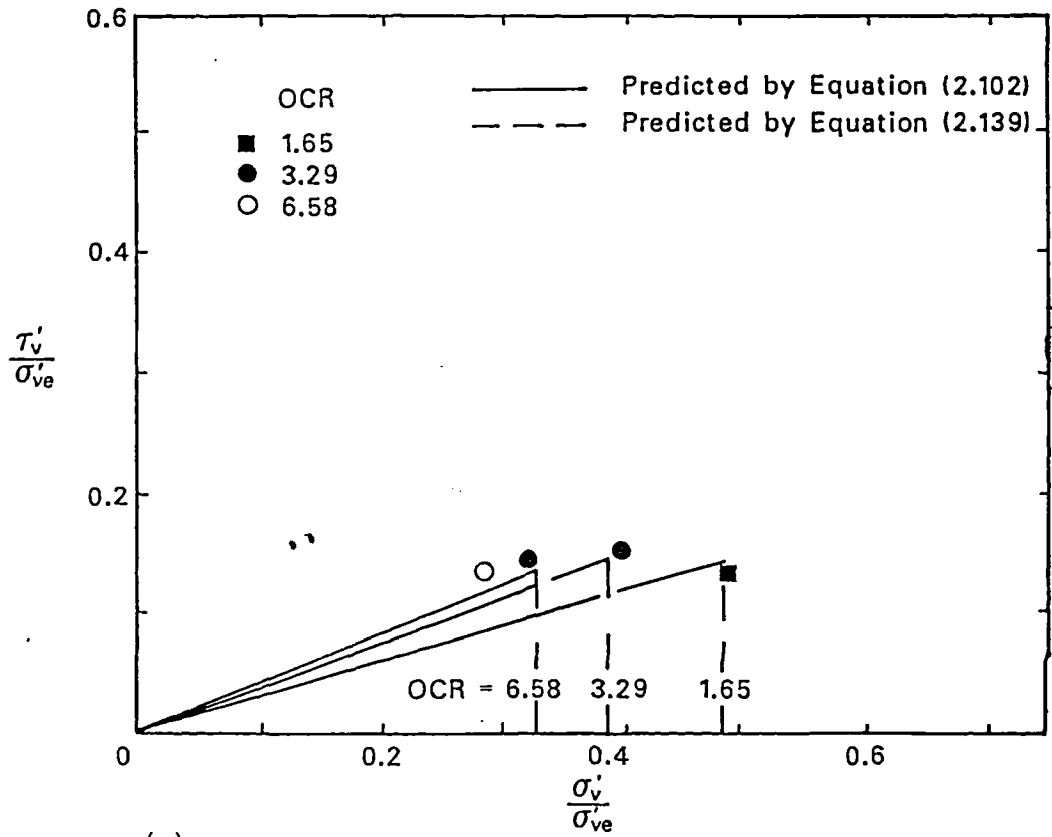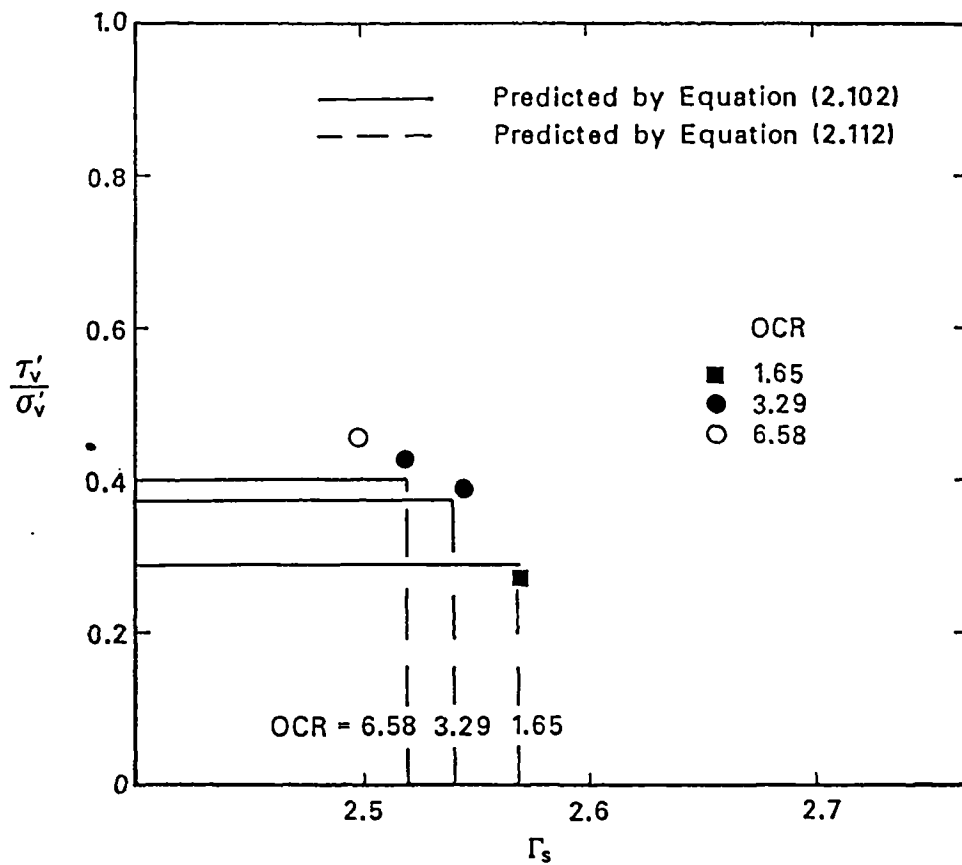
Figure 7.37   Normalised critical states for simple shear tests
on undisturbed London clay (blue)
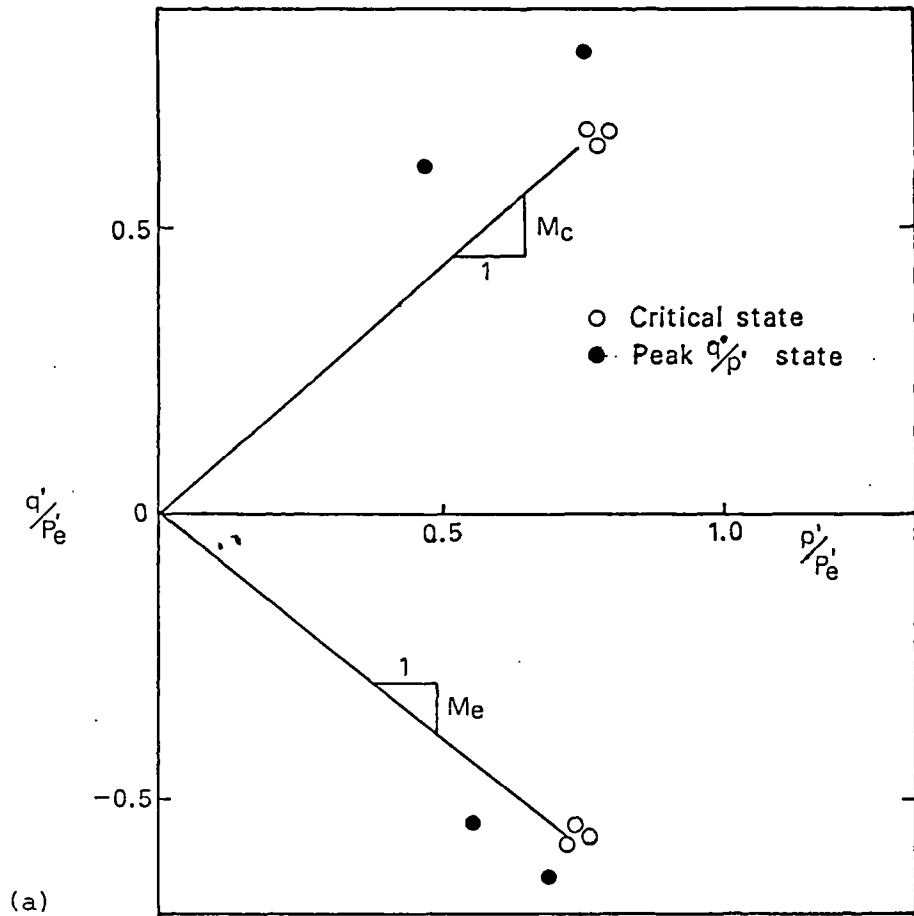
(a)
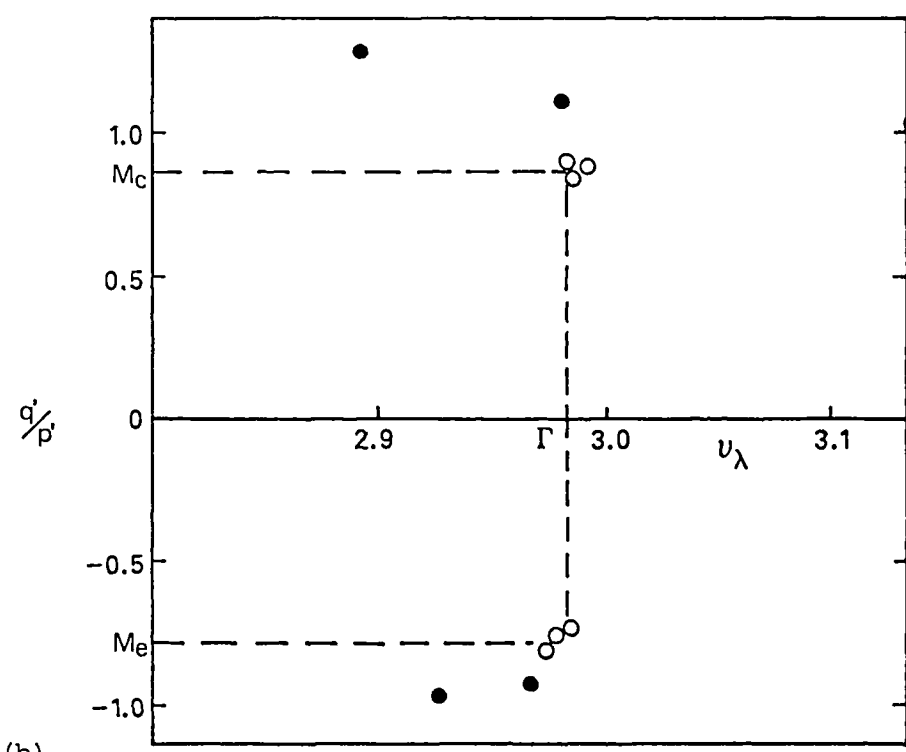
(b)

Figure 7.38   Normalised critical and peak states for stress path
tests on 38 mm reconstituted London clay (blue)
samples
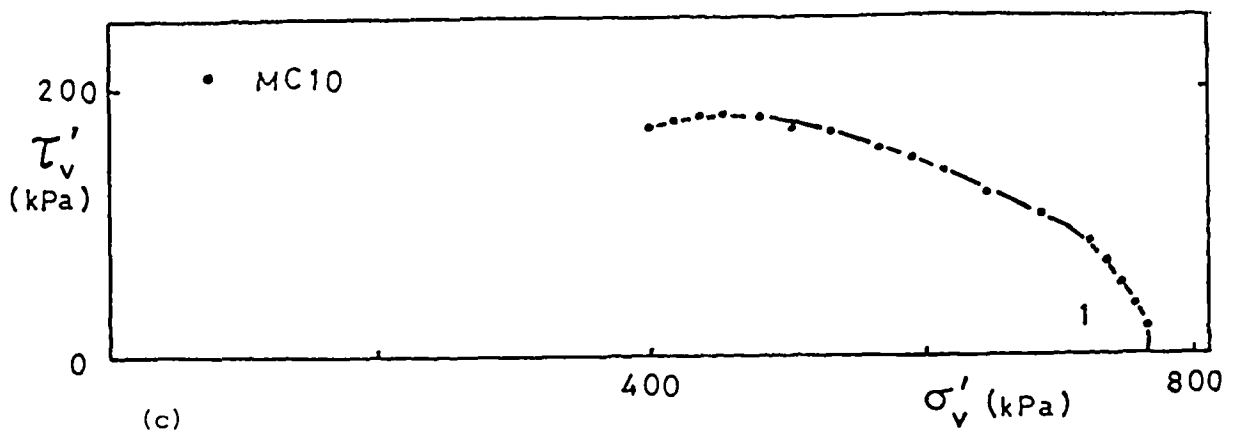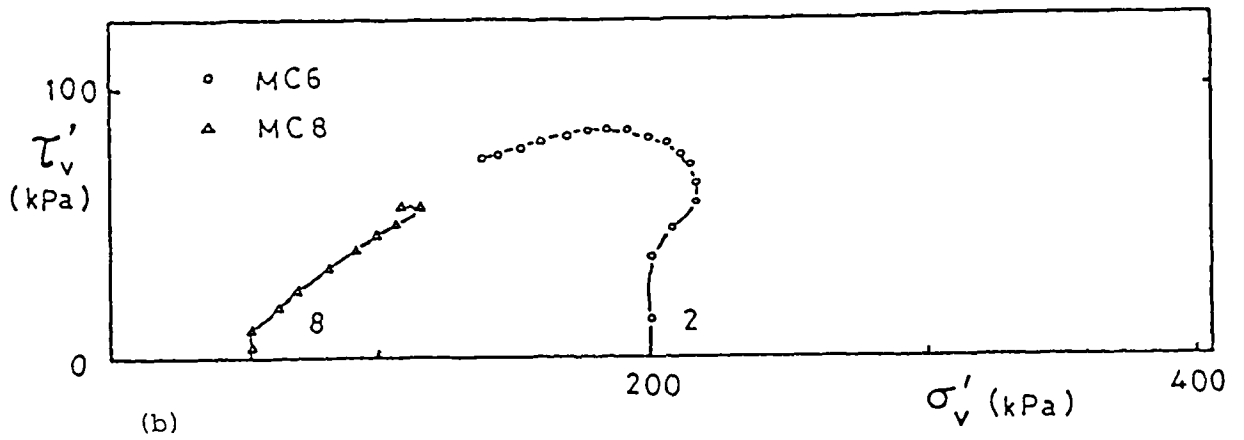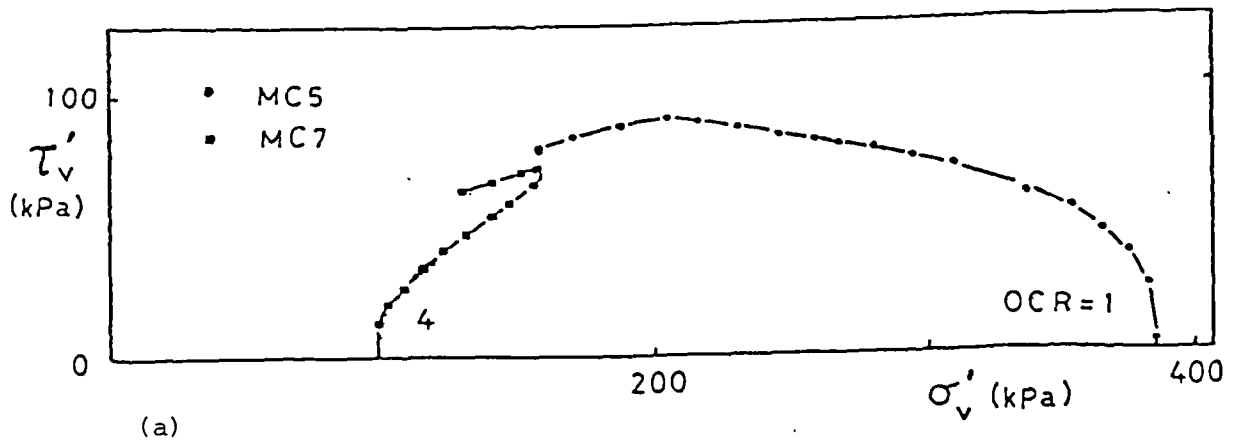
Figure 7.39 State paths for remoulded Cowden till simple shear samples
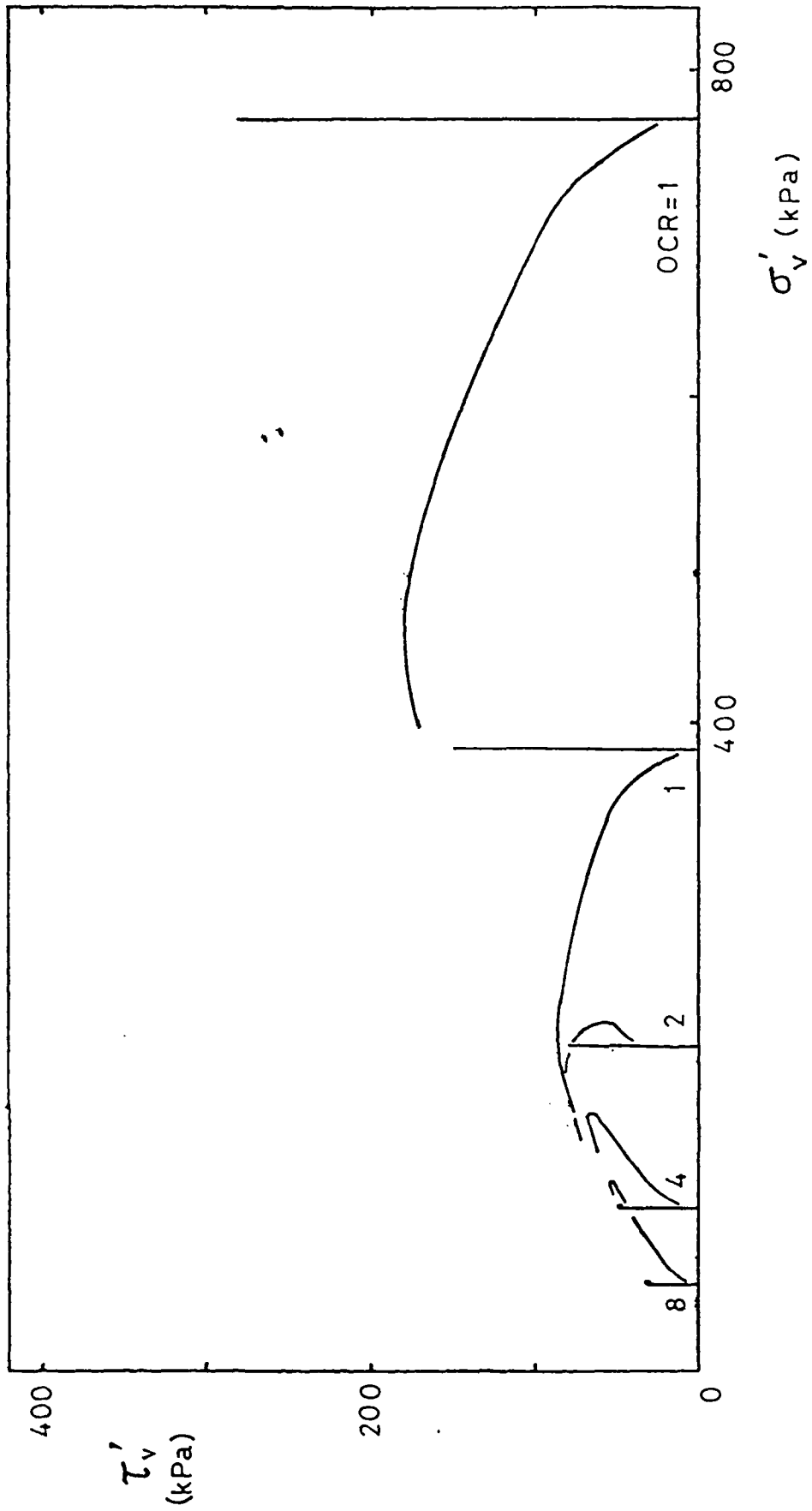
(d)   Summary of all tests

Figure 7.39 continued

(e)

(f)

Figure 7.39 continued

(a)

(b)

(c)   Summary of tests CC1 to CC8
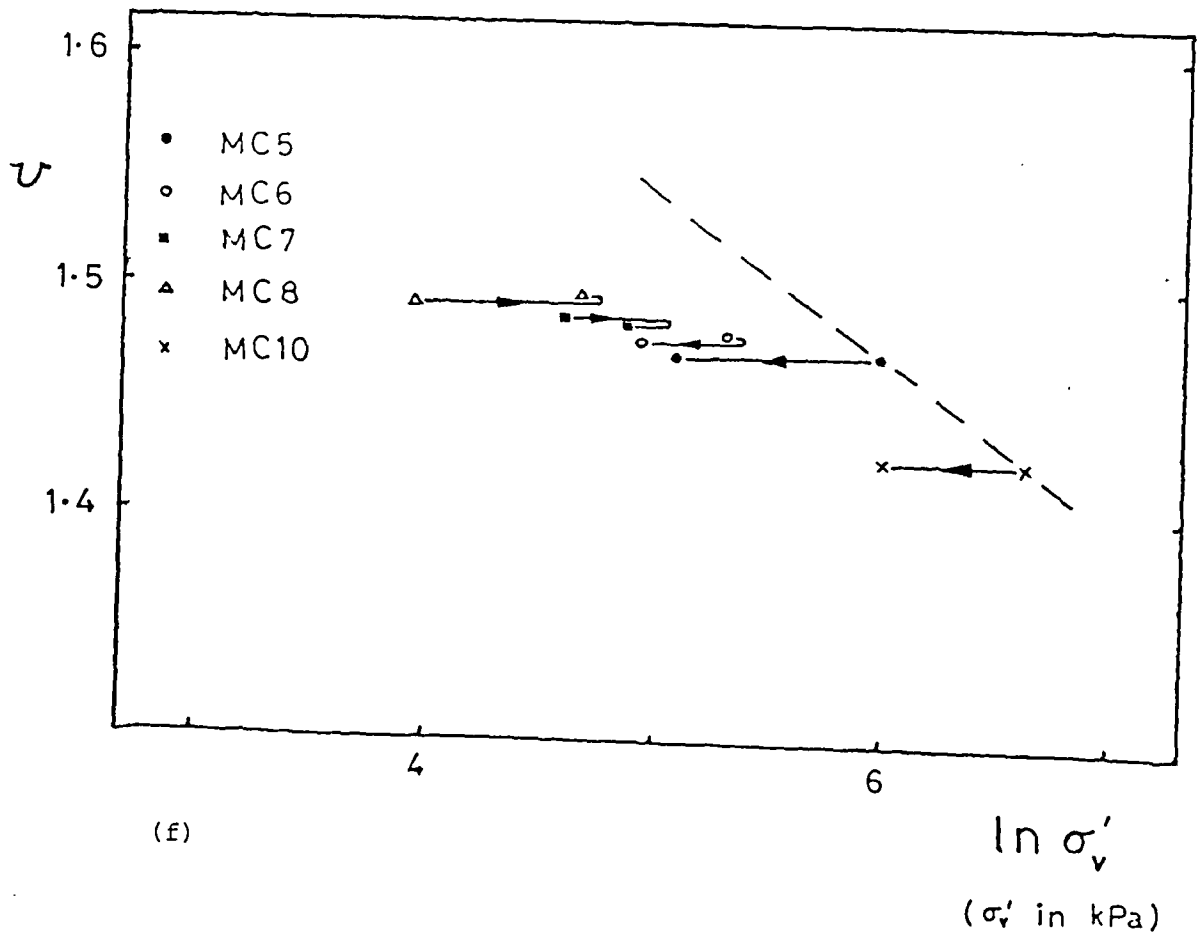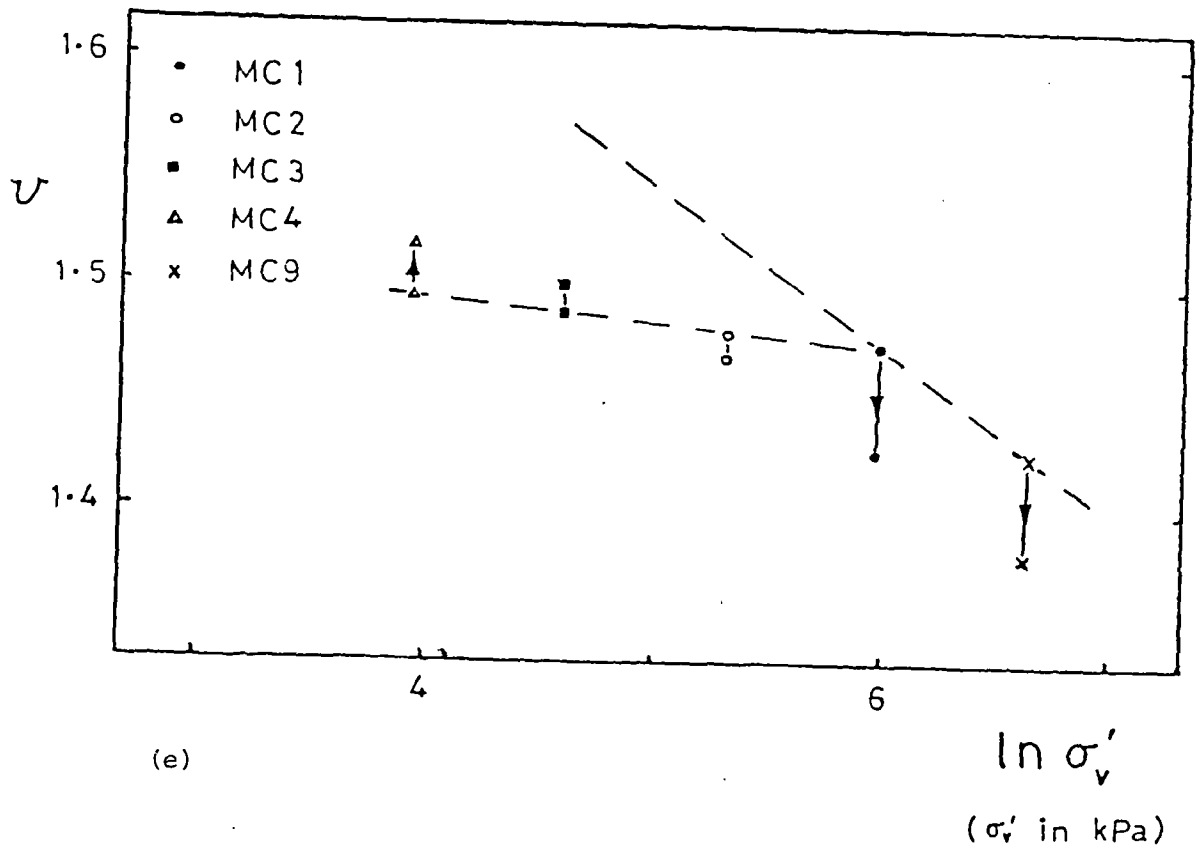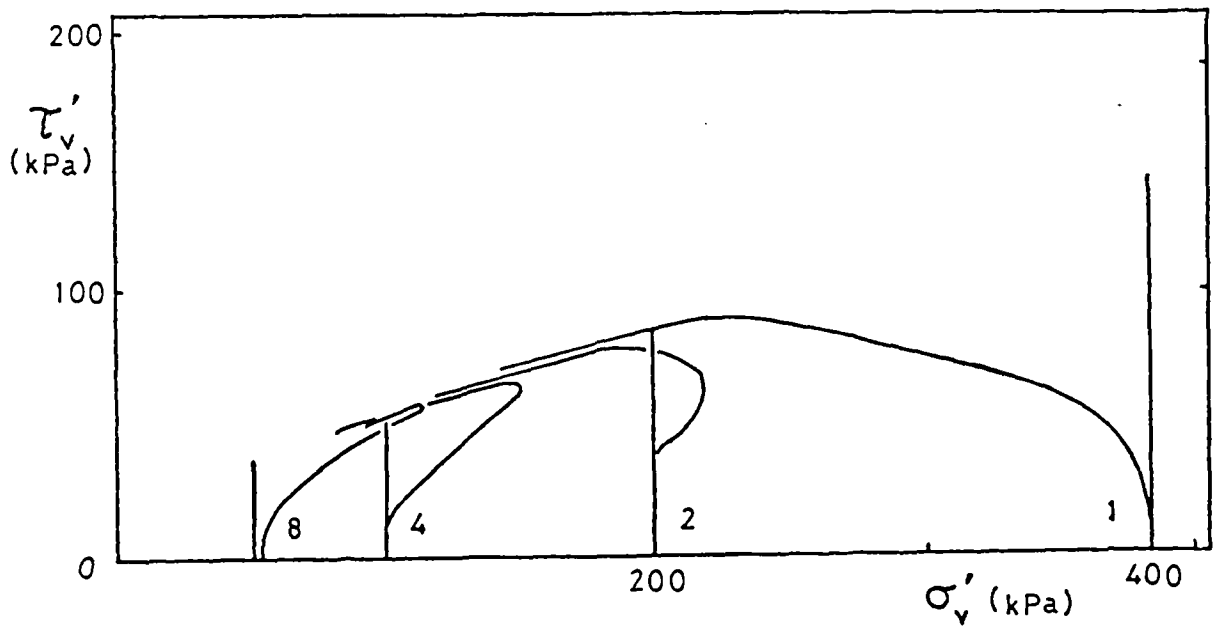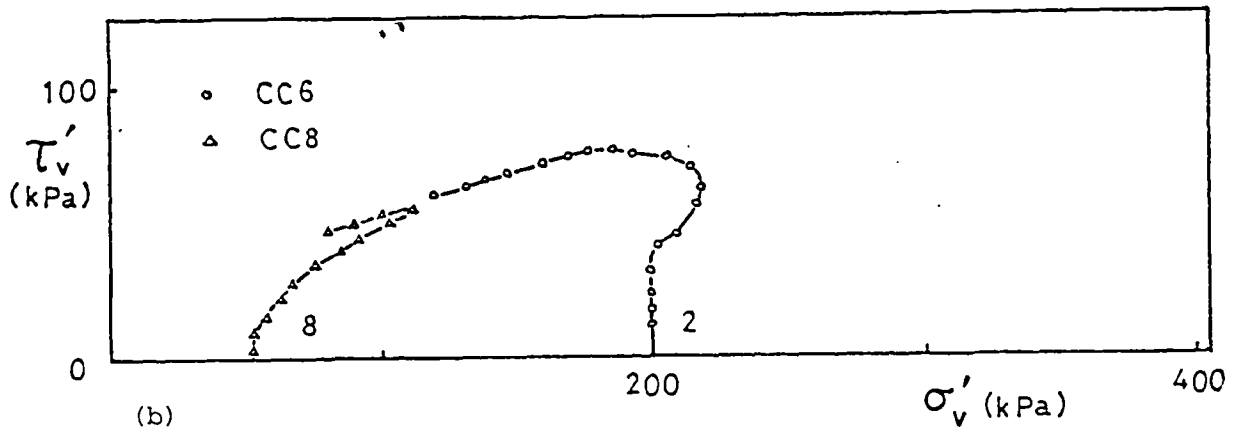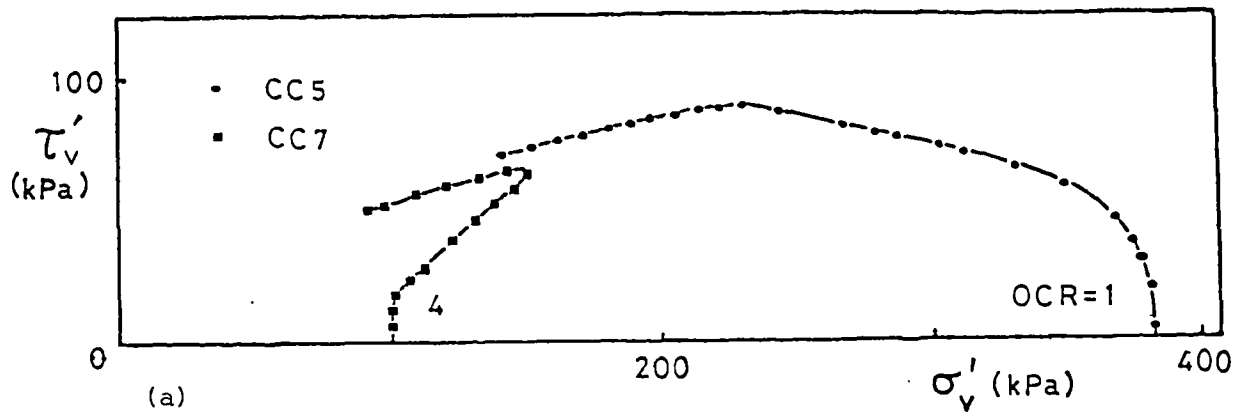
Figure 7.40   State paths for reconstituted Cowden till simple
                  shear samples

(d)

$\ln \sigma_v'$

$(\sigma_v'$ in kPa)

(e)

$\ln \sigma_v'$

$(\sigma_v'$ in kPa)
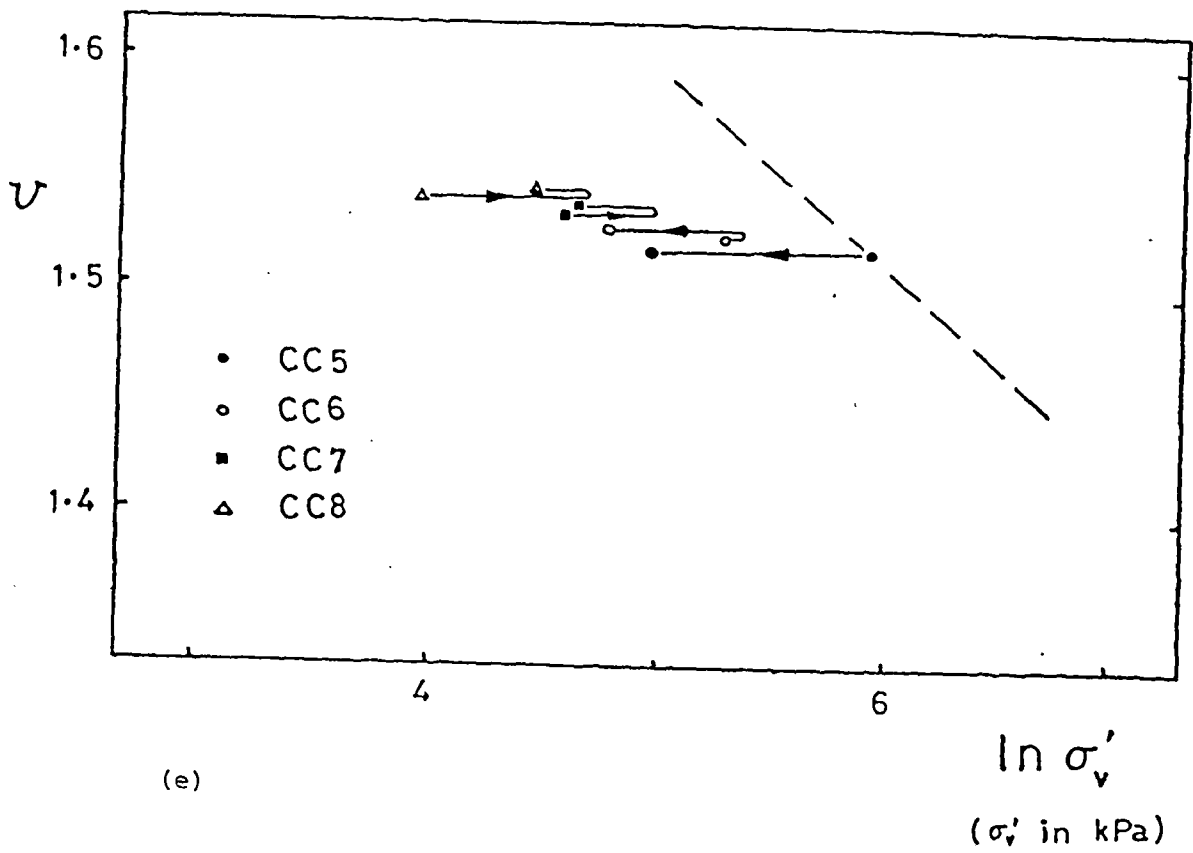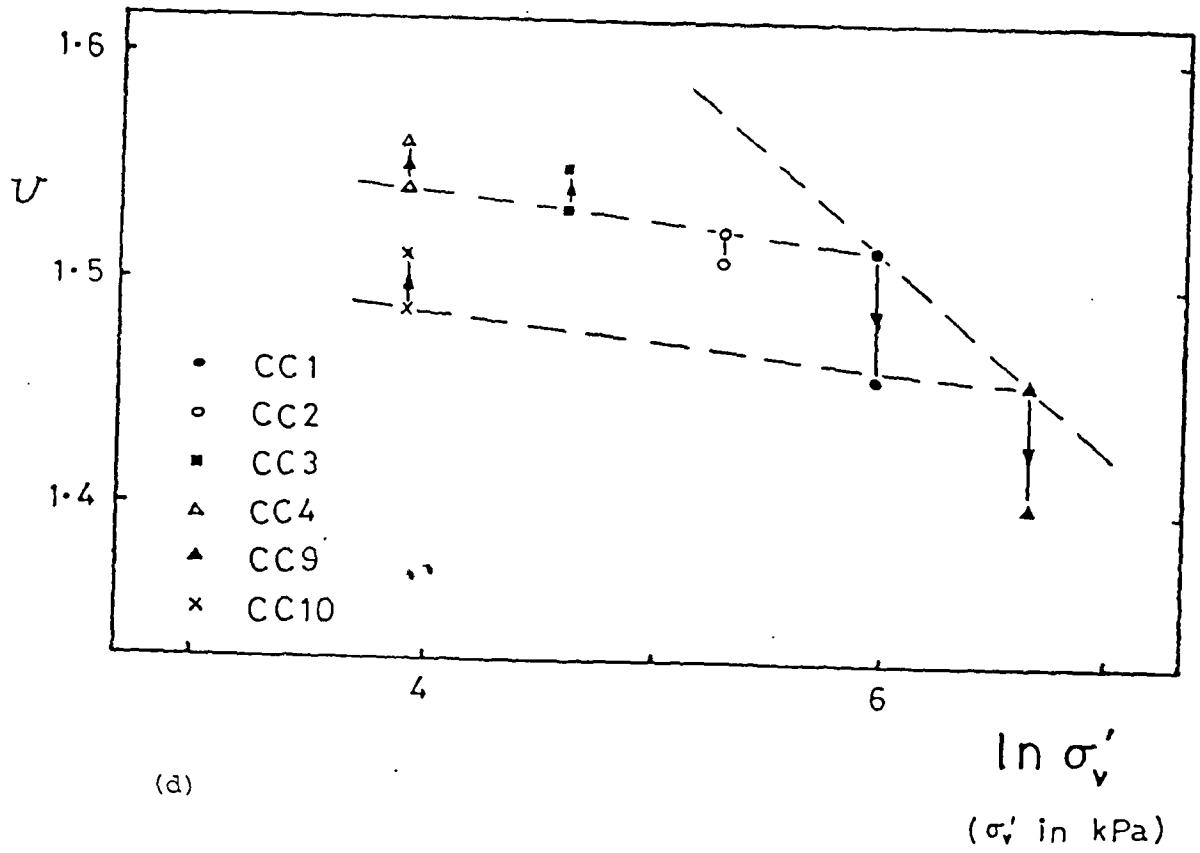
Figure 7.40 continued
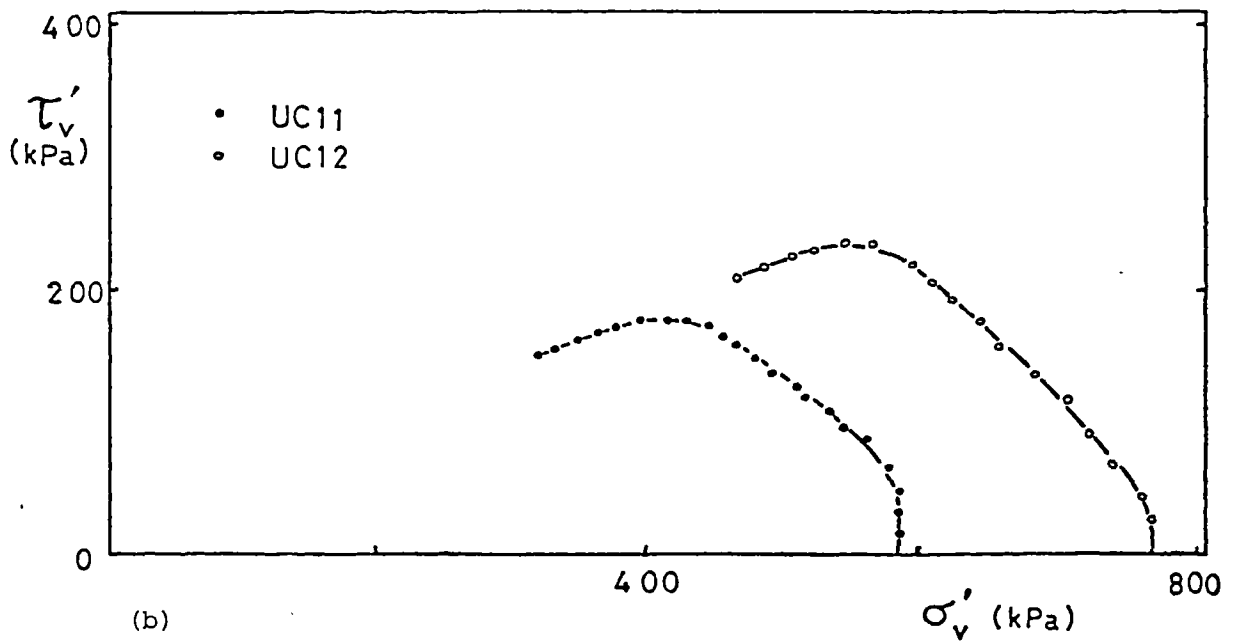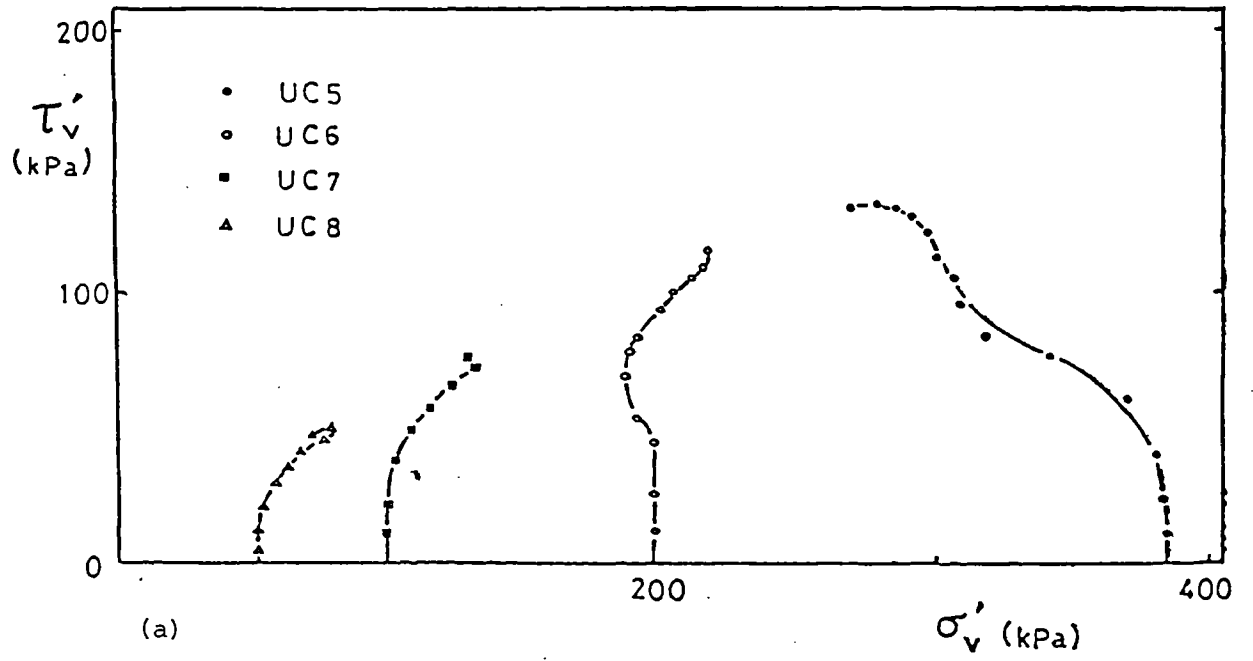
Figure 7.41   State paths for undisturbed Cowden till simple shear
samples
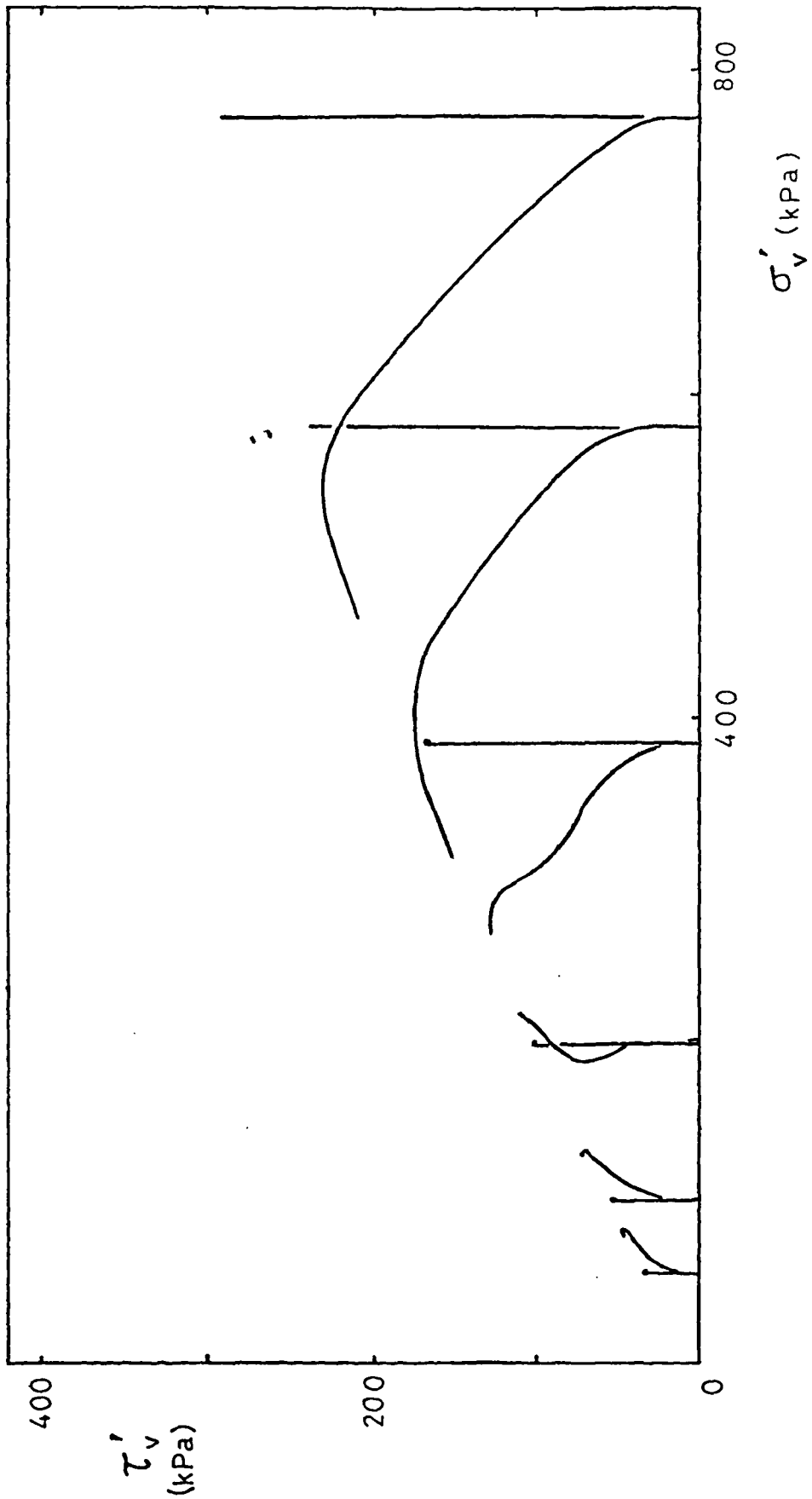
(c)   Summary of all tests

Figure   7.41   continued

(d)

$(\sigma_v'$ in kPa$)$

(e)

$(\sigma_v'$ in kPa$)$
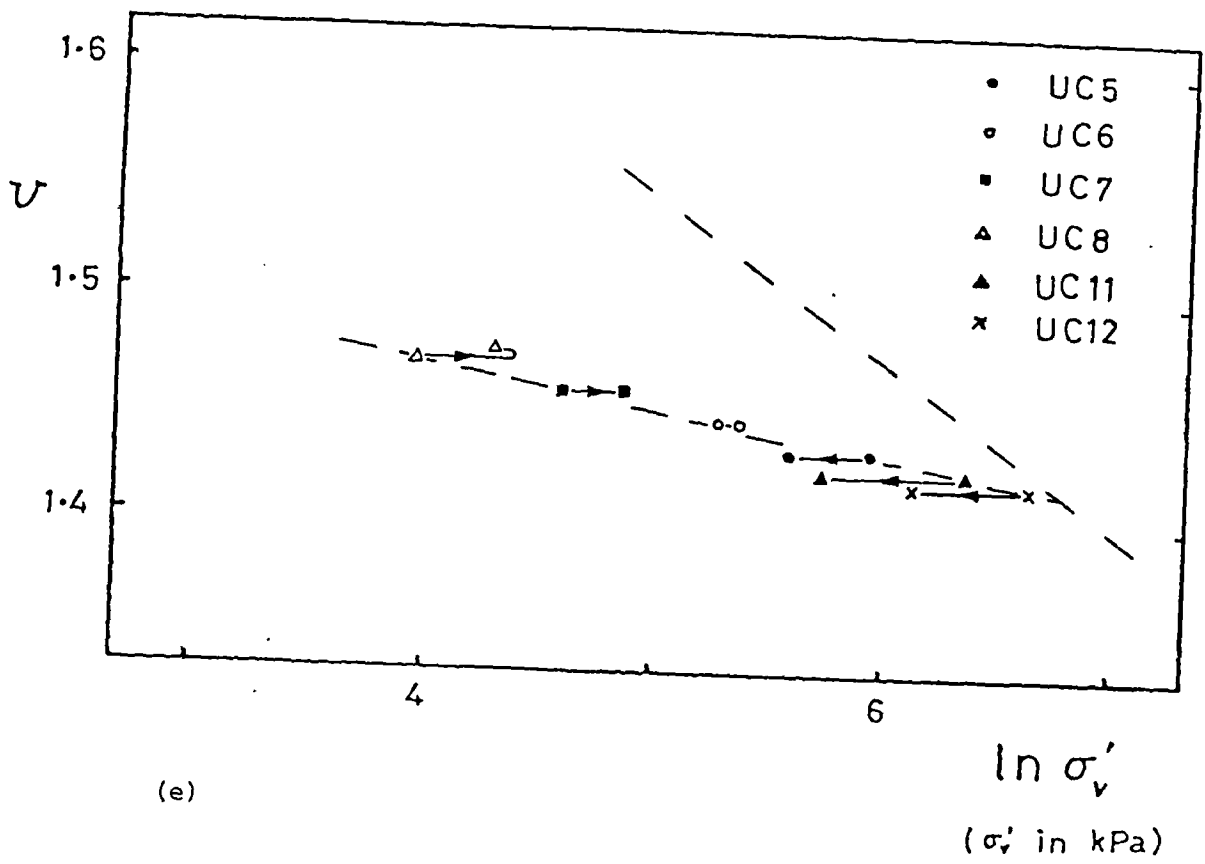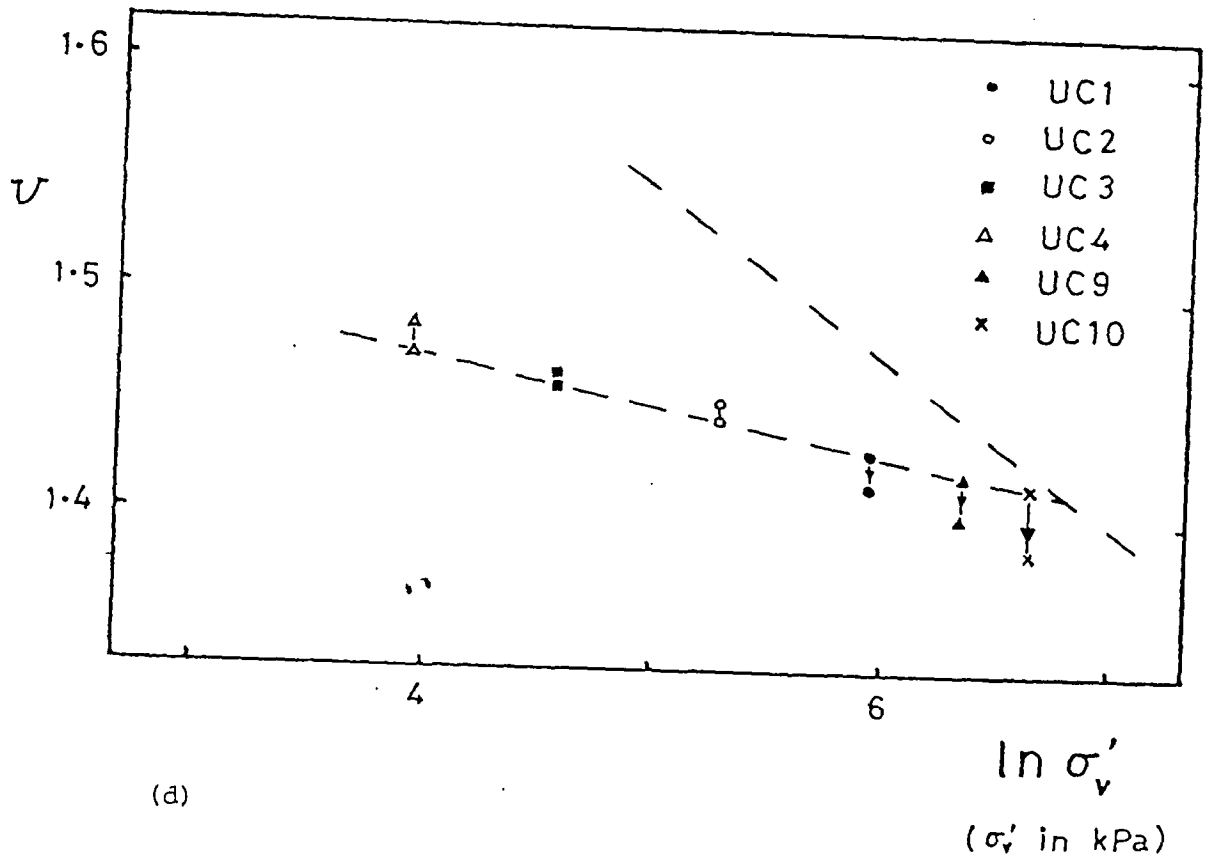
Figure 7.41 continued
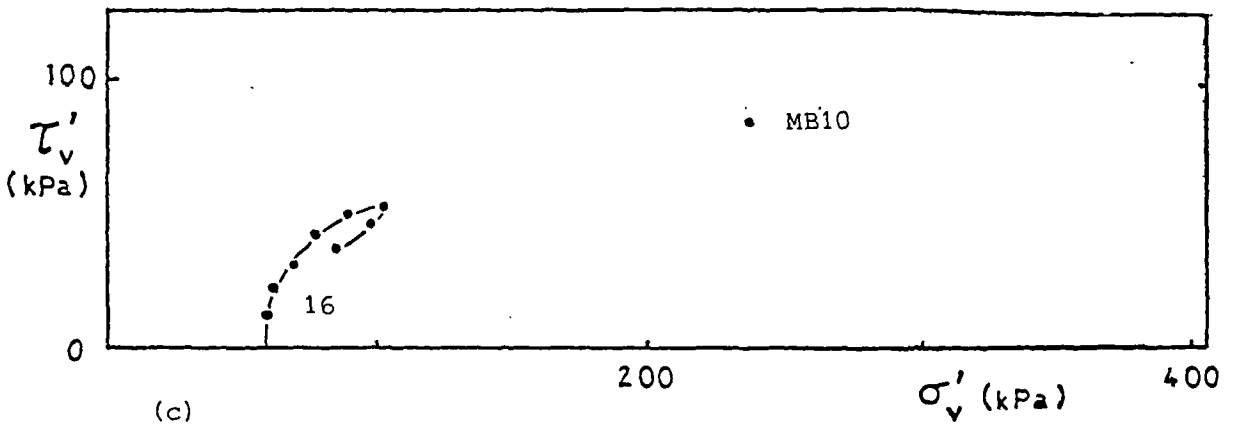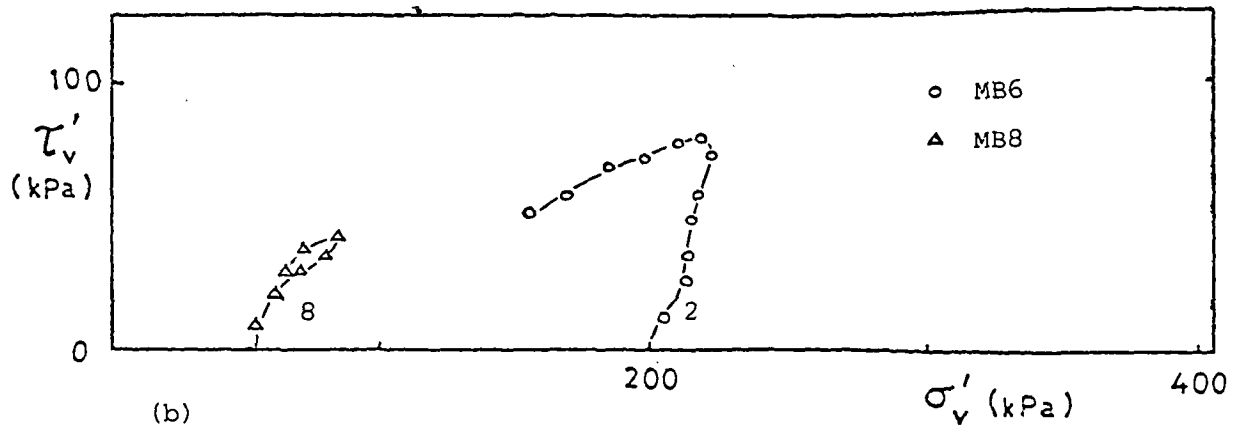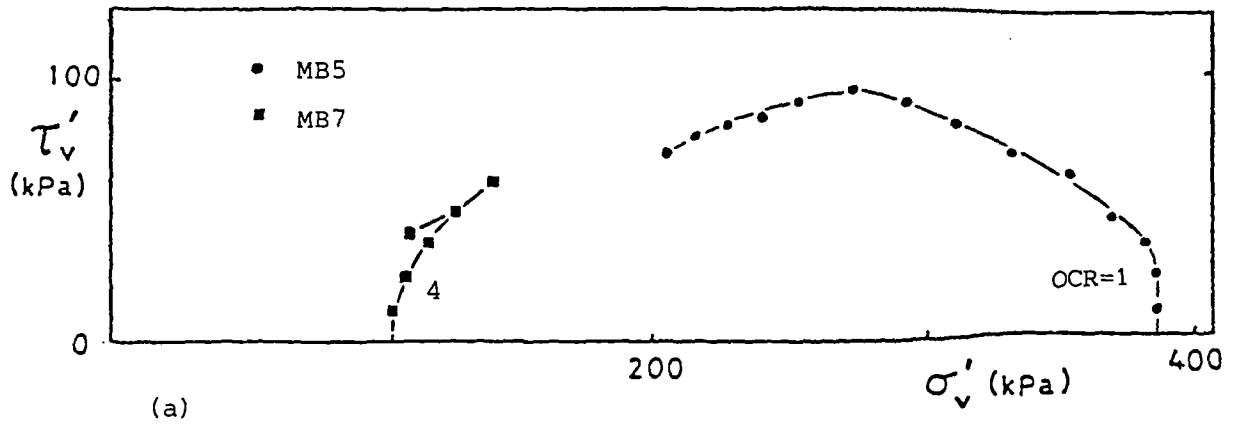
Figure 7.42   State paths for remoulded London clay (brown) simple
                shear samples

(d)

(e)
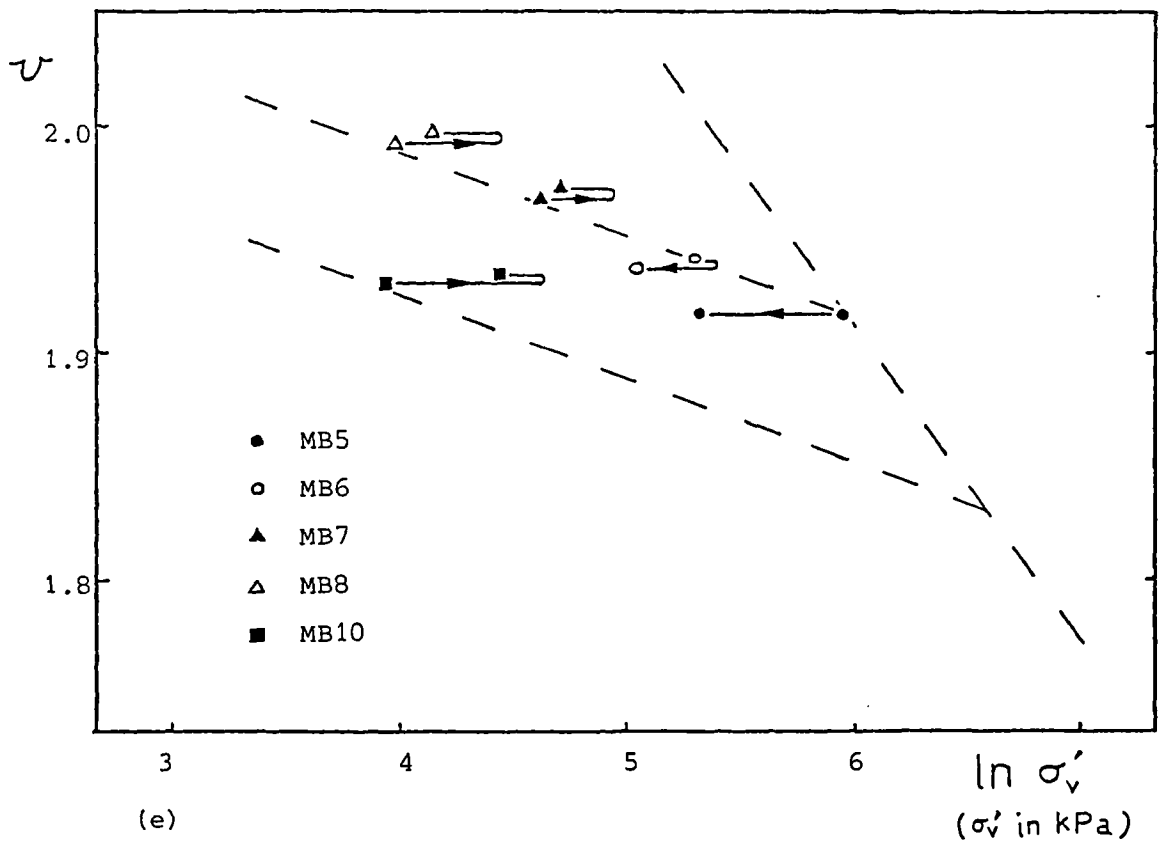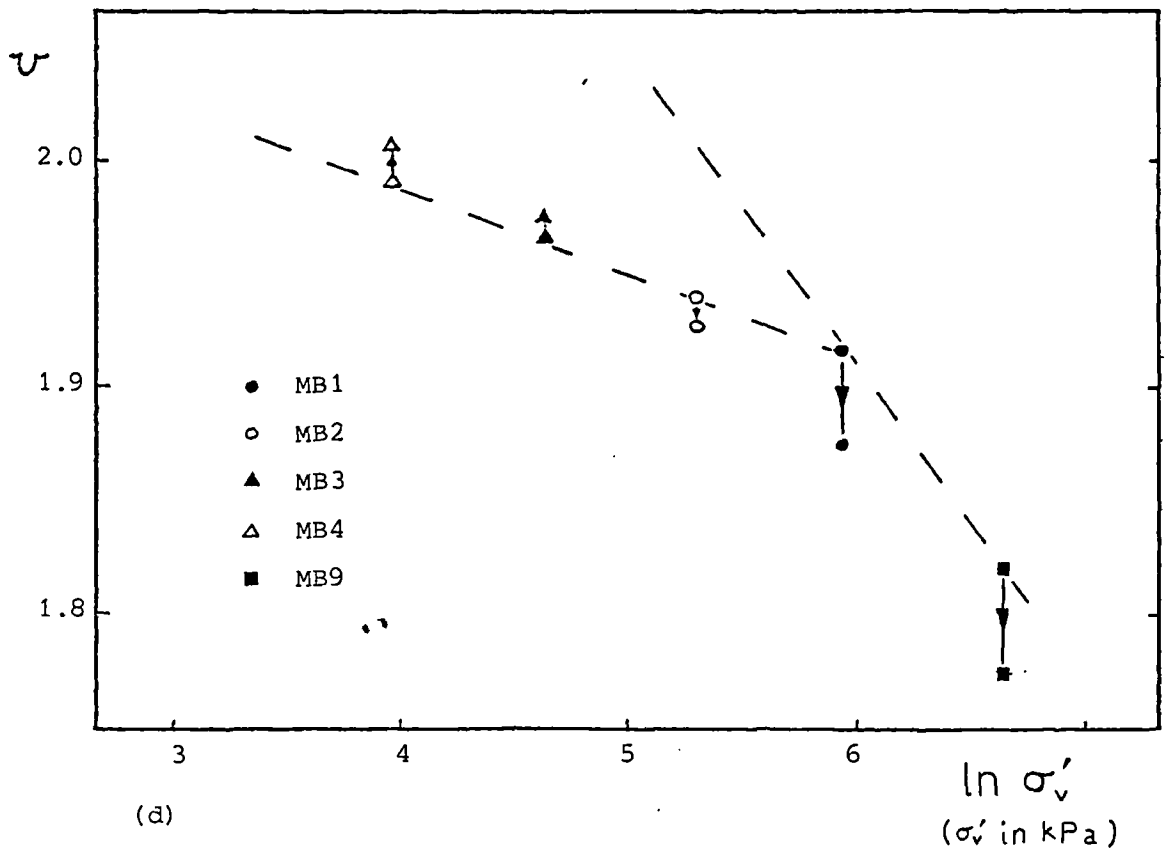
Figure 7.42 continued
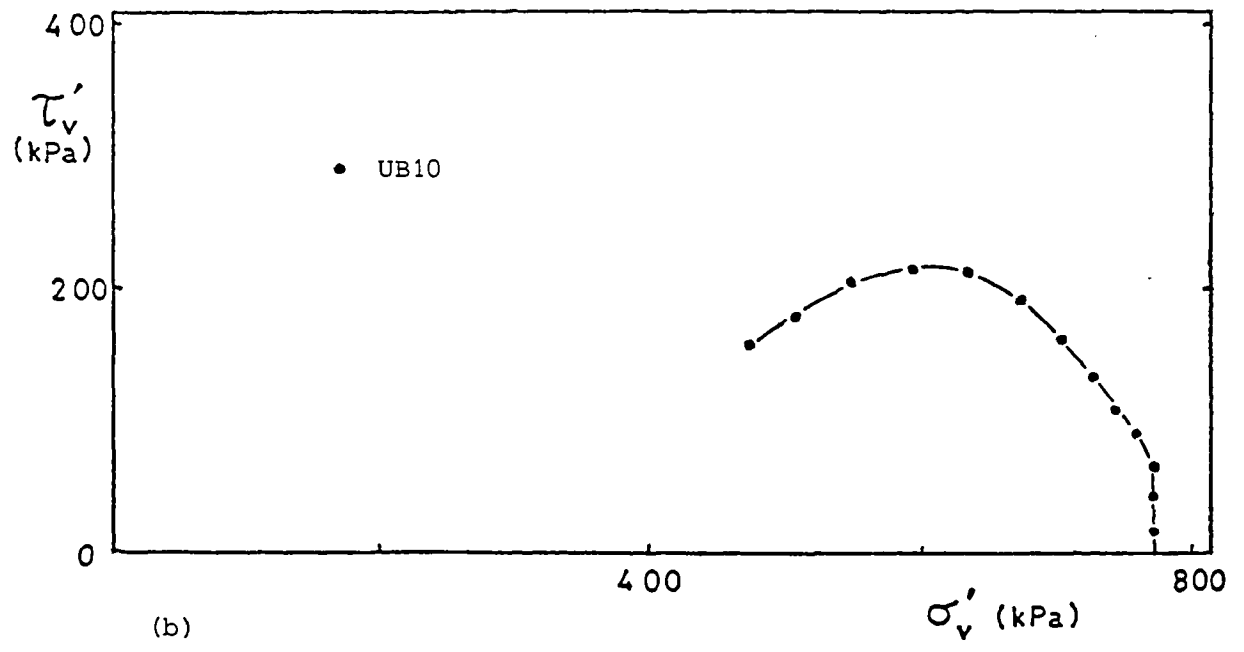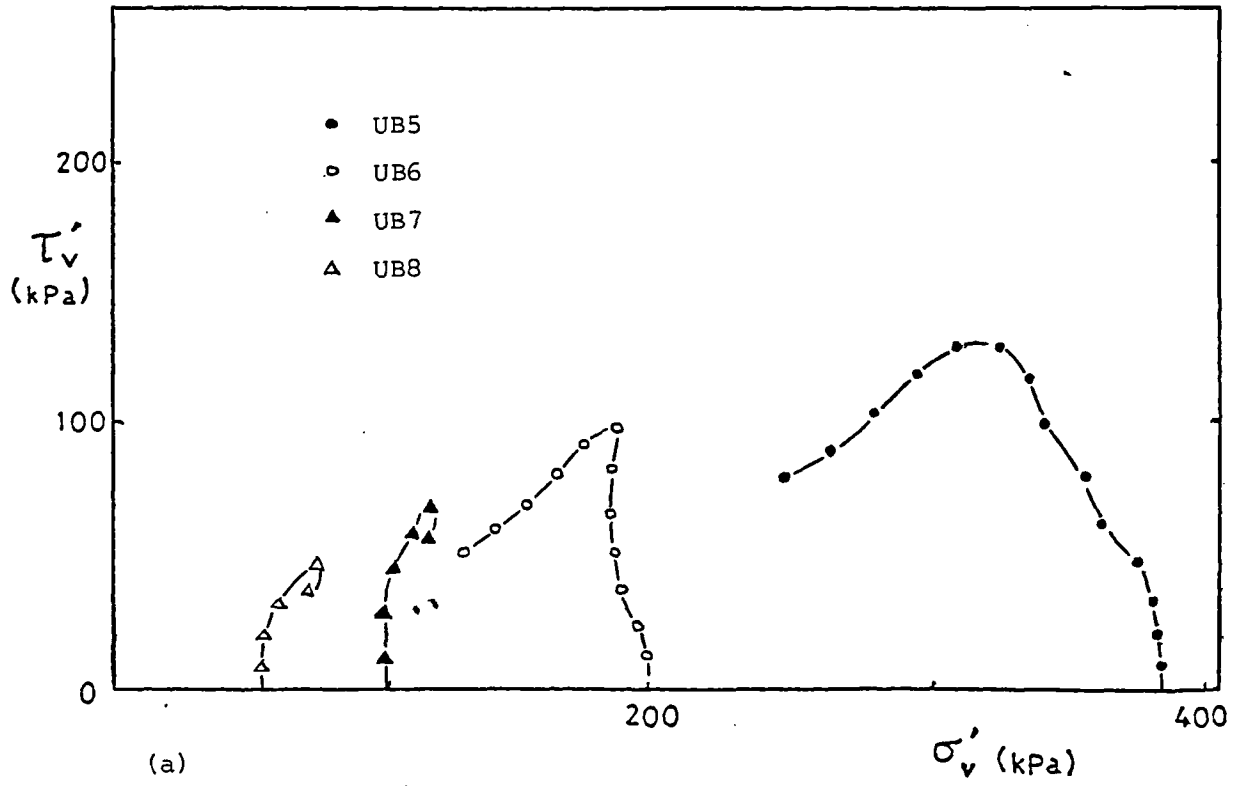
Figure 7.43   State paths for undisturbed London clay (brown) simple shear samples

(c)

(d)
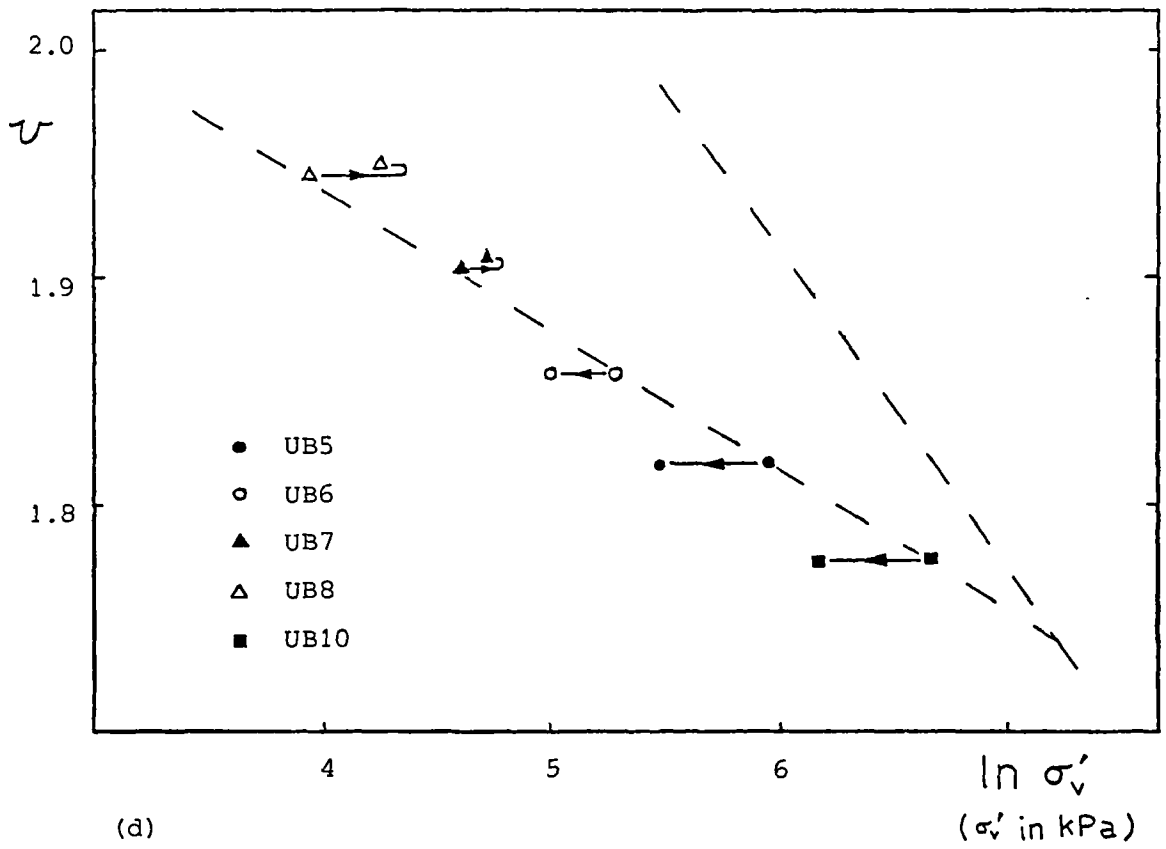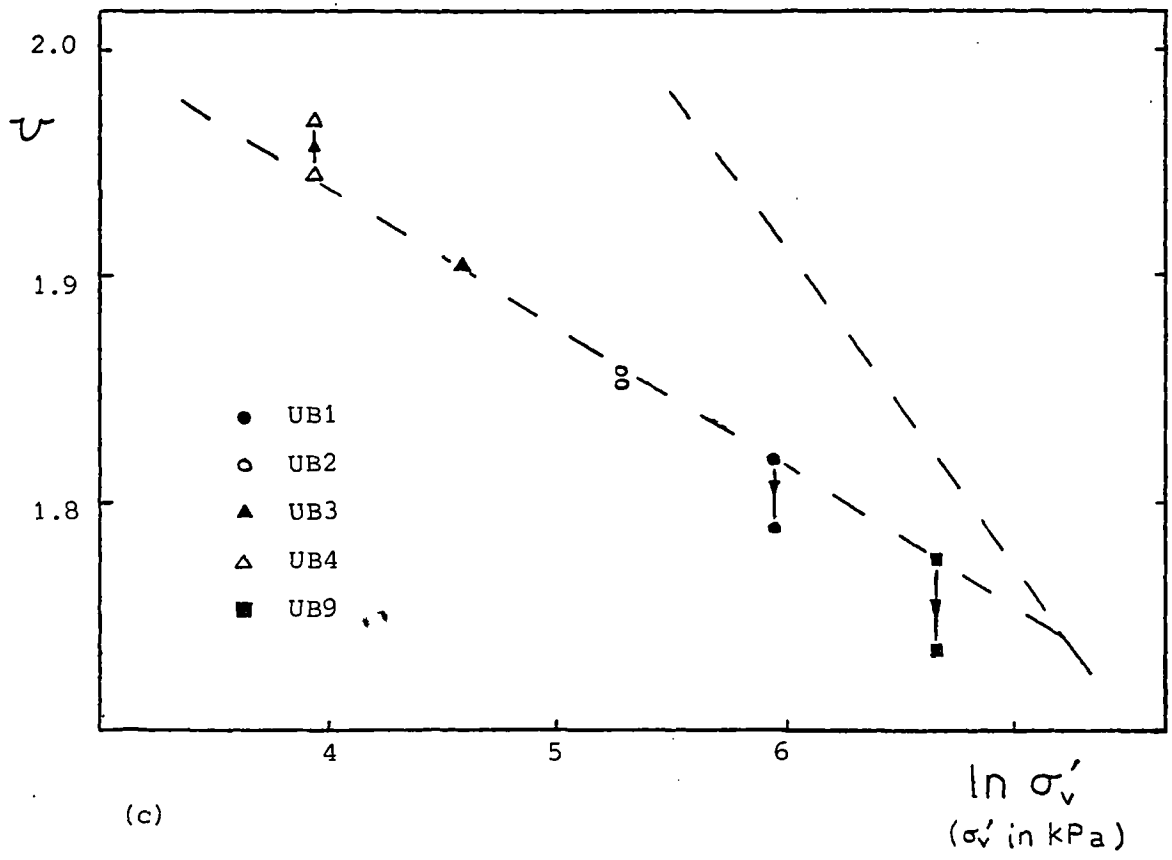
Figure 7.43 continued
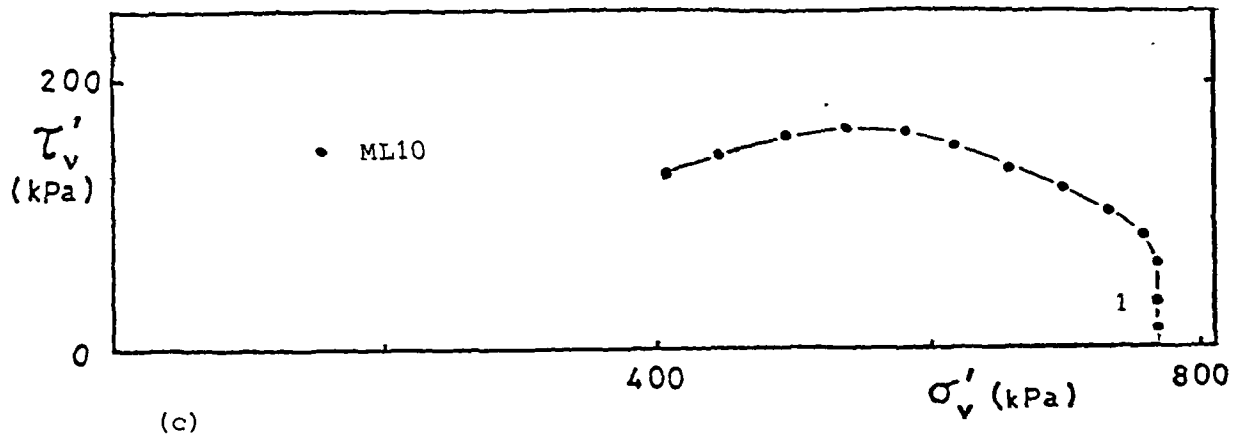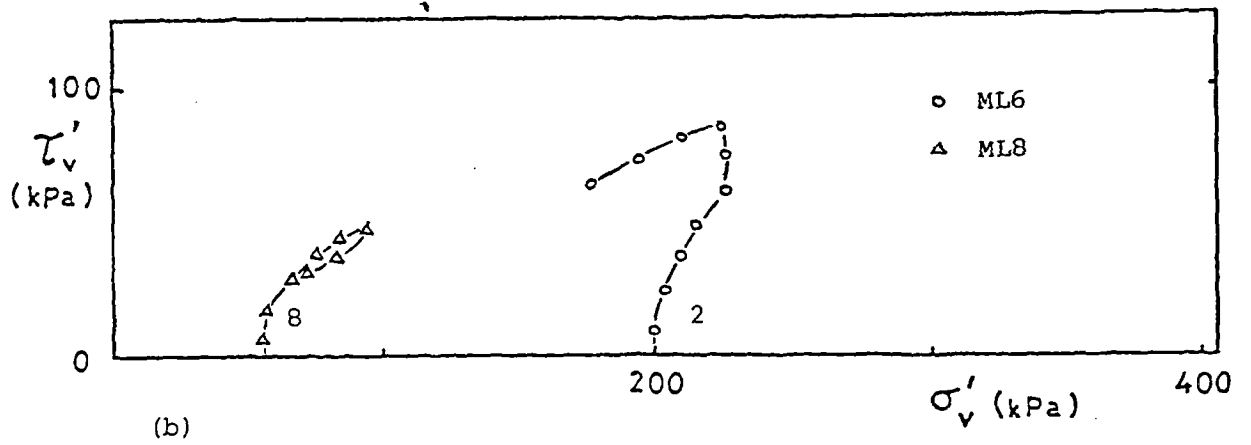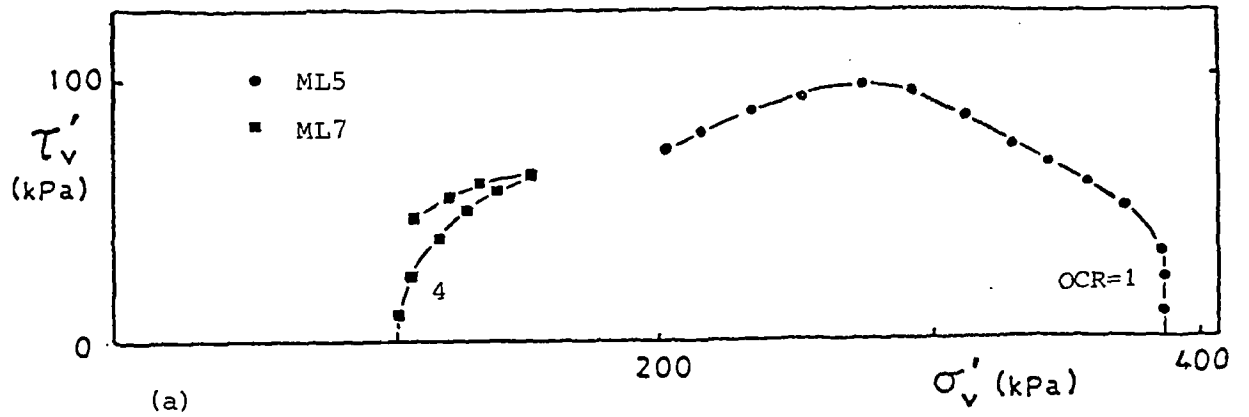
Figure 7.44   State paths for remoulded London clay (blue) simple shear samples

(d)

(e)
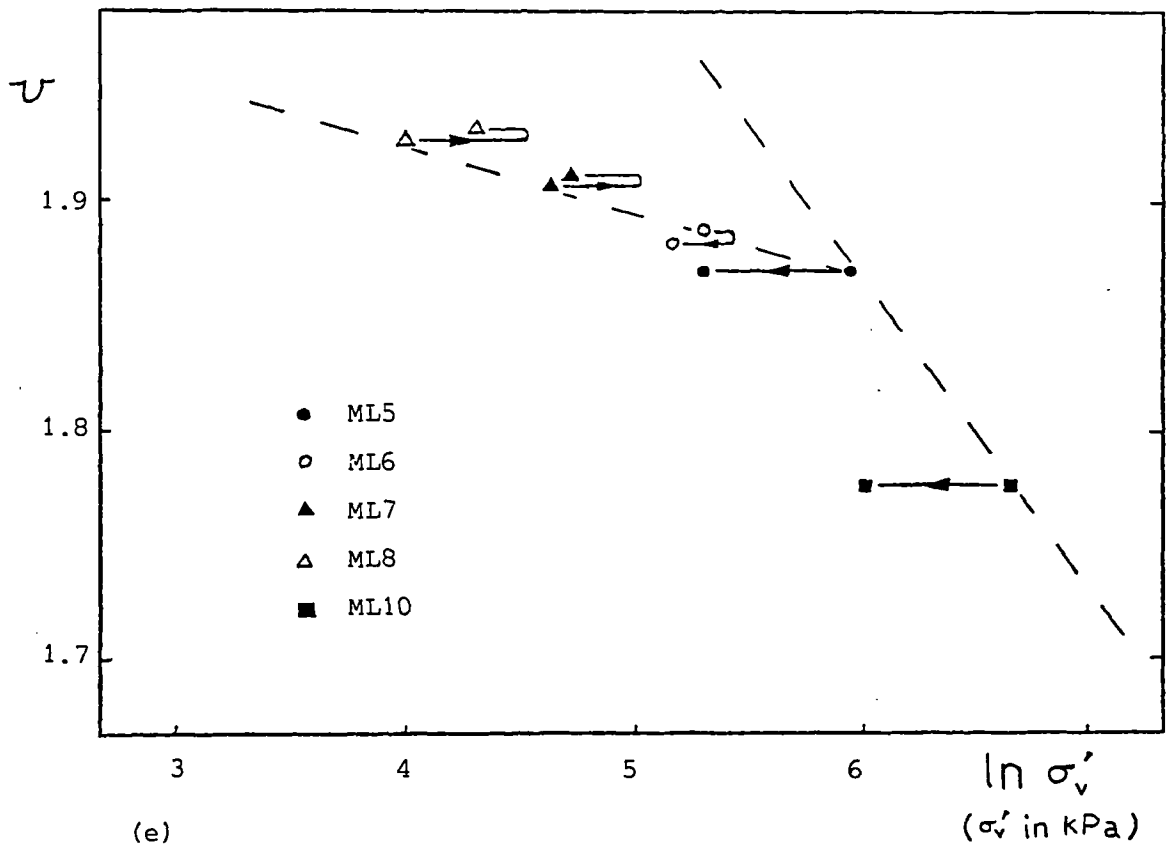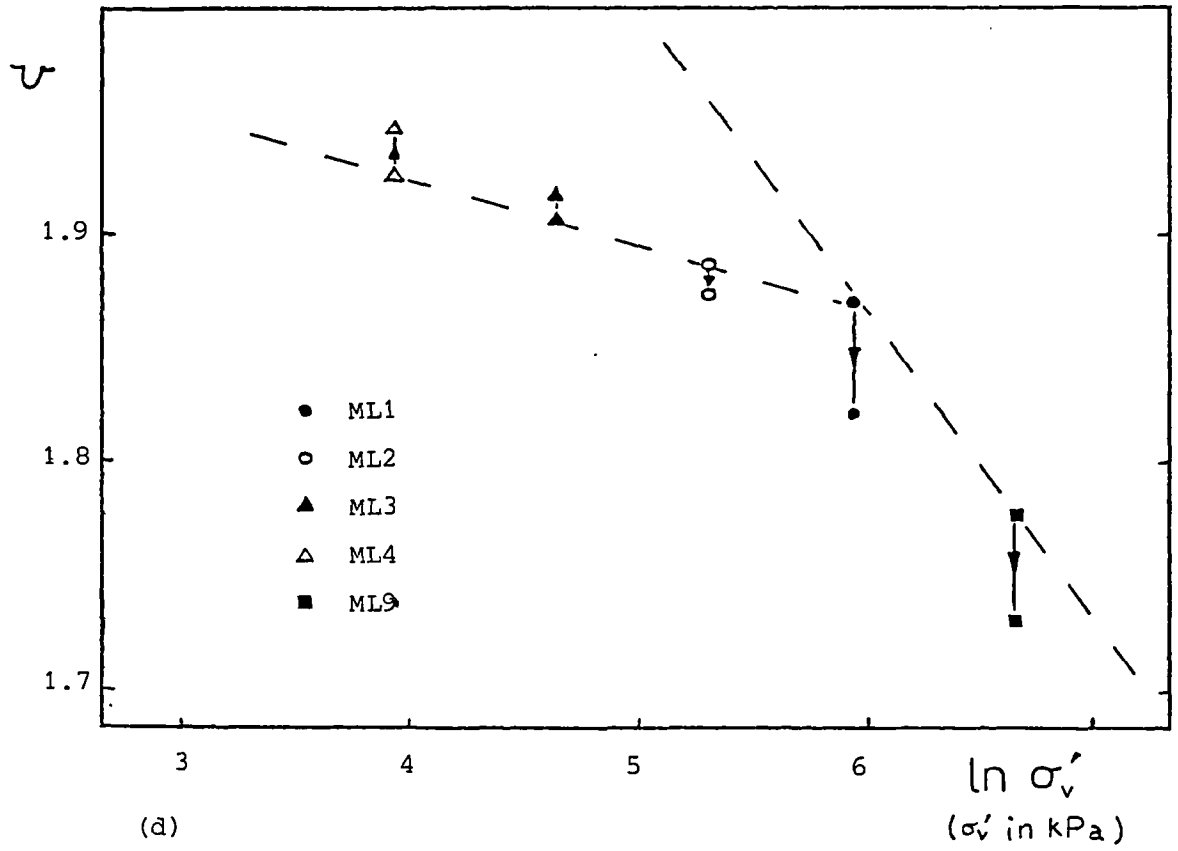
Figure 7.44 continued
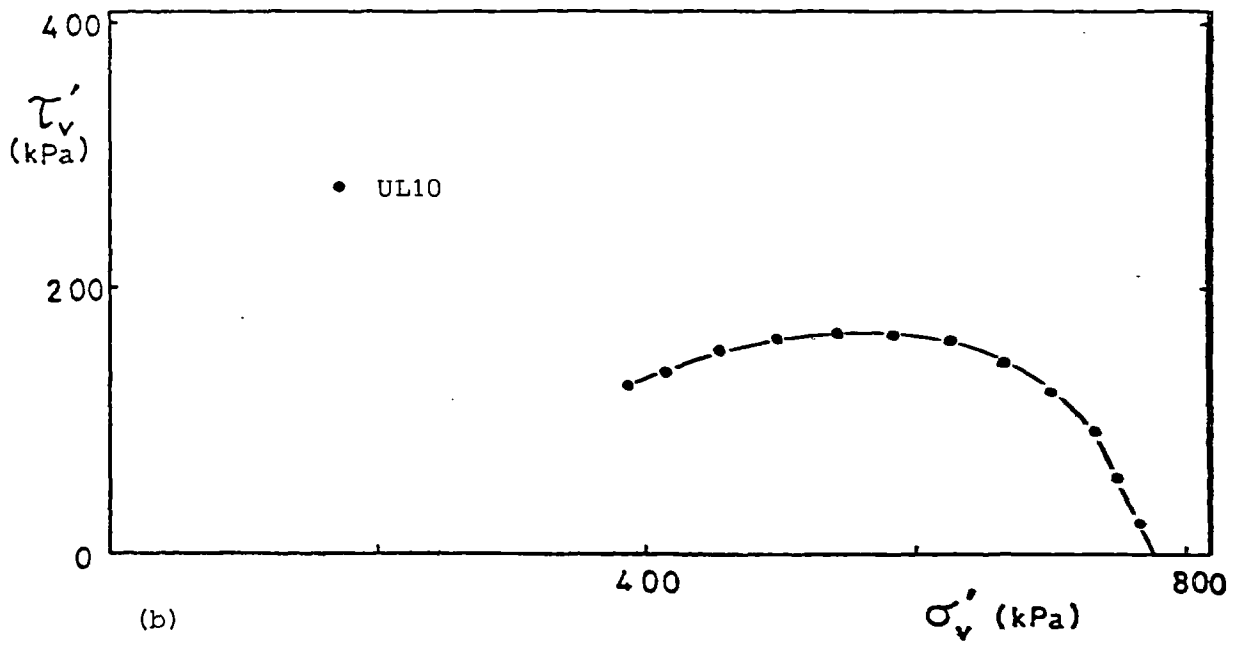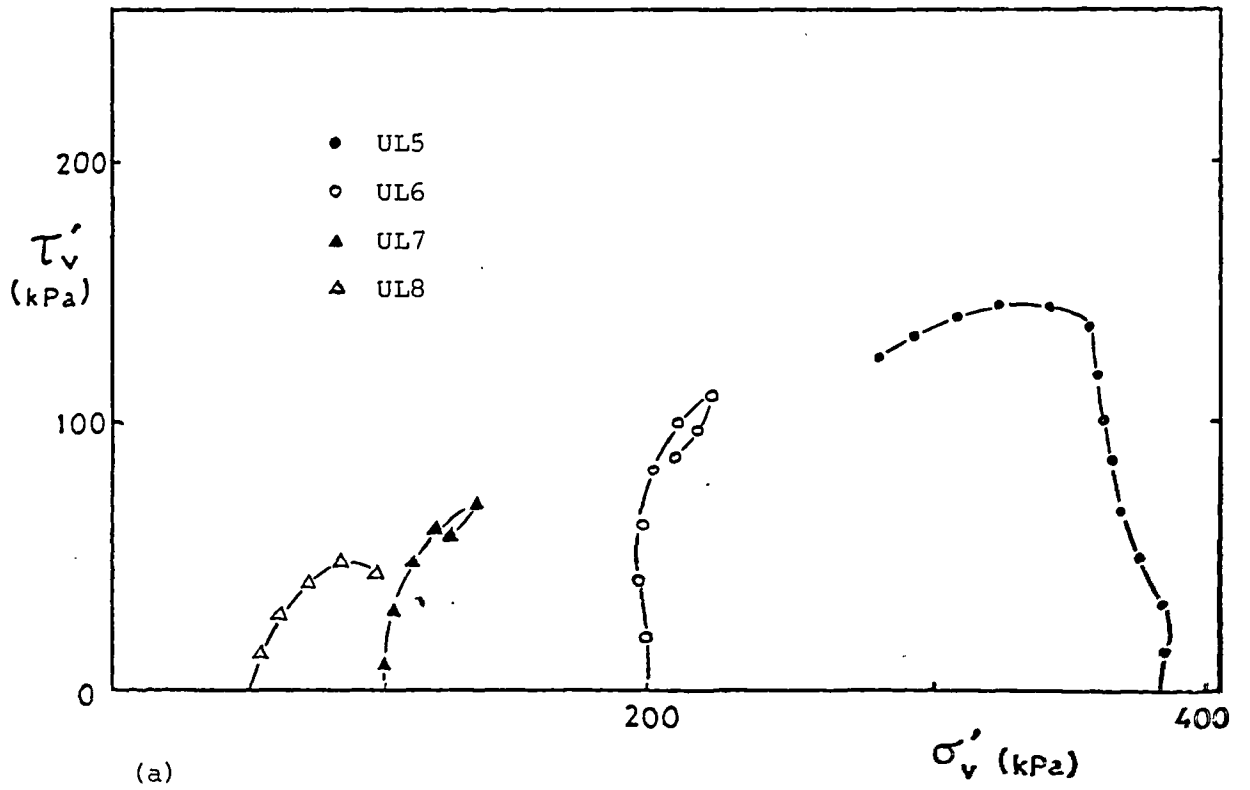
Figure 7.45 State paths for undisturbed London clay (blue) simple shear samples

(c)

$\ln \sigma_v'$

$(\sigma_v' \text{ in } kPa)$

(d)

$\ln \sigma_v'$

$(\sigma_v' \text{ in } kPa)$
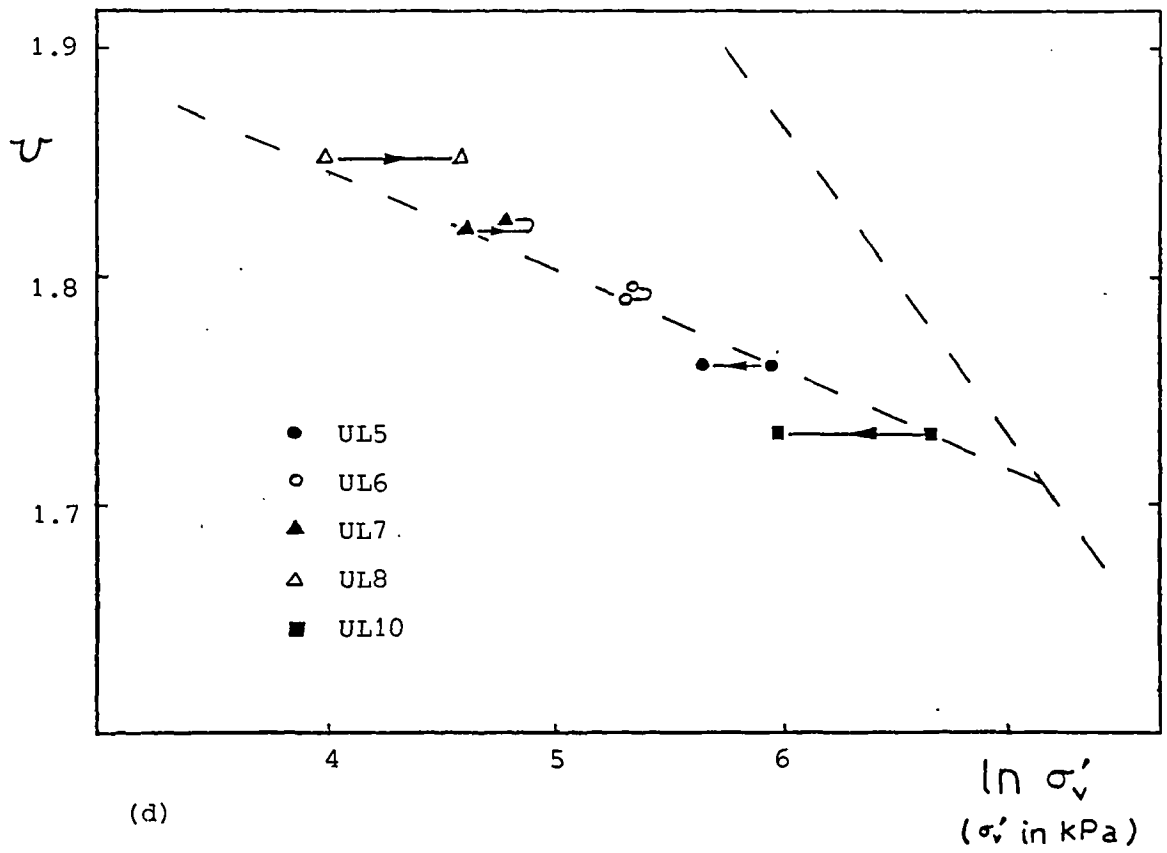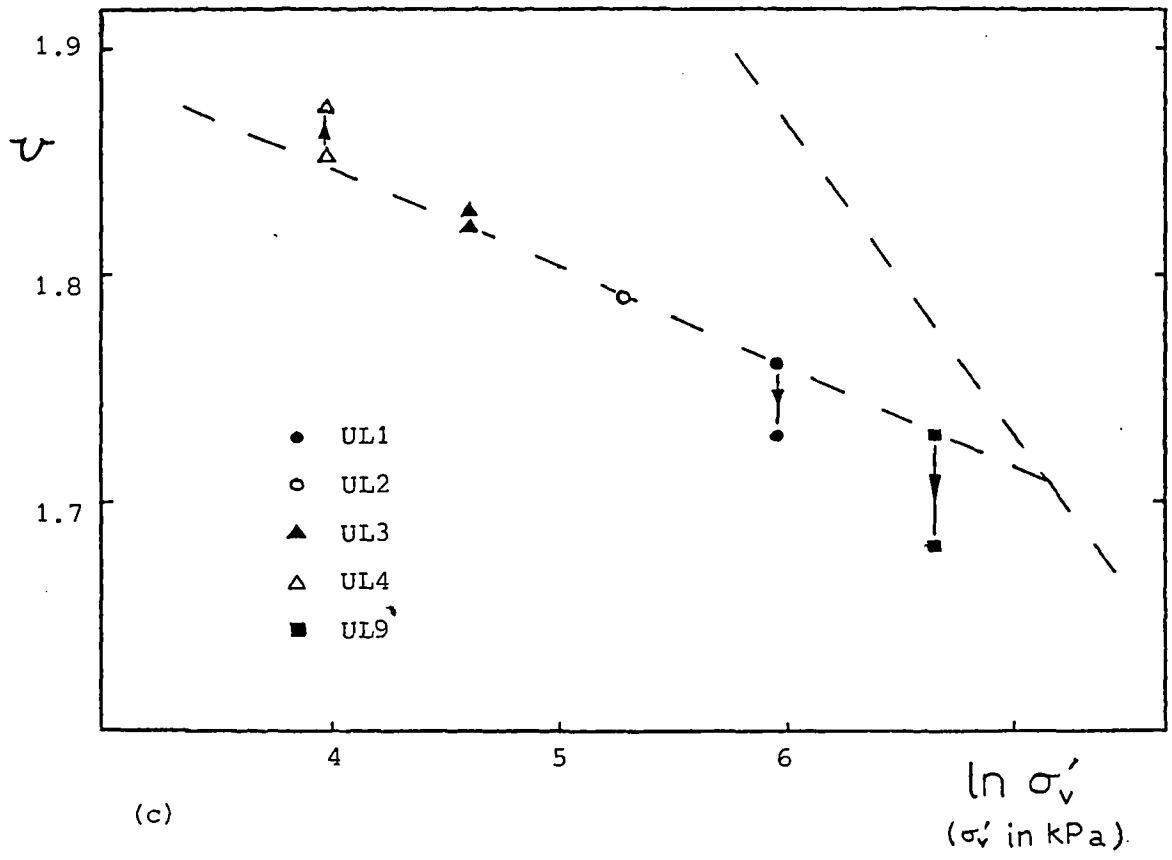
Figure 7.45 continued
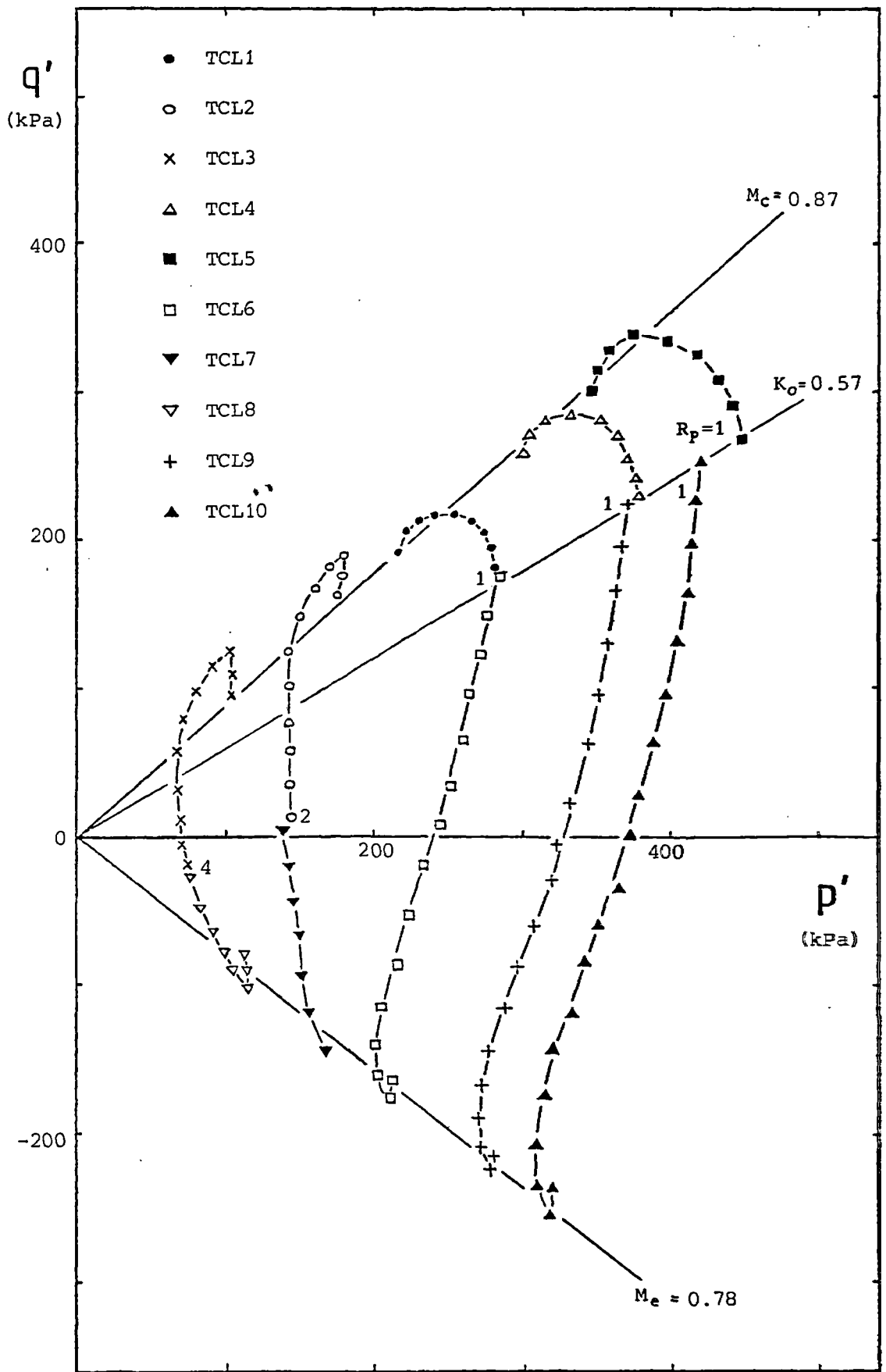
Figure 7.46   State paths for 38 mm reconstituted London clay (blue)
triaxial samples

(b)

(p' in kPa)
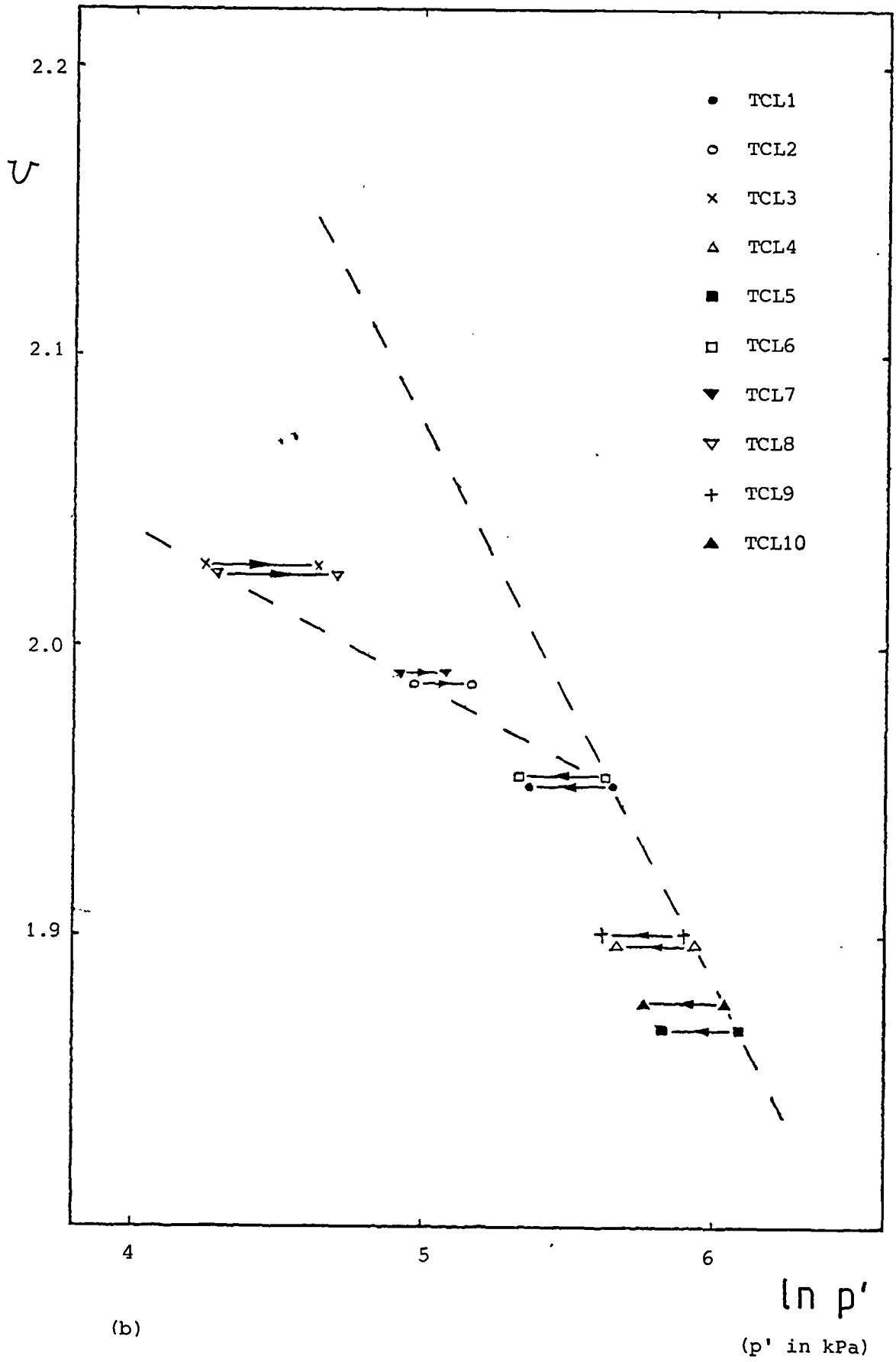
Figure 7.46 continued
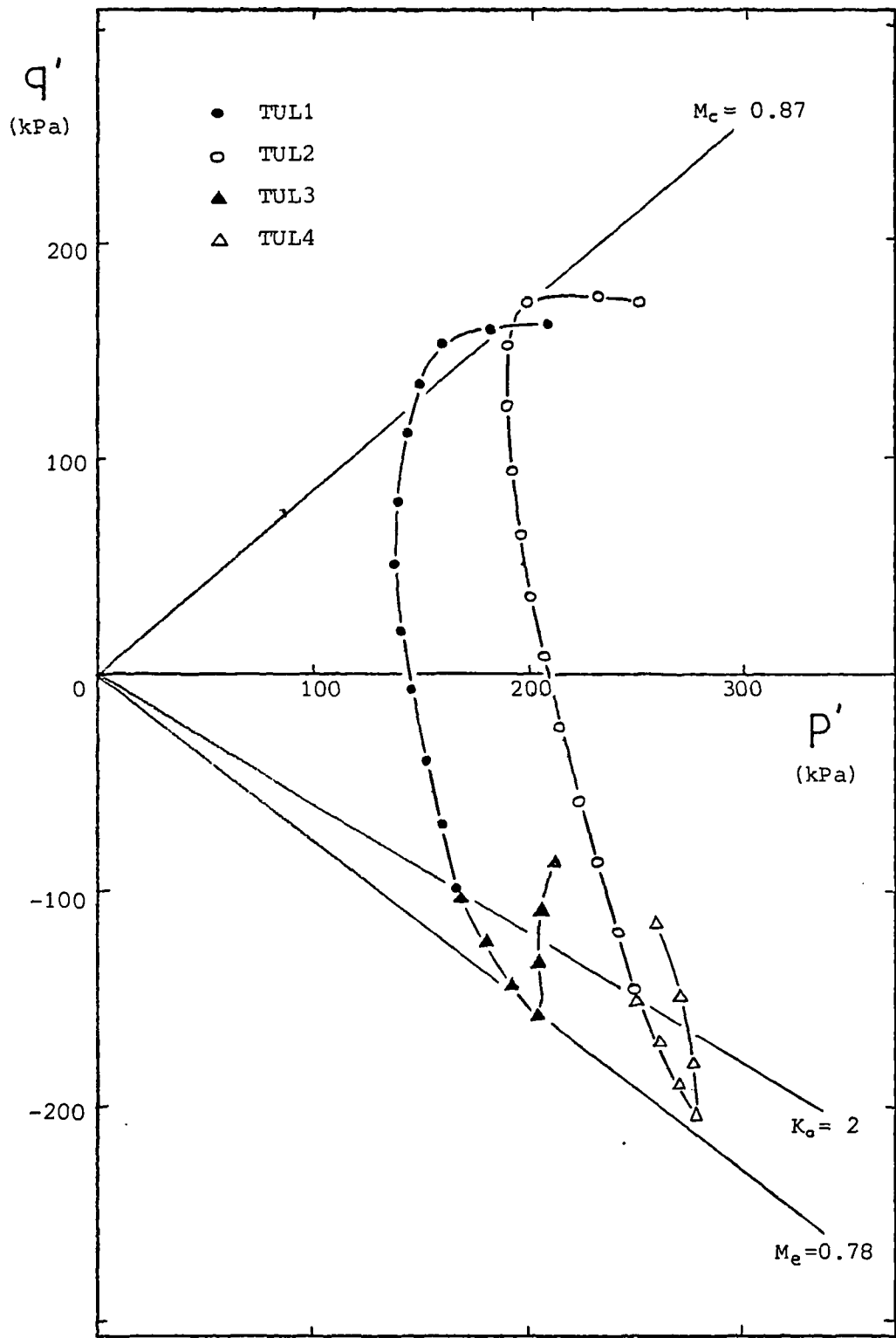
Figure 7.47   State paths for 100 mm undisturbed London clay
(blue) triaxial samples

(b)

(p' in kPa)
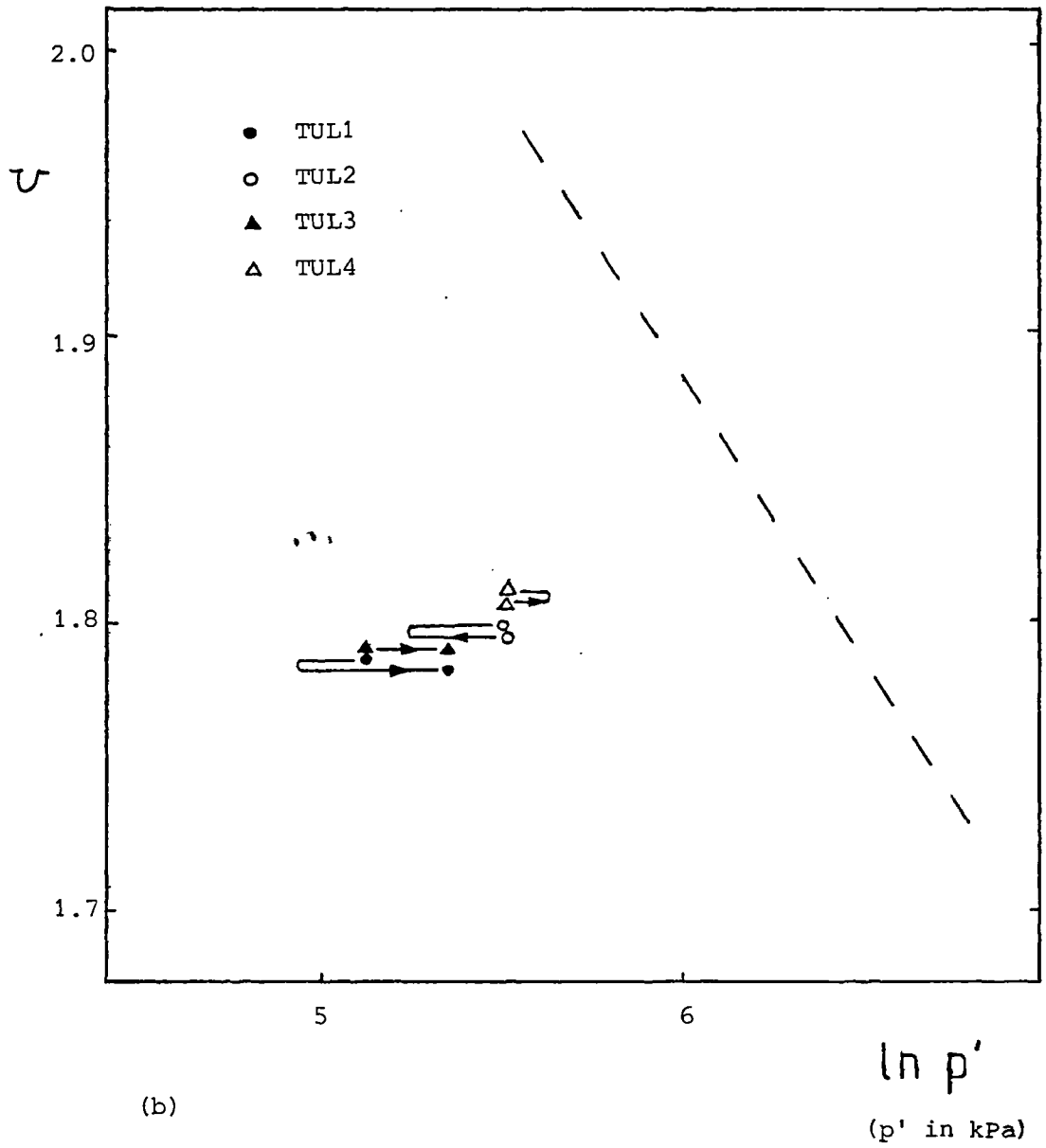
Figure 7.47 continued
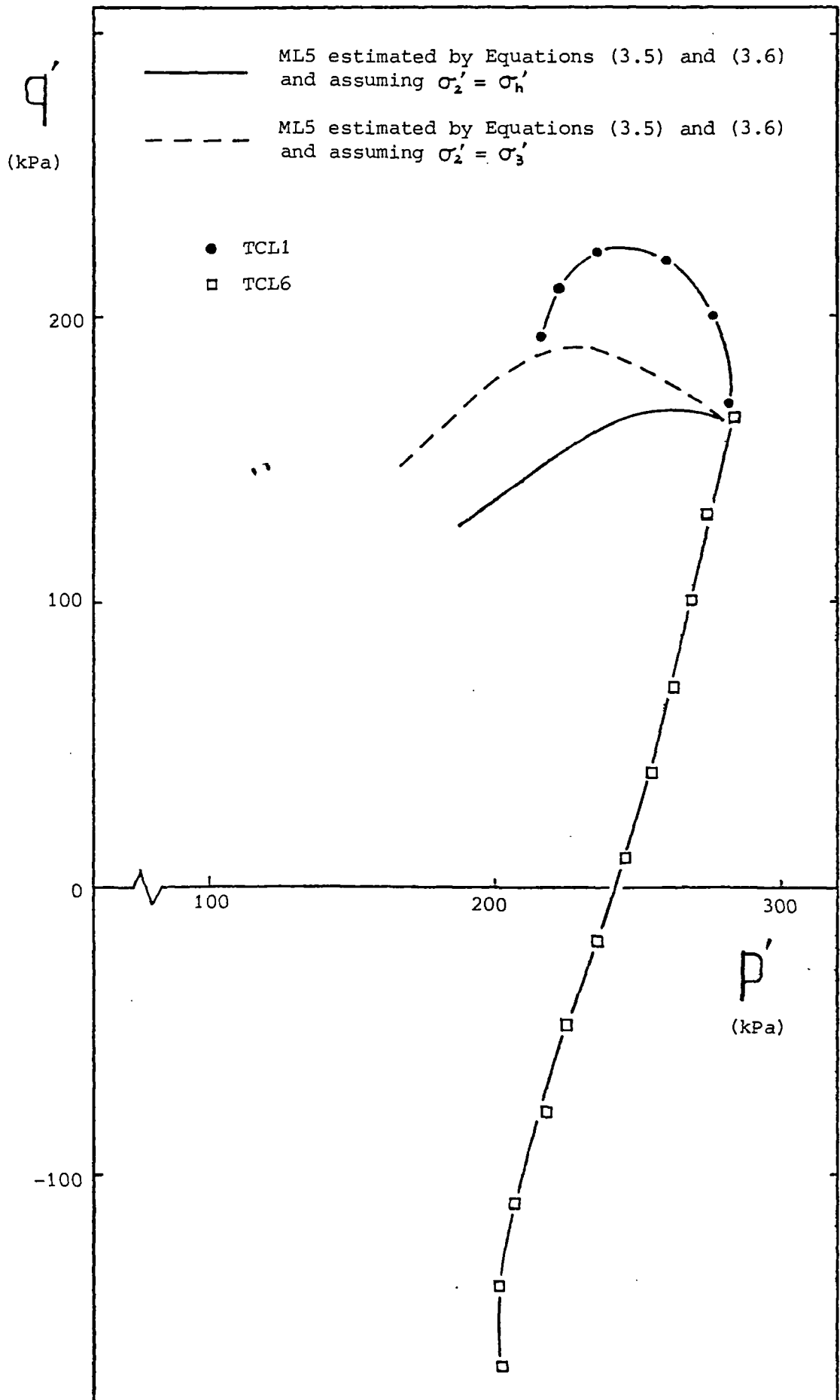
Figure 7.48   Estimated simple shear stress paths on p',q' plane
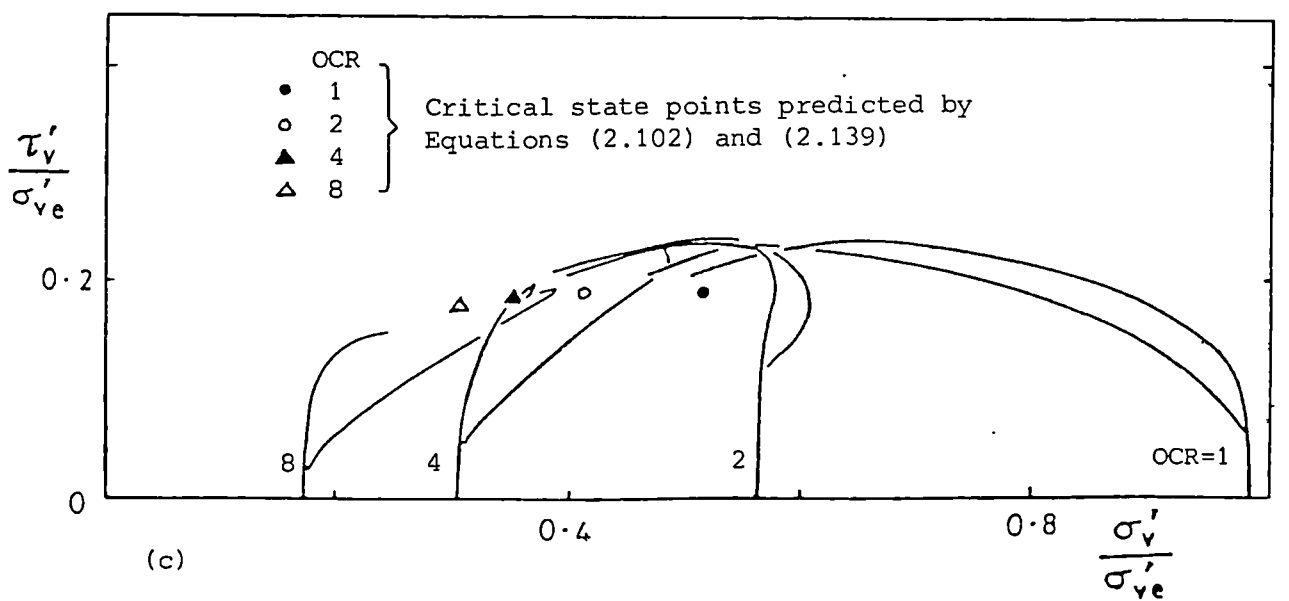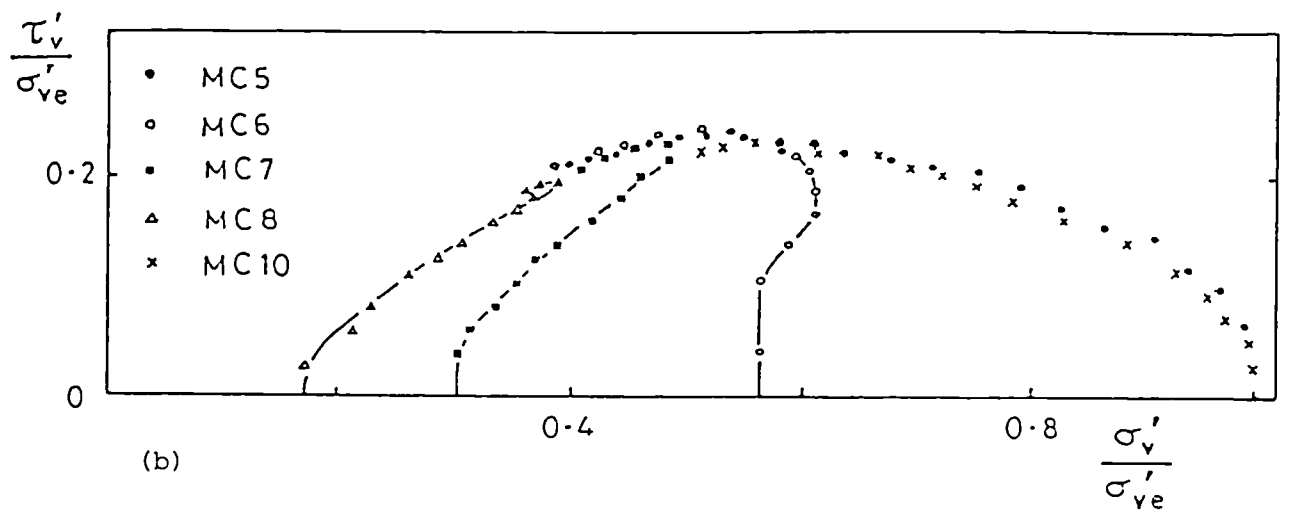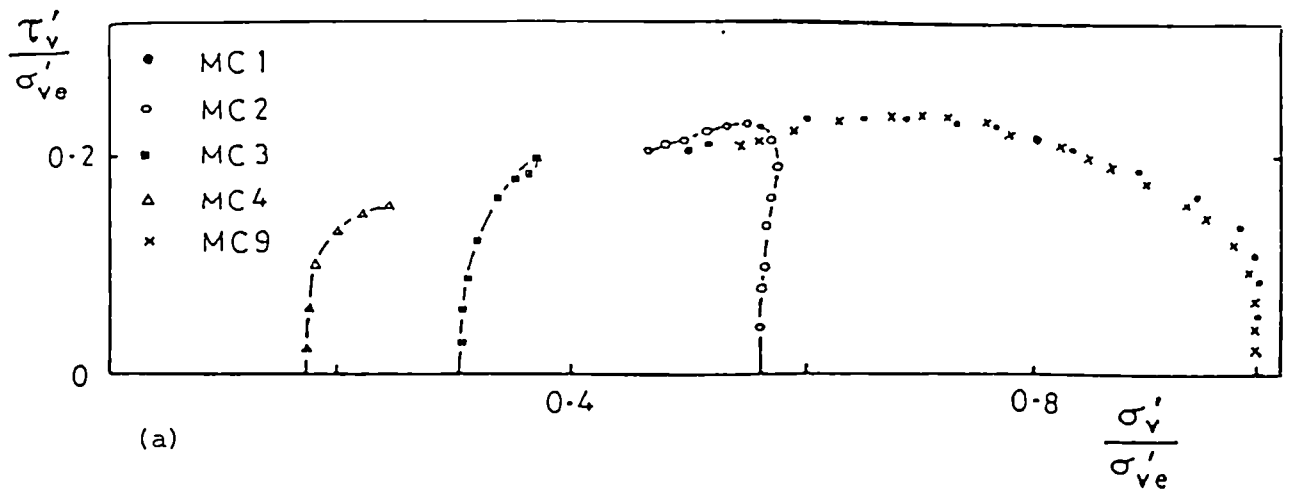
Figure 7.49 Normalised state paths for remoulded Cowden till simple shear samples

(d)

(e)

(f)
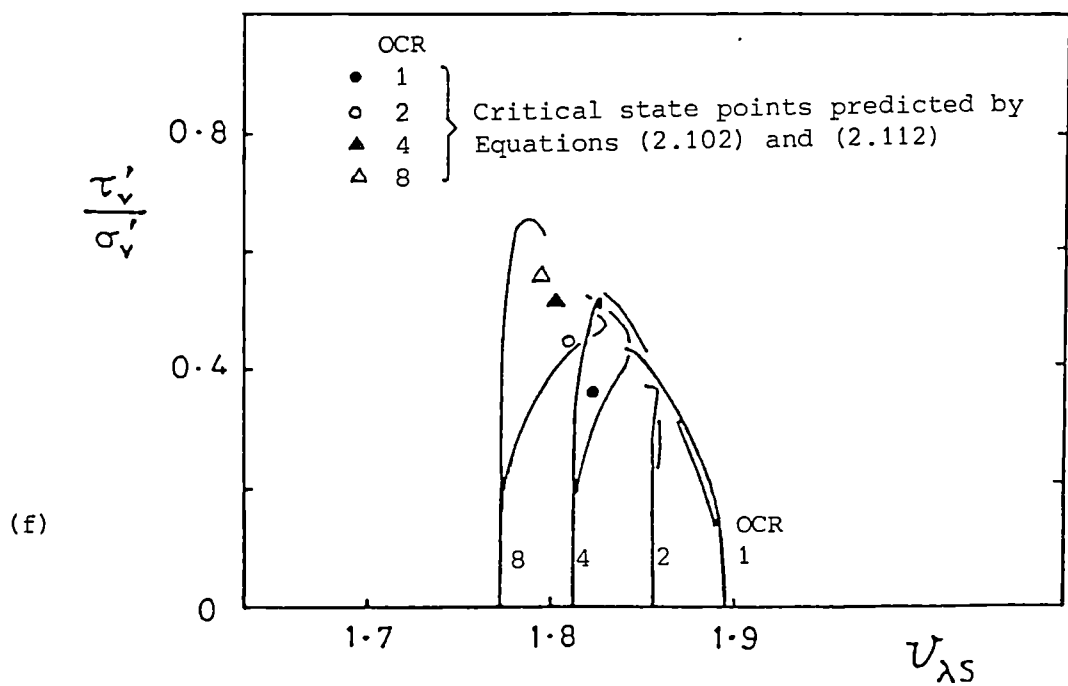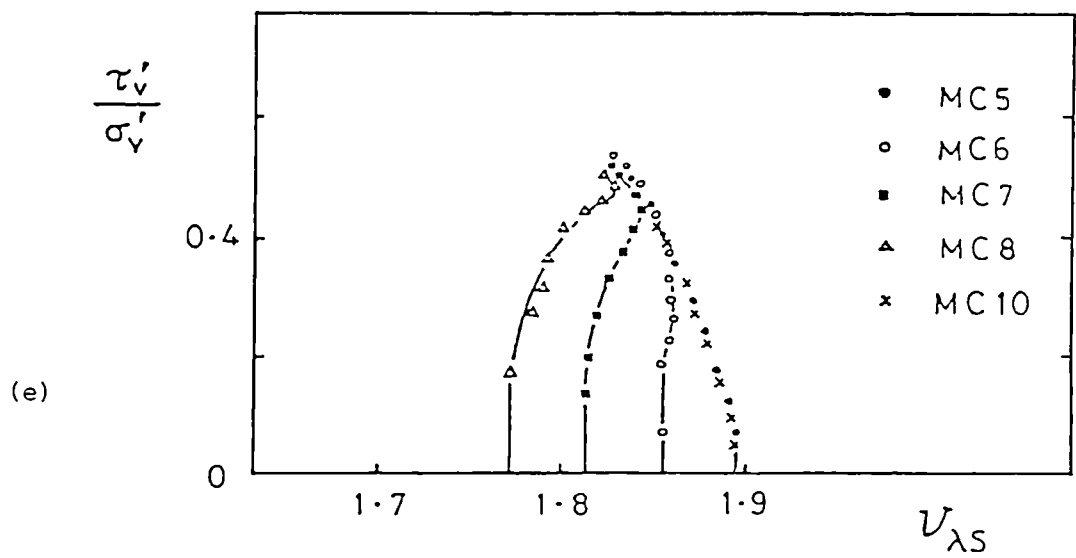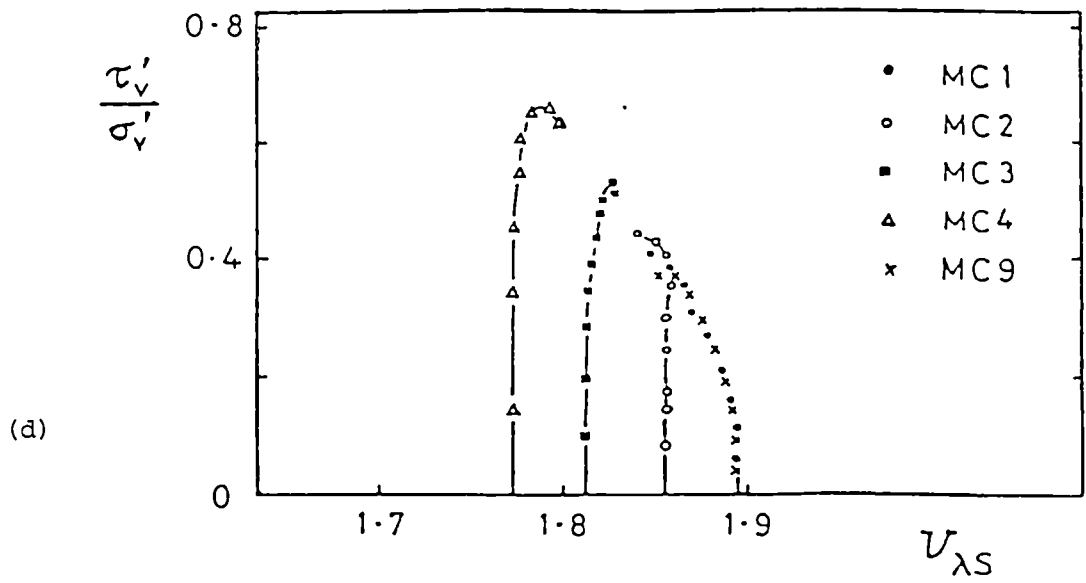
Figure 7.49 continued
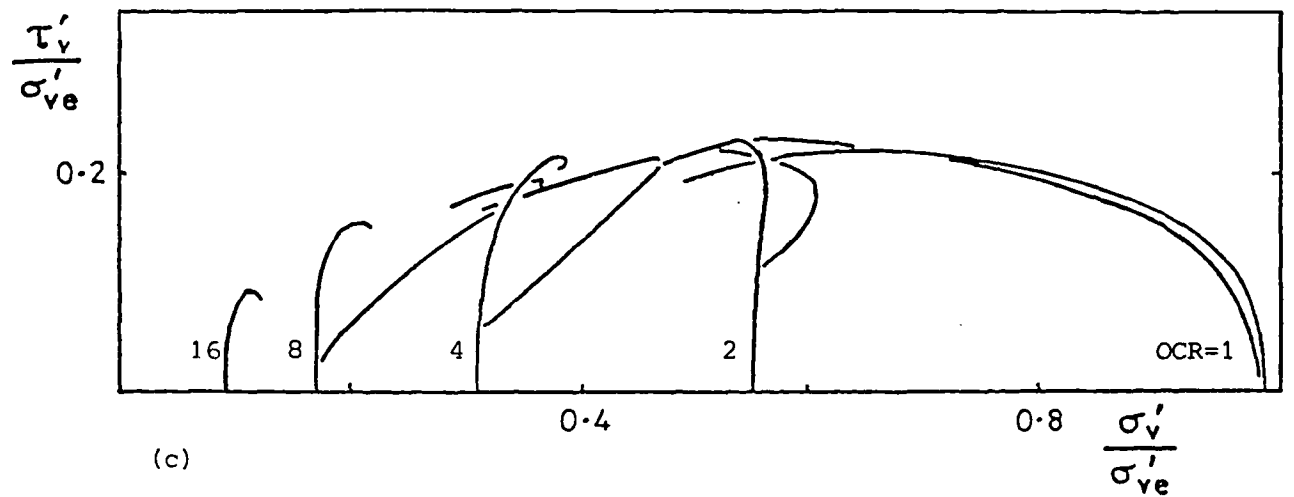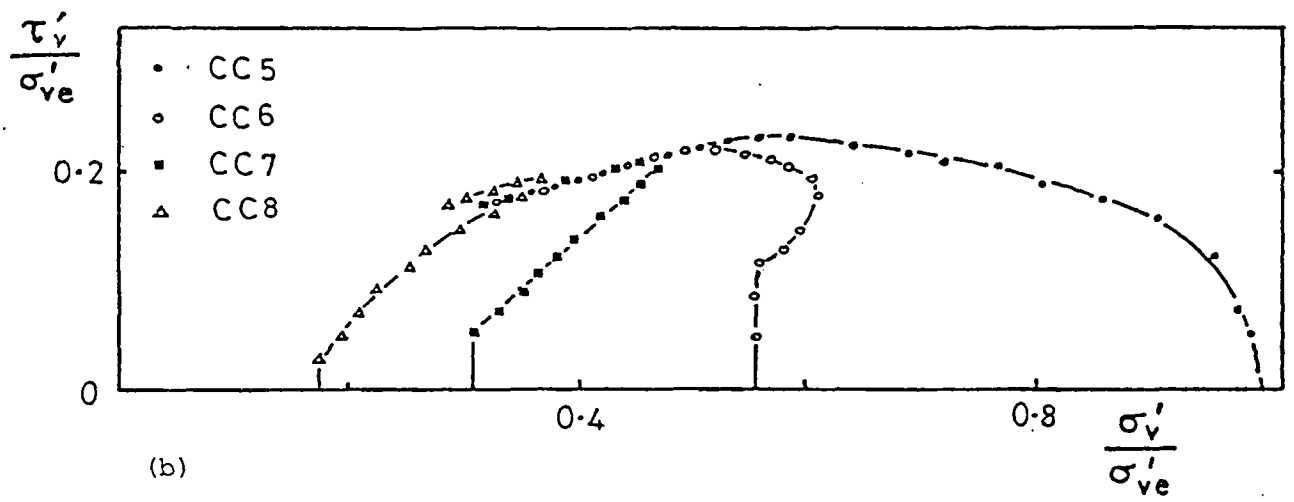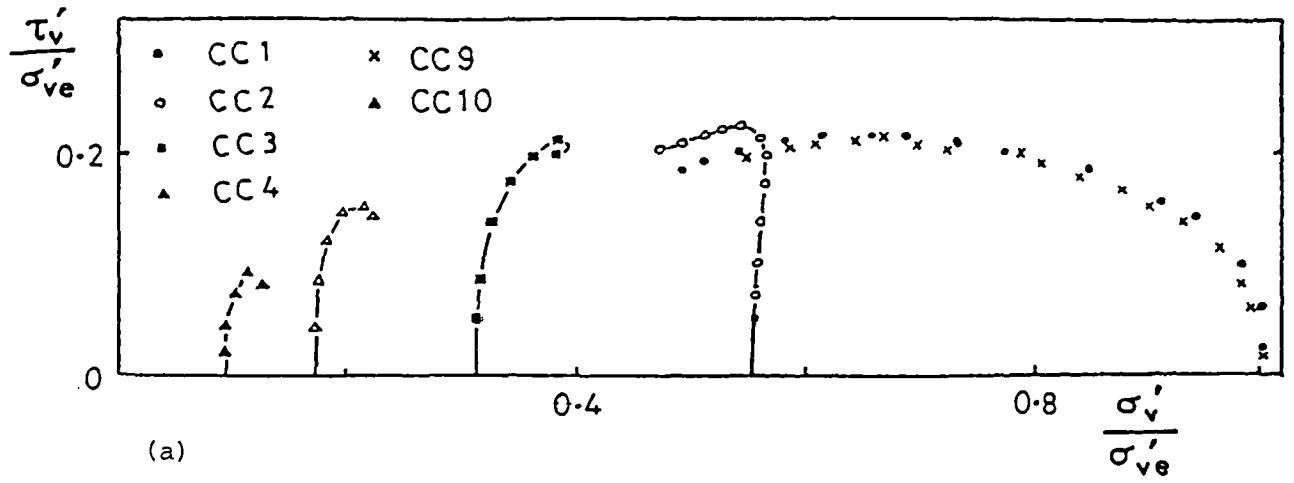
Figure 7.50   Normalised state paths for reconstituted Cowden till
simple shear samples

(d)

(e)

(f)
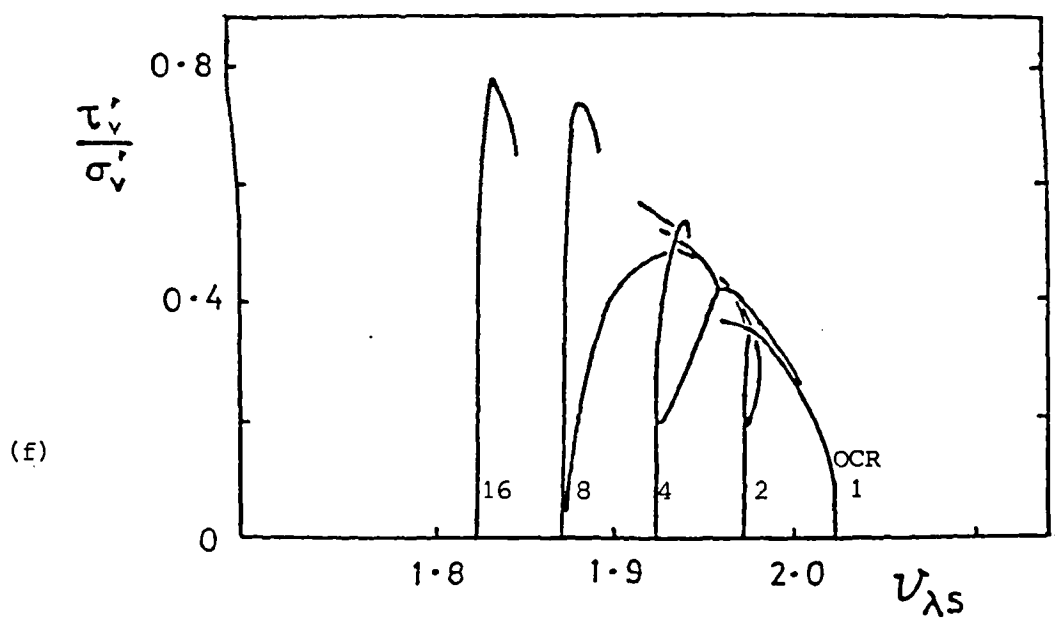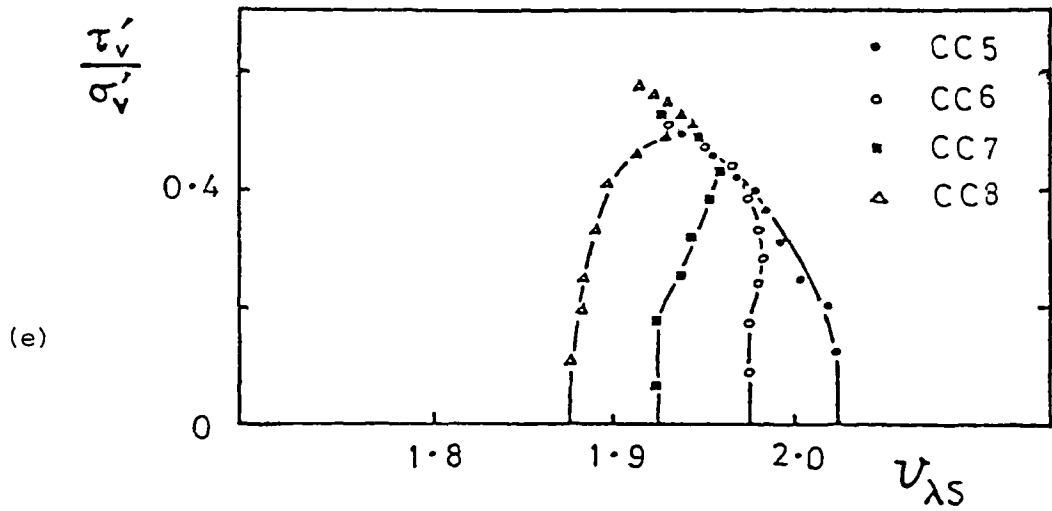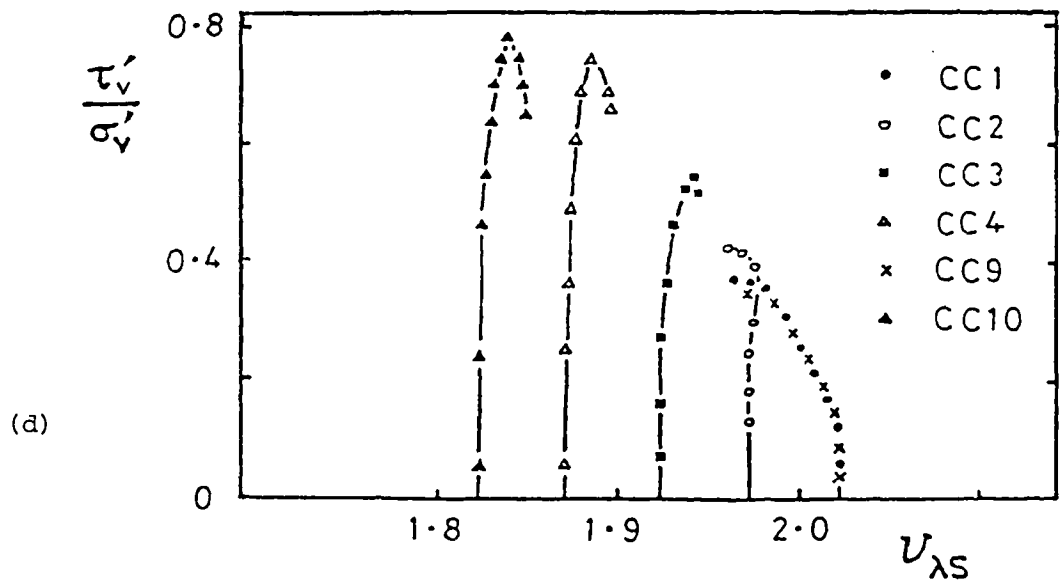
Figure 7.50 continued
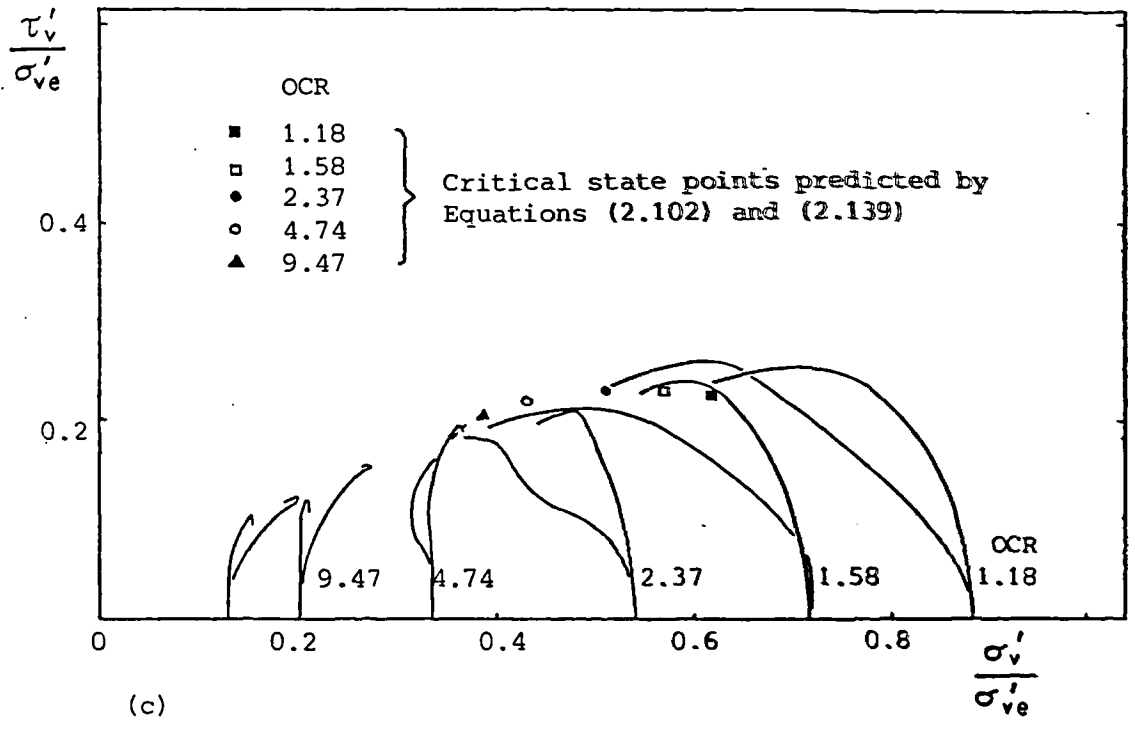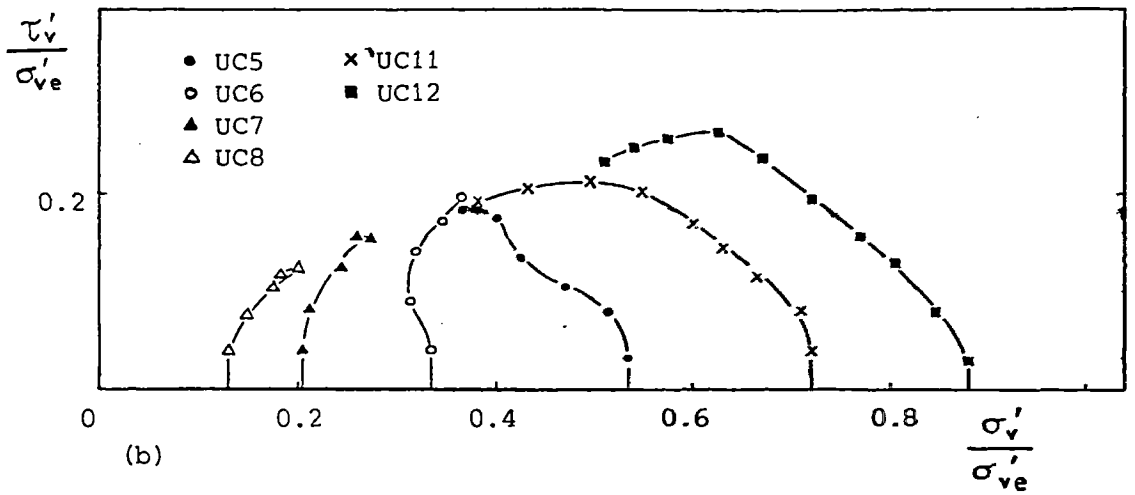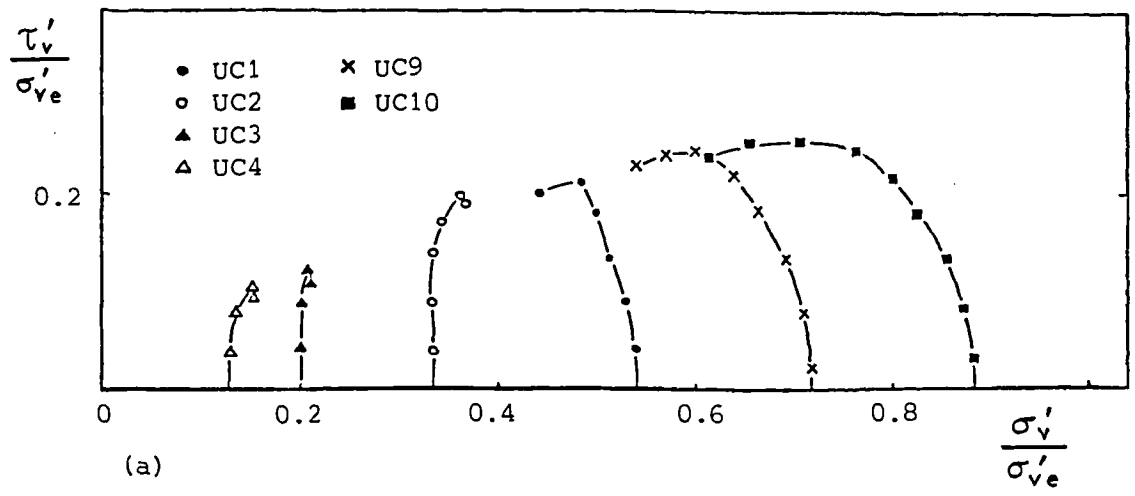
Figure 7.51 Normalised state paths for undisturbed Cowden till simple shear samples

(d)

(e)

(f)
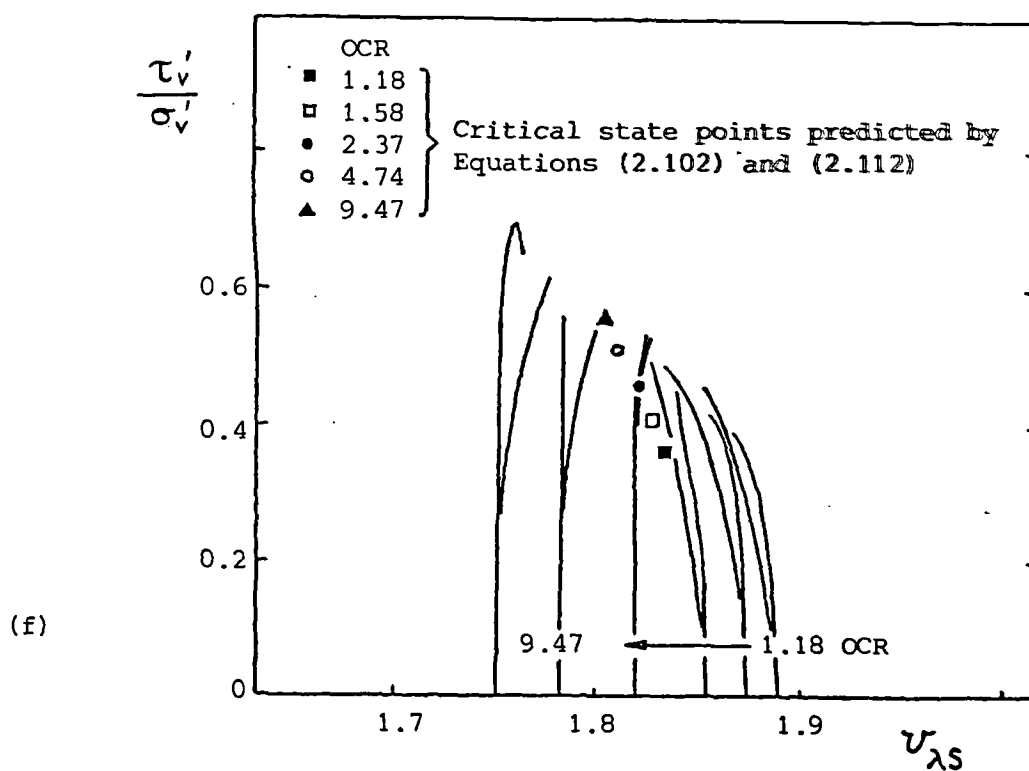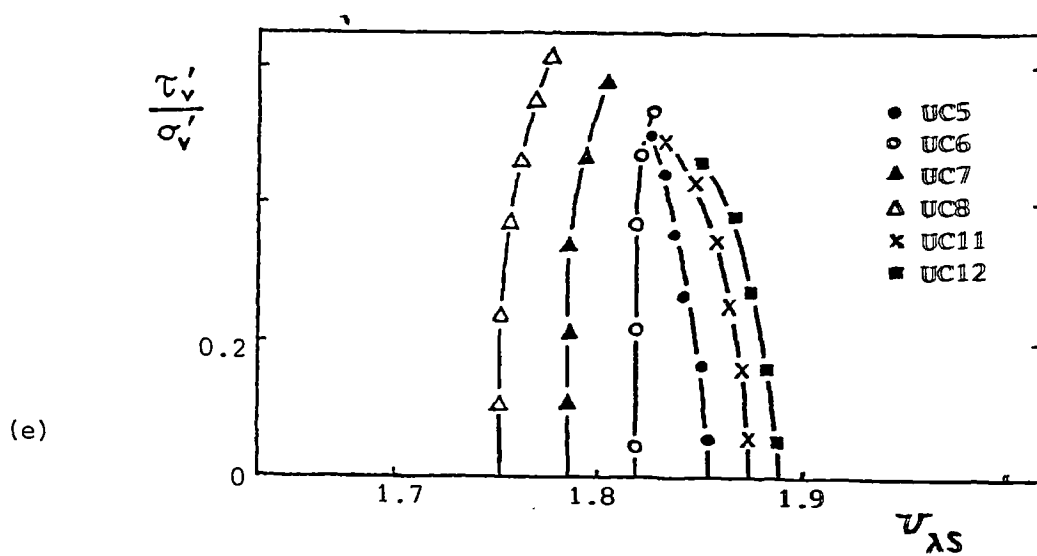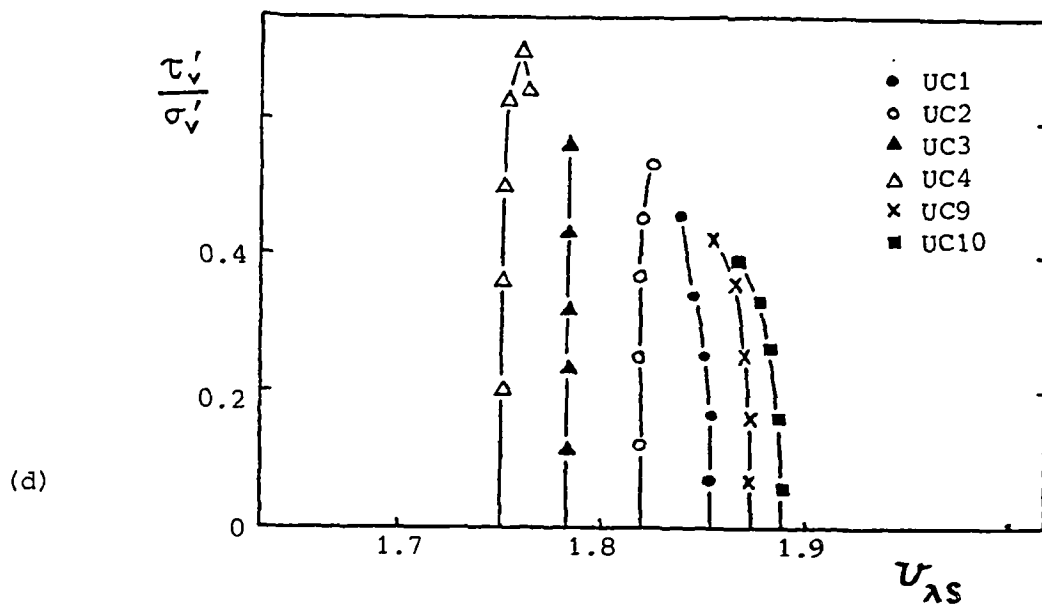
Figure 7.51 continued
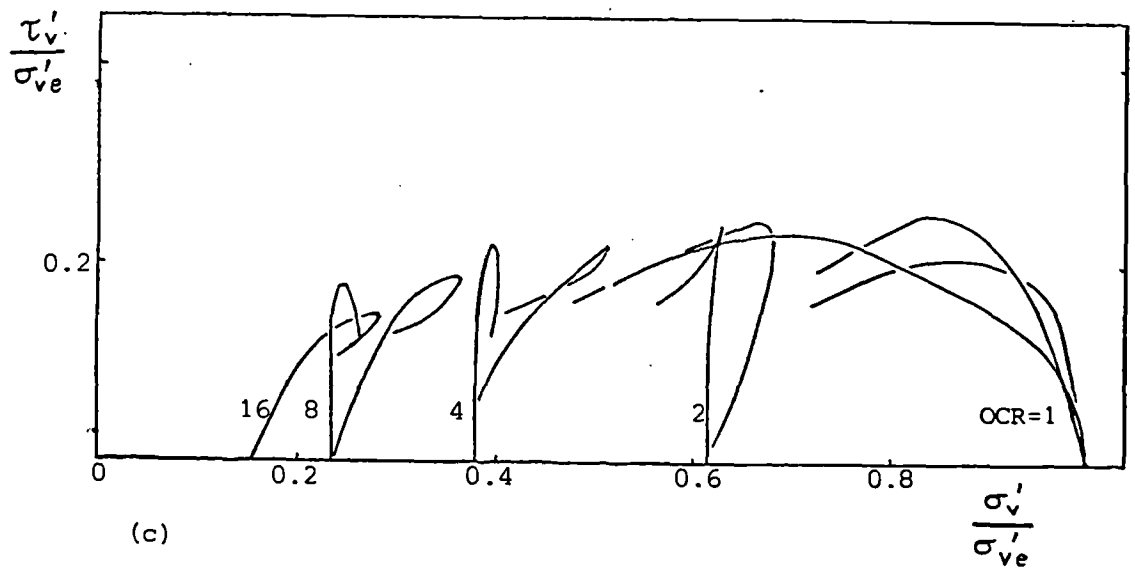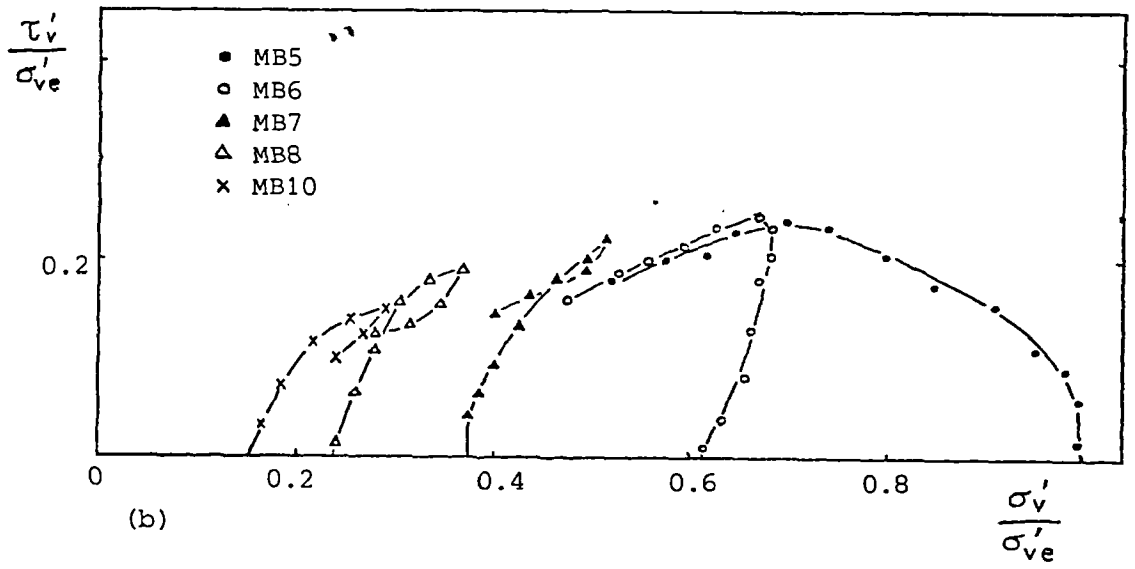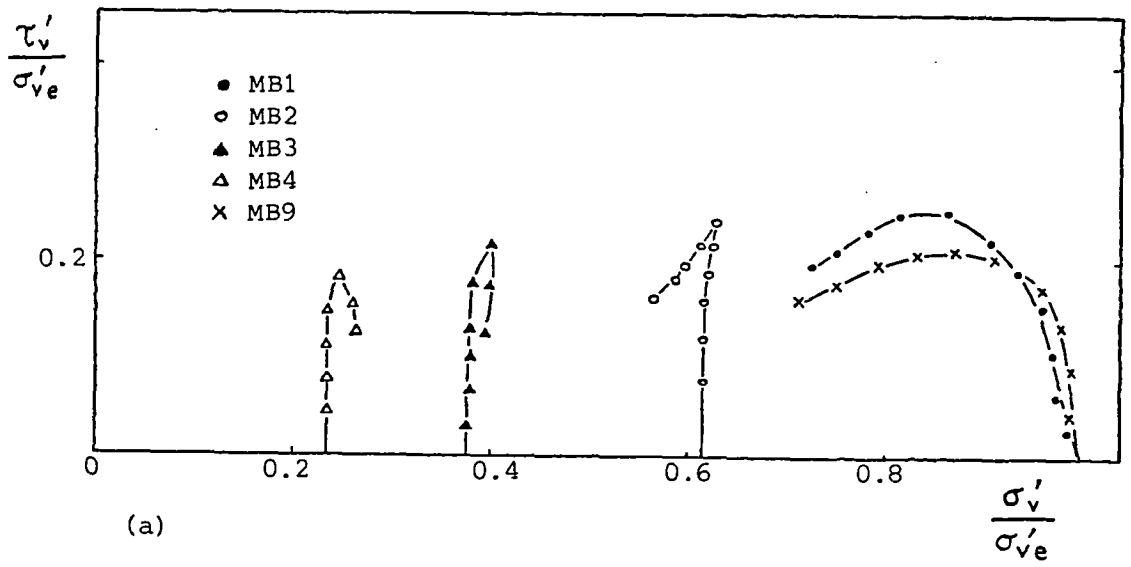
Figure 7.52   Normalised state paths for remoulded London clay
(brown) simple shear samples

(d)

(e)

(f)
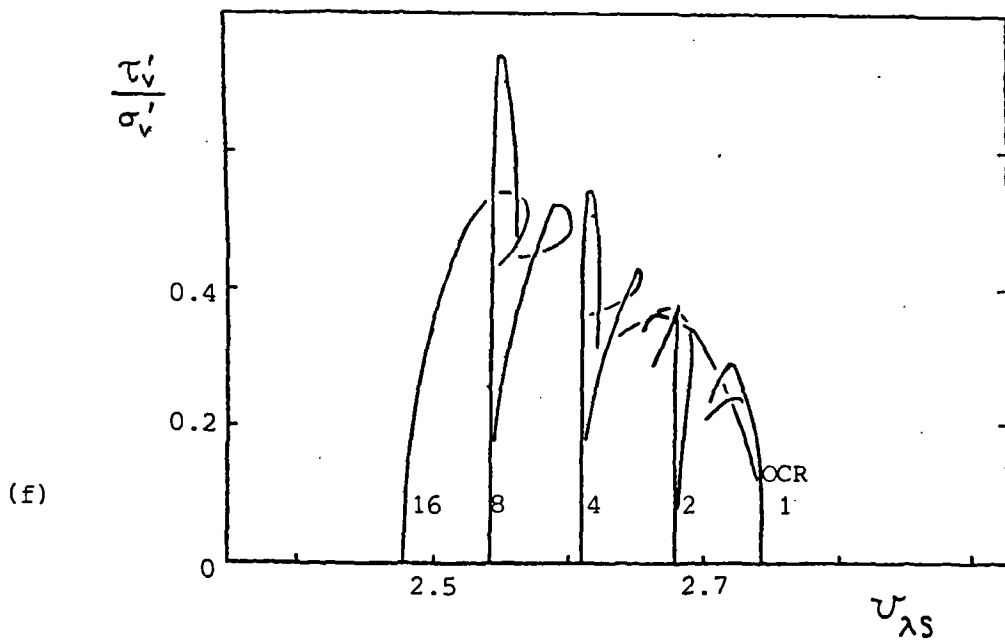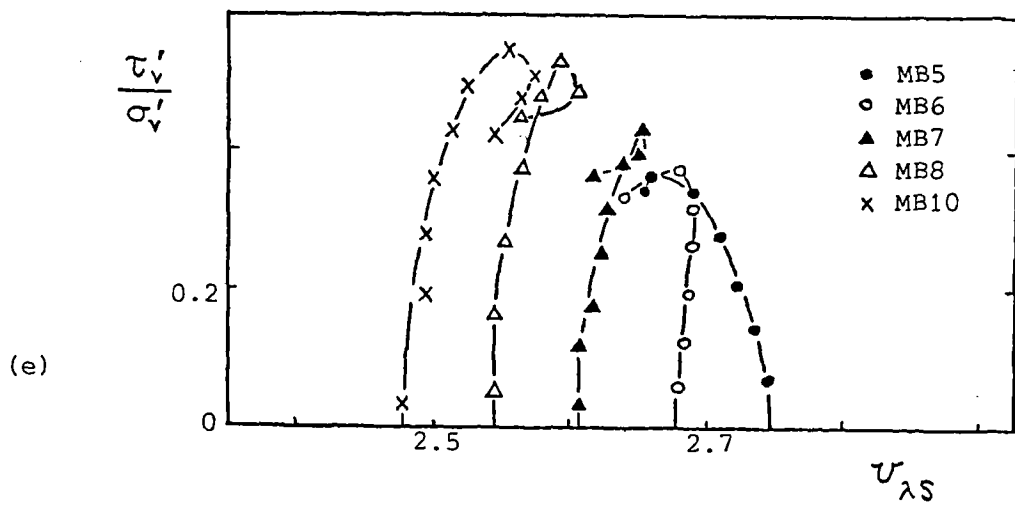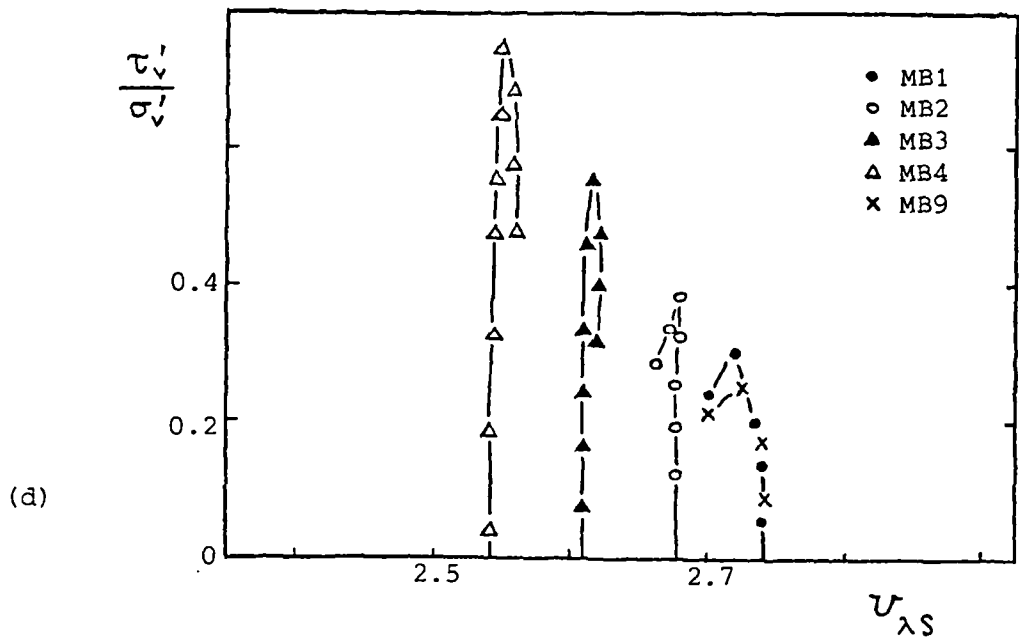
Figure 7.52 continued
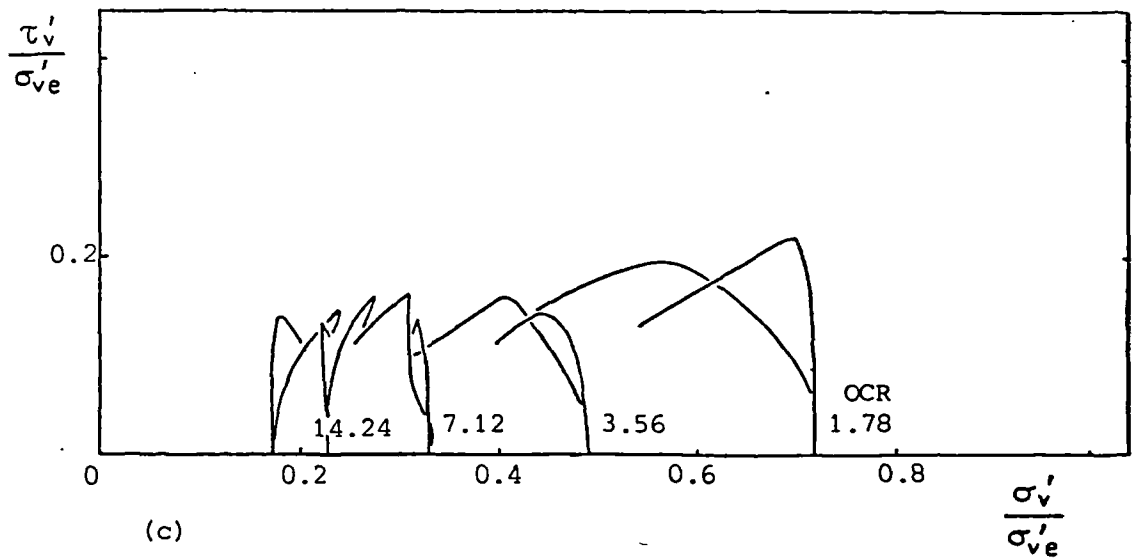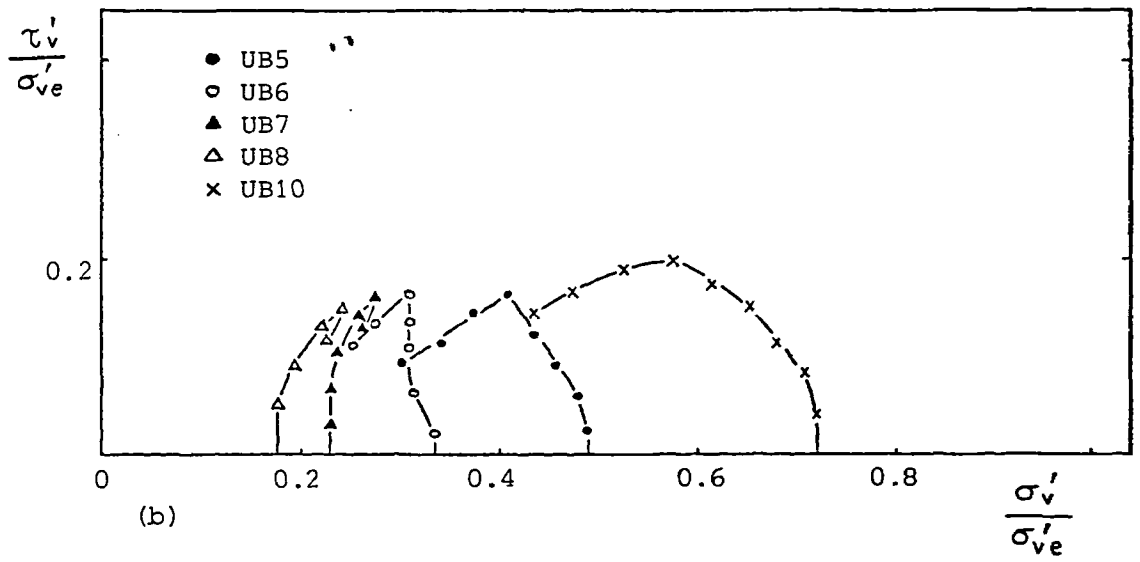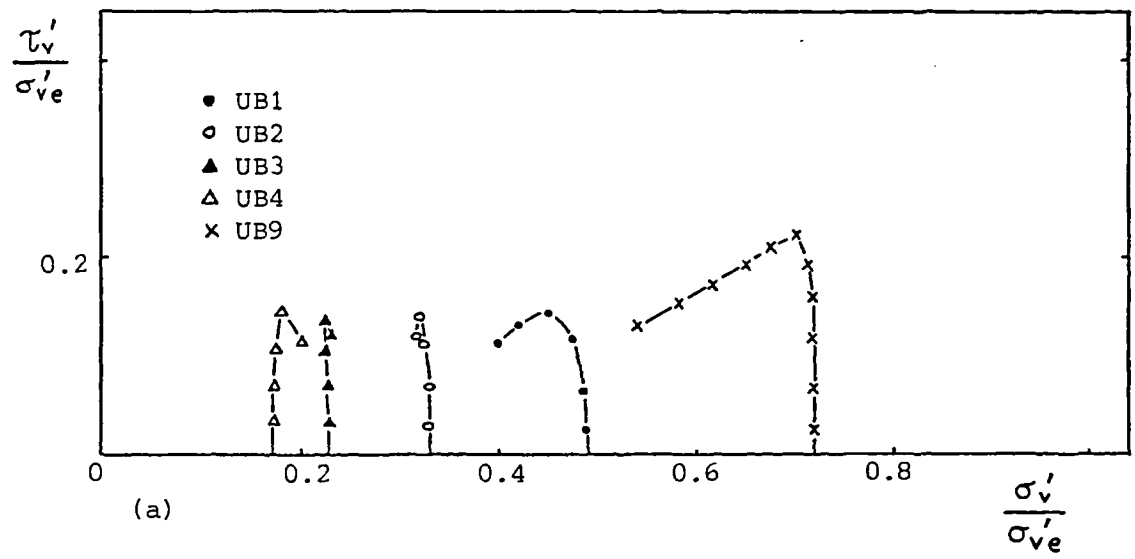
Figure 7.53 Normalised state paths for undisturbed London clay (brown) simple shear samples

(d)

(e)

(f)
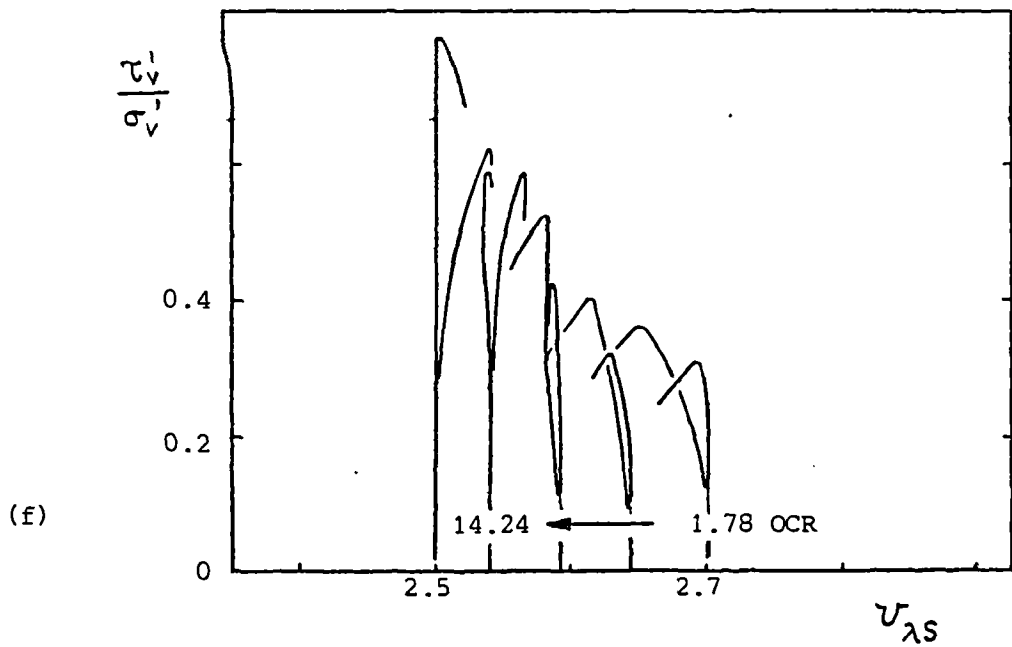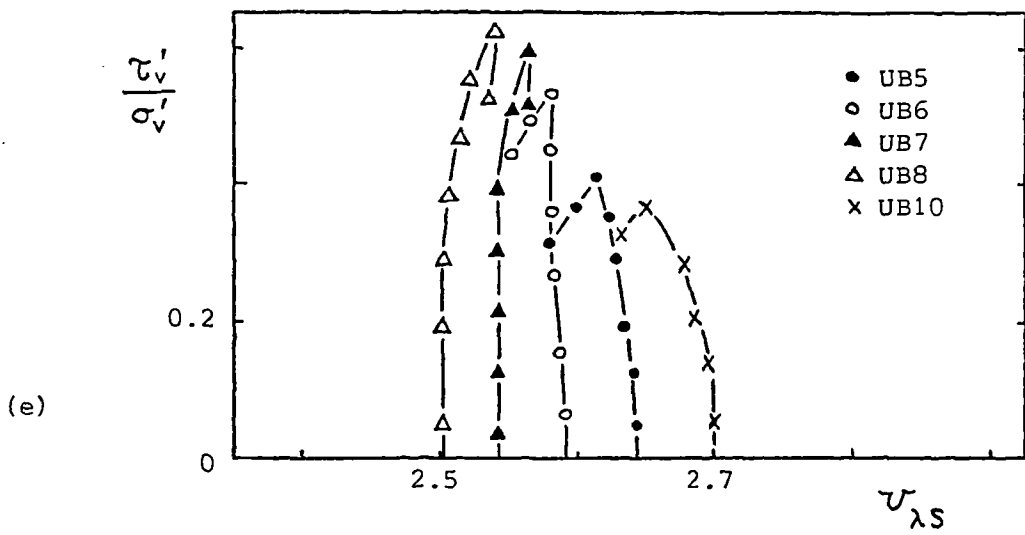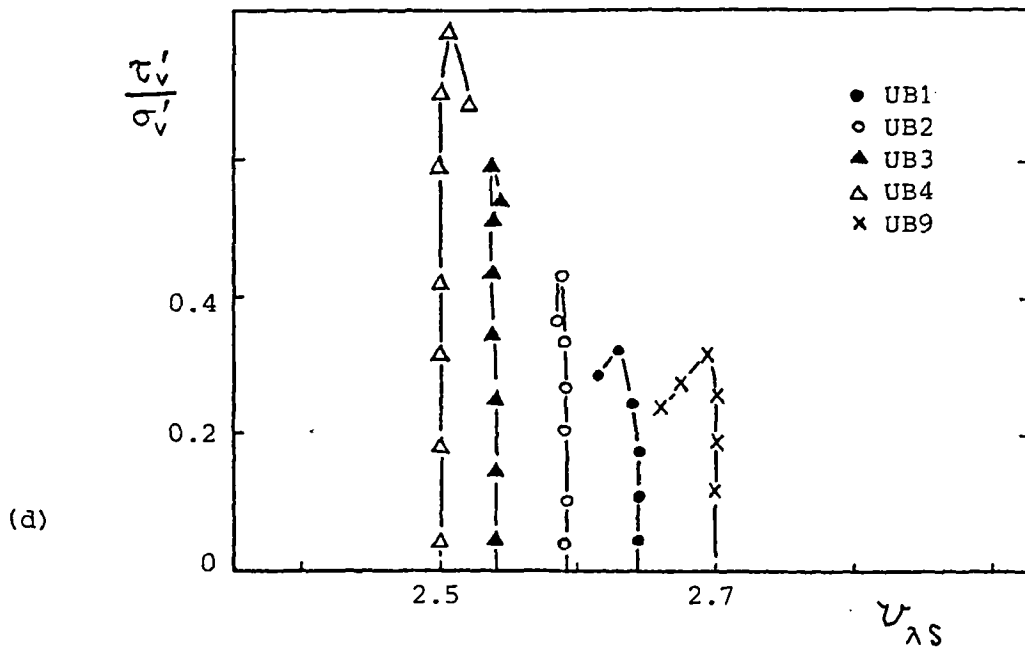
Figure 7.53 continued
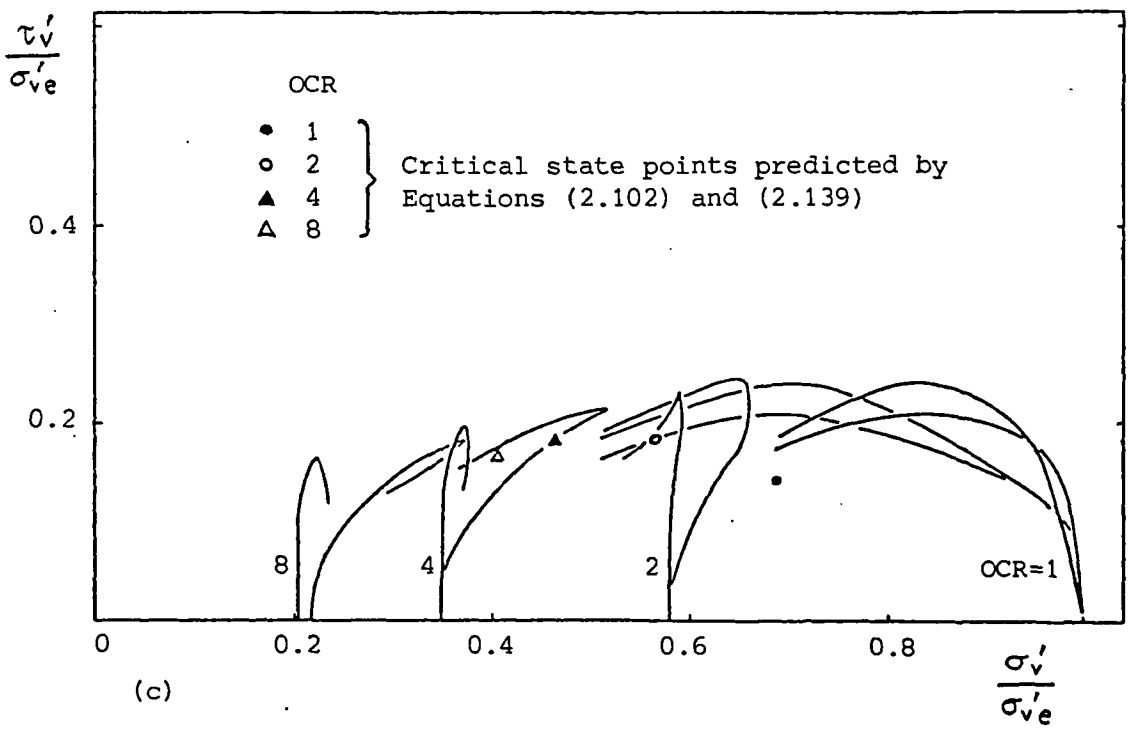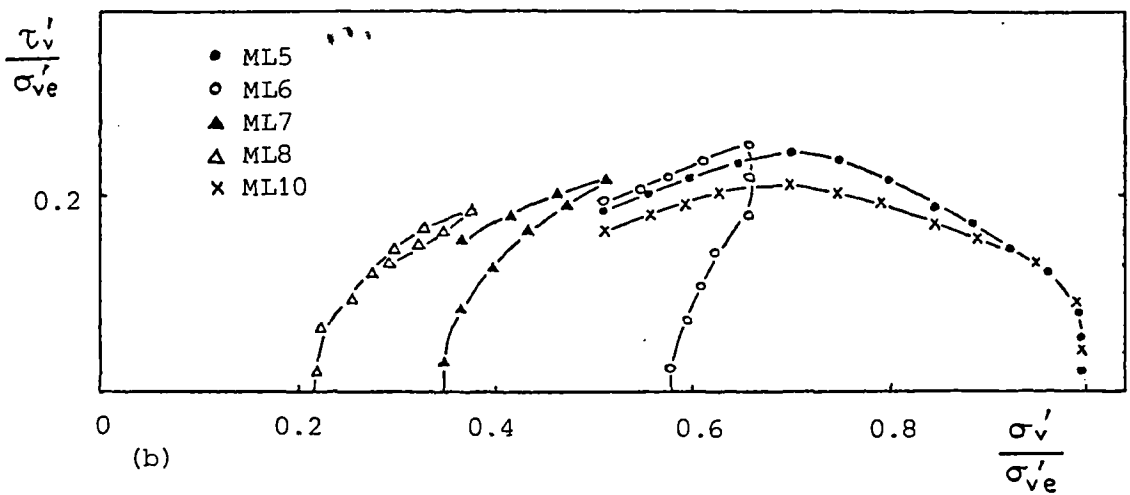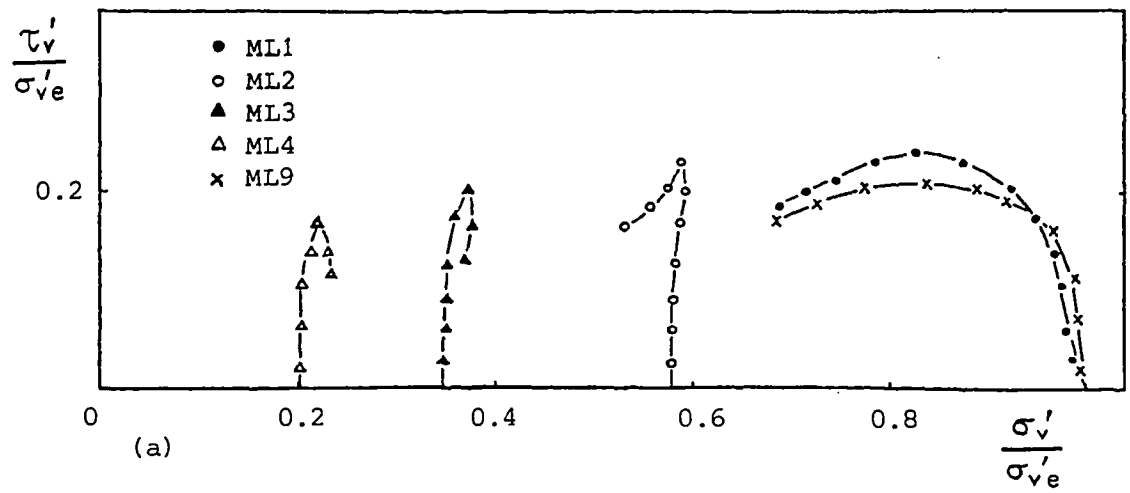
Figure 7.54   Normalised state paths for remoulded London clay
(blue) simple shear samples

(d)

(e)

(f)
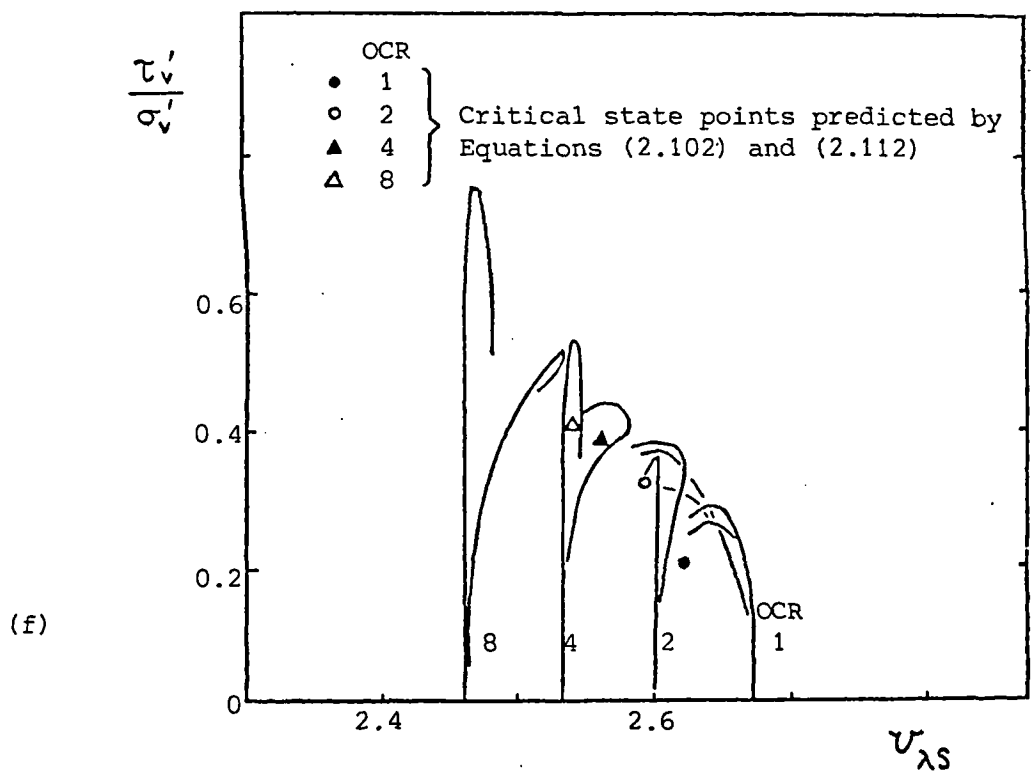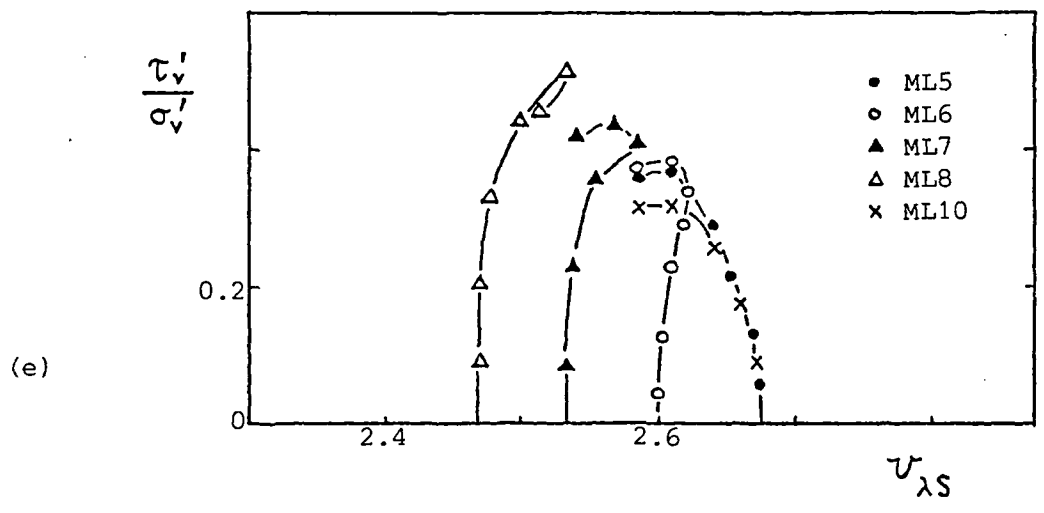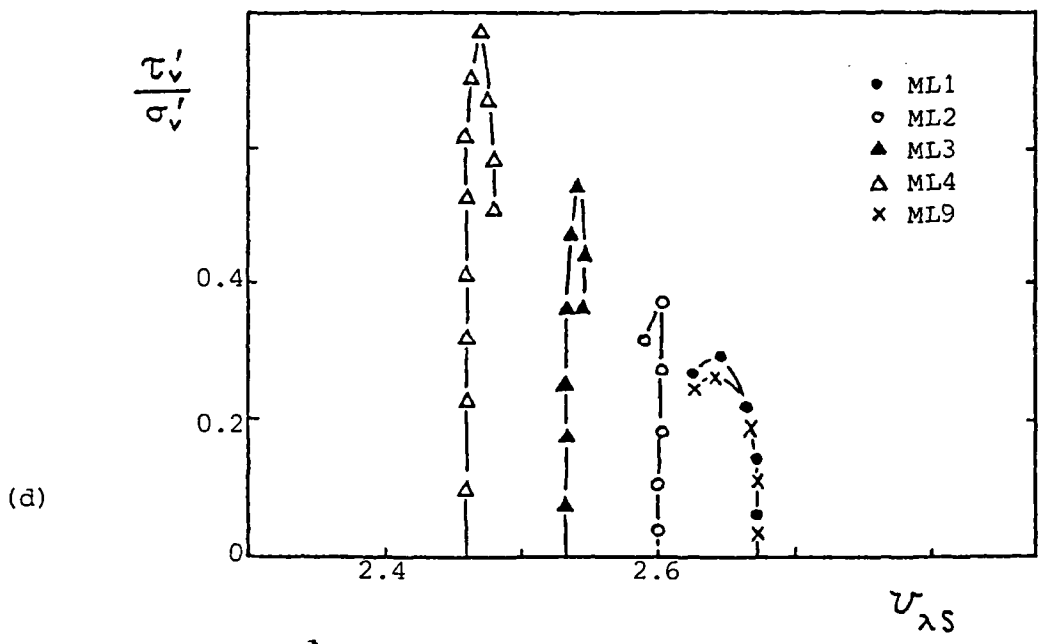
Figure 7.54 continued
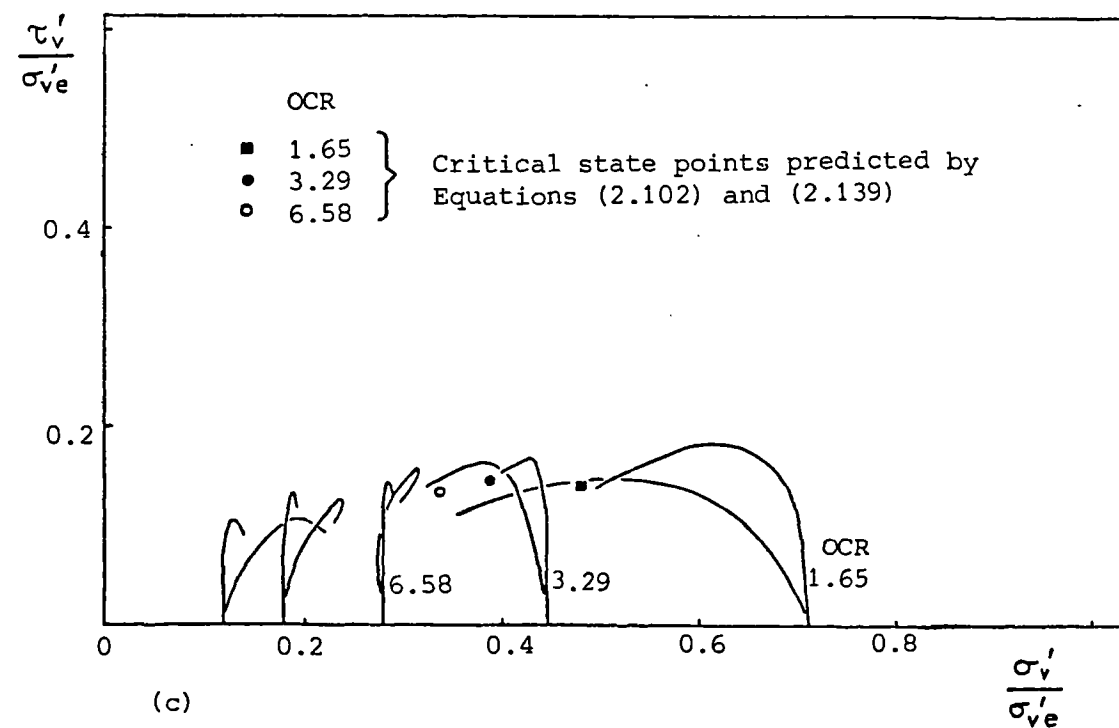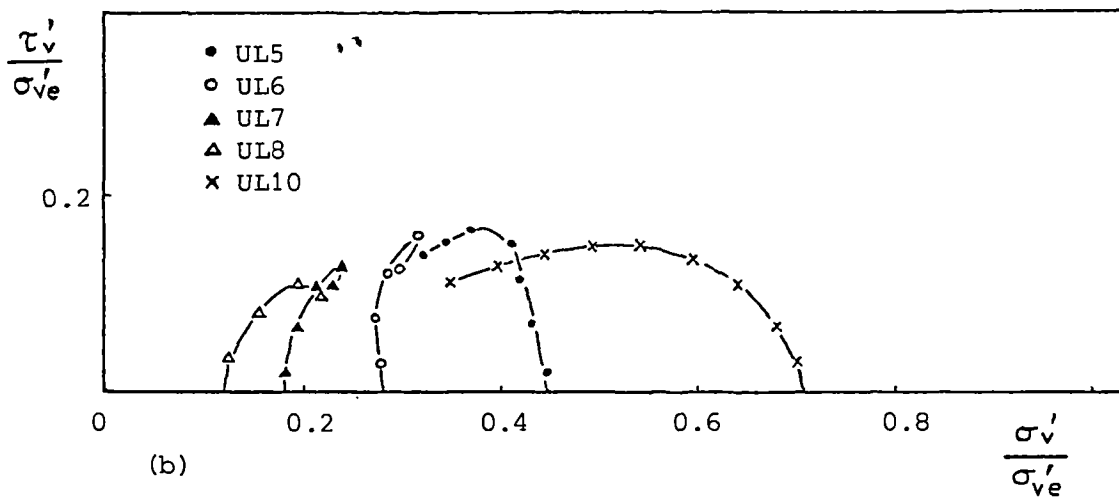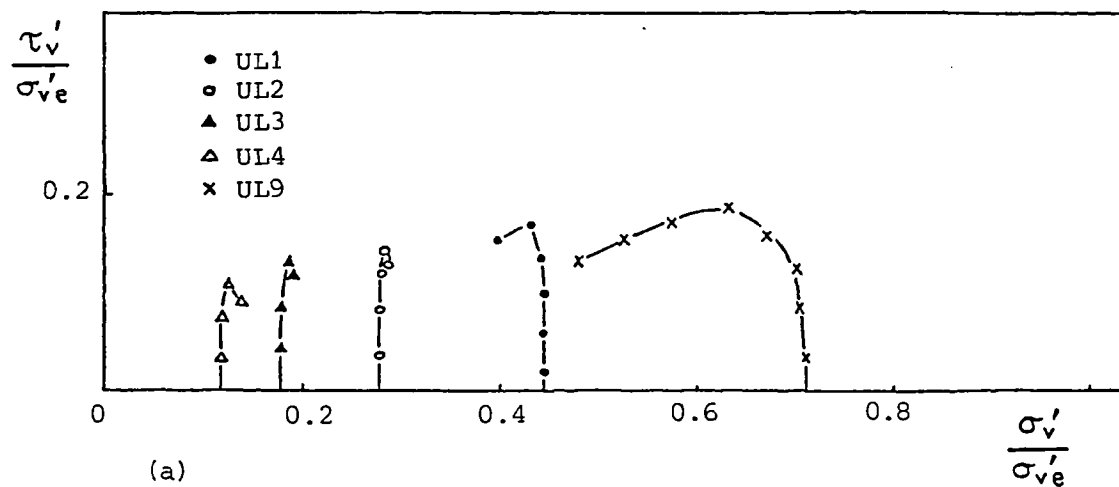
Figure 7.55 Normalised state paths for undisturbed London clay (blue) simple shear samples

(d)

(e)

(f)
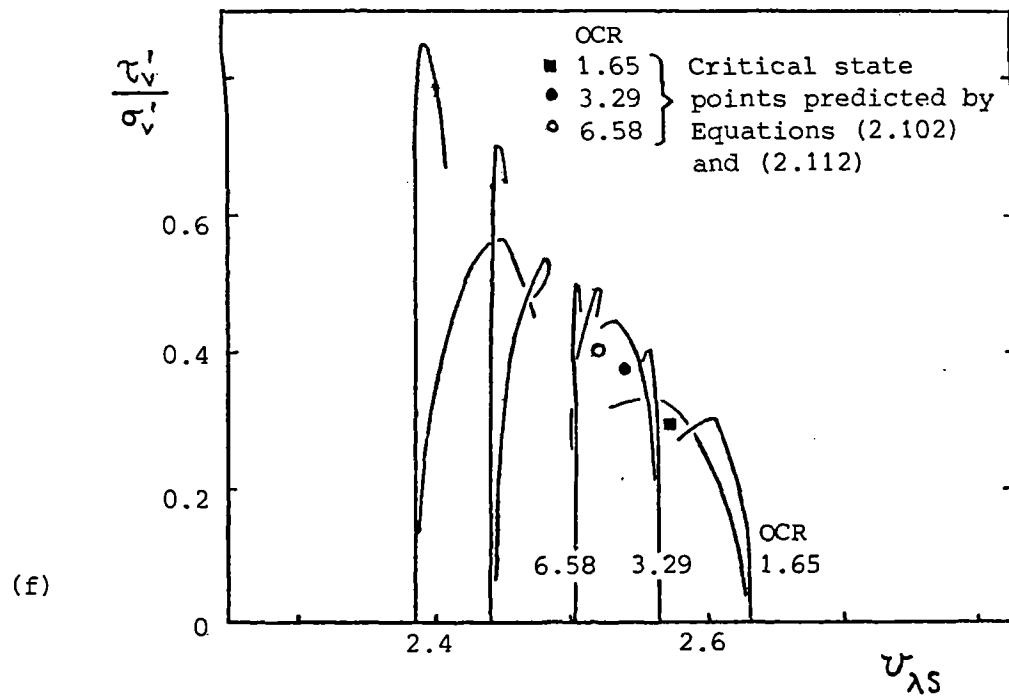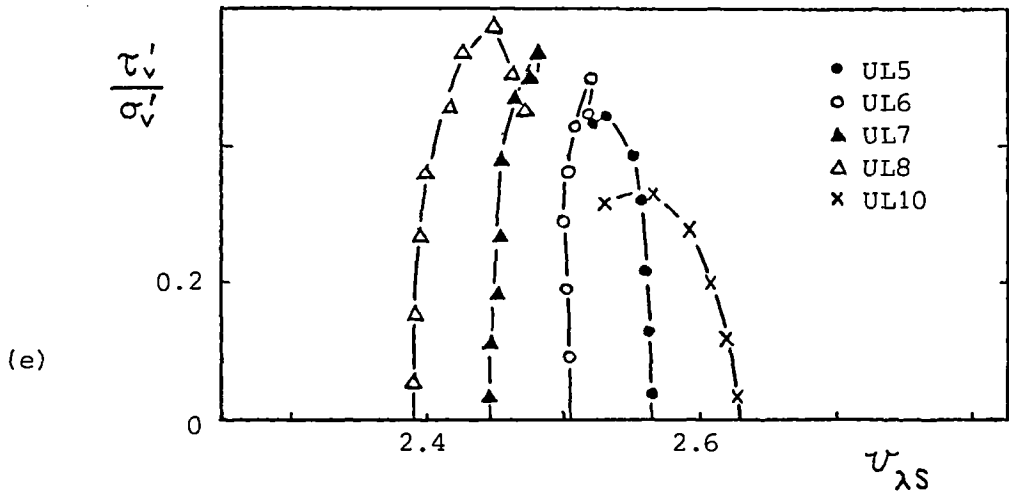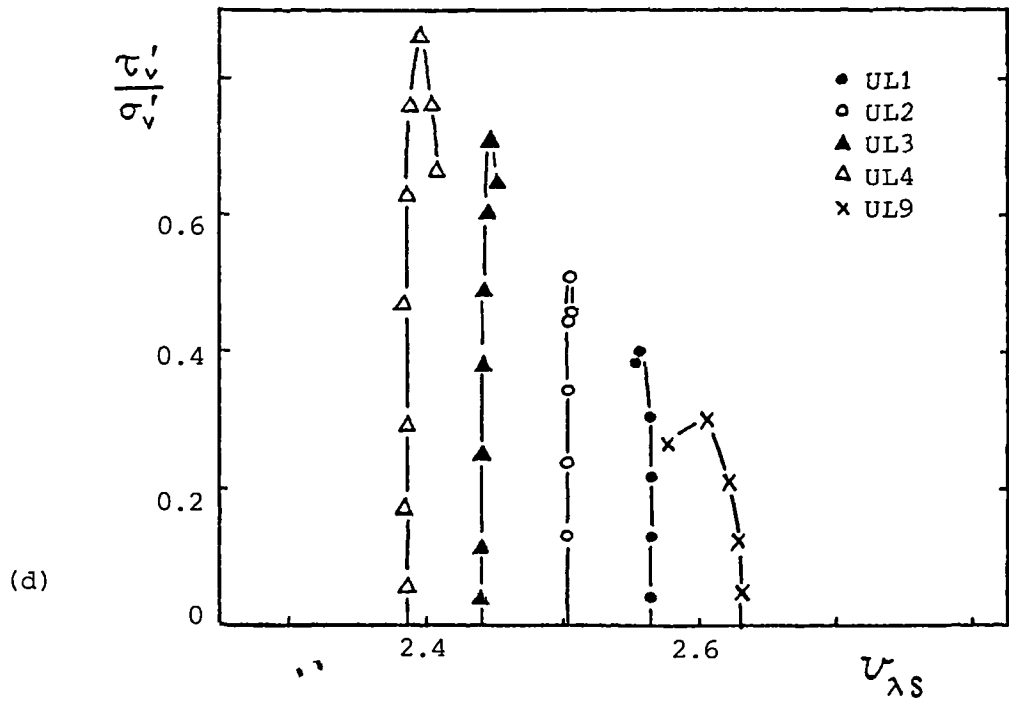
Figure 7.55 continued
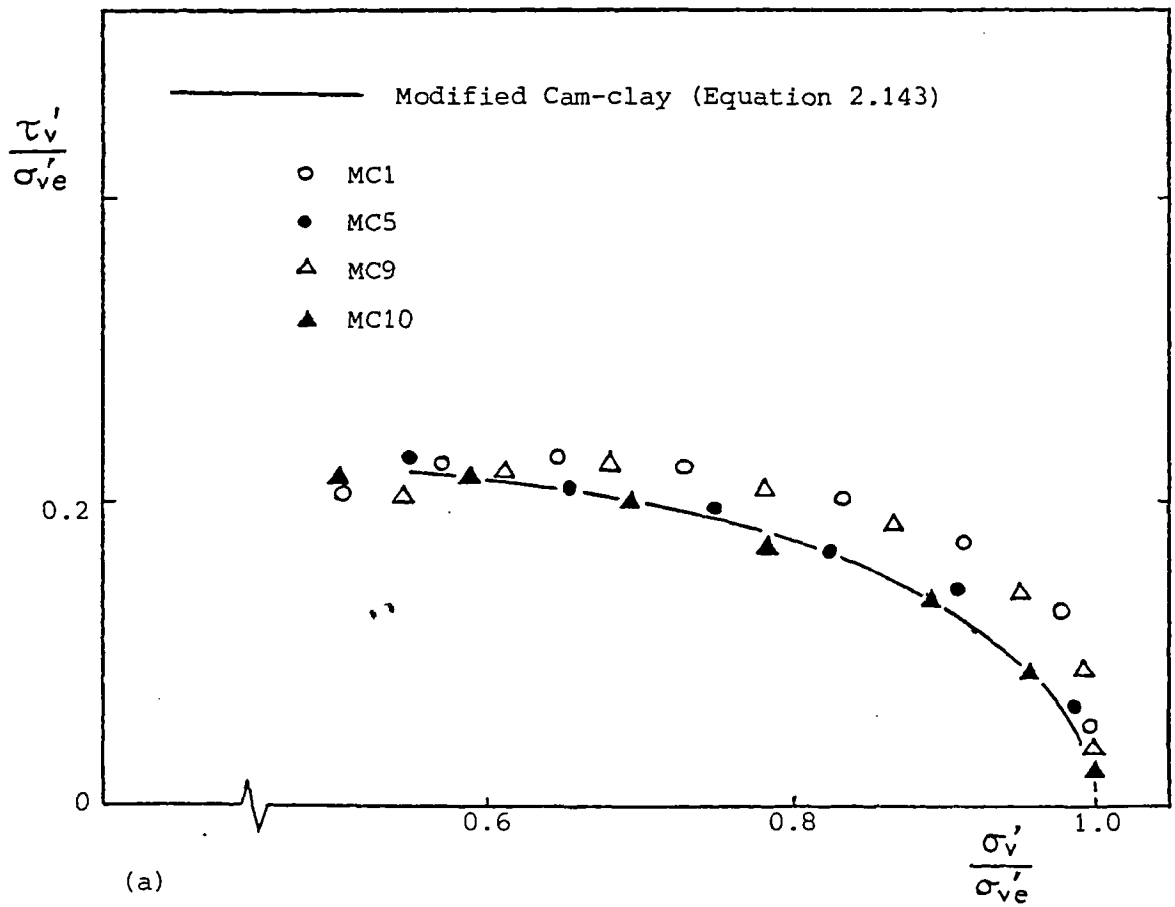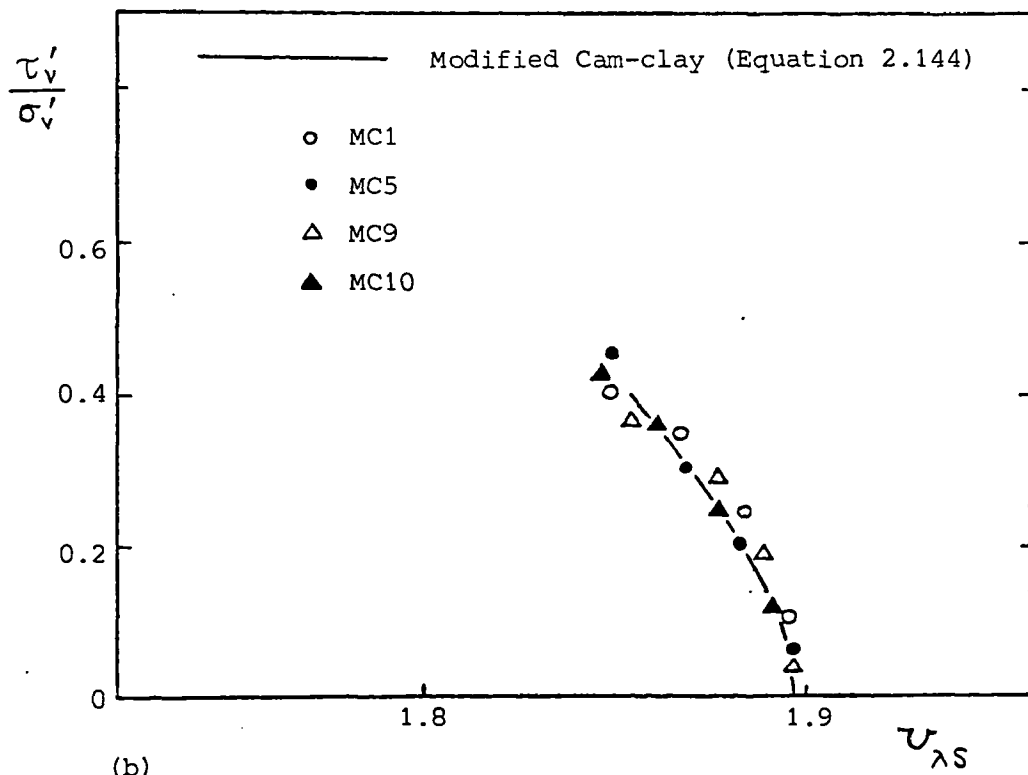
Figure 7.56   Roscoe surface for remoulded Cowden till
simple shear samples
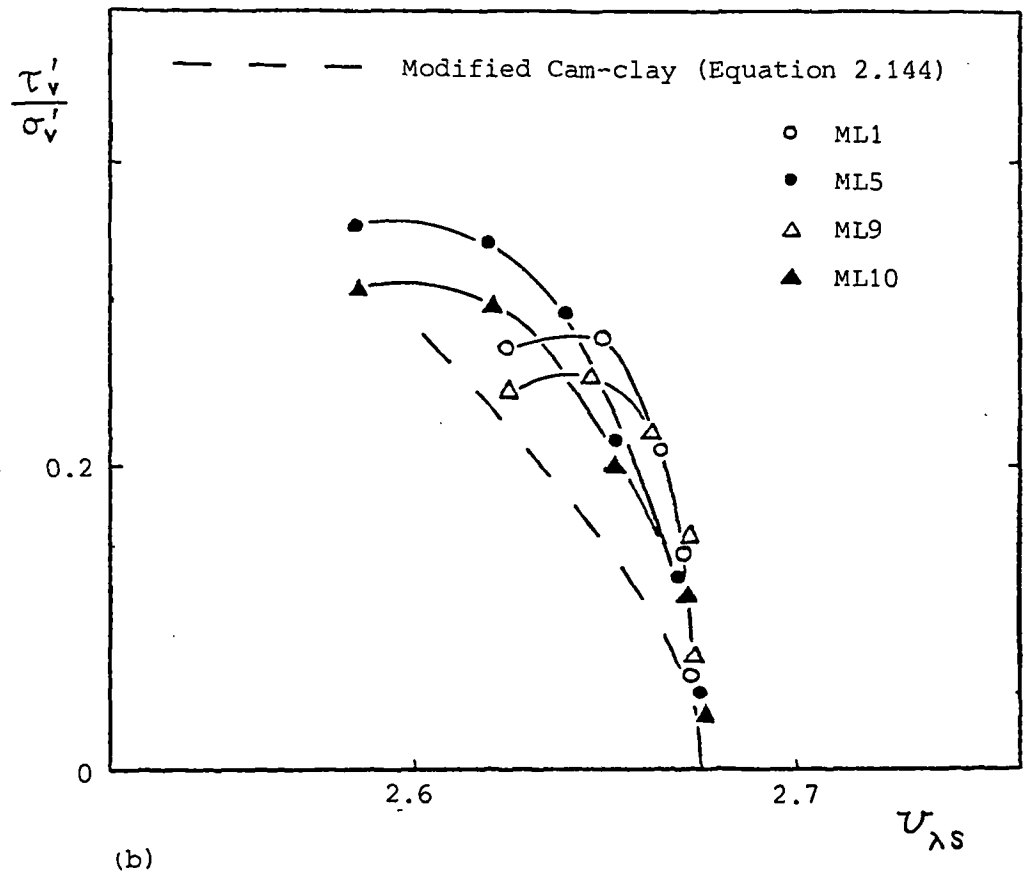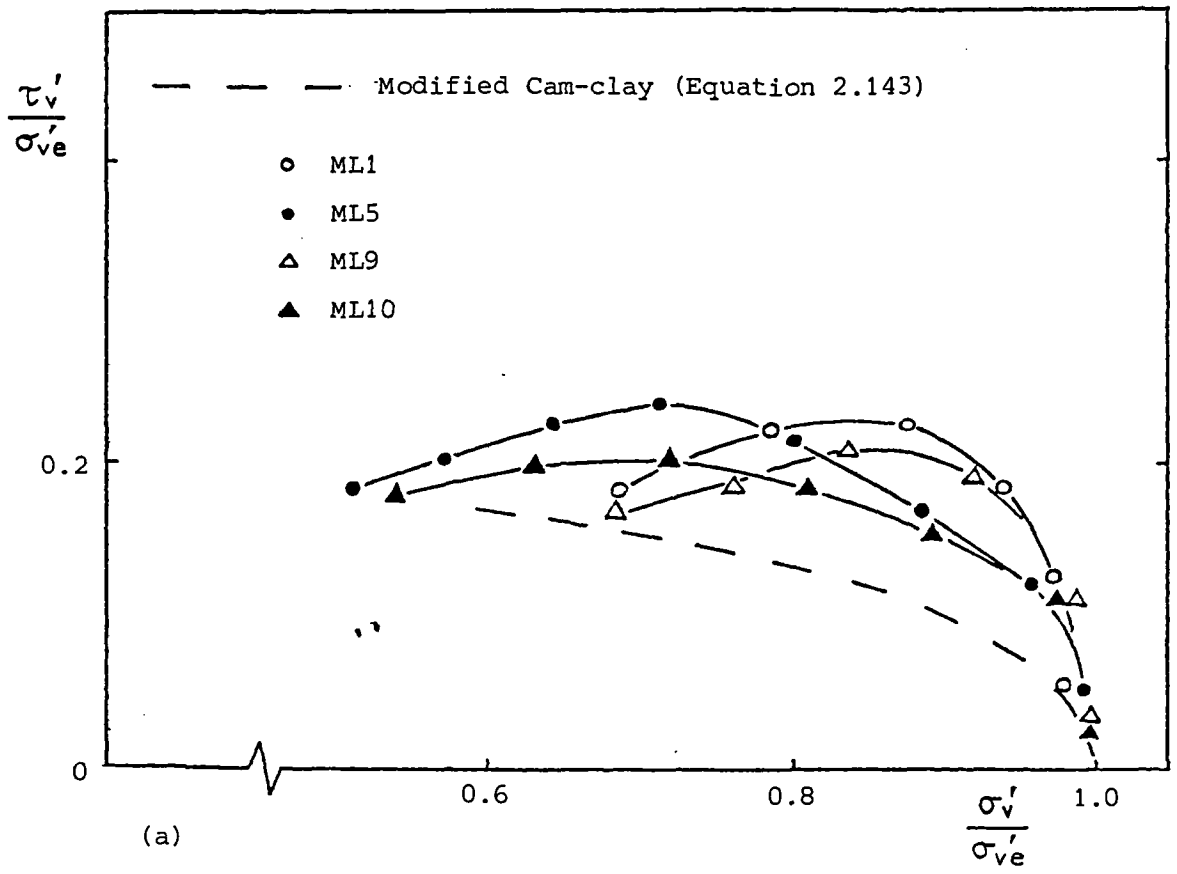
Figure 7.57 Roscoe surface for remoulded London clay (blue) simple shear samples
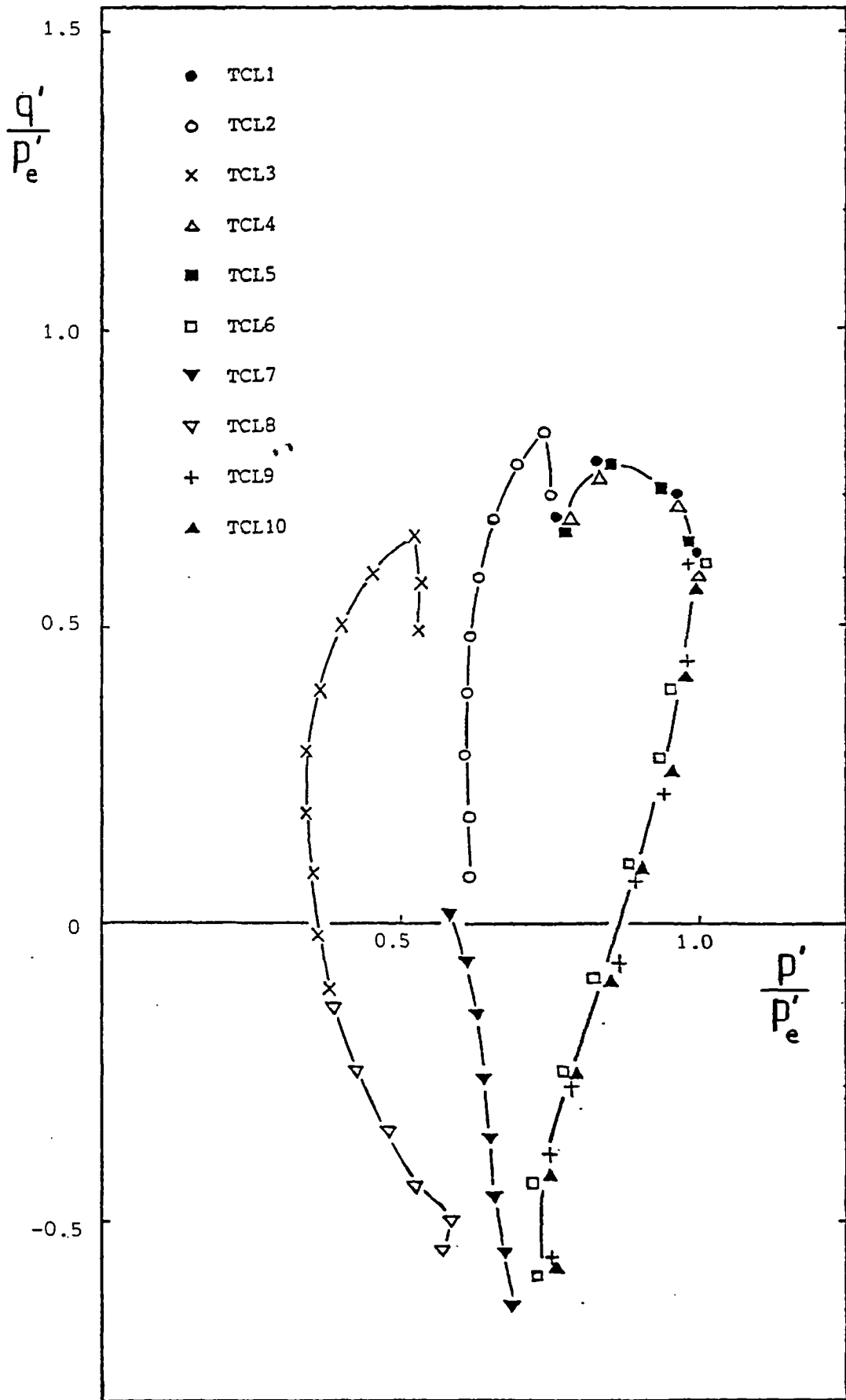
Figure 7.58   Normalised state paths for 38 mm reconstituted
               London clay (blue) triaxial samples
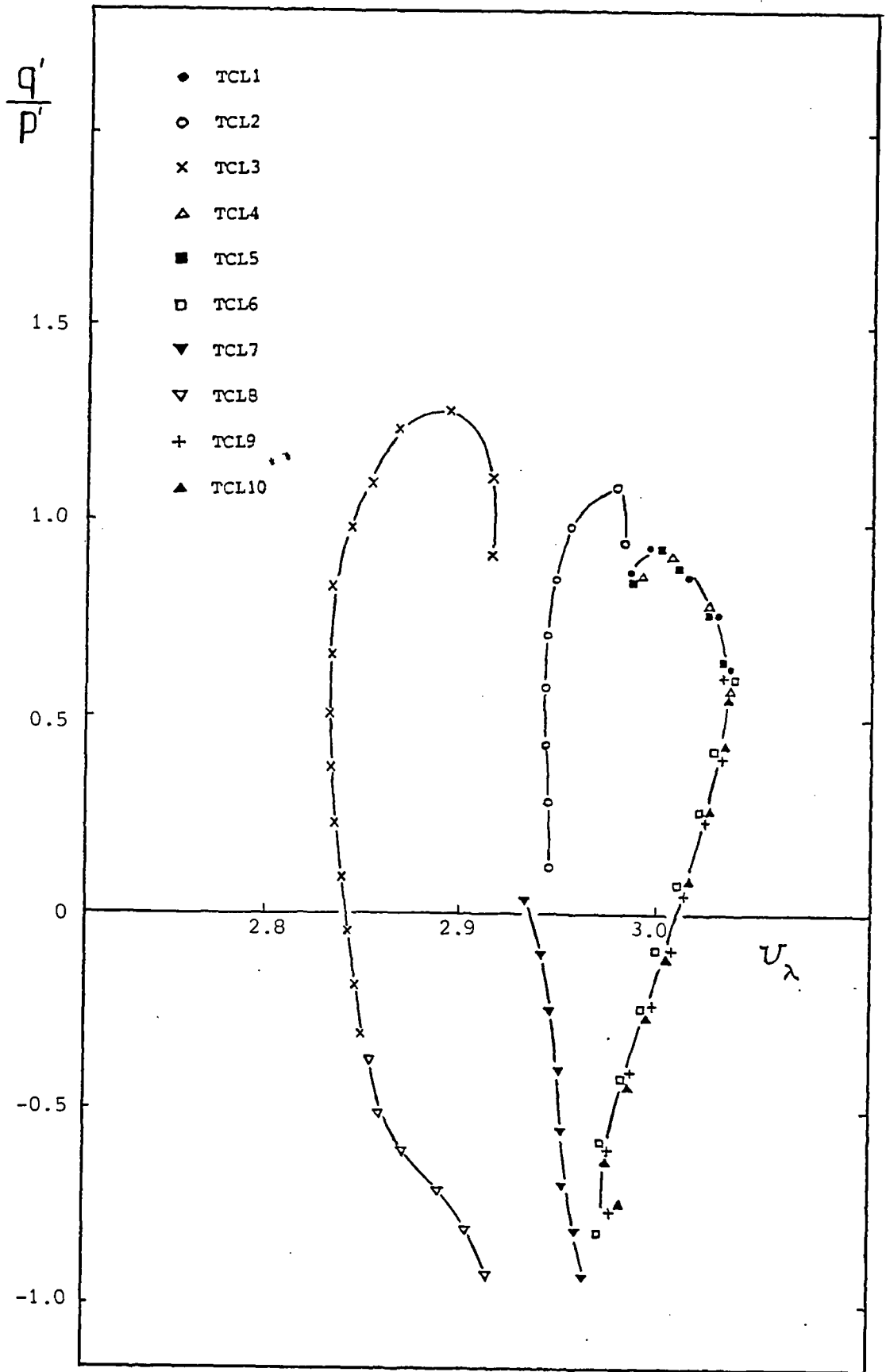
(b)

Figure 7.58 continued

(a)

(b)
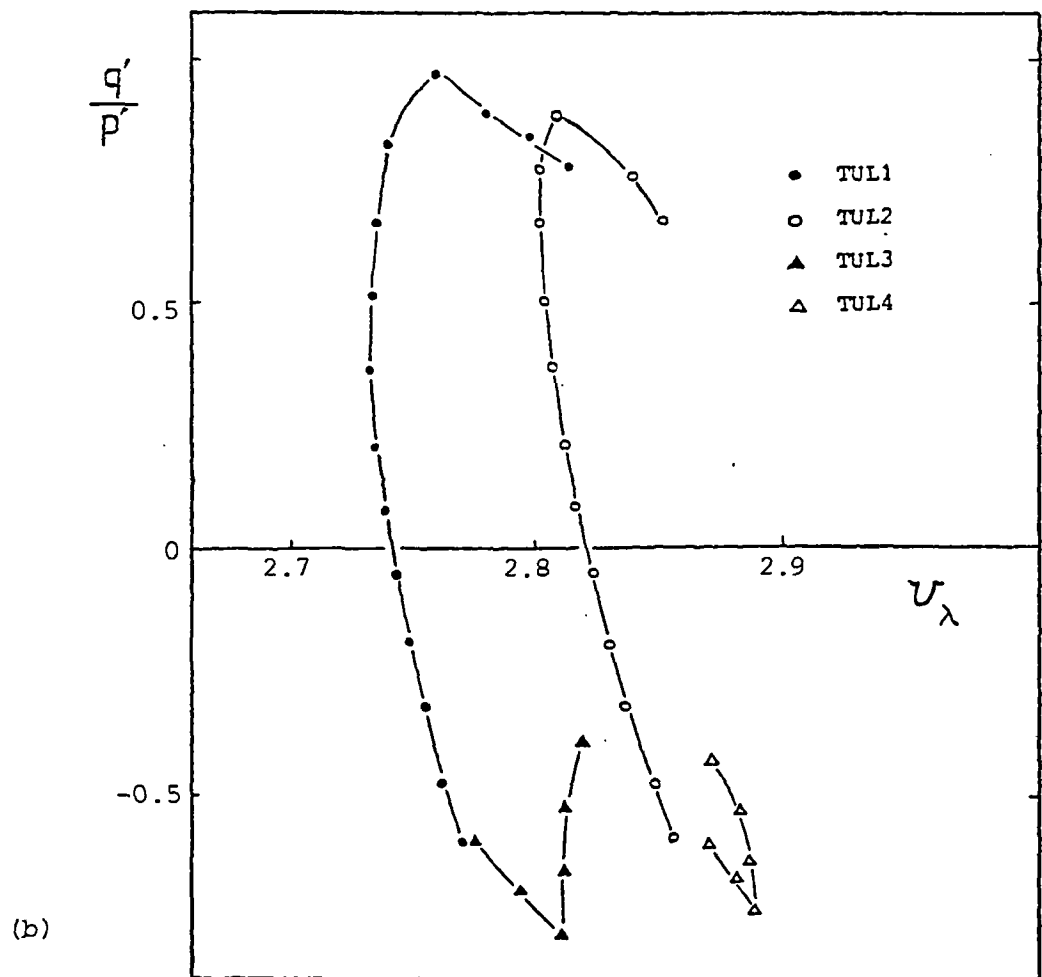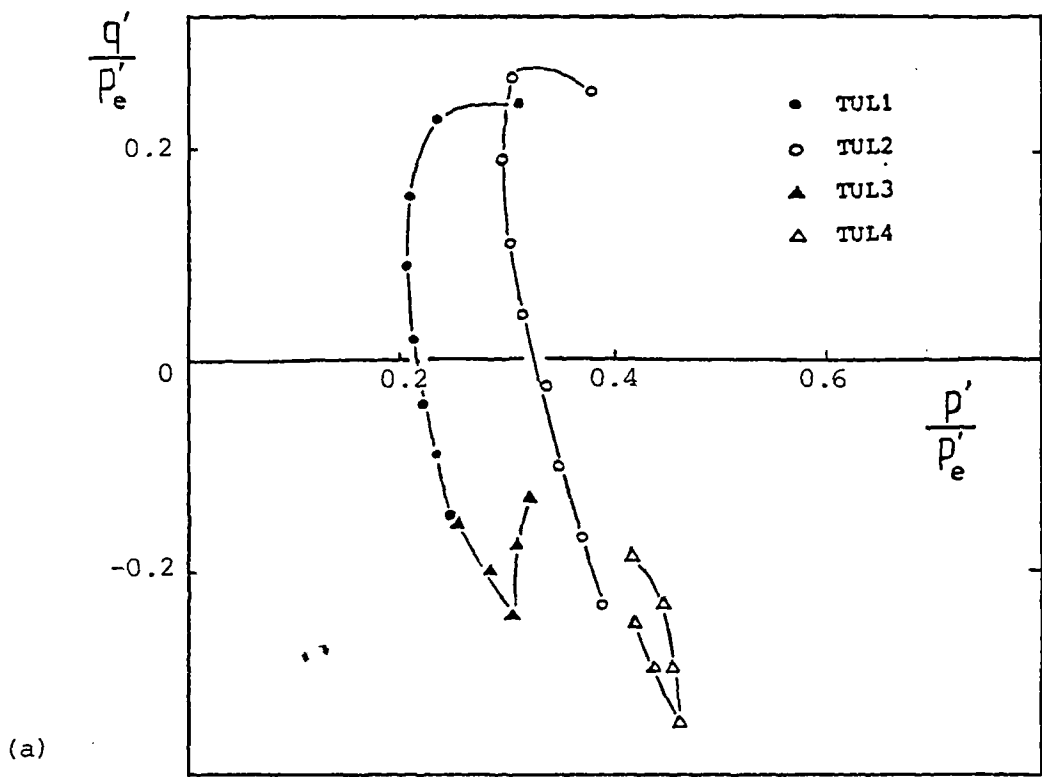
Figure 7.59   Normalised state paths for 100 mm undisturbed
London clay (blue) triaxial samples
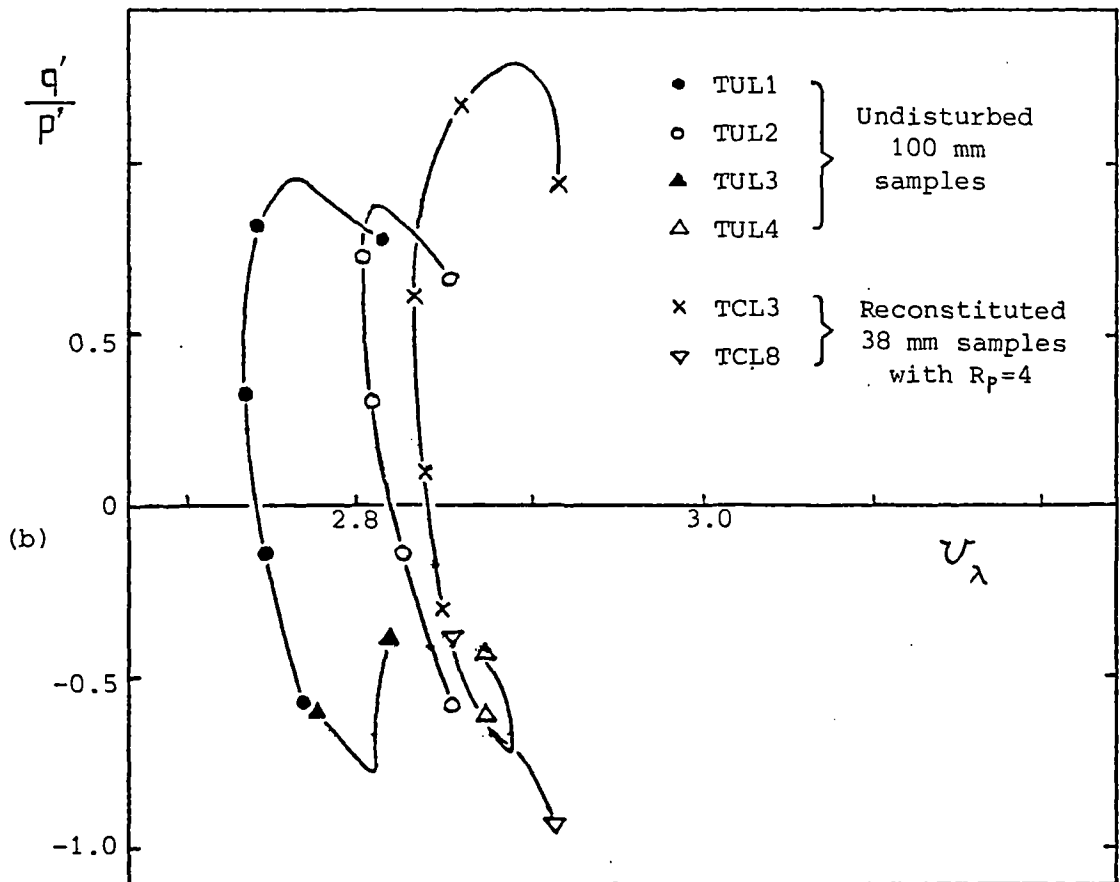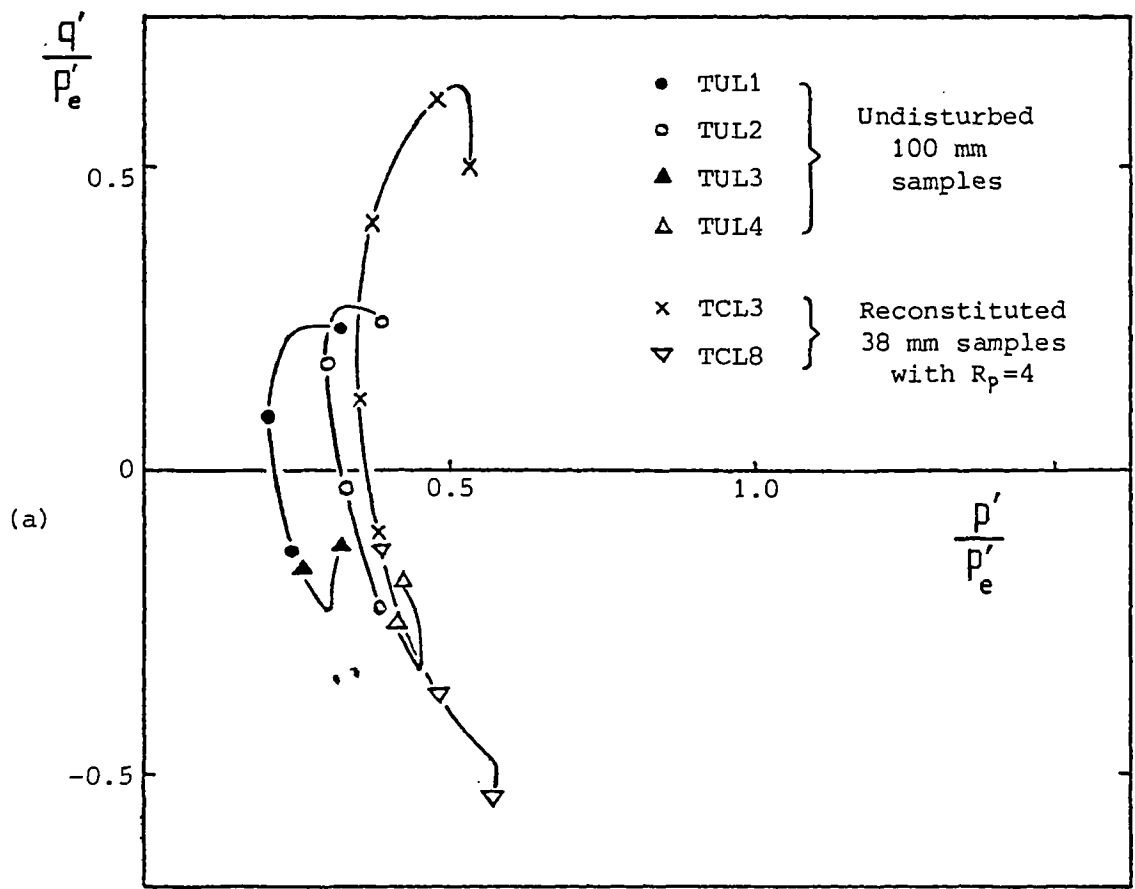
Figure 7.60   Comparison of normalised state paths for undisturbed
   and reconstituted London clay (blue) triaxial samples
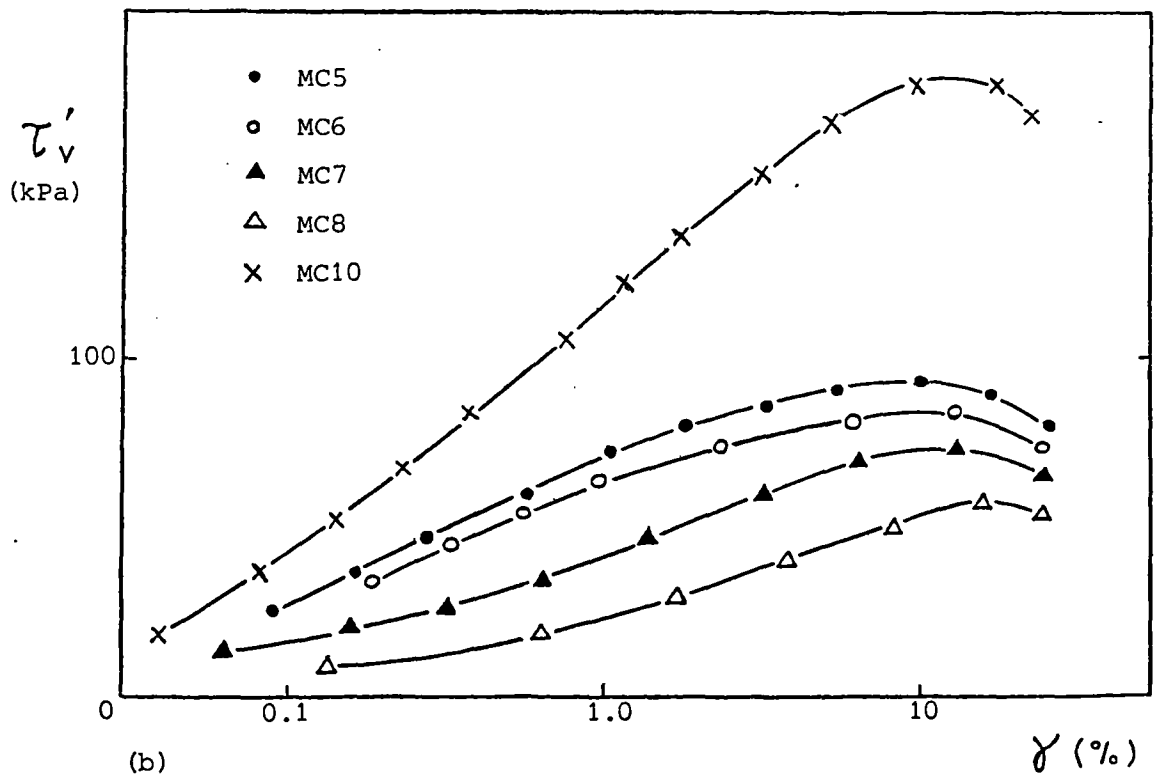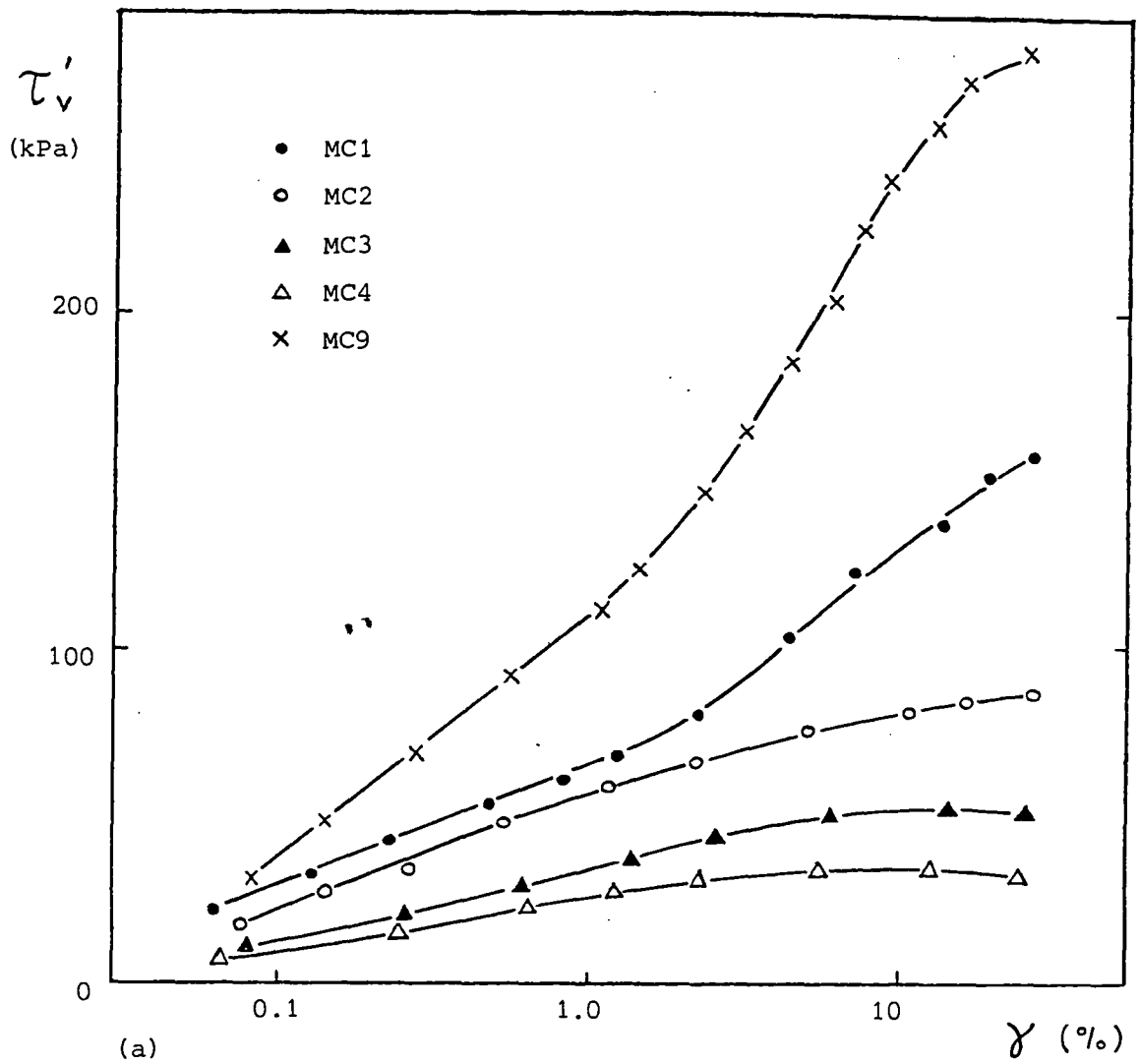
Figure 7.61 Variation of shear stress with logarithm of shear strain for remoulded Cowden till simple shear samples
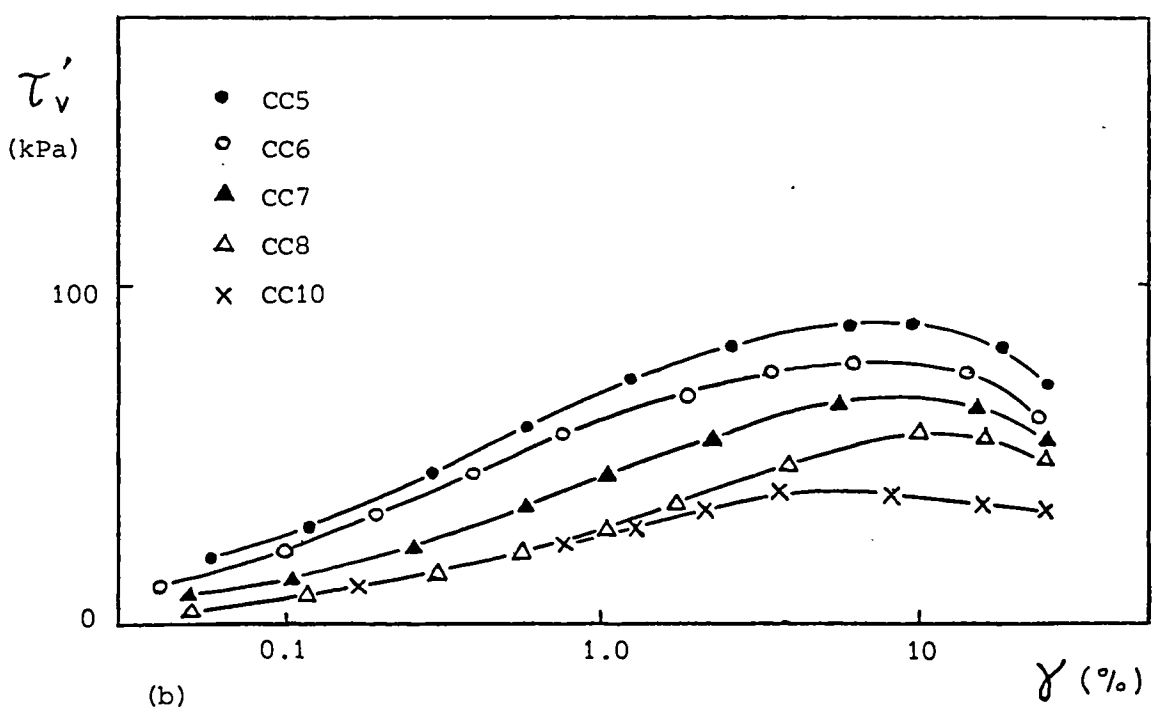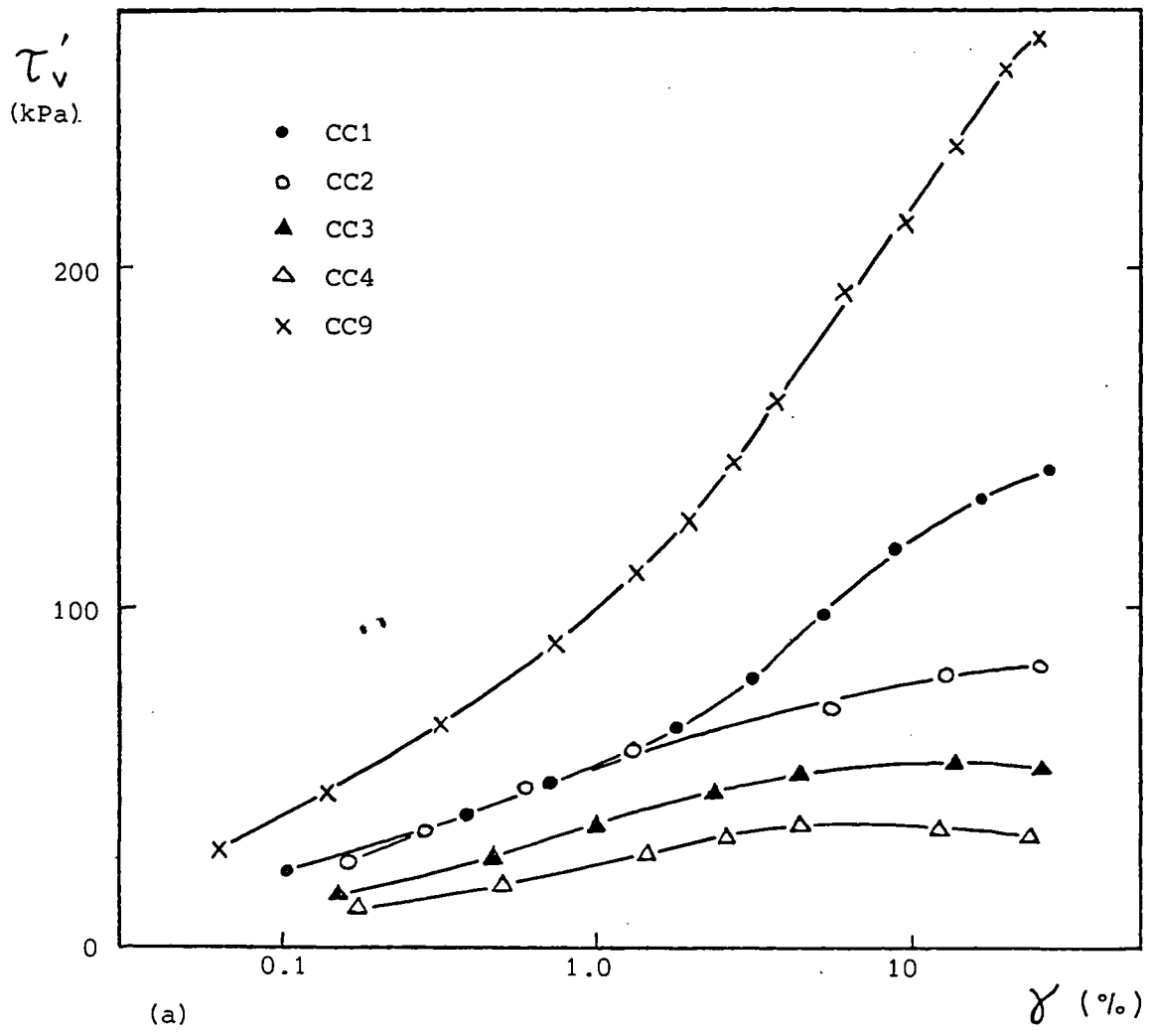
Figure 7.62 Variation of shear stress with logarithm of shear strain for reconstituted Cowden till simple shear samples
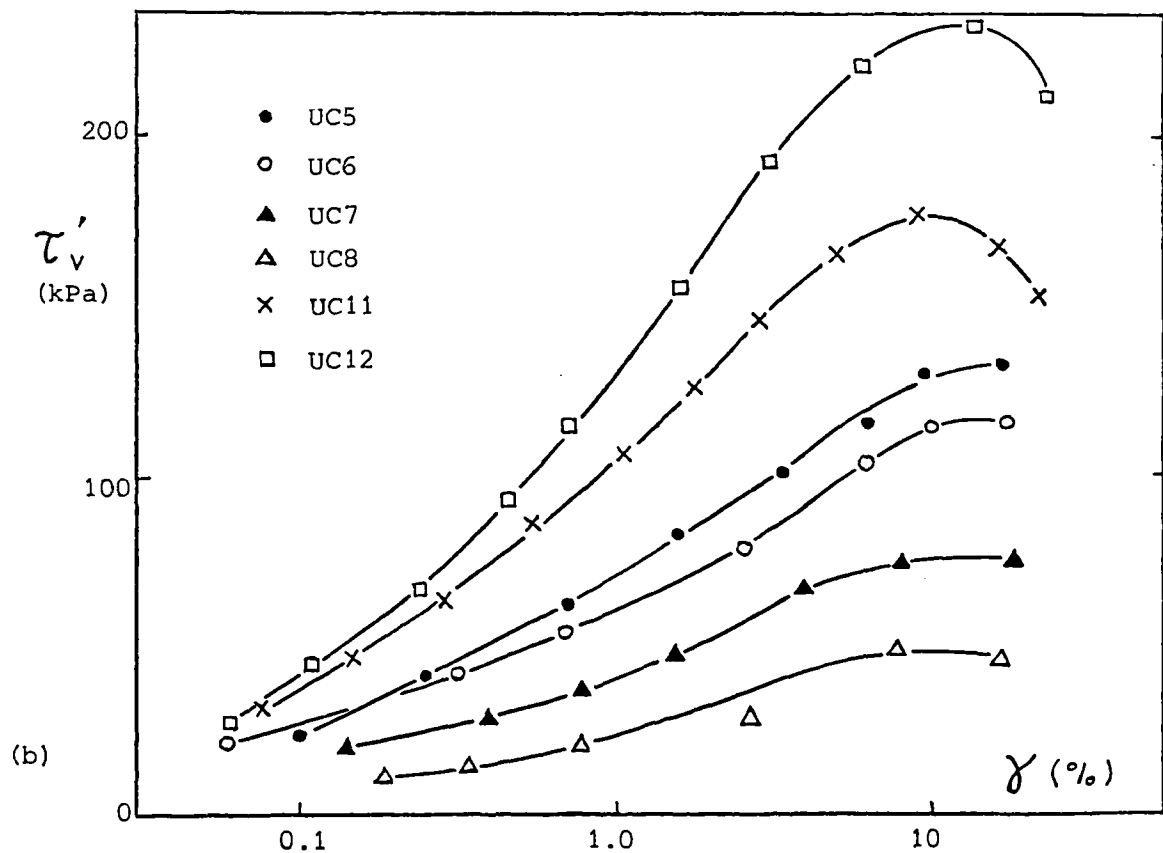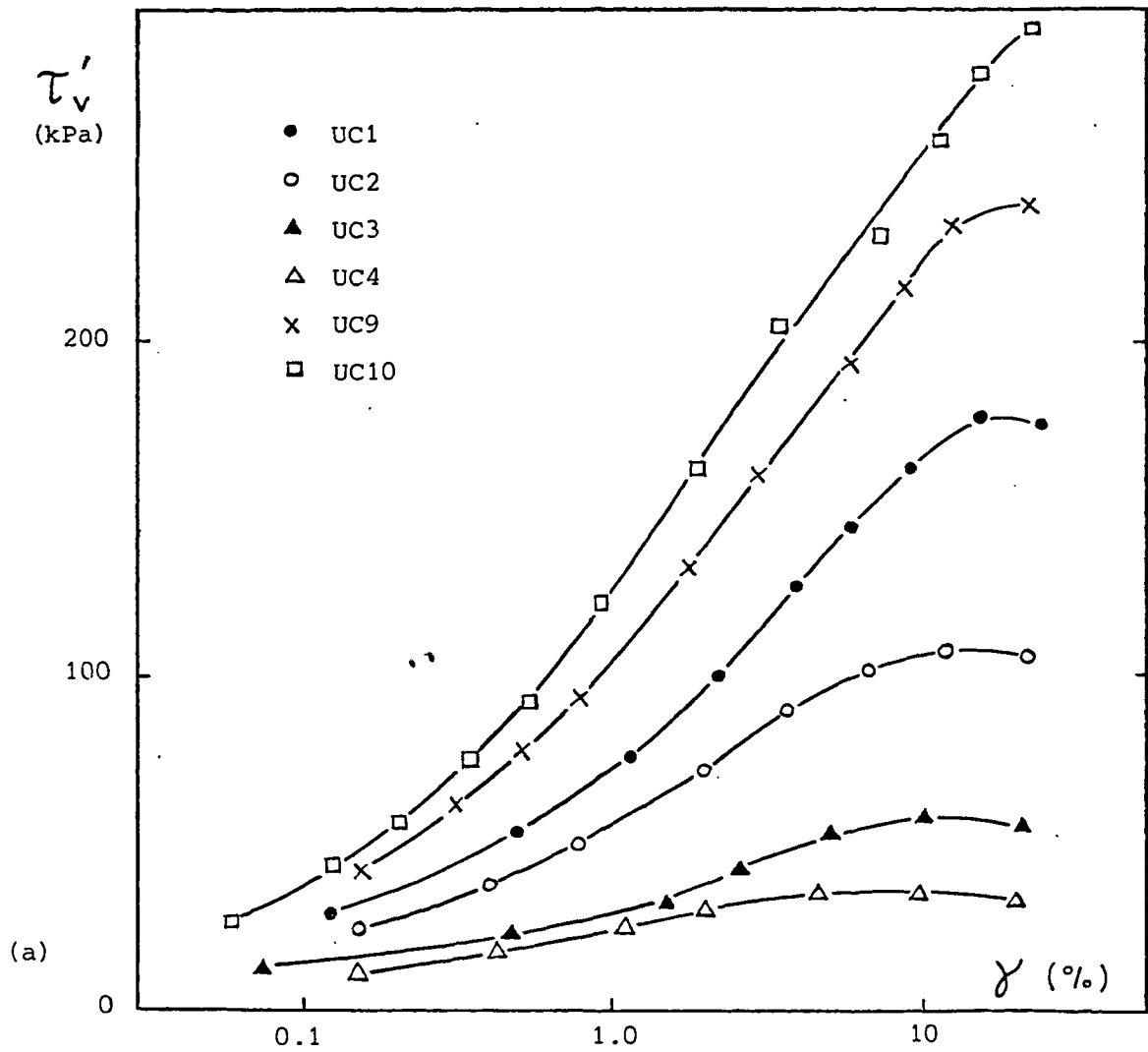
Figure 7.63   Variation of shear stress with logarithm of shear strain
for undisturbed Cowden till simple shear samples
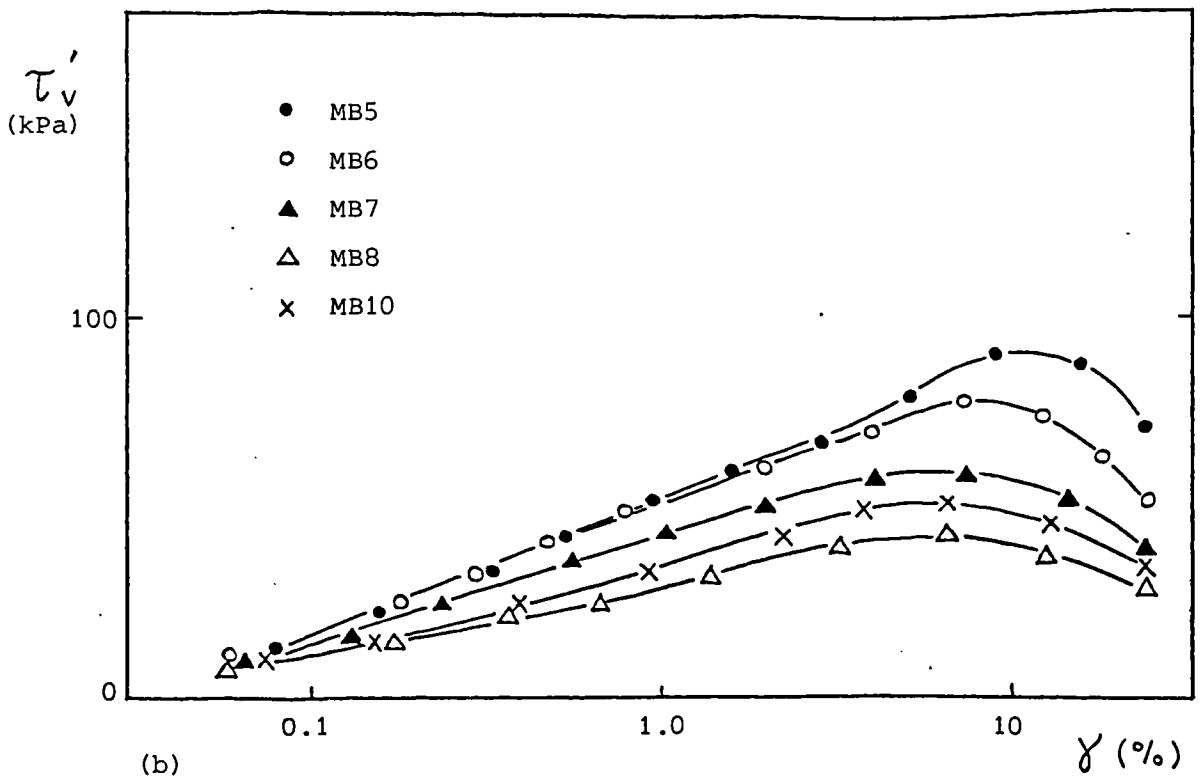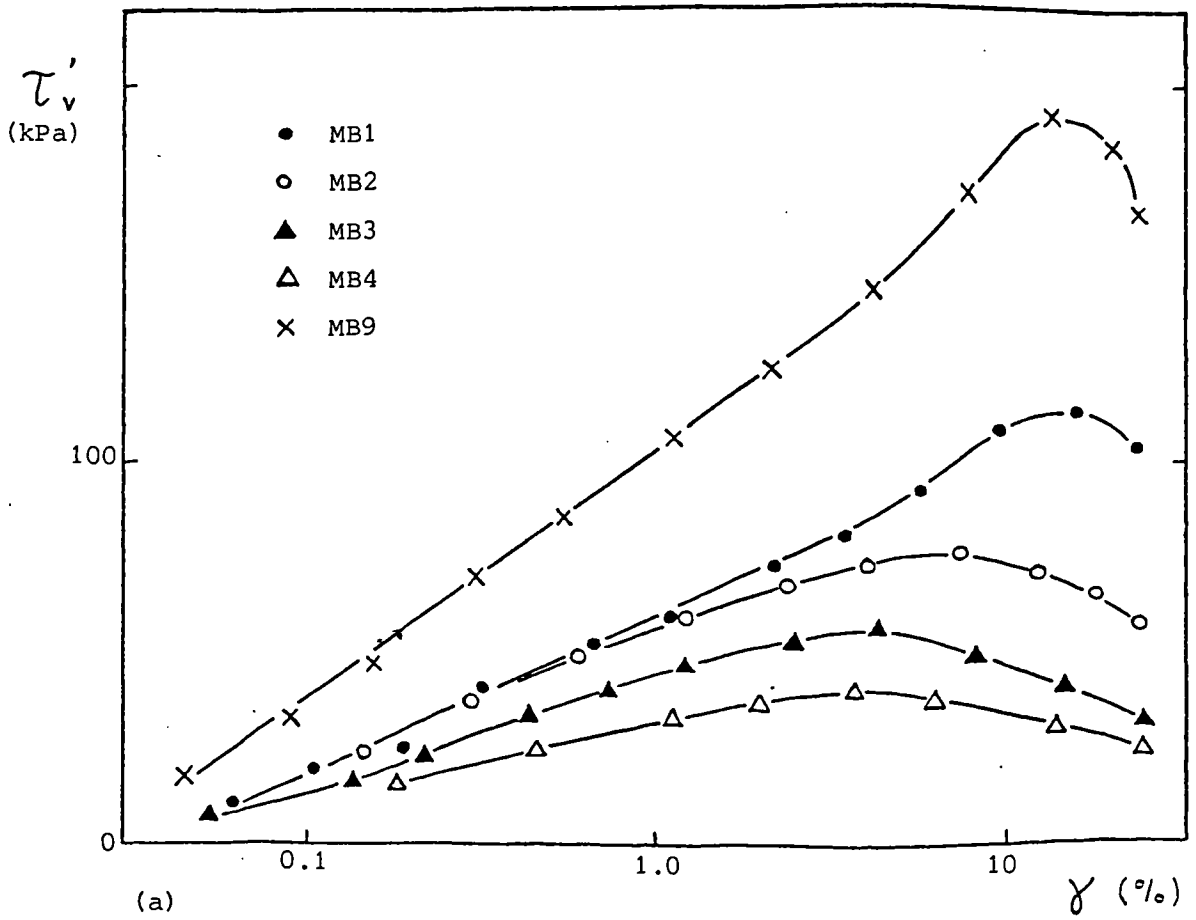
Figure 7.64   Variation of shear stress with logarithm of shear strain
for remoulded London clay (brown) simple shear samples
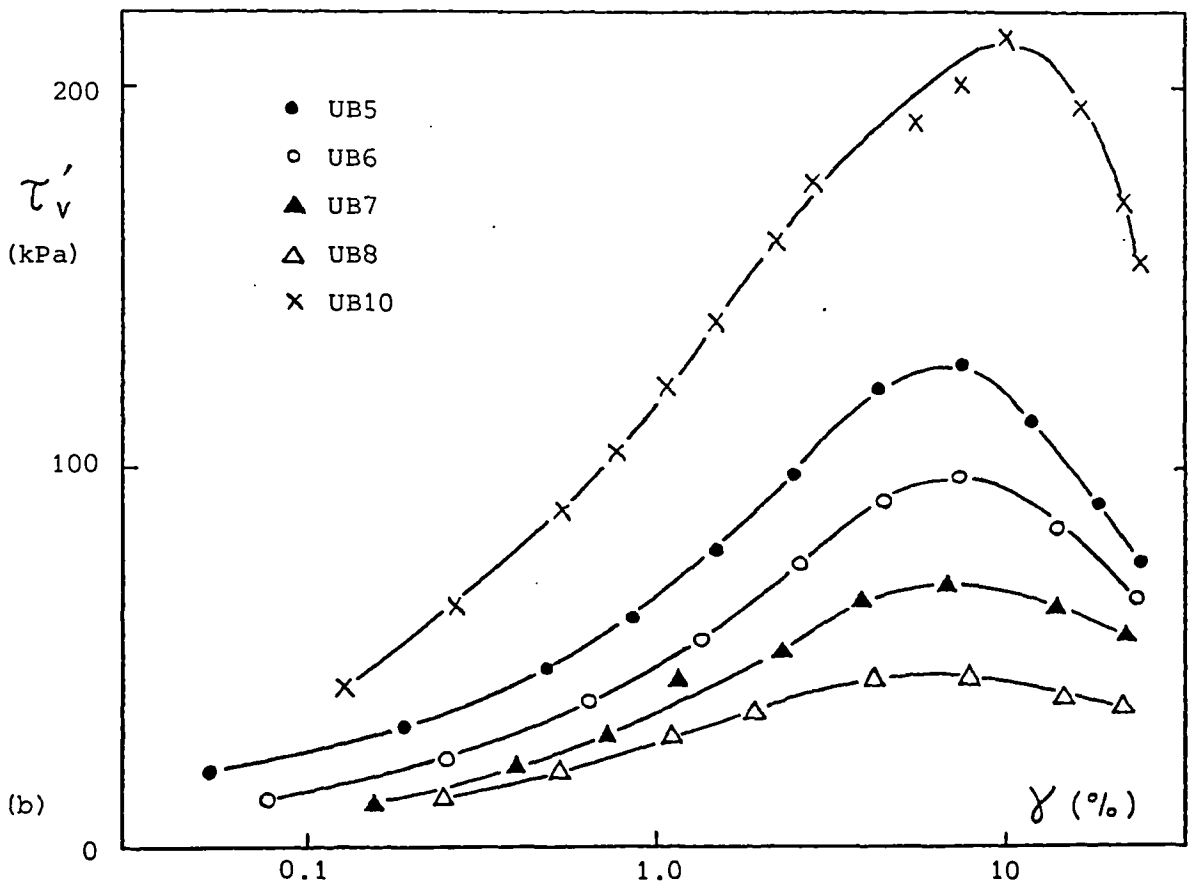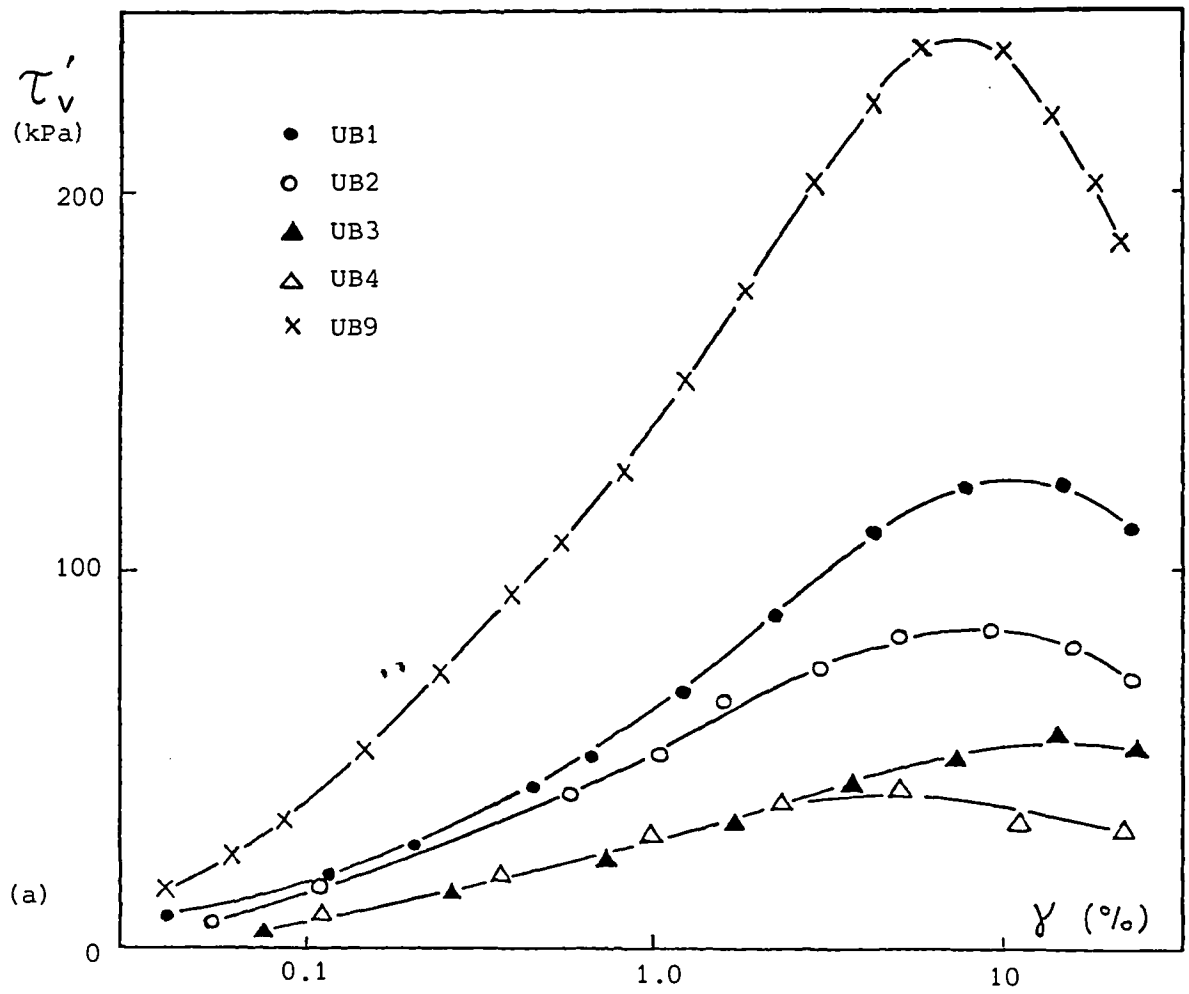
Figure 7.65   Variation of shear stress with logarithm of shear strain
for undisturbed London clay (brown) simple shear samples
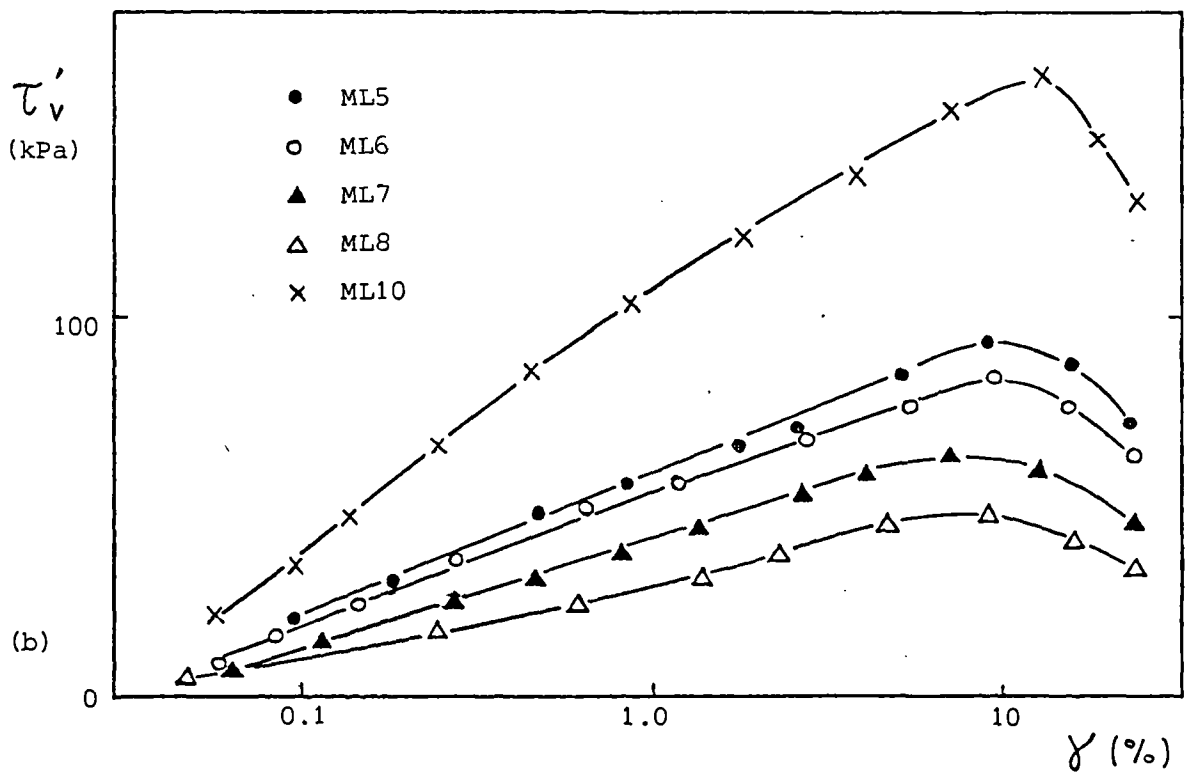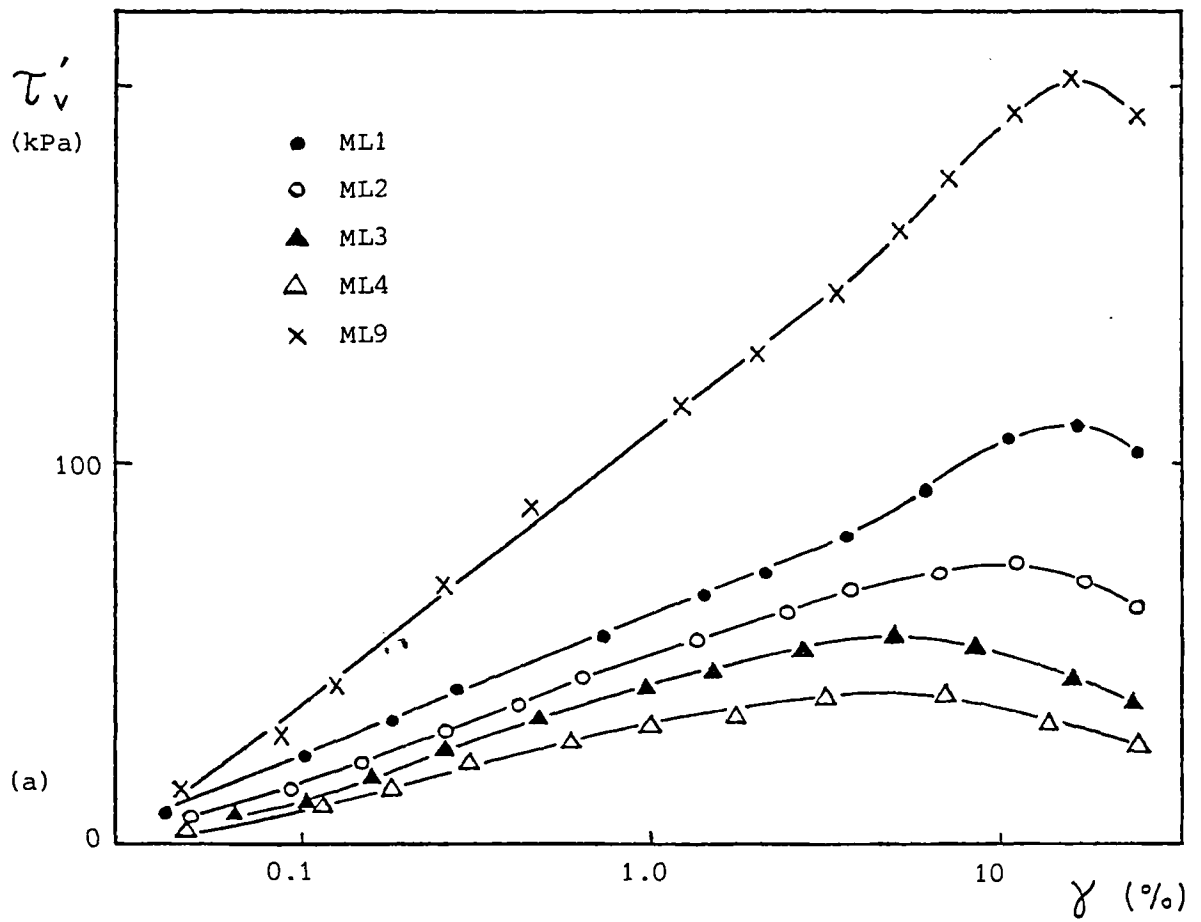
Figure 7.66   Variation of shear stress with logarithm of shear strain
              for remoulded London clay (blue) simple shear samples
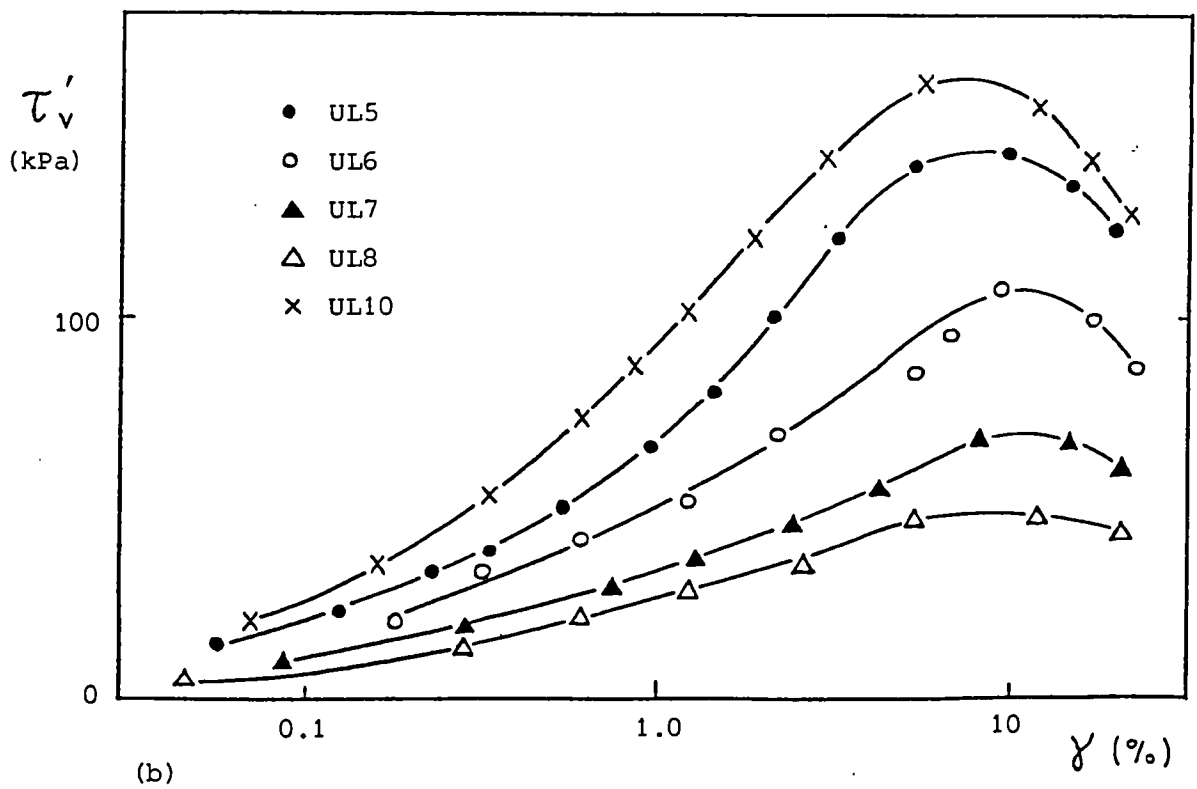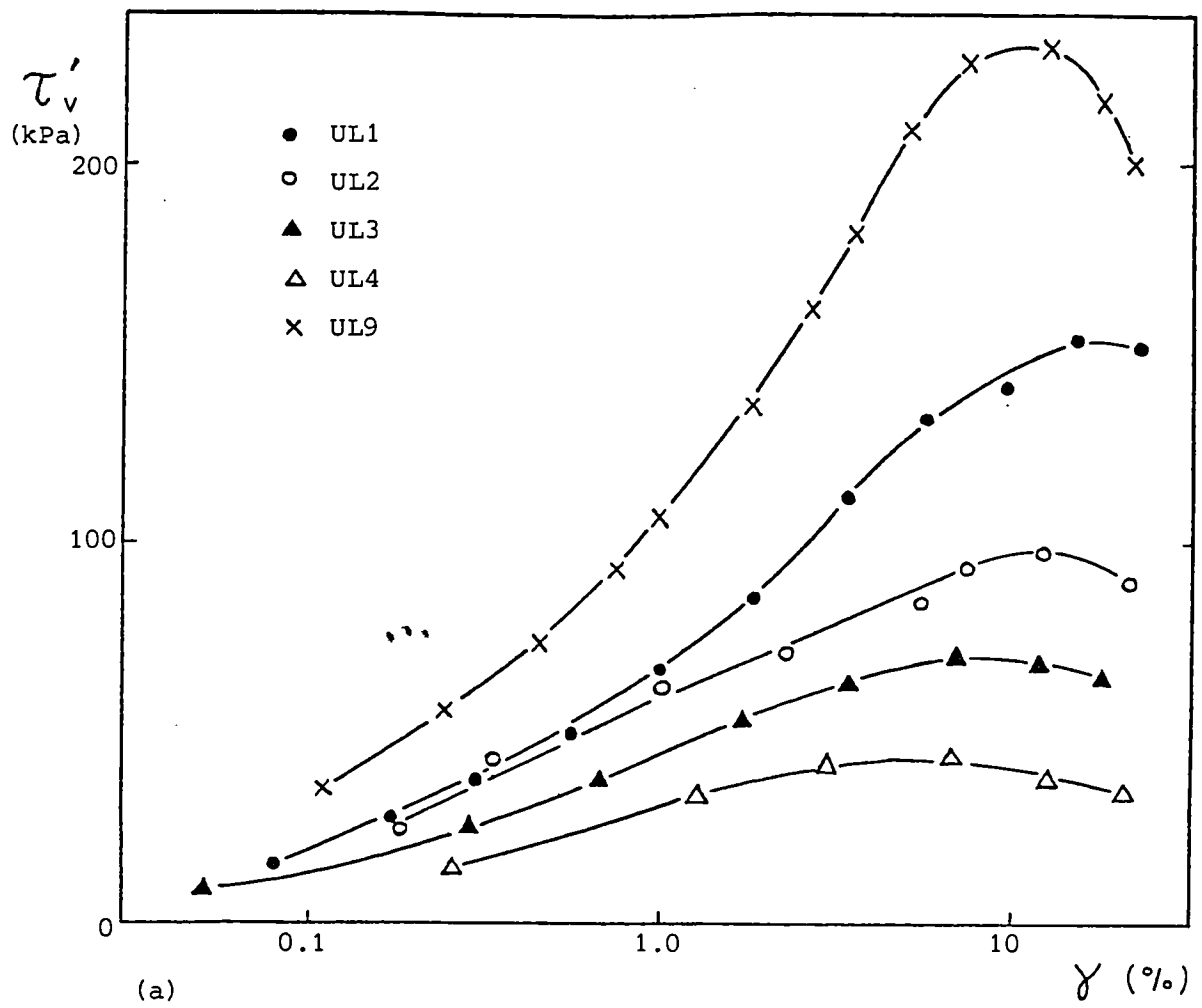
Figure 7.67 Variation of shear stress with logarithm of shear strain for undisturbed London clay (blue) simple shear samples
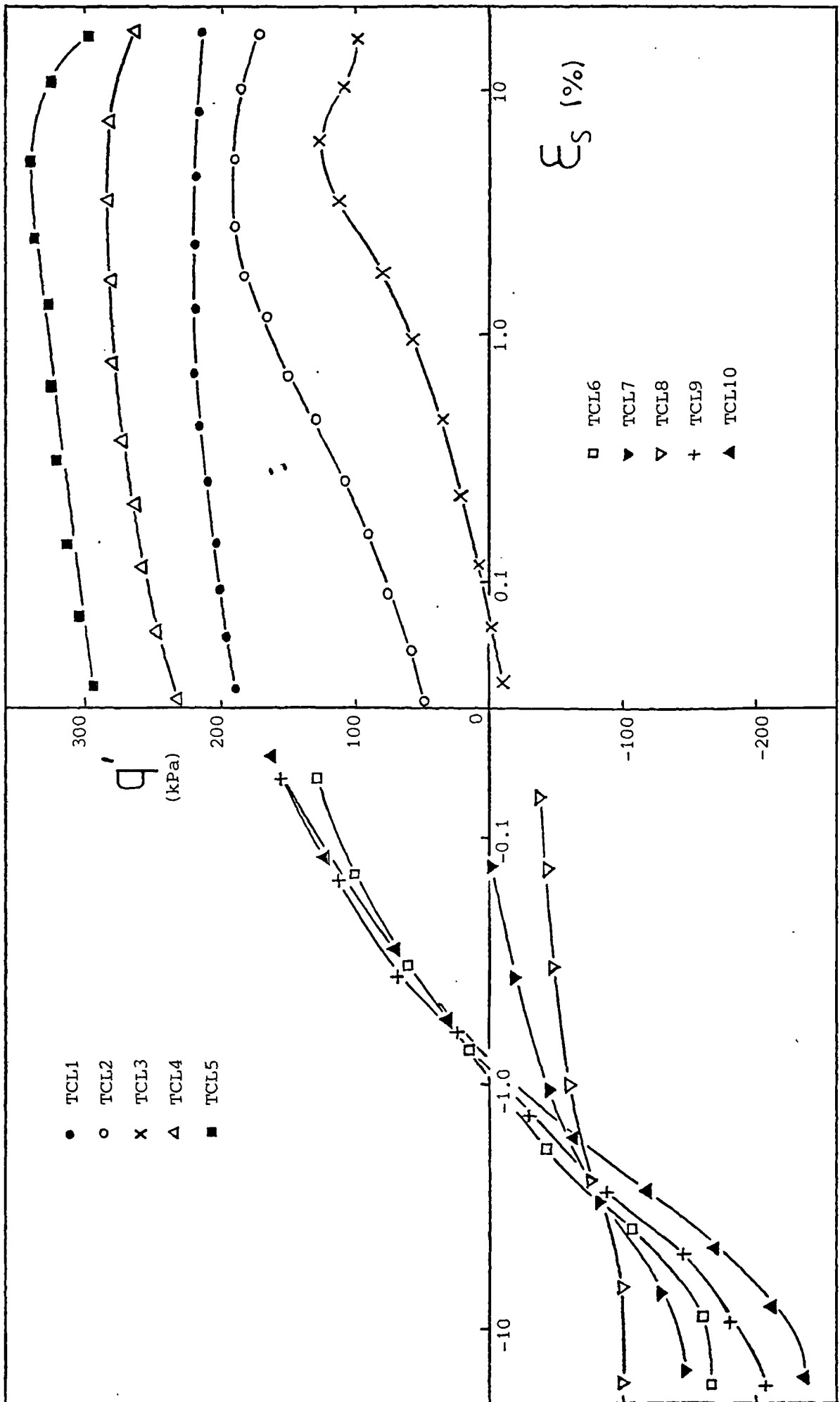
Figure 7.68   Variation of shear stress with logarithm of shear strain
               for 38 mm reconstituted London clay (blue) triaxial samples
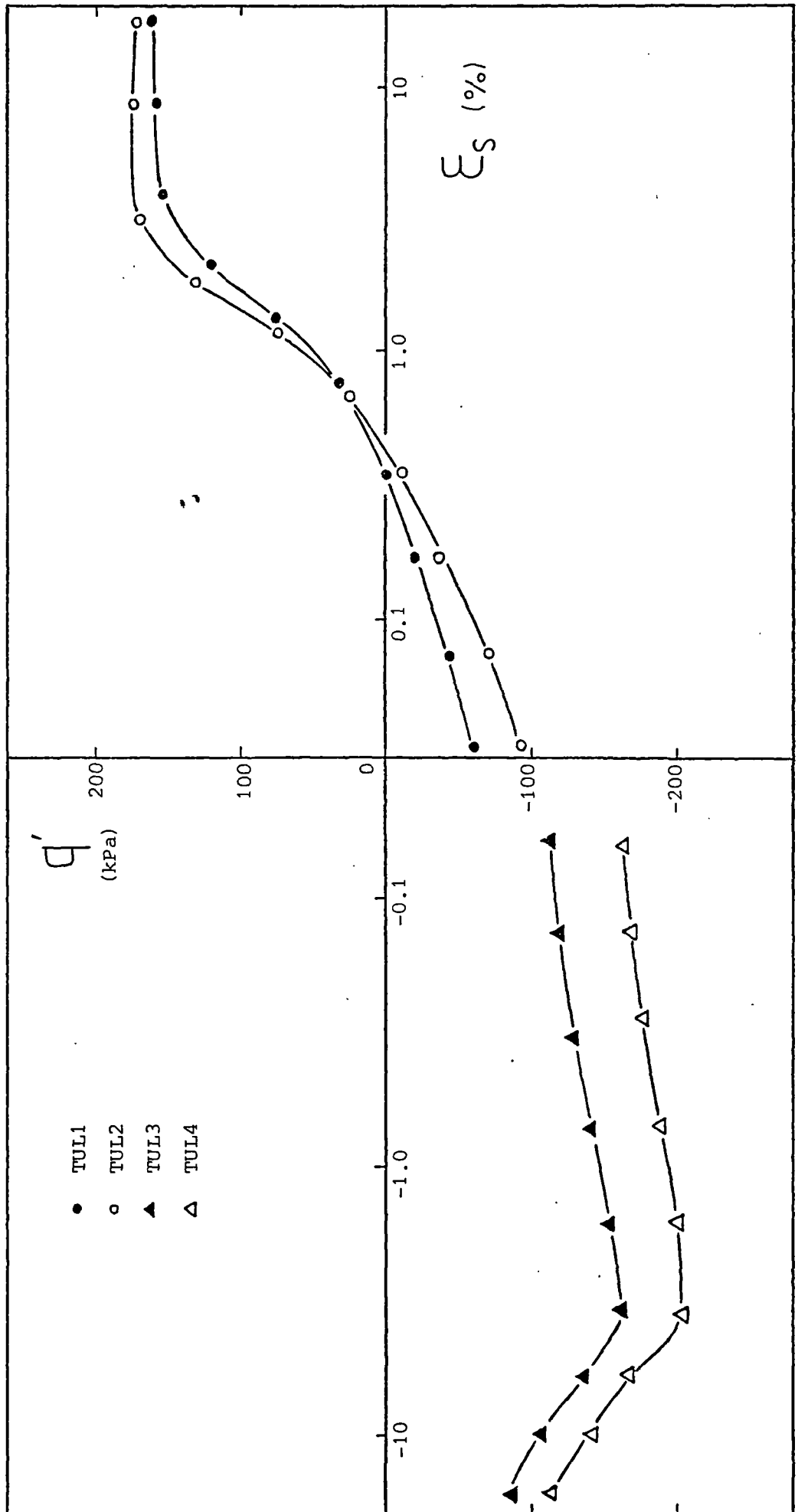
Figure 7.69   Variation of shear stress with logarithm of shear strain
for 100 mm undisturbed London clay (blue) triaxial samples
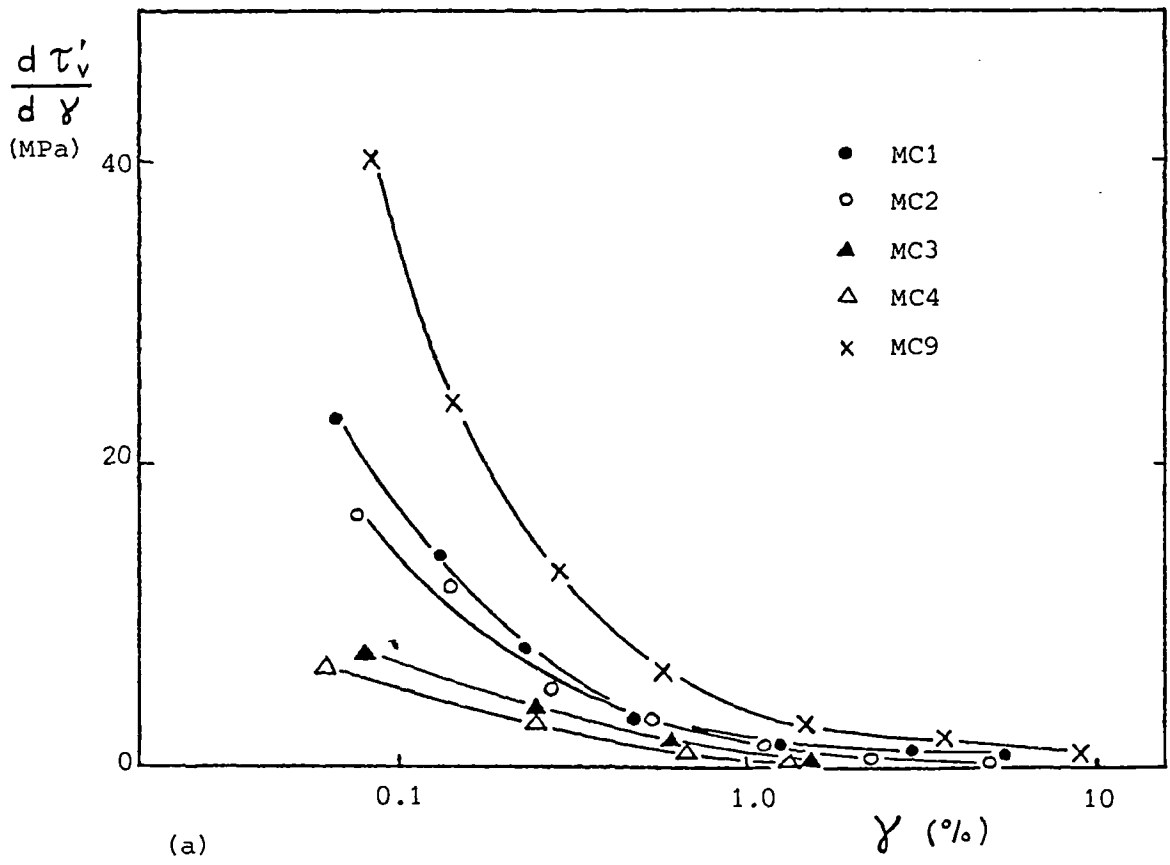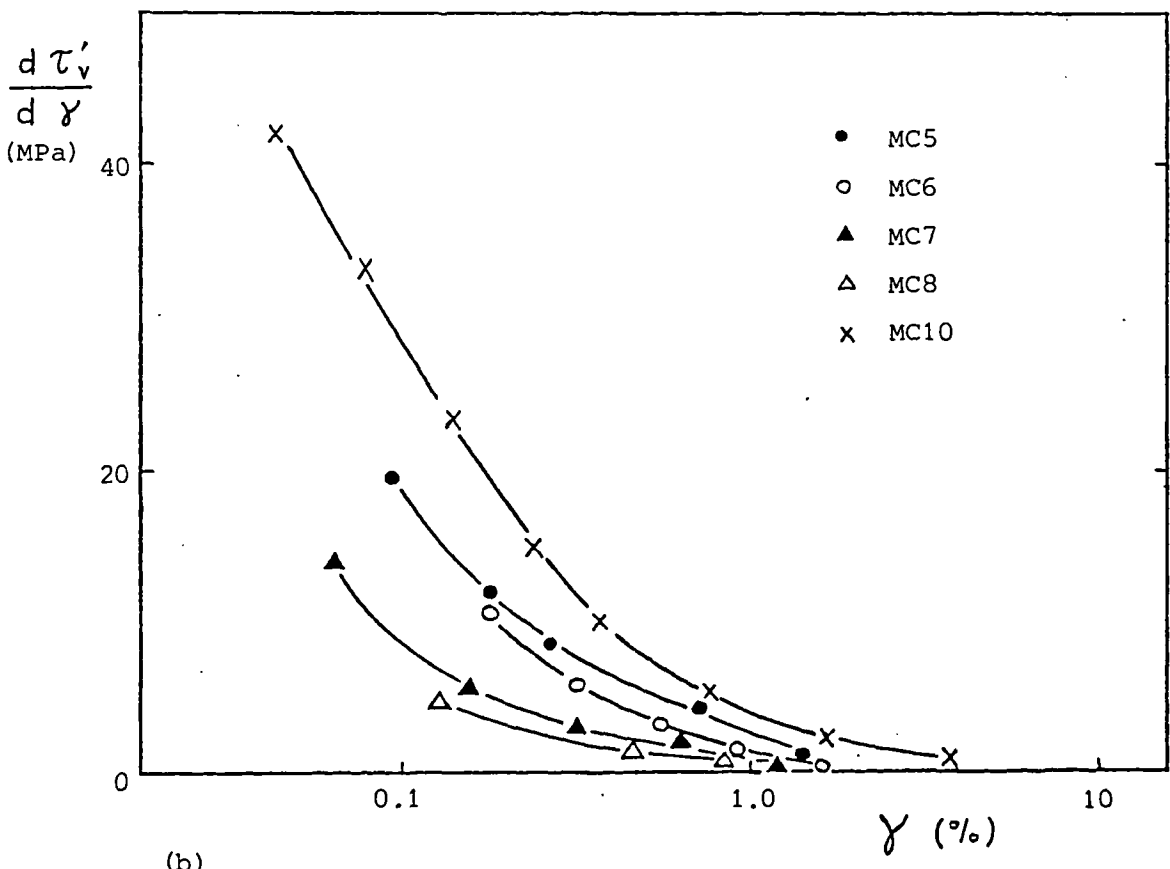
Figure 7.70 Variation of tangent shear stiffness with logarithm
of shear strain for remoulded Cowden till simple
shear samples
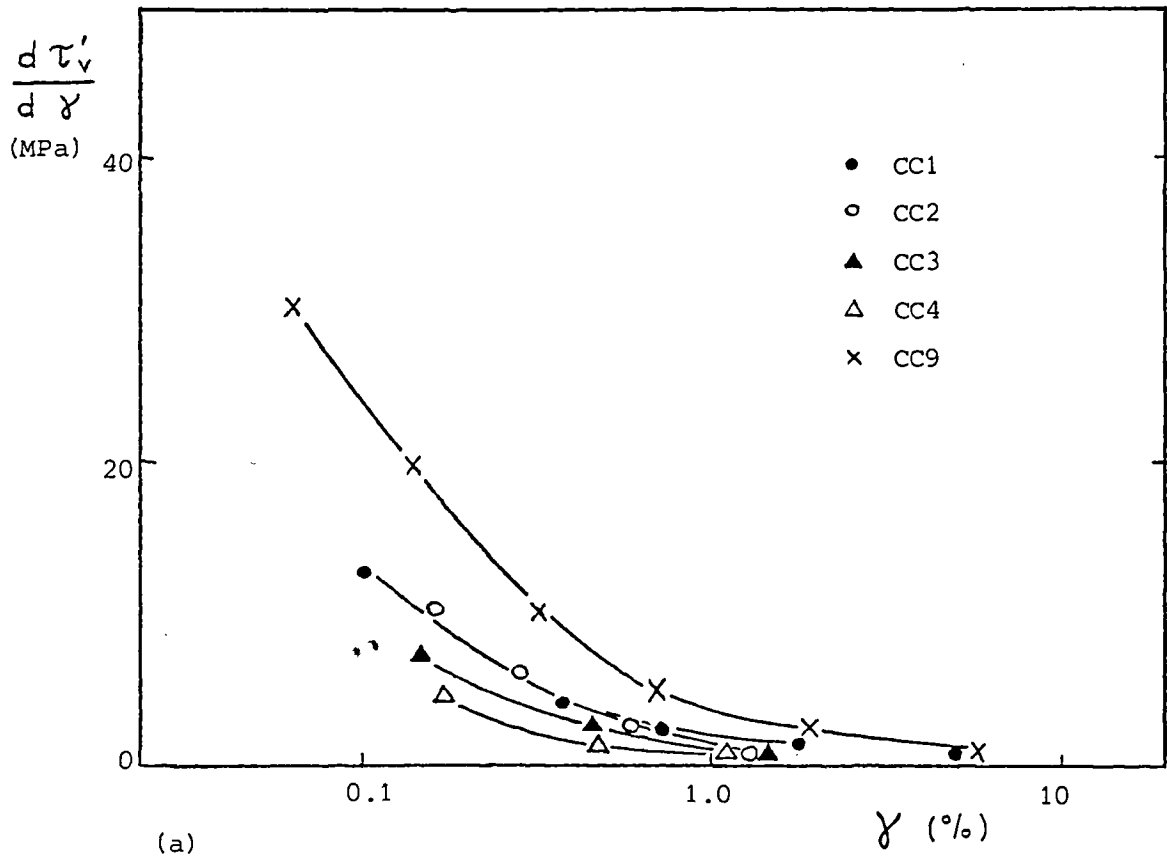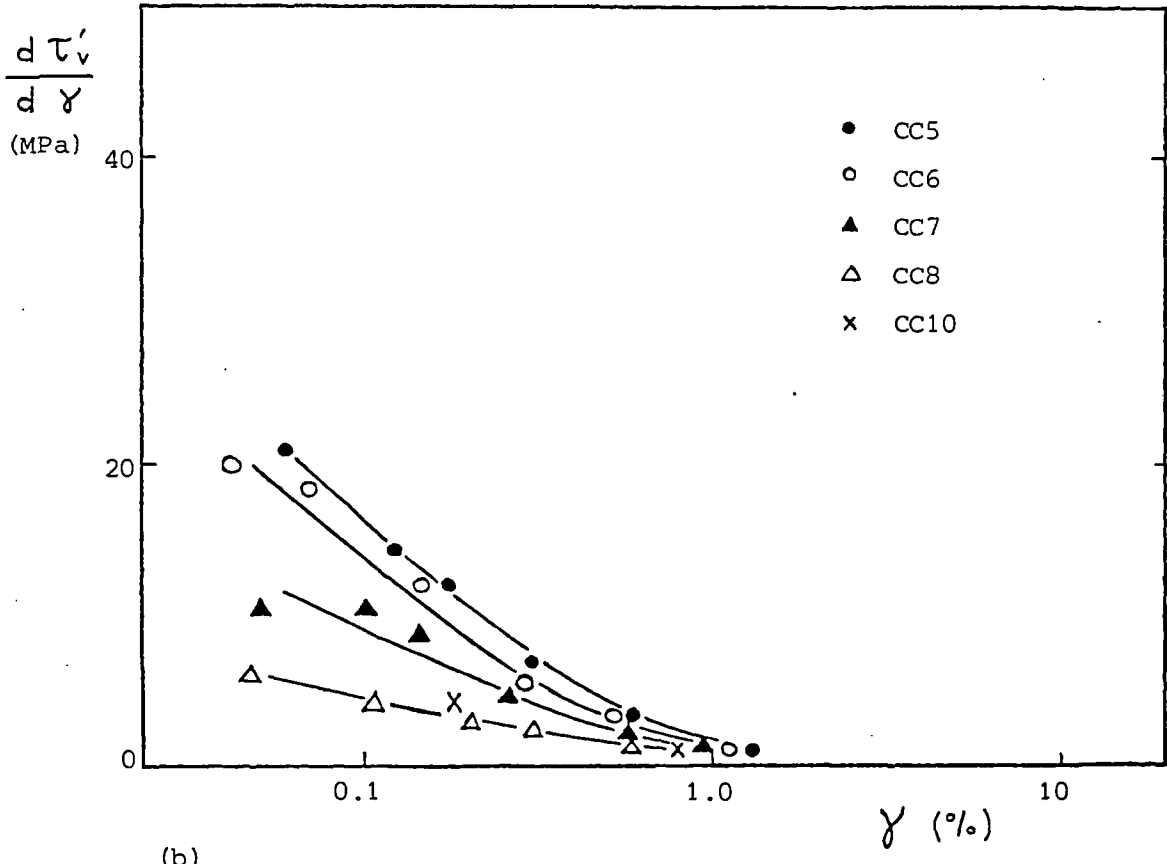
Figure 7.71   Variation of tangent shear stiffness with logarithm
of shear strain for reconstituted Cowden till simple
shear samples
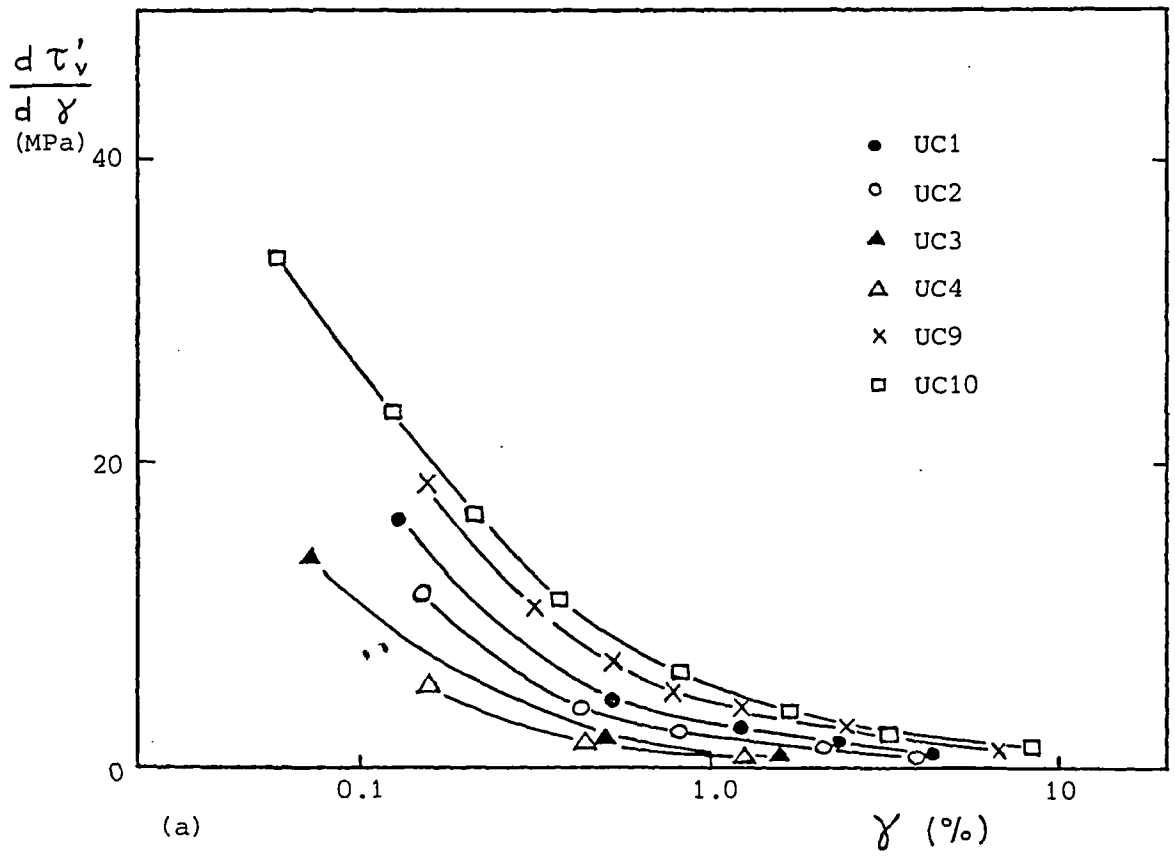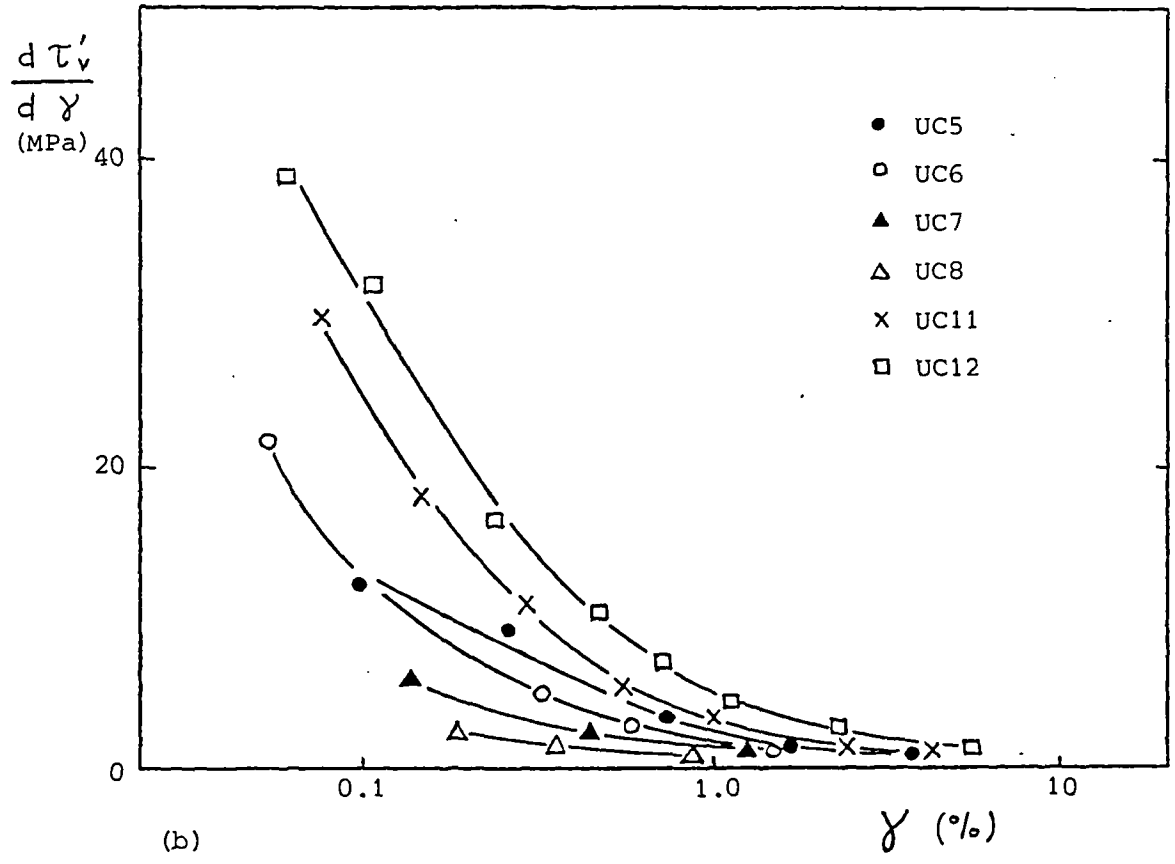
Figure 7.72   Variation of tangent shear stiffness with logarithm of shear strain for undisturbed Cowden till simple shear samples
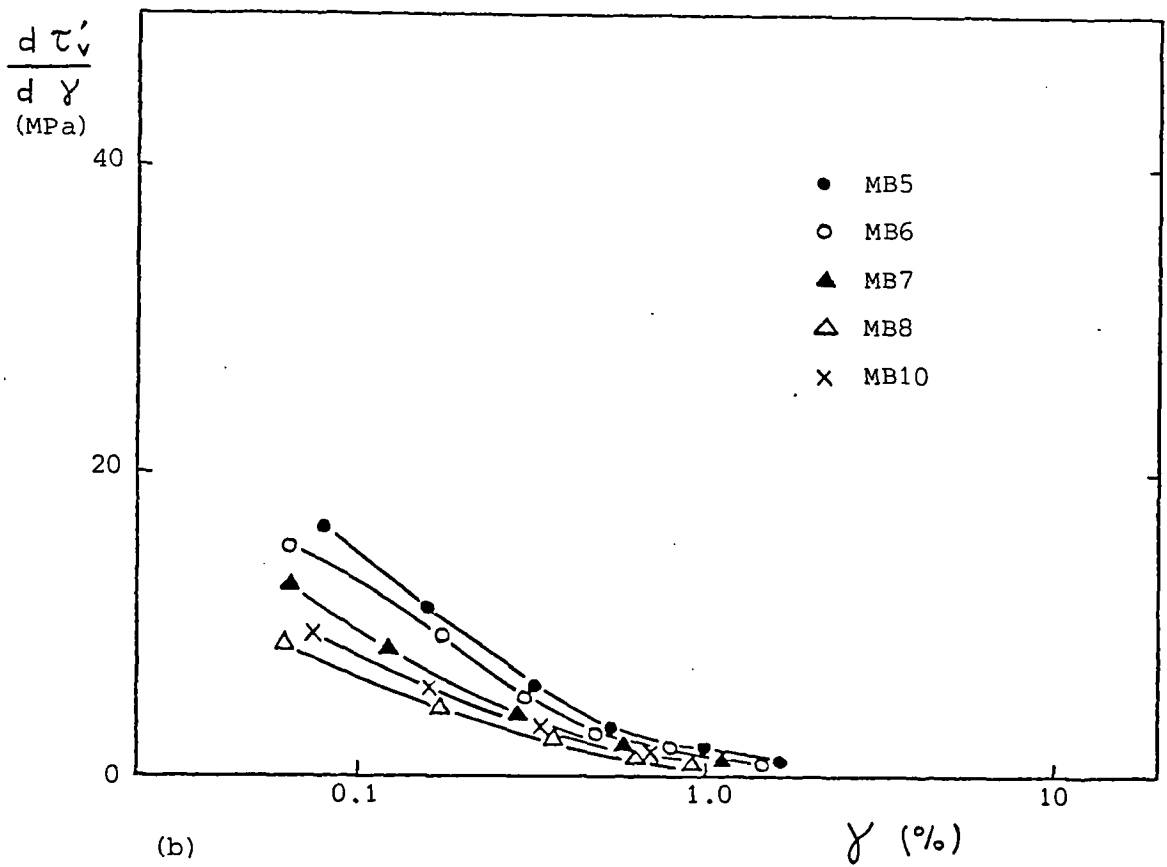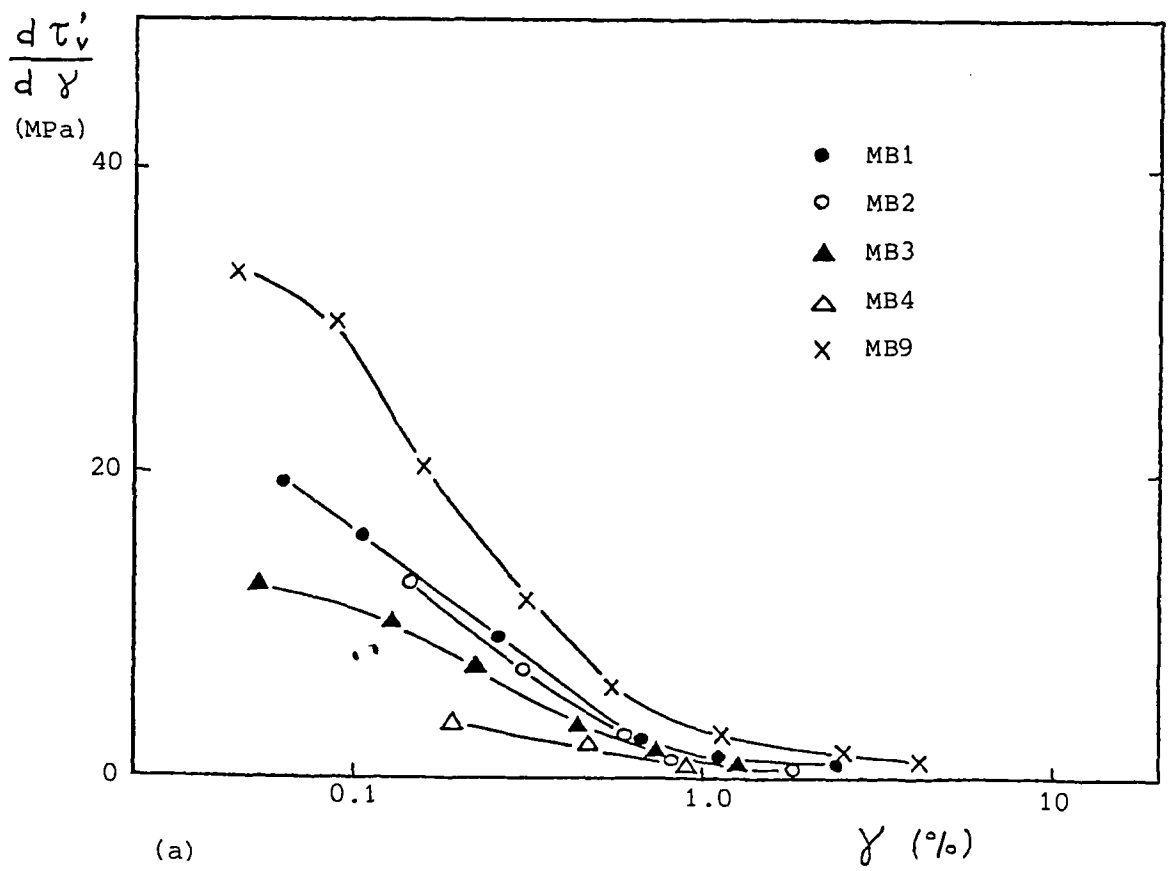
Figure   7.73   Variation of tangent shear stiffness with logarithm
of shear strain for remoulded London clay (brown)
simple shear samples
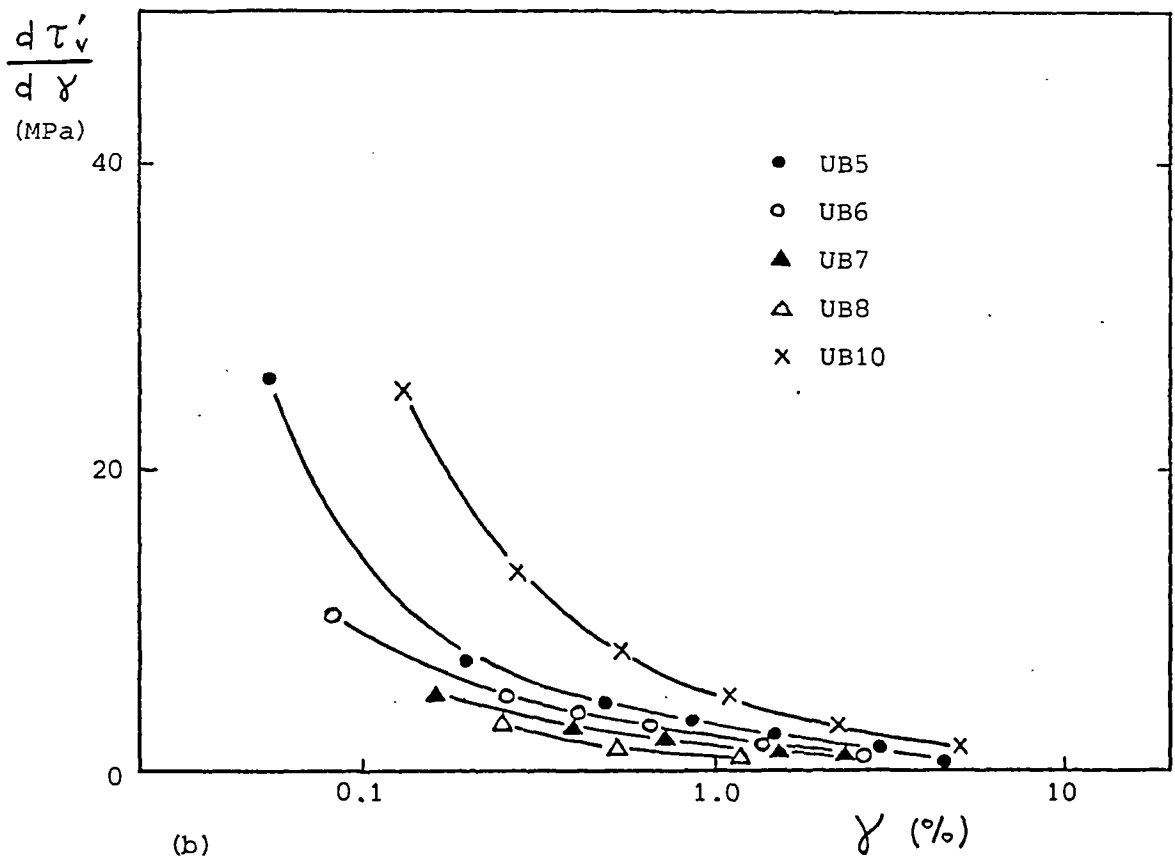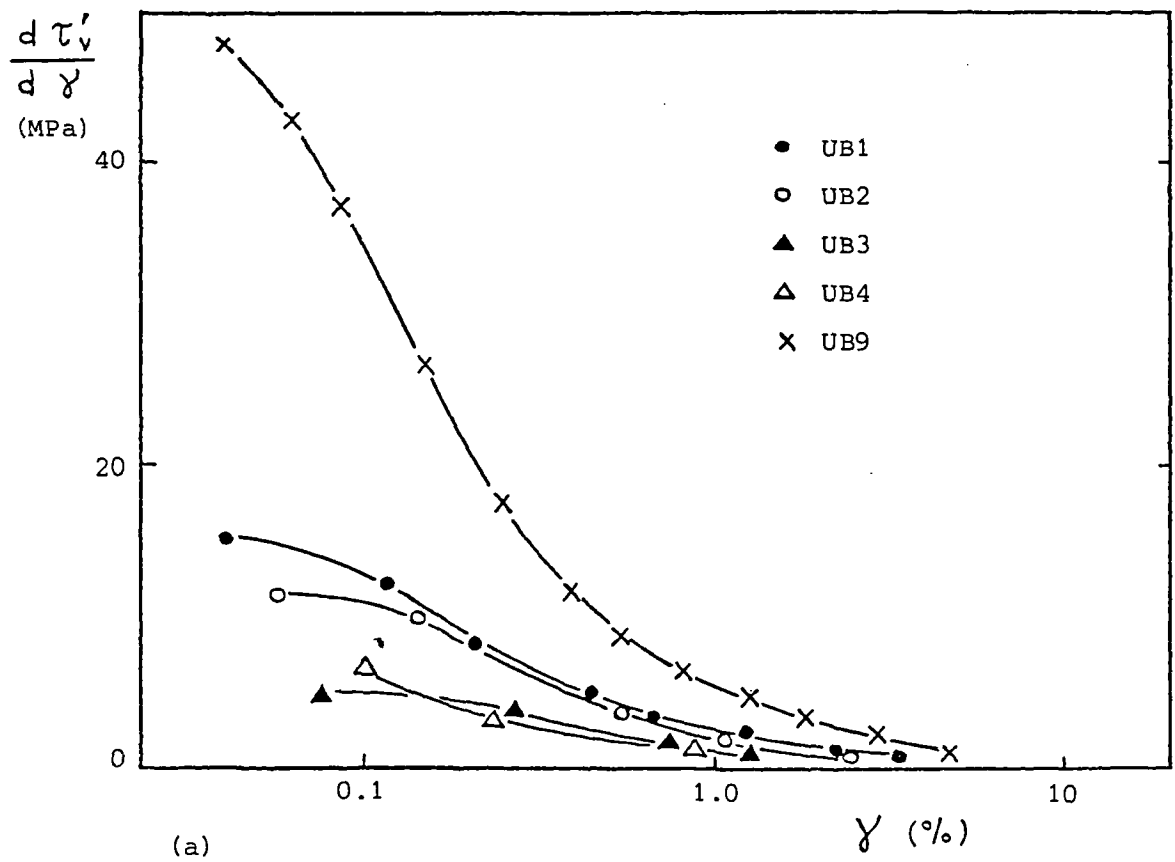
Figure 7.74   Variation of tangent shear stiffness with logarithm
of shear strain for undisturbed London clay (brown)
simple shear samples
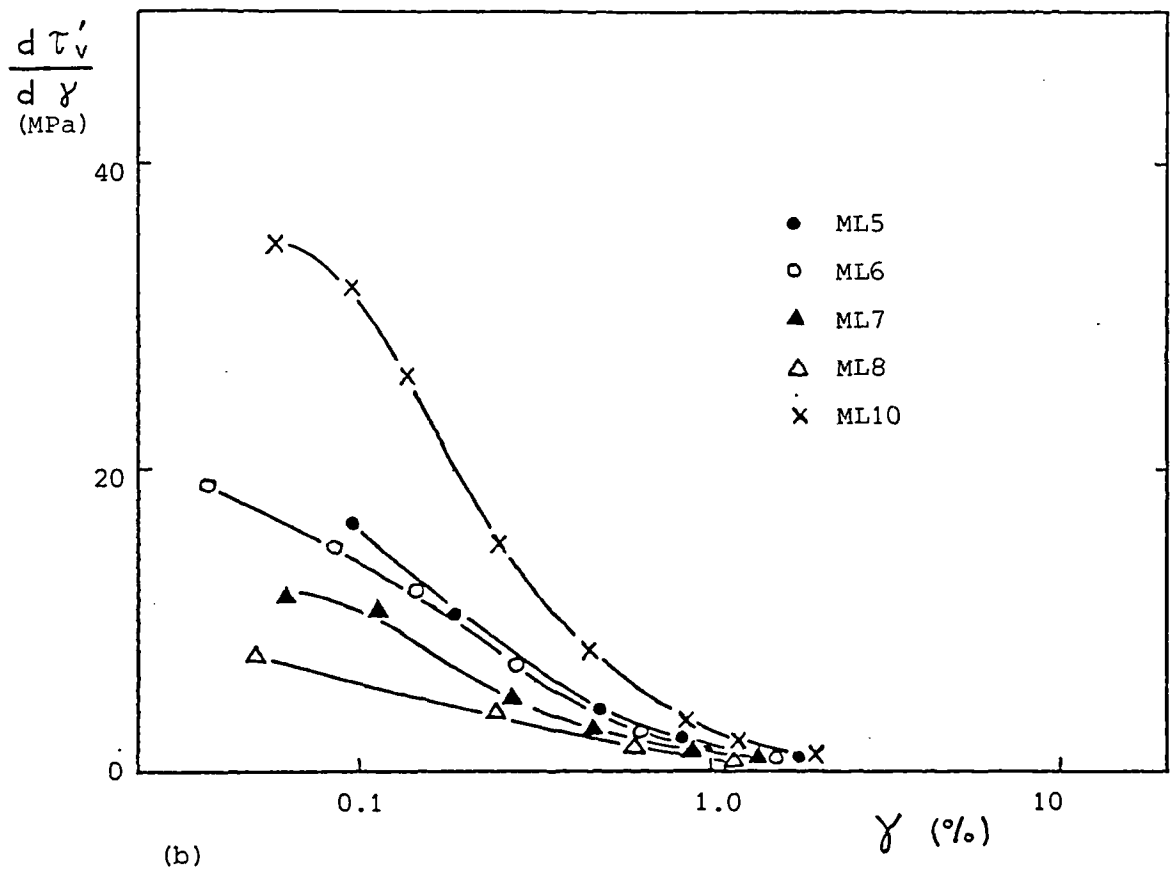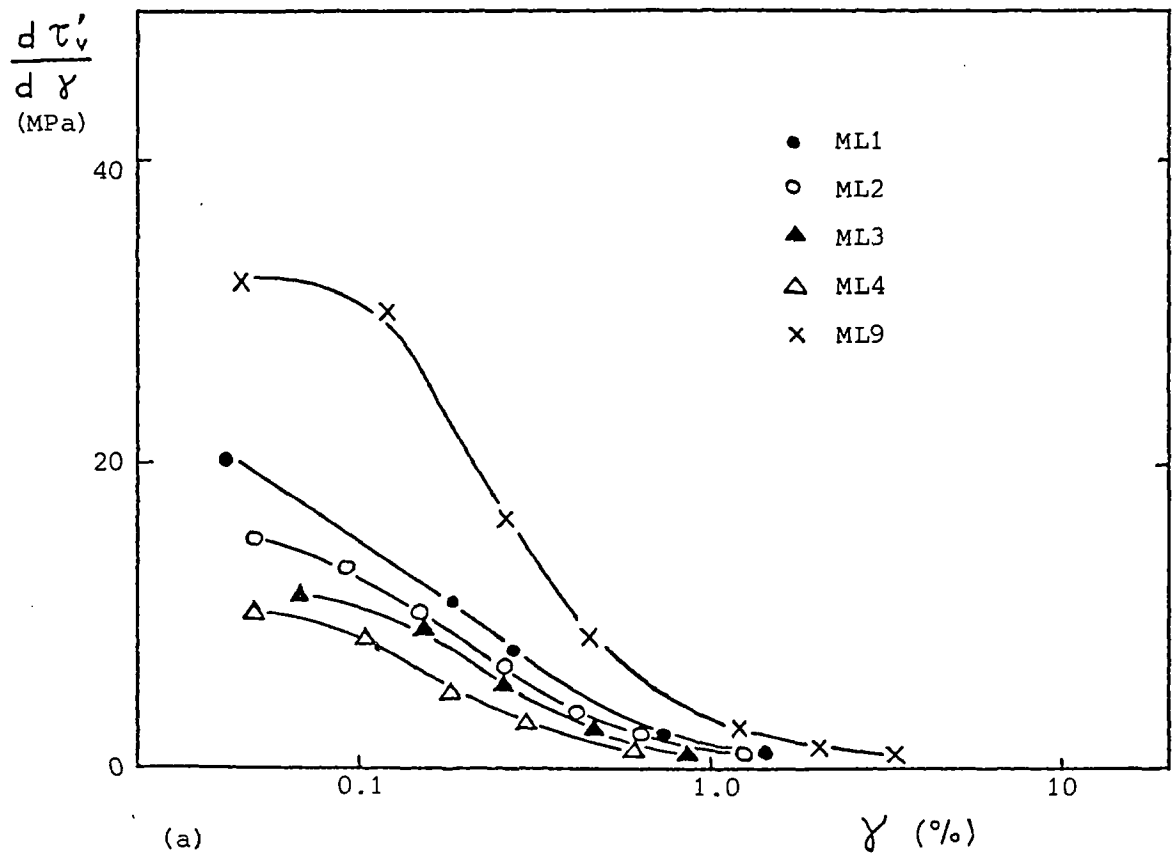
Figure 7.75 Variation of tangent shear stiffness with logarithm of shear strain for remoulded London clay (blue) simple shear samples
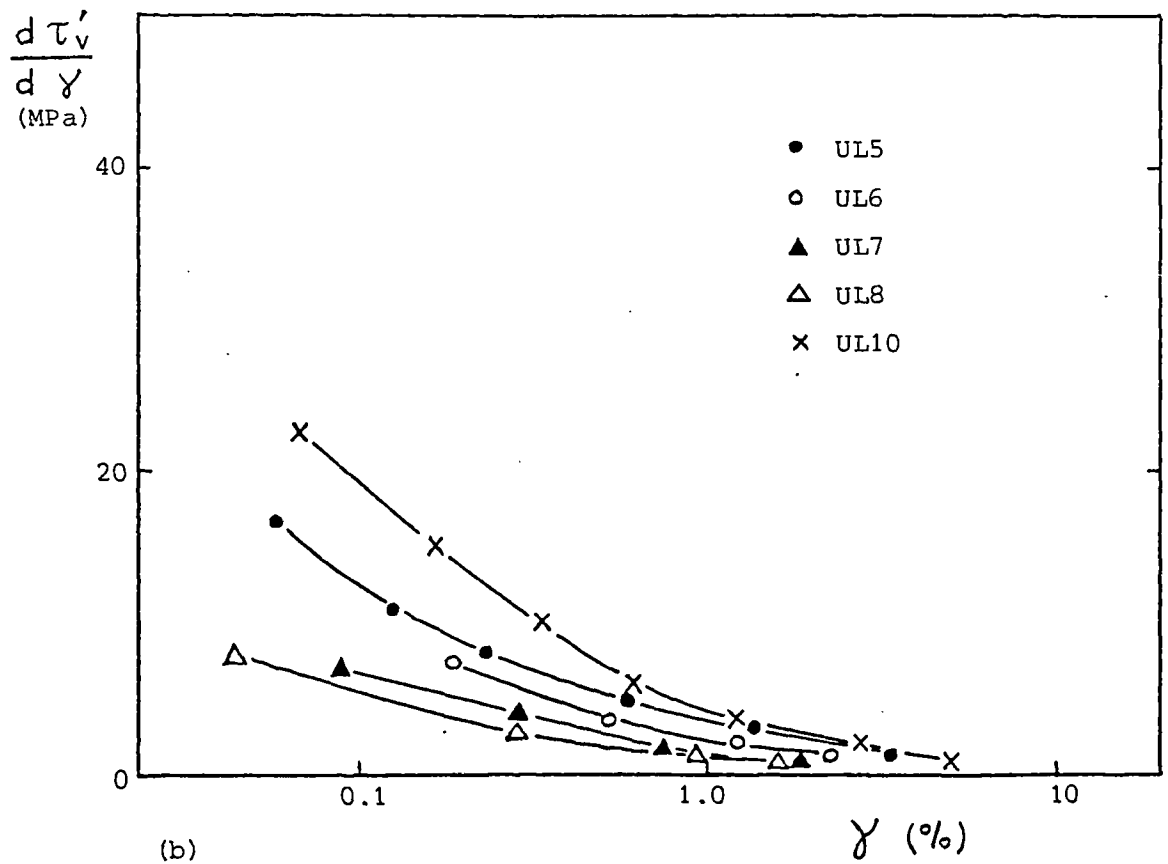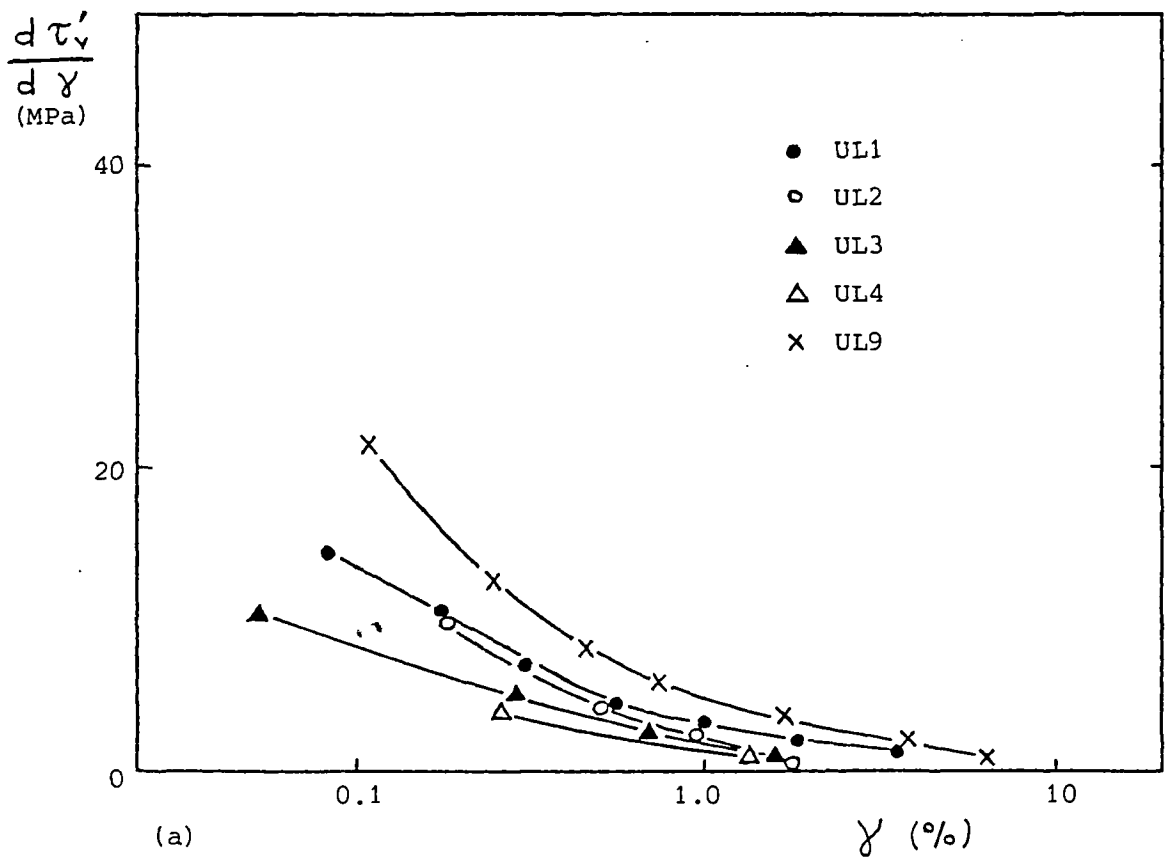
Figure 7.76   Variation of tangent shear stiffness with logarithm
of shear strain for undisturbed London clay (blue)
simple shear samples
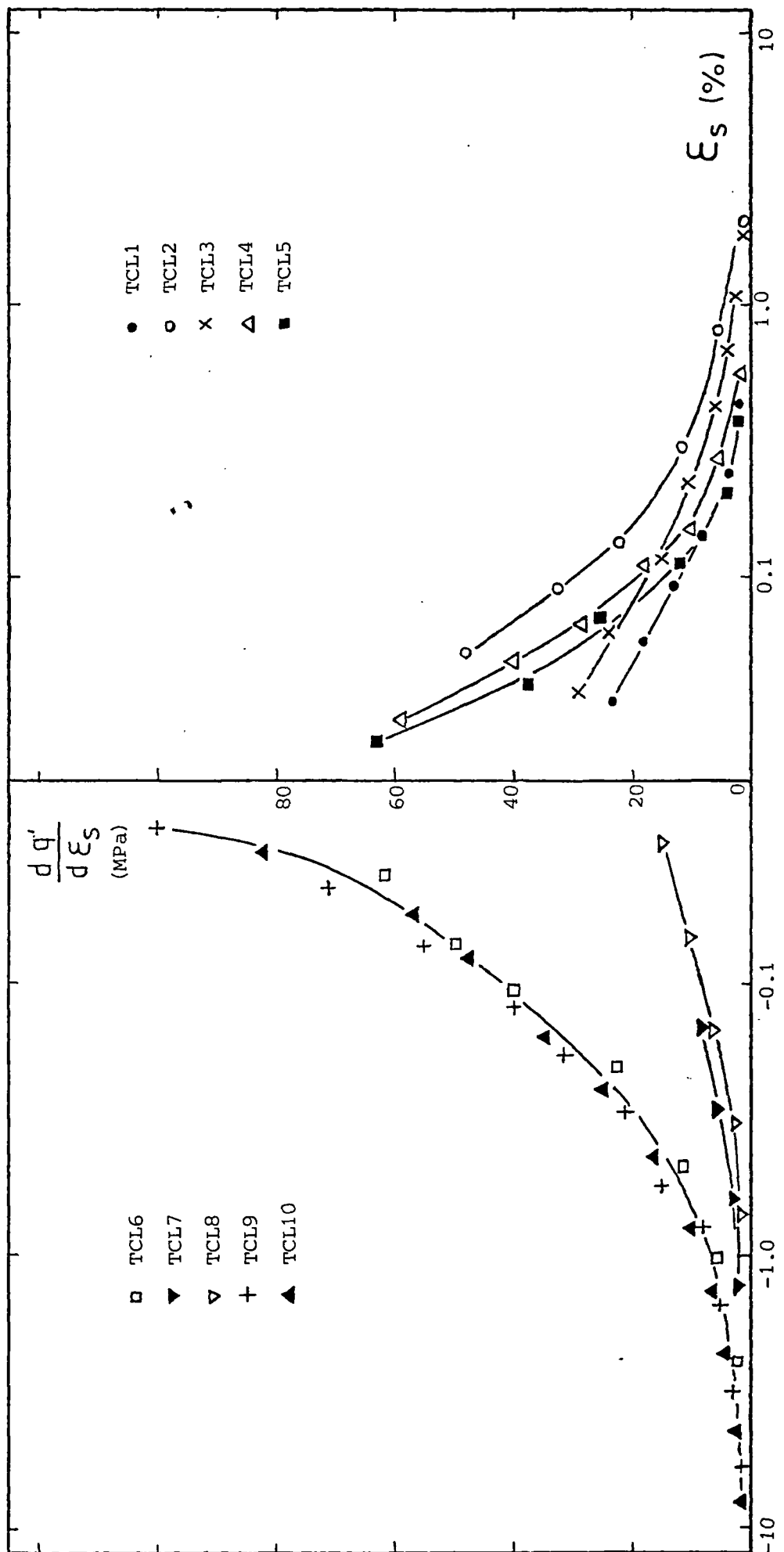
Figure 7.77   Variation of tangent shear stiffness with logarithm of shear strain for 38 mm reconstituted London clay (blue) triaxial samples
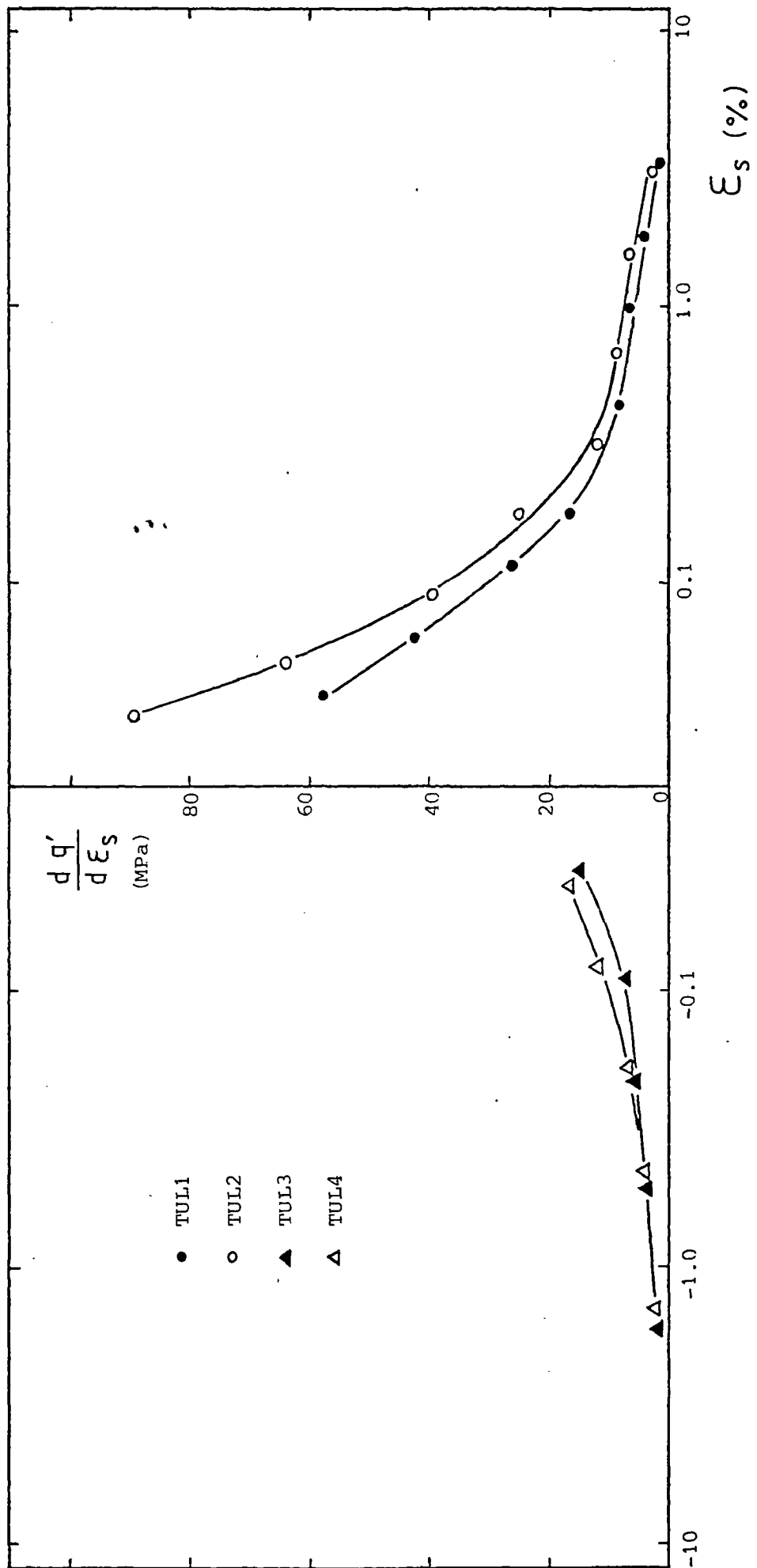
Figure 7.78   Variation of tangent shear stiffness with logarithm of
shear strain for 100 mm undisturbed London clay (blue)
triaxial samples
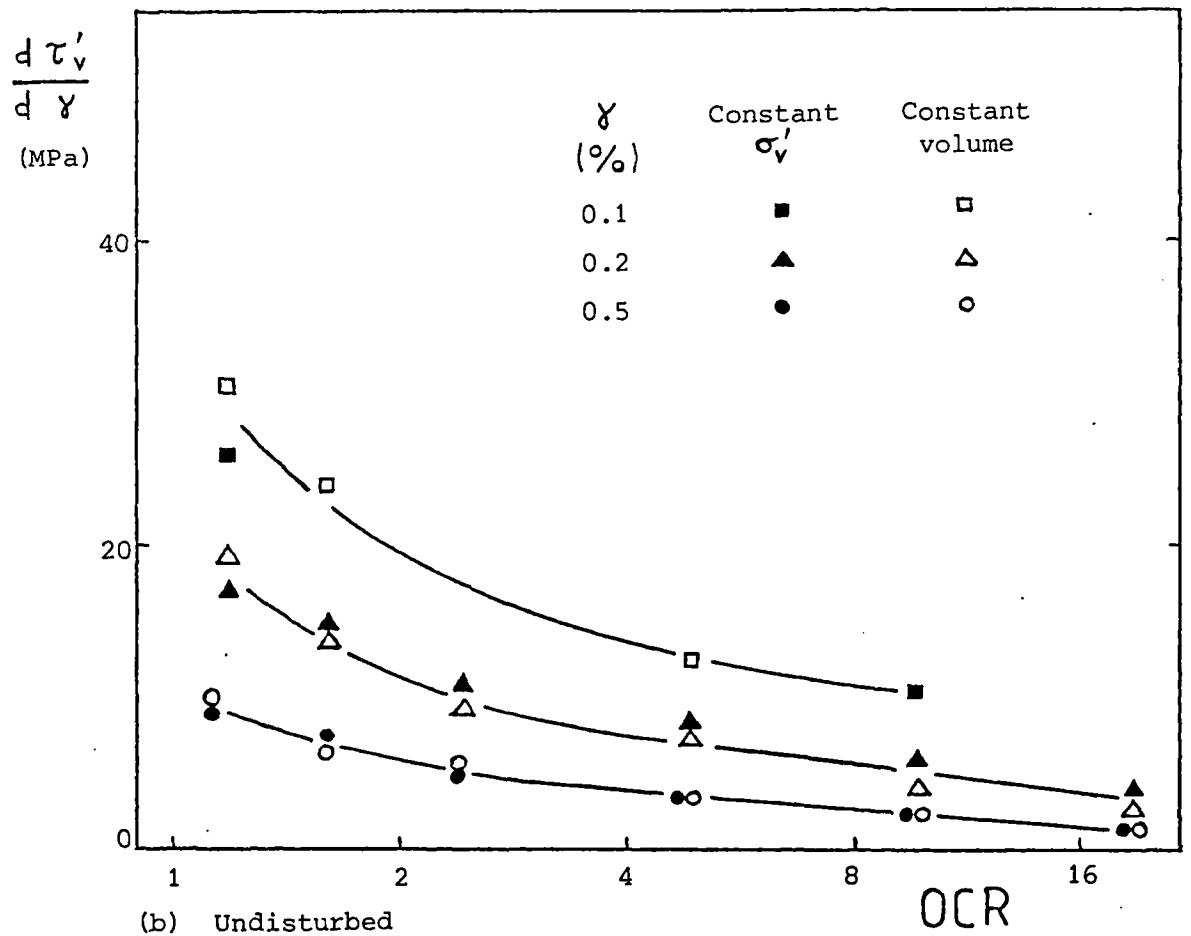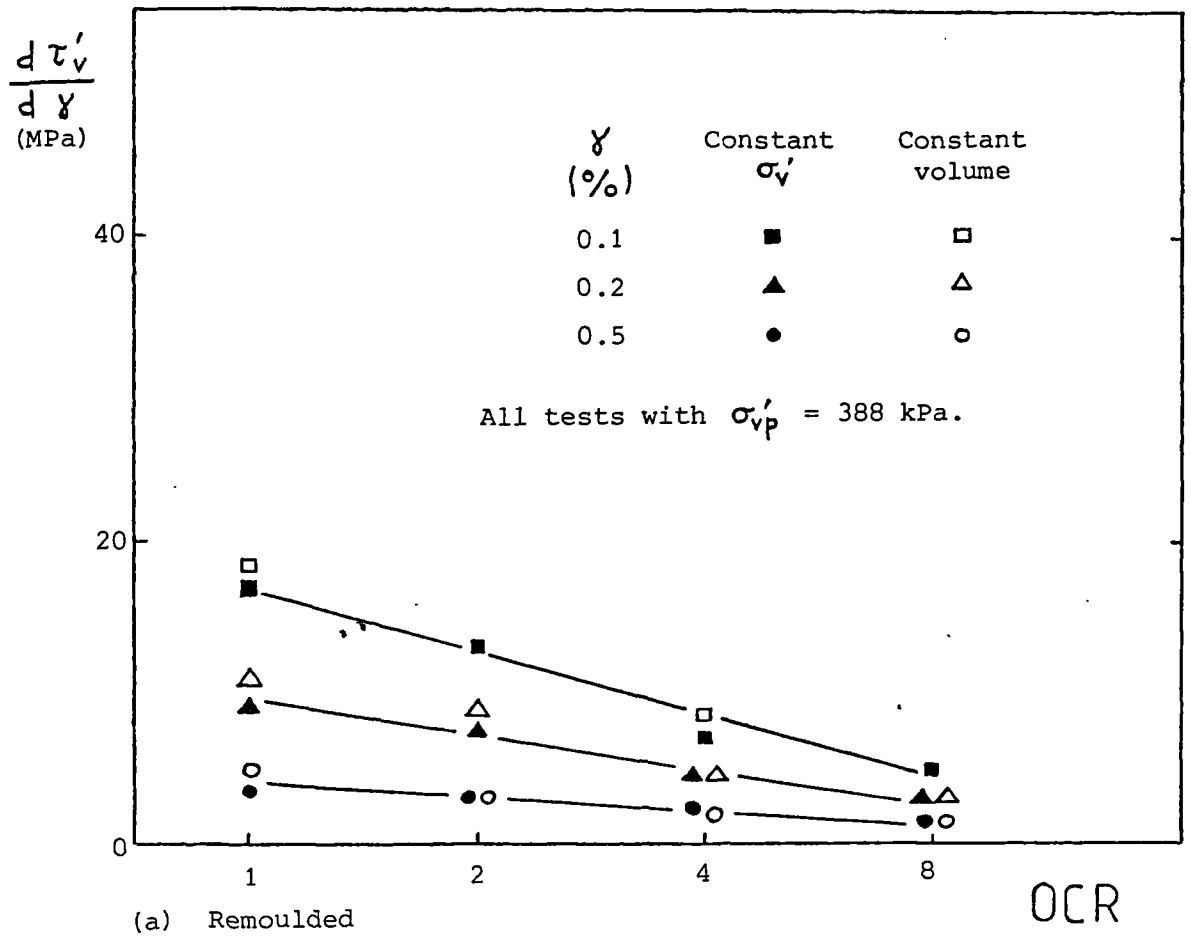
Figure 7.79   Comparison of tangent shear stiffnesses from constant σ_v' and constant volume simple shear tests on Cowden till
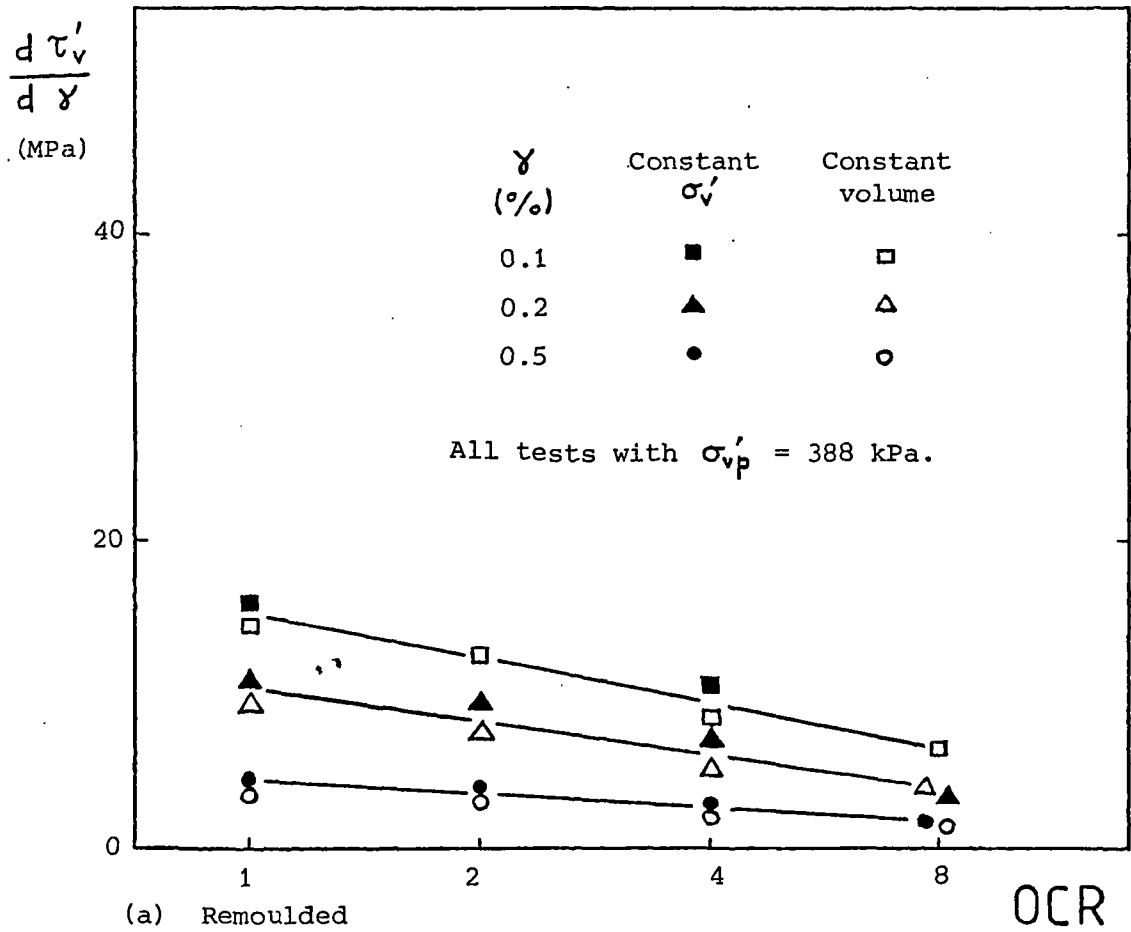
(a) Remoulded
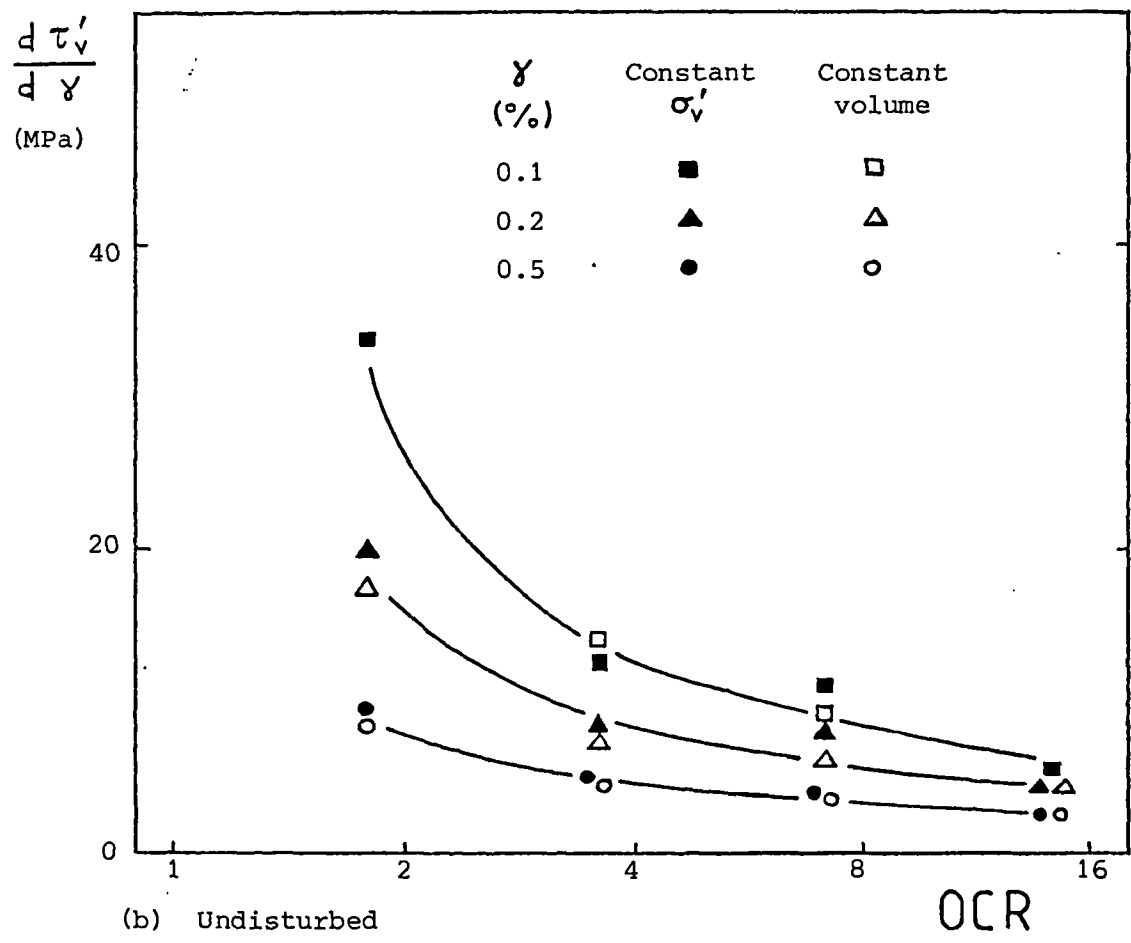
(b) Undisturbed

Figure   7.80   Comparison of tangent shear stifnesses from constant σ_v'
                   and constant volume simple shear tests on London clay
                   (brown)

(a)   Remoulded

(b)   Undisturbed
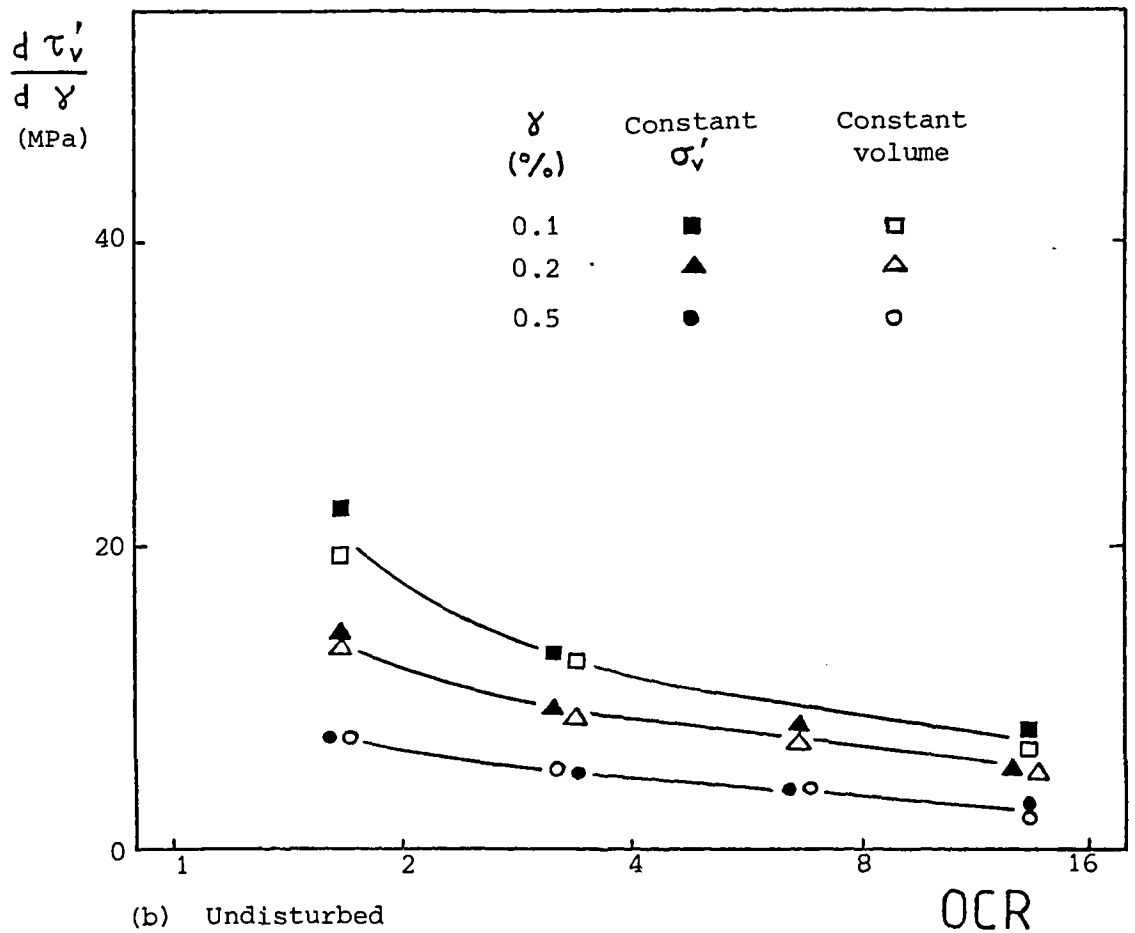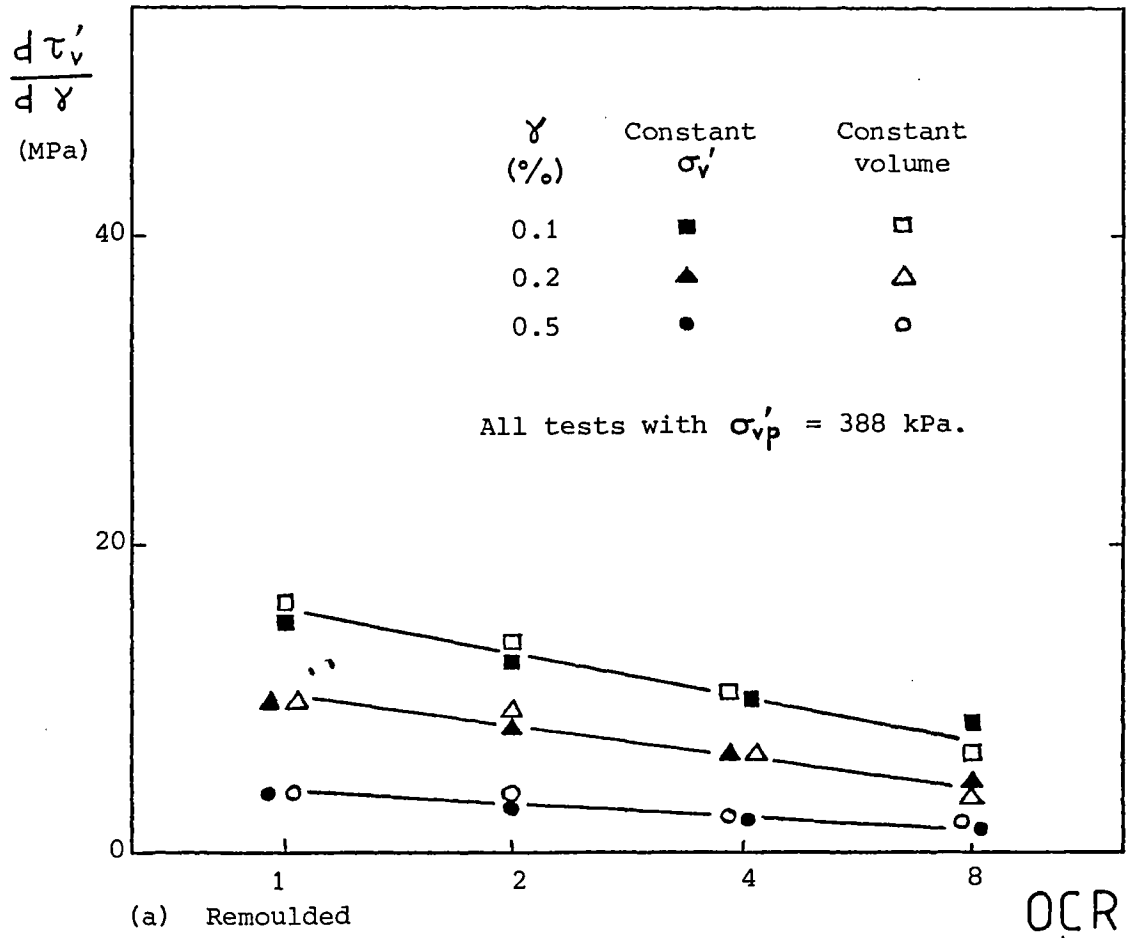
Figure   7.81   Comparison of tangent shear stiffnesses from constant σ_v'
and constant volume simple shear tests on London clay
(blue)
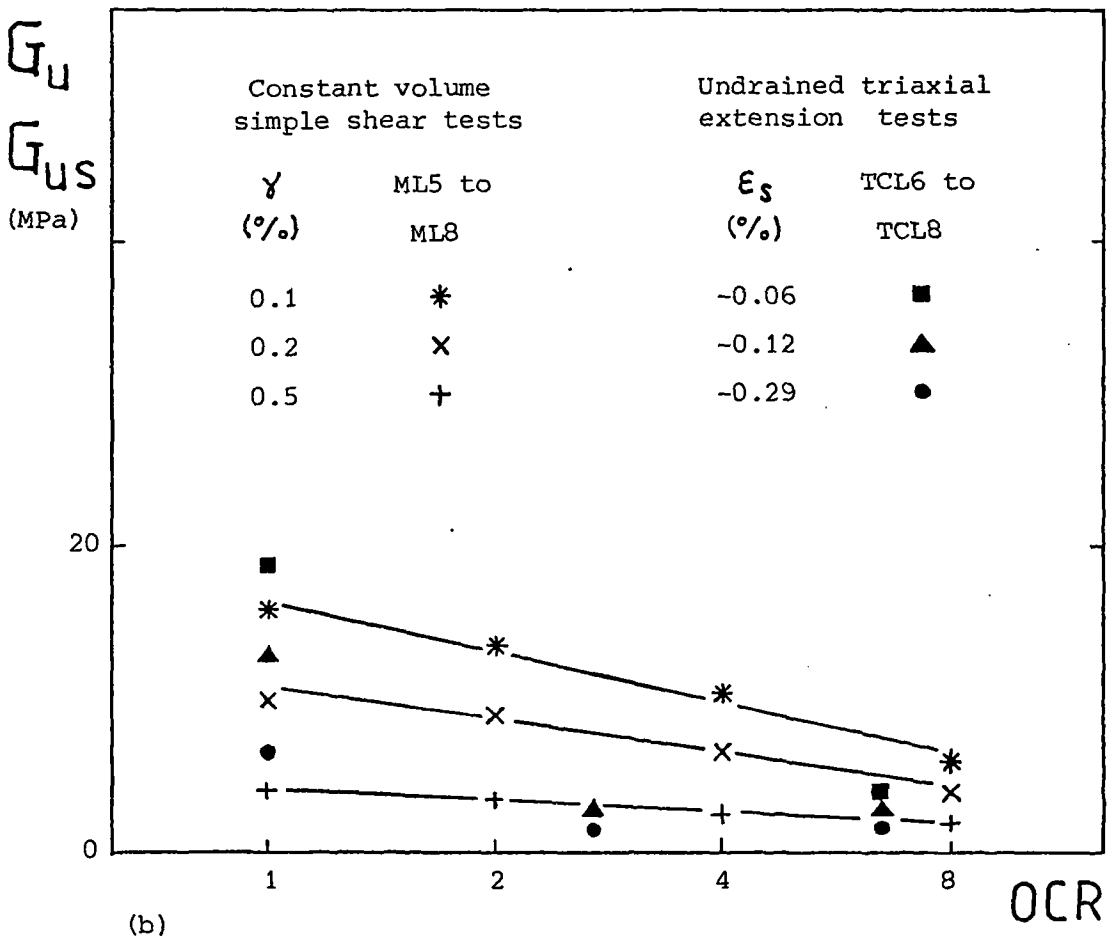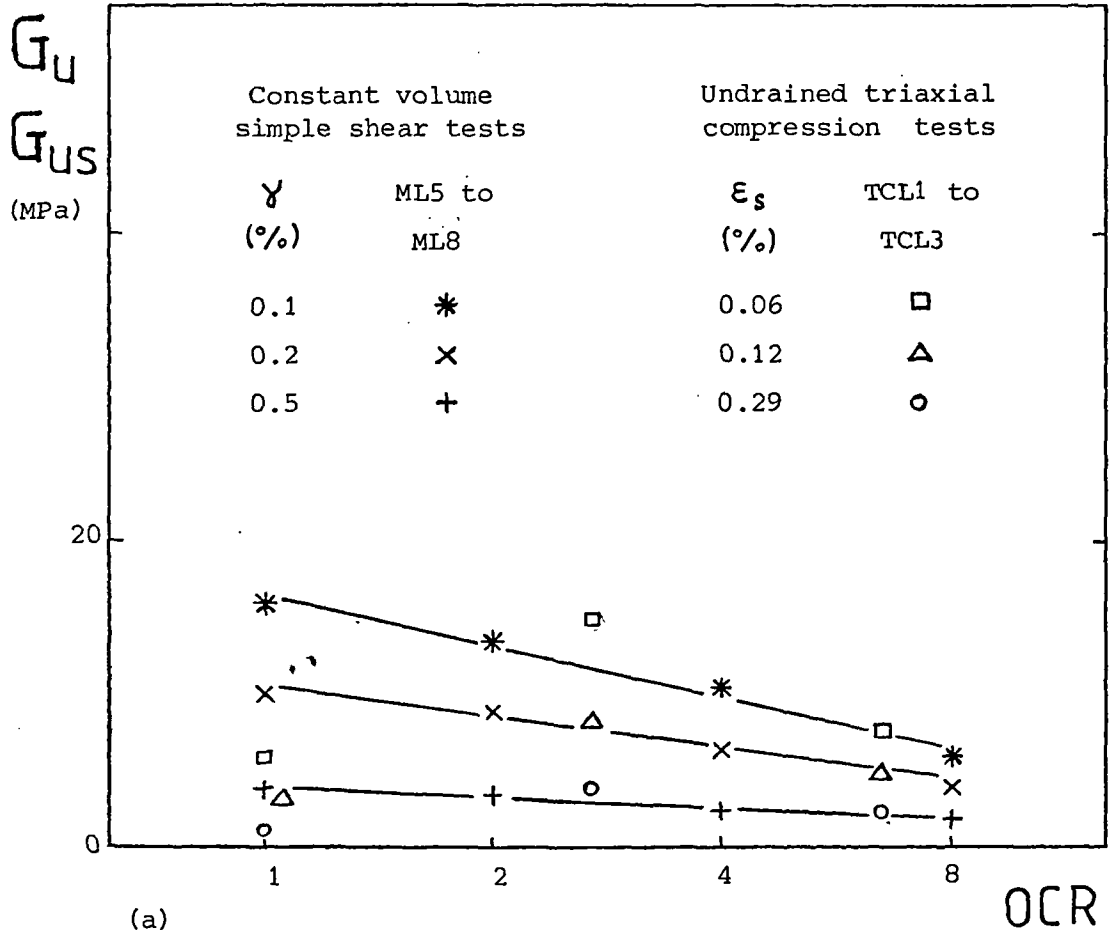
Figure 7.82   Comparison of tangent shear moduli from constant volume
simple shear and undrained triaxial tests on London clay
(blue)
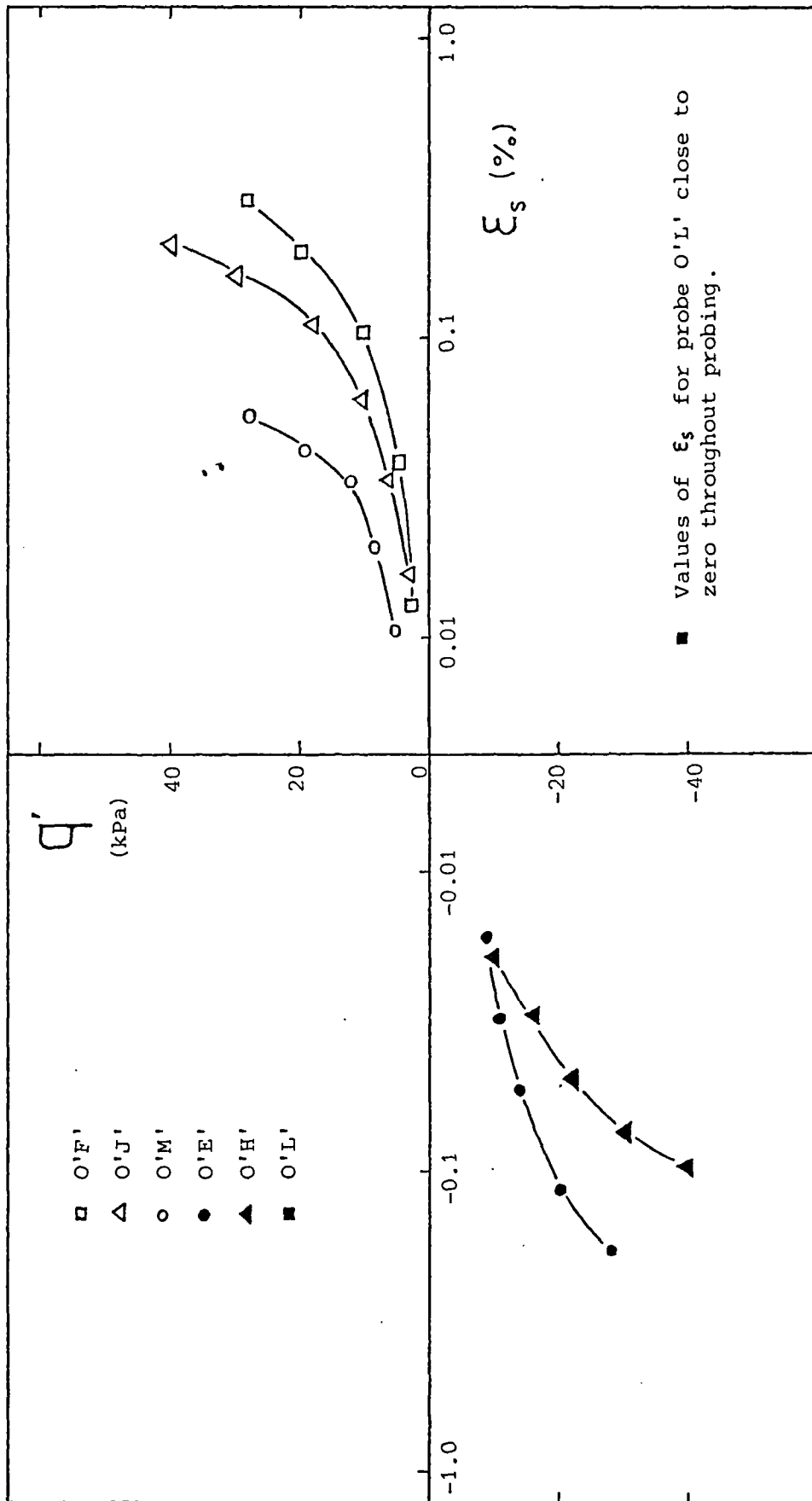
Figure 7.83   Variation of shear stress with logarithm of shear
strain for probing test on 100 mm undisturbed
London clay (brown) triaxial sample TUB1
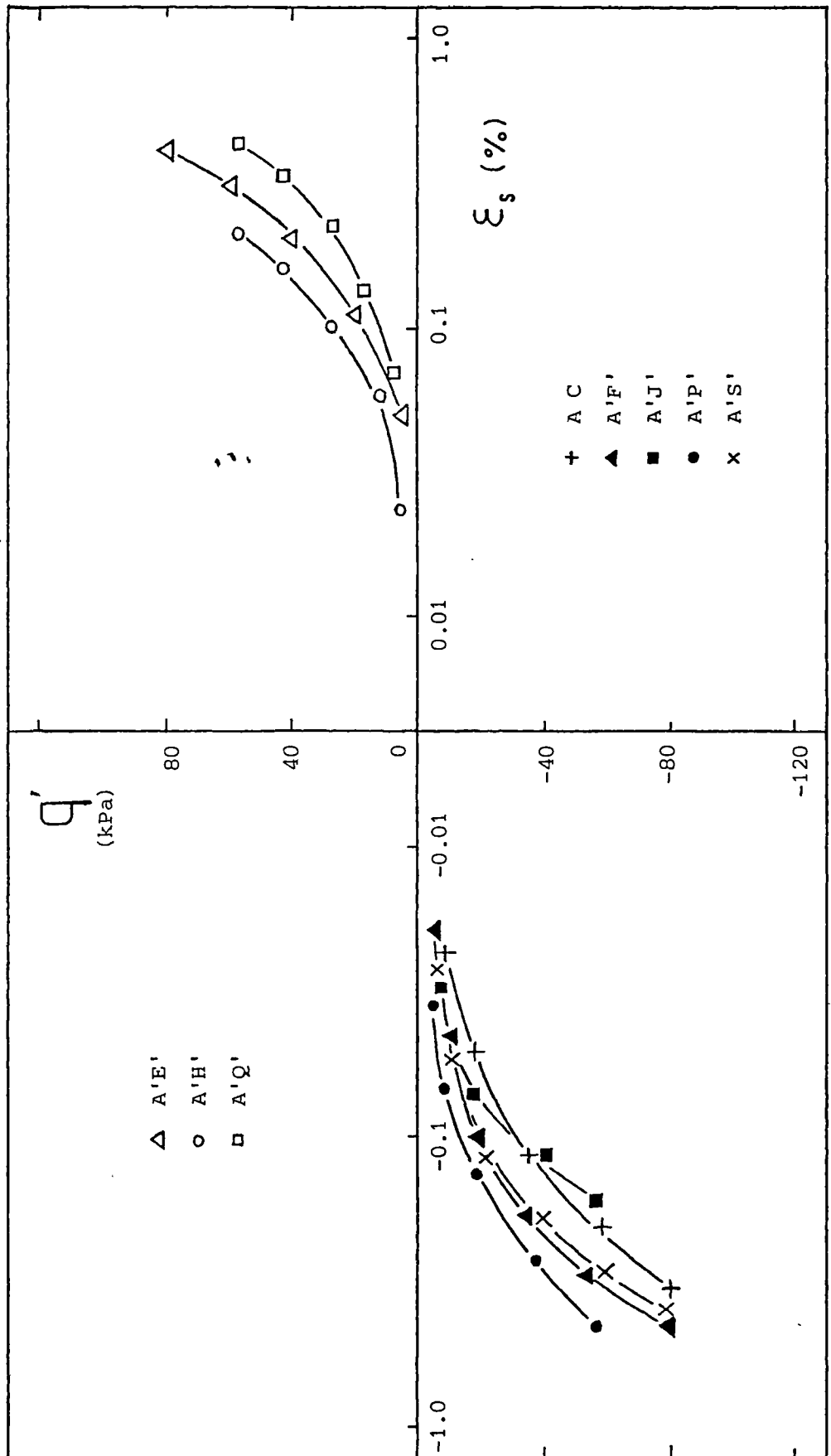
Figure 7.84   Variation of shear stress with logarithm of shear
                 strain for probing test on 100 mm undisturbed London
                 clay (blue) triaxial sample TUL5
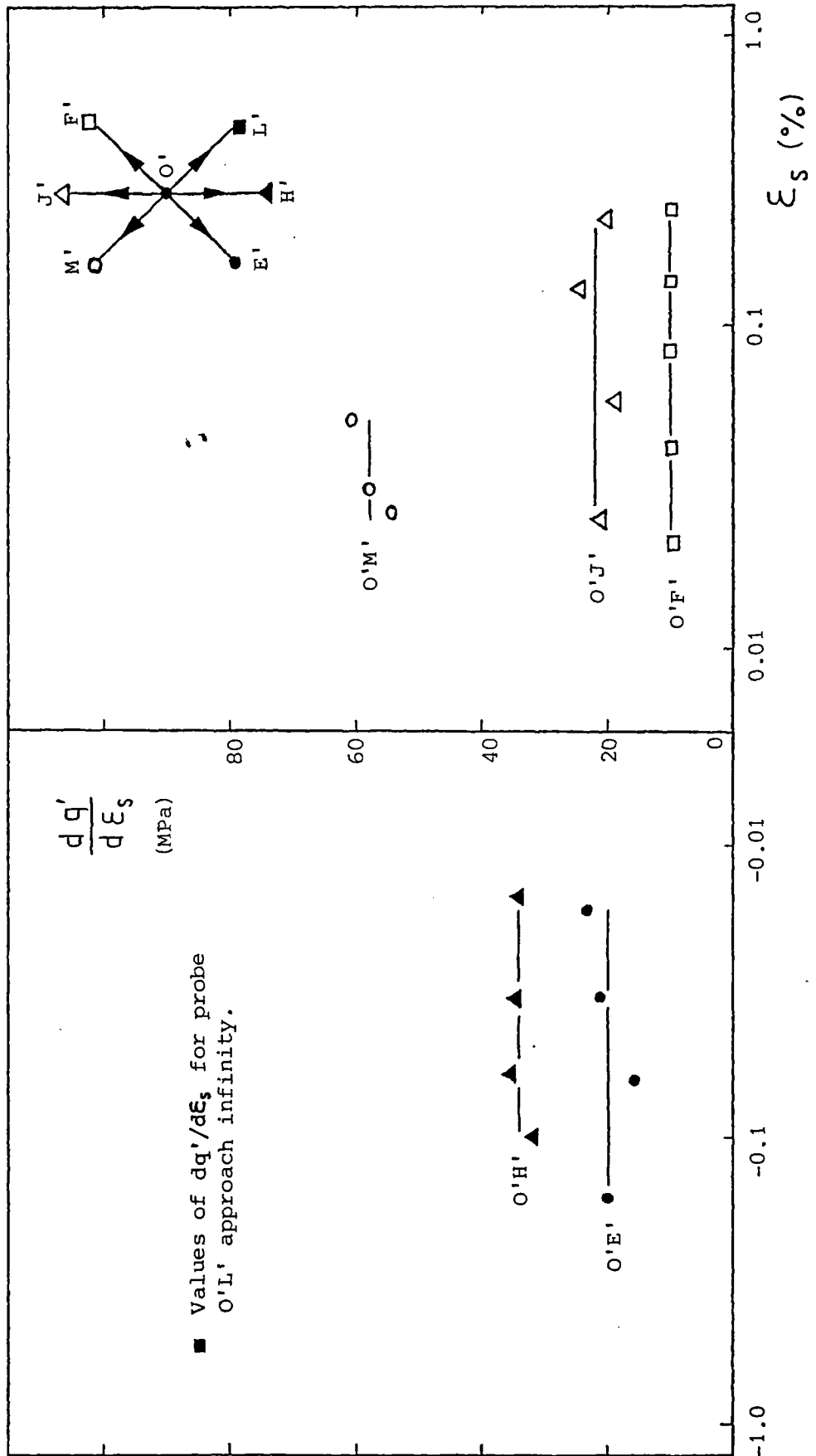
(a)

Figure 7.85   Tangent stiffnesses from probing test on 100 mm undisturbed London clay (brown) triaxial sample TUB1
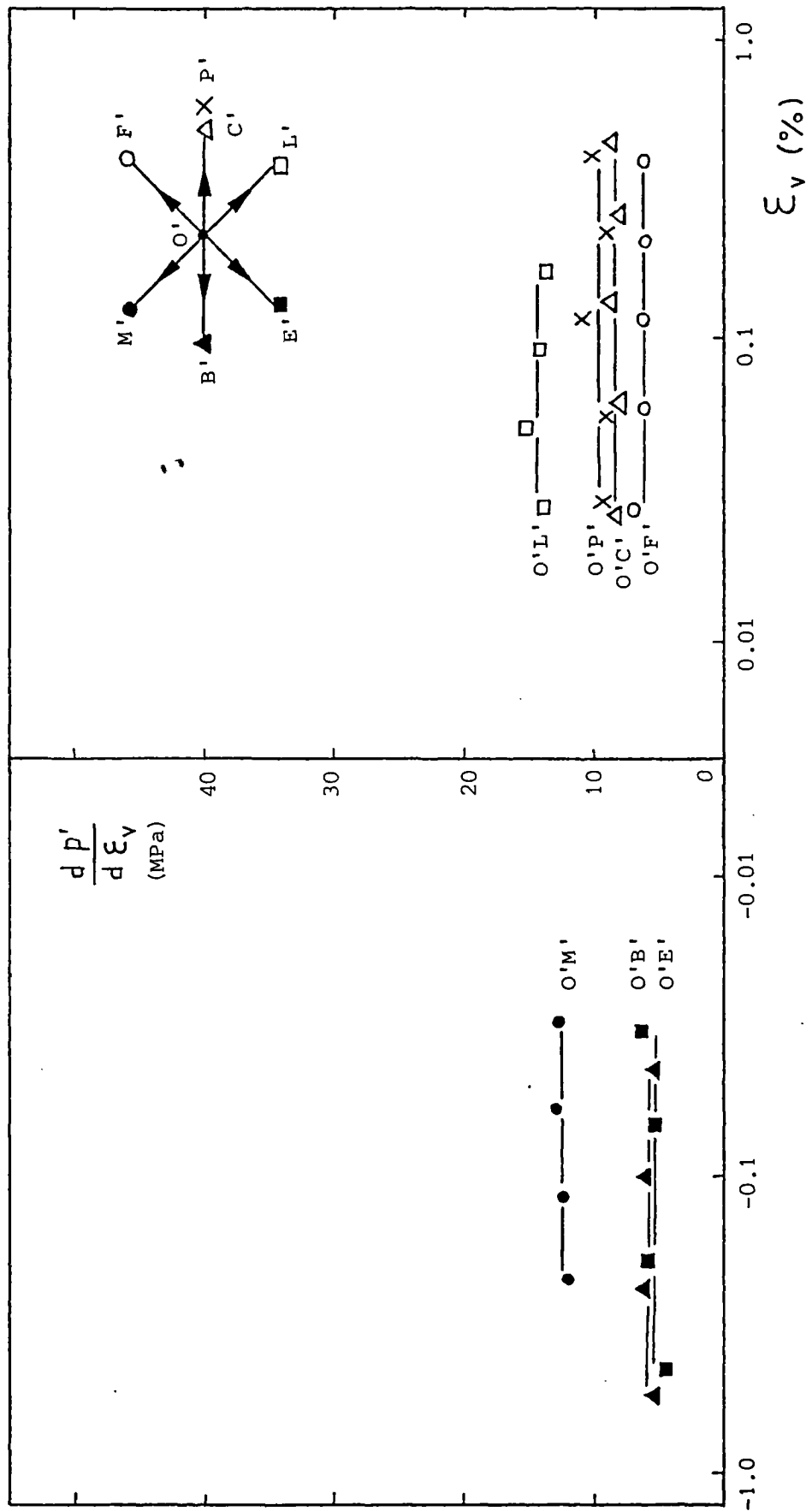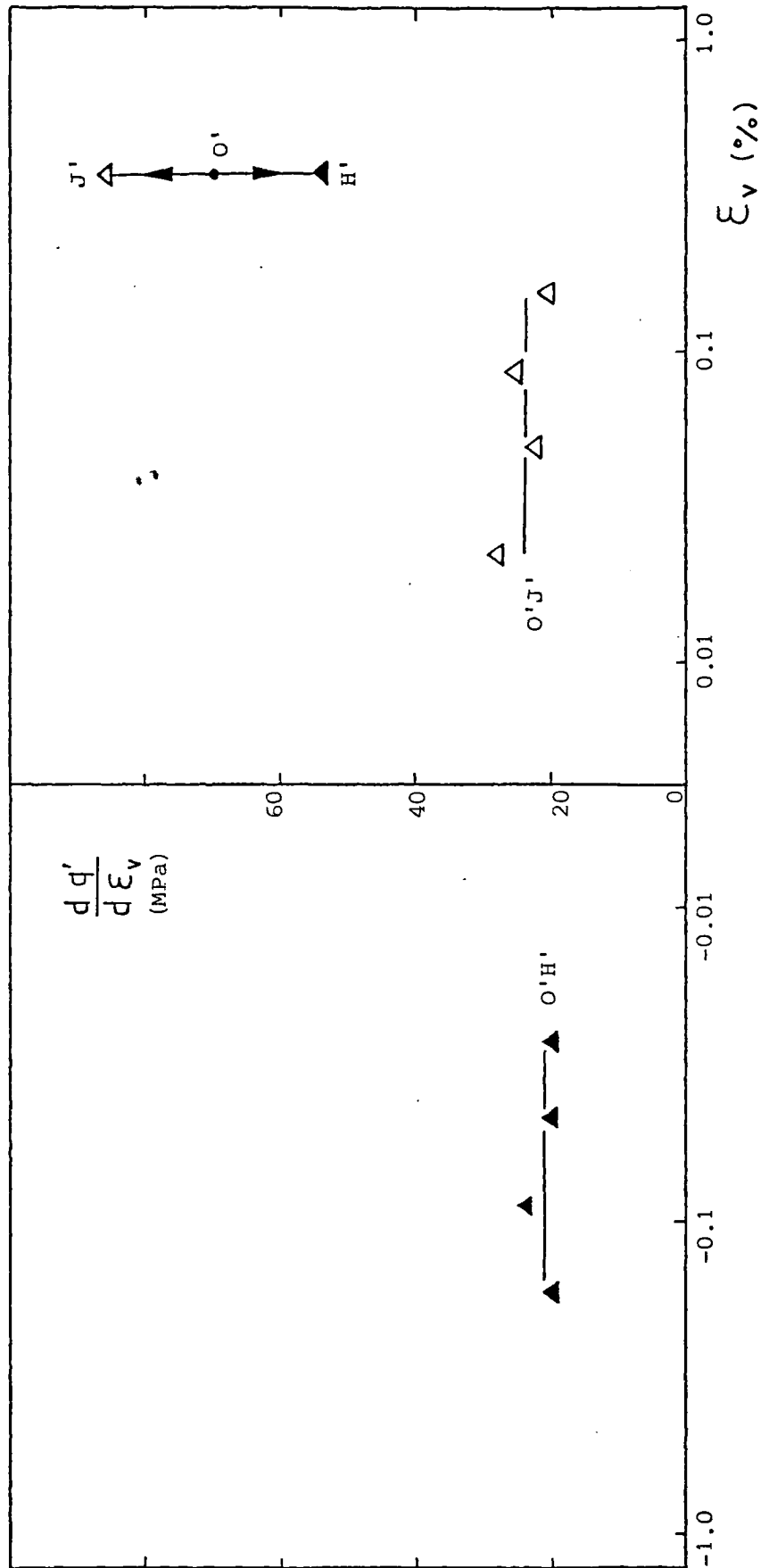
Figure 7.85 continued
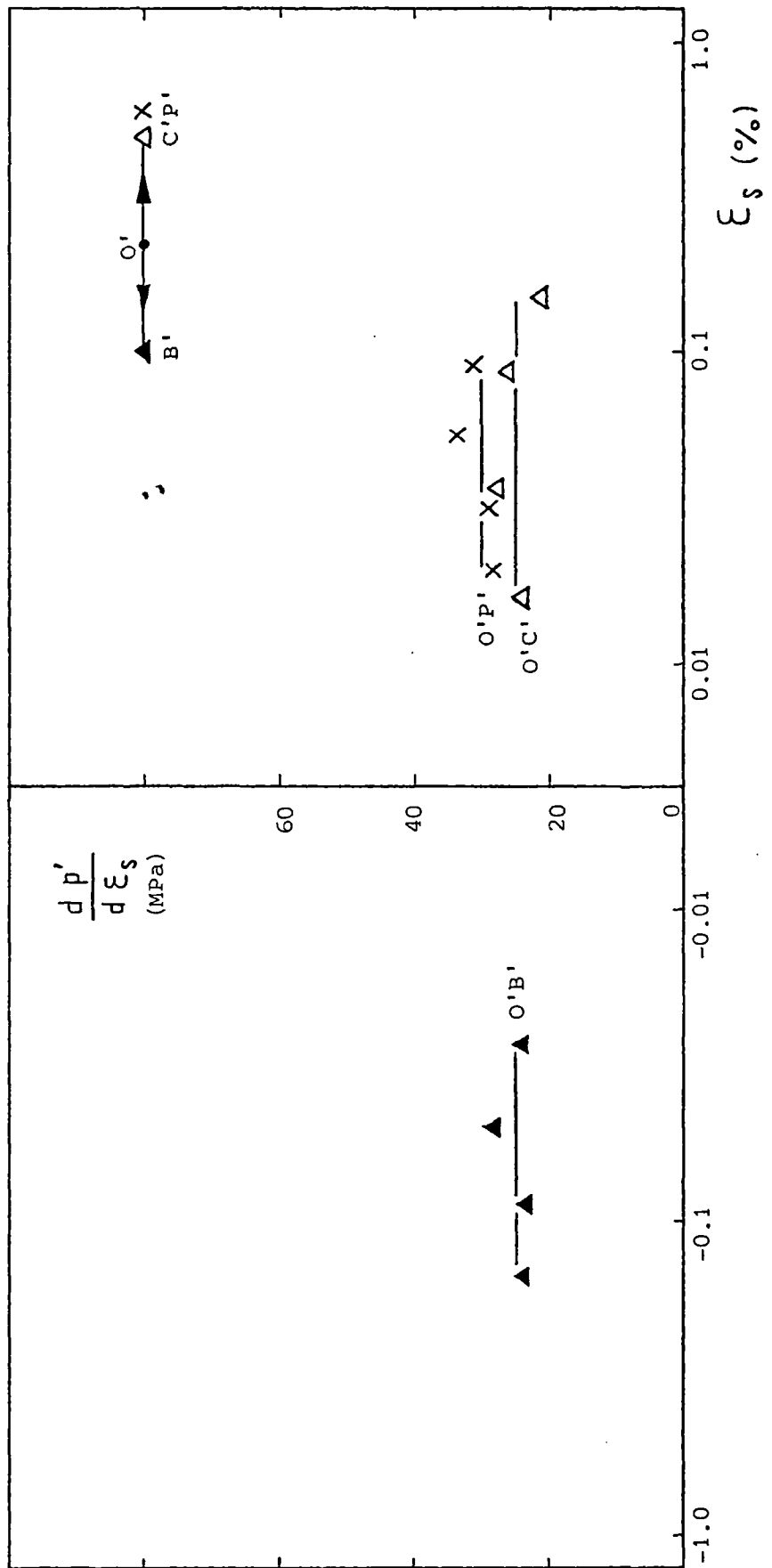
Figure 7.85 continued

Figure 7.85 continued
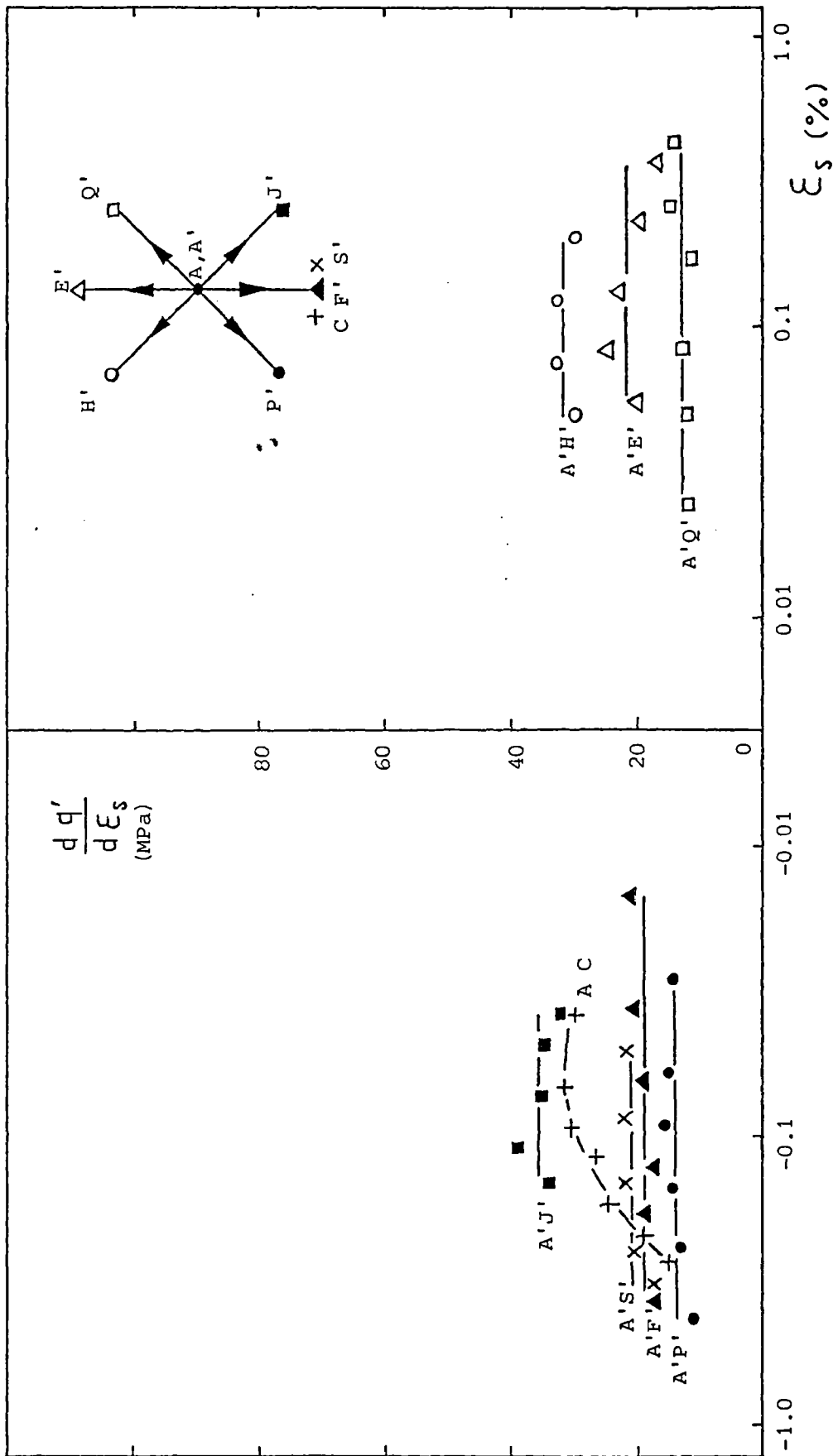
Figure   7.86   Tangent stiffnesses from probing test on 100 mm
undisturbed London clay (blue) triaxial sample
TUL5
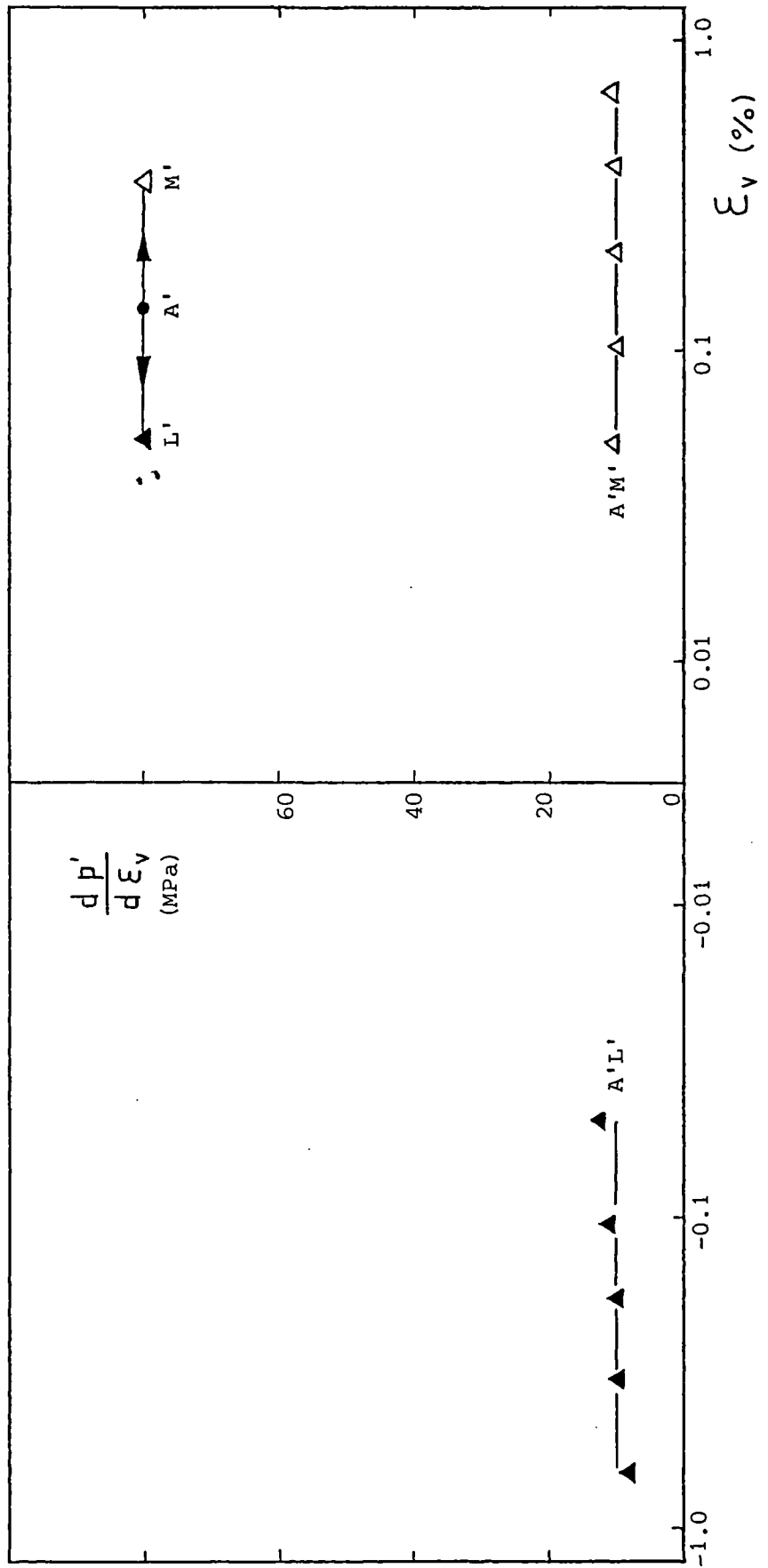
(b)

Figure 7.86 continued
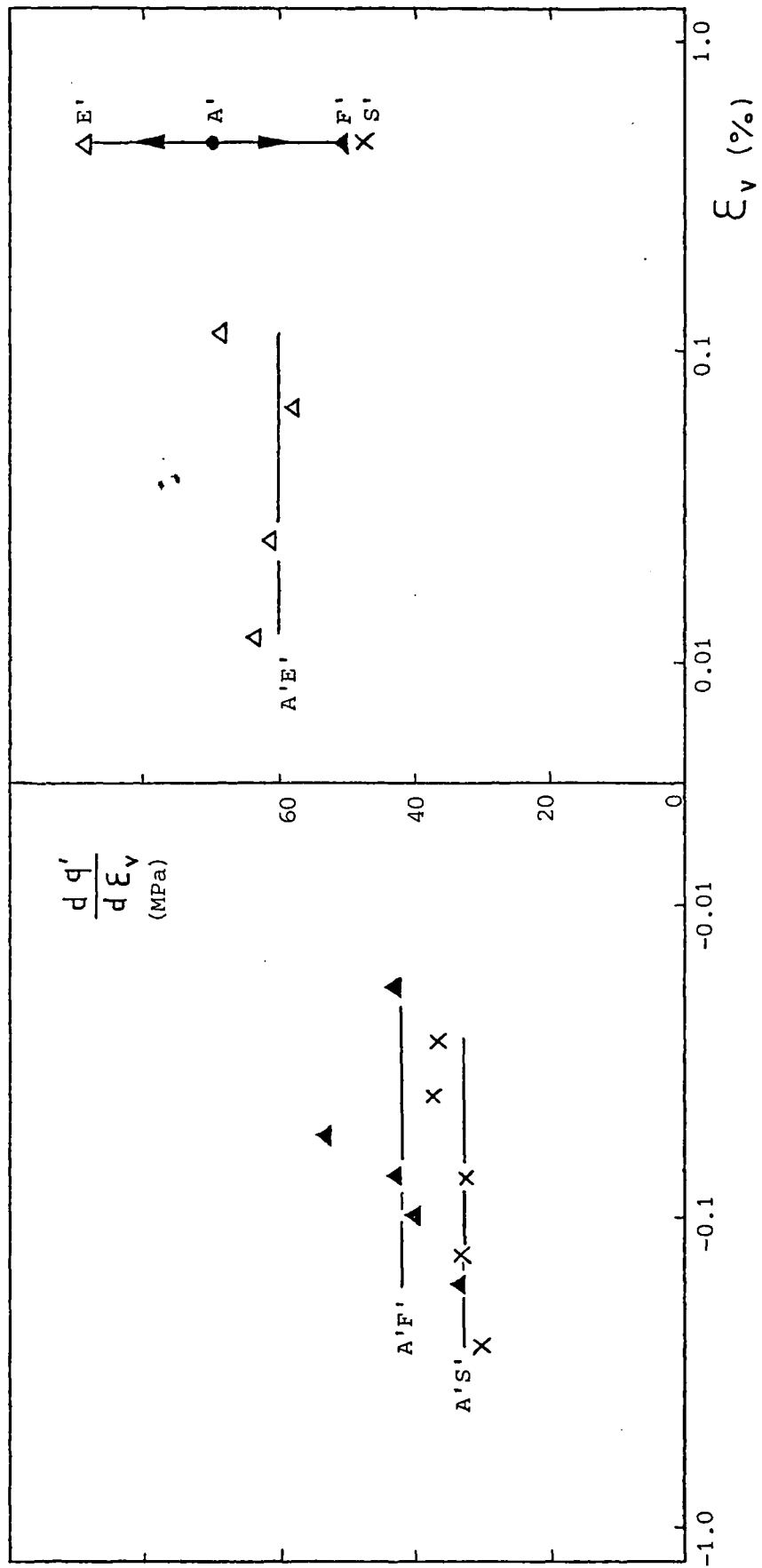
Figure 7.86 continued

(d)
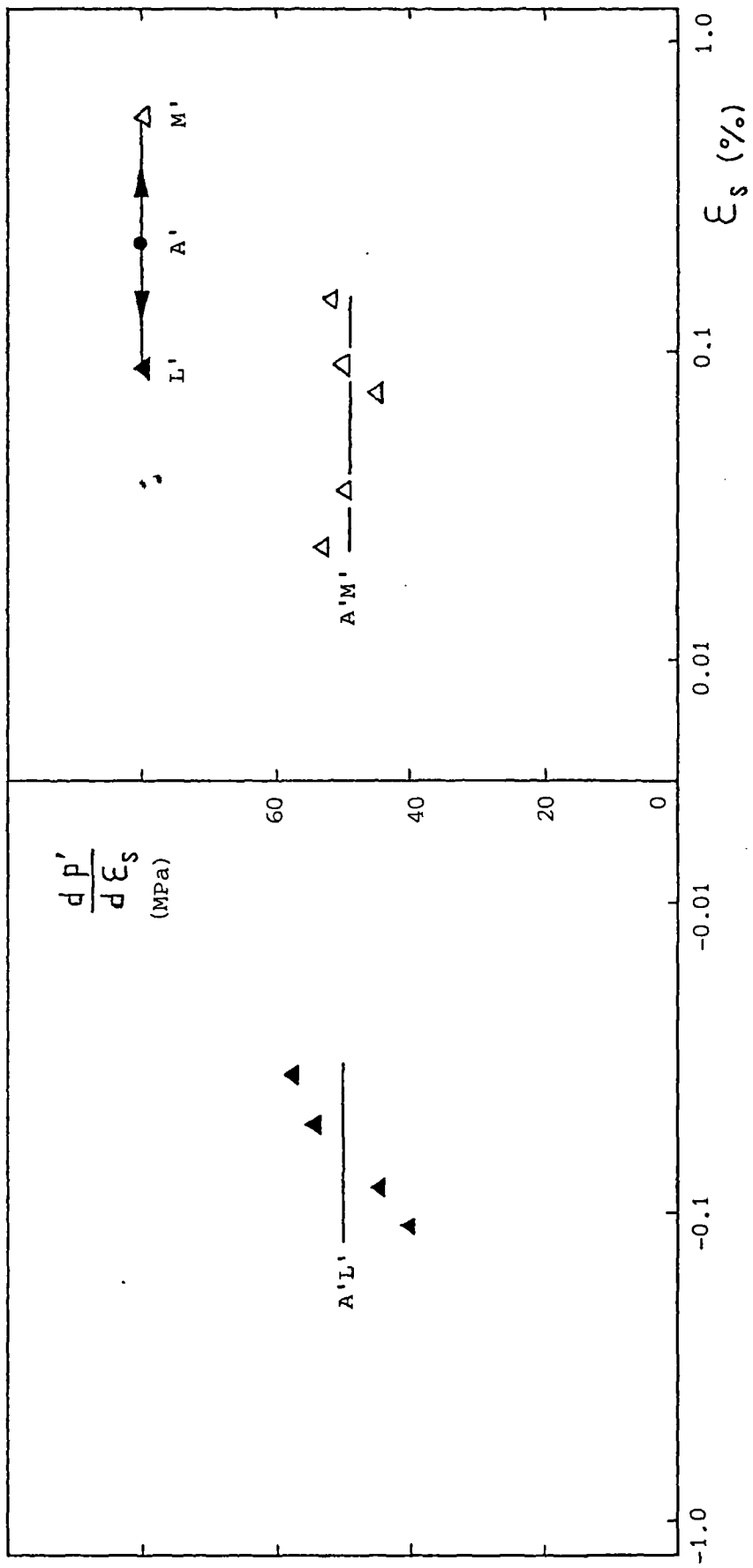
Figure 7.86 continued
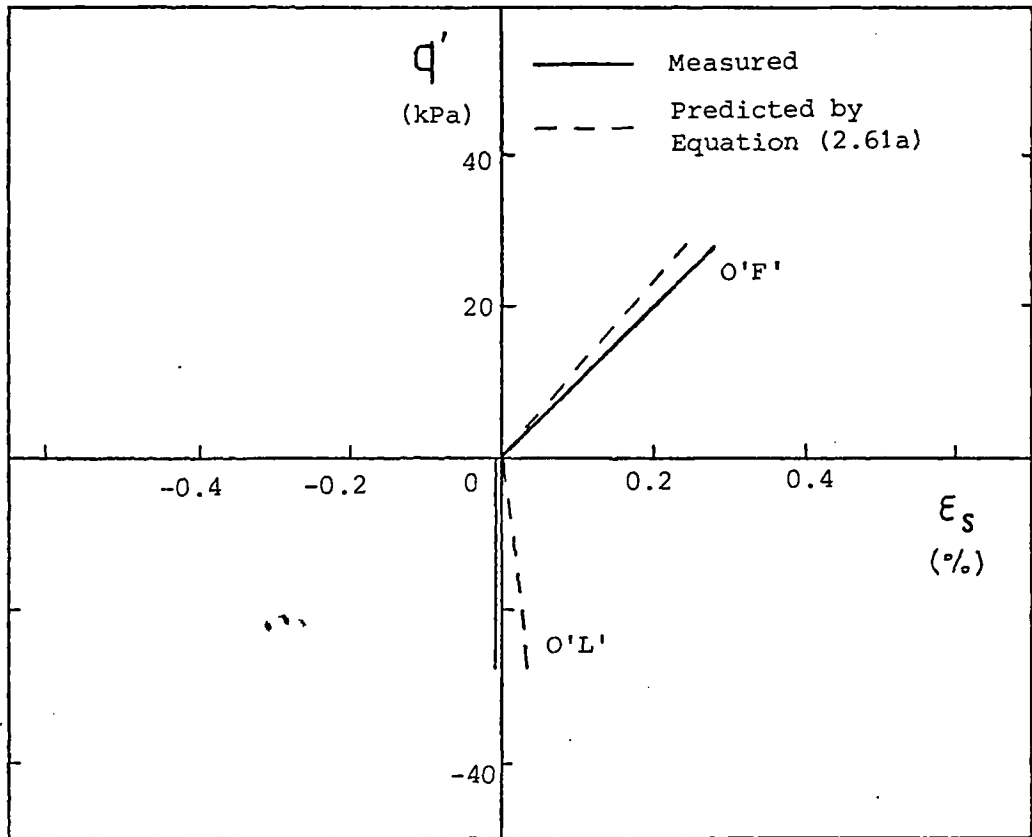
(a)
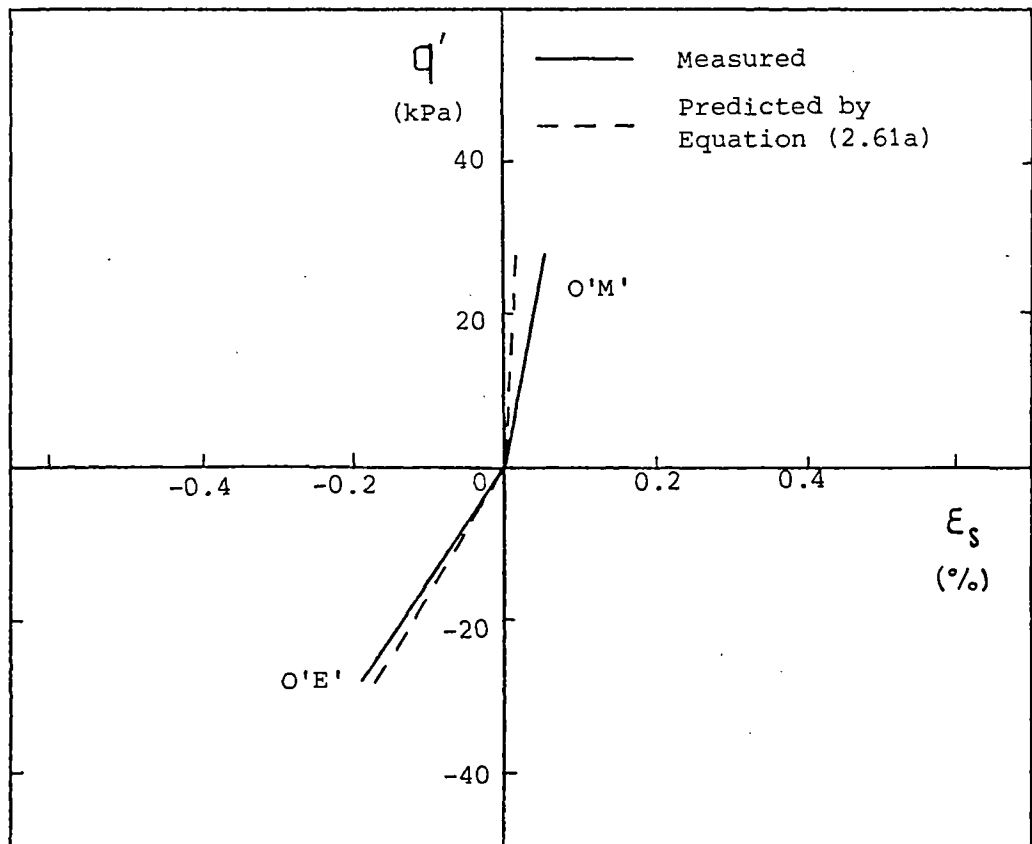
(b).

Figure 7.87   Comparison of measured and predicted shear strains for
probing test TUB1
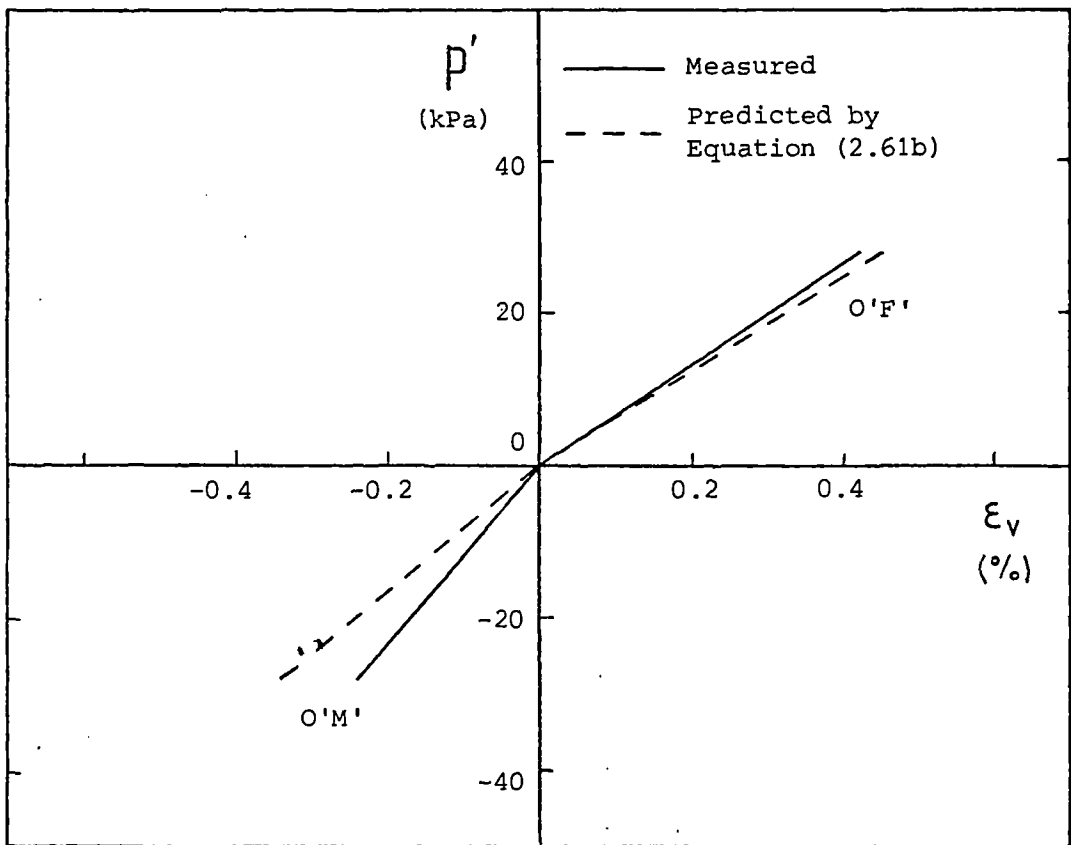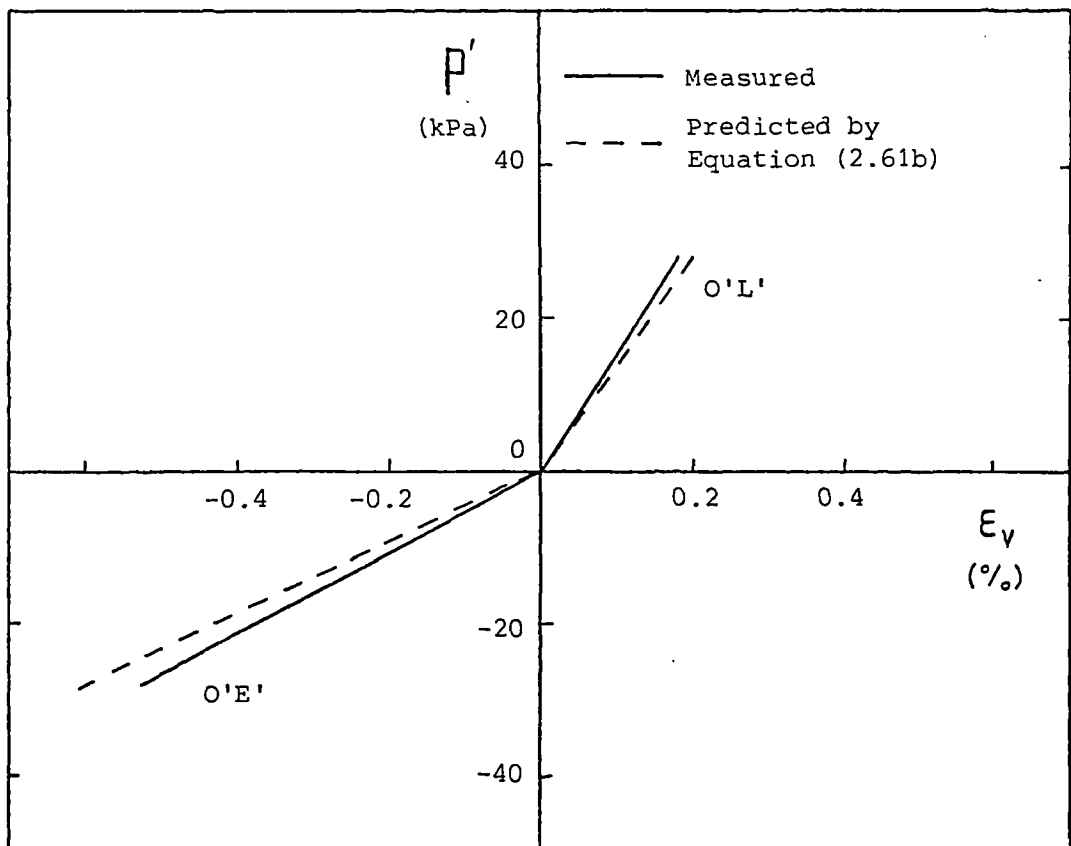
Figure 7.88   Comparison of measured and predicted volumetric strains
for probing test TUB1
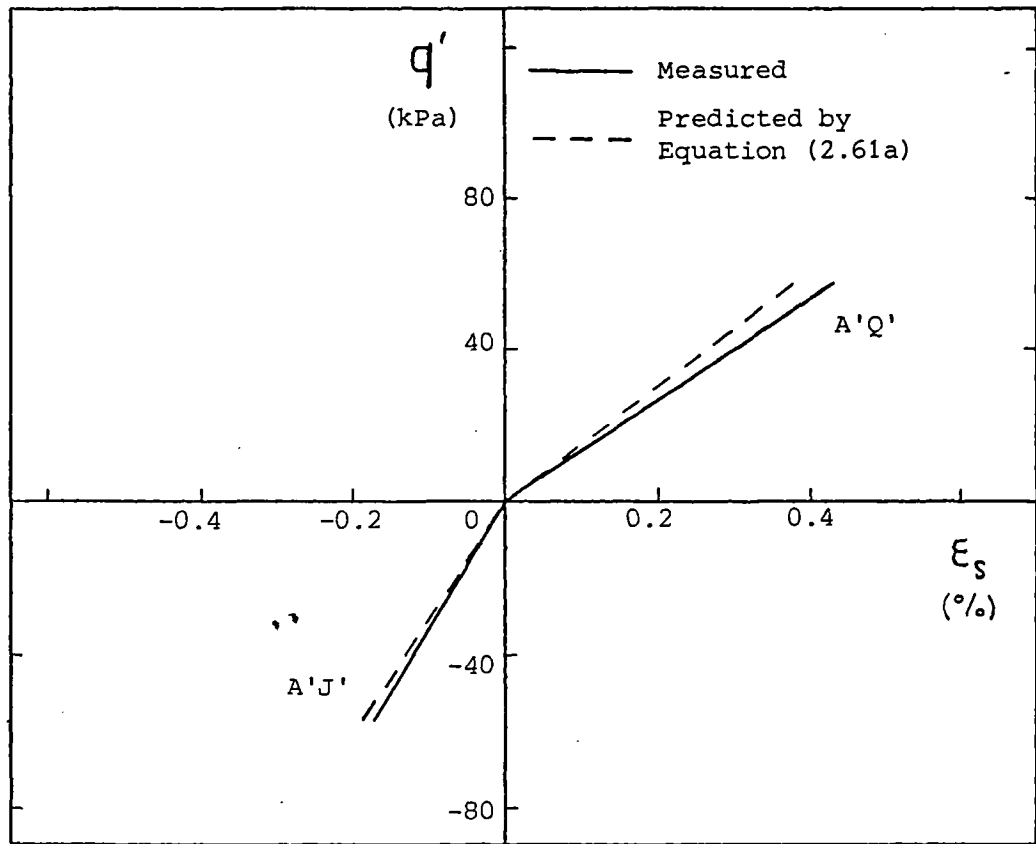
(a)
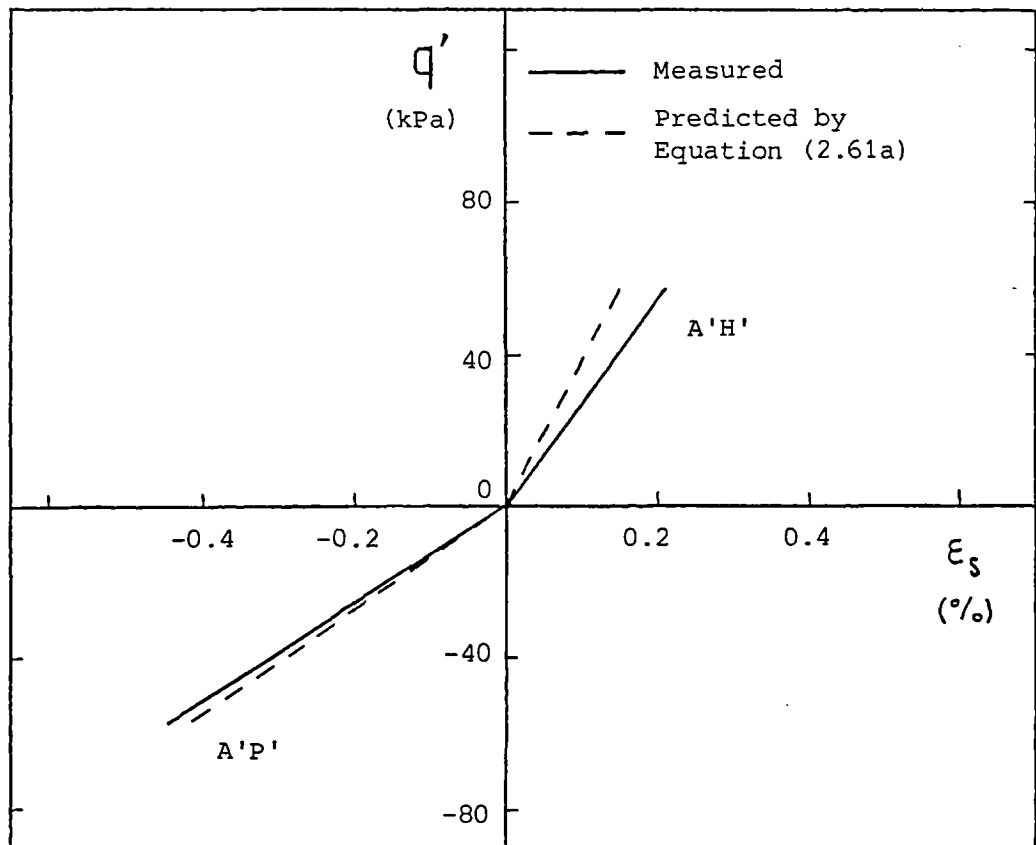
(b)

Figure 7.89   Comparison of measured and predicted shear strains for probing test TUL5
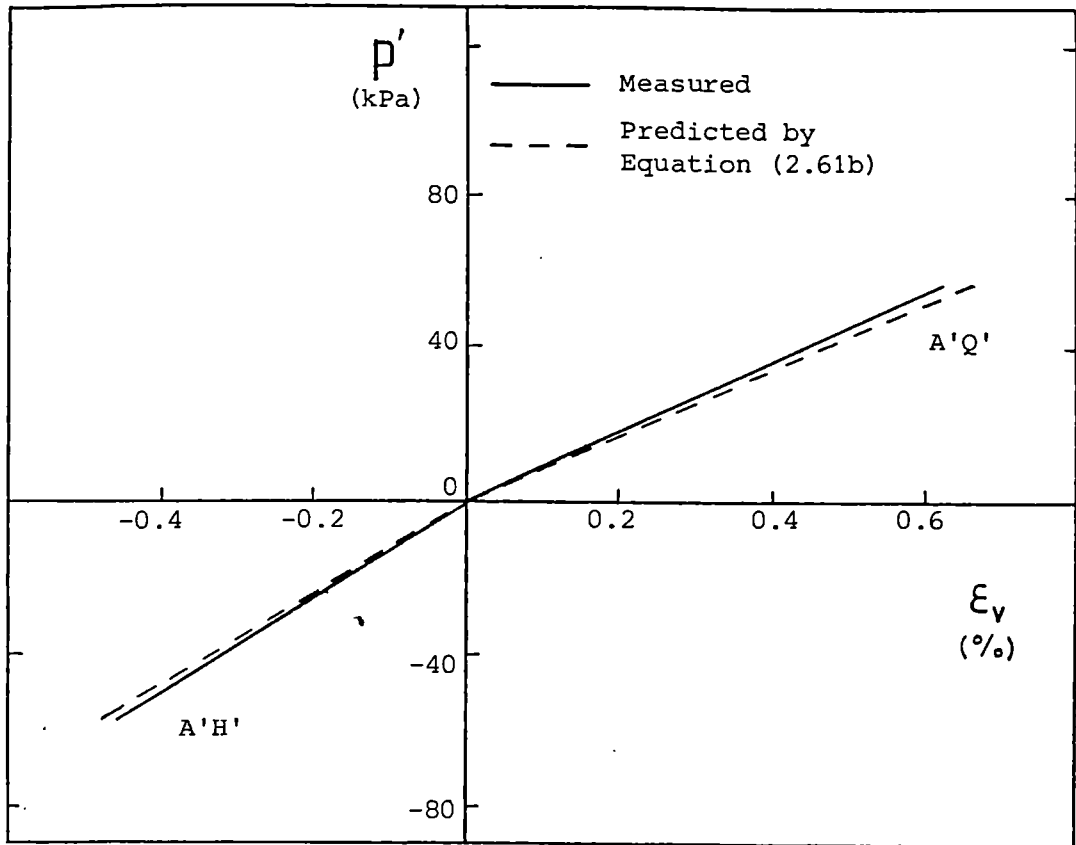
(a)
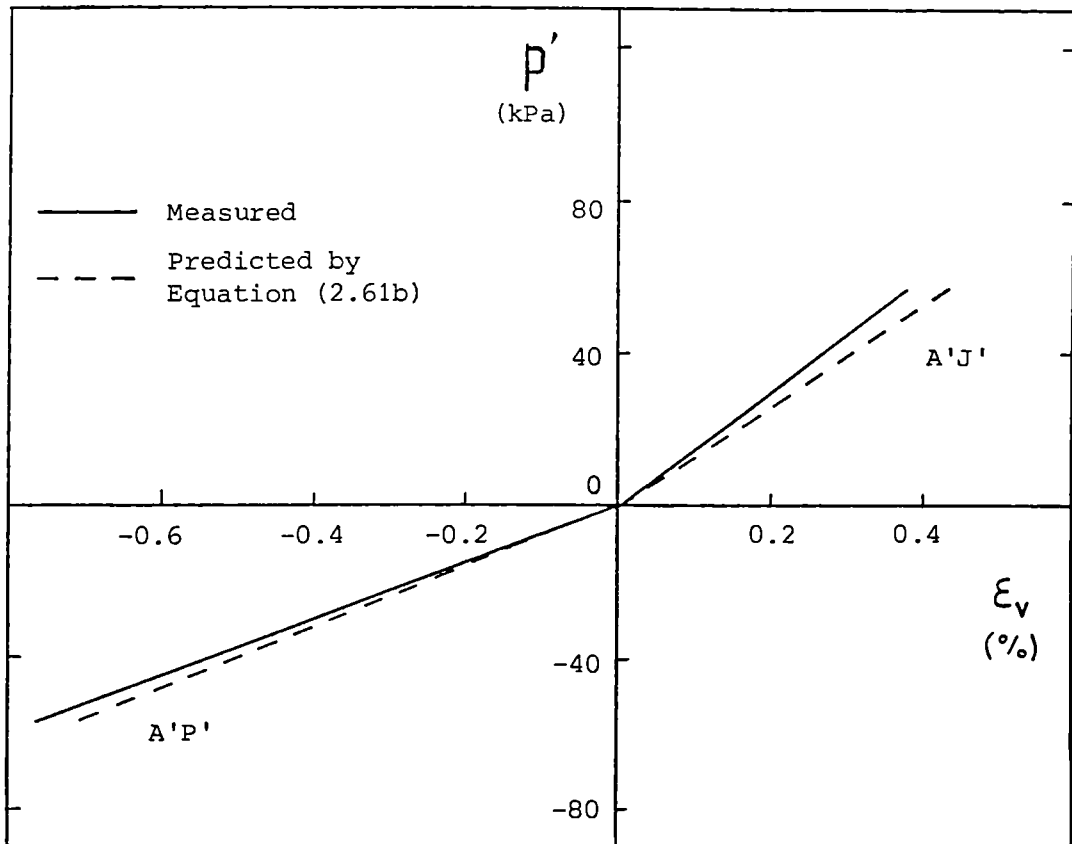
(b)

Figure   7.90   Comparison of measured and predicted volumetric strains
                   for probing test TUL5
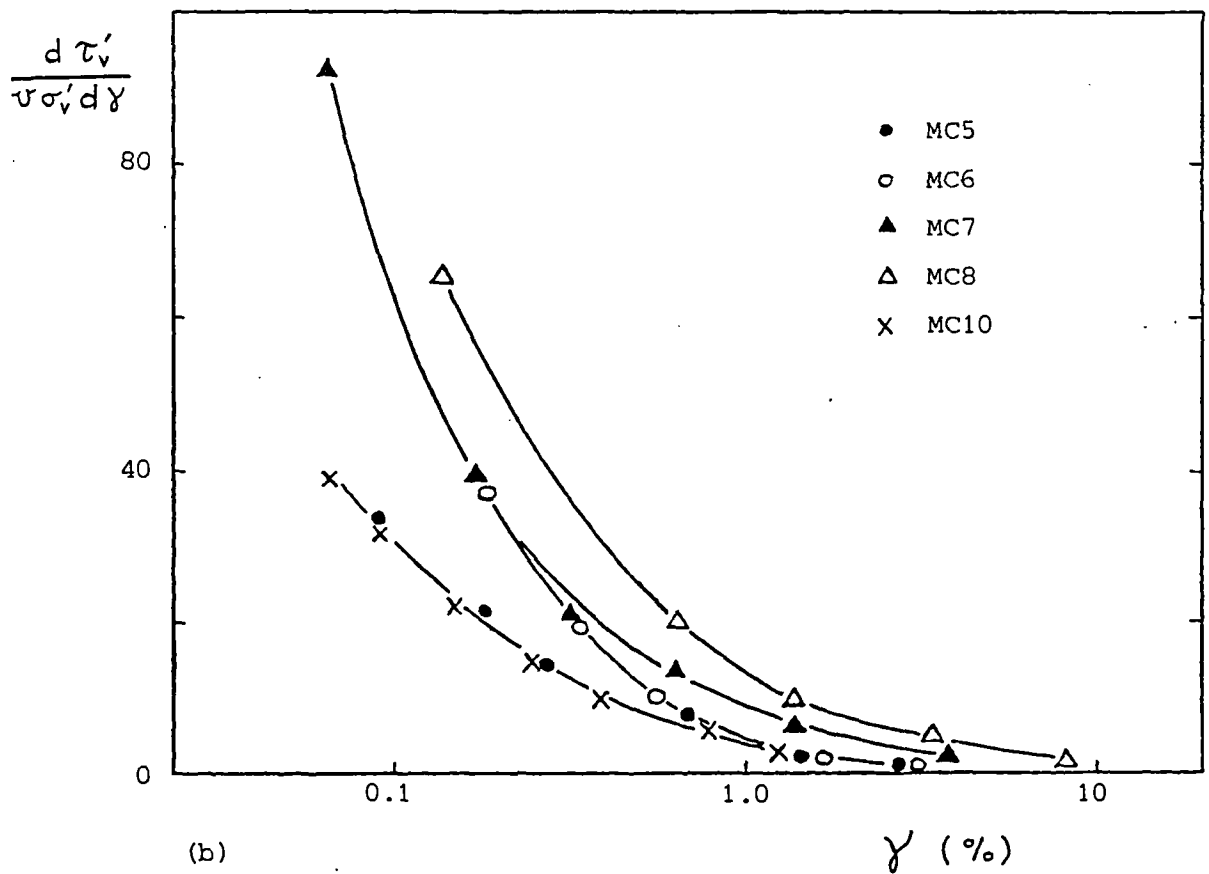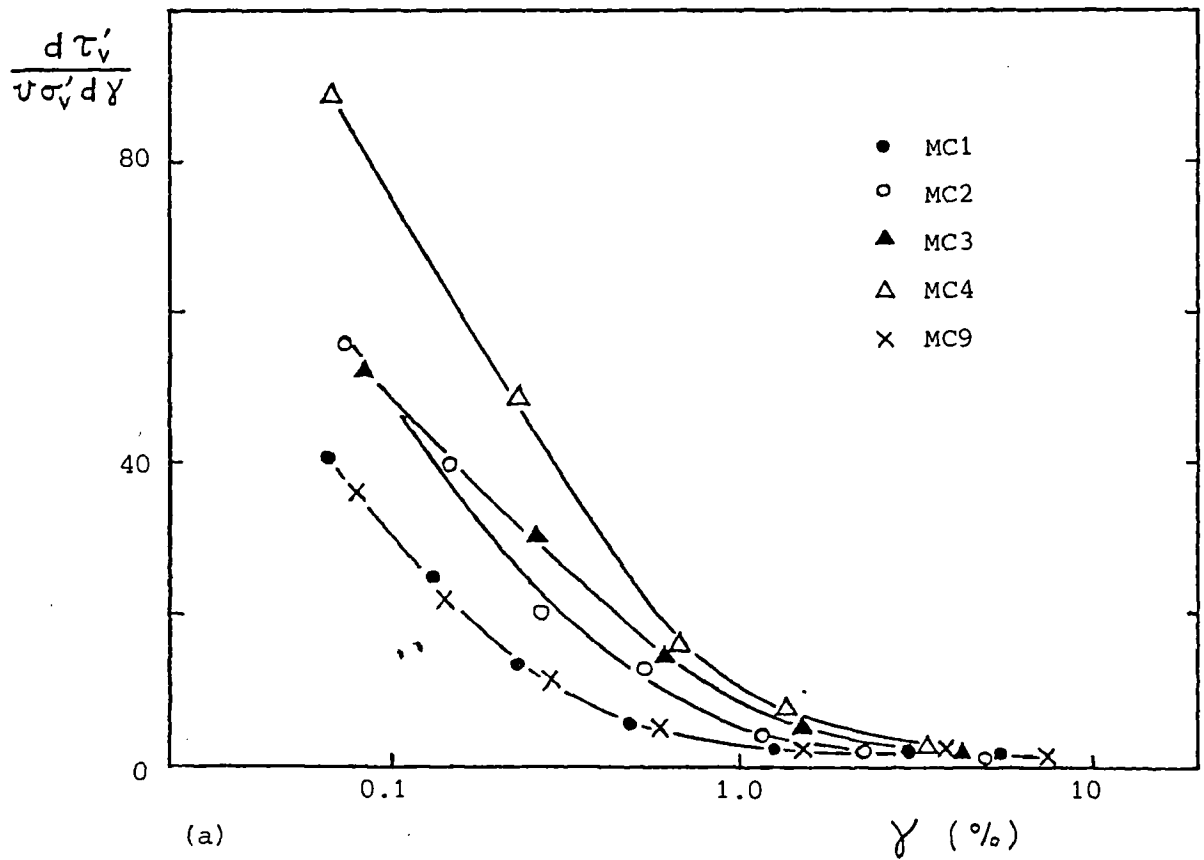
Figure 7.91   Variation of normalised tangent shear stiffness with
logarithm of shear strain for remoulded Cowden till
simple shear samples
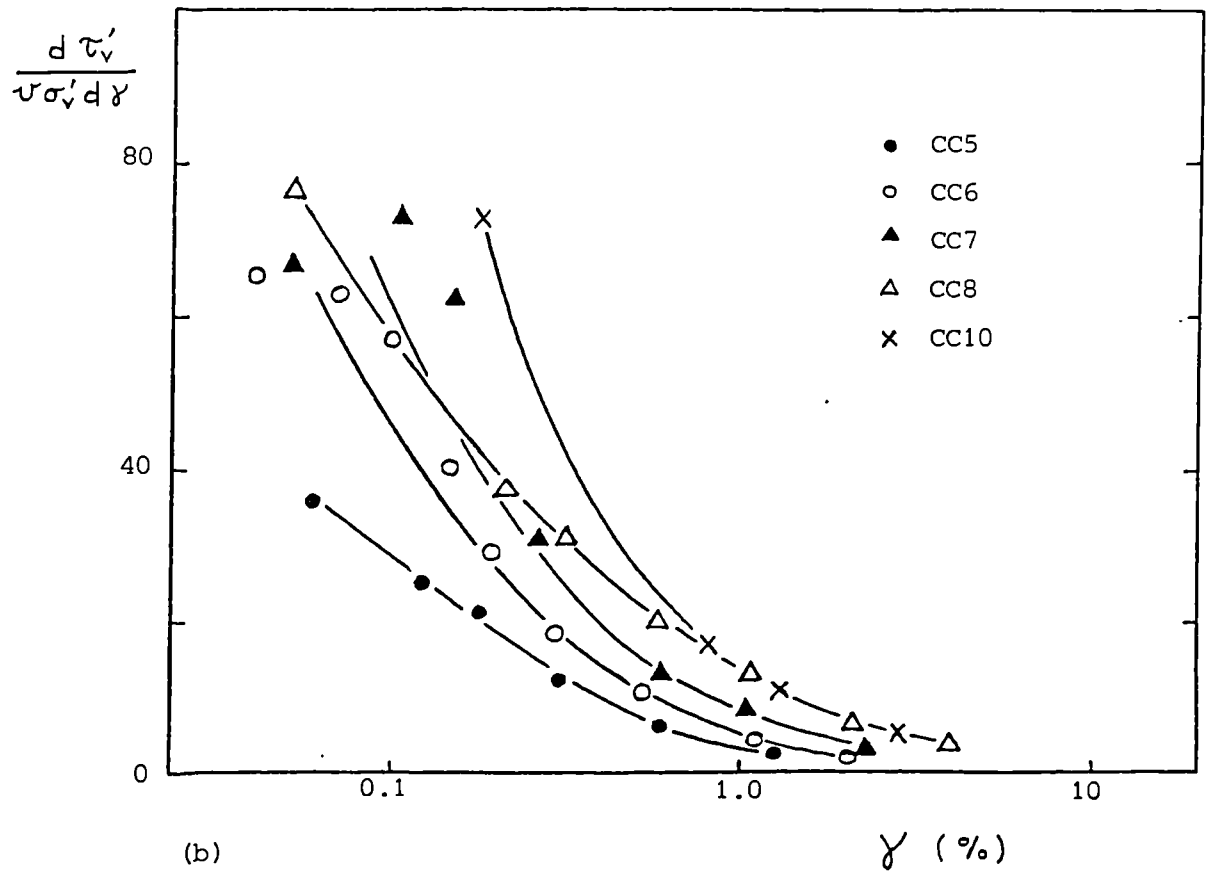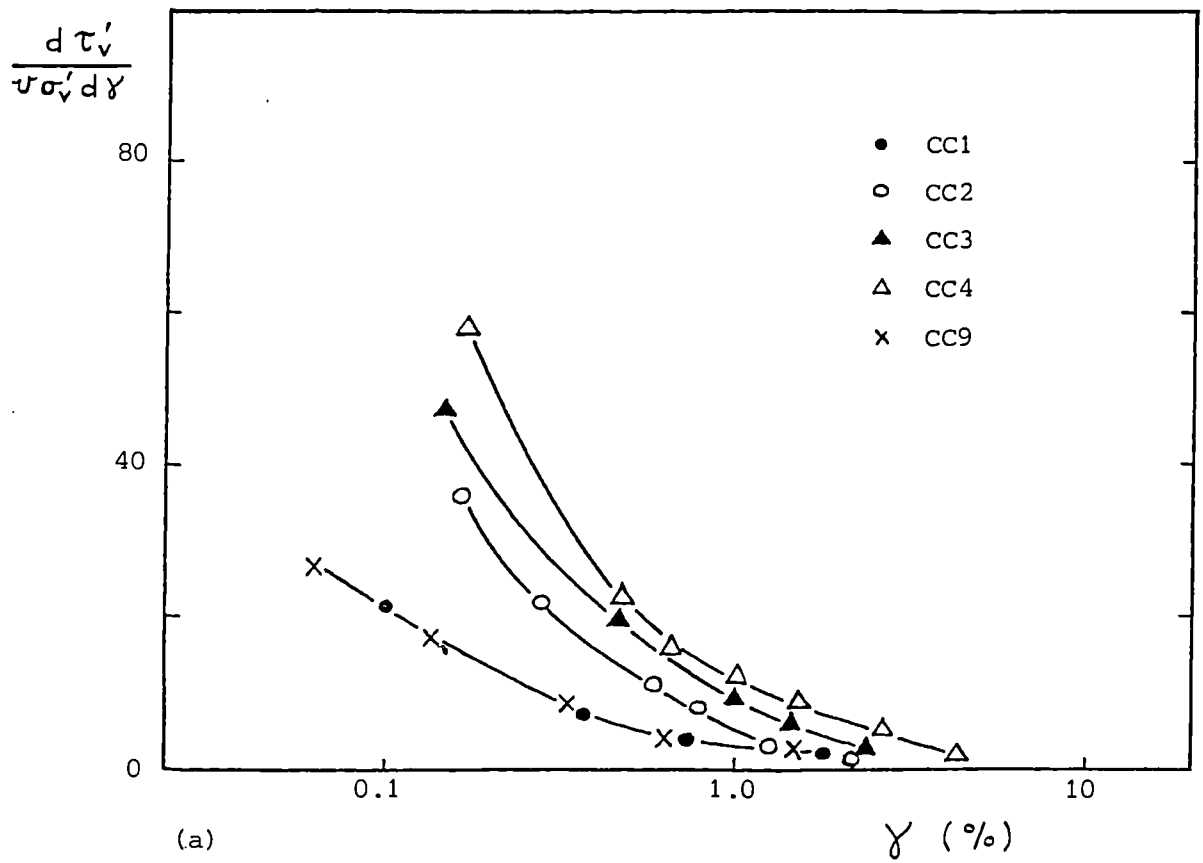
Figure 7.92   Variation of normalised tangent shear stiffness with
logarithm of shear strain for reconstituted Cowden
till simple shear samples
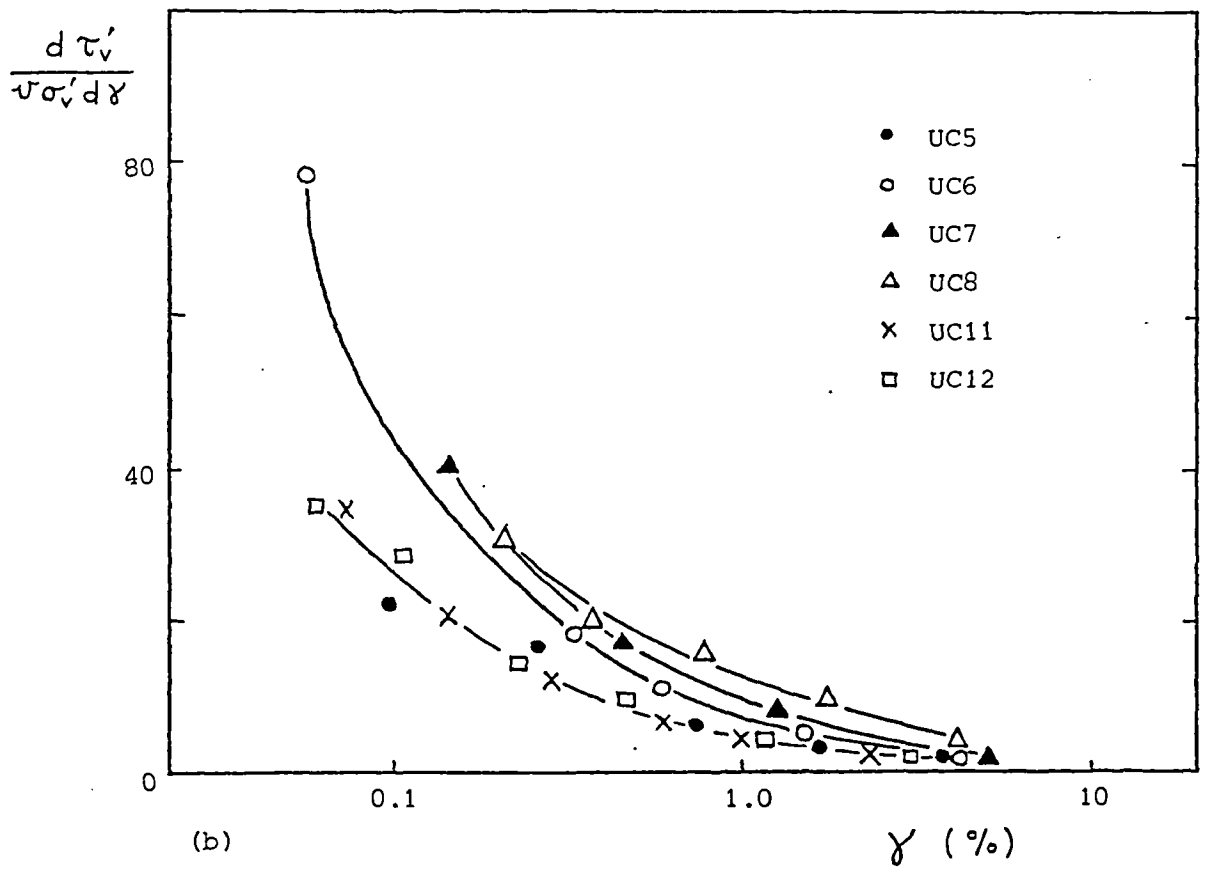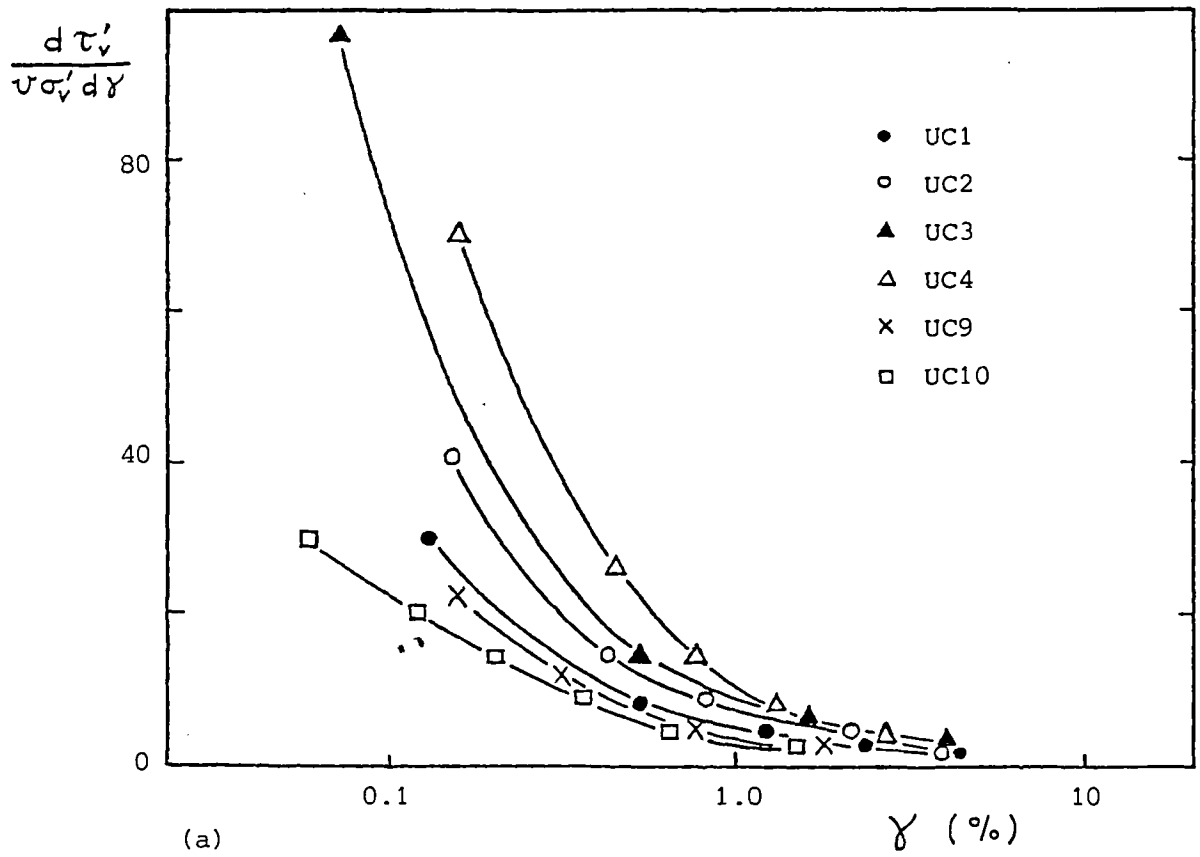
Figure 7.93   Variation of normalised tangent shear stiffness with logarithm of shear strain for undisturbed Cowden till simple shear samples
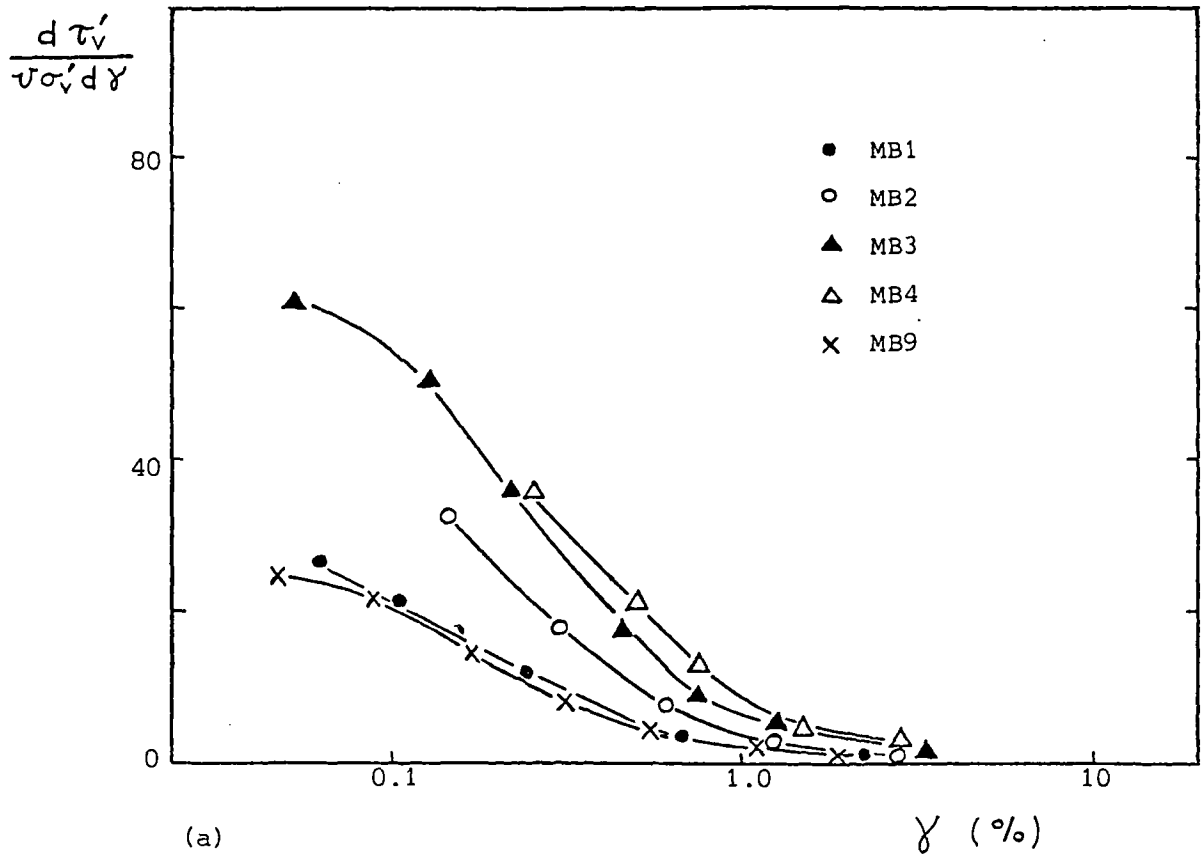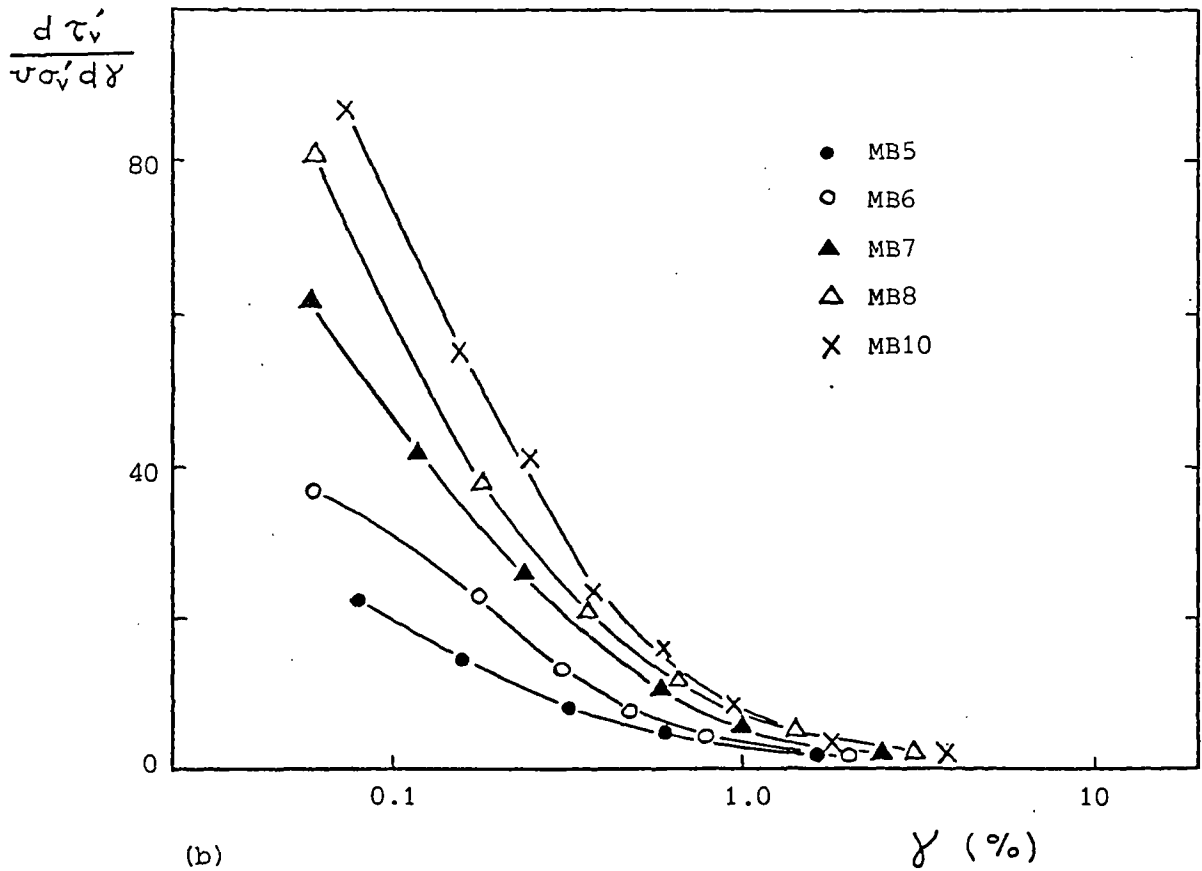
Figure 7.94   Variation of normalised tangent shear stiffness with
logarithm of shear strain for remoulded London clay
(brown) simple shear samples
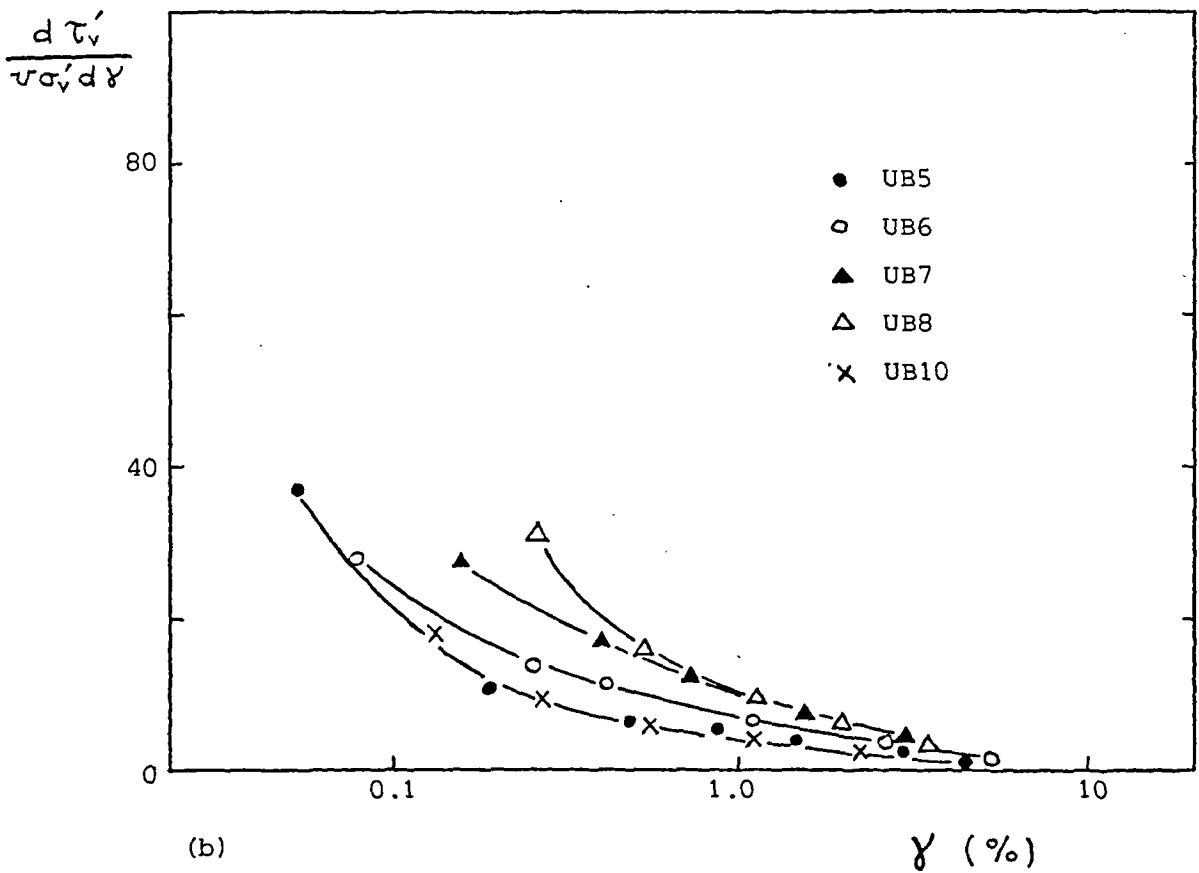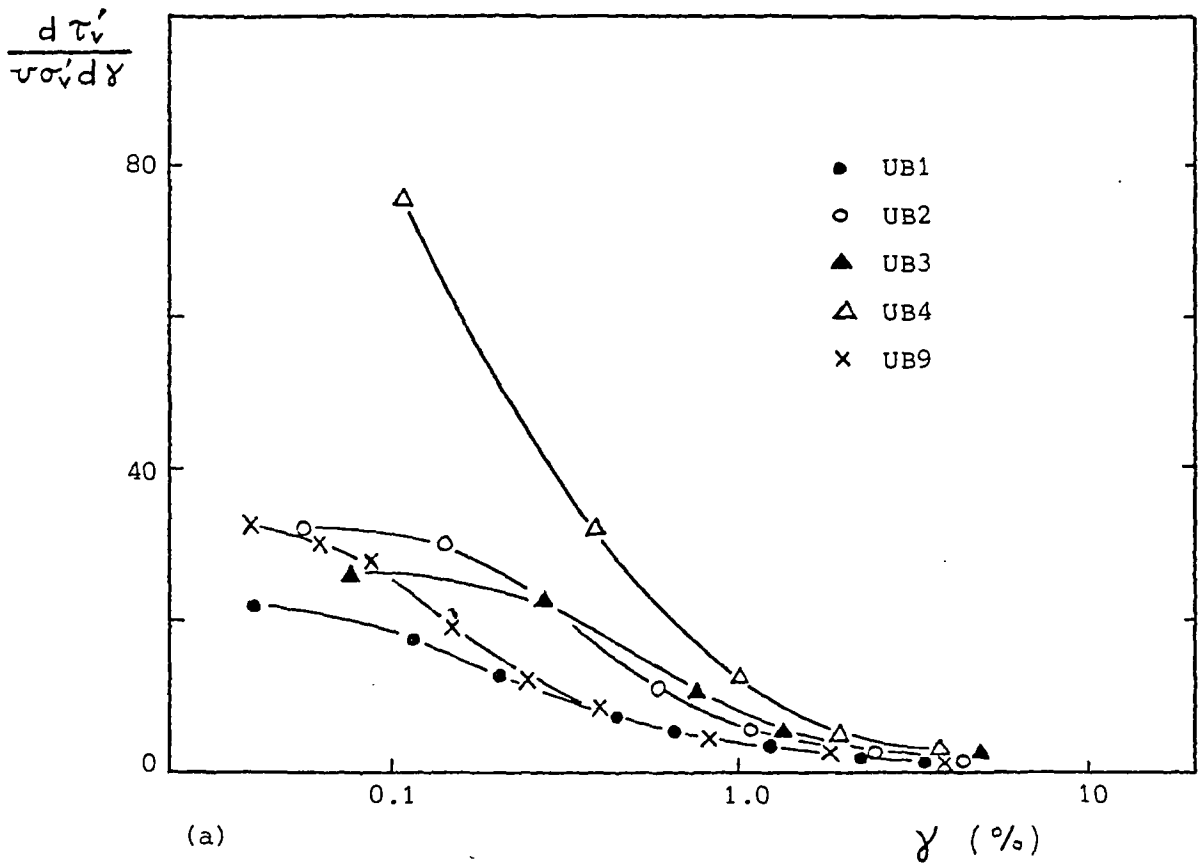
Figure 7.95   Variation of normalised tangent shear stiffness with logarithm of shear strain for undisturbed London clay (brown) simple shear samples
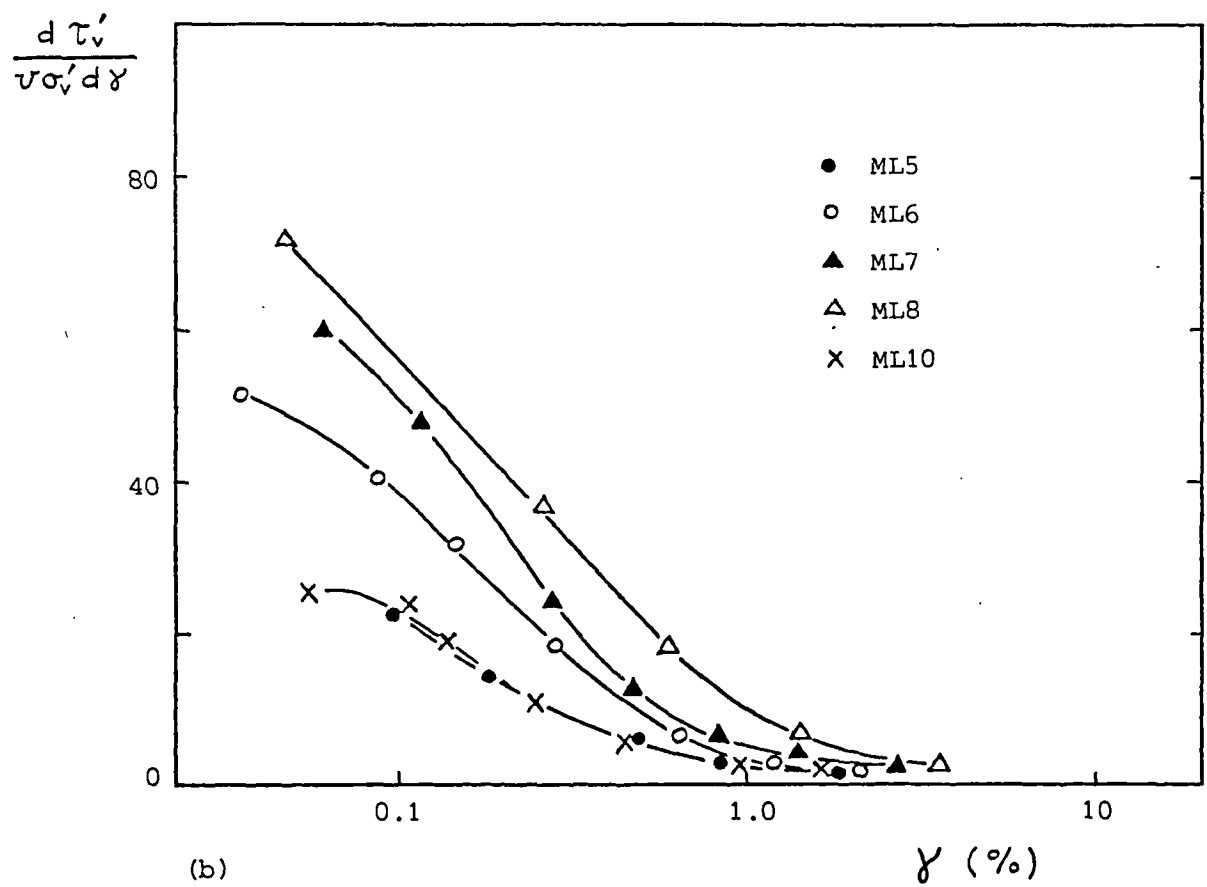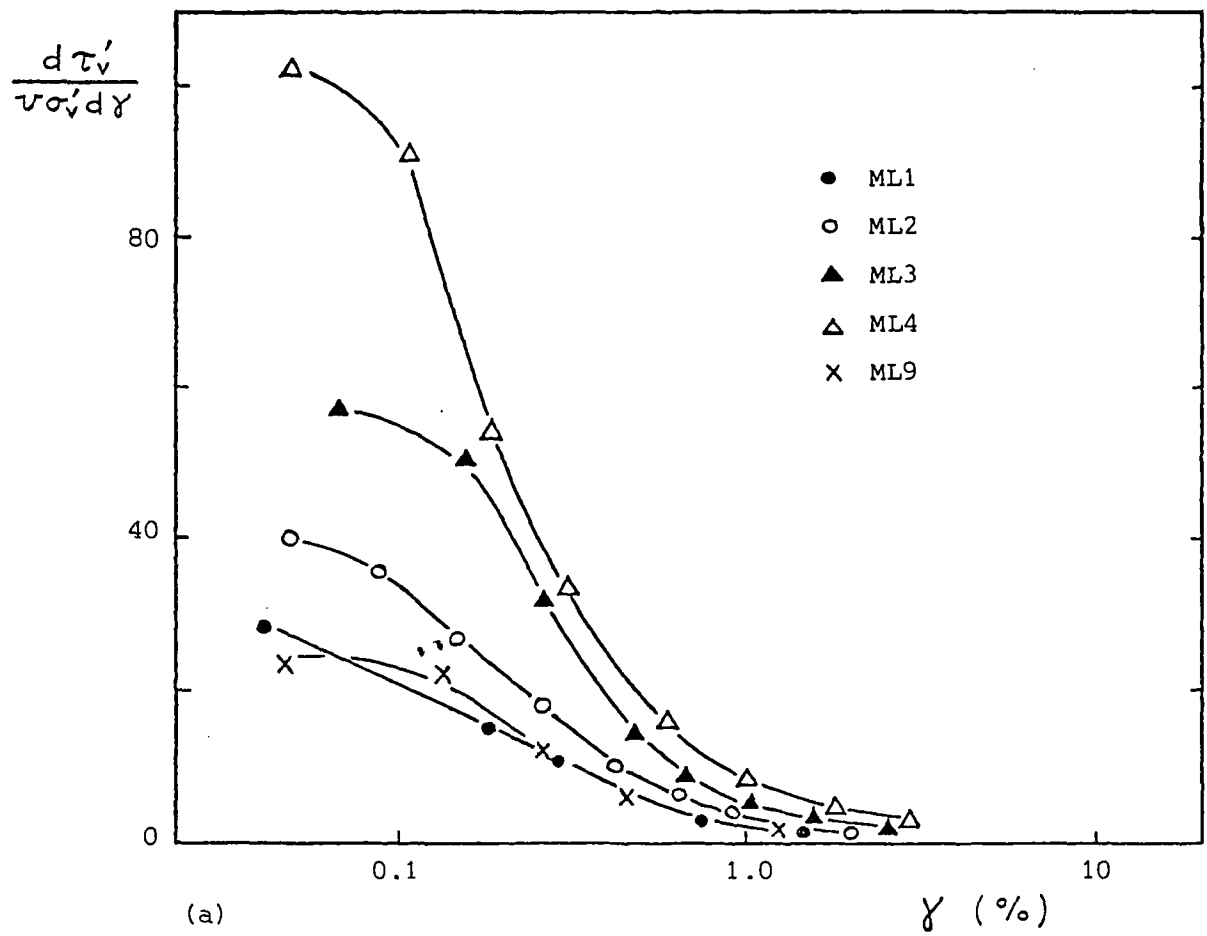
Figure 7.96 Variation of normalised tangent shear stiffness with logarithm of shear strain for remoulded London clay (blue) simple shear samples
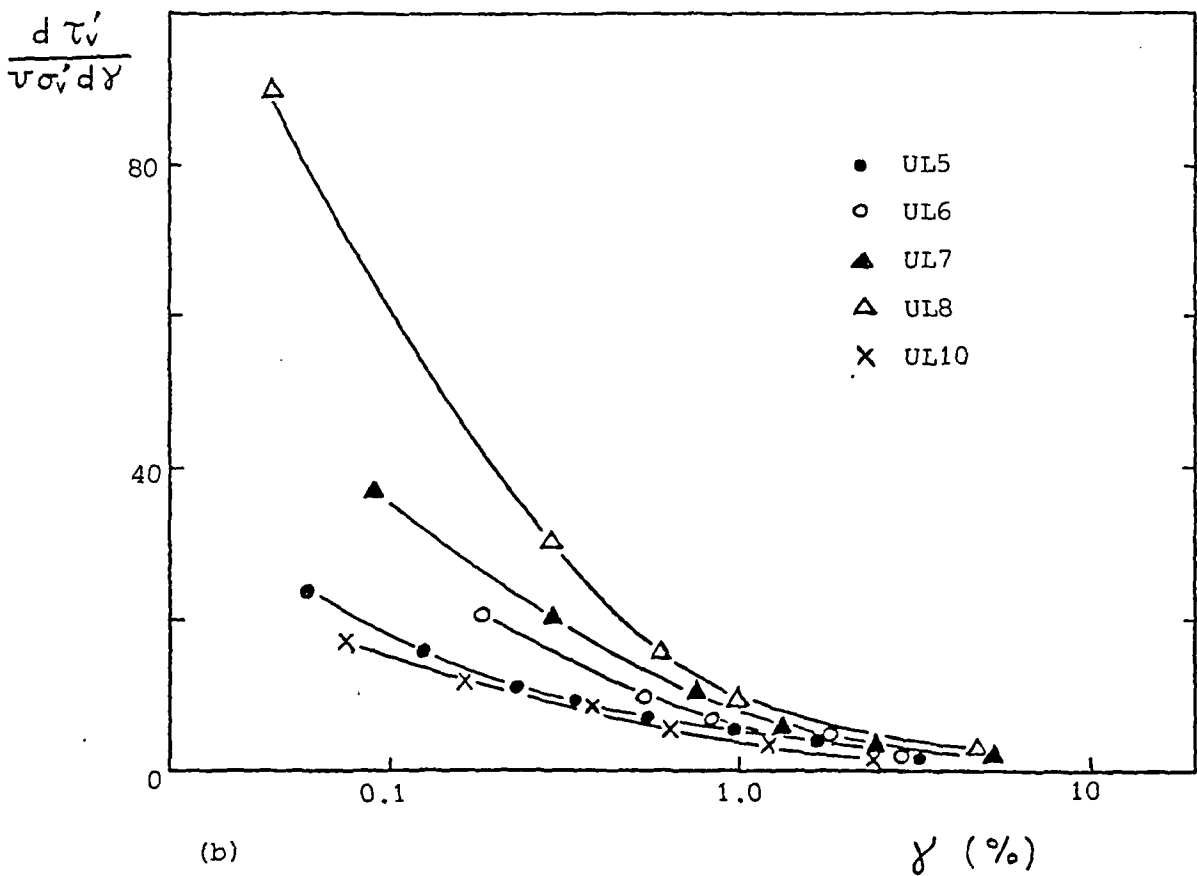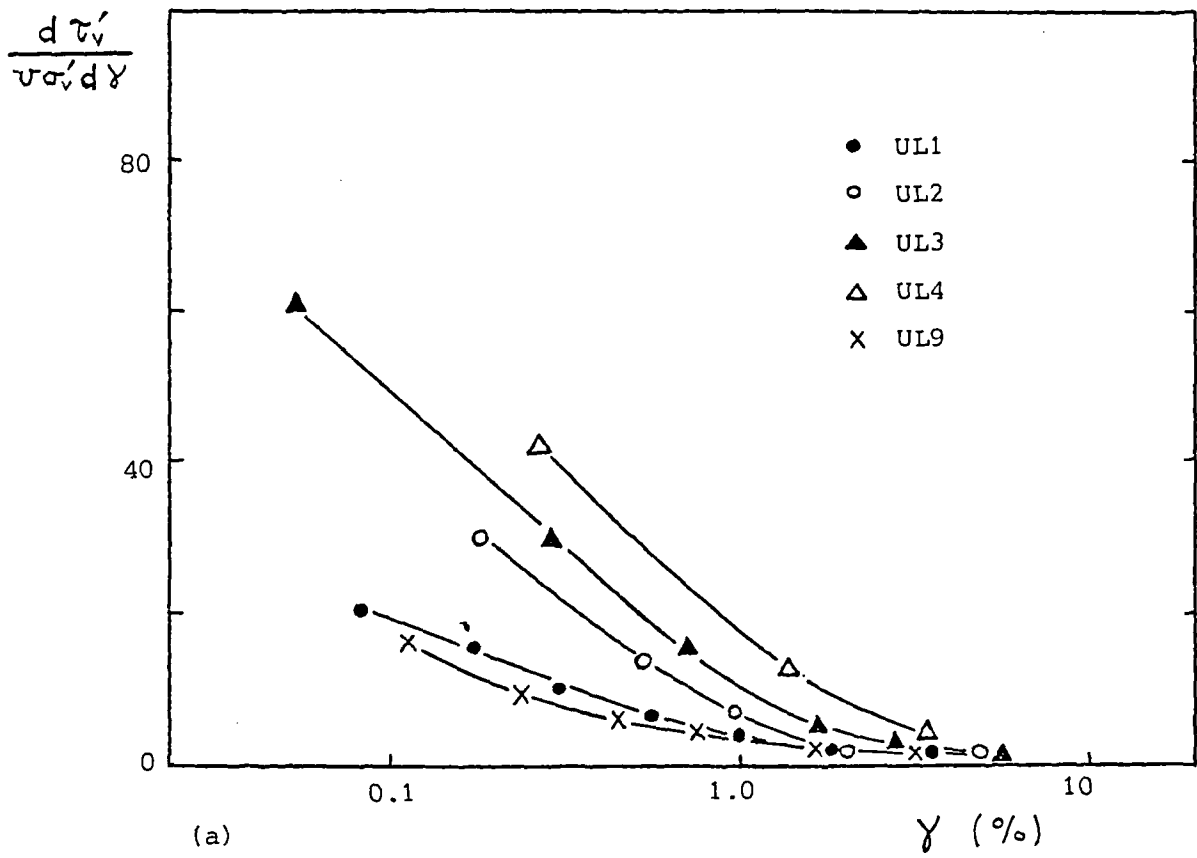
Figure   7.97   Variation of normalised tangent shear stiffness with
                 logarithm of shear strain for undisturbed London clay
                 (blue) simple shear samples
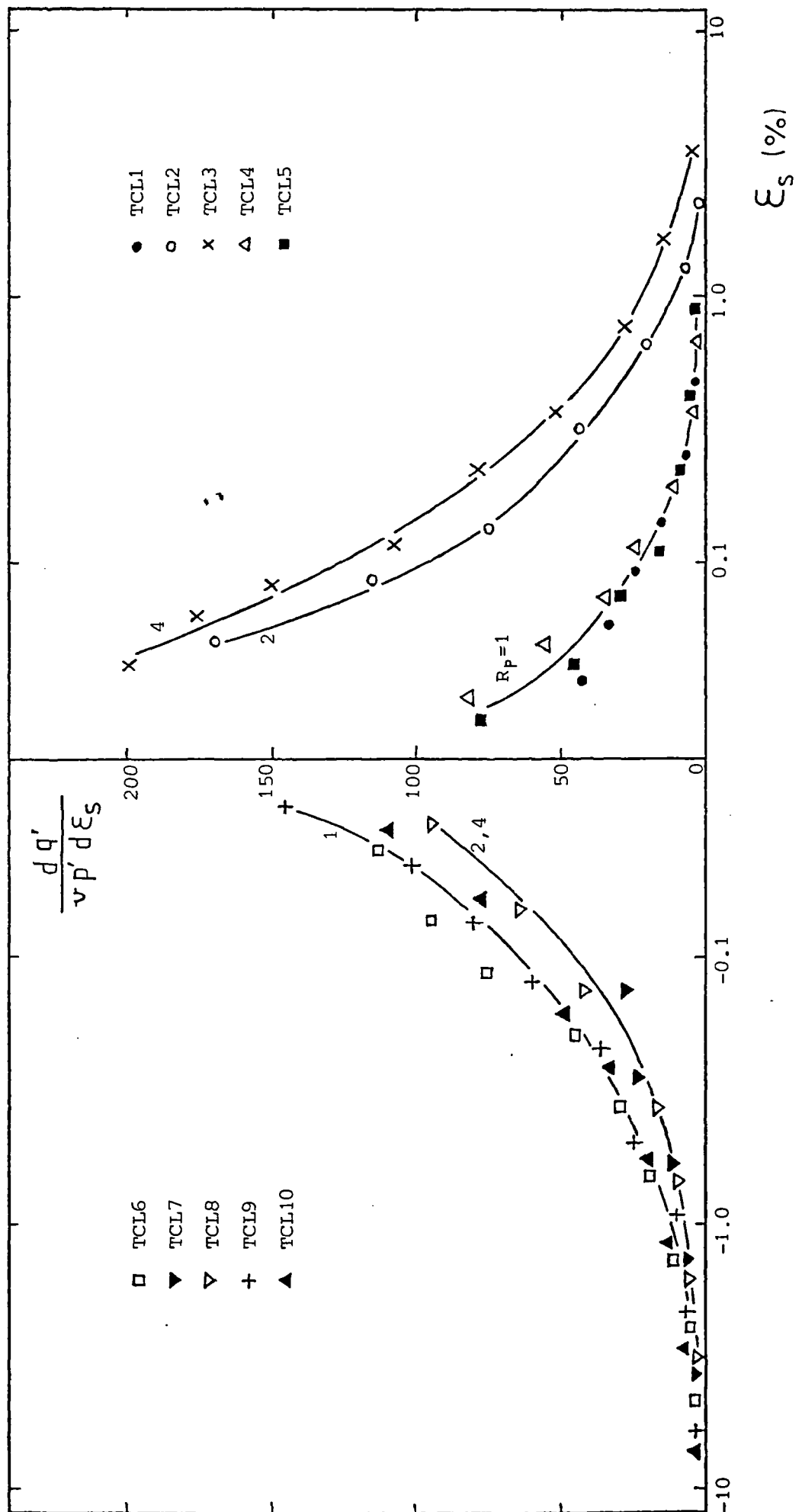
Figure 7.98   Variation of normalised tangent shear stiffness with logarithm of shear strain for 38 mm reconstituted London clay (blue) triaxial samples
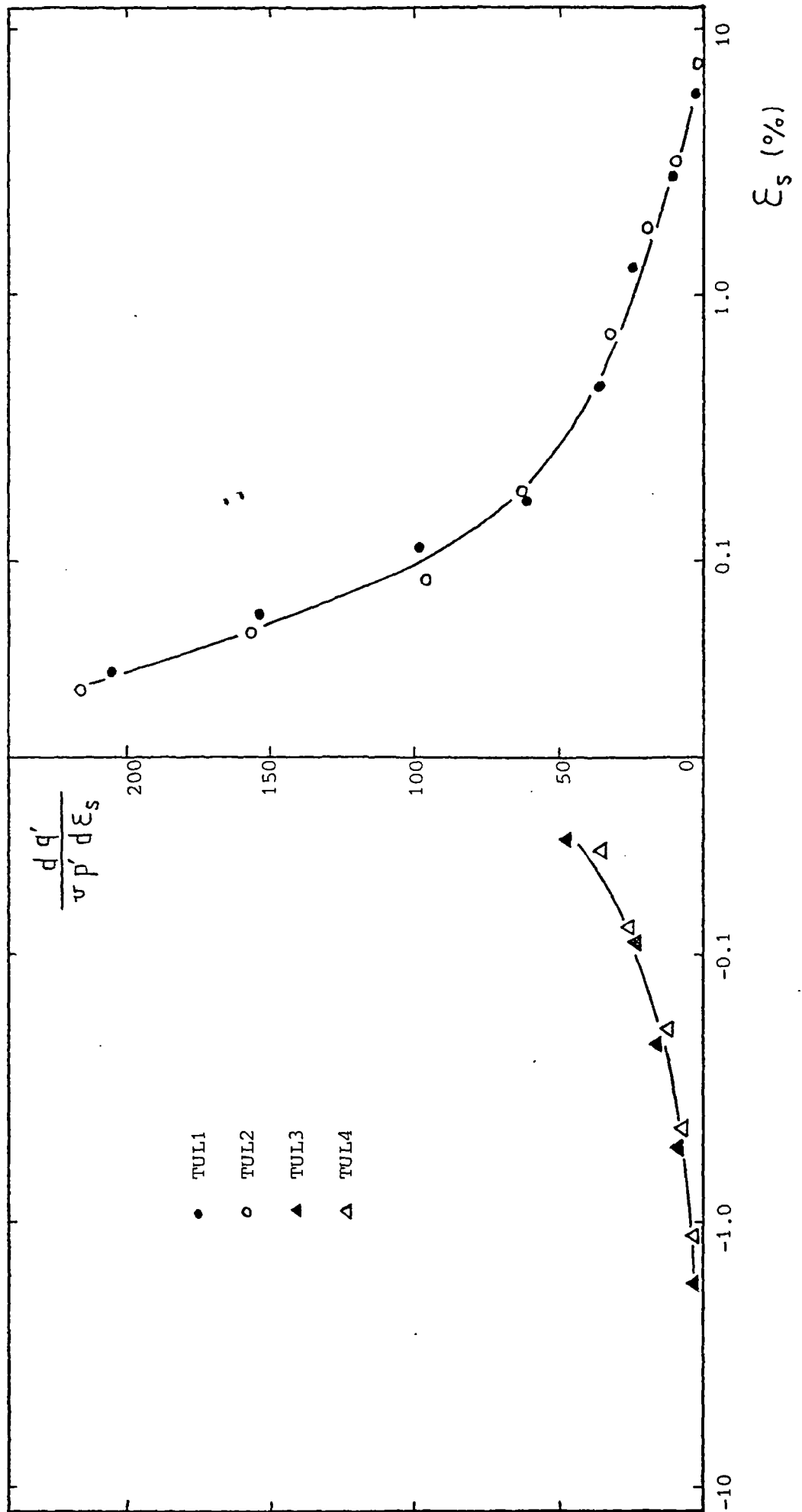
Figure 7.99 Variation of normalised tangent shear stiffness with logarithm of shear strain for 100 mm undisturbed London clay (blue) triaxial samples

(a)   Remoulded
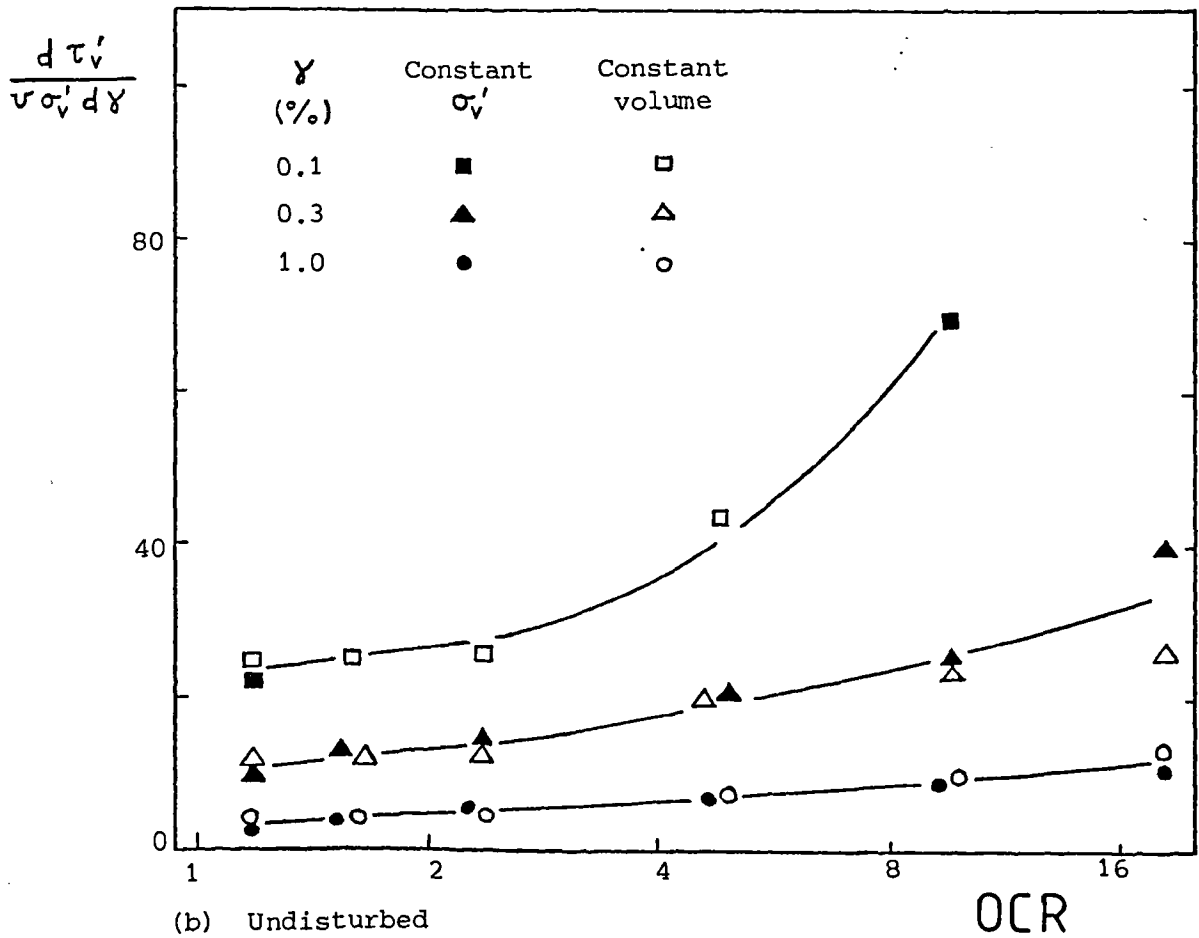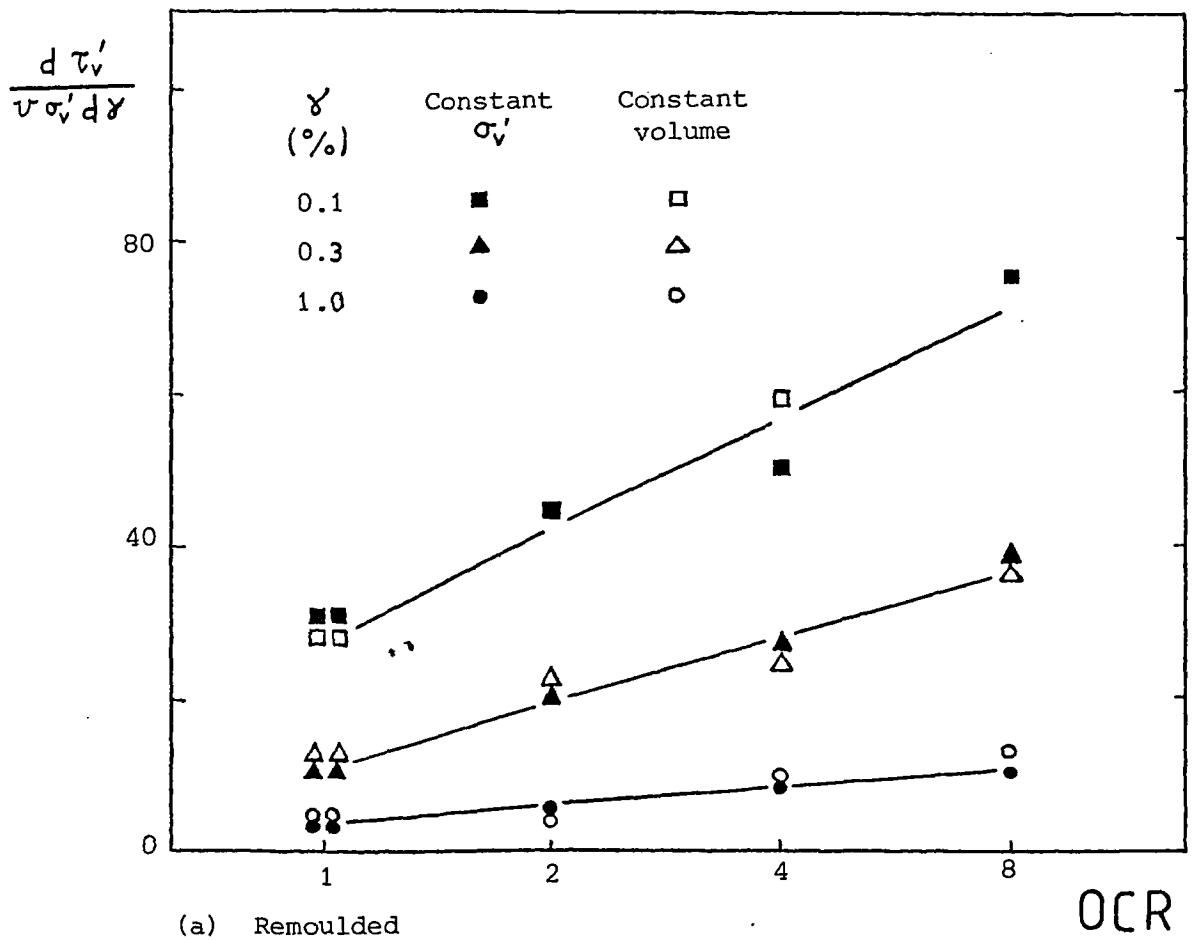
(b)   Undisturbed

Figure   7.100   Comparison of normalised tangent shear stiffnesses from constant σ_v' and constant volume simple shear tests on Cowden till
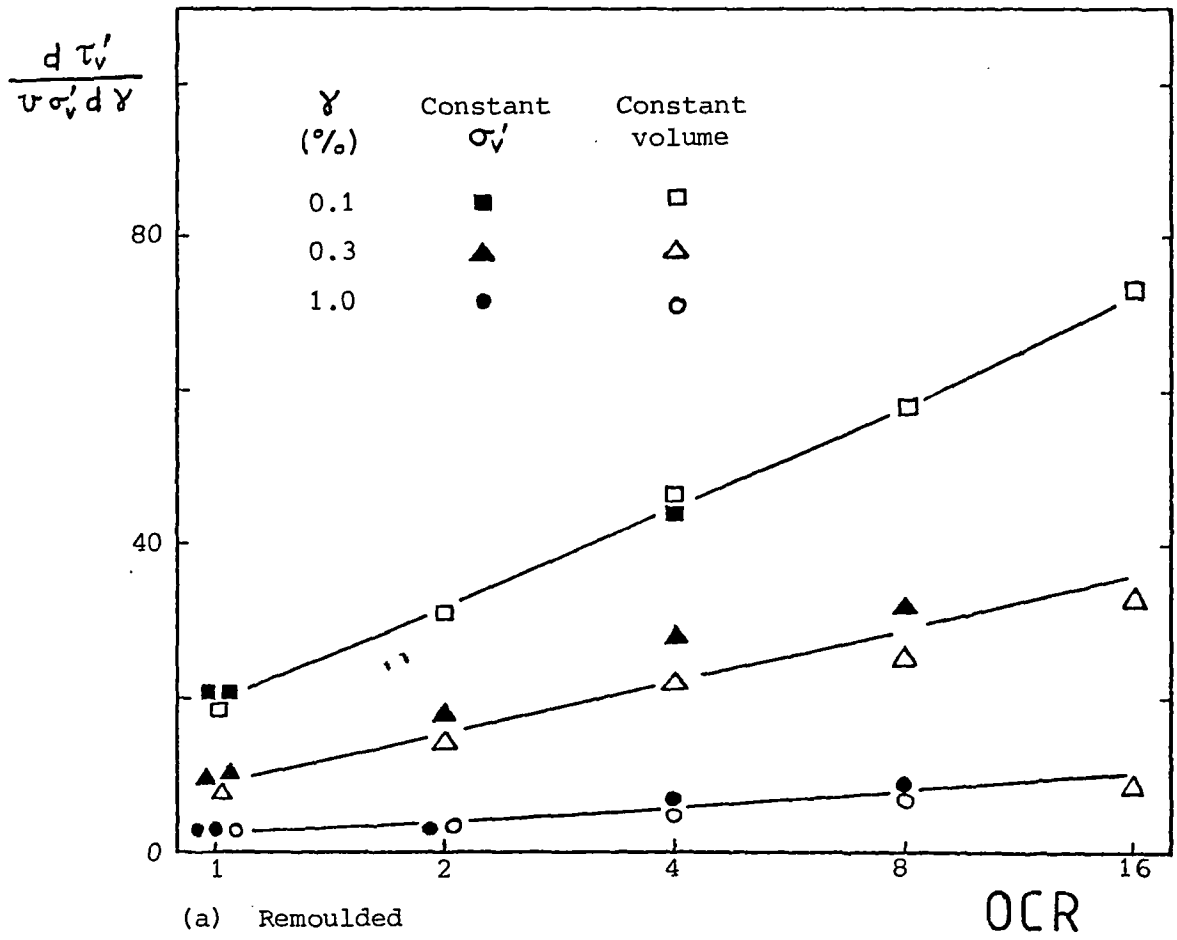
(a) Remoulded
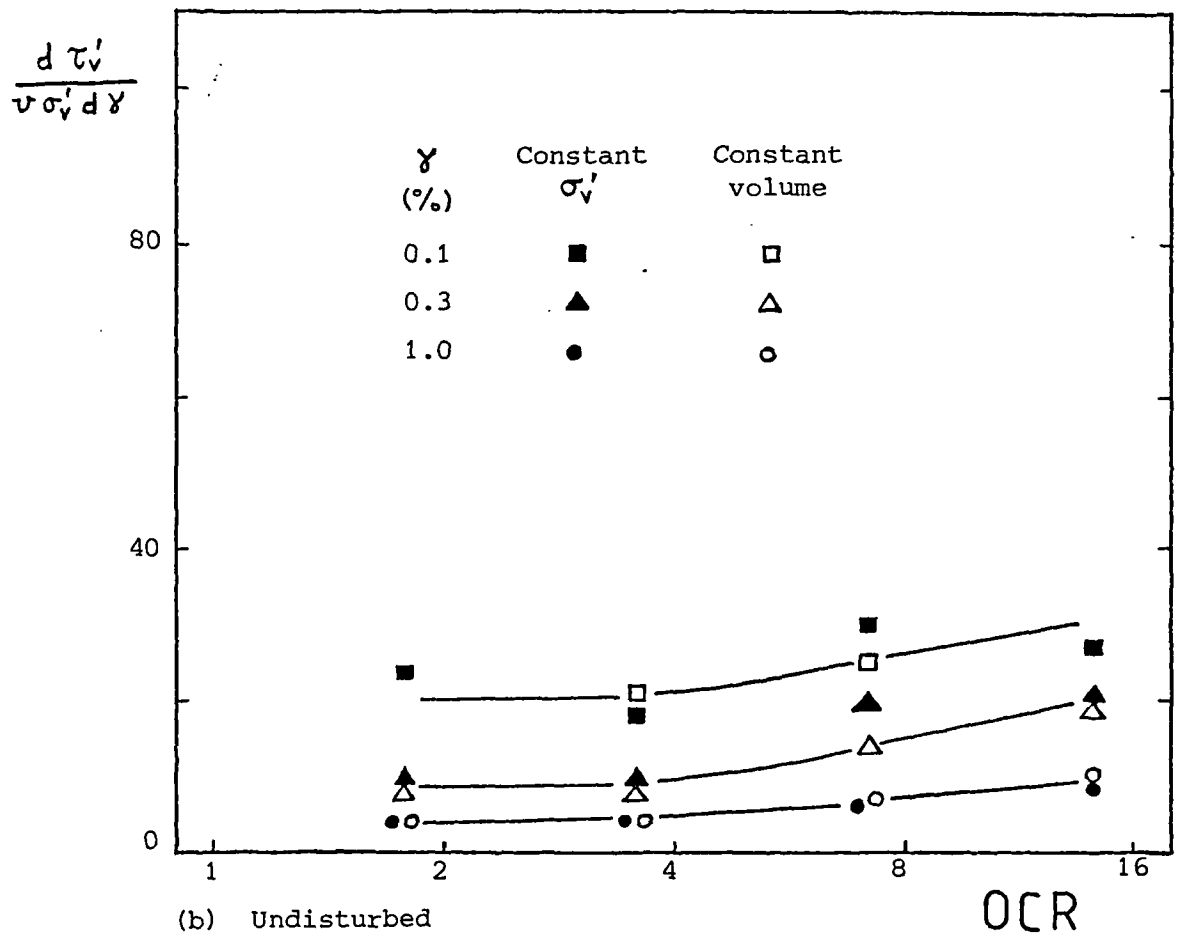
(b) Undisturbed

Figure 7.101 Comparison of normalised tangent shear stiffnesses from constant σ_v' and constant volume simple shear tests on London clay (brown)
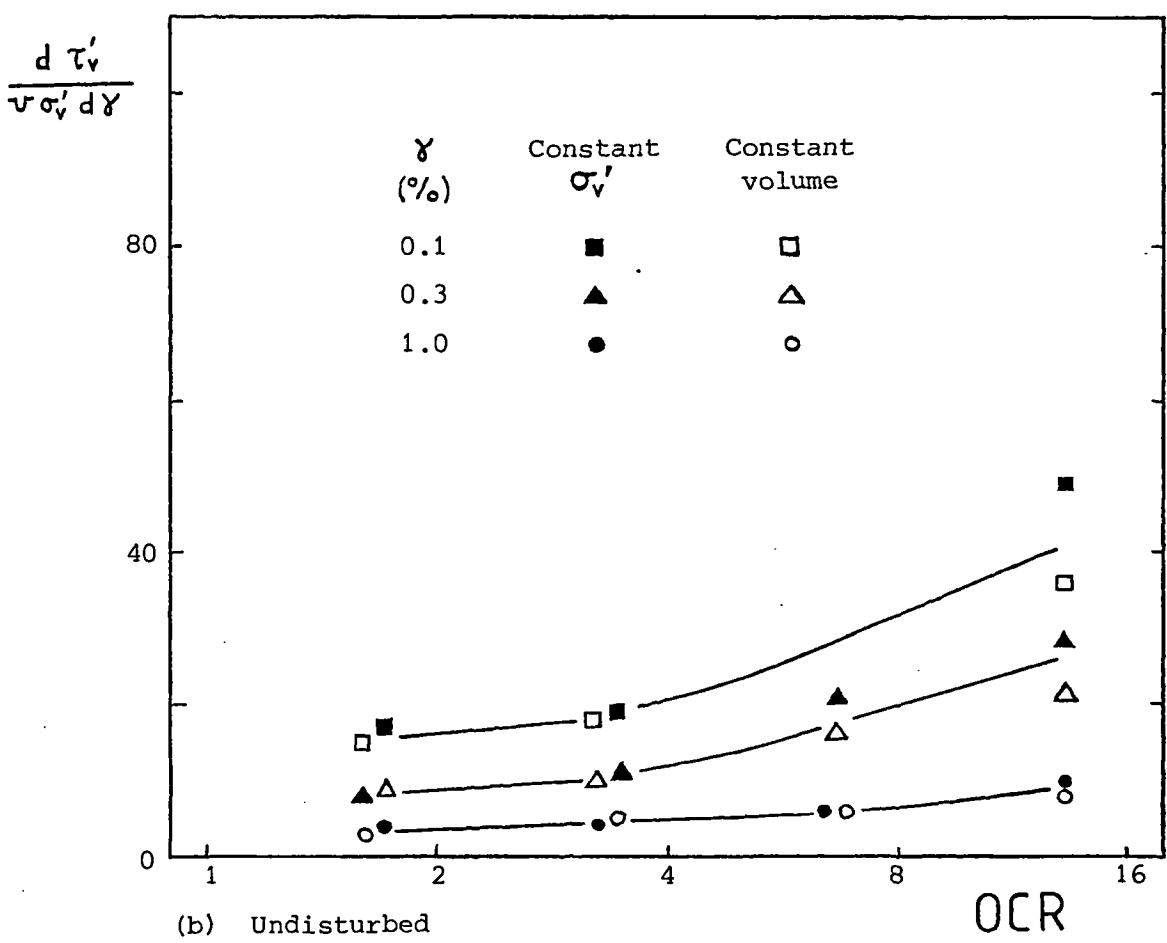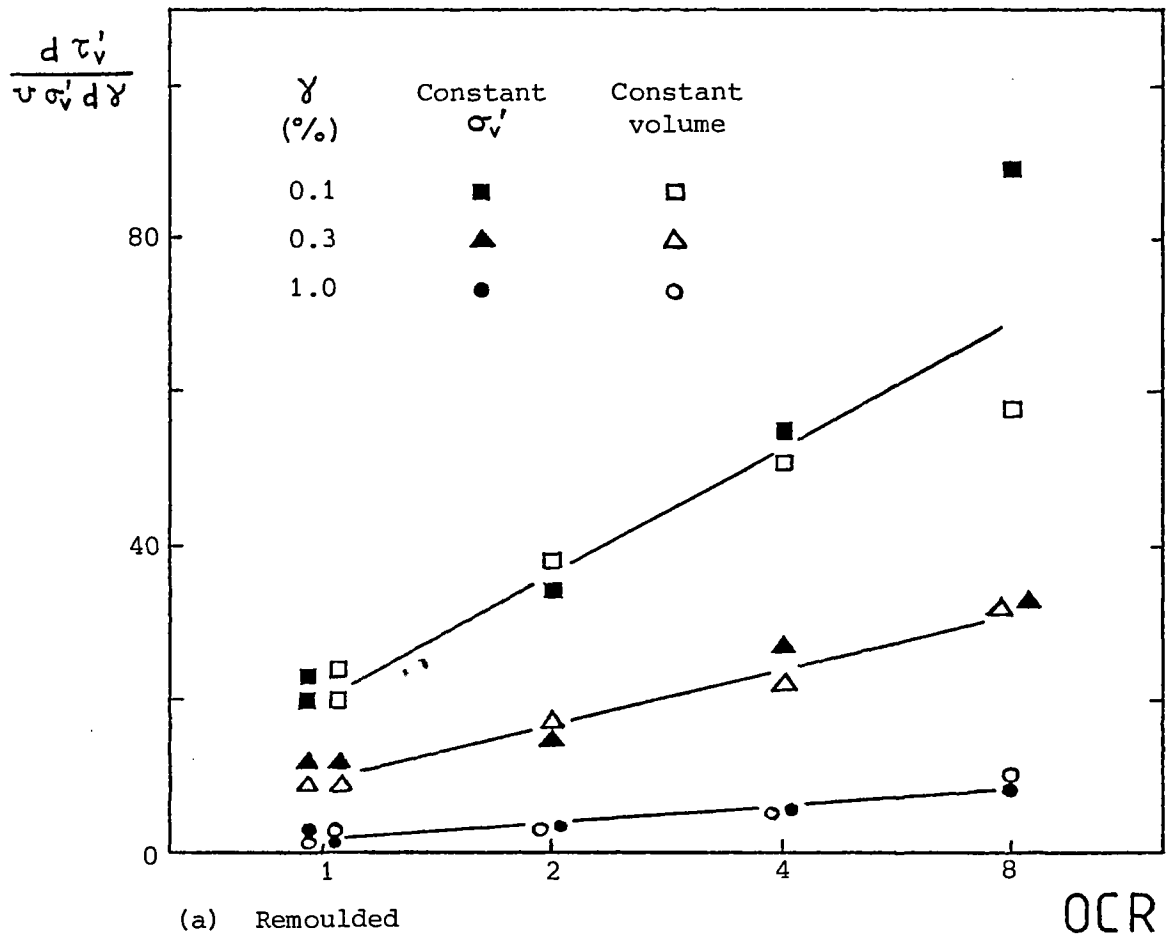
Figure 7.102 Comparison of normalised tangent shear stiffnesses from constant σ_v' and constant volume simple shear tests on London clay (blue)

(a) Compression tests

(b) Extension tests
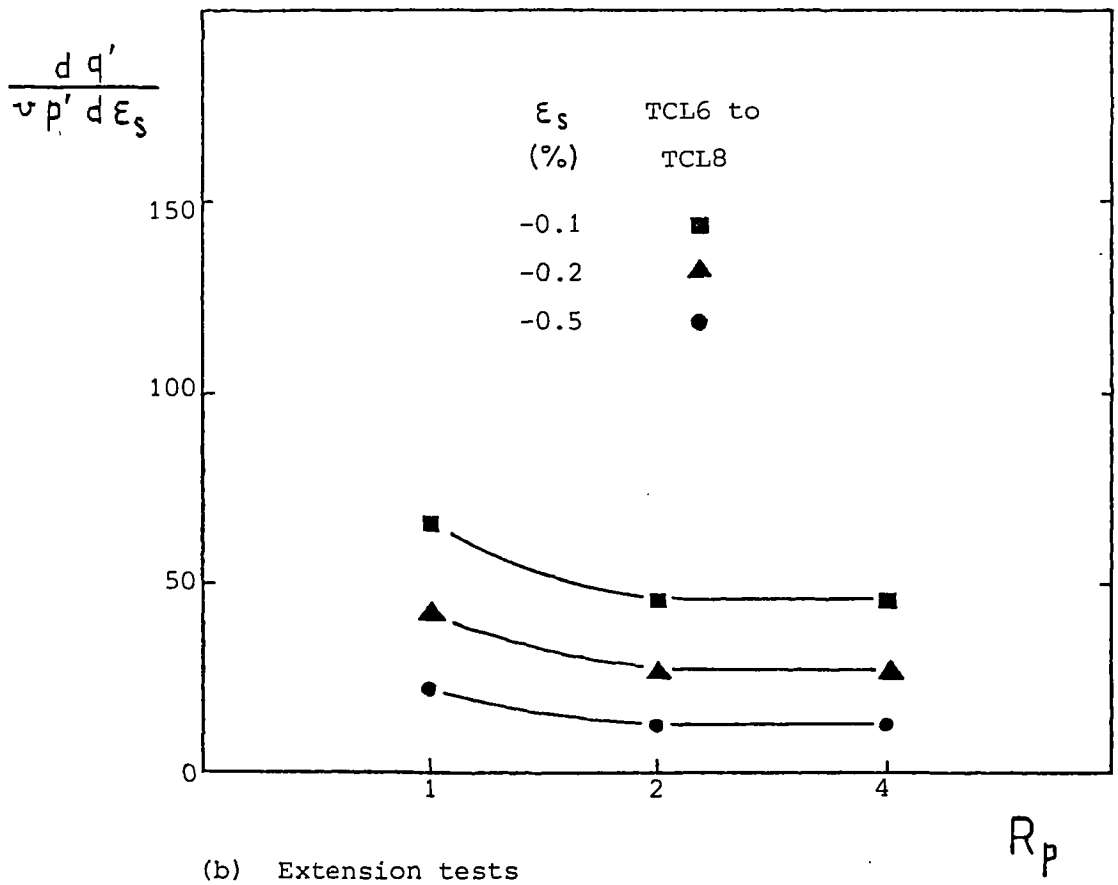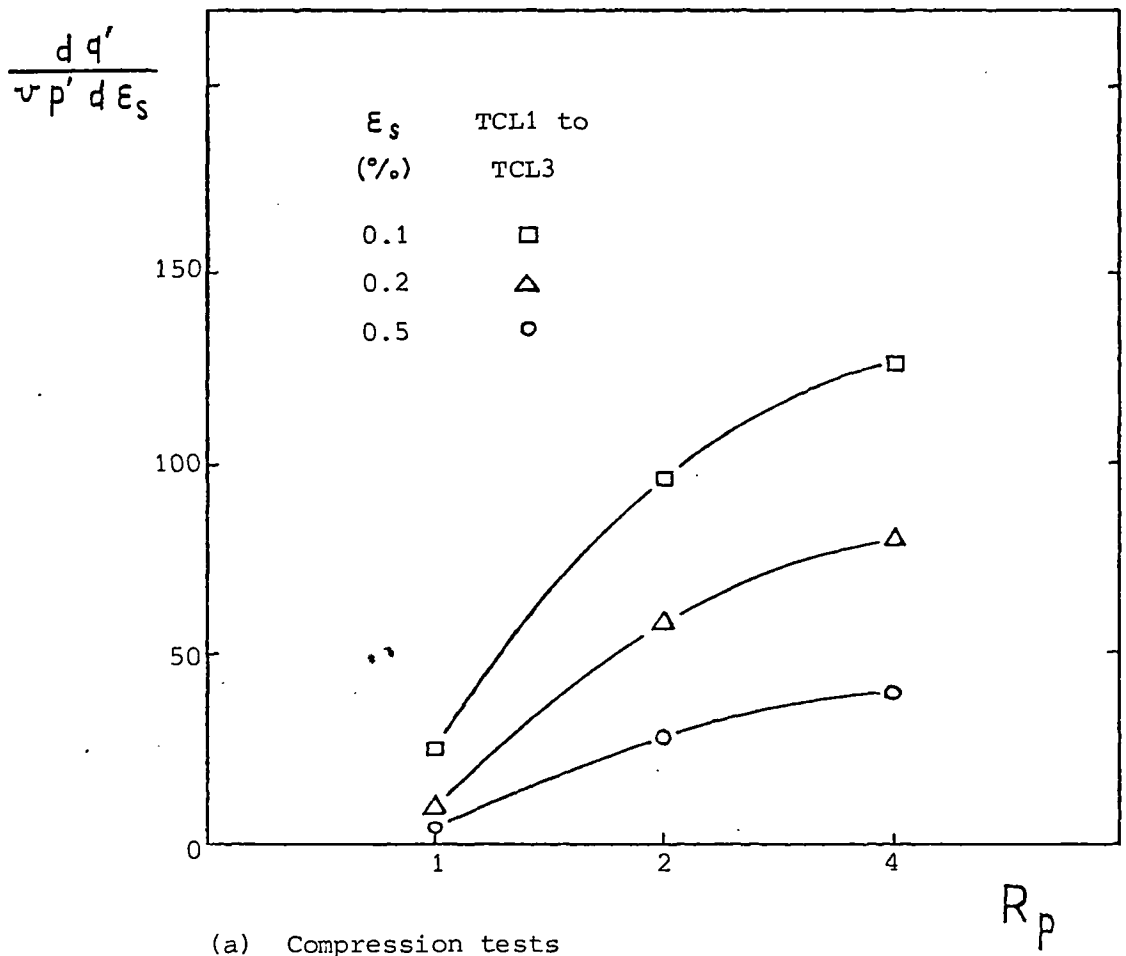
Figure 7.103   Variation of normalised tangent shear stiffness with
                   overconsolidation ratio for 38 mm reconstituted
                   London clay (blue) triaxial samples
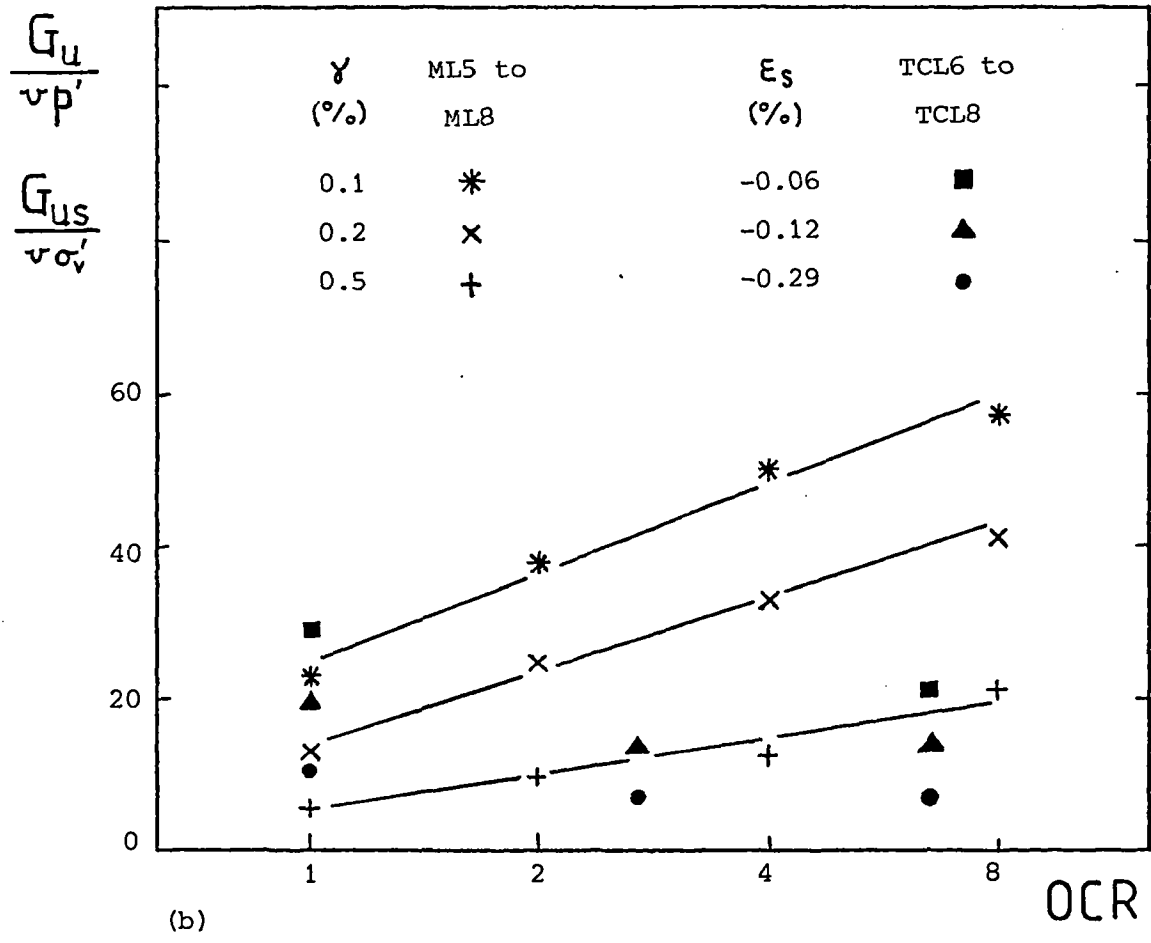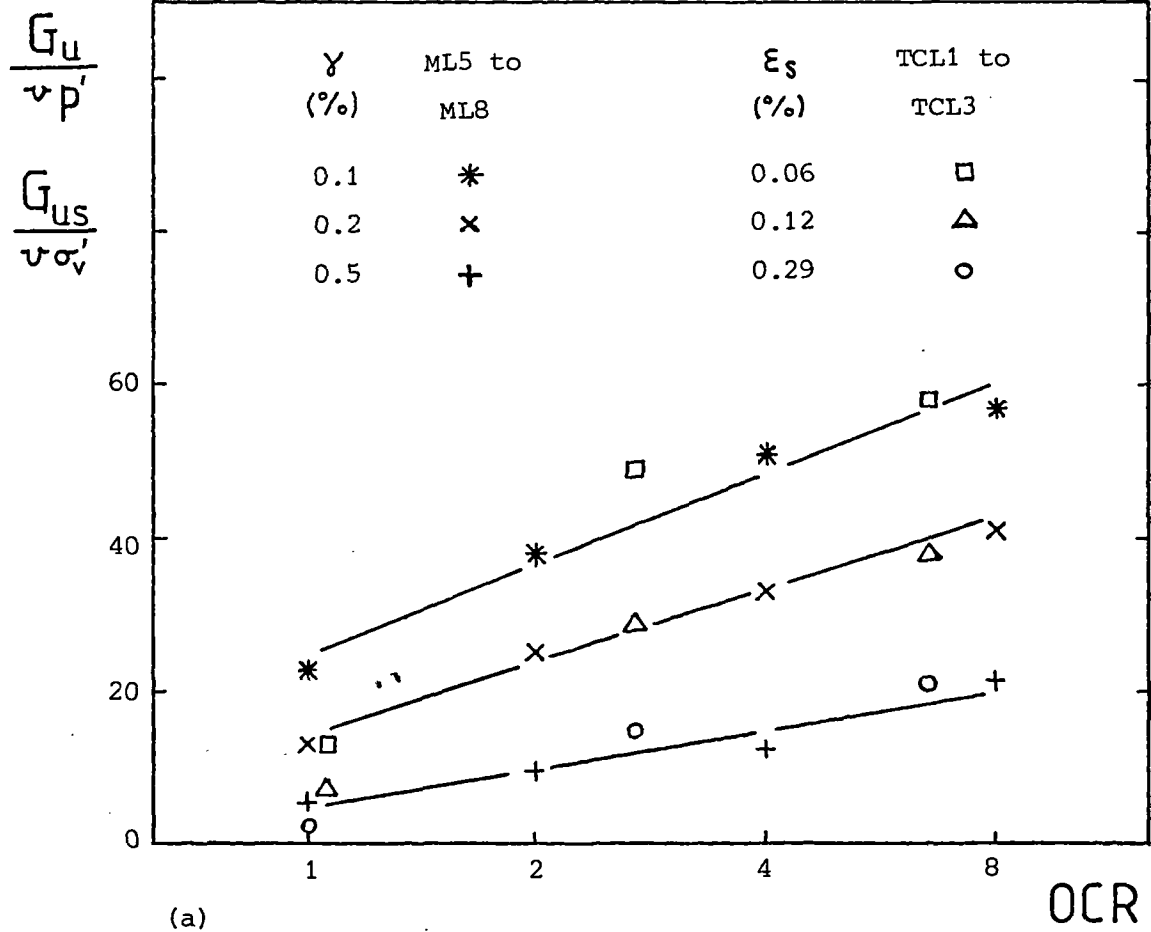
Figure 7.104   Comparison of normalised tangent shear moduli from
constant volume simple shear and undrained triaxial
tests on London clay (blue)
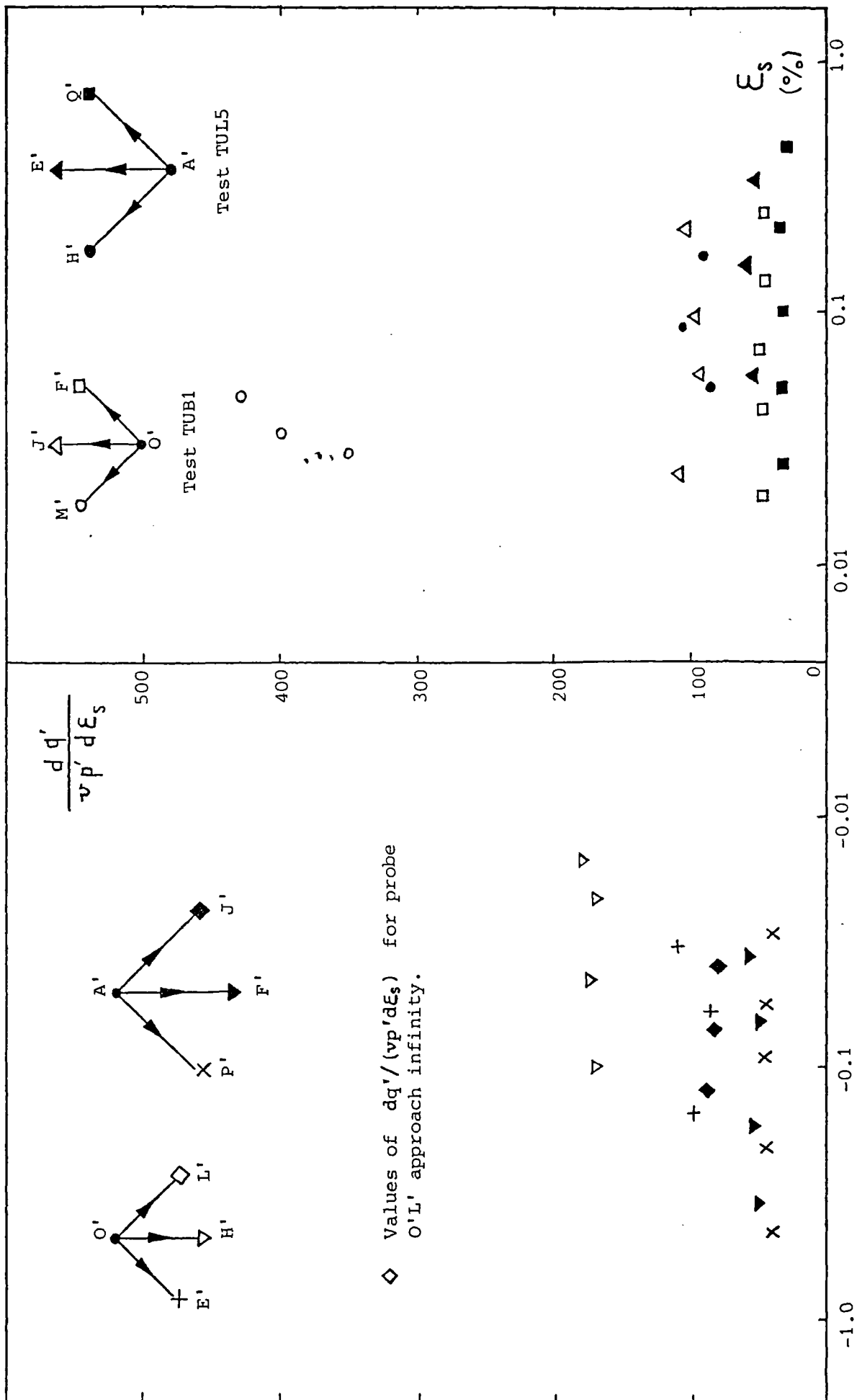
Figure 7.105   Comparison of normalised tangent shear stiffnesses
from probing tests TUB1 and TUL5
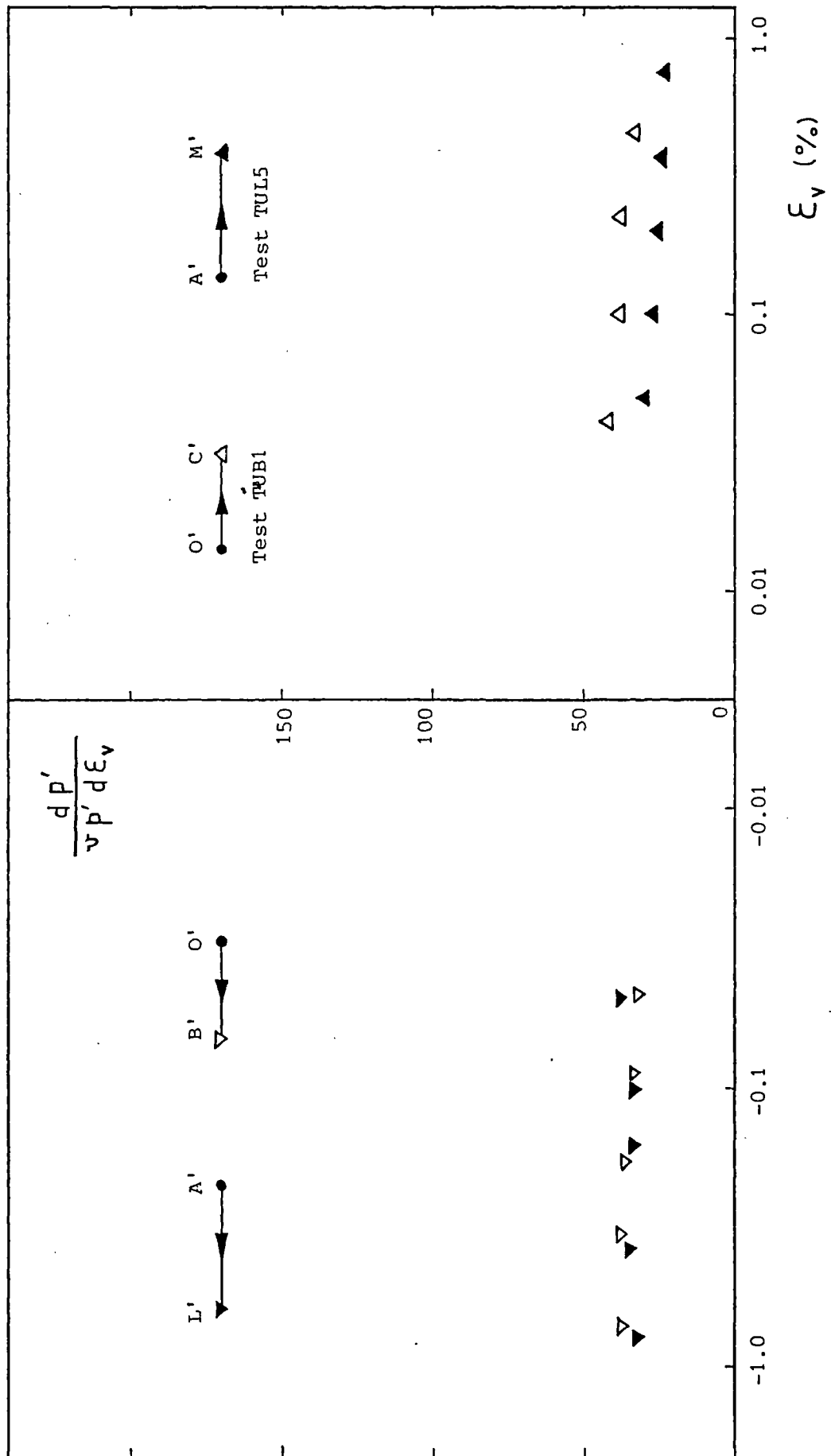
Figure 7.106   Comparison of normalised tangent bulk stiffnesses
                from probing tests TUB1 and TUL5
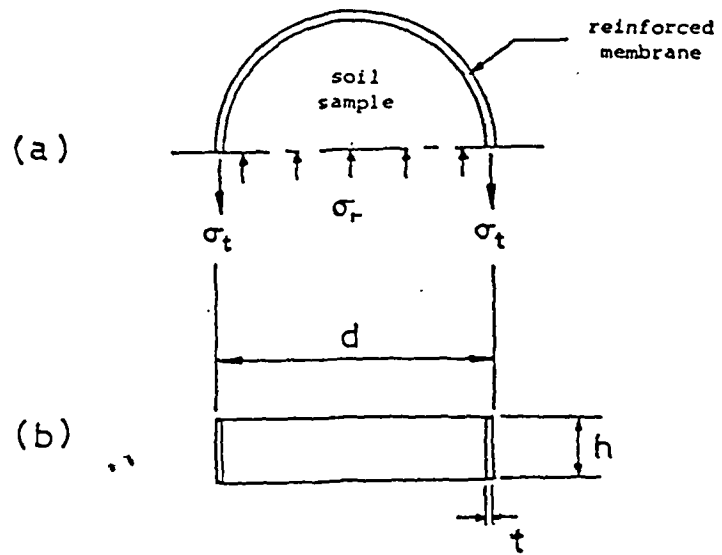
Figure C.1   Reinforced membrane approximated
as thin ring
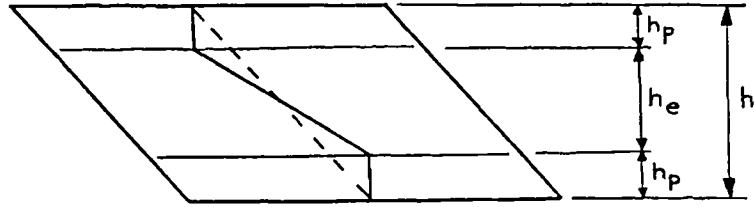
h_p = height over which no shear straining occurs

h_e = effective sample height

— — — — — soil fibre unaffected by pins

—————— soil fibre affected by pins

Figure D.1   Effect of pins on shear straining
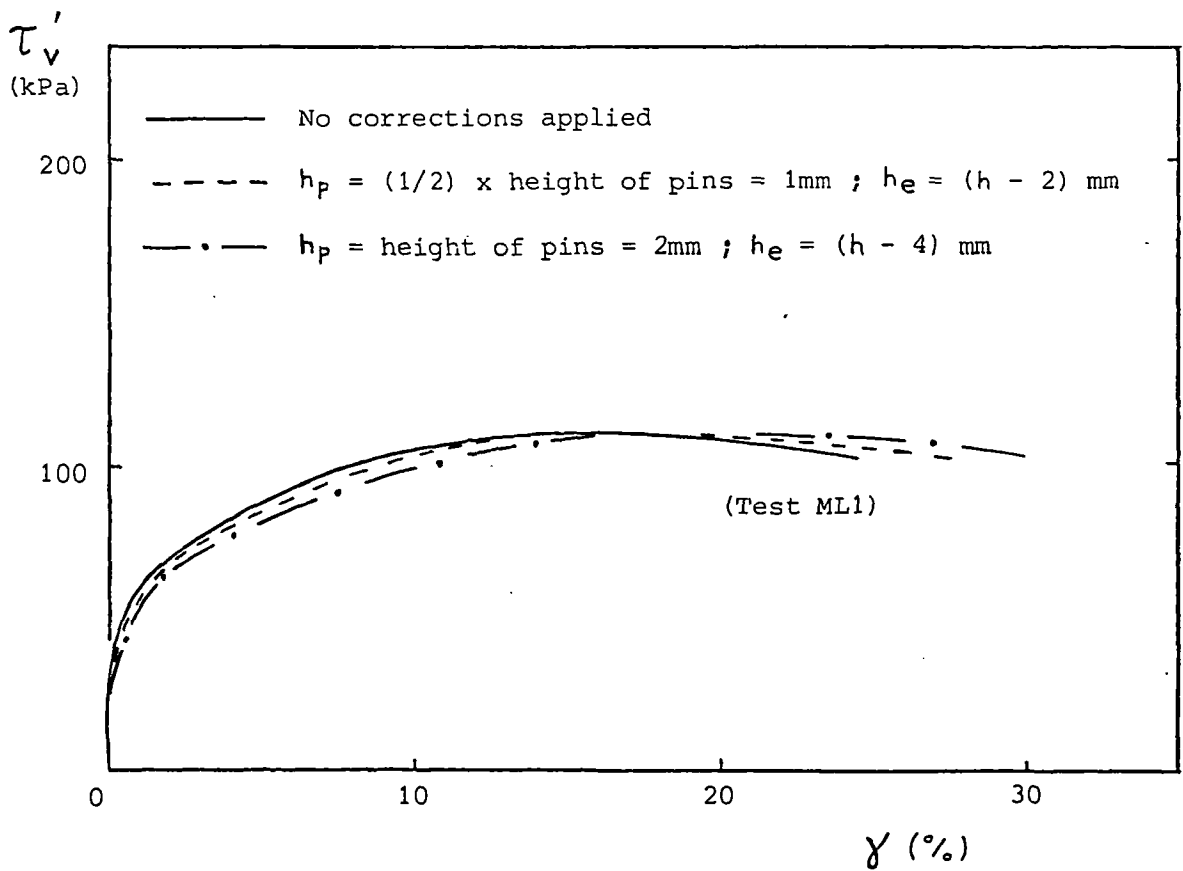
Figure D.2   Effect of pins on a typical shear stress versus
. shear strain curve
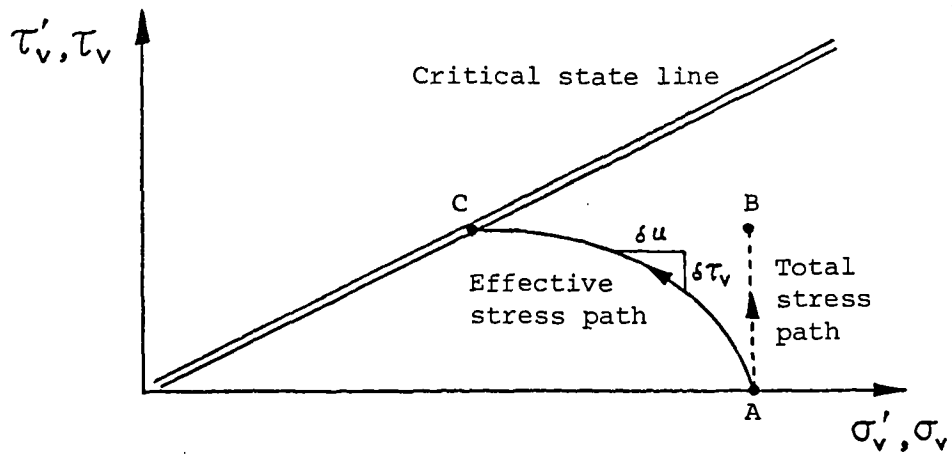
(a) undrained test
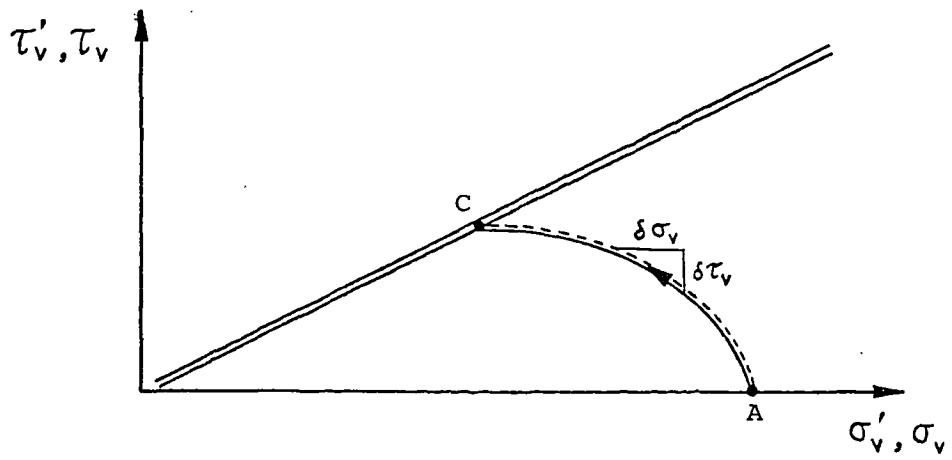
(b) constant volume test
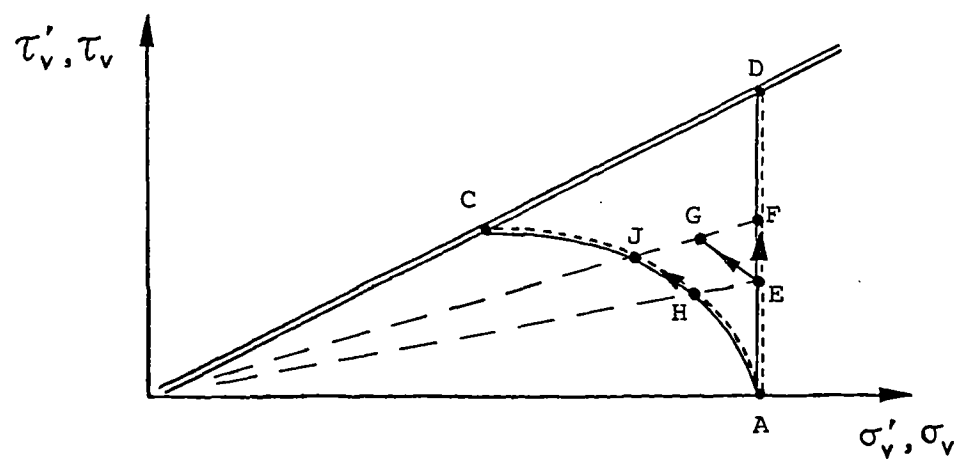
(c) constant σ_v' test

Figure E.1   Determination of α_s for simple shear tests on
normally consolidated samples
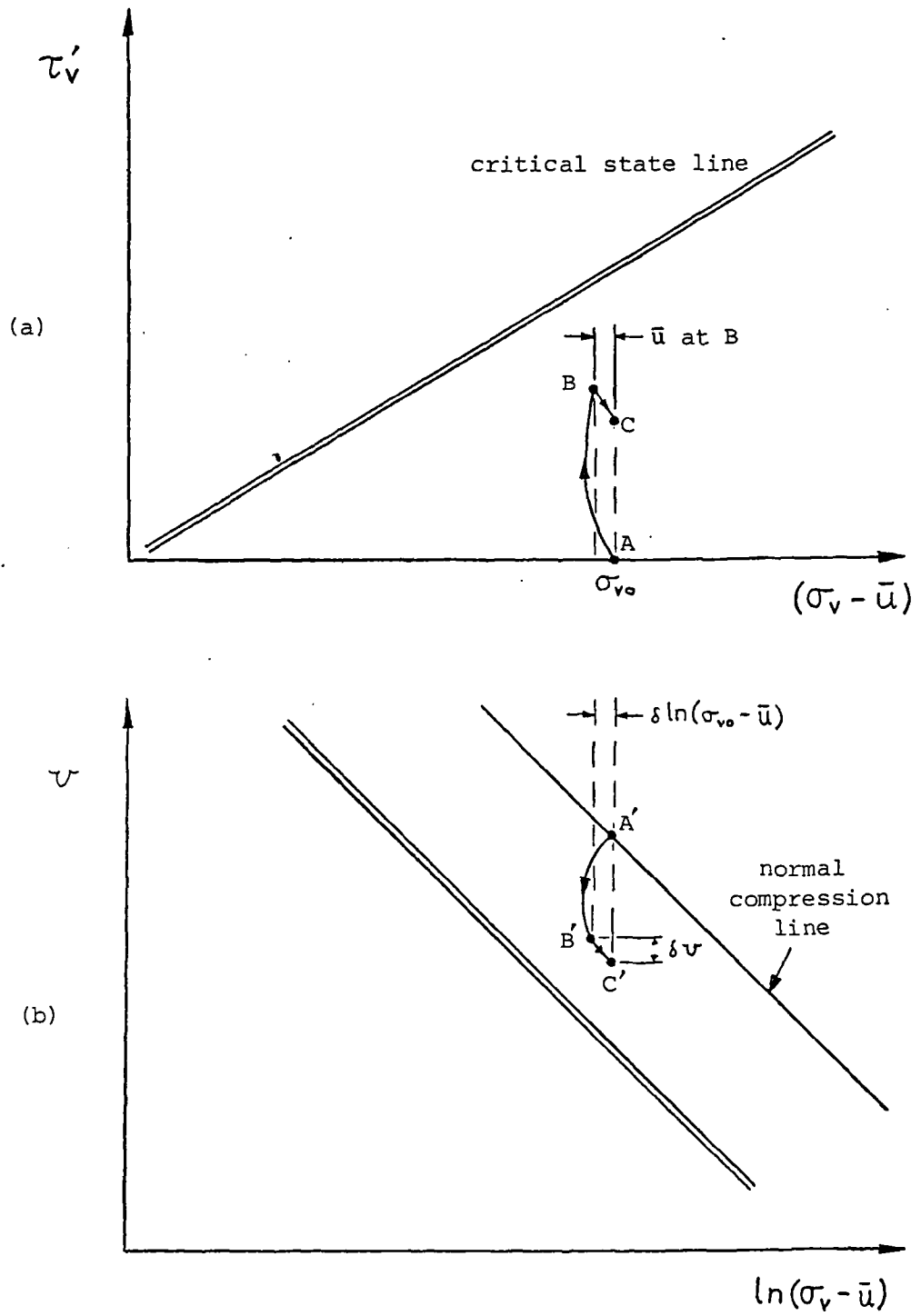
Figure E.2   Estimation of excess pore pressures in normally
consolidated simple shear samples during shearing
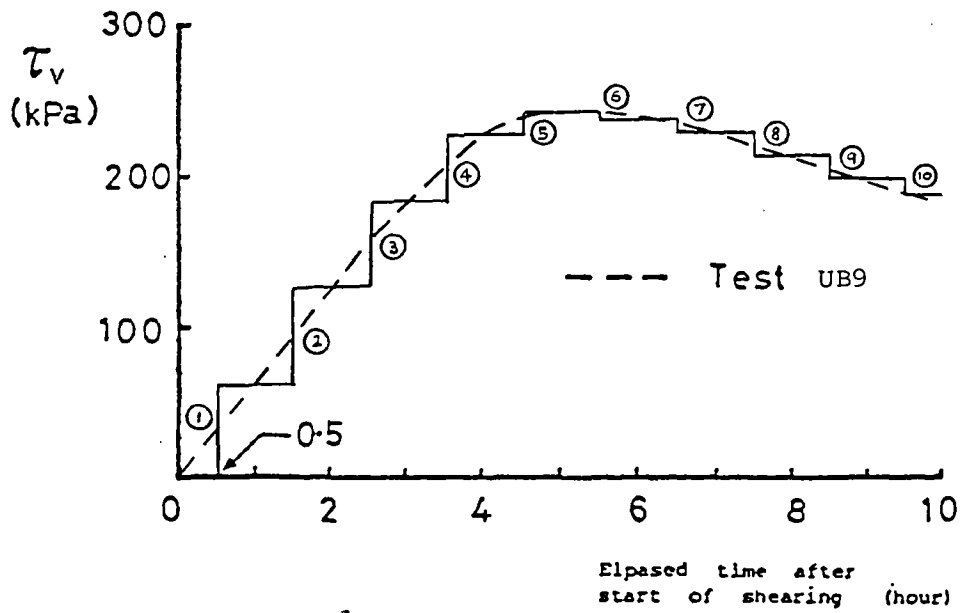
Figure E.3   Changes in τ_v with time approximated as a series of step increments for test UB9
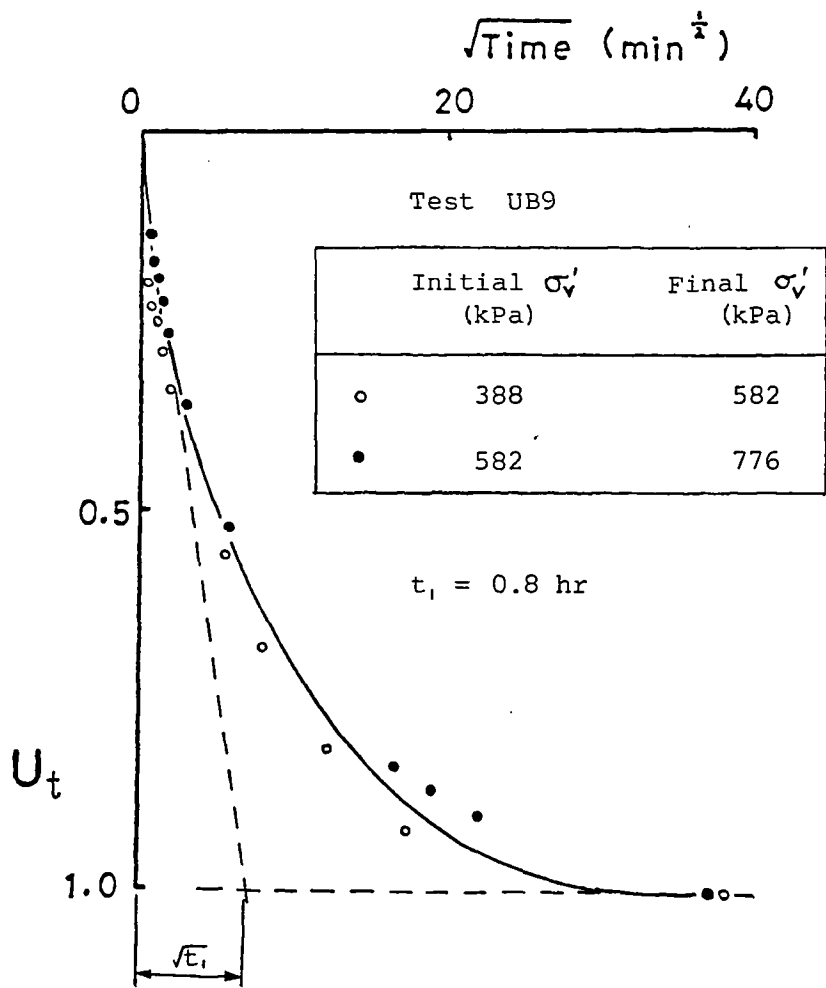
Figure E.4   Determination of t_i from one-dimensional consolidation data by $\sqrt{(time)}$ curve fitting method
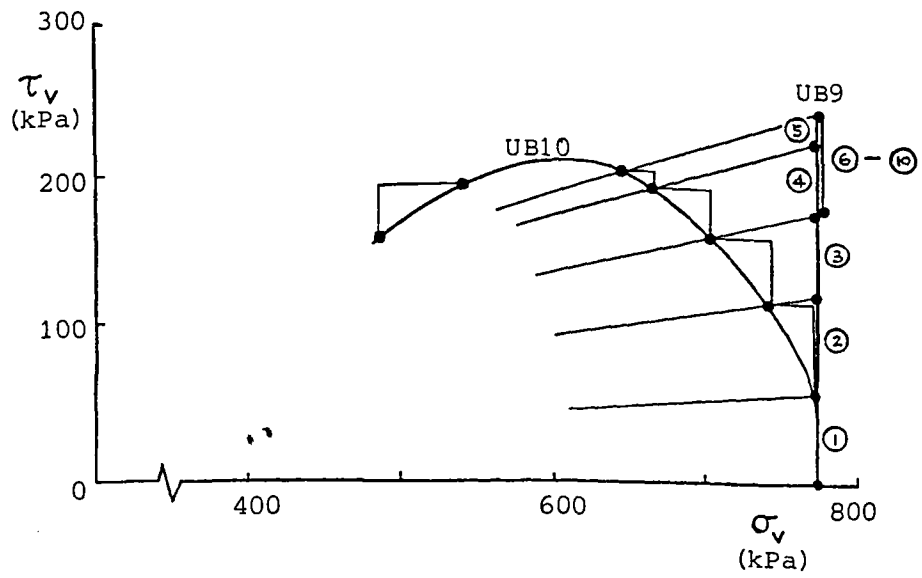
Figure E.5   Determination of α_s for each increment of τ_v
in test UB9
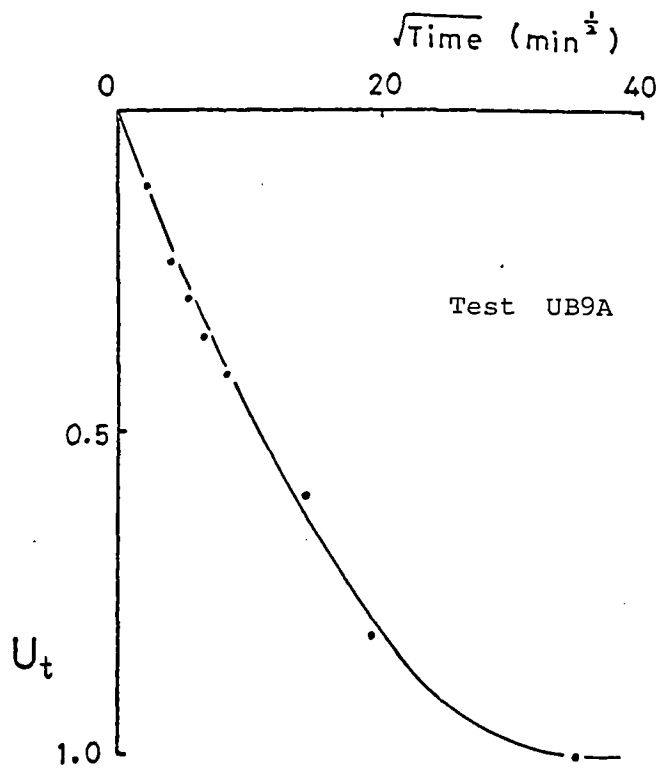
Figure   E.6   Variation of average degree of consolidation
with $\sqrt{\text{(time)}}$ during consolidation after
shearing suddenly stopped
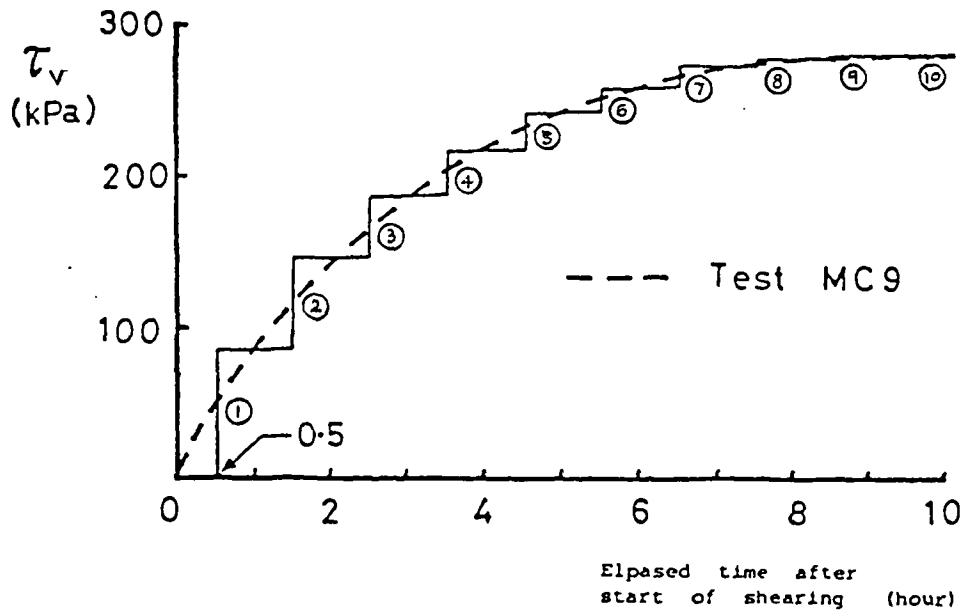
Figure E.7   Changes in τ_v with time approximated as a
series of step increments for test MC9
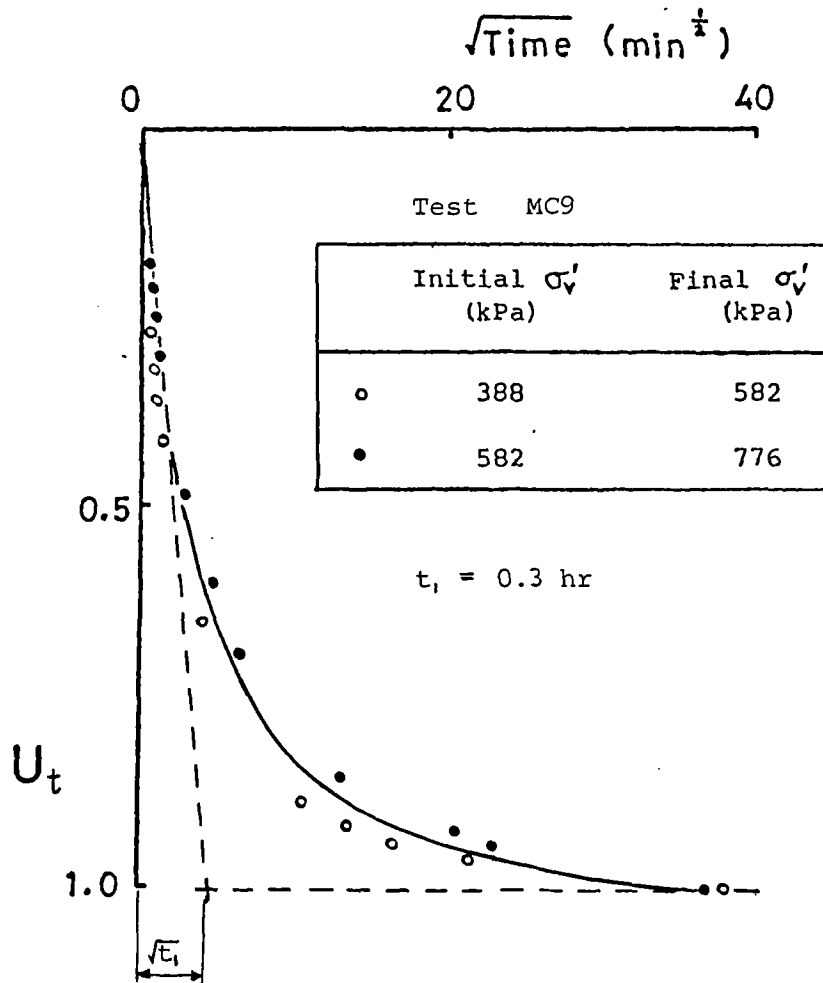
Figure E. 8   Determination of t_i from one-dimensional
consolidation data by $\sqrt{(time)}$ curve fitting
method
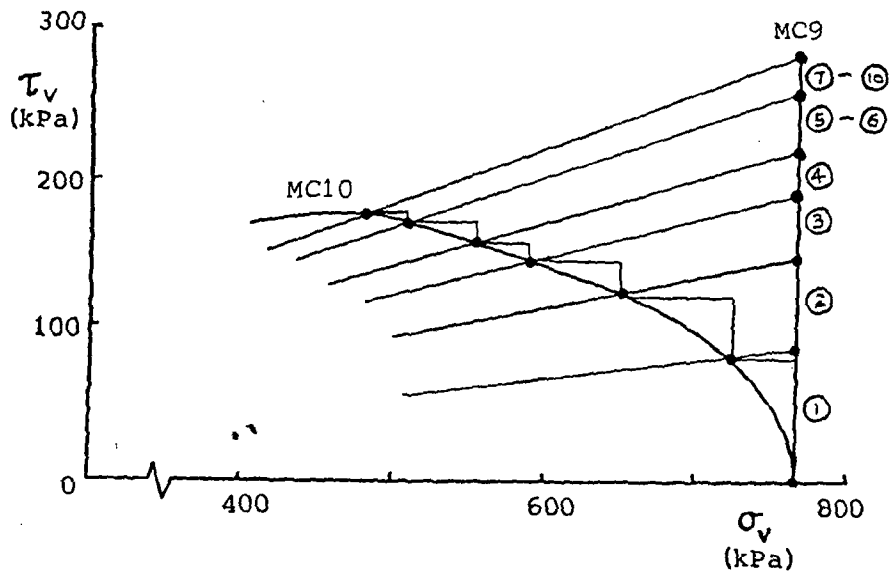
Figure   E.9   Determination of α_s for each increment
of τ_v in test MC9
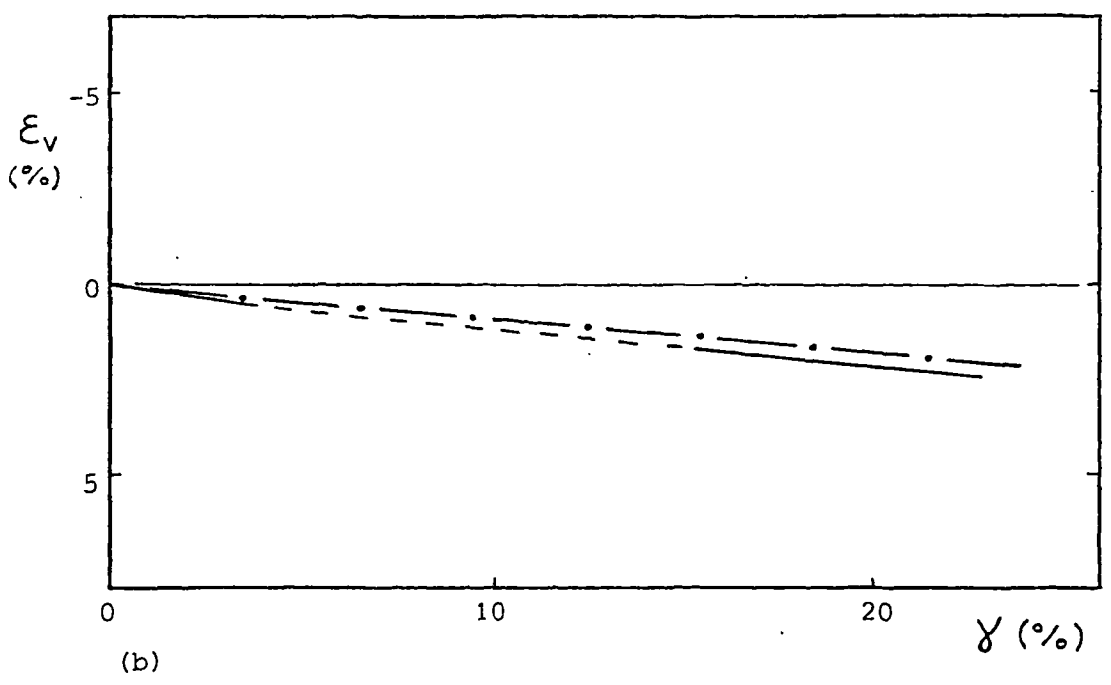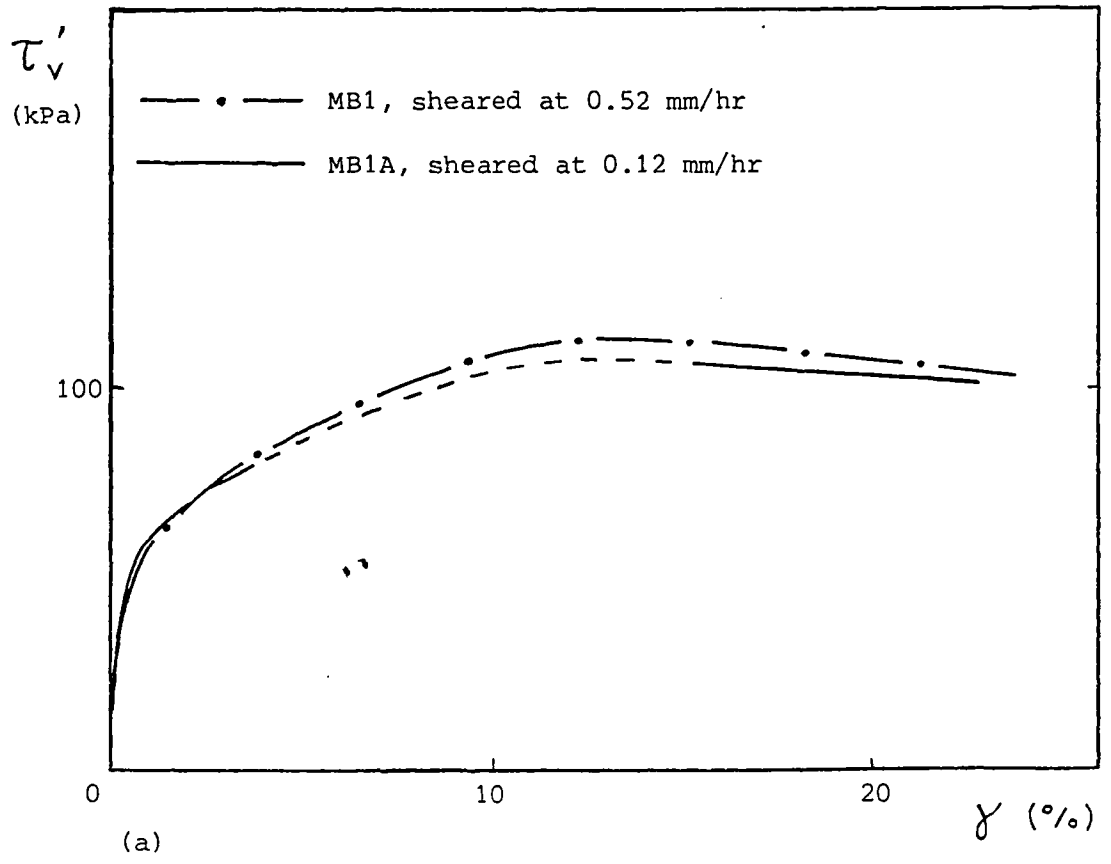
Figure   E.10   Comparison of results obtained from two samples
with same pre-shearing state sheared at different
rates under constant σ_v' condition